

32ND ANNUAL PRECISE TIME AND TIME INTERVAL (PTTI) SYSTEMS AND APPLICATIONS MEETING



*Proceedings of a meeting held at
the Hyatt Regency Hotel
at Reston, Virginia
28 — 30 November 2000*

The U.S. Naval Observatory
Washington, DC



32ND ANNUAL PRECISE TIME AND TIME INTERVAL (PTTI) SYSTEMS AND APPLICATIONS MEETING

Editor
Lee A. Breakiron
U.S. Naval Observatory

Proceedings of a meeting sponsored by
the U.S. Naval Observatory
the U.S. Naval Research Laboratory
the NASA Jet Propulsion Laboratory
the Defense Information Systems Agency
the U.S. Coast Guard Navigation Center
and the U.S. Army Research Office

and held at
the Hyatt Regency Hotel
at Reston, Virginia
28 — 30 November 2000



United States Naval Observatory
Washington, DC 20392-5420

2001

ORDER FORM FOR PROCEEDINGS

You can order back issues of the Proceedings from either PTTI or NTIS

Year	PTTI Price	NTIS Number	NTIS Price in U.S.; higher elsewhere
5 - 1973	\$ 25.00	AD-A010786/2	inquire
6 - 1974	\$ 25.00	AD-A018192/5	inquire
7 - 1975	unavailable	AD-A040774/2	inquire
8 - 1976	unavailable	AD-A043856/4	inquire
9 - 1977	unavailable	AD-A123920/1	inquire
10 - 1978	\$ 25.00	N79-24731/8	inquire
11 - 1979	unavailable	N80-29096/8	inquire
12 - 1980	\$ 25.00	N81-27467/2	inquire
13 - 1981	\$ 25.00	N82-20494/2	inquire
14 - 1982	unavailable	N83-35351/6	inquire
15 - 1983	\$ 25.00	AD-A149163/8	inquire
16 - 1984	unavailable	N85-29221/7	inquire
17 - 1985	\$ 25.00	inquire	inquire
18 - 1986	\$ 25.00	inquire	inquire
19 - 1987*	\$ 25.00	inquire	inquire
20 - 1988	\$ 25.00	AD-A217145/2INZ	\$ 77.50
21 - 1989	\$ 25.00	inquire	inquire
22 - 1990	\$ 50.00	N91-25755/0INZ	inquire
23 - 1991	\$ 50.00	AD-A255837/7INZ	\$ 31.50
23 - Tutorial	included	AD-A254745/3INZ	\$ 45.00
24 - 1992	\$ 50.00	AD-A267301/0INZ	\$ 86.50
25 - 1993	\$ 50.00	N94-30639/6INZ	\$ 103.50
26 - 1994	\$ 50.00	N95-32319/2INZ	\$ 86.50
27 - 1995	\$ 50.00	N19960042616INZ	\$ 69.50
28 - 1996	\$ 50.00	inquire	inquire
28 - Tutorial	\$ 15.00	inquire	inquire
29 - 1997	\$ 100.00	inquire	inquire
30 - 1998	\$ 100.00	inquire	inquire
31 - 1999	\$ 135.00	inquire	inquire
32 - 2000	\$ 135.00	Inquire	inquire

*Includes an Errata volume

When ordering from PTTI, return order form with payment to:

Treasurer, PTTI
 U.S. Naval Observatory
 3450 Massachusetts Avenue, NW
 Washington, DC 20392-5420
 Tel: 202-762-1414, Fax: 202-762-1511

Do not send cash. We cannot accept credit card orders.
 When you register for the PTTI meeting or order the
 Proceedings, your name is added to the PTTI mailing list to
 receive future meeting information.

When ordering from NTIS, contact:

U.S. Department of Commerce
 Technology Administration
 National Technical Information Service
 5285 Port Royal Road
 Springfield, VA 22161
 Tel: 800.553.6847, Fax: 703.605.6900

E-mail: orders@ntis.fedworld.gov
 WWW: www.ntis.gov

NTIS prices are subject to change without notice. There is
 also a handling fee. Microfiche is available.

EXECUTIVE COMMITTEE

DR. JOSEPH D. WHITE, CHAIRMAN
U.S. NAVAL RESEARCH LABORATORY

MR. RONALD L. BEARD
U.S. Naval Research Laboratory

LIEUTENANT DAVID FOWLER
U.S. Coast Guard Navigation Center

CAPTAIN THOMAS R. RICE
U.S. Coast Guard

DR. HOWARD SCHLOSSBERG
Deputy Assistant Secretary
U.S. Air Force/AQR

DR. ROBERT L. TJOELKER
NASA Jet Propulsion Laboratory

DR. LEE A. BREAKIRON
U.S. Naval Observatory

DR. DENNIS D. McCARTHY
U.S. Naval Observatory

MR. WILLIAM J. RYAN
Defense Information Systems Agency

MR. GEORGE SHATON
Department of Defense

Ms. FRANCINE M. VANNICOLA
U.S. Naval Observatory

ADMINISTRATIVE ASSISTANCE

Ms. NICOLETTE M. JARDINE
U.S. Naval Observatory

MRS. CARMEN DOMINIQUEZ
U.S. Naval Research Laboratory

OFFICERS

GENERAL CHAIRMAN

MR. HUGO FRUEHAUF
Zyfer, Inc.

TECHNICAL PROGRAM COMMITTEE

DR. PAUL KOPPANG

Datum — Timing, Test & Measurement

DR. ANDY WU, Co-CHAIRMAN

The Aerospace Corporation

DR. LEONARD S. CUTLER
Agilent Laboratories

MR. PAUL F. KUHNLE
NASA Jet Propulsion Laboratory

MR. DONALD H. MITCHELL
TrueTime, Inc.

Ms. FRANCINE M. VANNICOLA
U.S. Naval Observatory

MR. S. CLARK WARDRIP
SFA, Inc.

EDITORIAL COMMITTEE CHAIRMAN

DR. LEE A. BREAKIRON
U.S. Naval Observatory

TREASURER

DR. LEE A. BREAKIRON
U.S. Naval Observatory

EXHIBITS AND PUBLICITY COMMITTEE CHAIRMAN

MR. DONALD H. MITCHELL
TrueTime, Inc.

AUDIO-VISUAL CHAIRMAN

MR. HAROLD A. CHADSEY
U.S. Naval Observatory

TECHNICAL ASSISTANCE

MR. PAUL F. KUHNLE
NASA Jet Propulsion Laboratory

MEETING ARRANGEMENTS

Ms. SHEILA FAULKNER
SFA, Inc.

ADMINISTRATIVE ASSISTANCE

Ms. NICOLETTE JARDINE
U.S. Naval Observatory

Mrs. CARMEN DOMINGUEZ
U.S. Naval Research Laboratory

Mrs. BRENDA McHALE
Datum — Timing, Test & Measurement

DISTINGUISHED PTTI SERVICE AWARD COMMITTEE

DR. JOSEPH D. WHITE, CHAIRMAN
U.S. Naval Research Laboratory

DR. LEONARD S. CUTLER
Agilent Laboratories

DR. DENNIS D. McCARTHY
U.S. Naval Observatory

MR. DONALD H. MITCHELL
TrueTime, Inc.

DR. RICHARD L. SYDNOR
NASA Jet Propulsion Laboratory

PAST RECIPIENTS OF THE DISTINGUISHED PTTI SERVICE AWARD

1994

DR. GERNOT M. R. WINKLER
U.S. Naval Observatory (Ret.)

1995

DR. JAMES A. BARNES
National Institute of
Standards and Technology (Ret.)

1996

PROFESSOR SIGFRIDO M. LESCHIUTTA
Politecnico di Torino and
Instituto Elettrotecnico
Nazionale G. Ferraris

1997

PROFESSOR BERNARD R. GUINOT
Bureau International des
Poids et Mesures (Ret.)
Honorary Astronomer, Paris Observatory

1998

DR. JACQUES VANIER
National Research Council, Canada (Ret.)

1999

DR. LEONARD S. CUTLER
Agilent Laboratories

ADVISORY BOARD MEMBERS

MR. S. CLARK WARDRIP, CHAIRMAN
SFA, Inc.

Professor Carroll O. Alley
University of Maryland

Mr. Martin B. Bloch
Frequency Electronics, Inc.

Mrs. Mary Chiu
The Johns Hopkins University
Applied Physics Laboratory

Dr. Leonard S. Cutler
Agilent Laboratories

Mrs. Sheila C. Faulkner
SFA, Inc.

Mr. Hugo Fruehauf
Zyfer, Inc.

Mr. Robert H. Kern
KERNCO, Inc.

Dr. William J. Klepczynski
Innovative Solutions International

Dr. Paul A. Koppang
Datum — Timing, Test & Measurement

Mr. Paul F. Kuhnle
NASA Jet Propulsion Laboratory

Mr. Peter R. Lopez
TrueTime, Inc.

Mr. Donald H. Mitchell
TrueTime, Inc.

Mr. Jerry R. Norton
The Johns Hopkins University
Applied Physics Laboratory

Dr. Bradford W. Parkinson
Stanford University

Dr. Victor S. Reinhardt
Hughes Space and
Communications Company

Mr. William J. Riley
Datum — Timing, Test & Measurement

Dr. Henry Robinson
Duke University

Mr. Ronald C. Roloff
Geil Marketing Associates

Dr. Samuel R. Stein
Timing Solutions Corporation

Dr. Richard L. Sydnor
NASA Jet Propulsion Laboratory

Dr. Andy Wu
The Aerospace Corporation

SESSION CHAIRMEN

SESSION I

MR. ALECK HOLCOMB
TrueTime, Inc.

SESSION II

DR. WILLIAM J. KLEPCZYNSKI
Innovative Solutions International

SESSION III

Ms. LISA NELSON
National Institute of Standards
and Technology

SESSION IV

DR. DEMETRIOS N. MATSAKIS
U.S. Naval Observatory

SESSION V

DR. FRANÇOISE BAUMONT
Observatoire de la Côte d'Azur
Grasse, France

SESSION VI

DR. DENNIS D. MCCARTHY
U.S. Naval Observatory

SESSION VII

DR. DEMETRIOS N. MATSAKIS
U.S. Naval Observatory

SESSION VIII

DR. ROBERT L. TJOELKER
NASA Jet Propulsion Laboratory

SESSION IX

CDR CHRIS GREGERSON
U.S. Naval Observatory

SESSION X

MR. ED BUTTERLINE
Symmetricom

POSTER SESSION

DR. ANDY WU
The Aerospace Corporation

ARRANGEMENTS

MRS. SHEILA FAULKNER
SFA, Inc.

MR. PAUL F. KUHNLE
NASA Jet Propulsion Laboratory

FINANCE COMMITTEE

MR. RONALD L. BEARD
U.S. Naval Research Laboratory

DR. LEE A. BREAKIRON
U.S. Naval Observatory

DR. JOSEPH D. WHITE
U.S. Naval Research Laboratory

THE RECEPTIONISTS AT THE 32ND ANNUAL PTTI MEETING WERE:

**Ms. Brenda Hicks
Ms. Nicolette Jardine
Mrs. Aline Kuhnle
Mrs. Betty Wardrip**

TABLE OF CONTENTS

THE TIME AND FREQUENCY CONTROL COMMUNITY LOSES ONE OF ITS PIONEERS AND LEADERS	1
Dr. Helmut Hellwig (1938 — 2000)	
PTTI OPENING ADDRESS	3
Captain Benjamin J. Jaramillo, Superintendent, U.S. Naval Observatory	
PTTI DISTINGUISHED SERVICE AWARD	5
Presented by Dr. Joseph D. White U.S. Naval Research Laboratory to Roger L. Easton U.S. Naval Research Laboratory (Ret.) and ROBARCO	
IN THE BEGINNING OF GPS	7
Roger L. Easton, U.S. Naval Research Laboratory (Ret.) and ROBARCO	

SESSION I

PTTI VENDOR PRESENTATIONS

**Aleck Holcomb, Chairman
TrueTime, Inc.**

Presentations were made by representatives of Allen Osborne Associates, Inc.; Datum, Inc.; EndRun Technologies; Femtosecond Systems; Lange-Electronic GmbH; Oscilloquartz/Mme.; Quartzlock UK, Ltd.; SpectraDynamics, Inc.; Synergy Systems; Syntomics, LLC; TimeTech, GmbH; Timing Solutions Corporation; TRAK Systems; TrueTime, Inc.; and Zyfer, Inc.

SESSION II

GPS AUGMENTATION

**William J. Klepczynski, Chairman
Innovative Solutions International**

Modernization of the Global Positioning System

M. Shaw, U.S. Department of Transportation; K. Sandhoo, MITRE Corporation; and D. Turner, The Aerospace Corporation 17

WAAS, EGNOS, and MSAS for TELECOM SYNC

H. Fruehauf, Zyfer, Inc. 31

Modelization and Extrapolation of Time Deviation of USO and Atomic Clocks in GNSS-2 Context

J. Delporte, Centre National de'Etudes Spatiales, France; F. Vernotte, Observatoire de Besançon, France; M. Brunet, and T. Tournier, CNES 45

SESSION III

GPS AND GLONASS TIME TRANSFER

**Lisa Nelson, Chairman
National Institute of Standards and Technology**

Examining GPS Carrier-Phase Analyses to Evaluate the Accuracy of Frequency Transfer Using Data from NIST and PTB

L. Nelson and J. Levine, National Institute of Standards and Technology 57

A Transatlantic GETT Time Transfer Experiment — Latest Results

R. Dach, T. Schildknecht, T. Springer, Astronomical Institute, University of Berne, Switzerland; G. Dudle, and L. Prost, Swiss Federal Office of Metrology 67

Evaluation and Preliminary Results of the New USNO PPS Timing Receiver

M. Miranian, E. Powers, L. Schmidt, K. Senior, and F. Vannicola, U.S. Naval Observatory; J. Brad, and J. White, U.S. Naval Research Laboratory ... 79

Results From Time Transfer Experiments Based on GLONASS P-CODE Measurements From RINEX Files

F. Roosbeck, P. Defraigne, and C. Bruyninx, Royal Observatory of Belgium ... 91

Recovering UTC (USNO,MC) with Increased Accuracy Using a Fixed, L1-CA Code, GPS Receiver

R. Giffard, Agilent Laboratories 97

Progress on a New GPS Common-View Receiver M. Weiss, National Institute of Standards and Technology	111
The Infusion of MCS Kalman Filter Data into GPS Block II/IIA Frequency Standard Analysis Techniques G. Dieter, G. Hatten, and J. Taylor, Boeing Space and Communication Services	117
The Development of Multi-channel GPS Receivers at the CSIR — National Metrology Laboratory E. Marais, CSIR-NML, South Africa	129
One-Way GPS Time Transfer 2000 A. Gifford, National Institute of Standards and Technology; S. Pace, Rand Corporation; and J. McNeff, Science Applications International Corporation	137
Common-View and Melting-Pot GPS Time Transfer with the UT+ F. Meyer, Observatoire de Besançon, France	147
GPS-Based Time Error Estimates Provided by Smoothing, Wiener, and Kalman Filters: A Comparative Study Y. Schmaliy, Guanajuato University, Mexico; and A. Marienko, "Sichron" Center, Ukraine; M. Torres-Cisneros, and O. Ibarra-Manzano, Guanajuato University	157
Clock Synchronization Using GPS/GLONASS Carrier Phase K. Tu, H. Peng, C. Liao, National Standard Time and Frequency Laboratory and Chunghwa Telecom Company, Taiwan; and F. Chang, National Taiwan University	171

SESSION IV

TIME SCALES I

**Demetrios N. Matsakis, Chairman
U.S. Naval Observatory**

Time Links for the Construction of TAI J. Azoubib and W. Lewandowski, Bureau International des Poids et Mesures, France	181
A Revised Way of Fixing an Upper Limit to Clock Weights in TAI Computation J. Azoubib, Bureau International des Poids et Mesures, France	195

SESSION V

TWO-WAY SATELLITE TIME TRANSFER

**Françoise Baumont, Chairman
Observatoire de la Côte d'Azur, Grasse, France**

Results of a Continuous Transatlantic Two-Way Time Transfer Test Using Commercial Satellite Modems

T. Celano, Timing Solutions Corporation; S. Francis, Zeta Associates; A. Gifford, National Institute of Standards and Technology; B. Ramsey, and T. Erickson, Timing Solutions Corporation 211

TWSTFT Network Status in the Pacific Rim Region and Development of a New Time Transfer Modem for TWSTFT

M. Imae, M. Hosokawa, Y. Hanado, Communications Research Laboratory, Japan; Z. Li, Shaanxi Astronomical Observatory, China; P. Fisk, National Measurement Laboratory, Australia; Y. Nakadan, National Research Institute of Metrology, Japan; and C. Liao, Telecommunication Laboratories, Taiwan .. 221

Report on the 8th Meeting of the CCTF Working Group on Two-Way Satellite Time and Frequency Transfer

W. Lewandowski, Bureau International des Poids et Mesures, France 229

SESSION VI

LEAP SECONDS: PANEL DISCUSSION

**Dennis D. McCarthy, Chairman 235
U.S. Naval Observatory**

Relating Time to the Earth's Variable Rotation

H. Chadsey and D. McCarthy, U.S. Naval Observatory 237

SESSION VII

TIME SCALES II

**Demetrios N. Matsakis, Chairman
U.S. Naval Observatory**

A Total Estimator of the Hadamard Function Used for GPS Operations	
D. Howe, National Institute of Standards and Technology; R. Beard, U.S. Naval Research Laboratory; C. Greenhall, NASA Jet Propulsion Laboratory; F. Vernotte, Observatoire de Besançon, France; and W. Riley, Datum — Timing, Test & Measurement	255
Performance and Characterization of U.S. Naval Observatory Clocks	
L. Breakiron and D. Matsakis, U.S. Naval Observatory	269

SESSION VIII

ADVANCED FREQUENCY AND TIME SYSTEMS

**Robert L. Tjoelker, Chairman
NASA Jet Propulsion Laboratory**

USNO Alternate Master Clock Steering	
S. Hutsell, U.S. Naval Observatory Alternate Master Clock, and P. Koppang, Datum — Timing, Test & Measurement	289
Observing a Gravitational Wave Background with LISA	
M. Tinto, J. Armstrong, and F. Estabrook, NASA Jet Propulsion Laboratory ..	301
Theoretical and Experimental Study of Light Shift in a CPT-Based RB Vapor Cell Frequency Standard	
M. Zhu and L. Cutler, Agilent Laboratories	311
Preliminary Results from the USNO Atomic Fountain Development Project	
T. Swanson, E. Burt, and C. Ekstrom, U.S. Naval Observatory	325
Stabilized Reference Frequency Distribution for Radio Science with the Cassini Spacecraft and the Deep Space Network	
M. Calhoun, R. Wang, A. Kirk, W. Diener, G. Dick, and R. Tjoelker, NASA Jet Propulsion Laboratory	331
Multi-Purpose Time Analyzer and Monitor for Deep Space Network Time Synchronization	
J. Gonzalez, M. Calhoun, S. Cole, and R. Tjoelker, NASA Jet Propulsion Laboratory	341

Development of a Primary Reference Clock C. Green, Quartzlock, Ltd., UK	355
---	-----

POSTER SESSION

Andy Wu, Chairman
The Aerospace Corporation

(Papers have been reassigned in these Proceedings
to Sessions I, III, VII, VIII, and XI)

SESSION IX

FUTURE APPLICATIONS

Chris Gregerson, Chairman
U.S. Naval Observatory

Common Time Reference Technology for Systems Inter-Operability R. Beard and J. White, U.S. Naval Research Laboratory	367
--	-----

Development and Evaluation of GPS Space Clocks for GPS III and Beyond A. Wu and W. Feess, The Aerospace Corporation	389
---	-----

Global Positioning System (GPS) Modernization Lt. Col. C. McGinn, Capt. S. Rajotte, GPS Joint Program Office; and D. Latterman, Science Applications International Corporation	401
---	-----

Frequency Stability Requirements for Narrow Band Receivers W. Klepczynski, Innovative Solutions International; and P. Ward, Navward Systems	415
--	-----

SESSION X

TELECOM AND NETWORK TIMING

Ed Butterline, Chairman
Symmetricom

The Nanokernel D. Mills, University of Delaware; and P. Kamp, FreeBSD Project	423
---	-----

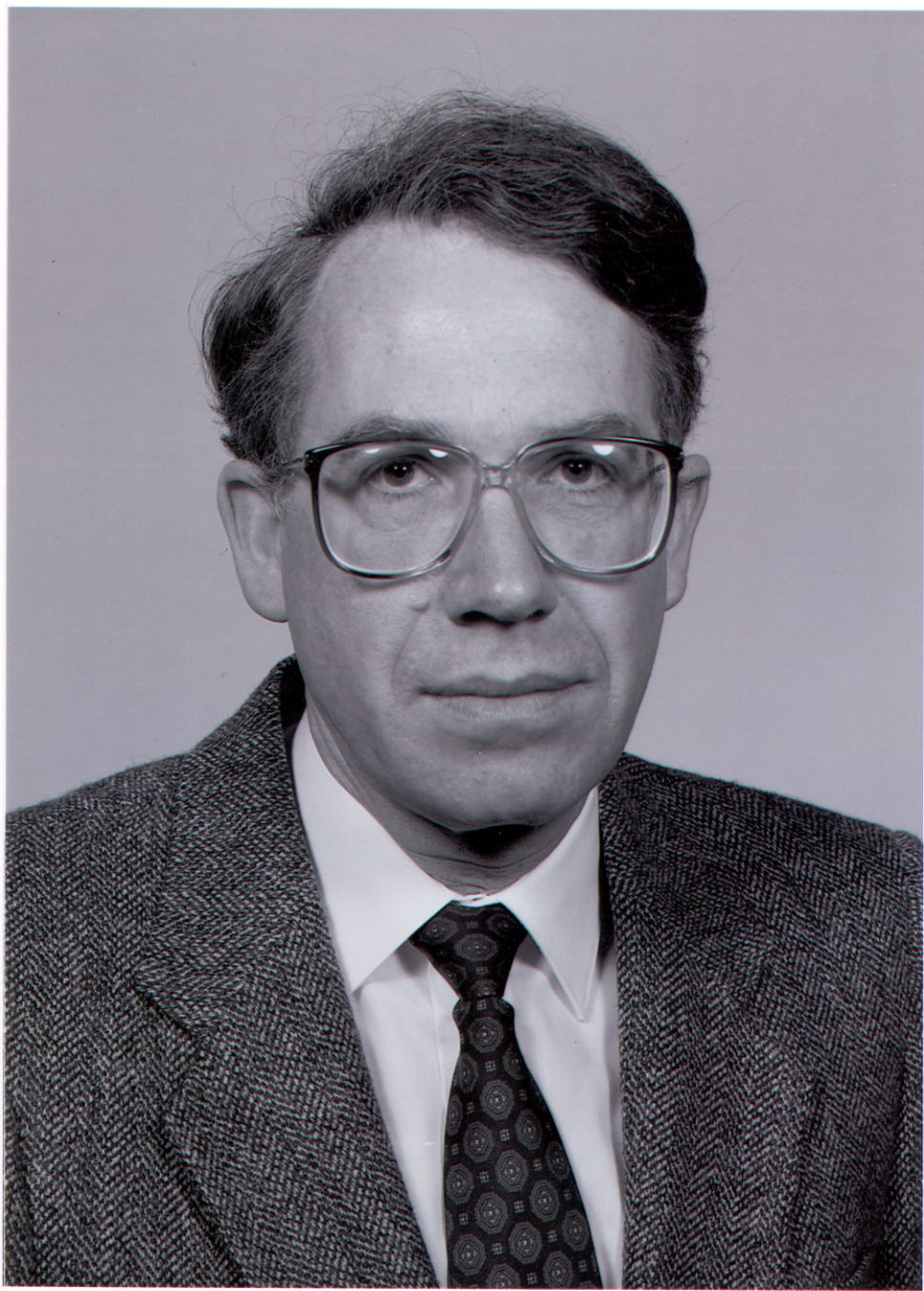
Using the Network Time Protocol (NTP) to Transmit International Atomic Time (TAI)	J. Levine, National Institute of Standards and Technology and University of Colorado; and D. Mills, University of Delaware	431
New Issues in Telecommunications	E. Butterline, Symmetricom	441
Primary Reference Clocks Using Indoor Antennas	D. Mitchell, TrueTime, Inc.	445

SESSION XI

NATIONAL LABORATORY REPORTS

(Reassigned in these Proceedings from the Poster Session)

The Time Link Between CSAO and CRL	L. Huanxin and W. Zhengming, Shaanxi Astronomical Observatory, China . . .	449
Time and Frequency Activities at the CSIR — National Metrology Laboratory	E. Marais, CSIR-NML, South Africa	455
Detection of the Gravitational Redshift of the Cesium Frequency Standard at CRL	M. Hosokawa, N. Kotake, K. Imamura, and N. Kurihara, Communications Research Laboratory, Japan	463
Millisecond Pulsar Observation at CRL	Y. Hanado, Y. Shibuya, M. Hosokawa, M. Sekido, and M. Imae, Communications Research Laboratory, Japan	471
List of Attendees	479



The Time and Frequency Control Community Loses One of its Pioneers and Leaders:

HELMUT HELLWIG (1938-2000)

The time and frequency control community lost one of its leaders on July 22, 2000 when Helmut Hellwig passed away. Helmut made many scientific and management contributions to our field and he will be missed by his many friends and colleagues.

Helmut Hellwig was born on May 7, 1938 in Berlin, Germany. His professional education in Germany included a 1963 Master of Science degree in physics and a 1966 Doctorate in electrical engineering, both from the Technical University of Berlin. During that period Helmut was a Researcher at the Heinrich Hertz Institute in Berlin. He immigrated to the United States in 1966 and became a U.S. citizen in 1972.

Dr. Hellwig was a research physicist in the field of atomic frequency standards for the U.S. Army Electronics Command in Ft. Monmouth, NJ between 1966 and 1969, and a Time and Frequency Division Research Physicist, Section Chief and Associate Division Chief at the National Bureau of Standards (NBS) in Boulder, CO between 1969-1979. While there, Helmut established an organizational culture of advanced research in the field of atomic clocks which persists to this day.

In 1979, Helmut became the President of Frequency and Time Systems, Inc. (FTS, now part of Datum, Inc.), a research and manufacturing company in Beverly, MA. He led the successful qualification and production of satellite cesium clocks for the Global Positioning System (GPS).

In 1986, Helmut returned to NBS as Associate Director. Then, in 1990 he was appointed Director of the Air Force Office of Scientific Research, Bolling Air Force Base, DC, where he was responsible for managing the entire basic research program of the U.S. Air Force. He built a strong research infrastructure carried out by approximately 6,000 researchers in Air Force Laboratories, universities and industries.

In 1996, Helmut was appointed Deputy Assistant Secretary for Science, Technology and Engineering, Office of the Secretary of the Air Force (Acquisition) in Arlington, VA. In that position, he was responsible for all Air Force investments in science and technology. Helmut retired from this position in 1999.

He was a Fellow of the IEEE, a Member of the American Physical Society and Sigma Xi. He was also a member of the International Scientific Radio Union (URSI), the International Radio Consultative Committee (CCIR) and the International Astronomical Union (IAU)

Helmut was very active in IEEE and frequency control committees, including the I&M and UFFC Societies. He was an Associate Editor of the Transactions on UFFC, Chairman of the I&M Technical Committee on Time and Frequency, and a member of the PTTI Executive Committee. He has also organized or co-organized numerous national and international conferences.

He was granted several patents in the field of atomic frequency standards, and published about 100 technical and scientific articles and papers.

Helmut received a number of professional awards, including an honorary doctorate from the University of Besancon, France in 1989 for his work on atomic frequency standards, and a 1996 Air Force Senior Executive Service, Presidential Rank Award for exceptional performance over an extended period of time. He was also the recipient of the E.U. Condon Award, the IR-100 award and the United States Army Science Award.

Helmut is survived by his wife Thekla, his two sons Frank and Peter, and two granddaughters.

Donations may be made in Helmut Hellwig's name to RICA, a facility for children and adolescents with severe emotional disabilities at 15000 Broschart Road, Rockville MD 20850.

OPENING ADDRESS

**Capt. Benjamin Jaramillo
Superintendent
U.S. Naval Observatory
Washington, DC 20392, USA**

Ladies and gentlemen, good morning. It is a pleasure to open the 32nd Annual Precise Time and Time Interval (PTTI) Meeting.

Over the past 32 years, these meetings have continued to provide the timing community with an opportunity for users to present their ideas and requirements for improving the ability of the timing community to meet the nation's needs. Similarly, these conferences have allowed time and time interval providers to make system developers aware of the latest improvements in the field. The objectives of the series of meetings, namely to disseminate and coordinate PTTI information at the user level; to review present and future PTTI requirements; to inform government engineers, technicians, and managers of precise time and frequency technology; and, to provide opportunity for an active exchange of new technology associated with PTTI, are more important today than ever before.

Since the first PTTI meetings, the precision with which time and time interval are measured and transferred has improved by three orders of magnitude, a factor of 10 per decade. We have witnessed remarkable growth in the use of precise time and frequency. It is safe to say that the development of precise time has played a critical role in the growth of technology that touches all of our lives today. The Global Positioning System (GPS) is the prime example of a system based on timing that has had a remarkably extensive impact on all aspects of society. There are many others.

The program for this meeting includes topics that promise exciting, significant developments for the future. Sessions are devoted to issues related to time scales, advances in frequency and timing systems, future timing and frequency applications, telecommunications, utilities, Internet protocol, and GPS augmentation systems. All of these timing applications point out the need to recognize operational standards for timekeeping and time transfer. The Department of Defense (DoD) has clearly realized that the interoperability is a major issue.

It has become evident that standards for time and time interval play an increasingly important role in ensuring that modern defense systems can communicate among themselves without confusion and function effectively. We need to eliminate the costly practice of independent development and nonstandard terminology without regard for the requirement to operate with existing systems and without regard for the likely systems of the future. The U.S. Naval Observatory (USNO) is prepared to assist those who are improving current systems and those who are in the process of developing new systems to provide effective PTTI applications and eliminate needless and extensive duplication. The growing importance of GPS and GPS-based timing is evident. The papers in the sessions of this meeting will no doubt demonstrate the latest numbers characterizing the precision and accuracy of the systems that take advantage of

GPS for timing. The growing use of GPS, however, is not without its own issues.

We know that the dependency on GPS is slowing the development of improved clocks. It is also necessary to consider the requirement for additional sources of precise time and frequency, and the development of possible alternate time transfer methods will definitely be a concern for the future to mitigate the possibility of a single point of failure. Realize, too, that the increasing use of inter-operable systems will demand accurate, as well as precise, time to permit this inter-operability.

Finally, I would like to close with the concern that the PTTI community must continue to challenge system engineers to make use of the potential development of increasingly more accurate time and time interval. While we need to keep track of user requirements for PTTI, we also need to challenge users to take advantage of possible 10-picosecond timing or one part in 10^{16} in frequency.

We often hear that precise time is a utility and that we must recognize the need to manage this new utility to meet society's current and future requirements. Part of this management responsibility is to make sure that users are aware of current and projected PTTI capabilities. National and international laboratories must work together to make sure that the world's timing needs are met and that society can make use of what we expect to make available in the future. I hope that this and future meetings will continue to address these concerns. But, in addition, I would like to challenge users of time to think creatively about new possibilities that take advantage of our ability to provide time and time interval with improving precision. The utility of precise time will in the future provide improvements for us all, and we need to plan now to take advantage of this resource.

Thank you for giving me the opportunity to open this meeting. I know that it will be an interesting and productive meeting for all of us. I would like to introduce Mr. Joe White, who has a presentation.

PTTI DISTINGUISHED SERVICE AWARD

**Presented to
Roger L. Easton
U.S. Naval Research Laboratory (Retired)
ROBARCO**

**by
Dr. Joseph D. White
U.S. Naval Research Laboratory**

Captain, thank you for the opening remarks. I am the Chairman of the PTTI Executive Committee, and mostly what I get to do in that job is delegate things to others and stand back and watch things happen. But every now and then, I find a good job that I like to keep for myself, and this is one of them.

The PTTI has its Distinguished PTTI Service Award. We award this sometimes annually, sometimes less. It kind of depends on how we feel and whether we feel we have good candidates. In this case, this year we have an exceptional person that we're honoring, a man that I've been honored to work for and to know for 20-something years now. Roger Easton will be our award winner this year.

Most of you have known Roger at one time or another during his career, which has been quite long and distinguished. Some of you knew him before I have met him. I worked for him from 1973 to 1980, I guess it was. He's done a number of other things since he retired. And I thought I'd just take a minute to go over briefly some of Roger's accomplishments, and there are a lot; I'm reducing them to just the big ones here today.

Roger worked for NRL and the Navy continually from World War II up to 1980. Among his accomplishments there were the design and the construction of the first Vanguard satellite. An outgrowth out of that was a system called "Mini-Track," which was developed to track Vanguard and later expanded to do other things. Mini-Track grew into a system that became known as the "Naval Space Surveillance System." That all started around 1960 or so. "SpaceSur" is not well known in the community, but in fact if you look at NORAD's list of what's flying around in space today, most the items on that list, I think something like 75 or 80%, come out of SpaceSur. It's a system that's still going, still growing, and Roger is one of the people that made SpaceSur happen.

Roger also, shortly after SpaceSur, invented a one-way ranging concept that became a Navy program that was known as "Timation." For those of you that know the history of GPS, Timation was one of two programs, that and the Air Force 621B project, which became GPS. That's about the time I went to work for Roger. The things that make GPS work so well, the clocks, the orbits, a lot of the concepts all came from Roger. We owe him a great debt of

gratitude for the work he did there.

As I say, Roger retired from NRL around 1980; however, that was by no means the end of his career. He did a number of other things after that, including politics. Roger was elected twice to the New Hampshire General Court, which I believe is roughly the same thing as the State Assembly. And in 1986 he actually ran for Governor. He was beaten by an upstart by the name of John Sununu, and we understand that it had to do with the irregular voting in the southern part of the state and dimpled ballots. But he came close.

Roger has also received a number of awards over the years. I would like to list a few of those: in 1960, back in the SpaceSur days, as that started up, he won NRL's Distinguished Civilian Achievement Award. Roger was one of several people involved in the Collier Award, which is shared between NRL, Aerospace, the Air Force, and Rockwell for GPS.

Another award that I thought was very interesting was the Magellanic Premium Award from the American Philosophical Society. And I'll read the description to you of what this is: "a medal to be awarded from time to time to the author of the best discovery or most useful invention relating to navigation, astronomy, or natural philosophy." Roger is also a Fellow of the Institute of Navigation.

Sometimes, though, as you look through the list of people, a lot of people have won awards. One of the things that kind of gets your attention, as to how well recognized they are, is how many awards have been named after them. I know there are at least two in Roger's case: There's the Roger L. Easton Science and Engineering Award, which was out of Naval Space Surveillance, and the NRL Roger L. Easton Award for Engineering Excellence. I'm particularly interested in the NRL award because NRL, like most laboratories, is a hard science laboratory, but we have a group that does engineering. In hard science groups, the engineering people often get ignored. So it's very nice to see that award came for Roger and recognized not only his achievements, but also the achievements of the people who have followed.

So Roger, if I could you up here please, I'd like to make the award. You have to be aware of boxes that tick. I don't know how you are going to get this back on the airplane. This is the clock that is awarded as the PTTI Distinguished Service Award. It's inscribed "Distinguished PTTI Service Award 2000 to Roger Easton."

KEYNOTE ADDRESS: IN THE BEGINNING OF GPS

**Roger L. Easton
U.S. Naval Research Laboratory (Ret.)
and ROBARCO**

INTRODUCTION

Good morning. My talk is on the beginning of GPS. I've given this talk several times. Twice it went quite well. But the last time, it was a dead thud, so I'm warning you. A lot of its acceptance level had to do with the listener's age, because when one talks about 1969 to people who weren't born then, the talk has little current meeting.

GPS is a navigation system consisting of two dozen satellites in circular, inclined orbits. Each satellite contains a number of stable clocks. The satellites transmit clock-based synchronized signals continuously, allowing us to have a system unlimited by the number of participants. Further, in not needing interrogation, the user can observe radio silence. Having all the clocks synchronized is a big thing for GPS. At the time the idea of the satellites carrying the clocks was proposed, all the other proposals used interrogated schemes. Receivers detect signals from several satellites simultaneously (> three for x, y, z, and t). From these observations, position and time are calculated.

Where did GPS start? There have certainly been some wild comments about the beginning: (1) "It was developed by the DoD for the U.S. military," which is true; (2) "GPS can trace its heritage to the Navy's Transit program," which is not true; (3) "It began in 1973," while it actually began in 1964. Comment (1) is not especially helpful and comments (2) and (3) are not supported by the documented evidence. One is reminded of the quotation of Thomas Henry Huxley concerning "the slaying of a beautiful hypothesis by an ugly fact." Everything was going fine with these explanations until a fact came along and destroyed them all.

Let's look at some documented evidence. Early in the proposal stage of advanced navigation systems, in 1969, an EASCON meeting was held in Washington. Three different navigation proposals were discussed. (I've given Dr. White copies of these three proposals in case you would like to read them in full.)

LOW-ALTITUDE PROPOSAL

A paper by R. B. Kershner of APL studied the number of satellites necessary at different altitudes to have four-in-view to an observer on the earth's surface. At an altitude of 475 nautical miles (nm), 153 satellites are required. Seventy-eight are required at 1000 nm; 28

are needed at 5000 nm; 18 at 10,000 nm; and 18 at synchronous. Then Dr. Kerschner made a weight and cost comparison between satellites of a constellation at 480 nm and one at synchronous. As seen in the table below, the costs are not greatly different. The APL paper favored the low-altitude proposal.

Weight & Cost Comparison

Altitude	480 nm	Sync.
Tx Power	19 W	150 W
Weight	300 lb.	1100 W
Unit Cost	\$1.5 M	\$11.3 M
Constellation Cost	\$225 M	\$203 M

Conclusion: Costs About Equal

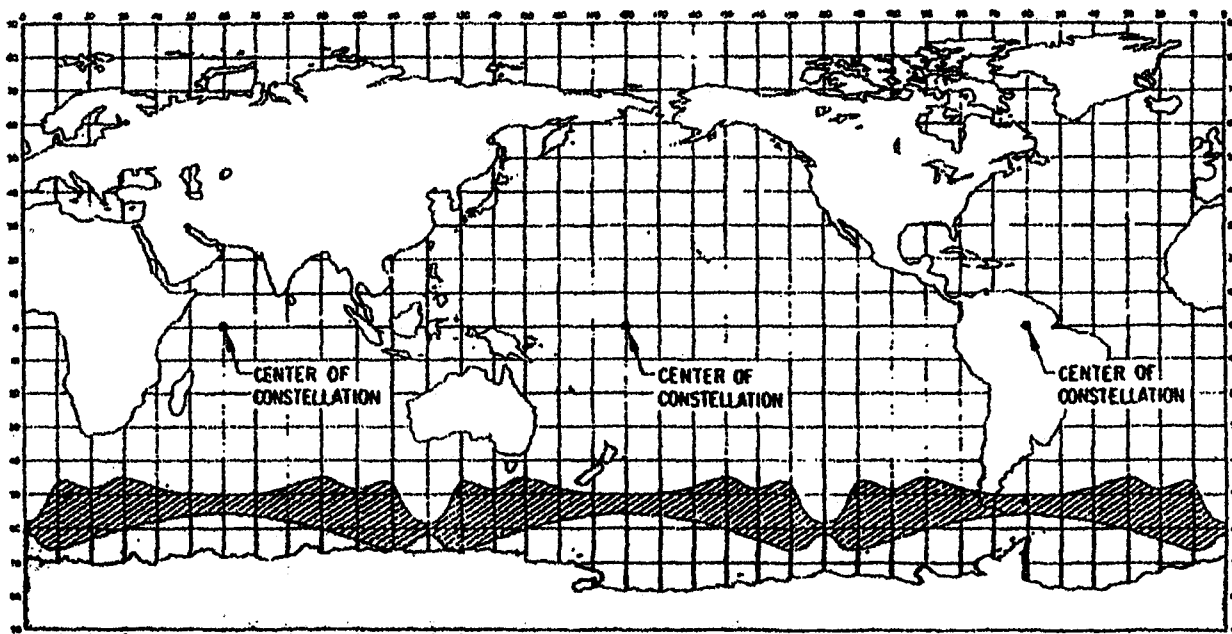
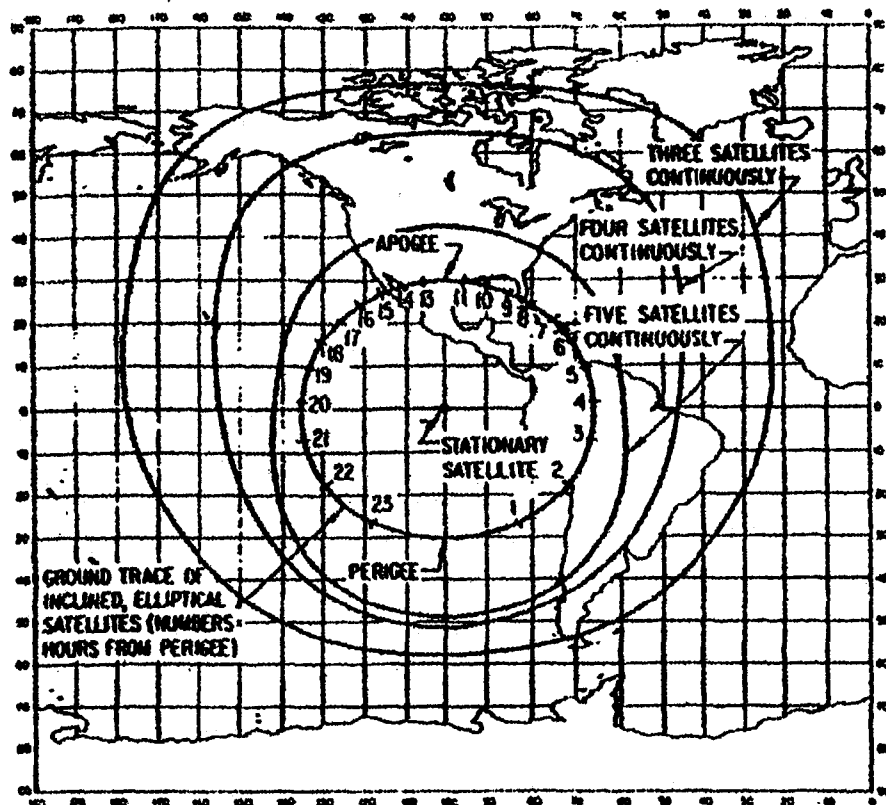
THE AEROSPACE 24-HOUR CONSTELLATION PROPOSAL

The Aerospace Corporation proposed a 24-hour constellation made up of several choices of sub-constellations and two orbital inclinations. The next figure shows the geometry of one sub-constellation. It consists of a single geostationary satellite with three (or four) satellites in circular ground tracks traveling with the geostationary satellite at the center. The non-geostationary satellites have inclinations of 30 degrees and eccentricities of 0.3 to give the circular ground tracks in the next figure.

The following figure shows the coverage results with three constellations similar to the one described above; for a viewer seeing four to seven satellites for three-dimensional (3D) navigation; for three satellites in view for two-dimensional (2D) navigation; and places near the South Pole with intermittent coverage. The coverage in the North was better because the apogees of the eccentric satellites were to the north. It was a clever system, but its coverage was not strictly global.

WHERE DID GPS START?

So where did GPS start? As I said before, not with the Transit program, though Transit has some similarities. And it started much before 1973. We claim that it can trace its ancestry to the radar "fence" of the Navy Space Surveillance System in 1964, long before some in our audience were born.

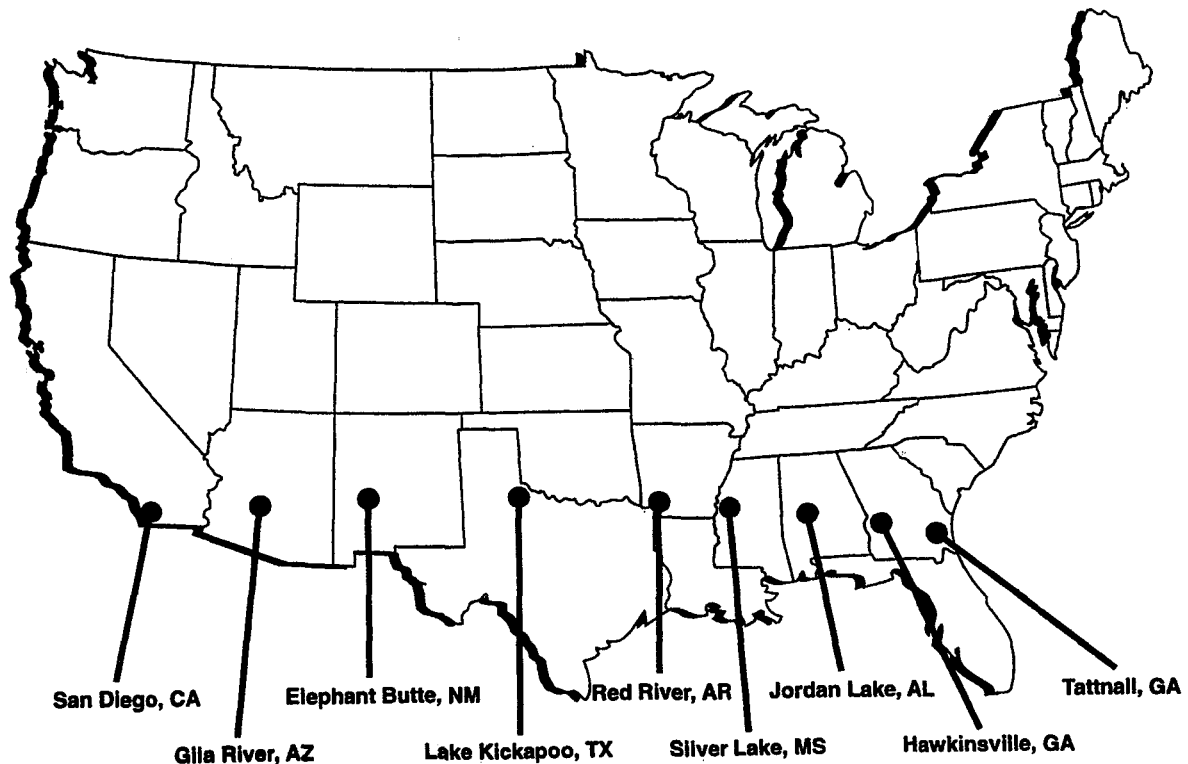


CODE	SATELLITES CONTINUOUSLY VISIBLE	NAVIGATION PROVIDED
■	3	2-DIMENSIONS
□	4 TO 7	3-DIMENSIONS
▨	INTERMITTENT COVERAGE	

COVERAGE FOR $i = 30 \text{ deg}$, $e = 0.30$
MINIMUM ELEVATION ANGLE = 5 deg

THREE CONSTELLATIONS OF FIVE SATELLITES EACH

For a few years in the early 1960s, we operated another fence in addition to the stations shown in the next figure. This second fence was in Southern Texas, with a transmitter near Rio Grande and a receiver near Raymondville. This second fence provided a second look at objects passing vertically through the two systems and permitted the determination of an orbit as soon as the second observation was received. This arrangement was especially valuable for the determination of orbits of multiple pieces.



There are at least two types of radars: pulse radars, which send and receive at one antenna, and continuous wave radars. We worked with the latter, having transmitter and receiver about 100 miles apart. We needed to know the modulation phase of the transmitter at the receiver as it was transmitted. We tried over-the-horizon transmission, which didn't work too well, as the signal was noisy. We tried carrying a cesium-beam clock between the two stations. The idea worked, but it was a continuous job, so we thought, why not put the cesium-beam clock in the satellite?

What else could such a satellite do besides transmit time? We decided it could be used for navigation. We were subjected to criticism because it was an idea looking for an application and not the other way around.

THE MID-ALTITUDE CONSTELLATION

At NRL we investigated a large range of altitudes, from low to synchronous and concentrated mainly on an integral number of ground tracks per day. We favored 8-hour orbits, but had done some work on the 12-hour orbits that GPS chose.

For a few years in the early 1960s, we operated another fence in addition to the stations shown in the next figure. This second fence was in Southern Texas, with a transmitter near Rio Grande and a receiver near Raymondville. This second fence provided a second look at objects passing vertically through the two systems and permitted the determination of an orbit as soon as the second observation was received. This arrangement was especially valuable for the determination of orbits of multiple pieces.

There are at least two types of radars: pulse radars, which send and receive at one antenna, and continuous wave radars. We worked with the latter, having transmitter and receiver about 100 miles apart. We needed to know the modulation phase of the transmitter at the receiver as it was transmitted. We tried over-the-horizon transmission, which didn't work too well, as the signal was noisy. We tried carrying a cesium-beam clock between the two stations. The idea worked, but it was a continuous job, so we thought, why not put the cesium-beam clock in the satellite?

What else could such a satellite do besides transmit time? We decided it could be used for navigation. We were subjected to criticism because it was an idea looking for an application and not the other way around.

THE MID-ALTITUDE CONSTELLATION

At NRL we investigated a large range of altitudes, from low to synchronous and concentrated mainly on an integral number of ground tracks per day. We favored 8-hour orbits, but had done some work on the 12-hour orbits that GPS chose.

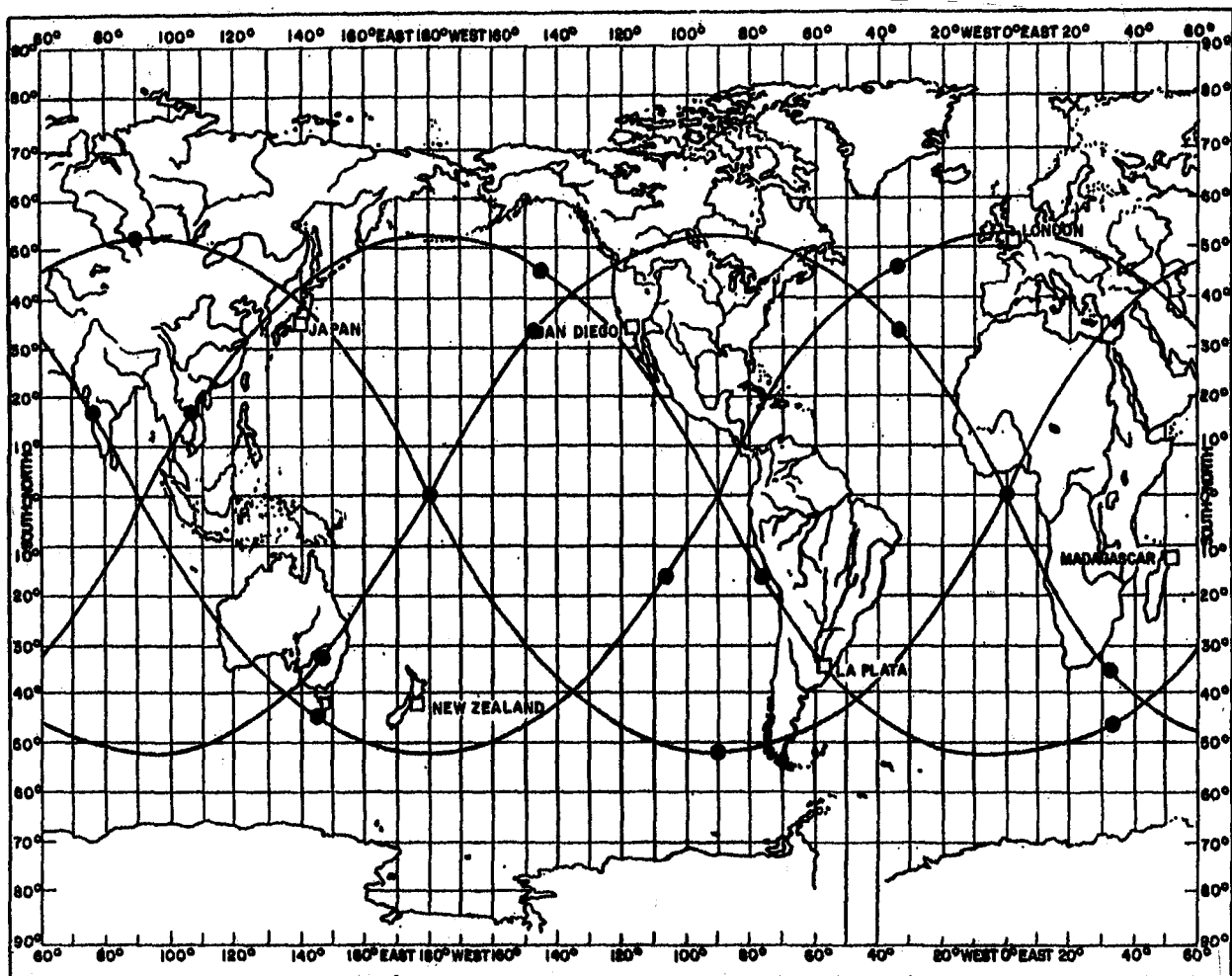
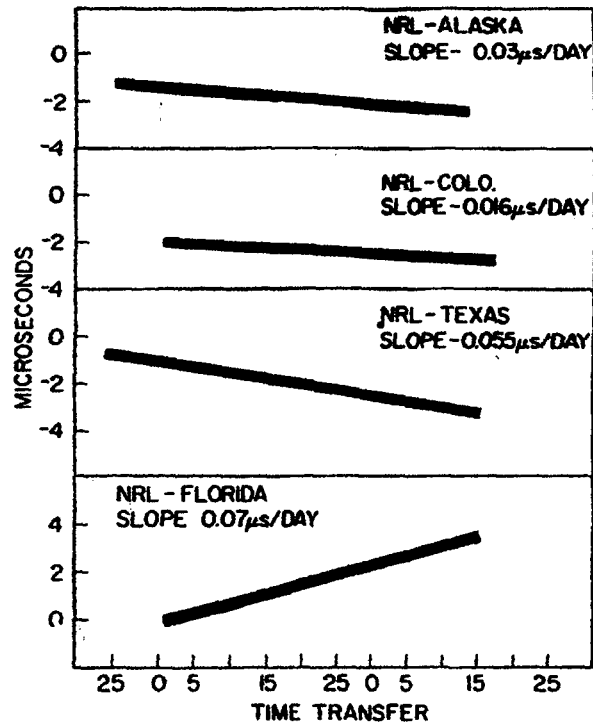
We demonstrated our TIMe navigATION (TIMATION) concept to the Naval Air Systems Command in 1964. As a result, NAVAIR sent us a \$35,000 Work Order. The reason the order was so small is that the project manager did not think he could get approval for a larger order.

We then demonstrated passive ranging for 2D and 3D and time which satisfied the navigation needs of aircraft, ships, and ground personnel. In the EASCON paper we favored polar orbits, intermediate altitudes, and circular orbits. We considered quartz and atomic oscillators and obtained the time transfer results in the next figure with the first TIMATION satellite, launched May 31, 1967.

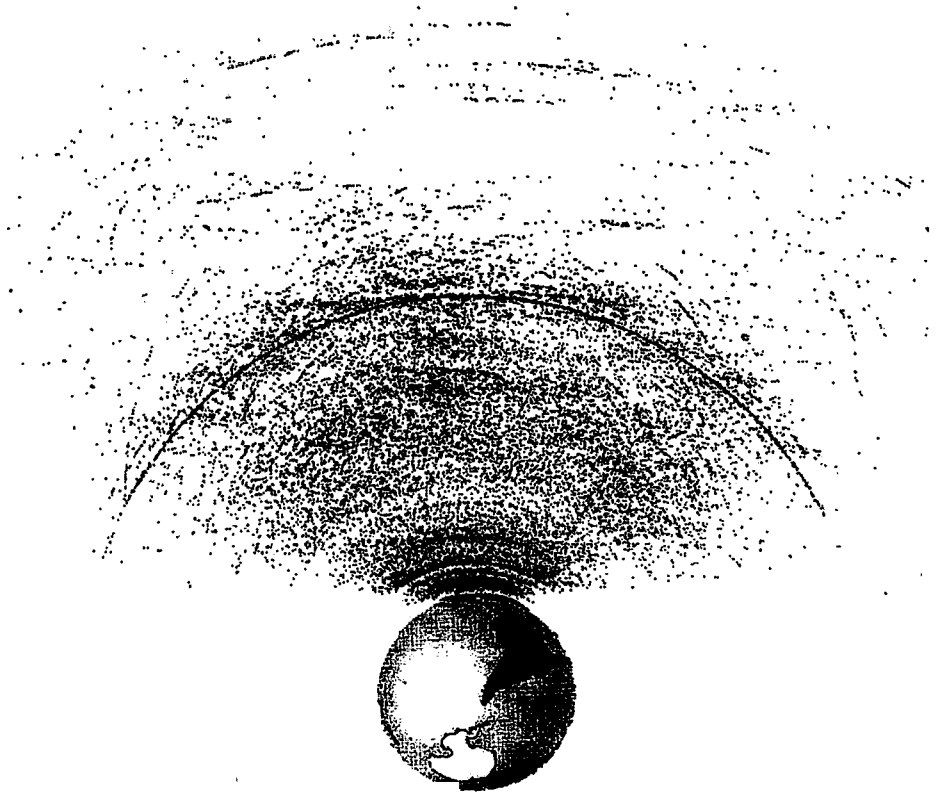
If I had my choice now I think I would go with polar inclinations. We went with 55 degrees because that came out as an optimum under the assumptions used. However, you miss something at that inclination. Unless you are at a low altitude, you see no satellites north (or south) of you. A polar satellite would also be advantageous for keeping the clocks on time.

ANOTHER MID-ALTITUDE PROPOSAL

There was another, somewhat similar mid-altitude proposal from General Electric that I must confess that I didn't know about. In a development led by Roy Anderson, it proposed two dozen satellites in 6-hour orbits. It was proposed to NASA and we didn't pay much attention to it. In the following figure are shown its ground tracks and you see it was at 55 degrees, just like GPS. It had both active and passive ranging and accuracies of 0.1 and 1 mile respectively.



The next figure shows observations seen from the present space surveillance fence. The arc about 12,000 miles from the earth represents the observations of the GLONASS satellites.



THE WINNER

Why did the mid-altitude proposal win? One could say because it was cheaper, more accurate, truly worldwide, and required fewer ground stations. The chart above relates the different proposals to the final design of GPS. One could say that since the GPS came from the NRL proposal, it naturally is most like the NRL TIMATION proposal. The next table compares the various proposals, showing which are most like the final choices (X) for GPS.

Proposal	Circular Orbit	Medium Altitude	Global Coverage	Atomic Clocks
GE	X	X	X	O
Aerospace (621B)	O	O	O	O
APL	X	O	X	O
NRL	X	X	X	X

Since the relevant patent may be of some interest, I've included a copy of the first page.

United States Patent [19]
Easton

[11] **3,789,409**
[45] **Jan. 29, 1974**

[54] **NAVIGATION SYSTEM USING SATELLITES
AND PASSIVE RANGING TECHNIQUES**

[76] **Inventor:** Roger L. Easton, 7704 Oxon Hill Rd., Oxon Hill, Md. 20021

[22] **Filed:** Oct. 8, 1970

[21] **Appl. No.:** 79,307

[52] **U.S. CL.... 343/112 R, 343/100 ST, 343/112 D**

[51] **Int. Cl..... G01s 5/14, G01s 11/00**

[58] **Field of Search..... 343/112 D, 112 R, 100 ST**

[56] **References Cited**

UNITED STATES PATENTS

3,643,259	2/1972	Entner	343/112 D X
3,384,891	5/1968	Anderson	343/100 ST UX
2,947,985	8/1960	Cooley	343/112 D UX
3,397,400	8/1968	Maass et al. . .	343/112 D UX
2,924,820	2/1960	Dishal et al.....	343/112 D UX
3,339,202	8/1967	Earp	343/112 D X

Primary Examiner—Richard A. Farley

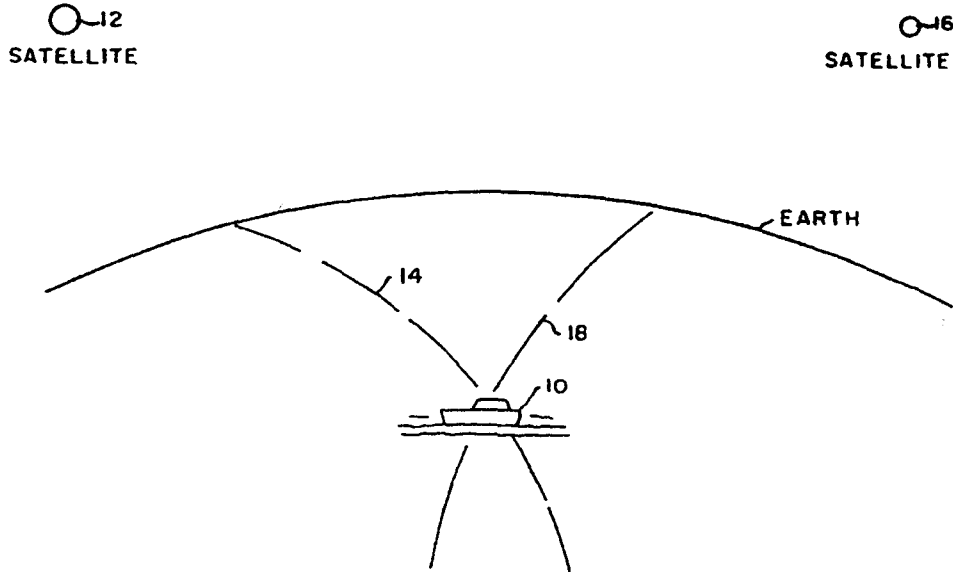
Assistant Examiner—Richard E. Berger

Attorney, Agent, or Firm—R. S. Sciascia; Arthur L. Branning; J. G. Murray

[57] **ABSTRACT**

A navigation system wherein the navigator's location is obtained by determining the navigator's distance (or range) from one or more satellites of known location. Each satellite transmits multifrequency signals that are derived from a stable oscillator which is phase synchronized with the navigator's equipment that produces similar multifrequency signals. Phase comparison between the signals received from the satellites and the locally produced signals indicates both the distance between the navigator and the satellites and the navigator's location. In determining his location, the presence of the navigator is not revealed since no interrogatory transmission by him is required.

6 Claims, 3 Drawing Figures



THE SECOND PART

This talk was made in two parts. You've have heard the first or technical part. The second part consists of a number of quotations. "The purpose of poetry is to persuade, fool, or compel God into speaking" is a favorite from Howard Nemerov. It is especially pertinent if you feel that some engineering approaches a class of poetry.

Then there are religious quotes coming from technical people. There's the famous one from Einstein: "Der Herrgott is subtle but not malicious." Two others, "Doing physics was walking the path of God" and "Doing physics was wrestling with the Champ," are by I. I. Rabi, who, of course, had much to do with atomic clocks.

John M. Zinman said, "Modern science is a successful social invention for acquiring, not truth, but reliable knowledge." I think Robert Frost's quote, "Two roads diverged in a wood and I took the one less travelled by," is perhaps a good way of looking at what we do in experimental fields. Of course, Frost is sort of a permanent poet laureate up New Hampshire and Vermont. He lived in both states, but was born in California and named for General Lee.

Some developments that were essential to GPS are small atomic clocks and integrated circuits. I was glad to see Mr. Fruehauf here. He was in on the very small atomic clocks, which we flew in satellites. Later, we went to Mr. Kern's cesium clocks.

I want to say something concerning awards: "Love of praise is, I believe, common to all men and whether it be a frailty or a virtue, I plead no exception from its fascination" (Capt. J. Eads, 1874). I like this one: "All anybody needs to know about awards is that Mozart never received one" (Henry Mitchell).

If you look at the awards mentioned in the World Almanac or any other almanac, you will see that there are almost none that apply to engineering. We know of the Pulitzer and Nobel prizes, but there are at least 29 entire categories of other awards. You won't find many scientific awards. When I was young, the Collier Award for Advances in Aviation was generally known. It's not well known now, nor is the oldest U.S. award, the Magellanic Premium (1786). So if you want an award, go into a field like entertainment, sports, or writing, and stay away from fields that change the world, like engineering.

In spite of what I have said about awards, I appreciate the one given me today. It's a beautiful clock. I will try to place it in its proper place. Thank you very much.

Questions and Answers

BRUCE MONTGOMERY (Syntomics, LLC): Who were the chaps at General Electric who were so prescient back in 1964? They got it pretty close to right.

ROGER EASTON: That was Roy Anderson. I got to know him very well since, and he's very impressive in this field.

HUGO FRUEHAUF (Zyfer, Inc.): The irony was that GE dropped out of the satellite business when it finally got to the satellite award. Even though they were so ahead of the game.

EASTON: You are saying **they** dropped out?

FRUEHAUF: Yes, the final bidders were Rockwell and RCA at the time, and General Electric ended up bowing out of the satellite race, which was kind of ironic.

EASTON: Then they ended up buying RCA, right?

FRUEHAUF: Right.

MODERNIZATION OF THE GLOBAL POSITIONING SYSTEM¹

Michael Shaw

Office of the Assistant Secretary of Defense for C3I
U.S. Department of Transportation

Kanwaljit Sandhoo

Center for Advanced Aviation System Development (CAASD)
MITRE Corporation

David Turner

The Aerospace Corporation

Abstract

More than two decades have now passed since the construction of the GPS operational control segment (OCS), including the Master Control Station (MCS) at Schreiber AFB, Colorado and worldwide monitoring stations, and launch of the first GPS satellites. During that time, several generations of satellites have been designed, built, and launched, and operations are routinely supported by the OCS.

Today, Global Positioning System (GPS) is entering into the new millennium with a far-reaching program to modernize the system on the ground and in space. This paper describes the goals, requirements, design objectives, and plans for implementing a \$1 billion-plus modernization program in the coming decade.

INTRODUCTION

The Department of Defense (DoD) originally conceived the Global Positioning System (GPS) in the 1970s as a satellite-based navigation system for joint-service military applications. Beginning in 1980, federal radionavigation planning conducted jointly by the DoD and the Department of Transportation (DOT) forever transformed this system into a global utility for positioning, navigation, and timing (PNT).

In 1996, federal policy and planning for GPS and its augmentations were significantly strengthened with the release of the Presidential Decision Directive (NSTC-6) "U.S. Global Positioning System Policy." The PDD provides the strategic vision for the management and use of GPS, addressing a broad range of military, civil, commercial, and scientific interests, both national and international. Further, specific roles and responsibilities were assigned to the DoD, DOT, and the State Department. The PDD also established the DoD-DOT-chaired Interagency GPS Executive Board (IGEB) to manage the GPS and its U.S. Government augmentations.

¹A version of this paper appeared in the September 2000 (Vol. 11, No. 9) edition of *GPS World Magazine* and this paper was previously presented at ION-GPS 2000, 13th International Technical Meeting of the Satellite Division of the Institute of Navigation, 19-22 September 2000.

The first meeting of the IGEB took place the following year. The major topic of discussion at that meeting was the need for additional civil GPS signals to improve services provided to a vast array of civil and commercial users. As a result, the IGEB agreed to identify a second civil frequency within a year. Combined with an effort already underway within the Air Force to incorporate both civil and military requirements into an updated GPS operational requirements document (ORD), these activities established the foundation of the current GPS modernization program.

MODERNIZATION GOALS

Civil Goals

The GPS Standard Positioning Service (SPS) refers to the signal-in-space provided free of direct user charges for peaceful civil, commercial, and scientific use on a continuous, worldwide basis. Today, only one fully accessible signal (the C/A-coded signal at L1) is available for civil applications through the SPS. Therefore, the principal objective of modernization from a civil perspective is to provide additional coded civil signals.

In 1998, Vice President Gore announced that a second civil signal would be broadcast at the 1227.6 MHz frequency, known as the GPS L2. Only a P (Y)-code, used by the U.S. military and other authorized users, is currently modulated on this frequency. (The Y-code refers to the encryption of the precise P-code to make it available only to authorized users.) The Vice President also stated that a third civil signal specifically designed for safety-of-life services would be broadcast beginning in 2005. Backed by the intense labors of interagency working groups formed under the auspices of the IGEB, the frequency of the third civil signal, now known as L5, was selected in January 1999. The L5 will be at 1176.45 MHz in a portion of the spectrum that is allocated for aeronautical radionavigation services (ARNS). The ARNS allocation is required for any signal used in support of any aviation safety-of-life application. The resulting changes to the GPS signal structure are illustrated in Figure 1.

For stand-alone (non-differential) real-time users of GPS, the addition of a second and third civil GPS signal will: provide signal redundancy, improve positioning accuracy, improve signal availability and integrity (timely notice of an "unhealthy" signal), improve continuity of service, and improve resistance to radio frequency (RF) interference.

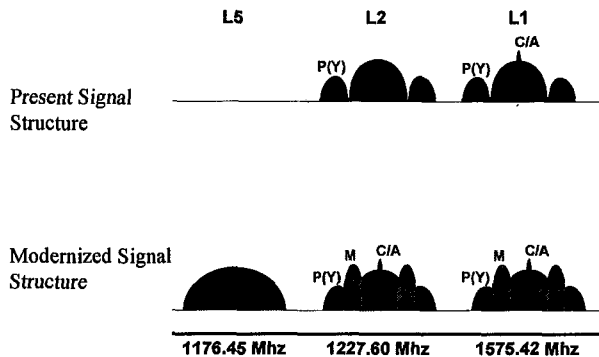


Figure 1
Current and Modernized Signal Structures

The two new additional coded civil signals (the C/A-code on the L2 frequency and the new signal at L5) will also assist high-precision (often called real-time kinematic) short- and long-baseline differential applications – such as aircraft precision approach and landing, mapping, surveying, precision farming, machine control, and earth science studies – by calibrating the spatially uncorrelated components of the ionosphere seen across the baseline and by speeding up ambiguity resolution to get accuracies of a decimeter or better.

Military Goals

In addition to providing an SPS, the 1996 GPS PDD and subsequent legislation ² also committed the U.S. government and the DoD to providing a Precise Positioning Service (PPS) for U.S. military and other authorized users. Further, the policy also called for the development of measures to prevent the hostile use of GPS and its augmentations, thus ensuring that the United States and its allies retain a military advantage without unduly disrupting or degrading legitimate, peaceful civil GPS uses.

This has been translated into what is often referred to as the 3 P's:

- Protection of military service in a theater of operation
- Prevention of adversarial exploitation of GPS services
- Preservation of civil service outside a theater of operations.

To successfully accomplish the 3 P's, the military must have the ability to selectively and locally deny GPS signals which could be potentially misused, while ensuring that authorized PPS users can continue military operations. Spectral separation of civil signals from military signals represents a key component of this capability. As a result, defense-oriented GPS modernization focuses on providing new military codes, referred to collectively as M-code, that will "reuse" portions of the radio spectrum already assigned to the L1 and L2 frequencies while remaining spectrally distinguishable from the L1 and L2 C/A-codes (see Figure 1).

The new military signal and code structure will also have improved cryptographic protection and changes in the broadcast data message. Based on validated military requirements for higher signal power, future GPS satellites will also be designed to broadcast the new M-code signals on a regional basis, when necessary, at 20 dB greater power (-138 dBW) than the existing P (Y)-code. These improvements will provide the U.S. military and its allies with both increased anti-jam capability and enhanced signal security for military worldwide operations.

SIGNAL STRUCTURE

Implementation of a new signal structure represents the cornerstone of improved GPS services for both military and civil communities. For civil users, however, the first real step towards modernizing GPS took place earlier this year when President Clinton directed that the intentional degradation of the GPS Standard Positioning Service (SPS), known as Selective Availability (SA), be discontinued at midnight Eastern Daylight Time on 1 May 2000. Figure 2 below illustrates the impact of this "magic moment."

Since SA was discontinued, GPS users have routinely observed horizontal SPS accuracy values of less than 10 meters. However, more conservative accuracy estimates (based on the conditions and constraints described in Ref. [2]) would be 22 meters horizontal (95% of the time), 33 meters

²National Defense Authorization Act for Fiscal Year 1998, Public Law 105-85, sec. 2281, 18 November 1997

vertical (95%), and 200 nanoseconds (95%) relative to Coordinated Universal Time (UTC), the international standard for timekeeping. The corresponding GPS horizontal positioning error budget is shown in Table 1.

Table 1
GPS Error Budget with and without SA

Error Source	Typical Range Error Magnitude (meters, 1σ)	
	SPS with SA	SPS with SA set to zero
Selective Availability	24.0	0.0
Atmospheric Delay		
Ionospheric	7.0	7.0
Tropospheric	0.2	0.2
Clock and Ephemeris Error	2.3	2.3
Receiver Noise	0.6	0.6
Multipath	1.5	1.5
Total User Equivalent Range Error (UERE)	25.0	7.5
Typical Horizontal DOP (HDOP)	1.5	1.5
Total Stand-Alone Horizontal Accuracy, 95%	75.0	22.5

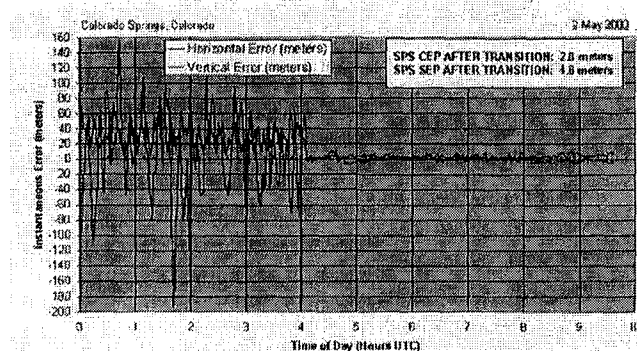


Figure 2
Performance with SA off

Without any additional equipment costs to users, discontinuing SA brings tangible benefits to millions of GPS users throughout the world in a wide range of applications. Some of these benefits are described below:

Car Navigation

Previously, GPS-based car navigation could give the location of the vehicle to within a hundred meters. This was a problem, for example in areas where multiple highways run in parallel, because the degraded signal made it difficult to determine which highway the car was on. Discontinuing SA will minimize such problems, leading to greater consumer confidence in the technology and higher adoption rates. It will also simplify the design of many systems (e.g., eliminating the need for certain map matching software), thereby lowering their retail cost.

Enhanced-911

The FCC will soon require that all new cellular phones be equipped with more accurate location determination technology to improve responses to emergency 911 calls. Removing

SA will boost the accuracy of GPS to such a degree that it could become the method of choice for implementing the 911 requirements. A GPS-based solution might be simpler and more economical than alternative techniques such as radio tower triangulation, leading to lower consumer costs.

Hiking, Camping, and Hunting

GPS is already popular among outdoorsmen, but the degraded accuracy has not allowed them to precisely pinpoint their location or the location of items (such as game) left behind for later recovery. With 20-meter accuracy or better, hikers, campers, and hunters should be able to navigate their way through unmarked wilderness terrain with increased confidence and safety. Moreover, users will find that the accuracy of GPS exceeds the resolution of U.S. Geological Survey (USGS) topographical quad maps.

Boating and Fishing

Recreational boaters will enjoy safer, more accurate navigation around sandbars, rocks, and other obstacles. Fishermen will be able to more precisely locate their favorite spot on a lake or river. Lobster fishermen will be able to find and recover their traps more quickly and efficiently.

SPS SIGNAL SPECIFICATION

The GPS SPS Signal Specification is the definitive source regarding the expected performance levels of the civil GPS navigation service. While important to all civil users, these performance levels are particularly crucial in determining the system design for civil GPS augmentation systems that are required to meet the stringent performance criteria for safety-of-life use.

The current signal specification was published in 1995. Many of the performance parameters in that document – such as coverage, availability, and reliability – originated prior to the GPS constellation reaching initial operating capability in December 1993. Consequently, the SPS Signal Specification needs to be updated to reflect operational experience and observed performance over the last 6.5 years and to include the dramatic change in accuracy resulting from the discontinuation of SA. The DOT and DoD are working to revise the specification in a manner that reflects accurate yet consistently obtainable GPS service. The next version of (Edition 3) of Ref. [2] is expected to have been released by the end of 2000.

OVERCOMING THE ATMOSPHERE

With the elimination of SA, the next largest contributor to the GPS positioning error budget is the signal delay caused by the Earth's atmosphere (see Table 2). Since the military currently has full access to two signals and frequencies through the PPS, military users can correct the ionospheric error by forming a linear combination of L1 and L2 pseudorange measurements to mathematically estimate and remove almost all the ionospheric bias from the L1 measurements. To compensate for the ionospheric error in limited civilian applications, some receiver manufacturers have developed innovative techniques for using components of the encrypted Y-code signal to calculate the ionospheric effects. However, to function effectively, these so-called "semi-codeless" receivers require a signal-to-noise ratio (SNR) for the L2 signal that is considerably higher than the SNR required by a dual-frequency military PPS receiver.

As a result, although the higher SNR can be achieved in stationary positioning applications, many situations preclude effective use of these techniques. For example, when a receiver is

in a moving vehicle or ionospheric scintillation is present, the receiver may lose its ability to track incoming signals and take several minutes to recover the signal needed for precise positioning. The same is true when the receiver must view satellites through foliage or in the presence of multipath signals. As a result, civilian access to additional coded signals will enable improved accuracy through ionospheric corrections for dynamic applications even in sub-optimal environments with RF interference and multipath (reflected GPS signals).

As shown in Table 2, the use of C/A-code on the L2 frequency in conjunction with L1 will reduce the typical ionospheric error of 7.0 meters to 0.01 meters (1σ). This will result in a stand-alone accuracy as low as 8.5 meters (95%) compared with approximately 22.5 meters (95%) with L1 alone.

Table 2
SPS with Two Coded Civil Frequencies

Error Source	Typical Range Error Magnitude (meters, 1σ)	
	SPS with SA set to zero	SPS with two coded civil signals
Selective Availability	0.0	0.0
Atmospheric Delay		
Ionospheric	7.0	0.1
Tropospheric	0.2	0.2
Clock and Ephemeris Error	2.3	2.3
Receiver Noise	0.6	0.6
Multipath	1.5	1.5
Total User Equivalent Range Error (UERE)	7.5	2.8
Typical Horizontal DOP (HDOP)	1.5	1.5
Total Stand-Alone Horizontal Accuracy, 95%	22.5	8.5

To implement C/A-code on L2, the GPS Block II Replenishment (Block IIR) satellite contract will be revised to direct Lockheed Martin to modify the last 12 Block IIR satellites. New earth-coverage military codes on L1 and L2 will also be added to these same satellites, as shown in Figure 3.

ADDING THE THIRD CIVIL SIGNAL

During the IGEB's civil signal selection process, it became clear that simply adding C/A-code to L2 would not be sufficient to allow its use for civil aviation safety-of-life applications because of

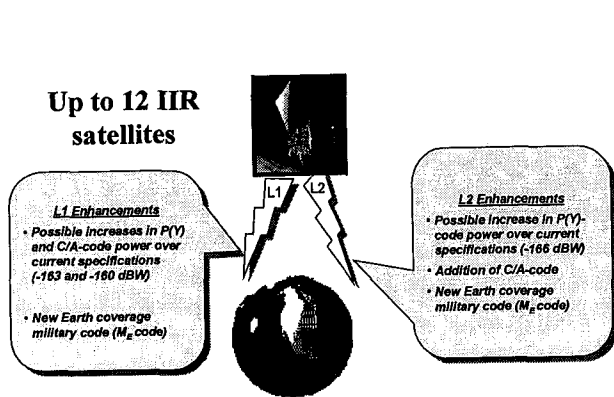


Figure 3
GPS Block IIR Satellites with New Signals

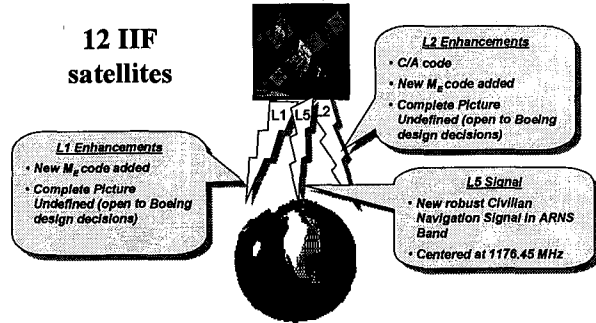


Figure 4
GPS Block IIF Satellites with New Signals

potential interference from existing ground radars that broadcast in and near the GPS L2 band. Obtaining an internationally accepted ARNS designation for L2 (necessary for all aviation safety-of-life applications) would require that many of these systems would have to be moved out of the band. U.S. agencies evaluated this approach, but concluded that the cost would be too high.

Instead, a new wide-band GPS signal offered the best option for civil aviation in the band from 1164-1188 MHz, a portion of the spectrum that already had an ARNS allocation. However, a new allocation, an RNSS (Radio Navigation Satellite Service – space to earth) allocation would have to be approved. That new allocation was thought to be attainable, and in May 2000, the World Radio Conference approved an RNSS allocation for the frequency band from 1164 to 1215 MHz.

The third civil signal at 1176.45 MHz, or L5, will be added to the first Boeing Block IIF satellite along with C/A-code on L2 and M-code on L1 and L2, as shown in Figure 4.

The L5 signal has been specifically designed to improve performance over the current L1 C/A-code signal in several ways. L5 power will be increased 6 dB compared to the current L1 signal (-154 dBW vs. -160 dBW). This is equally split between an in-phase (I) data channel and a quadrature (Q) data-free channel which will improve resistance to interference, especially from other pulse-emitting systems in the same band as L5 such as Distance Measuring Equipment (DME) systems already used for en-route and terminal area air navigation, and the military Joint Tactical Information System (JTIDS) used for critical military command and control communications. The data-free component of the new signal also provides for more robust carrier-phase tracking, which is desirable for many applications. A minimum 20-MHz broadcast bandwidth and a higher chipping rate will provide greater accuracy in the presence of noise and multipath. Finally, a longer code than the L1 and L2 C/A-codes will reduce system self-interference caused by CDMA cross-correlation. (See Ref. [1] for a full discussion of the L5 signal.)

The benefits of multiple ARNS signals in space will be significant. For instance, use of dual-frequency L1/L5 avionics will allow direct measurements of ionospheric delays directly by avionics equipment on-board aircraft. This will allow seamless global navigation and precision approach capability with minimal investment in ground infrastructure by many countries for

Space-based Augmentation Systems (SBAS). Less reference stations might be required for a worldwide SBAS coverage to meet navigational requirements for civil aviation as a result of availability of dual frequency avionics.

The Federal Aviation Administration (FAA) also plans to broadcast L5 from its SBAS known as the GPS Wide Area Augmentation System or WAAS. A design for the WAAS L5 signal structure has been proposed that is similar to the GPS L5 signal, except that only a single-channel carrier will be used (no Q channel), and the data rate will be increased.

As shown in Figure 5, L5 will be available for en-route navigation across the vast majority of the world even if the current worldwide DME infrastructure is maintained. Exceptions are limited to portions of the U.S., Europe, and Japan, which have a high density of DMEs. The FAA plans to reassign DMEs as necessary to protect L5 use at high altitudes in the U.S. national airspace system. At the surface of the earth, where the vast majority of non-aviation users of GPS reside, interference to L5 from DMEs is essentially nonexistent, as shown in Figure 6.

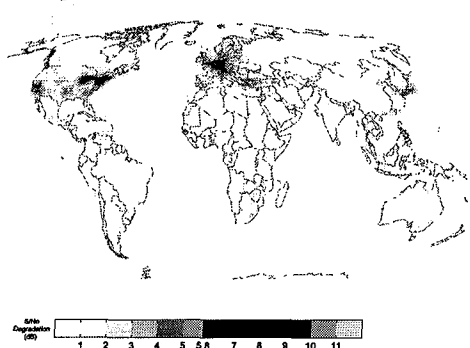


Figure 5
**Interference to L5 Service at High Altitude
(40,000 Ft)**

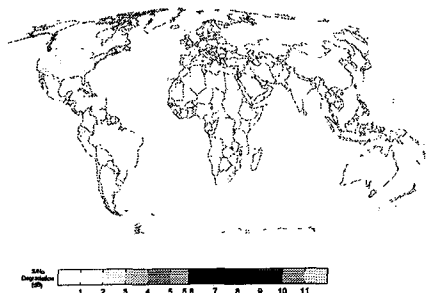


Figure 6
**Interference to L5 Service at Approximately
5,000 Ft And Below**

GROUND CONTROL NETWORK

Upgrading the operational control segment (OCS) as shown in Figure 7, represents an often overlooked but essential component of the overall modernization program. A number of improvements are under way that will improve the capability to monitor all signals broadcast from the constellation, make the control network more robust, improve the positioning accuracy of both the civil and military services, and add new functions that are necessary to control the modernized satellites. These improvements include:

- Upgrading the dedicated GPS monitor stations and associated ground antennas with new digital receivers and computers
- Replacing existing MCS mainframe computers with a distributed architecture
- Implementing the Accuracy Improvement Initiative (AII), Air Force Satellite Control Network integration, and full IIR capabilities
- Completing a fully mission-capable Alternate Master Control Station (AMCS) at Vandenberg Air Force Base

- Adding IIF command and control functionality.

Table 3
**SPS and PPS with the Implementation of
the Accuracy Improvement Initiative**

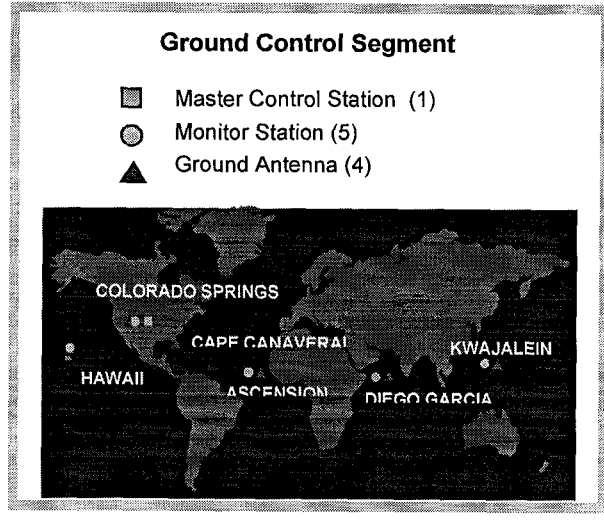


Figure 7
The GPS Ground Control Network

Error Source	Typical Range Error Magnitude (meters, 1σ)	
	SPS with two or more coded civil signals	SPS and PPS with the AII
Selective Availability	0.0	0.0
Atmospheric Delay		
Ionospheric	0.01	0.1
Tropospheric	0.2	0.2
Clock and Ephemeris Error	2.3	1.25
Receiver Noise	0.6	0.6
Multipath	1.5	1.5
Total User Equivalent Range Error (UERE)	2.8	2.0
Typical Horizontal DOP (HDOP)	1.5	1.5
Total Stand-Alone Horizontal Accuracy, 95%	8.5	6.0

In addition to other operational functions, such as satellite health monitoring and routine maintenance, the ground control network determines the ephemeris (orbital position) and clock parameters of the satellites in the GPS constellation and uploads these data to the GPS spacecraft. In its current configuration, the MCS uses individual "mini Kalman filters," known as partitions, to estimate the orbit and clock errors for each of the GPS satellites as well as the clock errors for the monitor site receivers. Updated orbit and clock corrections are uploaded to each satellite at least once a day.

Once atmospheric errors have been eliminated (by the dual-frequency methods discussed earlier), ephemeris and clock errors become the largest contributors to the GPS positioning error budget. With the current GPS constellation, the clock and ephemeris errors contribute approximately 1.8 and 1.4 meters (1σ), respectively, to user equivalent range error (UERE) for a combined error of 2.3 meters (1σ), as shown in Table 3. A new technique, called the Accuracy Improvement Initiative (AII), is expected to reduce the GPS clock and ephemeris contribution to UERE to approximately 1.25 meters. This will be accomplished by incorporating data from 6 to 14 additional monitoring stations operated by the National Imagery and Mapping Agency (NIMA) into a new, fully correlated, single-partition Kalman filter at the GPS Master Control Station. This is projected to result in stand-alone horizontal accuracies for all GPS users of 6 meters (95%) or better. (See Ref. [3] for more information about AII.)

GPS BLOCK III PROGRAM

The current GPS modernization efforts should carry the constellation through approximately the year 2010 (using up to 12 GPS Block IIF satellites). To meet military and civil requirements through 2030, the IGEB has accepted a DoD recommendation to develop a new generation of satellites (GPS Block III) and associated ground control network for use beyond 2010.

The objective of the GPS III program is to deliver a GPS architectural solutions that will satisfy the current and evolving military and civilian needs. The DoD is initiating a study in late summer of 2000 that will examine candidate acquisition and architectural concepts that refine and validate the system requirements trade space. For the military, a key requirement that will not be met until the Block III satellites are in orbit is the need for a higher power M-code signal (-138 dBW vs. -158 dBW) to further improve resistance to both intentional and unintentional interference in a geographically limited area of operations.

The GPS III architecture study will also address concepts that optimize cost (to include economic benefits), schedule, performance, risk, and technology insertion. These concepts will consider alternative solutions and interfaces both inside and outside the traditional GPS, including interoperability with, incorporation of, and/or utilization of various existing or developing military and civil systems.

IMPLEMENTATION TIMETABLE

The current schedule for GPS Modernization activities is depicted in Table 4. Using this timetable, an initial operational capability for dual-frequency navigation, would occur in 2008, which is based on a constellation of 18 properly placed satellites broadcasting C/A-code on L2. Similarly, the L5 signal should be available on 18 GPS satellites by approximately 2012. Reaching this service level will require the launch of 6 to 12 GPS III satellites. Operational Control Segment improvements will be carried out in multiple stages from 2000 through 2008 in support of the evolution of GPS IIR, IIF, and Block III.

SUMMARY

GPS is being modernized in order to further improve positioning, navigation, and timing capabilities for both civil and military users. The first step in the modernization process, the elimination of Selective Availability, will be followed by a series of steps that include:

- The near-term revision of the GPS SPS signal specification
- The addition of C/A-code to L2 and M-codes on both L1 and L2 beginning in 2003
- The addition of a third civil signal (L5) designed with aviation and other safety-of-life users beginning in 2005
- Ground Control Network upgrades to improve operational robustness and system accuracy
- A GPS Block III program to add more power to the military M-code signals and to address additional civil and military positioning, navigation, and timing requirements unmet by the current program.

As shown in Figure 8, these actions will improve the stand-alone GPS horizontal accuracy for all users from 100 meters to 6 meters or better. For non-dynamic or non-real-time scientific and survey applications, centimeter-level accuracies should be achievable more quickly and cost

effectively than is possible today through the existence of three frequency "wide lanes" (L1 - L5, L1 - L2, and L2 - L5) to resolve integer ambiguities in making precise carrier-phase measurements. Most importantly, the existence of three spectrally separated civil frequencies, when combined with improved signal design characteristics, will significantly reduce the chance of unintentional interference to GPS services.

Table 4
GPS Modernization Schedule

Activity	Implementation Date
SA set to zero	May 2000
GPS IIR Enhancements - C/A Code on L2 - M-code on L1 & L2	2003 – 2006
GPS IIF Enhancements - C/A Code on L2 - M-code on L1 & L2 - L5	2005 – 2010
GPS III Enhancements - C/A Code on L2 - M-code on L1 & L2 with greater power - L5 - Future Capabilities	2010 – TBD
OCS Enhancements	2000 – 2008

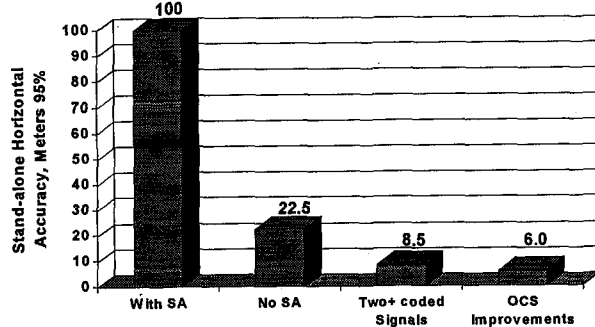


Figure 8
Improvements in GPS Accuracy

The spectral separation of civil and military GPS services through implementation of new military signals is an additional improvement. It will provide operational benefits to all users of GPS and will help to maintain the system's dual role as a military force multiplier and as a global information utility for peaceful civil use throughout the globe. The modernization of GPS will be a challenging endeavor that will demand the full commitment and dedication of the entire military and civil GPS communities. However, given the tremendous potential for both civil and military benefits, it will be well worth the effort for future generations.

REFERENCES

- [1] "Innovation" column, GPS World, September 2000.
- [2] *Global Positioning System Standard Positioning Service Signal Specification*, Second Ed., 2 June 1995.)
- [3] "Innovation" column, GPS World, June 2000.

Questions and Answers

MARC WEISS (NIST): Could you say something about the jam resistance for civilians in GPS modernization?

MIKE SHAW: There are a number of factors that go into jam resistance, and I'm glad you used the word "resistance" rather than "prevention." But, as we look at the power increases, on L5 as well as possibly on the other signals, that will certainly increase the jam resistance. If you look at the improved bandwidth, if you will, on L5 as well as the code lengths and all that, that will again make it more resistant to jam. And just by virtue of fact that you had more than one signal certainly improves resistance to jamming or the unintentional interferer, as we talked about.

Again, there is not a way, if you will, to prevent totally the ability for an intentional interferer to interfere on any of these. What you've got to do is implement backup systems, whether it's through multiple signals coming through GPS; alternative technologies, in particular in the use of safety of life; internal reference systems; or other ground radio systems. It's a combination of all that. Does that answer your question?

WEISS: It answers it. There's a lot more I would like to know, but it is a good start.

SHAW: There's a lot more we would all like to know.

THOMAS CLARK (NASA Goddard Space Flight Center): This is a slight follow-on on the last question. You're showing that in the GPS III constellation, that the M-code power will be increased. That could very easily become a source of jamming for the civilian users, especially if you turn up the M-code by 20 dB. Is that problem being considered in all of this new design work?

SHAW: Absolutely. I mean, as we find out in this interesting dual-use system, there's a balance here. What is good for one often affects the other and visa versa. We clearly understand that as we increase the power on the M-code, the desire is to increase that power in the theater of operations. We would like to minimize, if you will, the impact on the rest of the world that's not in that theater of operations. The problem, of course, is that radio signals don't necessarily, in fact, rarely recognize borders, and so that is a problem with the implementation. Certainly as we implement M-code, it complicates just by virtue of the fact they're on the same signals, or it's the same frequency as the L1 and L2.

CLARK: Is it the civil or military community that is to be kept in balance?

SHAW: I think it will be a balance between both interests, and it's my hope that we will make the best decision in the nation. How's that?

CLARK: Sounds like a political answer.

SHAW: But that's the truth.

WILLIAM KLEPCZYNSKI (Innovative Solutions International): But Tom, there is no M-code on L5, so that signal won't be affected at all.

CLARK: But it affects both L1 and L2. We ultimately rely on L1 band, and L2 or L5 to do the ionosphere corrections. Part of the reason I asked.

SHAW: I gave you a political answer, but I also think a very truthful answer. But I also say that we know that that's a very trying issue. Right now, the DoD has been very proactive in including the civil community in their acquisition, if you will, of the modernized capability

in the GPS III. I'm going to use a term that I don't necessarily like to use; it's called the "acquisition program baseline," which, if you will, is the report card by which we will judge success on modernization in GPS III. One of those issues in there that we're struggling with, even as we speak today, is the term of backward capability. To ensure that as we bring on new modernized capability, we don't unduly, negatively impact the current capability that is there, which is what the issue is that you talk about. But in the final analysis, the GPS is a dual-use system that is fielded both for national security reasons as well as, I would say, our economic security reasons. And we've got to achieve an equitable balance between those. We are aware, very, very intimately, with the detail that you talked about.

WAAS, EGNOS, AND MSAS FOR TELECOM SYNC

Hugo Fruehauf
Zyfer Inc., an Odetics Company
Tel: 714-780-7960
E-mail: Hxf@zyfer.com, www.zyfer.com

Abstract

The WAAS, EGNOS, and MSAS GPS Augmentation Systems bridge the gap between the military applications of GPS and the needs of civil aviation navigation. These USA, Europe, and Asian systems consist of a network of differential GPS ground stations, using principally the Inmarsat-3 geosynchronous satellite constellation as the means of relaying the differential corrections to the users. In the process of providing precise navigation signals, GPS time is maintained through the Inmarsat-3 downlinks. It is this functionality that provides for robust time retrieval for the synchronization needs of the telecommunications community. This paper discusses:

- The basic makeup and performance of the system
- How time and frequency can be extracted for the telecom terminals
- Added functionality and noise rejection capabilities using these signals for telecom timing applications
- How the system offers the first true backup to the GPS C/A signal for telecom synchronization users.

The Basic Makeup and Performance of the System

THE BASIC MAKEUP AND PERFORMANCE OF THE SYSTEM

First, let's define the meaning of the terms used (Figure 1).

Figure 1 - Definitions

WAAS, EGNOS, and MSAS is a Differential GPS, Ground-Based Augmentation System designed to fulfill the needs of Civil Aviation Navigation

- WAAS - Wide Area Augmentation System (USA)
- EGNOS - European Geostationary Navigation Overlay System
- MSAS - Multifunctional Transport Satellite Space-Based Augmentation System (Japan)

The GPS program began in 1973 with the design of the Block-I satellites at what was then Rockwell International, which won the contract award in 1974. Launches began in 1978 and have continued since then to form a worldwide, 24-hour, three-dimensional military navigation, positioning, and timing system. The civil community has from the beginning benefited from the use of the GPS clear (or coarse) acquisition signal (C/A) for both navigation and timing but only in an unofficial, uncertified manner as to navigation. The question might be asked, why has it taken 22 years for the civil aviation community to embrace the GPS capability in an official, certified manner for commercial aviation? The answer lies in the difference between warfighting requirements and the safety requirements for commercial aviation, as shown in Figures 2 and 3.

Figure 2 - Issues With GPS-SPS for Civil Aviation

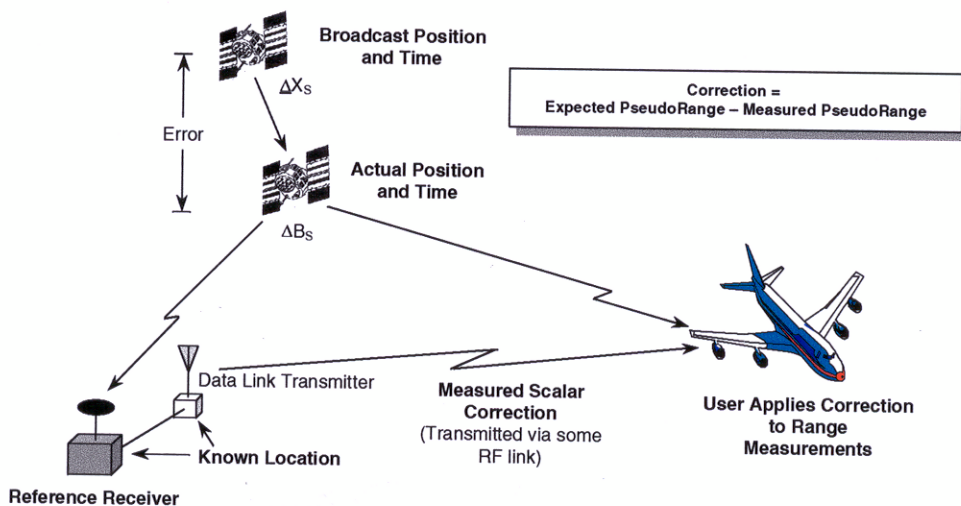
- With SPS, and in case SA is ON, accuracies are not good enough to meet FAA's Category I, II, and III requirements
 - Needs Differential Corrections (DGPS) and elimination of SA (in case SA is activated)
 - Needs improved Vertical Accuracy through use of added Range Signals from overhead satellites
 - Needs improved Ionospheric Corrections
- With SPS, Signal Reliability is not good enough; Can be out of limits without real-time user knowledge
 - Needs to be forward looking enough to allow a safe abort
 - Remote/Receiver Autonomous Integrity Monitoring (RAIM) addresses this need

Figure 3 - FAA Navigation Requirements vs. GPS Performance

Parameter	GPS with past SA	GPS w/o SA	FAA Requirements			WAAS
			CAT I	CAT II	CAT III	
Horizontal Position Accuracy (2σ)	100 m 300 m (99.99%)	20 m	16 m	6.9 m	6.1 m	7.6 m
Vertical Position Accuracy (2σ)	140 m	30 m	7.7m	2 m	2 m	7.6 m
Time Accuracy to UTC (2σ)	340 ns	40 ns	N/A	N/A	N/A	25 ns 12.5 ns (1σ)
Decision Height (DH)	—	—	200 ft	100 ft	50 ft	—

To accomplish the requirements of civil aviation navigation, a GPS augmentation system is required to bring the performance and signal reliability in line with the needs. The chosen method to accomplish this is the implementation of massive, worldwide ground-based differential GPS network supported by geosynchronous satellites to transmit the correction signals to the users. Differential GPS can be demonstrated by Figure 4.

Figure 4 - Local Area Differential GPS (DGPS) Concept



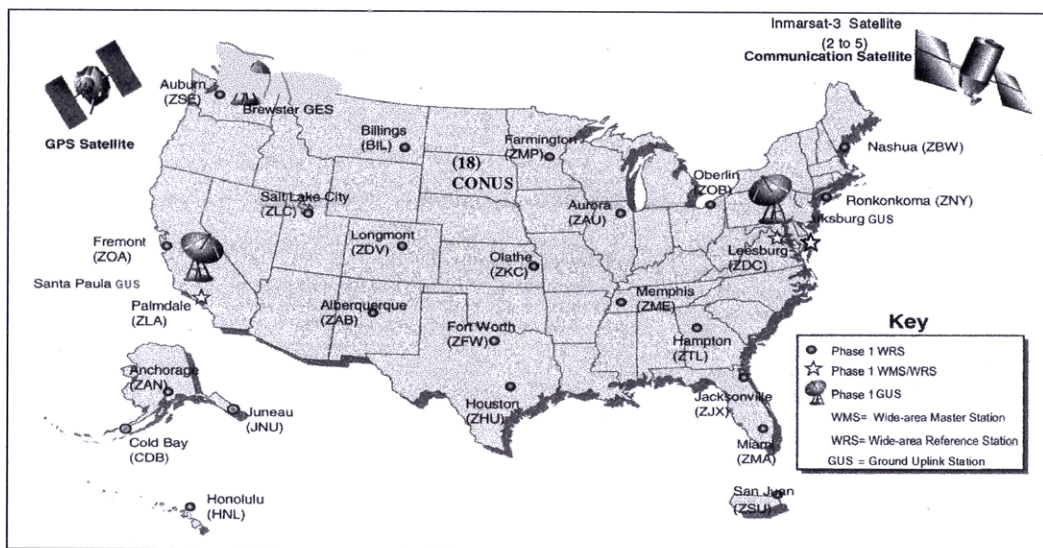
The GPS signals are measured by one or more ground reference stations that have been located precisely through surveying methods. There will be a difference between the GPS signal versus the known position of the ground station. This differential correction is then transmitted by some means to the user. The accuracy of the correction is best when the user is over the ground reference station, of course, but then degrades somewhat proportionally with the distance away from the reference. Local area augmentation, referenced in Figure 4, often called LAAS, is to differentiate between a specific local area and a wide area, country-wide system, called WAAS.

The North American portion of the world-network Wide Area Augmentation System (WAAS) is shown in Figure 5.

The basic functionality of the world-network GPS augmentation system concept is shown in Figure 6.

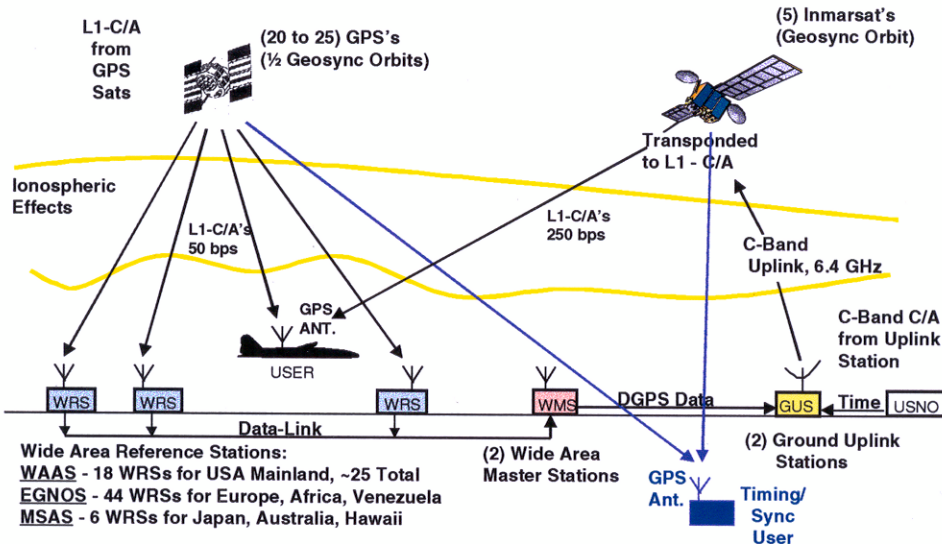
The data collected from the WRSs is fused at the WMS and sent to the GUSs for uplink. The Inmarsat-3 or equivalent geosynchronous constellation acts as a “bent-pipe,” transponding the correction signals from the 6.4 GHz C-Band uplink to the L1-C/A GPS look-alike downlink signal. The signals do not originate in the Inmarsats, but come from the GUSs. The genius of the WAAS system is the GPS “look-alike” signals from the geosync satellites, which are received by the GPS receivers at the same signal strength and with the same antenna. This eliminates an otherwise separate and complex worldwide RF infrastructure that would be needed to transmit corrections to the users. There is a catch, however. Although the same GPS receiver can receive and process the RF portion of the Inmarsat signal as if it were a GPS satellite, it cannot process the data portion of the signal because of the data rate difference: GPS 50 bps and WAAS 250 bps.

Figure 5 - WAAS Network*



* From 'WAAS Briefing', Michel Gonthier, CMC/BA

Figure 6 - Wide Area Augmentation System Concept



The "times 5" data rate is needed to handle the added differential corrections, along with an approximate 6-second refresh rate versus the 30 seconds for GPS. As a minimum, then, the GPS receiver requires an updated software set, including among other things, recognition of the new WAAS signals (satellite numbers 100 and up, versus the GPS SV 01 to 40) and the 250 bps data processing.

The WAAS System downlink is a culmination of formidable parameters that augment the existing GPS System to meet the civil aviation navigation challenges. Figure 7 lists these parameters.

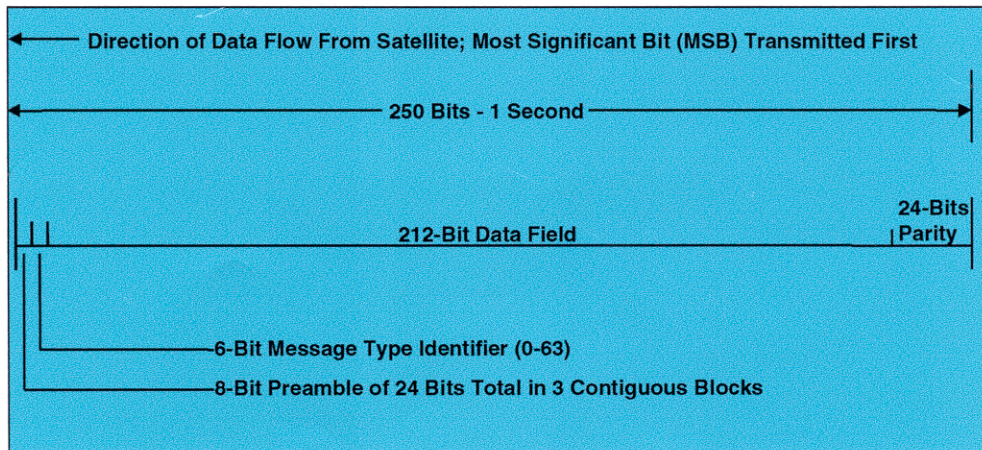
Figure 7 - WAAS Downlink

- L1-C/A GPS 'Look-Alike' signal from each GEO-Satellite with no SA (same signal strength as GPS satellites)
- DGPS Vector Corrections for each GPS Satellite
- Added Pseudo Range Signals via each GEO-Satellite
- Receiver Autonomous Integrity Monitor (RAIM) in Airborne WAAS receivers (a "Use/Don't Use" Flag)
- Improved Ionospheric Correction Model
- 250 bps data rate rather than the GPS 50 bps
 - Needed to transmit DGPS correction data for each GPS Sat
 - More frequent update - every 5 to 6 Sec. for DGPS and RAIM
 - Time to "Not-Use" alarm < 5.2 sec.

The Receiver Autonomous Integrity Monitor (RAIM) shown in Figure 7 is a very important part of making WAAS navigation useful for civil aviation. It provides the reliability function to give the signal integrity. In other words, the standard GPS navigation solution may be unreliable at times, unknown by the user in real time. RAIM considers a host of navigation data from GPS and WAAS and predicts for the next 5 to 6 seconds that the signal is correct. If the forward-looking calculations show an upcoming (estimated) out-of-spec conditions, the user has a 5 to 6 second warning before a "Not-Use" flag appears. This time is deemed sufficient to abort a critical operation, such as a landing or other critical flight phases.

The signal data structure of WAAS is referenced in Figures 8 and 9. The format of the WAAS signal is actually 500 bps, from which the usable 250 bps is formulated. There are a host of reasons for this, among which is jamming considerations. It may be prudent that the WAAS signal goes down before the GPS C/A signal becomes unusable in friendly military jamming scenarios.

Figure 8 - WAAS Block Format*

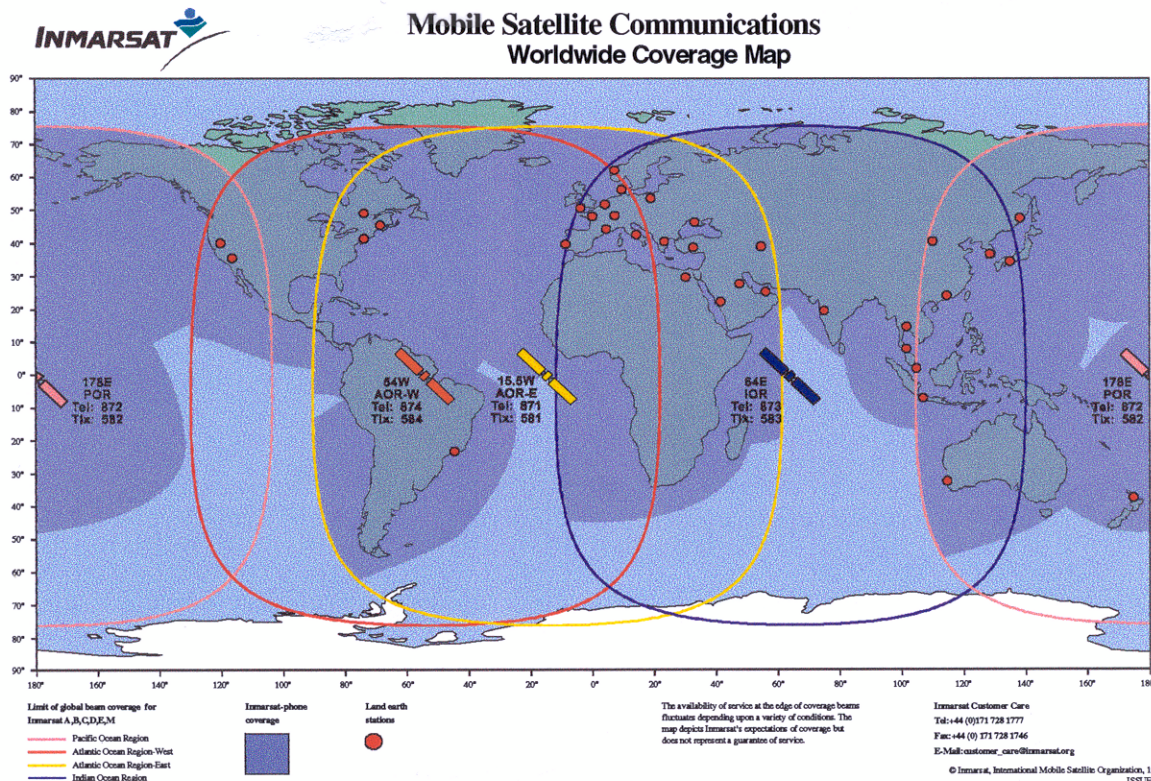


* From 'WAAS Briefing', Michel Gonthiar, CMC/BA

Figure 9 - WAAS Message Type

Type	Contents
0	Don't use this GEO for anything (for WAAS testing)
1	PRN Mask assignments, set up to 51 of 210 bits
2-5	Fast corrections
6	Integrity information
7	UDRF Degradation factor
8	Estimated RMS Error message
9	GEO navigation message (X, Y, Z, time, etc.)
10-11	Reserved for future messages
12	WAAS Network Time/UTC offset parameters
13-16	Reserved for future messages
17	GEO almanacs message
18	Ionospheric grid point masks
19-23	Reserved for future messages
24	Mixed fast corrections/long term satellite error corrections
25	Long term satellite error corrections
26	Ionospheric delay corrections
27	Reserved (WAAS Service Message)
28-61	Reserved for future messages
62	Reserved (Internal Test Message)
	Null Message

The Inmarsat-3 constellation is geosync and covers the earth. By this means, WAAS, EGNOS, and MSAS are linked to form a worldwide, 24-hour civil aviation navigation system that will eventually replace the existing and aging navigation aids. Since the satellite ground traces have significant coverage overlap, a robust redundancy is provided. The ground stations in each geographic area provide the navigation corrections to the user via the associated Inmarsat. The aircraft GPS/WAAS receiver extracts the applicable correction data which applies to the ground stations closest to its flight path.



With existing information WAAS officially began September 2000 with 2 to 5 Inmarsat-3 GEOS. A second C/A will be added to some GPS Sats (BLK IIR/F) at 1176.45 MHz (below GPS L2 of 1227.6 MHz) for direct Ionospheric Correction Solution in the year 2005(?). EGNOS officially begins in the year 2002. EGNOS uses two Inmarsat-3s and one Artemis GEOS (controlled by EU + ESA). There are 44 stations in Europe, Africa, and Venezuela. MSAS is expected to begin in the year 2003 (controlled by Japan). There are six stations in Japan, Australia, and Hawaii. Interoperability between WAAS, EGNOS, and MSAS is expected in the years 2002 to 2003.

HOW TIME AND FREQUENCY CAN BE EXTRACTED FOR THE TELECOM TERMINALS

So What's New for Timing/Sync? The WAAS/EGNOS/MSAS capability is designed for large/high-end airborne GPS receivers for civil aviation navigation (\$5K to 10K?). There are no thoughts given to other users. Making the typical low cost (\$100), small telecom GPS timing receiver capable of receiving and processing WAAS will be new. Some of the advantages are a more accurate timing signal, greater robustness in noisy environments using low-cost commercial DBS dish antennas, and an alternate timing signal in case of GPS C/A loss. Refer to Figure 11 for more details.

Figure 11 - Advantages for Timing/Sync

A more accurate UTC Timing Signal (<100 ns GPS vs. <25 ns for WAAS/EGNOS/MSAS)	<ul style="list-style-type: none"> - Due to the D-GPS corrections - If SA is ON, it is removed from C/A - Added Ranging Signals with the WAAS/EGNOS/MSAS Geo-Stationary Satellites
A more robust timing signal in noisy environments	<ul style="list-style-type: none"> - Contrary to GPS, WAAS/EGNOS/MSAS Geo-stationary Inmarsats allow the use of a fixed DBS dish aimed at the satellite - This can reduce ambient noise, multi-path, intentional and unintentional jamming - A 2 ft. DBS can achieve upwards of 18 dB of added noise rejection (Pat Fenton - NovAtel)
An alternate UTC Timing Signal to GPS L1-C/A (A WAAS/EGNOS/MSAS "only" mode)	<ul style="list-style-type: none"> - WAAS/EGNOS/MSAS Systems generate their own L1-C/A GPS "look-alike" signals - Uplink Station Clocks are referenced to UTC via Ground-Link to USNO - If position is known through GPS or other surveying means, a single WAAS/EGNOS/MSAS Inmarsat Satellite signal can maintain Network Sync, independent of GPS L1-C/A

ADDED FUNCTIONALITY AND NOISE REJECTION CAPABILITIES USING THESE SIGNALS FOR TELECOM TIMING APPLICATIONS

There are some additional benefits using the WAAS signal for telecom. First, it provides two to three more range signals from the geosync Inmarsats, which improves the timing accuracy by at

least a factor of 2 to 3. With SA turned off, the improvement is not as dramatic as it was earlier when SA was still active. Second, and more significant, is the ability to reduce ambient noise, multipath, and intentional and unintentional jamming. This can be accomplished through the use of commercially available low-cost Direct Broadcast Satellite dishes (DBS). Unlike GPS, the Inmarsats are stationary and, therefore, allow for the pointing of a DBS antenna toward the Inmarsats. Due to the higher gain nature of a dish antenna, telecom terminals can be made more robust in high noise areas or in areas where significant GPS signal obstruction occurs, such as high-rise downtown buildings, etc. Figures 12, 13, and 14 show antenna options.

Figure 12 shows the standard GPS antenna used with a WAAS-capable receiver. As stated earlier, since the Inmarsat signal is a GPS "look-alike," the antenna of course receives both. Since it sees all available GPS satellites, the terminal locates itself and then corrects the timing to the WAAS-capable levels.

**Figure 12 - Antenna Options,
GPS Antenna Only**

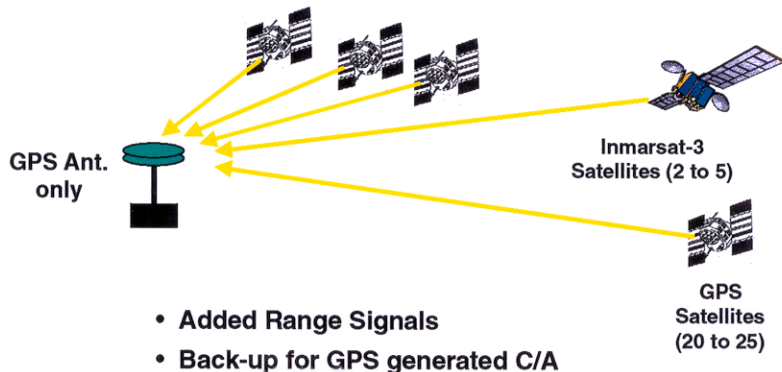


Figure 13 shows a combination of both standard GPS antenna and a DBS dish. The Figure 12 mentioned capabilities apply, in addition to significantly higher noise rejection from the dish. This means that the terminal is not likely to go down due to extreme permanent or temporary electromagnetic conditions. The potential problem with this configuration, however, is the 2 to 3 dB loss from an RF splitter between the GPS antenna and the dish. This can be mitigated, however, by various means in addition to multiplexing the antenna's signals.

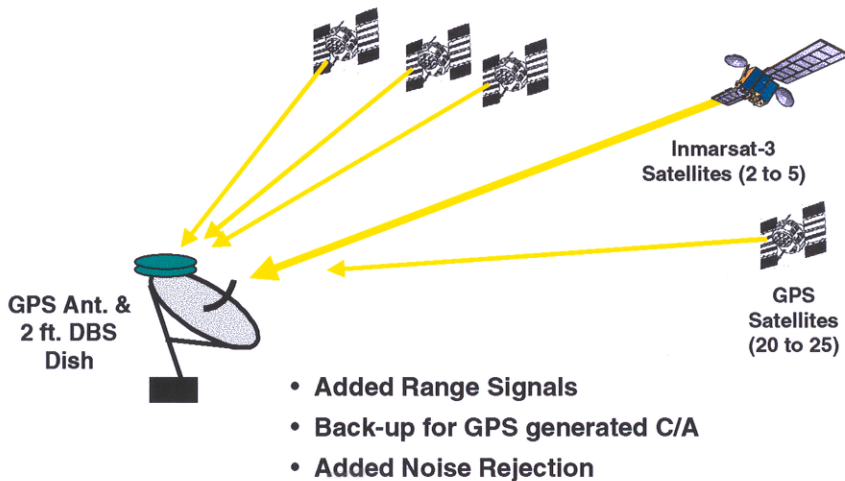
Figure 14 shows a DBS Dish only. This configuration may not always be self-erecting. In other words, it may not be able to position itself due to lack of GPS satellites in view of the directional dish. If the position is known and programmed in, the DBS can completely support the timing requirement without any further need to see GPS satellites. This confirmation also eliminates the need for a RF splitter.

Figure 15 provides a summary of setup and performance requirements versus antenna options.

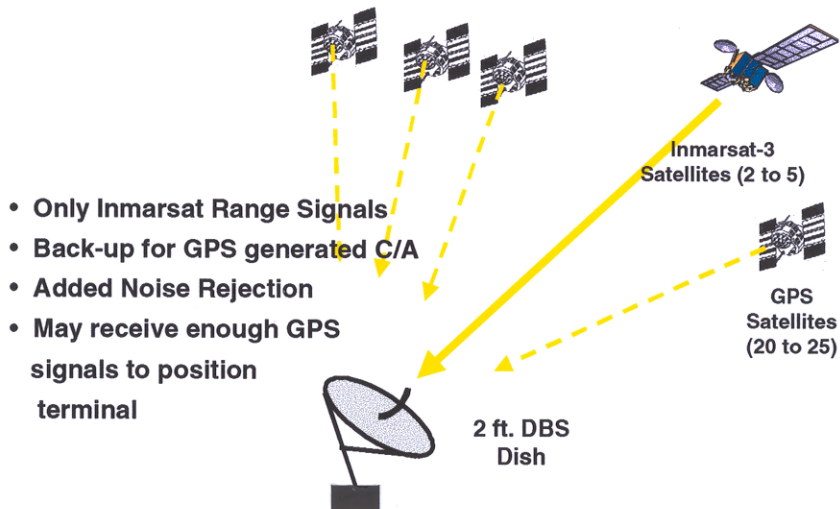
HOW THE SYSTEM OFFERS THE FIRST TRUE BACKUP TO THE GPS C/A SIGNAL FOR TELECOM SYNCHRONIZA- TION USERS

In retrospect, the telecom sync community has done a terrific job selling GPS as the main synchronization tool worldwide in light of the fact that it is military system. The question,

**Figure 13 - Antenna Options,
GPS and DBS Dish Antennas**



**Figure 14 - Antenna Options,
DBS Dish Only**



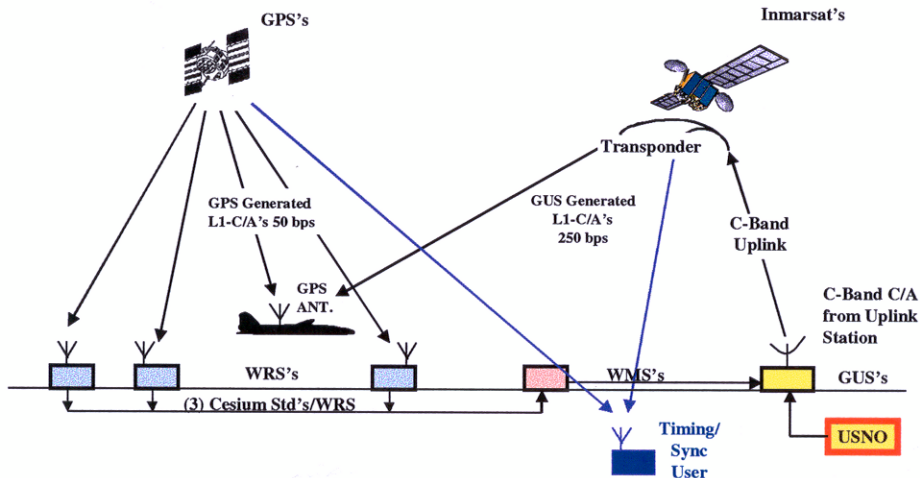
especially from foreign customers, is continually raised, "What if the military significantly degrades or even turns off the clear, civil C/A signal?" Since the U.S. government could do this without notice, the question has been addressed by the use of flywheel precision oscillators which can carry the network for some time. Cost-cutting service providers demand no more than 1 day of flywheel without a GPS C/A signal. More responsible providers demand a week or more, requiring more expensive atomic oscillators. In any event, neither option could handle a protracted military event. But this is where the most significant advantage for telecom comes in, the unintentional WAAS backup to the GPS C/A signal for timing.

Figure 15 -GPS/WAAS Receiver System Configurations

Parameters	Standard GPS RCVR, L1, C/A-Code (SPS) Reception	Standard GPS RCVR, L1, C/A-Code (SPS), + WAAS Reception	Standard GPS RCVR, L1, C/A-Code (SPS), Receiving only WAAS Signal; (1 to 5 Inmarsats)
Self-Erect GPS System (from Cold Start)	Needs minimum of (4) GPS Sats in view for position location	Needs minimum of (4) GPS Sats in view or (3) GPS Sats and (1) WAAS Signal	Cannot determine position on its own
	Needs at least 15 min. to filter SA, if ON	Needs only seconds to meet Time Spec (WAAS has no SA)	N/A
Manual Erect with surveyed position accuracy of 10 m or better	Needs only (1) GPS Sat; Time Spec depends on Fly-Wheel Osc.	Needs Only (1) GPS Sat or (1) WAAS Signal Not both. Time Spec determined by WAAS and Fly-Wheel Osc.	Meets WAAS Time Spec w/o GPS signals
	Needs only seconds to meet Time Specs	Needs only seconds to meet Time Specs	Needs only seconds to meet Time Specs.
Antenna Options	- (1) Standard GPS Antenna	- (1) Standard GPS Antenna (Omni-Dir, receives both GPS and WAAS) or - (1) Standard GPS Ant. on a DBS type com'l Antenna. Dish for high performance WAAS reception	DBS Dish for High Performance Reception (reduction of ambient noise, multipath, and intentional and unintentional jamming.)
Timing Accuracy	50 to 100 ns	~25 ns, 95%; 12 ns 1σ	~25 ns, 95%; 12ns 1σ

No C/A or a significant degradation of C/A will bring down the civil community navigation. Inmarsats are only transponders for correction data and cannot be used for navigation. In this event however, a “don’t-use” flag must be transmitted by WAAS, telling the community not to use the signal. This “don’t-use” signal comes from the ground station system which creates the L1-C/A look-alike signal relayed to the users via Inmarsat. This C/A signal is generated from the C-band uplink, transponded to L1 by the Inmarsats. In addition, this C/A is synchronized to USNO, the same agency which time-syncs all the GPS satellites. In this respect, the telecom terminals will remain on line when the GPS C/A is severely degraded by SA or even denied. Since this capability is inherent in EGNOS and MSAS as well, the backup to C/A can be realized worldwide. See Figure 16 for an illustration of this significant feature.

Figure 16 - The Independent L1-C/A Signal from WAAS/EGNOS/MSAS



Figures 17 and 18 portray potential military scenarios and the operation of the GPS and WAAS systems in light of these threats. Particular emphasis should be noted in the far right column, where a telecom terminal is equipped with a WAAS capable GPS timing receiver.

Figure 17 - GPS Signals vs. WAAS Signals Availability

Conditions	Navigation Users			T/F Users
	GPS SPS (CIVIL)	GPS PPS (MIL)	WAAS/EGNOS/ MSAS Signals	At Telecom Terminal (for T/F Sync)
Normal GPS Service Under Standard Conditions	C/A, No SA (Nav. Solution <10 m, Time Error ~100 nanosecs)	P(Y)	C/A w/o SA, even if SA is On, DGPS Corrections (Nav. Solution <7.6 m)	GPS + WAAS/ EGNOS/MSAS C/A w/o SA + Corrections (Time Error <25ns)
Foreign Tactical Conflict (USA Jams GPS C/A in Local Battlefield Area)	No GPS C/A (SPS Goes Down in Local Jammed Area)	Normal PPS P(Y) Continues (Need Direct P(Y) Acquisition Receivers for Cold-Start in Jammed area)	No WAAS/ EGNOS/MSAS C/A in local Jammed area (Civil Navigation goes down in the local area only)	Terminal in Local Jammed Area Goes on "Hold-Over" (Jammer may be defeated with a DBS aimed at GEO Inmarsat)

Figure 18 - GPS Signals vs. WAAS Signals Availability

Conditions	Navigation Users			T/F Users
	GPS SPS (CIVIL)	GPS PPS (MIL)	WAAS/EGNOS/ MSAS Signals	At Telecom Terminal (for T/F Sync)
Broader Foreign Conflict (Satellite SA is On and cranked High)	C/A with sever SA (Nav. Solution 1000 m?? Time Error >1 sec ??)	Normal PPS P(Y) Continues Increased SA does not materially affect P(Y)	C/A w/o SA from Inmarsat, but DGPS Corrections may be out of 7.6 m Spec (Most SA is filtered by DGPS Grd. Sta.) Note (1)	Terminal filters much of the GPS SA, WAAS/ EGNOS/MSAS C/A is w/o SA, Time Error may stay in 25ns area
Strategic Conflict (C/A is Unavailable from Satellite, unthinkable scenario, but possible)	No GPS C/A (SPS Goes Down Worldwide)	Normal PPS P(Y) Continues (Need Direct P(Y) Acquisition Receivers for Cold-Start)	GPS/WAAS/EGNOS/ MSAS Civil Aviation Navigation goes down Worldwide. (GUS generated C/A continues to transmit "Don't Use" message)	WAAS/EGNOS/ MSAS- GUS generated C/A will maintain Timing/Sync - GUS Cesiums locked to USNO via Ground-link Note (2)

Note (1): USA may ask EGNOS/MSAS to be turned off because it filters out some of the SA

Note (2): With no GPS C/A, all civil navigation is down. No need to shut down WAAS, EGNOS & MSAS; signals cannot be used for navigation.

CONCLUSION

The WAAS, EGNOS, and MSAS system is a significant step forward in expanding the use of the military GPS system to a reliable, certified civil navigation system. It brings a very robust 3σ military capability to a 6σ and beyond civil system. In the process, the telecom synchronization community is an unintentional beneficiary when the low cost time receivers are made WAAS-capable. But more than the improved accuracy in timing for this community is the proposed C/A backup, a fallout certainly not contemplated by the very capable WAAS systems designers—we thank you.

ACRONYMS

WAAS	Wide Area Augmentation System (USA)
EGNOS	European Geostationary Navigation Overlay System
MSAS	Multifunctional Transport Satellite Space-Based Augmentation System (Japan)
GPS	Global Positioning System
C/A	Clear (or Coarse) Acquisition Signal
P(y)	Precision Code When Crypto Keyed
SPS	Standard Positioning Service
PPS	Precise Positioning Service
SA	Selective Availability
DGPS	Differential GPS
Inmarsat	International Maritime Satellite
WRS	Wide Area Reference Station
WUS	Wide Area Master Station
GUS	Ground Uplink Station
USNO	United States Naval Observatory
RAIM	Receiver (Remote) Autonomous Integrity Monitor
DBS	Direct Broadcast Satellite

Questions and Answers

THOMAS CLARK (NASA Goddard Space Flight Center): Well, I'll play devil's advocate and ask another unpopular question, Hugo. There's one jamming scenario you didn't cover, and that is the fact that the Inmarsat satellites are functioning as a bent-pipe repeater with a 6.4 gigahertz uplink standard C-band satellite uplink. We have had the experience with C-band uplinks when Captain Midnight jammed the TV and was able to somehow generate a signal on the right frequency and jam things.

It would seem to me that probably the greatest vulnerability that this type of WAAS system faces comes at two different levels. One is that you generate enough uplink signals that spoof the WAAS signal, giving you invalid corrections, but still legal WAAS readings. The data become invalid.

The second is that you crank up the power even a bit more. In which case the bent-pipe transponder that is sitting there in geostationary orbit now has enough signal to actually capture many of the GPS downlinks. This is because of the limited dynamic range that you end up with in this type of spread-spectrum situation. So to me, it looks like the most vulnerable part of this, not by U.S. Government jamming, which was the scenario that you talked about, but malicious jamming, whether from a terrorist or a hacker, lies with 6.4 gigahertz uplink.

HUGO FRUEHAUF: Okay, very good points. Remember, though, that Johns Hopkins did a very detailed study on the susceptibility of the WAAS system as a whole to both smart and dumb jammers, and apparently the risk is acceptable. But, of course, your scenario certainly can play out.

CLARK: Yes, the Johns Hopkins study was basically a "trust me" type of study of the Inmarsat satellites; it was virtually impossible for someone on the ground to generate those powers. But that's where I find fault in this, that I could easily generate a signal that is stronger than the normal Inmarsat uplink that's carrying these things, in which case I can grab the link.

WILLIAM KLEPCZYNSKI (Innovative Solutions International): That's true, Tom. But there are some things within the architecture of the system which try to prevent that. There are two uplink stations to each of the geos, one on the East Coast, one on the West Coast. So there would have to be a simultaneous coordinated effort to simultaneously jam both uplink signals on the East and West Coast. In addition, the EGNOS signal is also being received in the US, too, as a supplement. They also have, within Europe, two uplink stations to the AOR East. They would have to simultaneously do that.

So yes, there are possibilities of doing that, but it might be a little difficult. The other aspect of it is that right now the Inmarsat satellites are being used, but that architecture won't necessarily be there in the future. The only thing that probably will stay the same is that the downlink frequency will be L1. However, the architecture might change. The uplinks and the satellites being used will probably also change in the future. At some point in time, the system will evolve and change.

But yes, for now, for the test, there is that possibility, but I think it's very small. It would have to really be a coordinated effort to do that.

MODELIZATION AND EXTRAPOLATION OF TIME DEVIATION OF USO AND ATOMIC CLOCKS IN GNSS-2 CONTEXT

J. Delporte
Centre National de'Etudes Spatiales
18 avenue Edouard Belin
31401 Toulouse Cedex 4, France
e-mail: jerome.delporte@cnes.fr

F. Vernotte
Observatoire de Besançon
41 bis avenue de'observatoire, BP 1615
25010 Besançon Cedex, France
e-mail: francois@obs-besancon.fr

M. Brunet and T. Tournier
CNES

Abstract

In Global Navigation Satellite Systems (GNSS), the on-board time has to be modeled and predicted in order to broadcast the time parameters to final users. As a consequence, the time prediction performance of the on-board clocks has to be characterized.

In order to estimate the time uncertainty of the on-board oscillator, a linear or parabolic fit is performed over the sequence of observed time difference and extrapolated during the prediction period. In 1998 the Centre National d'Etudes Spatiales (CNES) proposed specifications of orbit determination and time synchronization for GNSS-2. The needs of synchronization were specified as the maximum error of the time difference prediction from the extrapolated fit.

Using our work about the estimation of uncertainties in time error extrapolation, we have translated these time domain specifications into a noise level limit or an Allan deviation limit. Of course, these limits depend on the main type of noise for integration time of about 1 day and on the type of adjustment which is performed (linear for cesium clocks and quadratic for other oscillators).

A table summarizing these limits is presented. These values are compared to experimental results obtained with different types of oscillators (quartz, rubidium, and cesium).

INTRODUCTION

In Global Navigation Satellite Systems, the on-board time has to be modeled and predicted in order to broadcast the time parameters to final users. As a consequence,

the time prediction performance of the on-board clocks has to be characterized.

In order to estimate the time uncertainty of the on-board oscillator, a linear or parabolic fit is performed over the sequence of observed time difference and extrapolated during the prediction period, i. e. when the satellite is out of visibility. In 1998, CNES proposed specifications of orbit determination and time synchronization for GNSS-2. The needs of synchronization were specified as the maximum error of the time difference prediction from the extrapolated fit.

The question is then: how is this maximum error related to the noise levels of the clock? Despite several papers deal with this question [1, 2, 3, 4, 5], a new approach was chosen here because we are not only interested in the asymptotic trend of this maximum deviation, but also in its evolution close to the interpolated sequence.

In this paper, we will call Time Interval Error (TIE) the differences between the extrapolated parabola and the real time deviation $x(t)$. By definition, the TIE samples are then the residuals to this parabola. However, in the following, we will limit the use of the word "residuals" to the differences between the interpolated parabola and the real time deviation $x(t)$.

The TIE is due to two effects: the error of determination of the parabolic parameters and the error due the noise of the clock. Obviously, both of these errors may be positive or negative, and the ensemble average of the TIE is equal to zero. Moreover, it can be easily shown that the statistics of the TIE is Gaussian. Consequently, we only have to estimate the variance of the TIE in order to completely define its statistical characteristics.

Moreover, the removal of a quadratic fit from the time deviation sequence cancels out the non-stationarity problem of very low frequency noises [6, 7], and the variance of the TIE (i.e. the "true variance") converges for all types of noise without considering a hypothetic low cut-off frequency.

In order to determine an estimation of the TIE, we will already redefine the interpolation method. Then, we will compare the equations giving the theoretical estimates of the variance of the TIE to simulations and to real data.

ASSESSMENT PRINCIPLE OF THE INTERPOLATION AND EXTRAPOLATION ERRORS

Interpolating Functions |

Rather than performing a classical linear or quadratic fit, we used the Tchebytchev polynomials [8, 7]:

$$x(t) = P_0\Phi_0(t) + P_1\Phi_1(t) + P_2\Phi_2(t) + e(t). \quad (1)$$

where $e(t)$ is the noise, i.e. the purely random behavior of $x(t)$, $\{\Phi_0(t), \Phi_1(t), \Phi_2(t)\}$ are the first 3 Tchebytchev polynomials and the parameters $\{P_0, P_1, P_2\}$ have the same dimension as $x(t)$, i.e. time.

Estimation of the Residuals

The variance of the residuals σ_e^2 may be estimated by [8, 7]:

$$\sigma_e^2 = \sigma_X^2 - \frac{1}{N} (\sigma_{P_0}^2 + \sigma_{P_1}^2 + \sigma_{P_2}^2). \quad (2)$$

Correlation of the Samples

Obviously, the long-term behavior of the TIE depends greatly on the type of noise. The autocorrelation function $R_x(t)$ of the $x(t)$ data contains the information about this type of noise. The power spectral density (PSD) $S_x(f)$ is the Fourier Transform of the autocorrelation function $R_x(t)$.

Taking into account f_l , the low cut-off frequency and f_h , the high cut-off frequency, the autocorrelation function may be written [7]:

$$R_x(t_j - t_i) = \int_{f_l}^{f_h} S_x(f) \cos [2\pi f(t_j - t_i)] df. \quad (3)$$

We will use the power law model of $S_x(f)$:

$$S_x(f) = \sum_{\alpha=-4}^0 k_\alpha f^\alpha. \quad (4)$$

Calculation Method of the TIE

By hypothesis, we consider that the TIE is the difference between the true time deviation $x(t)$ at time t , and the extrapolation of the parabola (previously estimated from t_0 to t_{N-1}) up to this time $t > t_{N-1}$:

$$\text{TIE}(t) = x(t) - \hat{P}_0 \Phi_0(t) - \hat{P}_1 \Phi_1(t) - \hat{P}_2 \Phi_2(t) \quad \text{and } t > t_{N-1}. \quad (5)$$

Thus, the quadratic ensemble average of TIE may be estimated by:

$$\begin{aligned} \langle \text{TIE}^2(t) \rangle &= \langle x^2(t) \rangle + \langle \hat{P}_0^2 \rangle \Phi_0^2(t) + \langle \hat{P}_1^2 \rangle \Phi_1^2(t) + \langle \hat{P}_2^2 \rangle \Phi_2^2(t) \\ &\quad - 2 \left[\langle x(t) \hat{P}_0 \rangle \Phi_0(t) + \langle x(t) \hat{P}_1 \rangle \Phi_1(t) + \langle x(t) \hat{P}_2 \rangle \Phi_2(t) \right] \\ &\quad + 2 \left[\langle \hat{P}_0 \hat{P}_1 \rangle \Phi_0(t) \Phi_1(t) + \langle \hat{P}_0 \hat{P}_2 \rangle \Phi_0(t) \Phi_2(t) + \langle \hat{P}_1 \hat{P}_2 \rangle \Phi_1(t) \Phi_2(t) \right]. \end{aligned} \quad (6)$$

Consequently, for each type of noise, we have to know:

- $\langle x^2(t) \rangle = R_x(t)$, the autocorrelation function of $x(t)$;
- the 3 variances $\langle \hat{P}_i^2 \rangle = \sigma_{P_i}^2$;
- the 3 covariances $\langle \hat{P}_i \hat{P}_j \rangle = \text{Cov}(\hat{P}_i, \hat{P}_j)$: actually, only $\langle \hat{P}_0 \hat{P}_2 \rangle \neq 0$;
- the 3 covariances $\langle x(t) \hat{P}_i \rangle = \text{Cov}(x(t), \hat{P}_i)$.

THEORETICAL RESULTS

Only the final results are given here, but the calculation details are available upon request to the authors.

In the following, T_m designates the measurement time, i. e. the duration of the interpolated sequence:

$$T_m = N\tau_0. \quad (7)$$

and T_p is the prediction time whose origin is the beginning of the extrapolated sequence (and the end of the interpolated sequence).

Case of a Quadratic Interpolation

Variance of the residuals

From (2) we got the following results versus $T_m = N\tau_0$:

- White FM :

$$\sigma_e^2(T_m) \approx \frac{3\pi^2 k_{-2} T_m}{35}. \quad (8)$$

- Flicker FM:

$$\sigma_e^2(T_m) \approx \frac{\pi^2 k_{-3} T_m^2}{24}. \quad (9)$$

- Random walk FM:

$$\sigma_e^2(T_m) \approx \frac{\pi^4 k_{-4} T_m^3}{315}. \quad (10)$$

All the above equations were obtained under the assumption $N \gg 1$, i. e. $T_m \gg \tau_0$.

Estimation of the TIE using the noise levels

The theoretical calculation of (6) yields the following variances versus the measurement time T_m and the prediction time T_p :

- White FM:

$$\langle \text{TIE}^2(T_m, T_p) \rangle \approx \frac{6\pi^2 k_{-2} T_m}{35} \left(50 \frac{T_p^4}{T_m^4} + 100 \frac{T_p^3}{T_m^3} + 69 \frac{T_p^2}{T_m^2} + 19 \frac{T_p}{T_m} + 1 \right). \quad (11)$$

- Flicker FM:

$$\begin{aligned} \langle \text{TIE}^2(T_m, T_p) \rangle &\approx \frac{\pi^2 k_{-3} T_m^2}{8} \left[192 \frac{T_p^6}{T_m^6} + 576 \frac{T_p^5}{T_m^5} + 692 \frac{T_p^4}{T_m^4} + 424 \frac{T_p^3}{T_m^3} + 136 \frac{T_p^2}{T_m^2} + 20 \frac{T_p}{T_m} + 1 \right. \\ &\quad \left. + 96 \frac{T_p^3}{T_m^3} \ln \left(\frac{T_p}{T_m + T_p} \right) \left(2 \frac{T_p^4}{T_m^4} + 7 \frac{T_p^3}{T_m^3} + 9 \frac{T_p^2}{T_m^2} + 5 \frac{T_p}{T_m} + 1 \right) \right]. \end{aligned} \quad (12)$$

- Random walk FM:

$$\langle \text{TIE}^2(T_m, T_p) \rangle \approx \frac{2\pi^4 k_{-4} T_m^3}{315} \left(450 \frac{T_p^4}{T_m^4} + 690 \frac{T_p^3}{T_m^3} + 303 \frac{T_p^2}{T_m^2} + 42 \frac{T_p}{T_m} + 2 \right). \quad (13)$$

All the above equations were obtained under the assumption $N \gg 1$. Thus, under this assumption, the dependence versus N cancels out: the variance of the residuals only depends on the length of the interpolated sequence T_m , and the variance of the TIE only depends on the ratio $\frac{T_p}{T_m}$, whatever the number of samples N is.

Case of a Linear Interpolation

Cesium clocks are not affected by a quadratic drift. If such clocks are used, we may limit the fit to a linear interpolation. In this case, for long term, the main contribution to the TIE will be due to the error on the parameter P_1 and then will be lower than for a quadratic interpolation. It is then strongly recommended to extrapolate the time deviation of a cesium clock from a linear fit. On the other hand, the variance of the residuals will be higher because a quadratic adjustment remains closer to the time data than a linear one.

Variance of the residuals

- White FM:

$$\sigma_e^2(T_m) \approx \frac{2\pi^2 k_{-2} T_m}{15} \quad (14)$$

- Flicker FM:

$$\sigma_e^2(T_m) \approx \frac{\pi^2 k_{-3} T_m^2}{9} \quad (15)$$

- Random walk FM¹:

$$\sigma_e^2(T_m) \approx \frac{2\pi^4 k_{-4} T_m^3}{105} \quad (16)$$

All the above equations were obtained under the assumption $N \gg 1$, i. e. $T_m \gg \tau_0$.

Estimation of the TIE using the noise levels

- White FM:

$$\langle \text{TIE}^2(T_m, T_p) \rangle \approx \frac{4\pi^2 k_{-2} T_m}{15} \left(9 \frac{T_p^2}{T_m^2} + 9 \frac{T_p}{T_m} + 1 \right). \quad (17)$$

- Flicker FM:

$$\langle \text{TIE}^2(T_m, T_p) \rangle \approx \frac{\pi^2 k_{-3} T_m^2}{3} \left[12 \frac{T_p^4}{T_m^4} + 24 \frac{T_p^3}{T_m^3} + 20 \frac{T_p^2}{T_m^2} + 8 \frac{T_p}{T_m} + 1 \right]$$

¹The random walk FM is treated here for homogeneity, but a cesium clock is never affected by this type of noise.

$$\begin{aligned}
& +2 \ln \left(1 + \frac{T_p}{T_m}\right) \left(6 \frac{T_p^2}{T_m^2} + 6 \frac{T_p}{T_m} + 1\right) \\
& +2 \frac{T_p^3}{T_m^3} \ln \left(\frac{T_p}{T_m + T_p}\right) \left(6 \frac{T_p^2}{T_m^2} + 15 \frac{T_p}{T_m} + 8\right) \Big].
\end{aligned} \tag{18}$$

- Random walk FM¹:

$$\langle \text{TIE}^2(T_m, T_p) \rangle \approx \frac{8\pi^4 k_{-4} T_m^3}{105} \left(35 \frac{T_p^3}{T_m^3} + 39 \frac{T_p^2}{T_m^2} + 11 \frac{T_p}{T_m} + 1\right). \tag{19}$$

All the above equations were obtained under the assumption $N \gg 1$, i.e. $T_m \gg \tau_0$.

Estimation of the TIE Using the Variance of the Residuals

The relationships (11) to (13) and (17) to (19) needs an explicit knowledge of the noise levels k_α . However, for very-long-term interpolation (several days), we may be sure of the dominant type of noise: the flicker FM for a cesium clock or the random walk FM for a quartz oscillator.

Thus, the variance of the TIE may be directly estimated from the variance of the residuals.

As an example, the variance of the TIE for a random walk FM and a quadratic fit may be rewritten from (13) and (10):

$$\langle \text{TIE}^2(T_m, T_p) \rangle \approx 2\sigma_e^2 \left(450 \frac{T_p^4}{T_m^4} + 690 \frac{T_p^3}{T_m^3} + 303 \frac{T_p^2}{T_m^2} + 42 \frac{T_p}{T_m} + 2\right). \tag{20}$$

However, such a method is less precise than the use of a correct estimation of the noise levels. This is due to the statistics of the estimate of the variance of the residuals (see section “CONFIDENCE INTERVALS”).

Relationships With the Time Variance

The Time Variance (TVAR), and its square root, the Time Deviation (TDEV), are commonly used for time analysis [9]. Table 1 gives the relationships between the variance of the residuals σ_e^2 and TVAR(τ) for an integration time $\tau = T_m = N\tau_0$. It is interesting to notice that, for a given type of noise, the ratio $\sigma_e^2/\text{TVAR}(\tau)$ is constant.

EXPERIMENTAL VALIDATION

Monte-Carlo Simulations

In order to verify the equations (11) to (13) and (17) to (19), we simulated time deviation sequences of different types of noise (white FM, flicker FM, and random walk FM) and we used quadratic and linear fits. For each type of noise, 10,000 realizations were calculated with

- the same noise level: $k_{-2} = 1.4 \cdot 10^{-4}\text{s}$, $k_{-3} = 3.3 \cdot 10^{-8}$ or $k_{-4} = 5.0 \cdot 10^{-12}\text{s}^{-1}$ for the quadratic fit, $k_{-2} = 3.5 \cdot 10^{-3}\text{s}$, $k_{-3} = 4.8 \cdot 10^{-7}$ or $k_{-4} = 3.3 \cdot 10^{-11}\text{s}^{-1}$ for the linear fit,

$S_x(f)$	$k_{-2}f^{-2}$	$\frac{k_{-3}f^{-3}}{\pi^2 [27 \ln(3) - 32 \ln(2)] k_{-3}\tau^2}$	$\frac{k_{-4}f^{-4}}{11\pi^4 k_{-4}\tau^3}$
$\text{TVAR}(\tau)$	$\frac{\pi^2 k_{-2}\tau}{3}$	$\frac{\pi^2 [27 \ln(3) - 32 \ln(2)] k_{-3}\tau^2}{6}$	$\frac{11\pi^4 k_{-4}\tau^3}{15}$
Quadratic interpolation			
σ_e^2	$\frac{3\pi^2 k_{-2}\tau}{35}$	$\frac{\pi^2 k_{-3}\tau^2}{24}$	$\frac{\pi^4 k_{-4}\tau^3}{315}$
$\frac{\sigma_e^2}{\text{TVAR}(\tau)}$	$\frac{9}{35}$	$\frac{1}{4 [27 \ln(3) - 32 \ln(2)]}$	$\frac{1}{231}$
$\frac{\sigma_e^2}{\text{TDEV}(\tau)}$	0.51	0.18	0.066
Linear interpolation			
σ_e^2	$\frac{2\pi^2 k_{-2}\tau}{15}$	$\frac{\pi^2 k_{-3}\tau^2}{9}$	$\frac{6\pi^4 k_{-4}\tau^3}{315}$
$\frac{\sigma_e^2}{\text{TVAR}(\tau)}$	$\frac{2}{5}$	$\frac{2}{3 [27 \ln(3) - 32 \ln(2)]}$	$\frac{2}{77}$
$\frac{\sigma_e^2}{\text{TDEV}(\tau)}$	0.63	0.30	0.16

Table 1: Comparison between the Time Variance $\text{TVAR}(\tau)$ and the variance of the residuals σ_e^2 for different types of noise and for quadratic and linear interpolation.

- the same number of data: 65,536,
- the same number of data taken into account for the fit: $N = 8640$,
- the same time of estimation of the TIE: $\frac{T_m+T_p}{\tau_0}$ equals to $\{8640, 9900, 11350, 13000, 14900, 17000, 19500, 22400, 25700, 29400, 33700, 38600, 44300, 50700, 58100, 65535\}$.

The noise levels were chosen for getting a variance of the residuals equal to 1.

Figure 1 shows the curves corresponding to the square root of equations (11) to (13) and (17) to (19) compared to the standard deviation estimated from the 10,000 simulations. The simulations exhibit a quite good agreement with the theoretical curves.

The asymptotic behaviors are reached at the end of the log-log graphs. The benefits of the linear interpolation are obvious.

Real Clocks (Quartz USO and Atomic Clocks)

Figure 2 compares the long-term behavior of a real ultra-stable quartz oscillator (denoted “quartz 1” in table 2) to the bounds given by the estimated standard deviation of the TIE (the square root of Equations (11) to (13)).

The data from the oscillator are time deviations sampled with a sampling period $\tau_0 = 10$ s, obtained at CNES Toulouse (France) with their own reference clocks (Cs HP 5071A option 001 and H-maser EFOS-16).

Allan variance revealed that 2 types of noise must be taken into account: white FM ($h_0 = 10^{-22}$ s, i.e. $k_{-2} = 2,5 \cdot 10^{-24}$ s) and random walk FM ($h_{-2} = 1,5 \cdot 10^{-31}$ s $^{-1}$, i.e.

Clock	$\sigma_y(24h)$	h_{-2}	h_{-1}	h_0	σ_e exp.	σ_e theo.	σ_{TIE} exp.	σ_{TIE} theo. (from h_α)	σ_{TIE} theo. (from σ_e)
		(s^{-1})		(s)	(ns)	(ns)	(ns)	(ns)	(ns)
Quartz 1	$1.8 \cdot 10^{-13}$	0	$2.2 \cdot 10^{-26}$	$7.5 \cdot 10^{-23}$	1.4	1.4	7.1	6.2	6.6
Quartz 2	$2.9 \cdot 10^{-12}$	$1.4 \cdot 10^{-29}$	$1.6 \cdot 10^{-25}$	0	9.6	9.2	56.5	52.0	56.0
Quartz 3	$3.0 \cdot 10^{-12}$	$1.4 \cdot 10^{-29}$	$6.4 \cdot 10^{-25}$	0	10.2	11.0	55.7	59.0	59.5
Rb 1	$2.7 \cdot 10^{-13}$	$1.2 \cdot 10^{-31}$	0	$5.3 \cdot 10^{-22}$	1.2	1.3	6.2	5.7	7.1
Cs 1	$9.2 \cdot 10^{-14}$	0	0	$1.5 \cdot 10^{-21}$	1.7	1.6	5.5	5.5	5.6
Cs 2	$3.0 \cdot 10^{-14}$	0	$2.1 \cdot 10^{-28}$	$1.1 \cdot 10^{-22}$	0.6	0.5	1.9	1.6	3.0

Table 2: Comparison between measured and estimated values of σ_e and σ_{TIE} for several clocks with a quadratic interpolation.

Clock	$\sigma_y(24h)$	h_{-1}	h_0	σ_e exp.	σ_e theo.	σ_{TIE} exp.	σ_{TIE} theo. (from h_α)	σ_{TIE} theo. (from σ_e)
			(s)	(ns)	(ns)	(ns)	(ns)	(ns)
Cs 1	$9.2 \cdot 10^{-14}$	0	$1.5 \cdot 10^{-21}$	2.0	2.1	4.1	4.6	4.5
Cs 2	$3.0 \cdot 10^{-14}$	$2.1 \cdot 10^{-28}$	$1.1 \cdot 10^{-22}$	0.8	0.6	1.5	1.4	1.8

Table 3: Comparison between measured and estimated values of σ_e and σ_{TIE} for two cesium clocks with a linear interpolation.

$k_{-4} = 4 \cdot 10^{-33} \text{ s}^{-1}$). Thus, the bounds of Figures 2 were obtained by using the square root of the sum of (11) and (13). This fit was performed over a 24-hour sequence, but the interpolated sequence was shifted along the 90-hour data sequence. At each step ($\tau_0 = 10\text{s}$) of this shift, the fit was extrapolated over 3.5 hours. The TIE measured at this instant ($T_p = 3.5$ hours) was plotted (solid line) and the interpolated sequence was shifted again.

The TIE bounds of the left figure (dashed lines) were estimated from the noise levels as in Figure 2. In the right figure, the TIE bounds were estimated from the variance of the residuals, which was calculated at each step of the shift. In this case, we assumed that the random walk FM was dominant and we used the square root of (20).

The experimental TIE curves remain generally in the theoretical bounds. The few moments where the TIE is outside the bounds is fully compatible with the statistics of TIE (see next section).

Table 2 shows experimental results obtained with several clocks and a quadratic interpolation. The noise levels were estimated from Allan variance measurements. This table compares “ σ_e exp.”, the standard deviation of the residuals, with “ σ_e theo.”, the estimate of σ_e obtained from the square root of (8), (9), (10) and the noise level coefficients.

This table compares also “ σ_{TIE} exp.”, the measured error between the parabola extrapolated over 3.5 hours and the real-time deviation of the clock at this instant, with

" σ_{TIE} theo. (from k_α)" estimated from the square root of (11), (12), (13), and with " σ_{TIE} theo. (from σ_e)" estimated from the square root of the expression using the variance of the residuals such as (20).

Table 3 shows the same type of results but limited to the cesium clocks and with a linear interpolation.

Here also, the agreement between measurements and estimates is quite good.

On the other hand, Table 2 and 3 confirm that the standard deviation of the residuals is higher for a linear interpolation than for a quadratic one, whereas it is the opposite for the standard deviation of the TIE.

CONFIDENCE INTERVALS FOR THE INTERPOLATION AND EXTRAPOLATION ERRORS

Figure 2 shows that the real TIE may be outside the bounds of the estimated $\hat{\sigma}_{TIE}$. Thus, it is important to know the probability for the real TIE to be inside or outside these bounds. Moreover, it may be useful to improve the TIE bounds by using confidence intervals. This may be achieved by studying the statistics of the TIE.

We want to obtain a coefficient c_β ensuring the following confidence interval:

$$-c_\beta \cdot \hat{\sigma}_{TIE} < \text{TIE}(T_m, T_p) < +c_\beta \cdot \hat{\sigma}_{TIE} \quad \text{with } \beta\% \text{ of confidence.} \quad (21)$$

By definition, c_β follows a Student distribution with ν degrees of freedom [10]. Consequently, for building the confidence interval (21), we have to use the Student coefficients for c_β . These coefficients are given in tables [10].

However, it is then necessary to know the number of degrees of freedom of the Student distribution, or, and this is equivalent, the number of degrees of freedom of the χ^2 distribution followed by $\langle \text{TIE}^2(T_m, T_p) \rangle$. Obviously, this number depends on how $\langle \text{TIE}^2(T_m, T_p) \rangle$ is estimated, i. e. from the variance of the residuals or from the noise levels k_α .

Estimation From the Variance of the Residuals

Equation (20) shows that $\langle \text{TIE}^2(T_m, T_p) \rangle$ is the product of a random variable $\hat{\sigma}_e^2$ by a constant number. Thus, the distribution of $\langle \text{TIE}^2(T_m, T_p) \rangle$ is the same as the distribution of $\hat{\sigma}_e^2$, i. e. a χ^2 distribution.

From Monte-Carlo simulations, we observed that the degrees of freedom of the distribution of $\hat{\sigma}_e^2$ only depend on the type of noise but, curiously, neither on the number of data N , nor the sampling period τ_0 .

We measured the following degrees of freedom ν for the χ^2 distribution of $\hat{\sigma}_e^2$:

- White FM: $\nu \approx 8$;
- Flicker FM: $\nu \approx 3$;
- Random walk FM: $\nu \approx 2$.

$S_x(f)$	ν	$c_{70\%}$	$c_{95\%}$
$k_{-2}f^{-2}$	8	1.1	2.3
$k_{-3}f^{-3}$	3	1.2	3.2
$k_{-4}f^{-4}$	2	1.4	4.3

Table 4: Degrees of freedom of $\hat{\sigma}_e^2$ and $\hat{\sigma}_{TIE}$, and confidence coefficients c_β for 70% and 95% versus the types of noise [10].

Therefore, the c_β Student coefficient must be chosen with these degrees of freedom, according to the type of noise. Table 4 gives these coefficients for a 70% confidence interval (1σ) and for a 95% confidence interval (2σ).

Large Estimation From the Noise Levels

In this case, the degrees of freedom of $\langle TIE^2(T_m, T_p) \rangle$ are equal to the ones of the estimated noise level \hat{k}_α and then depend on the accuracy of its estimation. For instance, if \hat{k}_α was estimated by using the Allan variance, its degrees of freedom depend on the length of the sequence and on the number of sample used by the Allan variance [11, 12]. If this sequence is long enough, the degrees of freedom may be much greater than the values obtained from the variance of the residuals. The degrees of freedom have to be estimated at each noise level measurement [11, 12].

Therefore, if the noise levels are precisely determined, the estimation of $\hat{\sigma}_{TIE}$ is far better by using this method than from the variance of the residuals.

CONCLUSION

The first application of this work may be the selection of clocks according to their time stability performances. We may fix a limit for the maximum acceptable σ_e and TIE for a given interpolation sequence and extrapolation time. Let us consider that for an interpolated period $T_m=24h$ and for an extrapolated time $T_p=3.5h$, we fix : $\sigma_e < 2.1$ ns and $TIE < 5$ ns. The use of Equations (8) to (13) allows us to translate the above specifications into specifications on the noise levels k_α (for instance, for a random walk FM, these specifications become $k_{-4} < 3.7 \cdot 10^{-33} s^{-1}$). Furthermore, these specifications may be translated again in term of Allan variance over 1 day (in the case of the random walk FM, it yields $\sigma_y(24h) < 3 \cdot 10^{-13}$). Thus, we can obtain a very simple criterion by using the Allan variance, ensuring that the specifications for σ_e and TIE will be respected.

Besides the interest of this method for navigation satellite systems, it may be used for defining a new method for very-long-term stability analysis.

A clock may be continuously measured during a few days (e.g. a time deviation measurement with a sampling period of 1 minute during 10 days). From these data, the noise levels of this clock could be precisely determined and a quadratic fit could be carried out. Thus, if the clock is continuously running in the same conditions, it could be possible to extrapolate the difference of this clock with the parabolic fit after a few months or 1 year.

This analysis could be helpful to low-accuracy purposes of time keeping, for instance for industrialists who periodically send their clock to an accreditation laboratory, or for applications which need a large autonomy.

REFERENCES

- [1] J. A. Barnes et al., "Characterization of frequency stability," *IEEE Transactions on Instrumentation and Measurement*, IM-20(2):105–120, May 1971.
- [2] D. W. Allan, "Time and frequency (time-domain) characterization, estimation, and prediction of precision clocks and oscillators," *IEEE Transactions on Ultrasonics, Ferroelectrics, and Frequency Control*, UFFC-34(6):647–654, November 1987.
- [3] L. G. Bernier, "Linear prediction of the non-stationary clock error function," *Proceedings of EFTF 88*, pages 125–137, Neuchâtel, Switzerland, March 1988.
- [4] L. Di Piro, E. Perone, and P. Tavella, "Random walk and first crossing time: applications in metrology," *Proceedings of EFTF 98*, pages 388–391, Warsaw, Poland, March 1998.
- [5] A. Lepek, "Clock prediction uncertainty," In *Proceedings of EFTF 98*, pages 205–208, Warsaw, Poland, March 1998.
- [6] J. E. Deeter and P. E. Boynton, "Techniques for the estimation of red power spectra. I. Context and methodology," *The Astrophysical Journal*, 261:337–350, October 1982.
- [7] F. Vernotte, J. Delporte, M. Brunet, and T. Tournier, "Uncertainties of drift coefficients and extrapolation errors: Application to clock error prediction," *Metrologia*, 2000, submitted.
- [8] F. Vernotte, J. Delporte, M. Brunet, and T. Tournier, "Estimation of uncertainties in time error extrapolation," *Proceedings of the 31st PTI*, pages 305–316, Dana Point, California USA December 1999.
- [9] D.W. Allan, M.A. Weiss, and J.L. Jespersen, "A frequency-domain view of time-domain characterization of clocks and time and frequency distribution systems," *Proceedings of the 45th IEEE Frequency Control Symposium*, pages 667–678, May 1991.
- [10] G. Saporta. *Probabilités, analyse des données et statistique*. Editions Technip, Paris, 1990. ISBN 2-7108-0565-0.
- [11] P. Lesage and C. Audoin, "Characterization of frequency stability: uncertainty due to the finite number of measurements," *IEEE Transactions on Instrumentation and Measurement*, IM-22(2):157–161, June 1973. See also comments in IM-24 p. 86 and correction in IM-25 p. 270.
- [12] D. A. Howe, D. W. Allan, and J. A. Barnes, "Properties of signal sources and measurement methods," *Proceedings of the 35th IEEE Frequency Control Symposium*, pages A25–A35, Philadelphia, PA, USA, May 1981.

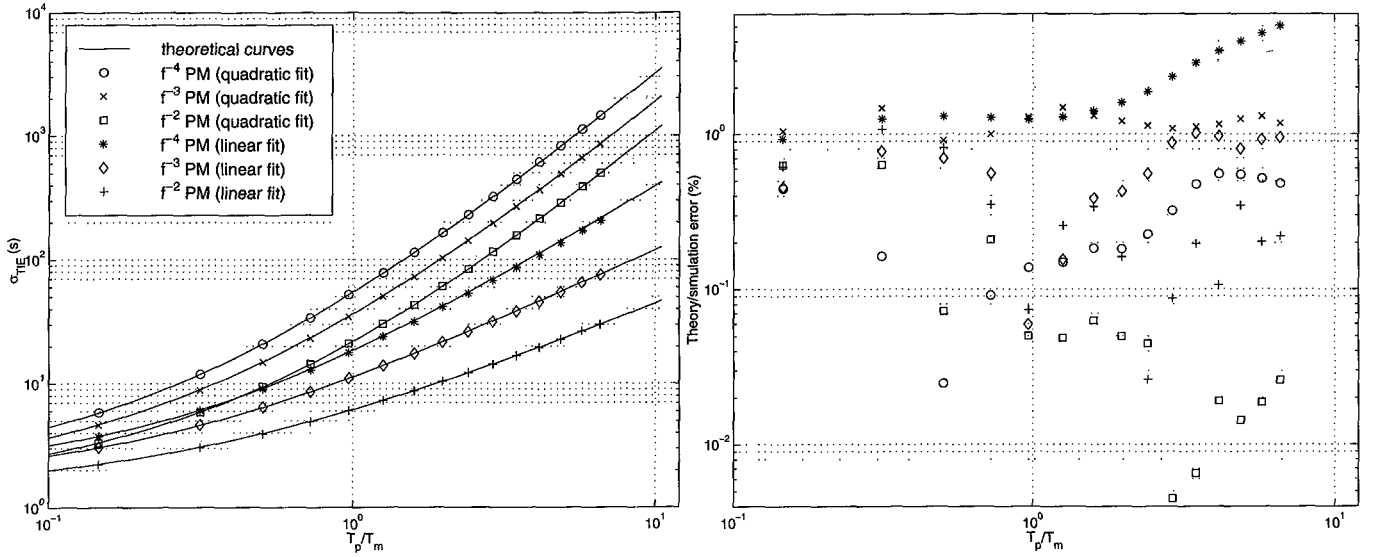


Figure 1: Comparison of the estimation of the standard deviation of the TIE calculated from the equation (11), (12), (13), (17), (18), (19) (solid lines) and estimated over 10000 realizations of simulated noise for a quadratic interpolation (\circ , \times , and \square) and for a linear interpolation ($*$, \diamond and $+$). In order to use the same scale, the noise levels were defined in such a way that the variance of the residuals is equal to one ($k_{-2} = 1.4 \cdot 10^{-4}\text{s}$, $k_{-3} = 3.3 \cdot 10^{-8}$ and $k_{-4} = 5.0 \cdot 10^{-12}\text{s}^{-1}$ for the quadratic interpolation, $k_{-2} = 3.5 \cdot 10^{-3}\text{s}$, $k_{-3} = 4.8 \cdot 10^{-7}$ and $k_{-4} = 3.3 \cdot 10^{-11}\text{s}^{-1}$ for the linear interpolation). The error bars corresponding to the estimates of the simulated noises are too small to be plotted on this graph. The right plot shows the differences between the theoretical curves and the simulation points: the larger error is equal to 5% but most of them are below 1%.

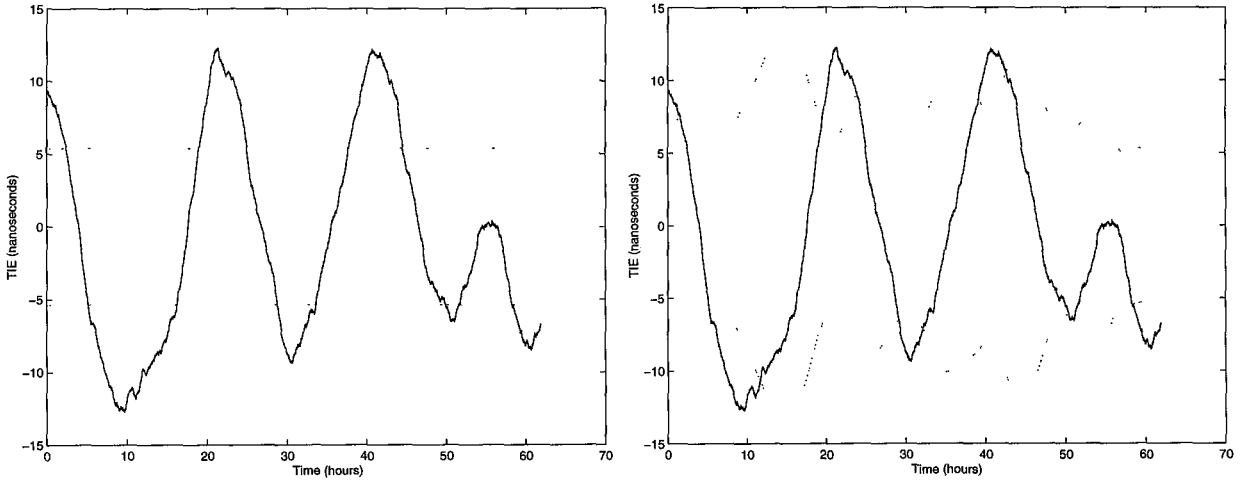


Figure 2: Estimation of the TIE for an ultra-stable quartz oscillator. The fit was performed over a 1-day sliding window. The TIE was measured 3.5 hours after the fitted sequence (solid line). The TIE bounds (dashed lines) were estimated from the noise levels (left) or from the variance of the residuals (right).

EXAMINING GPS CARRIER-PHASE ANALYSES TO EVALUATE THE ACCURACY OF FREQUENCY TRANSFER USING DATA FROM NIST AND PTB*

Lisa Nelson and Judah Levine
Time and Frequency Division
National Institute and Standards and Technology
Boulder, CO 80305, USA

Abstract

In recent work, comparisons were made between the primary frequency standards at the National Institute of Standards and Technology (NIST) and the Physikalisch-Technische Bundesanstalt (PTB) using dual-frequency geodetic receivers that measure the phase of the GPS carrier relative to the local standard. In this work we report on studies of the effects of data analysis lengths, bias vs. non-bias fixing, and troposphere estimation on the final solution. This was done in an effort to determine the effect of data merging routines and atmospheric modeling on these comparisons. Initial results indicate that these effects currently contribute to the error budget at parts in 10^{15} . We also show initial results using two different analytical software packages for the NIST/PTB baseline. This analysis was made in an effort to lower the overall error budget of the comparison technique.

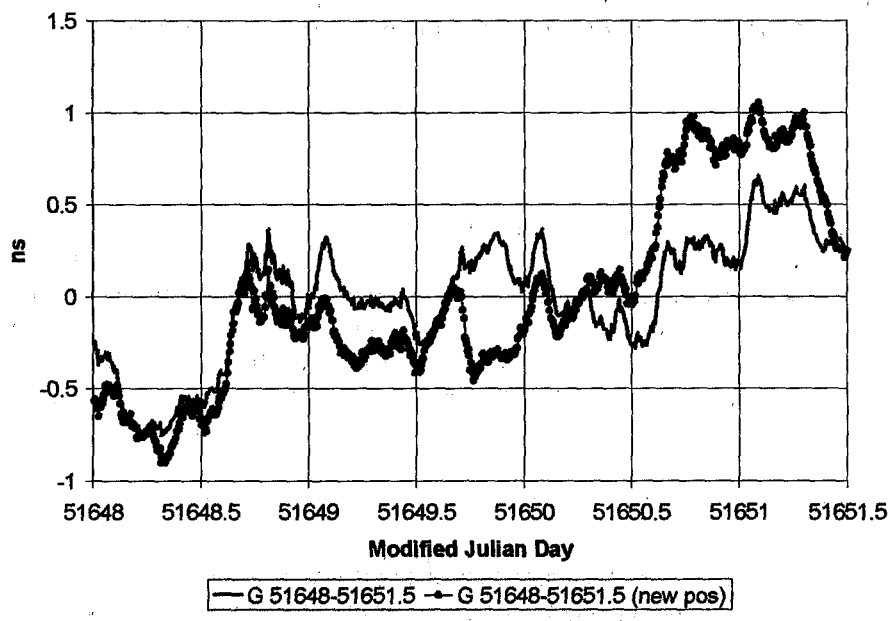
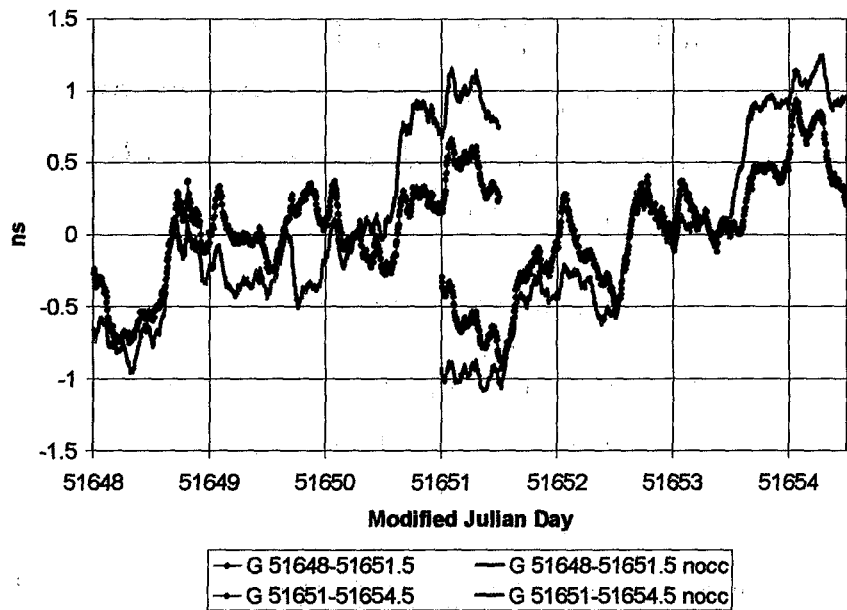
INTRODUCTION

Our previous work has shown that it is possible to compare frequency standards at a few parts in 10^{15} using the GPS carrier phase technique [1]. However, we found that as we merged consecutive data series a frequency change appeared. This prompted us to investigate possible reasons for this rate difference. In this paper we investigate errors that mixing cross-correlating and non-cross-correlating receiver data in our network produces in the analysis. Also, we present the differences between the bias and non-bias fixed solutions, and look at the troposphere estimation to see what effect that has on the network solution. Initial results comparing two different software analysis packages are also presented.

CROSS-CORRELATING AND NON-CROSS-CORRELATING RECEIVER DATA

In our initial comparisons of NIST and PTB frequency standards we used both cross-correlating and non-cross-correlating receiver data in our network analysis. Figure 1 shows the results of making all the receiver data in our network non-cross-correlating. This change was made because of the way different receivers deal with the P1-C1 bias [2]. Over two runs of 3.5 d comparing the hydrogen maser at PTB, called H2(PTB), and UTC(NIST) we see a maximum difference of approximately 750 ps, largely near the start and stop times of the run. The difference in the two solutions is a few parts in 10^{15} .

* U. S. Government work not protected by U. S. Copyright.



Using the all non-cross-correlating data format we also compared solutions when we entered the final estimated coordinates of PTB back in as the a priori values. Figure 2 shows the differences in the solution made by changing the position according to the estimation results. Once again in the short term the structure is consistent, but over the length of the data span there are differences on the order of parts in 10^{15} .

LENGTH OF DATA RUN

To investigate why there is a significant difference in the frequency we looked at the length of data that we processed in each analysis. Figure 3 shows the differences in the solution when we processed each day separately, compared to the solution with the 3.5 d run. In the short term things are similar, but in the long term there are differences of parts in 10^{15} . Figure 4 shows the differences between runs of 1 and 1.5 days. These solutions also have significant frequency differences, even though the data spans differ by only half a day. From our previous work [1], it is also important to note the overlap regions of the data runs and the significantly different slopes there as well. It demonstrates the importance of determining exactly how the data are going to be merged together to form a multi-day solution, and why merging can contribute to a rate offset.

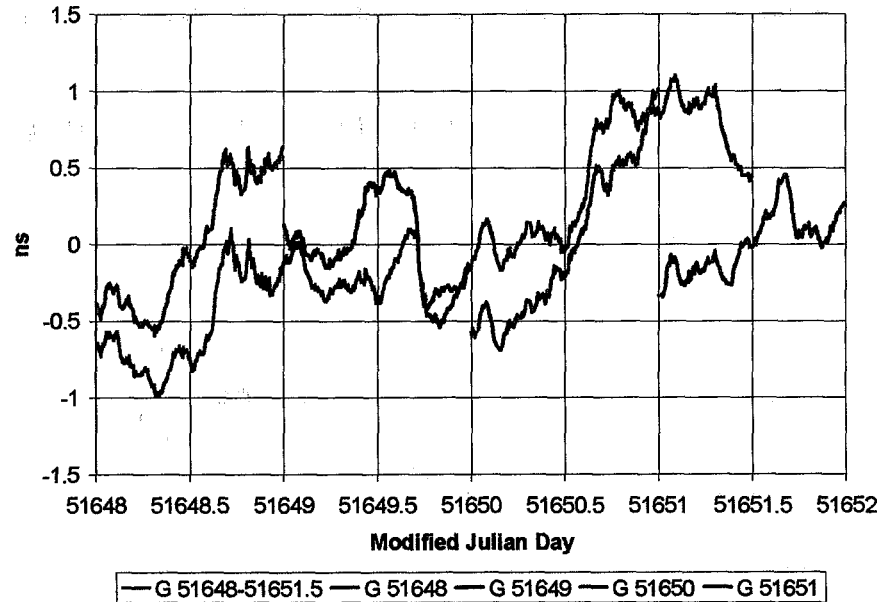


Figure 3: H2(PTB)-UTC(NIST) 1 d vs. 3.5 d run. The black line is the run of 3.5d. The gray lines are the runs of 1d, over the same time period.

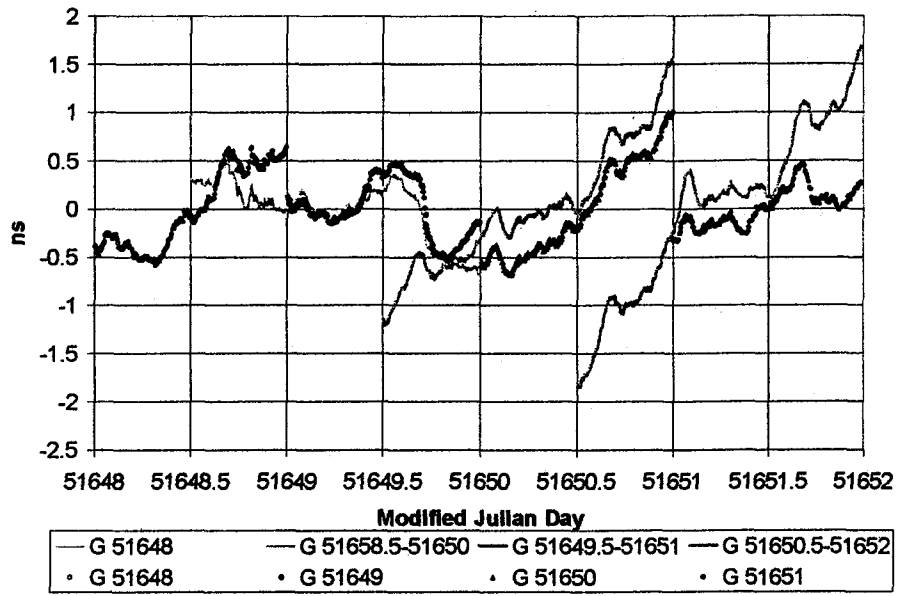


Figure 4: H2(PTB)-UTC(NIST) 1 d vs. 1.5 d runs. The black dots are the runs of 1d. The gray lines are the runs of 1.5 d.

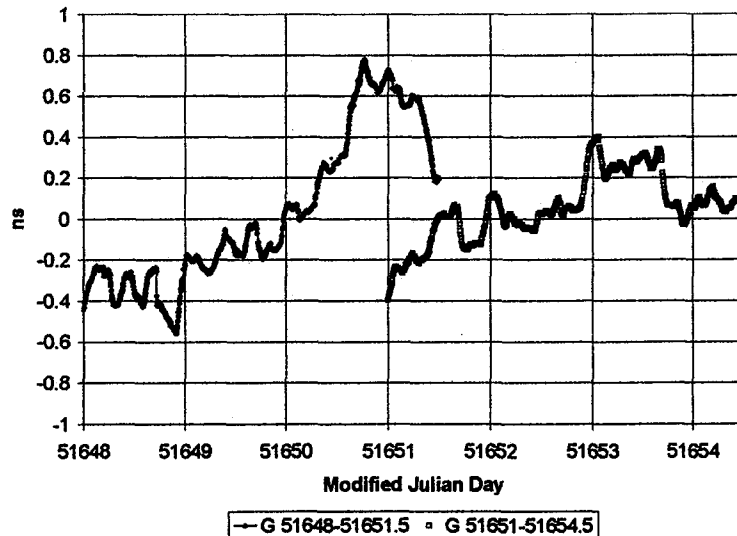


Figure 5: Difference in bias and non-bias fixed solutions runs of 3.5 d.

BIAS AND NON-BIAS FIXING

Our analysis also showed a significant difference in frequency between the bias and non-bias fixed solutions. Bias fixing is when we attempt to resolve the ambiguities, or integer number of cycles in the carrier phase observation, to a more accurately measure the range. If bias fixing is not performed we do not completely determine the unknown number of internal cycle slips, or loss of lock conditions, in the receiver. Figures 5–7 show the differences in the bias and non-bias fixed cases for the runs of 3.5 d, 1.5 d, and 1 d. There are significant differences between the lengths of the various data runs and the ways in which the ambiguities are being resolved. The solutions differ by parts in 10^{15} .

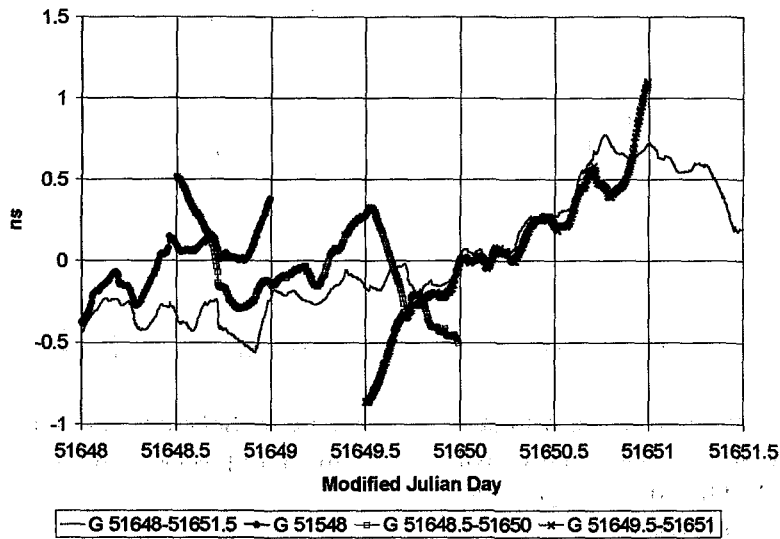


Figure 6: Difference in bias and non-bias fixed solutions runs of 1.5 d and 3.5 d.

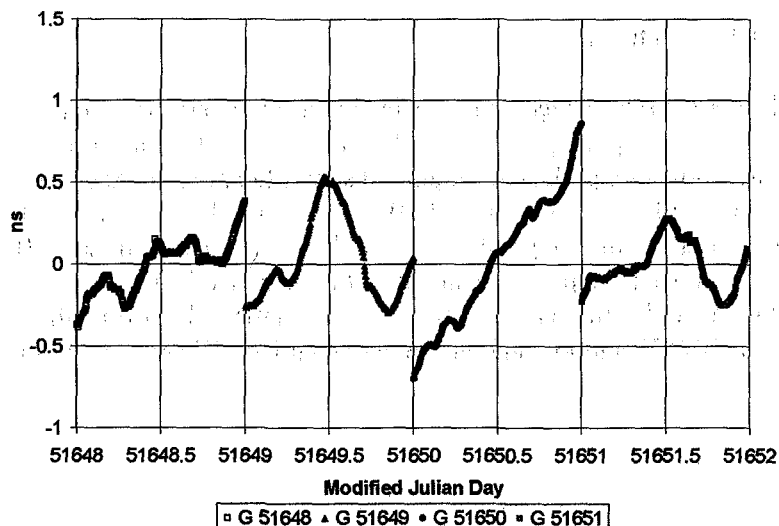


Figure 7: Difference in bias and non-bias fixed solutions for runs of 1 d.

TROPOSPHERE ESTIMATION

We also looked at the troposphere estimation parameters to determine their effects. We found them to be less than a part in 10^{15} over the 3.5 d interval and the shorter 1.5 d intervals, as shown in Figures 8 and 9. They do not appear to be the cause of the frequency change of the final solution.

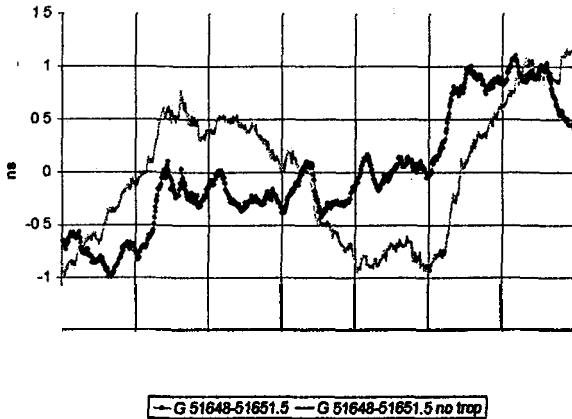


Figure 8: Solutions for the run of 3.5 d with and without troposphere estimation. The black dotted line is with troposphere estimation. The gray line is without troposphere estimation.

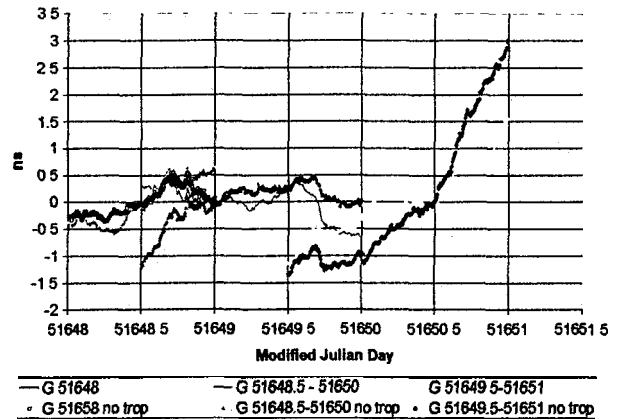


Figure 9: Solutions for runs of 1.5 d with and without troposphere estimation.

DIFFERENT SOFTWARE SOLUTIONS

In order to determine whether the rate change might be due to our processing technique we also explored the use of a different analytical software package, Bernese [4]. We performed the analysis on a daily basis using both the GIPSY and Bernese software packages. Figure 10 shows the differences between the two solutions for H2(PTB)-UTC(NIST) for both analyses. Days 51648, 51649, and 51651 all show differences of parts in 10^{15} , with the biggest differences at the endpoints of the analysis. On the third day, 51650, we found that the solutions had almost the opposite slopes. We are not yet clear why this is the case for this day, but first indications are that it might be in the differences in ambiguity resolution. Figure 11 shows the differences in the bias and non-bias fixed GIPSY solution and the Bernese solution. We are continuing to investigate the differences in the solutions.

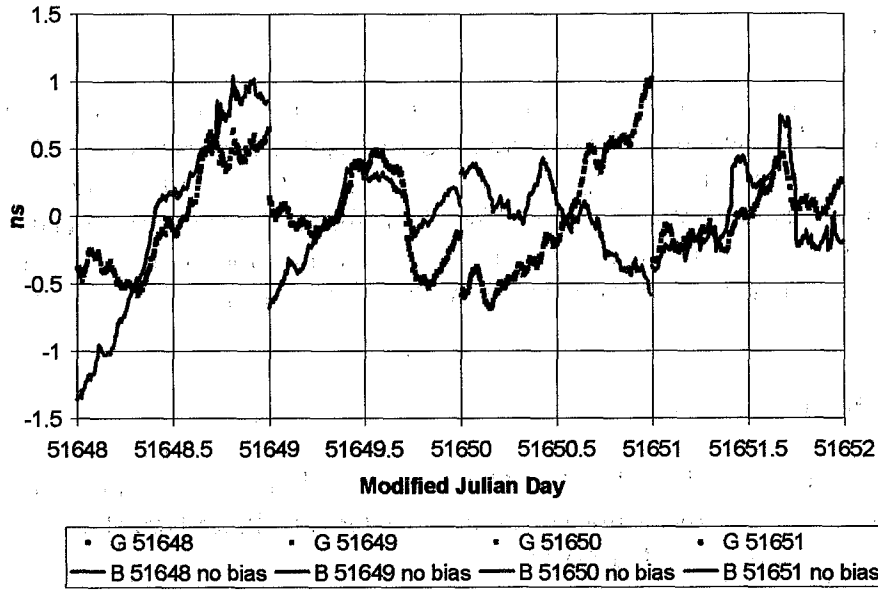


Figure 10: Different Software Solutions. Bias fixed GIPSY solutions are indicated by the black dots and Bernese solutions by the gray lines. Each is processed in daily batches. In the key the GIPSY solutions are indicated by G, and the Bernese solutions by B.

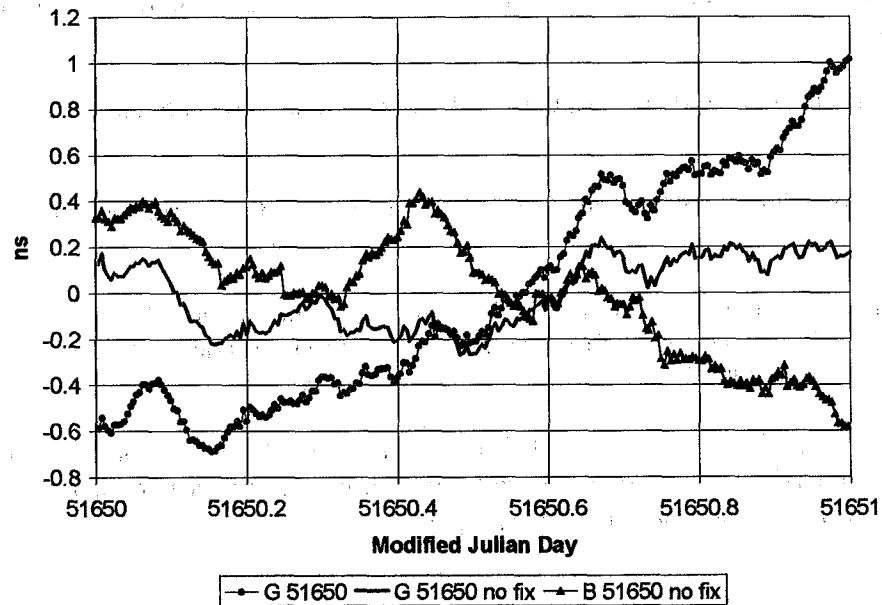


Figure 11: Different Software Solutions for Modified Julian Day 51650. The gray lines, with and without markers, indicate GIPSY solutions. The Bernese solution is the black line with triangle markers.

CONCLUSIONS

We have shown that some of the frequency differences are dependent on the length of the data series that is processed. The longer the data series the smoother the results. We have also shown that differences made by the bias fixing process significantly affect on the rate regardless of the length of the data series, and that the rate offset depends on the analysis procedure used. We have determined that the troposphere estimation is not a significant source of error. We plan to continue our investigation of the reason for these frequency changes in hopes of reducing the uncertainty to less than parts in 10^{15} .

ACKNOWLEDGMENTS

The authors thank John Braun from UNAVCO and Rolf Dach from AIUB for their help with the Bernese processing. We also thank our colleagues at PTB, Dr. Peter Hetzel and Jurgen Becker, for their continual help with our data retrieval.

REFERENCES

- [1] L. Nelson, J. Levine, and P. Hetzel 2000, "*Comparing primary frequency standards at NIST and PTB*," Proceedings of the 2000 IEEE/EIA International Frequency Control Symposium and Exhibition, 7-9 June 2000, Kansas City, Missouri, USA, pp. 622-628.
- [2] J. Ray (EO Dept., U.S. Naval Observatory), IGSMAIL-2744: new pseudorange bias convention, personal communication.
- [3] GIPSY-OASIS II software, NASA Jet Propulsion Laboratory, California Institute of Technology, Pasadena, CA, USA.
- [4] G. Beutler, E. Brockmann, R. Dach, P. Fridez, W. Gurtner, U. Hugentobler, J. Johnson, L. Mervart, M. Rothacher, S. Schaer, T. Springer, R. Weber, Bernese GPS Software, version 4.2, Astronomical Institute, University of Berne, August 2000.

Disclaimer: Any mention of commercial products is for information only; it does not imply recommendation or endorsement by the National Institute of Standards and Technology nor does it imply that any products mentioned are necessarily the best available for the purpose.

Questions and Answers

DEMETRIOS MATSAKIS (USNO): A few months ago, I heard a paper, and I think you did too, by Rolf Dach. I know he's talking next and will probably be repeating some things. I might be stealing some of his fire. He found there was a correlation between the position error and ambiguity-fixing that could result in funny things like you are seeing there. Have you looked at the actual values for the parameters you're getting?

LISA NELSON: Actually, because of such initial data, I haven't had a chance to look at all that yet. But yes, I am aware of what he's worked on. I just haven't gone through to check all this recent stuff out with that.

THOMAS CLARK (NASA Goddard Space Flight Center): I presume that this is all dual-frequency data. Did you assume the receiver offset between L-1 and L-2 was constant between these days or was that a solved-for parameter?

NELSON: I'm not sure about that; I would have to look.

A TRANSATLANTIC GETT TIME TRANSFER EXPERIMENT — LATEST RESULTS

R. Dach, T. Schildknecht, T. Springer
Astronomical Institute, University of Berne
Sidlerstr. 5, 3012 Bern, Switzerland
tel: +41-31-6313802; fax: +41-31-6313869
e-mail: dach@aiub.unibe.ch

G. Dudle and L. Prost
Swiss Federal Office of Metrology
Lindenweg 50, 3084 Wabern, Switzerland

Abstract

Two Geodetic Time Transfer terminals (GeTT) were installed at the Physikalisch-Technische Bundesanstalt (PTB), Braunschweig, Germany and at the U.S. Naval Observatory (USNO), Washington, DC. The receivers store GPS Carrier Phase (GPS CP) data as well as GPS Pseudorange (GPS PR) observations from both frequencies. This time and frequency transfer experiment over the Atlantic has now been running for more than 2 years. Comparisons of the results from our GPS-based time series with other, independent methods like Common View (CV) and Two-Way Satellite Time and Frequency Transfer (TWSTFT) allows one to study the long-term stability of these techniques.

The analysis of GPS data gives differences between two clocks with a high sampling rate (300 seconds or even less). Therefore, GPS permits the possibility of comparing two clocks nearly continuously over intercontinental distances.

High-quality GPS products, e.g. satellite orbits, are necessary to get good results for the clock estimation. We will compare the time transfer results using the final and the rapid products from the Center for Orbit Determination in Europe (CODE), one of the analysis centers of the International GPS Service (IGS). Using the rapid products the time transfer results are available at approximately 1800 UT the day after the observations. The final solution is usually available 1 week later.

INTRODUCTION

The Astronomical Institute of the University of Berne (AIUB) is operating the Center for Orbit Determination in Europe (CODE) which is one of the analysis centers of the International GPS Service (IGS). CODE routinely analyses a global network of GPS stations to produce improved orbits, Earth orientation parameters, ionosphere models, station coordinates/usnovelocities, as well as additional results for geodetic and other applications. Since summer 1998 a small subnetwork of stations is processed separately in the framework of a time transfer experiment (see Figure 1). The procedures used in this experiment are focusing on the estimation of receiver clocks using all available code and phase observations. The network has currently produced a time series of time transfer data of more than 2 years.

The network includes two special Geodetic Time Transfer terminals (GeTT) developed at the Swiss Federal Office of Metrology (OFMET) – see [1] for more details. They are located at the Physikalisch-Technische Bundesanstalt, Braunschweig, Germany (PTB; the GPS station is named PTBA) and at the U.S. Naval Observatory, Washington, DC (USNO; the GPS station is named USNB). These terminals are based on the geodetic Ashtech Z-XII receiver. These receivers provide not only the code measurements on both frequencies, but also the carrier phase. For time transfer purposes, the receiver is driven directly by an external clock. All electronic equipment is installed in a thermostatic box together with the receiver itself. This design should minimize the influence of temperature changes in the laboratories on the time transfer results. [2]

ANALYSIS STRATEGY

For the time transfer solution we presently use the Bernese GPS Software, Version 4.3. The general analysis steps are:

1. Double difference solution for the network to get coordinates and troposphere information
2. Data screening of the zero difference files
3. Phase and code observations are taken for the time transfer (network) solution.

A more detailed description is given in [3].

Because of the high correlation between the station height, troposphere estimates, and clock parameters only observations to satellites with an elevation angle of more than 10° are used for the analysis (see [4]). The data received from satellites with low elevations are more noisy and the occurrence of multipath becomes more probable. Therefore, we use an elevation dependent weighting of the data. These basic analysis options have never been changed since the beginning of the transatlantic time transfer experiment.

Since May 2000 (MJD 51670) the routine processing at CODE is running on a new operating system. In the course of the transfer of the processing, some new software options were implemented to improve the time transfer results. The most important changes concerning the time transfer solution are:

- Improved data screening
- A priori values for the receiver clocks can be introduced
- Overlapping sessions are processed to get the possibility for concatenation of the daily solutions.
- Additional time transfer solution based on the CODE rapid products.

RESULTS

Continuous Time Transfer Results

The noise behavior of the pseudorange observations may cause discontinuities between consecutive time transfer solutions. For daily solutions they can reach a magnitude up to 1 ns at the day boundaries (see Figure 2). To get a continuous series of time transfer results, we propose to use all data twice: in a first session (computing batch) from 0:00 UTC until 24:00 UTC of the day and in a second session from 12:00 UTC to 12:00 UTC of the next day. The overlapping periods may be used to estimate and remove the day boundary discontinuities.

After this concatenation of the individual session solutions, the GPS CP time transfer results constitute a nearly continuous series of time differences. The only remaining discontinuities stem from gaps in the data. Figure 3 shows the improvement of the Allan deviations caused by the concatenation of the time transfer results from the individual computing sessions. Because the receiver clock values are not corrected with local measurements, only the difference between the two curves in the diagrams can be interpreted – both curves contain, therefore, in addition the characteristic of the GPS receiver clocks. The improvement is nearly independent from the length of the baseline.

Comparing the concatenated GPS CP time transfer results with the results from TWSTFT, the scatter of the differences becomes smaller than the scatter of the differences between the non-concatenated GPS CP and the TWSTFT results. In both diagrams of Figure 4 a jump at MJD 51714 is visible when the antenna cable at USNB was changed. Another event shows up in the concatenated result only: a small jump in the order of 2 ns at MJD 51764. At this epoch the temperature stabilization electronics of the GeTT in USNB failed – the temperature dropped from 15°C to 4°C (e-mail 19 September 2000 from E. Powers, USNO). The magnitude of the jump can be explained with the calibration results of the temperature dependence of the receiver in [2].

Time Transfer Results Using CODE Rapid Products

Time transfer using GPS CP gives time differences with a high sampling rate and a high precision. Therefore, a large amount of data has to be transferred and analyzed (four measurements each 30 s to usually 6 to 10 satellites). This is done in a postprocessing mode. If the final orbits from one of the IGS analysis centers are used, it takes about 1 week from the measurement until the time transfer results are available. The CODE rapid orbits are available the day after the observation and have nearly the same accuracy as the CODE final orbits [5]. The time transfer solutions based on the CODE rapid orbits should, therefore, have nearly the same quality as those based on the final orbits.

Since May 2000 the time transfer network of Figure 1 is also processed the day after the observations based on the CODE rapid products. The time transfer results are available usually before 18 UTC of the day after the measurement. The overlapping sessions are also computed for rapid product. The processing is running in a completely automatic mode without manual interactions. The results have roughly the same accuracy as the final solution. This is confirmed by the Allan deviations for the rapid as well as for the final time transfer solutions based on 4 months of data (see Figure 5). Independent from the length of the baseline only small differences between the two solutions may be observed – even for the intercontinental baseline USNB→PTBA. This is essentially due to the high quality of the CODE rapid orbits.

COMPARISON WITH OTHER METHODS

From the beginning of this transatlantic time transfer experiment in summer 1998 until May 2000, neither the hardware installation on the sites nor the analysis strategy has been changed. Because the Ashtech receivers do not show any internal clock resets a continuous series of time transfer results between USNB and PTBA is available. This experiment offers, therefore, a good possibility to study the long-term stability of the GPS CP method in comparison with other time transfer methods.

In the Figure 6 the differences between the time transfer results from GPS CP and TWSTFT until September 2000 are shown when the GeTT terminal in Braunschweig was switched off and

shipped back to the OFMET for maintenance and calibration purposes. All differences are smaller than 4 ns – the standard deviation of the difference is 2 ns. Some systematic behavior may be observed in the plots. It can still not be explained, but it is also not significant. A correlation with the outside temperature – the GPS antennas are not temperature controlled – could not be found [6].

The differences between the GPS CP time transfer solution and the Circular T values – see Figure 7 – are of the same order of magnitude, but with an increased scatter. The evident jump of about 9 ns at MJD 51364 is explained by a changed ionosphere modeling in the Circular T computation from this date onwards (see [7]). For the time difference between UTC(USNO) and UTC(PTB), this change of the analysis model resulted in an offset of 9 ns (e-mail 10 January 2000 from G. Petit, BIPM).

A reprocessing of the 2 years from the beginning of the experiment until May 2000 is planned in order to generate a concatenated time transfer solution over the full period of observations. The comparison between the GPS CP and the other methods may then reveal more details on possible systematics in the differences between the results.

CONCLUSIONS

The time transfer using GPS CP is a very powerful method for clock comparisons. A network of about 15 stations in Europe and North America is processed at AIUB every day. Two of the stations are equipped with special GeTT terminals developed at OFMET.

Since May 2000 it is possible to concatenate the daily time transfer solutions to a continuous time series. This time series shows an improvement in the comparison with other time transfer methods such as TWSTFT. Independent from the length of the baseline, an improvement in the Allan deviation can be observed.

Because of the high quality of the rapid orbits from CODE the time transfer results based on the rapid orbits have nearly the same quality than the time transfer solutions based on the final CODE products. The rapid solution is available less than 18 hours after the last observation of a day, whereas the latency for the final solution is nearly 1 week.

Two years of data were collected with the GeTT terminals at USNO and at PTB without any changes in the hardware configuration or in the data analysis parameters. The acquired time transfer series is, therefore, very homogeneous. The differences to the results from TWSTFT have a standard deviation of about 2 ns. The differences to the Circular T values are a slightly more noisy and show a standard deviation of 3 ns.

ACKNOWLEDGMENTS

The authors wish to thank both USNO and PTB for accepting and maintaining the GeTT terminals in their laboratories. We are especially grateful to Dr. D. Matsakis and Dr. P. Hetzel and their co-workers for many helpful discussions and advice.

REFERENCES

- [1] G. Dudle, F. Overney, L. Prost, T. Schildknecht, and T. Springer 1999, “*First Results on a Transatlantic Time and Frequency Transfer by GPS Carrier Phase*,” Proceedings

of the 30th Annual Precise Time and Time Interval Systems and Applications Meeting, 1-3 December 1998, Reston, Virginia, USA, pp. 271-280.

- [2] F. Overney, L. Prost, U. Feller, T. Schildknecht, and G. Beutler 1997, "GPS Time Transfer using Geodetic Receivers: Middle-Term Stability and Temperature Dependence of the Signal Delays," Proceedings of the 11th European Frequency and Time Forum (EFTF), 4-7 March 1997, Neuchâtel, Switzerland, pp. 504-508.
- [3] R. Dach, T. Schildknecht, T. Springer, G. Dudle, and L. Prost 2000, "Recent Results with Transatlantic GeTT Campaign," Proceedings of the 31st Annual Precise Time and Time Interval Systems and Applications Meeting, 7-9 December 1999, Dana Point, California, USA, pp. 461-469.
- [4] M. Rothacher, and G. Beutler 1998, "The Role of GPS in the Study of Global Change," Physics and Chemistry of the Earth, **23**, 1029-1040.
- [5] U. Hugentobler, T. Springer, S. Schaer, G. Beutler, H. Bock, R. Dach, D. Ineichen, L. Mervart, M. Rothacher, U. Wild, A. Wiget, E. Brockmann, G. Weber, H. Habrich, and C. Boucher 2000, "CODE IGS Analysis Center Technical Report 1999," 1999 Technical Reports of the IGS (K. Gowey et al., eds.).
- [6] G. Dudle, L. Prost, R. Dach, T. Springer, and T. Schildknecht 2001, "Progress Report on the Transatlantic Time Transfer by GeTT," Proceedings of the 14th European Frequency and Time Forum (EFTF), 14-16 March 2000, Torino, Italy (in press).
- [7] P. Wolf, and G. Petit 2000, "Use of IGS Ionosphere Products in TAI," Proceedings of the 31st Annual Precise Time and Time Interval (PTTI) Systems and Applications Meeting, 7-9 December 1999, Dana Point, California, USA, pp. 419-429.
- [8] T. Springer, "Modeling and Validating Orbits and Clocks Using the Global Positioning System," Ph.D. theses at Philosophisch-naturwissenschaftliche Fakultät, University of Berne, Bern, Switzerland, 1999.

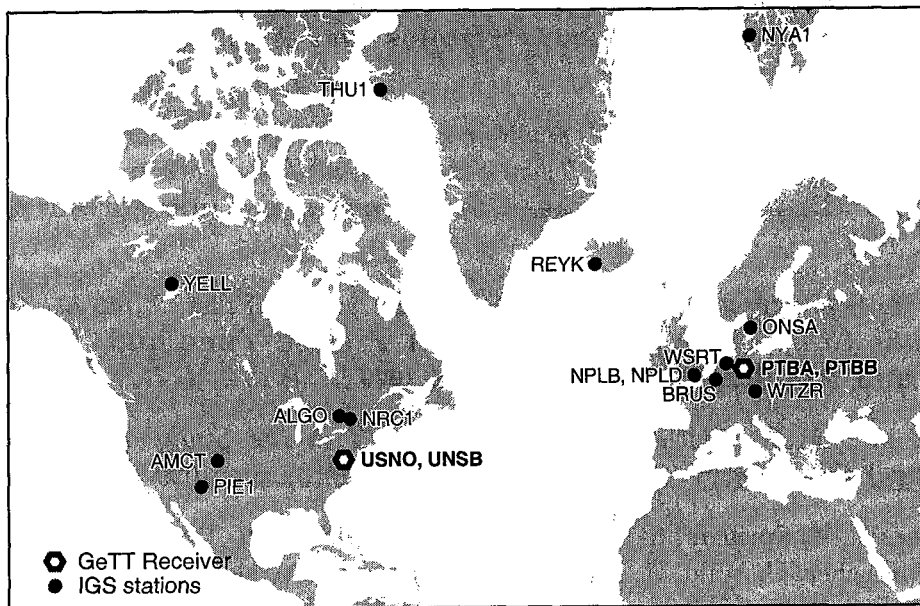
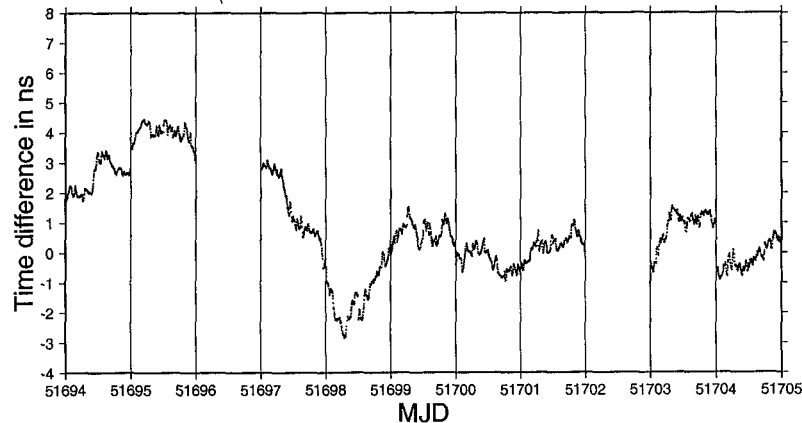
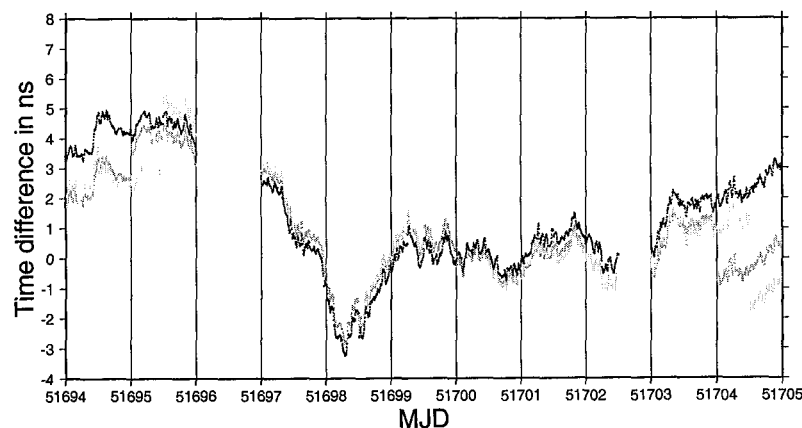


Figure 1: Geographical distribution of the stations in the network for the clock solution.



Daily solutions may show discontinuities at the day boundaries



Concatenated time transfer results without discontinuities (in black)

Figure 2: Effect of the concatenation of time transfer results to avoid the discontinuities at the day boundaries for the transatlantic baseline USNB \rightarrow PTBA – time window MJD: 51694 to 51705. (The values have been shifted by an arbitrary amount.)

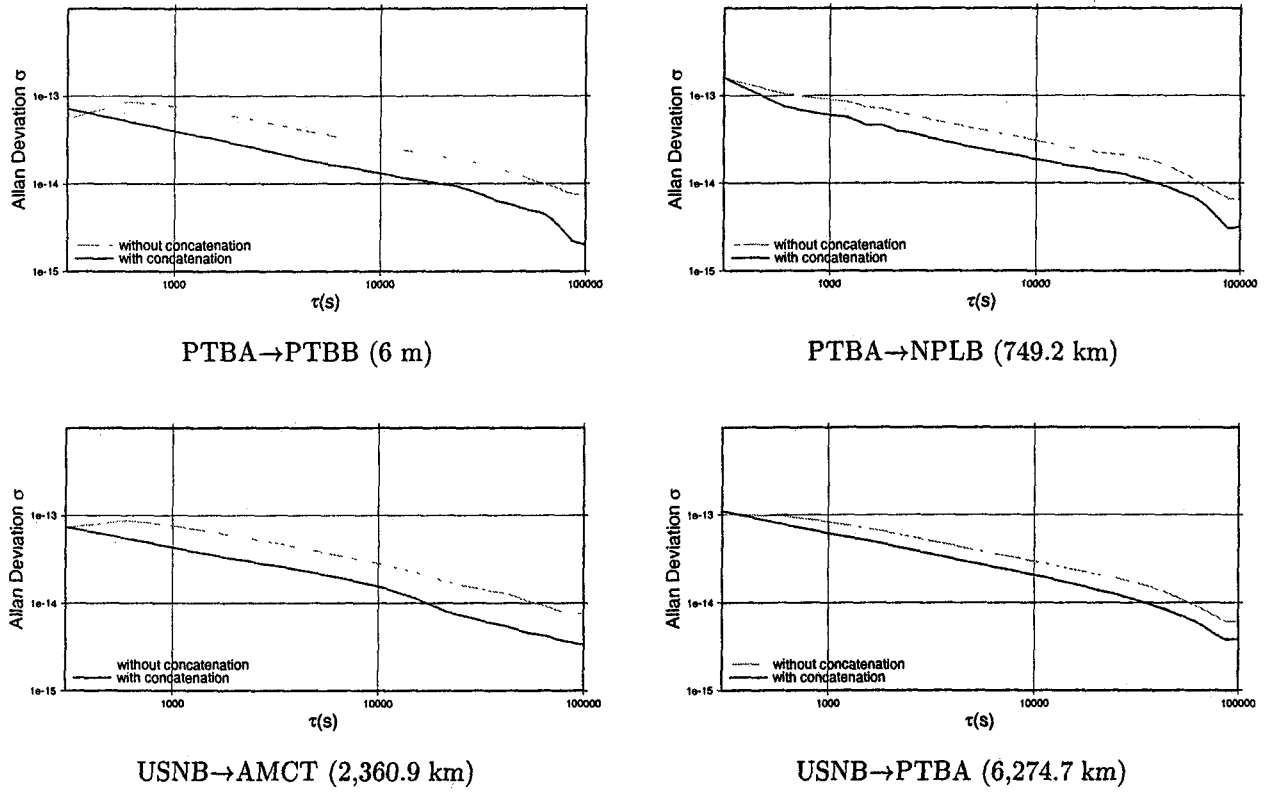
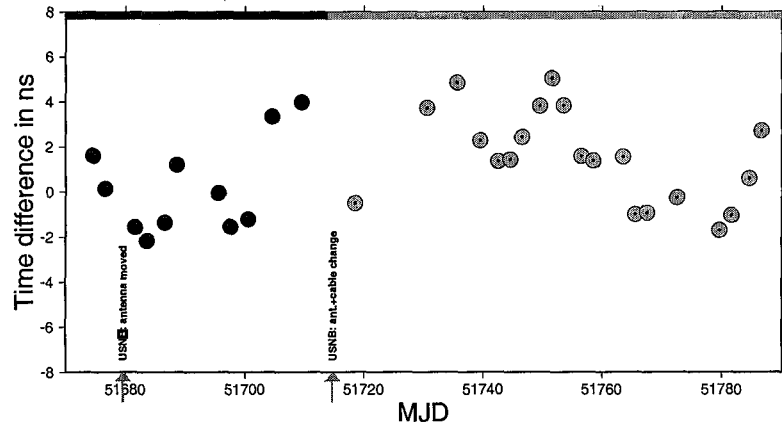
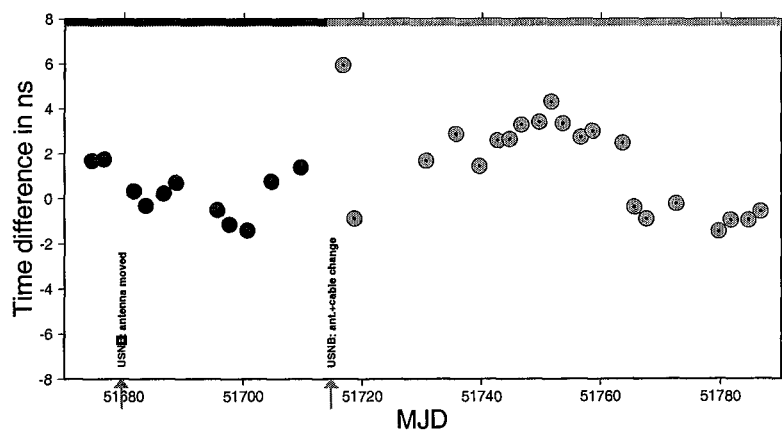


Figure 3: Allan deviations based on four months of time transfer solution using GPS CP for the original and the concatenated results for different baselines in the network.



Original GPS CP time transfer solution



Concatenated GPS CP time transfer solution

Figure 4: Differences between the time transfer solutions for the transatlantic baseline USNB \rightarrow PTBA obtained from TWSTFT and the GPS CP method. (The values have been shifted by an arbitrary amount, independent for black and gray symbols.)

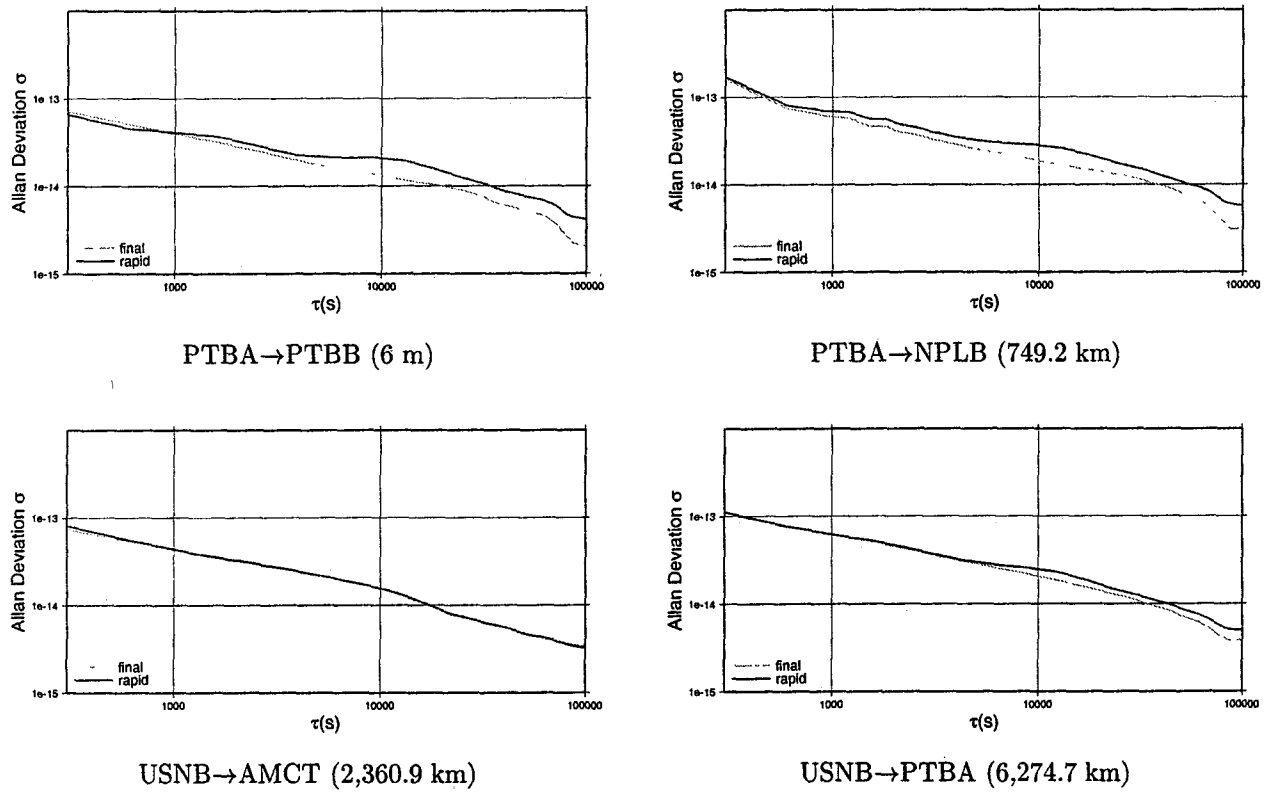


Figure 5: Allan deviations based on four months of time transfer solution using GPS CP for the results based on the CODE rapid resp. final orbits for different baselines in the network.

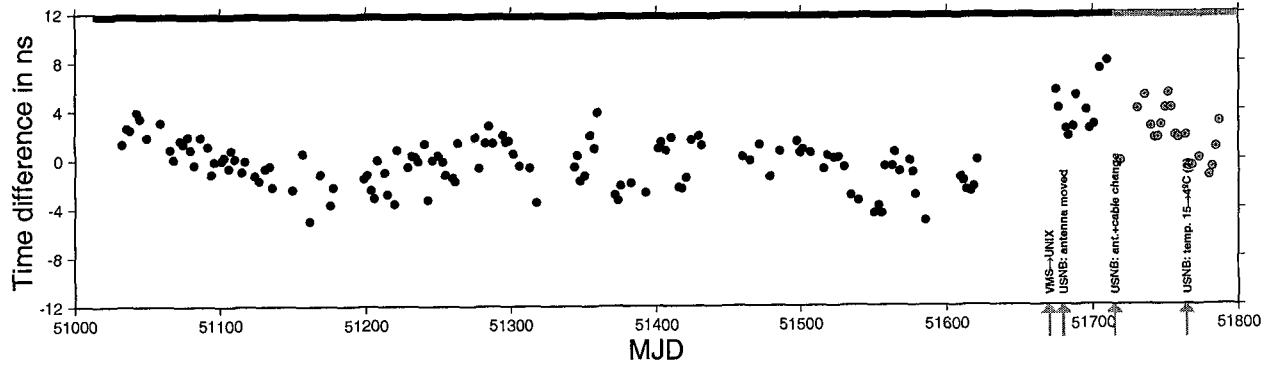


Figure 6: Differences between the time transfer solutions for the transatlantic baseline USNB \rightarrow PTBA obtained from TWSTFT and the GPS CP method. (The values have been shifted by an arbitrary amount, independent for black and gray symbols.)

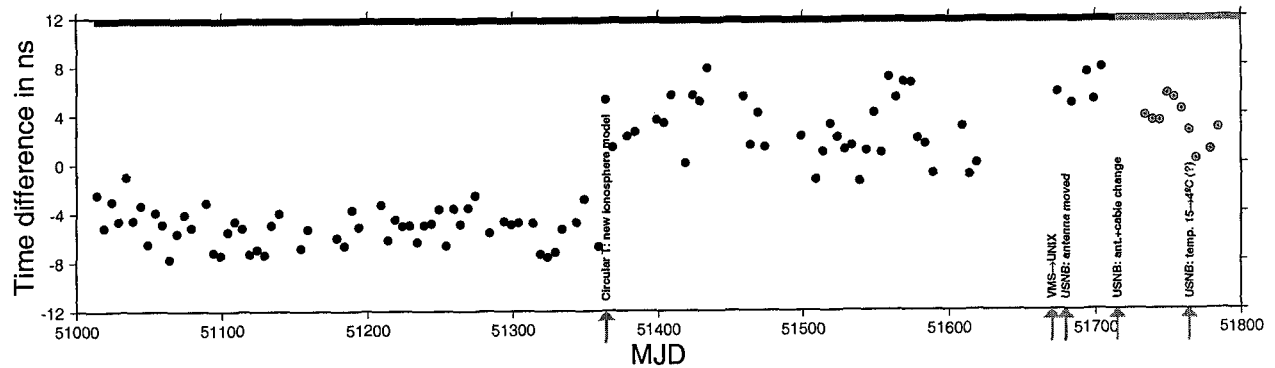


Figure 7: Differences between the time transfer solutions for the transatlantic baseline USNB \rightarrow PTBA obtained from Circular T and the GPS CP method. (The values have been shifted by an arbitrary amount, independent for black and gray symbols.)

Questions and Answers

DEMETRIOS MATSAKIS (USNO): I wonder if you could just clarify – maybe I misunderstood – earlier in the talk, I thought you had said that concatenating your results made things a little worse when compared to two-way. Is that right? In your conclusions, I thought you said that it made things a little better. This is comparing concatenated results with single-day results.

ROLF DACH: We could see an improvement. The difference was the two-way looked more systematic. The reason for this is one we don't have.

MATSAKIS: Which is better, of the two of them?

DACH: These are the concatenated results. Okay, these are smoother. But in this version you can see, for instance, this nanosecond jump. If we put it together, then the maximum and minimum values are smaller. But if you look at this blue part, then the maximum and minimum results are the same. But it comes from another epoch. The points between the maximum and minimum values look more systematic. We plan to recompute the 2 years of this experiment in a way that we can do a concatenation over the 2 years. Then we can see if we can really find systematic results. We can then look where it comes from, and hopefully it will be smoother over all this time.

But from this, it's hard to say. It became better this hour by 10 points, and the statistic from 10 points is nothing.

MATSAKIS: Okay, smoother is not better. Let me correct what I said.

DACH: Therefore, I would not say that this is better or this is better because in comparison to two-way, we have about 30 comparison points in these 4 months and not more. But I'm very encouraged from the deviation to do this reprocessing.

DAVID HOWE (NIST): Have you ever run a T-Dev statistic on that nice, very long run of data that you had toward the end?

DACH: Yes, we did all the 3-day solutions. Here we have the 1-day solutions. Then we can find, for instance for a 3-day solution, that they are through these 1-day solutions. The jumps between the end and the beginning of the next 3-day solution become smaller. This can be explained if this is a question of the behavior of the pseudo-range noise on this day.

So if you have a 3-day solution, then you have a mean of the pseudo-range noise behavior of these 3 days. If you have a longer time span, the jumps between the solutions become smaller. But 3 days of time transfer doesn't mean three times computing time, but much more.

HOWE: The question was really motivated to see whether you had a statistical summary using the time deviation statistic for that long run of data.

DACH: I have to look at the data again.

HOWE: Yes, underlying both yours and Lisa's talk, obviously, is that the mean is changing as a function of the length of the data set. T-Dev will allow you to interpret some of that, since it's a broad band spectral analysis. That was the reason for my question, and it might be very useful to run those data through that statistic.

DACH: I believe this loss over the different lengths of the computing figures is the same, the noise behavior of the pseudo-range. I hope this is right.

EVALUATION AND PRELIMINARY RESULTS OF THE NEW USNO PPS TIMING RECEIVER

**Mihran Miranian, Edward Powers, Lara Schmidt,
Ken Senior, and Francine Vannicola**
U.S. Naval Observatory
Washington, DC 20392, USA

Jimmie Brad and Joseph White
U.S. Naval Research Laboratory
Washington, DC 20375, USA

Abstract

The U.S. Naval Observatory (USNO) is tasked to provide the Global Positioning System (GPS) with a reliable and stable reference to UTC(USNO). This is accomplished using GPS Precise Positioning Service (PPS) timing receivers with a UTC(USNO) reference input. The USNO monitors GPS Time from all available healthy satellites. On a daily basis, the GPS Time correction, based on the entire constellation with respect to UTC(USNO), is determined and provided to the GPS Master Control Station (MCS) 2nd Satellite Operations Squadron (2 SOPS) at Schriever AFB in Colorado.

The USNO's GPS PPS operations have been limited to a single-channel receiver, which only allows tracking of one satellite at a time. Since February 2000, the USNO has been evaluating a 12-channel GPS PPS timing receiver, based on the GPS Monitor Station receiver. The unit is capable of tracking P(Y)-code and removes the effects of Selective Availability (SA). This paper describes the various tests conducted, the receiver's performance, and expected improvements to the USNO GPS PPS operations.

INTRODUCTION

The Master Clock of the U.S. Naval Observatory (USNO) is the official time reference of the United States as designated by the Joint Chiefs of Staff (JCS) Master Navigation and Timing Plan (MNTP) and the joint Department of Defense/Department of Transportation Federal Radionavigation Plan (FRP). The Department of Defense (DoD), most civilian government agencies, and private industry rely on the USNO Master Clock for their source of precise time. As part of the USNO timekeeping mission, the USNO serves as the precise time reference for the Global Positioning System (GPS).

The USNO measures the GPS time offset relative to the USNO Master Clock located in Washington, D.C. using specialized monitor station GPS timing receivers. These measurements are analyzed and sent daily to the GPS control segment, which then steers the GPS time scale to the DoD Master Clock at the USNO [1]. Over the last 5 years, the GPS time scale has been maintained to within +/-20 nanoseconds of UTC(USNO).

Currently the USNO uses STel 5401C GPS P(Y)-code timing receivers to monitor the GPS time offset. These receivers are based on a single satellite tracking, dual-frequency, P(Y)-code receiver that was developed in the mid 1980s. Because this receiver has only a single tracking channel, a tracking schedule must be used to ensure complete coverage of all GPS satellites. The

internal time-interval counter in these receivers has a resolution of only 9 nanoseconds. Therefore, to improve the precision of the measurements, an external counter with a resolution of 1 nanosecond is used. Also, the receivers are not GPS 1024 week number rollover-compliant. When the GPS week number rollover occurred, the receivers began displaying 6 January 1980 and the date in the receiver data record was incorrect. The USNO overcame this problem by simply correcting the epoch of the data before processing.

Due to the age and technical limitations of the STel 5401C receivers, it was apparent that a new state-of-the-art GPS time monitor receiver would have to be developed. The USNO requirements for the next generation time monitor receiver included P(Y)-code tracking of all GPS satellites in view on both L1 and L2 frequencies under all conditions of Selective Availability (SA), and providing the raw broadcast parameters, as well as code and carrier-phase measurements. In addition to tracking improvements, a modern all-digital design would have to provide sub-nanosecond time-interval measurements for improved long- and short-term stability. The receiver would also require stability to within 1 nanosecond over a temperature range of +/- 5 degrees centigrade.

RECEIVER DEVELOPMENT

In January 1998, Allen Osborne Associates (AOA) was contracted to develop a prototype receiver according to the USNO requirements [2]. Based on the Jet Propulsion Laboratory (JPL) Rogue family of Geodetic receivers, AOA's new BenchMark/TurboRogue geodetic GPS receiver with Advanced Codeless Tracking (ACT) technology and the AOA GPS Monitor Station Receiver Element (MSRE), the TTR-12 Security Module (SM) time monitor receiver was developed. The prototype was delivered to the USNO in August 1999 for test and evaluation. After months of testing, which included returning the receiver to AOA for modifications, it was apparent that the new receiver would be able to fulfill the requirements for a new USNO GPS time monitor receiver. Therefore, the USNO awarded AOA a contract to build four production models, which were delivered by May 2000. However, as of December 2000, the receivers were not in their final state.

The TTR-12 receiver tracks up to 12 GPS satellites simultaneously and provides all six code and carrier observables, whether the P-Code encryption (Anti-Spoofing) is on or off. It outputs carrier-phase and pseudo-range measurements derived from L1-C/A, L1-P(Y), and L2-P(Y) code with full carrier wavelength. The ACT code tracking technology improves upon the P-codeless technique of older generations of Rogue receivers, resulting in an increase of the signal-to-noise-ratio (SNR) on L2 and thus, reduces measurement noise. During normal operation, the TTR-12 receiver will track the true P(Y) code GPS signal. When the receiver is operated unkeyed, the TTR-12 will revert to the ACT code-tracking mode with minimal loss of precision. A commercial time-interval counter with the resolution of 100 picoseconds was integrated into the AOA design to allow the internal measurements to be related to an external clock.

In addition to the improved receiver hardware, USNO has also incorporated into the overall system the Andrews FSJ1-50A phase-stable antenna cable and modified the standard Dorne Margolin choke-ring antenna with temperature-stable electronics built by KW Microwave. The antenna cables and electronics are expected to provide a significant improvement to the temperature stability of the antenna portion of the system.

AOA TTR-12 TEST AND EVALUATION

During the period February 2000 through September 2000, USNO and the Naval Research Laboratory (NRL) conducted a series of tests to evaluate the TTR-12. USNO testing included comparisons with the STel 5401C and other TTR-12 receivers. NRL is the designated DoD agency for GPS timing receiver testing. Their testing was performed using a simulator capable of producing 10 simultaneous signals with SA and A-S. Numerous hardware and software problems were encountered with the testing and a majority were resolved.

SOFTWARE FIXES

When the STel and TTR-12 were compared using horizon-to-horizon tracks, the TTR-12 displayed an unusual trace. The expected trace of a GPS horizon-to-horizon track shows noise at the beginning and end of the track, and reduced noise in the middle. This was not the case for all TTR-12 tracks. After notifying AOA, it was discovered that the orbit iteration process was not being applied for satellites with large eccentricities. Figure 1 shows 5 days of horizon-to-horizon tracks of PRN02/SVN13 from the STel (top trace) and TTR-12 (bottom trace) receivers. Once the software was corrected, the TTR-12 horizon-to-horizon tracks showed an improvement. Figure 2 shows the STel track (top trace), the TTR-12 track before (middle trace) and after (bottom trace) the software fix. The authors would like to note that the AOA TTR-4P receiver continues to be plagued with this problem.

The remaining TTR-12 software fixes include the removal of SA dither at any selected sample output rate and SA epsilons. Live testing of the fixes would not be adequate since SA was set to zero on 2 May 2000, so verification will be done using the NRL simulator.

GPS CARRIER-PHASE TIME TRANSFER

Though software development for the TTR-12 has not yet been completed, in order to provide simultaneous real-time offload of GPS data necessary for the TTR-12 to function as both a GPS MSRE and a GPS carrier-phase timing receiver, one may currently obtain raw pseudorange and carrier-phase data by periodically downloading such data from a flashcard. Several preliminary experiments have been performed using data collected from the prototype TTR-12 receivers' flashcards and geodetic GPS carrier-phase techniques to further quantify the quality of the TTR-12.

TEMPERATURE SENSITIVITY OF GPS CARRIER-PHASE CLOCK ESTIMATES

A prototype TTR-12 was placed in a Tenney Environmental chamber oven while purposely varying the temperature in the oven in order to quantify the sensitivity to temperature of the TTR-12 when used for GPS carrier-phase time transfer. The phase-stable Andrews model FSJ1-50A antenna cable connecting the TTR-12 to its Dorne Margolin antenna has been shown to have a temperature coefficient of about $0.03 \text{ ps/m}^{\circ}\text{C}$ [3] while the temperature sensitivity of the Dorne Margolin choke-ring antenna has been inferred to be better than $2 \text{ ps}^{\circ}\text{C}$ [4]. Currently on loan to USNO from the Swiss Federal Office of Metrology is an Ashtech Z-12T (GeTT) GPS receiver (designated USNB). This receiver has the same type of antenna and antenna cable as that used with the TTR-12, but the USNB receiver is housed in a thermally shielded box whose temperature is controlled to within 0.1°C .

Temperature testing of the TTR-12 was conducted over a 4 day period (22-25 July 2000). The temperature in the Tenney chamber was changed every 6 hours in increments of 2.5 °C over a range of 20 to 38 °C. The 30-second pseudorange and carrier-phase data were used to obtain clock estimates between the TTR-12 and USNB at 5-minute intervals. These estimates were then combined with 1-minute temperature data, (T_{chamber}), which were collected from within the Tenney chamber and fit by least-squares to the simple model, $(\text{TTR12-USNB}) = k(T_{\text{chamber}})$. The resulting fit suggests a temperature coefficient for the TTR-12 receiver of $-77 \pm 6 \text{ ps}/^{\circ}\text{C}$. Figure 3 shows the temperature changes to the Tenney chamber and the reaction of the TTR-12 receiver.

POWER CYCLE TESTING

Power cycle testing of the TTR-12 receiver was conducted to verify that the receiver could maintain its calibration and receiver settings such as position and delays. Repeated power cycles indicate that the TTR-12 receiver has the capability to hold its calibration and receiver settings after loss of power.

PERFORMANCE EVALUATION

At the end of September when the USNO was confident that most of the hardware and software deficiencies had been resolved, performance evaluations focused on the GPS Time measurements and hardware stability.

GPS TIME MEASUREMENT STABILITY

Using one week of GPS Time measurements common to the STel and TTR-12, comparisons were made using broadcast clocks and orbits, and then applying the National Imagery and Mapping Agency (NIMA) precise orbit and clock corrections. The STel 13-minute UTC(USNO)-GPS values using broadcast corrections show a 30 to 35 nanoseconds peak-to-peak scatter in Figure 4. When the NIMA precise orbit and clock corrections were applied, the noise was reduced to about 15 nanoseconds peak-to-peak as seen in Figure 5. In Figure 6, the TTR-12 data using broadcast corrections, shows similar results to the STel, as well as an increase of data due to the multiple channels. After applying the NIMA precise corrections to the TTR-12 data, the noise was reduced to about 5 to 10 nanoseconds peak-to-peak, seen in Figure 7.

The Time Deviation (TDEV) plot in Figure 8 shows the STel and TTR-12 stability for UTC(USNO)-GPS using both broadcast and precise orbits and clocks as a function of averaging lengths. The dashed lines represent the STel performance and the solid lines represent the TTR-12 performance. The top two lines near the word "broadcast" represent the time deviation of UTC(USNO)-GPS using the standard broadcast clocks and orbits. The bottom two lines near the word "precise" represent the time deviation of UTC(USNO)-GPS after applying the NIMA precise clock and orbit corrections. In order to make a fair comparison with the STel, the TTR-12 data used are the same tracks used for the STel.

From this data set we can conclude that similar levels of performance of about 4.5 nanoseconds at 13 minutes and 2.5 nanoseconds at 1 hour can be seen in the TTR-12 and STel when measuring UTC(USNO)-GPS using the broadcast clocks and orbits. The noise in the broadcast corrections is larger than both the STel and TTR-12 hardware noise, evidenced by the fact that both the STel and the TTR-12 stability improved when precise corrections were applied. After applying the NIMA precise clock and orbit corrections, we see that the TTR-12 hardware is more stable than

the STel hardware, and that the stability of the TTR-12 UTC(USNO)-GPS measurements approaches 1 nanosecond at 13 minutes, and is sub-nanosecond thereafter.

RECEIVER HARDWARE STABILITY

Figure 9 is a TDEV plot which estimates the hardware stability of the receivers using GPS common-view. The two methods used were short baseline (co-located on the same roof, 2 to 3 meters apart) and common antenna. The dashed line is the time deviation of common-view between two STel receivers on a short baseline. The solid lines are time deviations for the TTR-12 receivers in several different situations. The top line represents the TTR-12 as if it were a single-channel receiver using the same tracks as the STel. The stability at one day for the STel is 400 picoseconds and the TTR-12 is 300 picoseconds. Although the short baseline common-view results are an estimate of the hardware stability, the results could be corrupted by multipath differences at the two antennas, differences in antenna hardware, cable quality and differences in the environment of the antennas and cables.

The Short Baseline Advanced Common-View (ACV) method represents the TTR-12 hardware stability where all common-view tracks for one single timestamp are averaged together. At 13-minutes, the stability drops down to 500 picoseconds and 90 picoseconds at 1 day.

The Common Antenna ACV represents the best estimate of the TTR-12 receiver hardware stability available. From this data set, it can be concluded that the TTR-12 hardware is quieter than the STel hardware over all averaging lengths, showing stabilities at or below 50 picoseconds over all averaging lengths.

REMAINING TESTS

The remaining tests to be completed at NRL with the simulator are the verification of the SA averaging and epsilons, and absolute calibration of the receivers, antenna cables and antenna electronics. Once these tests are completed, USNO will set up parallel operations with the STel receivers prior to going operational with the TTR-12 receivers.

CONCLUSION

For the future, a SAASM version of the TTR-12 receiver will be built, this being a DoD requirement. A phased array antenna is also being evaluated to decrease multipath and increase signal-to-noise strengths. USNO is encouraged with the hardware improvements that will enable the USNO to provide the GPS Control Segment with more stable and reliable timing corrections for the GPS.

ACKNOWLEDGMENTS

The authors would like to thank Art Dorsey, Lockheed Martin Company for his work applying the NIMA Estimated Range Deviations to the USNO data.

REFERENCES

- [1] ICD-GPS-202, Revision A, 01 May 1996.

- [2] M. Miranian, E. Powers, J. Brad and J. White 2000, "Initial Test Results for a New PPS GPS Timing Receiver," *Proceedings of the 31st Annual Precise Time and Time Interval (PTTI) Systems and Applications Meeting*, 7-9 December 1999, Dana Point, California, USA, pp. 357-364.
- [3] E. Powers, P. Wheeler, D. Judge and D. Matsakis 1999, "Hardware Delay Measurements and Sensitivities in Carrier-Phase Time Transfer," *Proceedings of the 30th Precise Time and Time Interval (PTTI) Systems and Applications Meeting*, 1-3 December 1998, Reston, Virginia, USA, pp. 293-305.
- [4] J. R. Ray and K. L. Senior 2001, "Temperature Sensitivity of Timing Measurements Using Dorne Margolin Antennas," to appear in *GPS Solutions* 2000/2001.

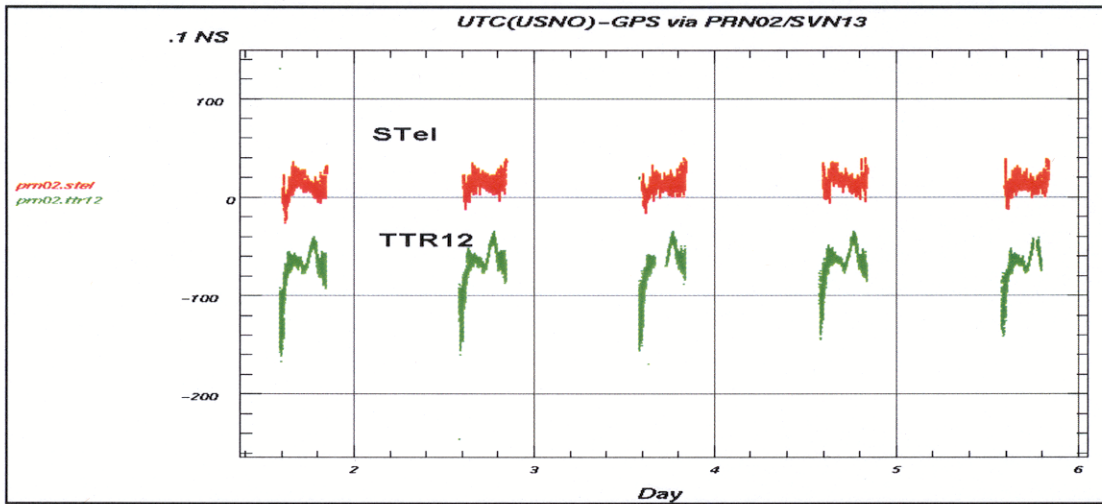


Figure 1. STel and TTR12 horizon-to-horizon tracks of PRN02/SVN13.

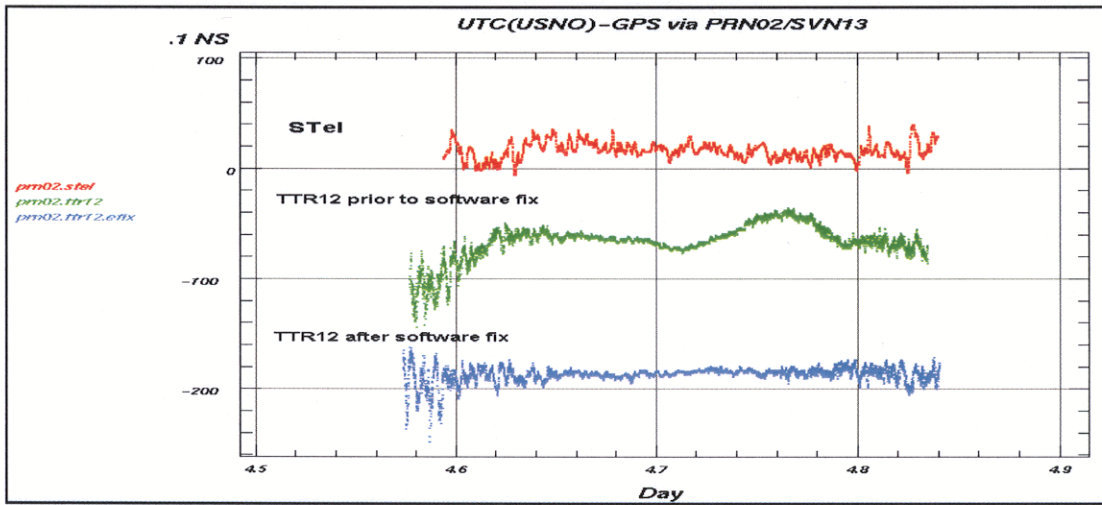


Figure 2. STel and TTR12 horizon-to-horizon tracks of PRN02/SVN13.

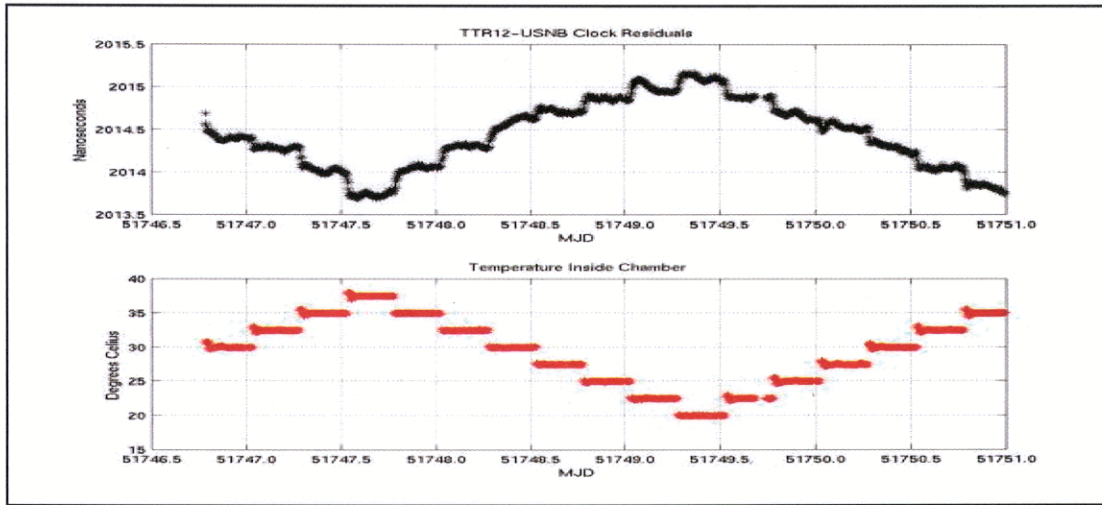


Figure 3. Clock residuals between TTR12 and USNOB, and temperature within Tenney Chamber for the period 22-25 July 2000.

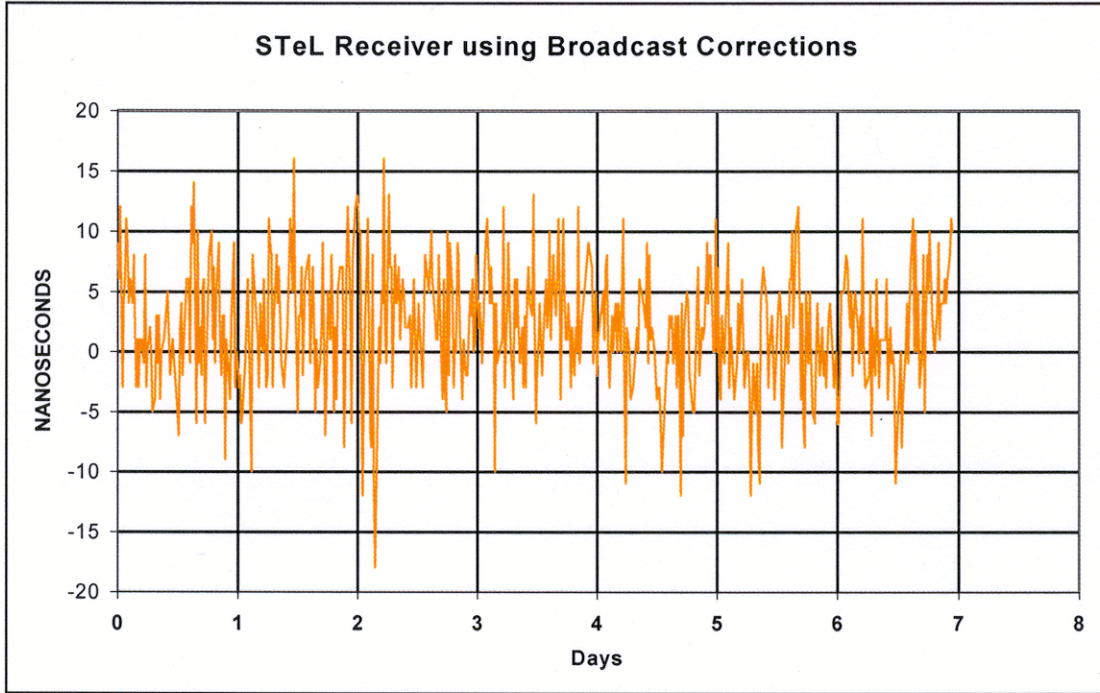


Figure 4. STeL 13-minute UTC(USNO)-GPS values using broadcast clocks and orbits.

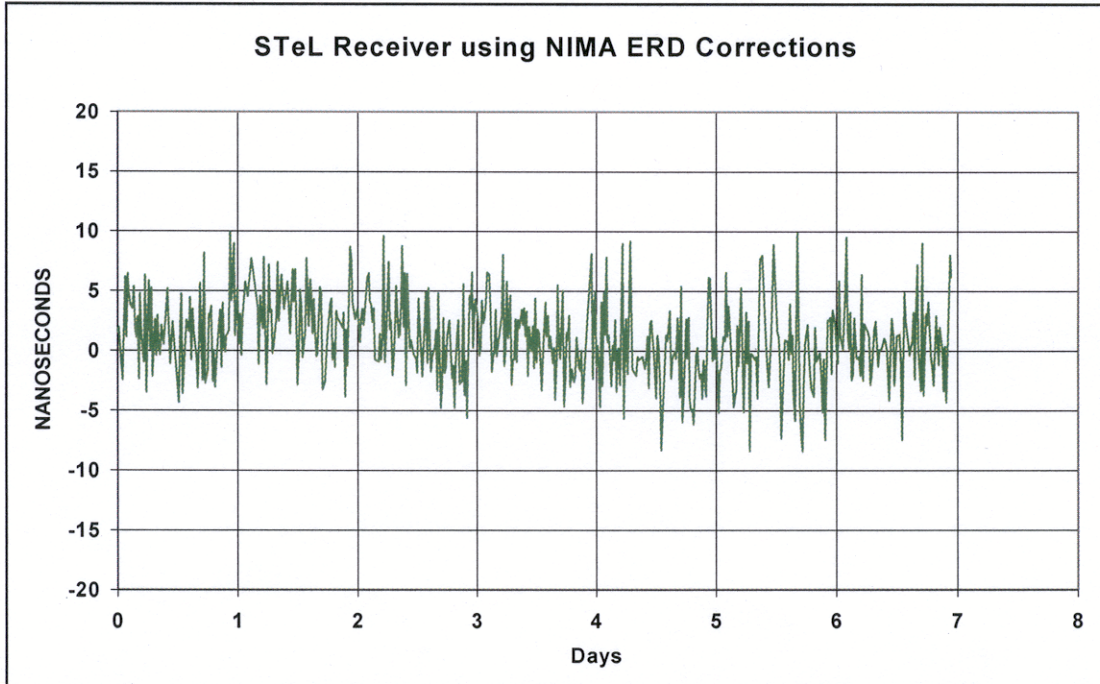


Figure 5. STeL 13-minute UTC(USNO)-GPS values using NIMA-corrected clocks and orbits.

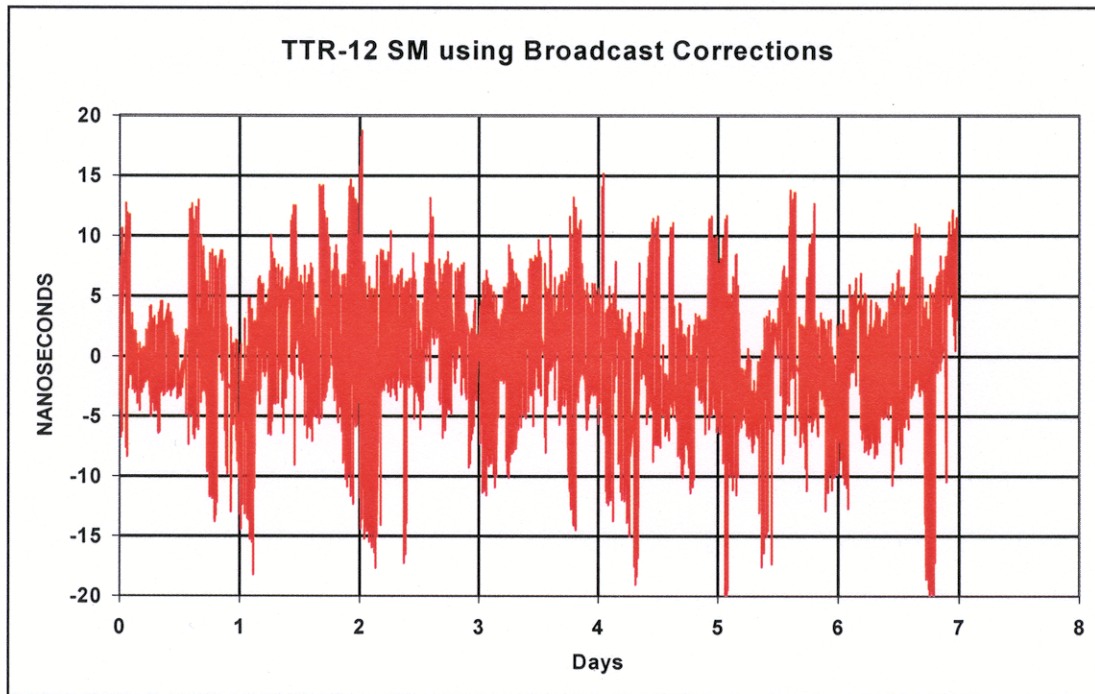


Figure 6. TTR-12 13-minute UTC(USNO)-GPS values using broadcast clocks and orbits.

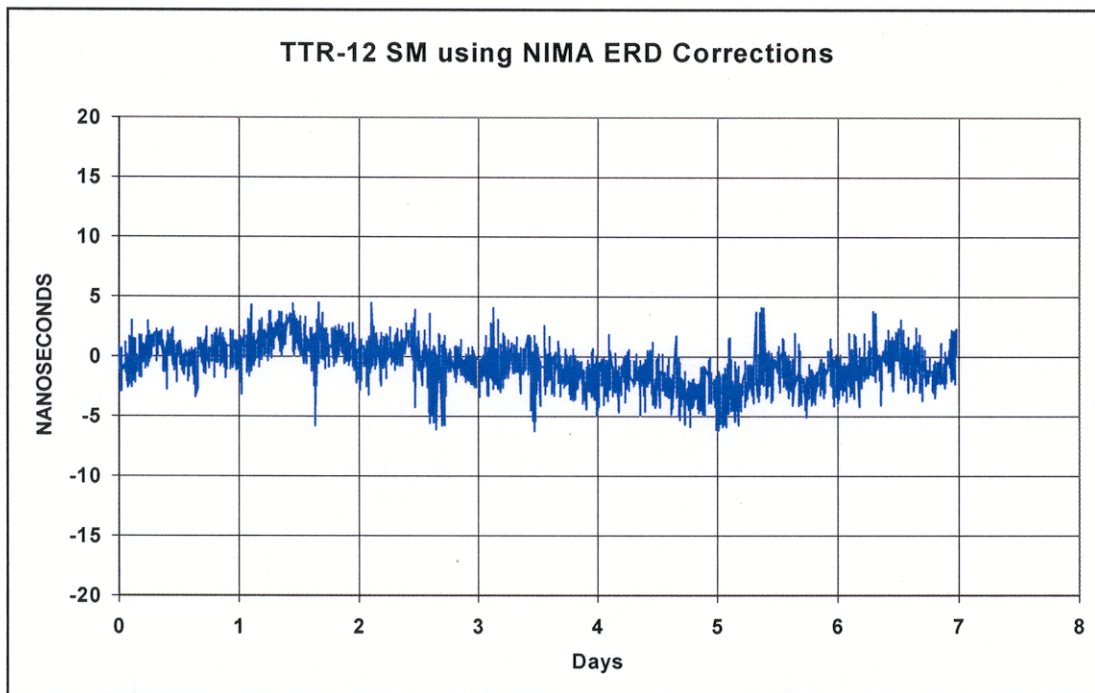


Figure 7. TTR-12 13-minute UTC(USNO)-GPS values using NIMA-corrected clocks and orbits.

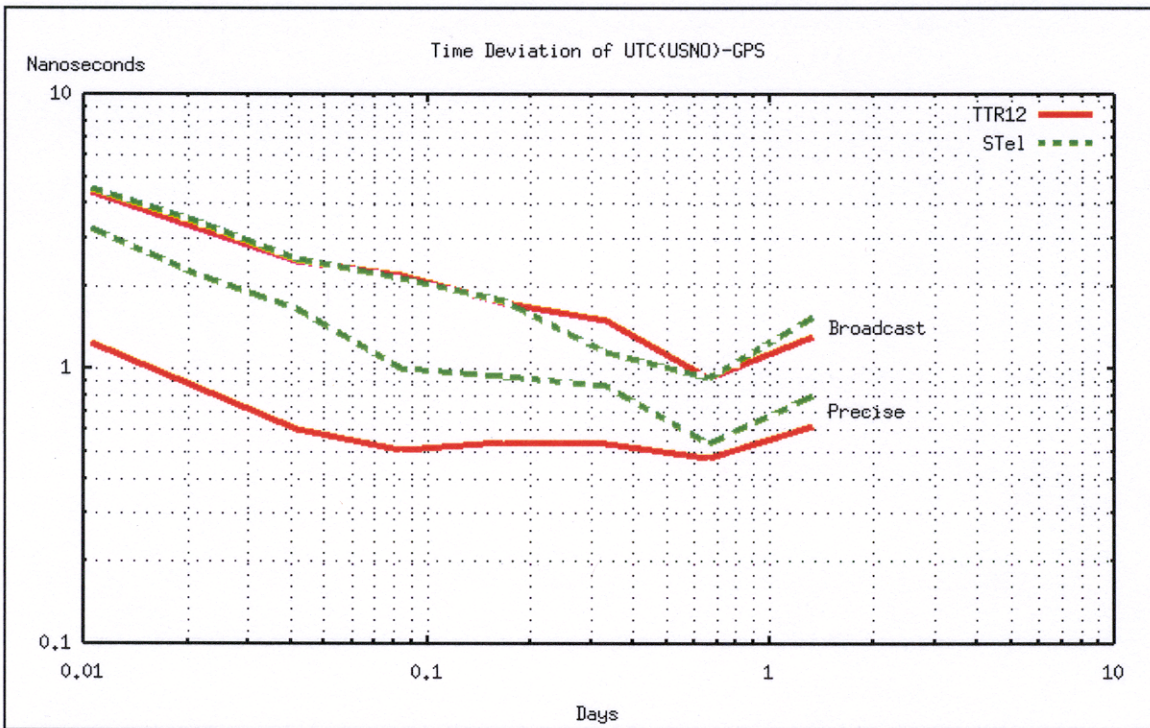


Figure 8. TDEV of UTC(USNO)-GPS for STel and TTR-12 using broadcast and precise orbits and clocks.

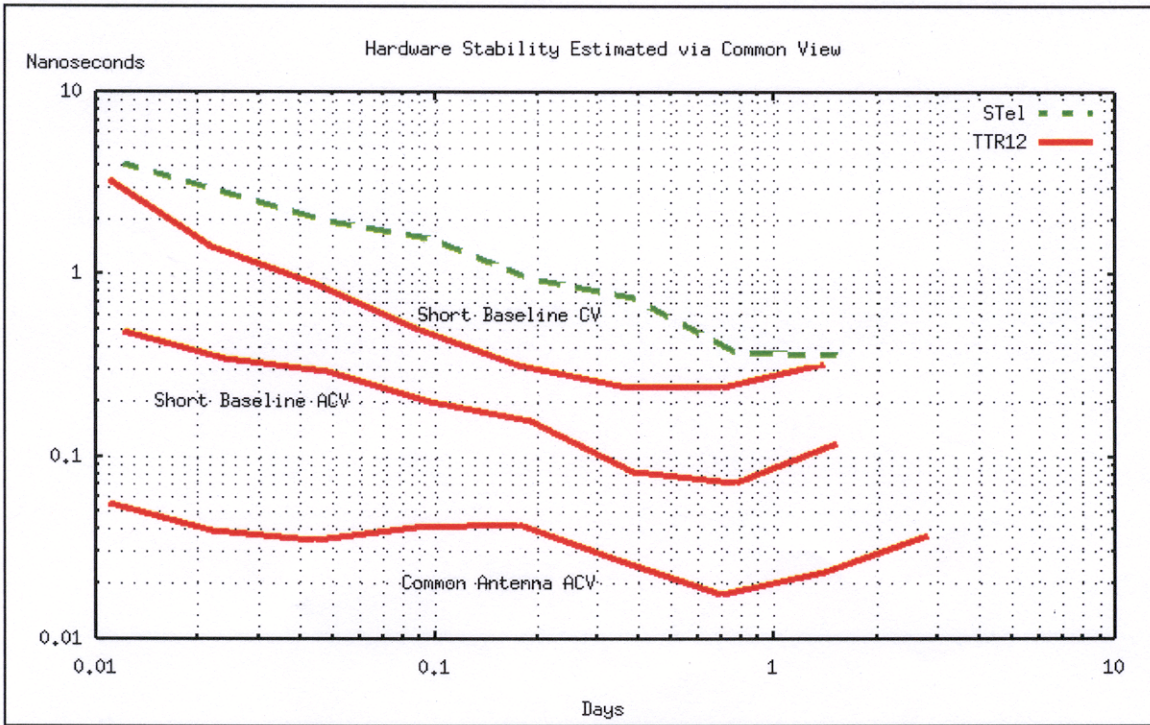


Figure 9. TDEV of STel and TTR-12 hardware stability estimated via common-view.

Questions and Answers

MARC WEISS (NIST): Can you say anything more about that phased array antenna—what are the plans? Is it in design, is it being built?

EDWARD POWERS: We reported last year on work we were doing at the time with NAVSYS to build a dual-frequency P(Y)-code receiver that could eventually be upgraded to the phased array. But since then, we went out and are in the process of awarding a contract. We haven't selected a vendor yet. So we can't talk a lot about that right now. But right now there are two vendors that we're looking at who will build a prototype of this system. It will be a 12-channel dual-frequency 16-element phased array which, the hope is, will get 10 or 12 dB of gain to each GPS satellite, along with maybe a factor of 50 or so reduction in multi-path.

JAMES WRIGHT (Computer Sciences Raytheon): I think in the beginning of your paper you said that there were two contractors that were building a receiver under this study.

FRANCINE VANNICOLA: Right.

WRIGHT: Has the second one materialized and are you testing that?

VANNICOLA: We have not received a prototype to this date, no.

THOMAS CLARK (NASA Goddard Space Flight Center): I'll ask the same question I asked Lisa earlier: How were the L1/L2 biases handled in the results you showed? Was it assumed to be a constant or was it solved for?

POWERS: Yes, right now this is basically handled in the same way as the TurboRogue—something of a calibration bias. For this particular day, the set are actually uncalibrated and mapped in as a clock error. It will be calibrated before we go operational with it. But they are treated right now as being stable with time, as far as the receiver calibration goes.

DAVID HOWE (NIST): Those are fantastic results. To what degree did you take out cable length problems between the antenna and your antenna when you were trying to determine the noise floor using the common antenna mode? Was there any special attention taken?

VANNICOLA: No. We had the antenna cable going into the splitter and then equal lengths going from the splitter to the receiver, so it all cancelled out.

HOWE: Okay, so it was split at the receiver.

VANNICOLA: Yes.

RESULTS FROM TIME TRANSFER EXPERIMENTS BASED ON GLONASS P-CODE MEASUREMENTS FROM RINEX FILES

F. Roosbeek, P. Defraigne, C. Bruyninx
Royal Observatory of Belgium
Avenue Circulaire 3, 1180 Brussels, Belgium
tel: +32-2-3730246; fax: +32-2-3749822
e-mail: f.roosbeek@oma.be

Abstract

The time transfer procedure presently used for the realization of TAI is based on the common view approach, using the CGGTTS data computed by an internal software of the time receivers. We choose here another approach and analyze the raw data available in the RINEX files produced by GPS/GLONASS geodetic receivers. We concentrate our analysis on the use of GLONASS P-code measurements. Because the frequency emitted by each GLONASS satellite is different, the measurements must be corrected for their frequency-dependent receiver hardware delays. These delays can be computed either from the CGGTTS files or directly from the raw P-code data. We show that the first approach is better than the second one. After this correction, time transfer (using the GLONASS P-codes) is realized with a rms of about 2 nanoseconds for a 1-day session between two receivers distant of a few hundred of kilometers.

INTRODUCTION

The use of the GLONASS P-codes for time transfer is very promising, as already shown by different studies ([2] [3] [4] [6] [7]). In all the mentioned studies, the time transfer results were obtained using CGGTTS (GPS/GLONASS Time Transfer Standard) data files provided by receivers designed for time transfer applications. The CGGTTS files ([1]) contain the clock differences between the GLONASS/GPS system time and the local clock of the time laboratory. These differences are computed by the receiver software for the satellites given in the international tracking schedules distributed by the BIPM (Bureau International des Poids et Mesures) and are used for the computation of TAI. On the other hand, the International GLONASS EXperiment (IGEX) ([10]) gave access to RINEX files from about 25 receivers in the world. Part of these combined GPS/GLONASS receivers are driven by precise frequency standards, and some of them contribute also to the realization of TAI. We have, therefore, investigated the possibility of performing time transfer using the GLONASS P-code data given in these RINEX data files.

Using a common view method, we determine the receiver clock offsets and consequently the time transfer between the external frequency standards driving these receivers. Compared to the method based on CGGTTS files, this method allows to work with a higher number of data points (about 3000 per day) and allows to control each aspect of the correction terms from the raw data to the final product.

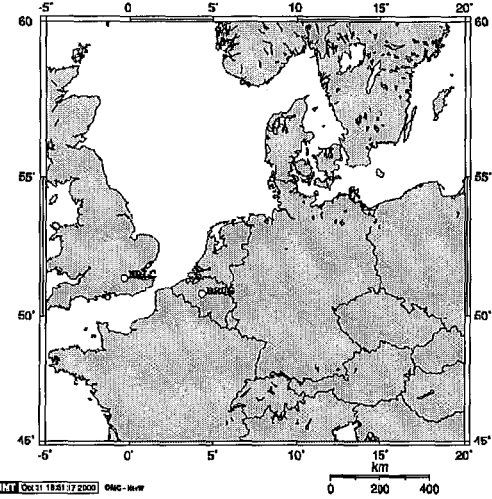


Figure 1: GPS/GLONASS sites used in this study.

In ([8]), the final precision of the time transfer between two 3S-Navigation R100 receivers distant of a few hundred of kilometers, obtained using the precise ephemerides, was about 10 ns . The main limitation was the receiver hardware delays which are different for each satellite because of the satellite dependency of L_1 and L_2 frequencies. Due to the fact that calibration values are not available, a first approach consisted in estimating the corrections of each satellite directly from the time transfer results produced by each satellite separately. However, this adjustment was not perfect due to the fact that we estimated the offset between the results of the different satellites on a time span of only 1 day. In ([9]), we used the CGGTTs delays determined on a time span of two weeks and showed that the final precision of the time transfer improves to 1.8 ns for a typical 1-day session between 2 receivers distant of a few hundred of kilometers. The disadvantage of this approach was that it could only be applied for time receivers.

In order to overcome this limitation, we try in this paper to determine these differential receiver hardware delays directly from the raw P-code measurements, but now using several days of measurements and we compare the results with those obtained from the CGGTTs data.

DATA SET DESCRIPTION

We have used the RINEX data of GPS/GLONASS receivers belonging to IGEX network, and operating at the same time as time laboratories participating in the realization of the international atomic time scale (TAI) (see Figure 1):

- BRUG, located at the Royal Observatory of Belgium, equipped with a combined GPS/GLONASS multi-channel receiver R100-30T from 3S-Navigation, connected to a H-maser for the geodetic part, and to a cesium clock HP5071A (=UTC(ORB)) for the participation to TAI;
- NPLC, located at Teddington (Greater London, UK), 336 km far from Brussels, equipped with a combined GPS/GLONASS multi-channel receiver R100-40T from 3S-Navigation, connected to a H-maser (=UTC(NPL)) for both the geodetic part and the participation to TAI.

As shown in ([8]), the R100 receivers exhibit regular artificial discontinuities in the computed receiver clock synchronization errors, which make it impossible to perform RINEX-based precise time transfer for more than 1 day. This is a typical situation for all receivers from this manufacturer.

RECEIVER HARDWARE DELAYS

Figure 2a shows that the time transfer signal obtained using a single day of observations with precise ephemerides still presents some small jumps or curvatures not attributable to the H-maser. These are due to changes in satellite configuration and to the uncorrected receiver hardware delays associated with the different satellites observed.

We have used two different methods for determining the hardware delays. The first one, already presented in ([9]), is based on the fact that the receivers used in our experiment (BRUG, NPLC) also provide CGGTTS files to the BIPM, so we used the time transfer results provided by these

Satellite number	hardware delays CGGTTS (ns)	hardware delays RINEX (ns)	Differences
1	-0.4	3.6	4
3	-2.9	-2.3	0.6
4	-0.4	-1.4	1
6	-0.9	-2.1	1.2
7	0.0	0.0	0
8	-0.5	1.4	1.9
9	7.2	7.9	0.7
10	1.4	5.3	3.9
11	-2.7	1.8	4.5
13	6.9	7.7	0.8
15	-2.1	-4.4	2.3
16	-3.8	-4.7	0.9
17	4.0	8.5	4.5
22	6.0	6.2	0.2

Table 1: Hardware delays. Satellite 7 is chosen arbitrary as the reference one.

CGGTTS files to estimate the differential receiver hardware delays. When using CGGTTS files, there are no jumps because these results give the offset between GPS time and the 1 *pps* (1 pulse per second) signal provided by the laboratory clock. Using the CGGTTS files, the calibration delays can now be determined using a longer time span containing more simultaneous observations. Note that we cannot assert that the hardware delays are the same for both geodetic data and the CGGTTS data; this depends on the receiver architecture and will be tested here by comparing with the hardware delays obtained directly from the raw data given in the RINEX files. Clock resets are not problematic because they do not alter the differential hardware delays computed from the RINEX files. This means that we can determine the calibration delays using RINEX data over a time span longer than 1 day.

We test both methods on the baseline BRUG – NPLC. A period of 14 days (51351–51365 MJD (Modified Julian Date) corresponding to GPS weeks 1015 and 1016) has been used to determine the calibration delays from the CGGTTS files (see ([9]) for details) as well as from the RINEX files. Table 1 lists the hardware delays determined by both methods.

In Figure 2, we have plotted the time transfer results between BRUG and NPLC for the first day of the GPS week 1016 (corresponding to MJD 51357). The first part of the graph shows results which are not corrected for the frequency dependent receiver hardware delays. In this case, the rms of the differences is equal to 2.6 ns. The second part is corrected for the receiver hardware delays using CGGTTS files and the corresponding rms is equal to 1.8 ns. The last part is corrected for receiver hardware delays obtained from the RINEX files and the corresponding rms is equal to 2.0 ns. We can say that this correction removes the curve variations induced by the variable ‘mean’ hardware delay, corresponding to the mean of the delays of the observed satellites at each

time. But, as seen from the graphs, although our correction sometimes reduces the jumps and variations, it leaves some variations at other times. This is due to the limited accuracy of the computed receiver hardware delays: the computed receiver calibration errors between the different satellites are of the same order of magnitude (from 0 to 10 ns) as the noise level of the clock differences computed with any satellite (2.5 ns). We see also that the results using the CGGTTS files for calibration are better than the ones using RINEX files (rms of 1.8 ns vs 2.0 ns). Indeed, even if the RINEX files provide a larger number of observation points, the noise level is higher than with the CGGTTS files (standard deviation of 5 ns instead of 2 ns). This is due to the data smoothing, which is part of the procedure applied to compute the CGGTTS files.

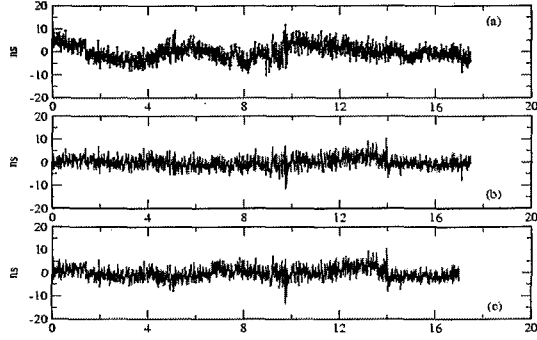


Figure 2: Time transfer (BRUG-NPLC). (a) Hardware delays not corrected, rms = 2.6 ns (b) Hardware delays corrected by CGGTTS files, rms = 1.8 ns (b) Hardware delays corrected by RINEX files, rms = 2.0 ns.

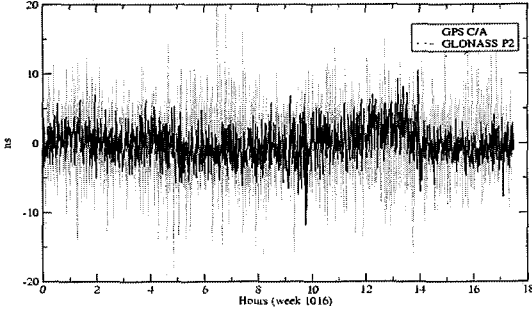


Figure 3: Time transfer (BRUG-NPLC).

COMPARISON BETWEEN GLONASS AND GPS RESULTS

In Figure 3, we have plotted the time transfer between BRUG and NPLC for the first day of the GPS week 1016. We see that the use of the GLONASS P-code (rms of 1.8 ns and maximum difference of 11.8 ns) reduces the noise level with a factor between 2 to 3 with respect to the use of GPS C/A code (rms of 4.4 ns and maximum difference of 31.9 ns).

Figure 4 shows the frequency stabilities of the frequency transfer performed with GPS C/A-codes, GLONASS P-codes and GPS phases. The GLONASS P-code results show a better stability than GPS C/A-code results at short time scales (below 1 hour). This is a direct consequence of the lower noise level of the GLONASS P-code compared to the GPS C/A-code. At longer time scales (larger

than 1 hour), we observe the opposite situation due to the imperfect correction of hardware delays in the GLONASS P-code results, inducing small undulations of the curve (as seen in Figure 3), which reduces the frequency stabilities. The results based on GPS carrier phases have frequency stability highly superior to the results based on codes (GPS or GLONASS). However, although carrier phases offer a huge potential for the frequency transfer applications, they still depend on the information in code data to determine the absolute synchronization offset (see ([5]) for more details).

CONCLUSION

We have used RINEX data from combined GPS/GLONASS receivers involved in the IGEX campaign to investigate the performances of the GLONASS P-codes for time transfer applications. We pointed out that it is necessary to correct the P-codes for the receiver hardware delays which are, for the GLONASS data, different for each satellite. Receiver calibrations are unavailable at the present time; the determination of the receiver hardware delays for each satellite must be done during the computation of the synchronization errors. However, due to the noise of measurements and the variability of the hardware delays, this determination cannot be done precisely enough with only 1 day of data. Using several days of data would allow a more reliable determination of the satellite dependent hardware delays. The CGGTTS files made available by some IGEX receivers give a long time series of synchronization errors determined on individual satellites and

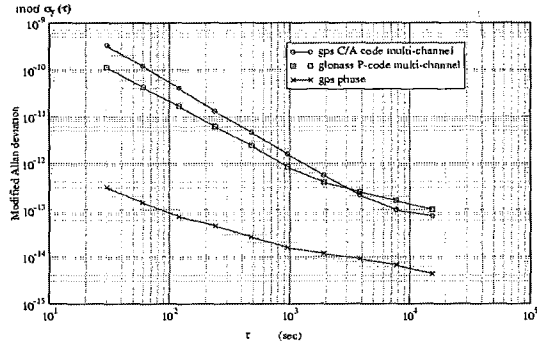


Figure 4: Frequency stabilities of the different time transfer results of Figure 3.

allow easier determination of the differential biases between the satellites. Another approach is to use the RINEX files themselves in order to use geodetic receivers and not only time receivers: in this case, clock resets occur, but are not problematic because they do not alter the differential hardware delays between the satellites. More problematic is the fact that the RINEX raw data are more noisy than the smoothed CGGTTS data, even with a larger number of observation points for the RINEX files. This leads to a better determination of the hardware delays with the CGGTTS files than with the RINEX files (rms of 1.8 ns instead of 2 ns for a typical 1-day session between two stations distant of a few hundred of kilometers). However, even with the knowledge of these calibration delays, a precise frequency transfer with RINEX data will be restricted to 1 day due to the jumps at the day boundaries due to the daily resets of the 3S-Navigation receivers. If a time transfer is needed for a time span longer than 1 day, the receiver clock jumps must be monitored with an external time-interval counter.

We can conclude that the present geodetic GLONASS receivers driven by a stable frequency standard can be used for time transfer applications only if (1) the satellite-dependent hardware delays are regularly monitored and, (2) the 1 pps output is monitored in order to measure the clock discontinuities.

REFERENCES

- [1] D. Allan, and C. Thomas 1994, "*Technical directives for standardization of GPS time receiver software,*" *Metrologia*, **31**, 69-79.
- [2] J. Azoubib, and W. Lewandowski 1999, "*A test of the use of GLONASS precise code for high-precision time transfer,*" Proceedings of the 30th Annual Precise Time and Time Interval (PTTI) Systems and Applications Meeting, 1-3 December 1998, Reston, Virginia, USA, pp. 201-206.
- [3] J. Azoubib, W. Lewandowski, and G. de Jong 1998, "*A new approach to international time transfer: multi-channel and multi-code GPS+GLONASS common-view observations,*" Proceedings of the 12th European Frequency and Time Forum, 10-12 March 1998, Warsaw, Poland, pp. 87-93.
- [4] J. Azoubib, W. Lewandowski, J. Nawrocki, and D. Matsakis 1999, "*Some tests of GLONASS precise-code time transfer,*" 1999 European Time and Frequency Forum/International Frequency Control Symposium, 13-16 April 1999, Besançon, France, pp. 263-267.
- [5] C. Bruyninx, P. Defraigne, and J.-M. Sleewaegen 1999, "*Time and frequency transfer using GPS codes and carrier phases: on-site experiments,*" *GPS Solutions*, **3/2**, 1-10.
- [6] G. de Jong, and W. Lewandowski 1998, "*GLONASS/GPS time transfer and the problem of the determination of receiver delays,*" Proceedings of the 29th Annual Precise Time and Time Interval (PTTI) Systems and Applications Meeting, 2-4 December 1997, Long Beach, California, USA, pp. 229-240.
- [7] F. Roosbeek, P. Defraigne, and C. Bruyninx 2000, "*Time transfer using P-code measurements from GPS/GLONASS receivers,*" Proceedings of the 31st Annual Precise Time and Time Interval (PTTI) Systems and Applications Meeting, 7-8 December 1999, Dana Point, California, USA, pp. 373-381.
- [8] F. Roosbeek, P. Defraigne, and C. Bruyninx 2000, "*Time transfer experiments using P-code measurements from RINEX files,*" submitted to *GPS Solutions*.
- [9] W. Lewandowski, J. Azoubib, G. de Jong, J. Nawrocki, and J. Danaher 1997, "*A new approach to international time and frequency comparisons: all-in-view multichannel GPS+GLONASS observations,*" Proceedings of the ION GPS-97, pp. 1085-1091.
- [10] P. Willis, and J. Slater 1998, "*International GLONASS experiment,*" Proceedings of the IGS Annual Report.

RECOVERING UTC (USNO,MC) WITH INCREASED ACCURACY USING A FIXED, L1-CA CODE, GPS RECEIVER

R. P. Giffard, Agilent Laboratories, Palo Alto, CA 94304, USA

Abstract

The accuracy with which a L1, single-frequency, GPS receiver can recover the time-scale UTC (USNO,MC) is well known to depend on many factors, including the accuracy of the signal in space, propagation path effects, the quality of the GPS/UTC (USNO,MC) correction, and the behavior of the receiver itself. Overall performance is now affected by a number of short- and medium-term noise sources that have hitherto been obscured by the intentional clock dither known as Selective Availability (SA). We report the development of a technique for periodically estimating the local ionospheric delay from observations of the code and carrier-phase GPS observables made with a multi-channel, L1, receiver module. An algorithm has been developed that uses information from several satellites to model the delay in real time. It is then possible to correct the raw time estimate from each satellite, improving the overall accuracy of the receiver's real-time estimate of GPS time or UTC(USNO,MC). With this technique it should be possible to approach the time accuracy obtained using a Precise Positioning Service (PPS) receiver. We have used a cesium standard ensemble related to UTC (USNO,MC) by common-view to measure the noise level obtained by applying the estimated corrections, and to compare this with the accuracy of the built-in single-frequency model.

1. INTRODUCTION

Single-frequency, L1, CA code, GPS receivers are often used to generate local time estimates synchronized either with the GPS system clock, or with UTC(USNO,MC). These receivers are modular, economical, and easy to operate. With a fixed receiver, and accurately known antenna coordinates, the time uncertainty can be minimized by averaging together individual time estimates from all of the satellites that are being tracked. This technique, which can be described as "Position-Hold, All-in-View," minimizes errors due to the accuracy of the "Signal in Space," multipath effects, and code correlator noise. Receivers operating in this way are often employed in "Disciplined Oscillators," which are widely used in telecommunications synchronization, calibration, science, and other applications [1,2].

Now that SA has been removed, the component of the inaccuracy in single-frequency time receivers that results from the effect of ionospheric delay has become more significant. Receivers can correct for the delay using a detailed model of the ionosphere, scaled by data contained in the 'navigation message' broadcast by the satellites. However, because of unpredictable variations of the ionosphere, this so-called single-frequency correction is only expected to absorb 50% of the effect. In timing receivers, the uncorrected ionospheric delay causes periodic daily time errors with amplitudes that change over a characteristic time of a few days. This unpredictable effect can cause significant errors in timing systems such as disciplined oscillators, and is of increasing importance with the approach of the solar activity maximum. In a previous publication [3] we have reported evidence for short-term and long-term errors at the level of 10 to 20 nanoseconds in disciplined oscillators that use the single-frequency model.

For users who are not qualified for the PPS, it is useful to explore ways of reducing the magnitude of ionosphere errors in single-frequency receivers. It is well known [4,5] that the

effect of many noise sources can be reduced by using the Common View (CV) technique, which is analogous to the use of differential GPS corrections (DGPS). The CV time transfer technique requires data exchange between the user and a reference station with a traceable time-scale. Since the technique does not easily work in real time, it requires the user to have a stable local clock. Uncorrected ionosphere effects are still important in common-view time transfer measurements over long baselines, although corrections can be applied after a delay of several days by using post-processed estimates from various sources, such as the IGS. The GLONASS system allows two-frequency operation, and is not encrypted. The GLONASS system is not synchronized with UTC or GPS time, and GLONASS time receivers are not yet economically available.

In this paper we will describe a technique for accurately estimating the local ionospheric delay using the GPS observables from an L1-C/A single-frequency receiver. The ionosphere estimate, which is made in near real time, is used to correct the averaged single-satellite time estimates and improve the accuracy of the receiver's time output. We will report measurements of the noise level obtained by comparison with a local time standard consisting of an active ensemble of two 5071A cesium standards referenced to UTC(USNO,MC) by common view. The measured real-time ionospheric delay was found to agree very well with the post-calculated "IONEX" products generated by the International GPS Service (IGS) network. The stability of the corrected time output indicates that the effect of the ionospheric delay has been reduced by at least an order of magnitude.

The technique that we have developed can be used to improve the performance of autonomous single-frequency time-transfer systems such as disciplined oscillators. The technique could also be used to improve the accuracy of common-view time transfer, particularly when the latency involved in using post-processed ionosphere results is objectionable. The technique requires some computation, but this can be performed in background because the ionosphere effect changes relatively slowly. A preliminary description of this work has been given elsewhere [6].

2. SINGLE-FREQUENCY IONOSPHERIC DELAY ESTIMATION

It is well known [7] that GPS code and phase ranges at a given frequency are affected with opposite signs by the dispersion due to free electric charges in the ionosphere. This principle has been used by Cohen et al. [8], and Tretheway et al. [9] to estimate the ionospheric delay using L1, single-frequency, observables. We have extended this work, and have developed a technique that is capable of generating an accurate estimate in real time. The new method uses the observables from several satellites to estimate the local ionospheric delay and its dependence on latitude and longitude with reduced uncertainty.

If the ionosphere is modeled as a thin slab, the expected difference Δ_i between the measured L1 code and carrier ranges for the i^{th} satellite, measured in meters can be written in the form:

$$\Delta_i = 0.325 \cdot F_i \cdot I + P_i + \varepsilon_i. \quad (1)$$

In this equation, I is the total electron content integrated along a vertical path through the ionosphere in 'TEC units' (10^{16} electrons per m^2). F_i is a dimensionless obliquity factor given by $1/\text{Cos}(\theta)$, where θ is the angle between the normal to the ionosphere and the line of sight to the satellite. P_i is equal to an integer number of L1 wavelengths, and remains constant as long as phase-lock on the satellite signal is not lost. Receiver noise and multipath effects are represented

by the noise term ε_i . The code-carrier divergence Δ_i is easily calculated from the GPS observables output by a suitable receiver.

Although F can be calculated from the elevation angle of the satellite, Equation(1)cannot be used to calculate I directly because of the unknown constant P_i . Cohen et al [8] have shown that I can be determined by fitting the observed time dependence of the divergence to the variation of F in a solar-fixed, rotating frame, in which I can be considered effectively constant. Tretheway et al. [9] have reported the possibility of a real-time calculation of I using a Kalman filter technique.

In the technique that we have previously described [6], we used the time dependence of the observed divergence, removing the constant phase uncertainty. For a continuously tracked satellite:

$$d\Delta_i/dt = 0.325 \cdot (I \cdot dF_i/dt + F_i \cdot dI/dt) + d\varepsilon_i/dt. \quad (2)$$

At least four satellites can usually be tracked simultaneously, giving a set of simultaneous equations, each of the form of Equation (2). For each satellite, the rate of change of Δ_i can be estimated from the GPS observables, and the values of F_i and dF_i/dt can be calculated from the satellite ephemeris. As long as two or more satellites are tracked, estimates of I and dI/dt may be determined by the usual process of inverting the set of equations. It is interesting to note that, unlike dual-frequency methods, the calculation of I by this method is independent of satellite and receiver inter-frequency biases. The method does, however, depend on the assumption of a slab model for the ionosphere.

The algorithm described above assumes that the ionosphere is effectively uniform over the area covering the points at which it is “pierced” by the lines of sight from the receiver to the satellites. We have now extended the method to allow the value of I to depend in first order on latitude and longitude. The variation with longitude can be found by assuming that most of the variation of I with time is associated with the effect of earth rotation with an ionosphere distribution that is changing relatively slowly in the solar-fixed frame. The rate of change with time in earth-fixed coordinates is then approximately equal to the rate of change with longitude multiplied by the rate of rotation of the earth.

The line of sight from the satellite to the receiving antenna passes through the idealized height of the ionosphere slab at a “pierce” point that is generally offset in longitude and latitude from the position of the receiver. If the offsets for the i^{th} satellite are λ_i and ϕ_i respectively, and the local variation of I is characterized by derivatives $dI/d\lambda$ and $dI/d\phi$ respectively, the divergence is given by:

$$\Delta_i = 0.325 \cdot F_i \cdot (I + \lambda_i \cdot dI/d\lambda + \phi_i \cdot dI/d\phi) + P_i + \varepsilon_i. \quad (3)$$

In this equation, I is the vertical TEC value at the position of the receiver, and it is assumed that the geometry may be treated as rectangular. This assumption should be satisfactory for mid latitudes.

To find the equivalent of Equation (2), we differentiate Equation (3). Keeping only first-order derivatives, and putting $dI/dt = \Omega \cdot dI/d\lambda$, where Ω is the rate of rotation of the earth we obtain:

$$\begin{aligned} d\Delta_i/dt &= 0.325 \cdot (I \cdot dF_i/dt + dI/d\lambda \cdot \{F_i \cdot [\Omega + d\lambda_i/dt] + \lambda_i \cdot dF_i/dt\} \\ &\quad + dI/d\phi \cdot \{F_i \cdot d\phi_i/dt + \phi_i \cdot dF_i/dt\}) + d\varepsilon_i/dt. \end{aligned} \quad (4)$$

There are now three unknowns: I , $dI/d\lambda$, and $dI/d\phi$. As before, with N satellites tracked, there are N such equations, which can be written in the form of a single matrix equation:

$$V = W \cdot G. \quad (5)$$

In Equation (5), V is a column vector containing the measured values of $d\Delta_i/dt$ for the N satellites normalized by the factor $1/0.325$, W is the $N \times 3$ matrix containing the calculated geometrical coefficients for the N satellites, and G is a column vector whose elements are the unknowns:

$$G = (I, dI/d\lambda, dI/d\phi)^T. \quad (6)$$

If N is equal to or greater than three, the set of equations can be inverted to obtain I , $dI/d\lambda$ and $dI/d\phi$. The least-squares solution is described by the matrix equation:

$$G = [W^T W]^{-1} W^T \cdot V. \quad (7)$$

The values of I , $dI/d\lambda$, and $dI/d\phi$ obtained from the solution are uncertain due to noise on the code-carrier differences. This is caused by receiver code correlator noise, and multipath noise that mostly affects the code ranges. The resulting noise on the output vector G can be estimated from the properties of the matrix $[W^T W]^{-1} W^T$. Under the simplifying assumption that the noise on the output quantities is not correlated, the mean square output noise is proportional to the diagonal elements and the rms noise on the divergences. Experimental data show that the magnitudes of the elements are, generally, slowly changing functions of the satellite constellation geometry. From time to time, the geometry becomes less satisfactory for determining one or more of the output quantities. This condition is associated with the appearance of unusually large values of the diagonal elements.

3. TESTS OF THE ALGORITHM

The system used in the experiments to be described consists of an 8-channel, modular, C/A code receiver [10] fed by a choke-ring antenna. As discussed elsewhere [6], the receiver's crystal oscillator is phase-locked to an external frequency standard in order to make it easier to detect loss of phase lock. Raw data from the receiver are reprocessed on-line by an external computer. The program calculates the code and phase ranges each second, and smoothes the code-carrier divergences using a filter with a pole frequency of 0.067 radian per second. Every 15 seconds, the value of the filtered divergence, the obliquity, the latitude offset, and the longitude offset for each satellite are stored in an array in memory. Pointers are maintained to indicate the start and finish of continuous tracking for each satellite.

Every 10 minutes, the stored data from all satellites that have been continuously tracked during the preceding 2400 seconds are analyzed in the on-line computer. Linear regressions of length

2400 seconds are used to estimate the rate-of-change of the code-carrier divergence and the rate-of-change of the obliquity. The obliquity and the offsets $d\lambda$ and $d\phi$ are averaged over the same interval. This data are then used to calculate the unknown vector G using the matrix relationship given in Equation (7). Although linear regressions may not be optimal for determining the rate of change, they are used in preference to IIR filters, because there is no settling time. The chosen length of the linear regressions represents a compromise between data latency and noise.

Comparing the noise variances on I and dI/dt (equal to $\Omega \cdot dI/d\lambda$) shows that a filter whose output approaches the integral of dI/dt in the short term, and the value of I in the long term can be used to reduce the noise on the estimate. A robust filter was devised to implement this principle using a cross-over time of 1 hour. The magnitudes of the diagonal elements of the matrix are used to determine whether the filter uses the current input quantities or values extrapolated from times at which the noise was satisfactory. The filter algorithm is based on the code-carrier smoothing filter typically used in GPS receivers.

To evaluate the performance of the filter and the algorithms described by Equations (1)-(7), stored raw GPS data were used to emulate the ionosphere delay given by the GPS built-in single-frequency model. In selected raw data files, the measured code-carrier differences for each satellite were replaced by calculated values obtained by doubling the delay given by the model [11] using the actual values of the satellite elevation and azimuth. The α and β parameters in the model were given the values contained in the satellite navigation message at the time. This modified raw data were then processed and filtered by the algorithms that were used for real-time data processing. The recovered variation of I was compared with values calculated directly using the model.

The success of the method is indicated by the data shown in Figure 1. The estimate of I found by the algorithm is in good agreement with the directly calculated value. It is clear that the use of a 2400-second processing span does not lead to serious rounding, although some ringing seems to occur where the second derivative of I is large. A linear regression between the two sets of data indicates that the values returned by the algorithm are smaller by a factor of 0.955. This may result from the use of a first-order time model. When there is no curvature, the model values are reproduced exactly by the algorithm. This is felt to be a good test of the data processing algorithm because the model represents the typical time variation of I , and the coefficient matrix values correspond to real satellite constellations.

When unmodified receiver raw data were processed in real-time, estimates of the three parameters included in the output vector G were obtained at 10-minute intervals. The outputs of the robust filter were written to a file. Data obtained over a 15-day period were used for a comparison with the IONEX ionosphere maps generated by the IGS from a worldwide array of dual-frequency receivers. The IONEX data could usually be obtained by Internet ftp after about 7 days. The data were interpolated for the latitude and longitude of the receiver at time intervals corresponding to 32 points per day.

Figure 2 shows a comparison between the output of the real-time single-frequency algorithm discussed above and the IGS data from the CODE center for a 3-day period. An ionosphere slab height of 450 km is assumed in both calculations. For the data shown, the agreement is very good. For the entire 15-day period for which both measurements are available, the mean difference is -0.52 TEC units, and the rms difference is 3.8 TEC units. There was no significant difference between the estimates from the two single-frequency receivers used, showing that

receiver noise had a negligible effect. The noise on the solution is probably mainly due to multipath effects.

4. CORRECTING THE RECEIVER TIME OUTPUT

Each second, the GPS receiver averages satellite tracking data to estimate the bias between its internal clock and GPS time. At the next second, this result is communicated to the user when the receiver emits a timing pulse aligned as closely as possible with the exact second. If the receiver is set to output UTC time, it applies the UTC/GPS correction contained in the navigation message, thereby relating the time of the output pulse to UTC(USNO,MC). To compensate the output using the measured ionospheric delay, the system calculates the amount by which the receiver output pulse has been delayed using the values of I , $dI/d\lambda$, and $dI/d\phi$. The result is provided numerically to the user, who can then use it to correct the result of the measurement of the time difference between the receiver output pulse and the 1 PPS pulse of the time-scale to be synchronized. The correction δt is given by a summation over the N satellites that are in the time solution for that second:

$$\delta t = 0.5416 \cdot F_i \cdot \sum (I + dI/d\lambda \cdot \lambda_i + dI/d\phi \cdot \phi_i) / N. \quad (8)$$

In these experiments, the time differences are averaged over the 600-second intervals between calculations of the ionospheric delay parameters. It is necessary to calculate a correctly averaged correction using the ionosphere values propagated to the mid point of the averaging interval, which is done as follows. The geometrical quantities F_i , $F_i \cdot \lambda_i$, and $F_i \cdot \phi_i$ are calculated each second, averaged over the satellites that are currently in the time solution, and stored in memory. After 600 seconds, the average of the accumulated counter readings is calculated. The averages of the three geometrical quantities over the previous 600 seconds are used with the delay parameters to calculate the estimated correction to the averaged time-difference, δt^* :

$$\delta t^* = 0.5416 \cdot (I \cdot \sum \langle F_i \rangle + dI/d\lambda \cdot \sum \langle F_i \cdot \lambda_i \rangle + dI/d\phi \cdot \sum \langle F_i \cdot \phi_i \rangle) / 600. \quad (9)$$

In this equation, triangular brackets denote averaging over the satellites that are used by the receiver in the time solution for a given second, and the summation is carried out over the most recent 600 solutions. The ionosphere estimates, the number of satellites in the estimate, the raw counter average, the counter rms, and the counter average corrected by δt^* are included in the file output.

5. TIME STABILITY EXPERIMENTS

To evaluate the success of the method, the time-differences between a local time-scale and the 1PPS outputs of the two receiver systems using the real-time ionosphere correction were measured for several weeks. One receiver was set to output UTC(USNO,MC) via GPS and the other was set to output GPS time. The built-in ionosphere correction was turned off in both of these receivers. The raw time differences, the real-time ionosphere estimates, and the corrected time differences were logged at 10-minute intervals. The time difference was also recorded for a conventional receiver system using the GPS single-frequency ionosphere correction. An independent receiver was used to log page 18, sub-frame 4, of the navigation message so that the current GPS-UTC correction and the ionosphere model parameters could be obtained for comparison. All receivers used the same choke-ring antenna.

The local time-scale consisted of an active ensemble of two high performance 5071As that was disciplined to UTC(USNO,MC) by a feedback loop with a time constant of 10 days. The time-difference between the 1 PPS output of the local ensemble and UTC(USNO,MC) was determined by common-view measurements as described elsewhere [3]. About 35 common-view passes could be compared daily using the BIPM USA (east coast) schedule. In the time comparison experiments to be described, a correction for the local time-scale was obtained by smoothing the common-view differences using a sliding filter with triangular weighting and a peak-to-peak width of 2 days [3].

The upper curve in Figure 3 shows the variation of the time difference between the corrected local time-scale and the raw output of a receiver with the GPS single-frequency model disabled, and the GPS/UTC correction enabled. The data have been shifted up by 50 ns for clarity. The time difference is dominated by the daily variation of the ionospheric delay, which has a fairly constant peak-to-peak amplitude during this period. The amplitude of the component at one cycle-per-day was determined by Fourier analysis to be 26 ns with a phase corresponding to a daily maximum at 21:05 UT.

The lower curve in Figure 3 shows the measured time difference for the same period between the corrected local time-scale and the receiver with the GPS single-frequency model and the GPS/UTC correction enabled. Daily effects can be seen, suggesting that the built in ionosphere correction was not completely effective at this time. The effects are significantly bi-modal, corresponding to the rising and falling edges of the actual delay. It appears that the effect is due to a phase difference between the real ionosphere delay, shown in the upper curve, and the single-frequency correction, which has a maximum at 22:14 UT at the longitude of the receiver, -122.15 degrees. This effect is characteristic of the data during this particular period, and is not always observed.

Correcting the measured raw time difference according to Equation (9), using the ionosphere model calculated in real-time, was found to reduce the effect of the ionosphere delay by a factor of 10, or 20 dB. Fourier analysis showed that, after correction, the time difference still contained a 1 cycle-per-day (cpd) component in phase with the original ionosphere effect. For both of the receivers studied, the 1 cpd component was minimized if the average correction δt^* was increased by a factor of 1.10. The rejection was then about 26 dB.

There are several possible explanations for this unexpected result. The results, shown in Figure 1 indicate that the algorithm has an effective scale factor of 95.5% when typical emulated data are used. It might be expected that the correction would have to be increased by about the reciprocal of this factor. Further inaccuracy may result from the use of a simple slab model for the ionosphere. Recent work has attempted to extend the ionosphere model to include its distribution with respect to height [12]. There is currently great interest in the use of advanced ionospheric models for aircraft navigation, but it is not yet clear how they would affect the compensation of a time receiver. The agreement between the ionospheric parameters and the IGS model is not surprising because both calculations are base on a slab ionosphere model with a height of 450 km. It should be pointed out that the accuracy of the IGS orbital and geodetic results does not depend on the ionosphere model used because the ionosphere delay is removed directly by dual-frequency ranging.

An alternative explanation is that some other daily variation such as a daily environmental change in the system group delay was being compensated. This seems unlikely because of the

stability of the effect, and its accurate agreement in phase with the ionosphere maximum. The same argument can be used with respect to any possible multipath effect, which would also have a 1 cpd periodicity.

Figure 4 shows the time differences with respect to the corrected local time-scale for the two receiver systems using real-time ionosphere correction increased by the experimentally determined factor 1.10. The upper curve is for the receiver operating in GPS time, and the data have been shifted up by 40 ns for clarity. (The 13-second integer time-difference between GPS time and UTC does not affect the data, which are modulo 1-second.) The data show a slow run-out of about 20 ns peak-to-peak between the local time-scale corrected to UTC(USNO,MC) and the receiver output during 14 days. The lower curve shows the time difference between the corrected local time-scale and the output of the ionosphere corrected receiver using the UTC/GPS correction. The data show significantly less long-term run-out, but the short-term variation appears to be less smooth. This is possibly due to the step-wise evolution of the GPS/UTC correction. The overall rms deviation over the 14-day period is 5 ns. Fourier analysis shows that the remaining amplitude at 1 cpd is less than 1 ns. Possible remaining sources of noise include satellite ephemeris errors, including clocks, and multipath effects. The magnitude of the noise is consistent with recent measurements of the accuracy of the signal in space [14].

The absolute values of the time-differences shown in Figures 3 and 4 are not significant. The CV receiver system has been accurately calibrated at NIST, but no attempt has been made to calibrate the absolute delays of the other receivers.

6. SUMMARY

We have demonstrated that the local GPS L1 ionospheric delay can be accurately estimated in real time with a single-frequency receiver by using the GPS observables from several satellites. The TEC values obtained assuming a slab ionosphere model at 450 km compare well with data from the IONEX maps produced by the IGS network. Our method currently involves averaging the raw data over 2400 seconds to minimize noise, and this does not seem to reduce the accuracy of the estimate significantly.

We have shown that the real-time delay estimate can be used to reduce the short-term effect of the ionosphere on the output of a single frequency time receiver. To optimize the correction of the ionospheric delay, it was found necessary to increase the magnitude of the delay estimate by a factor of 1.10. The reason for this is not yet completely understood, but it may be due to the use of a simple slab ionosphere model, and the neglect of second order time differences. This effect could possibly be studied by analyzing code-carrier divergences flattened with the calculated ionosphere model. At the latitude of the experiment, 37.68 degrees, the amplitude of the daily ionosphere effect could be reduced by 26 dB. More experiments would be useful to find out whether long-term effects that we have reported elsewhere [3], are also reduced.

In these experiments, a time correction was calculated every 10 minutes and applied to the average of the time differences measured over the same period. In an application such as a disciplined oscillator, where a less stable local clock must be steered, it would be possible to correct the time difference much more frequently without significantly increasing the computational load.

7. ACKNOWLEDGMENTS

It is a pleasure to acknowledge the enthusiastic support of Len Cutler, and the encouragement of the Precision Instrumentation Group at Agilent Laboratories. Ray Wong constructed the phase-lock circuitry.

8. REFERENCES

- [1] J.A. Davis and J. M. Furlong, "Report on the Study to Determine the Suitability of GPS Disciplined Oscillators as Time and Frequency Standards Traceable to the UK National Time-scale UTC (NPL)," Center for Time Metrology, National Physical Laboratory, Middlesex, TW11 0LW, U.K.
- [2] R.P.Giffard and R. Pitcock, "An Accurate Local Traceable Time-Scale for Calibrating GPS Time-Transfer Products," Proceedings of the Workshop and Symposium of the NCSL, Toronto, Canada, July 2000.
- [3] R.P. Giffard and R. Pitcock, "Comparison of Common-View and One-Way GPS Time Transfer Over a 4000 km East-West Baseline," Proceedings of the 31st Annual Precise Time and Time Interval (PTTI) Systems and Applications Meeting, Dana Point, California, USA, Dec. 1999, pp. 393-404.
- [4] D.W. Allan, D.D. Davis, M. Weiss, A. Clements, B. Guinot, M. Granvaud, K. Doren-wendt, B. Fischer, P. Hetzel, S. Aoki, M-K. Fujimoto, L. Charron, and N. Ashby, "Accuracy of International Time and Frequency Comparisons Via Global Positioning Satellites in Common-View," IEEE Trans. Inst. and Meas., Vol IM-34, 1985, pp. 118-125.
- [5] W. Lewandowski, "GPS Common-View Time Transfer," Proceedings of the 25th Annual Precision Time and Time Interval (PTTI) Applications and Planning Meeting, Marina Del Rey, USA, Dec. 1994, NASA Conference Publication 3267, pp. 235- 245.
- [6] R.P. Giffard, "Estimation of Ionospheric Delay Using L1 Code and Carrier Phase Observables," Proceedings of the 31st Annual Precise Time and Time Interval (PTTI) Systems and Applications Meeting, Dana Point, California, Dec. 1999, pp. 405-417.
- [7] J. A. Klobuchar, "Ionospheric effects on GPS", in Global Positioning System: Theory and Applications, Vol., Editors: B.W. Parkinson and J.J. Spilker, Progress in Astronautics and Aeronautics, Vol. 163, pp. 485-515.
- [8] C.E. Cohen, B. Pervan, and B.W. Parkinson, "Estimation of Absolute Ionospheric Delay Exclusively through Single-Frequency GPS Measurements," Proceedings of ION GPS-92, Institute of Navigation 1992, pp. 325-330.
- [9] M.L. Tretheway, I. Catchpole, and A. Hansla, "Single Frequency Ionosphere Determination Using GPS," Proceedings of ION GPS-93, Salt Lake City, UT, USA, Institute of Navigation 1993, pp. 1373-1381.

- [10] Motorola ONCORE-VP, 8-channel receivers with firmware versions 8.9 and 10.0 were used in this work. This receiver is currently obsolete, but any receiver with suitable outputs can be used.
- [11] GPS Interface Control Document ICD-GPS-200, Revision IRN-200C-002, Arinc Research Corporation, 10 Oct. 1993, pp. 124-127.
- [12] A.J. Hansen, "Real-time Ionospheric Tomography Using Terrestrial GPS Sensors," Proceedings of ION GPS-98, Nashville, TN, USA, Institute of Navigation 1998, pp. 717-727.
- [13] Robin P. Giffard, "Ionosphere Effects at the Nanosecond Level Observed in Common-View Time-Transfer," Navigation, Vol. 44, N0. 4, Winter 1997-1998, pp. 489-497.
- [14] Donghai Dai, Todd Walter, Per Enge, and J. David Powell, "Satellite-Based Augmentation System Signal-In-Space Integrity Performance Analysis, Experience, and Perspectives," Proceedings of ION GPS-99, Kansas City, MO, USA, September 1999.

9. FIGURES

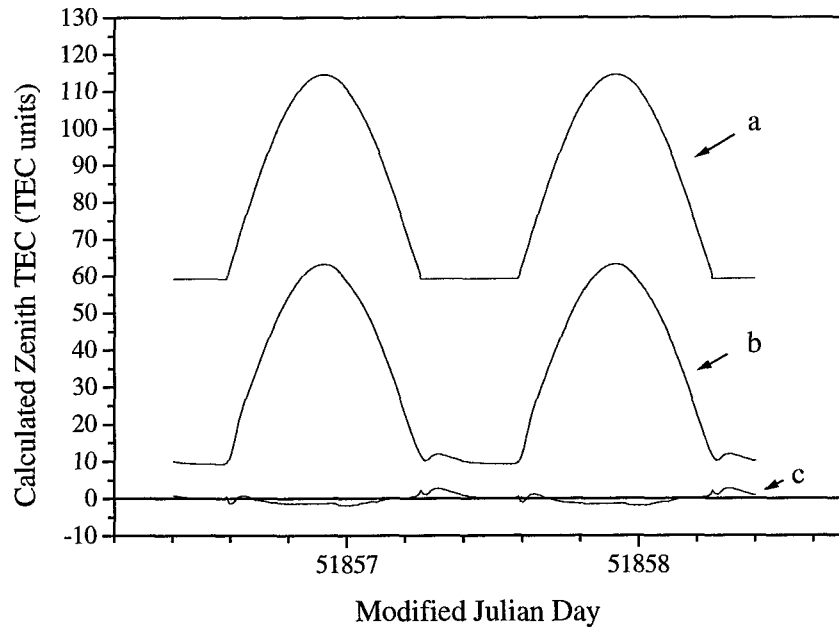


Figure 1. Curve a: Zenith TEC value calculated using the GPS single-frequency model. (Data shifted up 50 TEC units for clarity.) Curve b: The zenith TEC calculated by the real-time ionosphere algorithm from raw data emulating the single-frequency model, with the same values of α and β (from the current navigation message). Curve c: The difference between curves b and a.

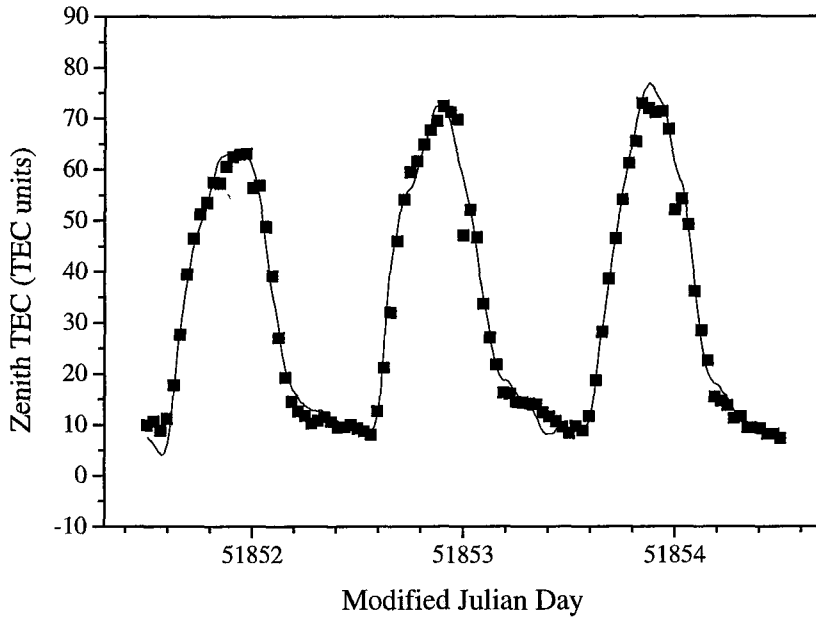


Figure 2. The figure shows a comparison between the output of the single-frequency algorithm and IGS data. The solid curve is the filtered output of the algorithm, calculated in real-time. The solid points represent IONEX data obtained about 7 days later from the IGS Berne computation center (CODE), interpolated to the latitude and longitude of the single-frequency receiver at a rate of 32 points per day.

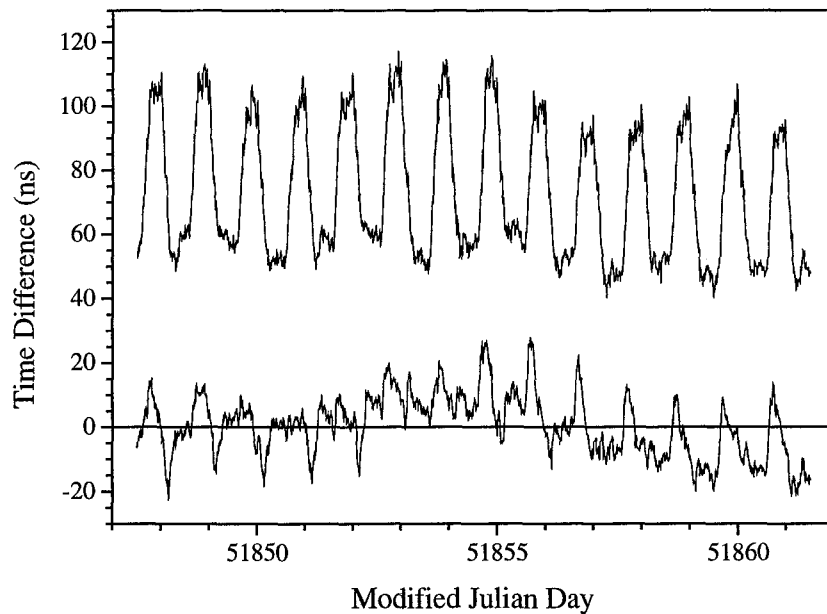


Figure 3. Upper curve: The measured time difference between the corrected local time-scale and the raw output of a receiver using no ionosphere compensation. The GPS/UTC correction is enabled. (Data shifted up by 50 ns for clarity.) The time difference is dominated by the daily variation of the uncorrected ionospheric delay. The lower curve shows the corresponding time-difference for a receiver with the GPS single-frequency model enabled.

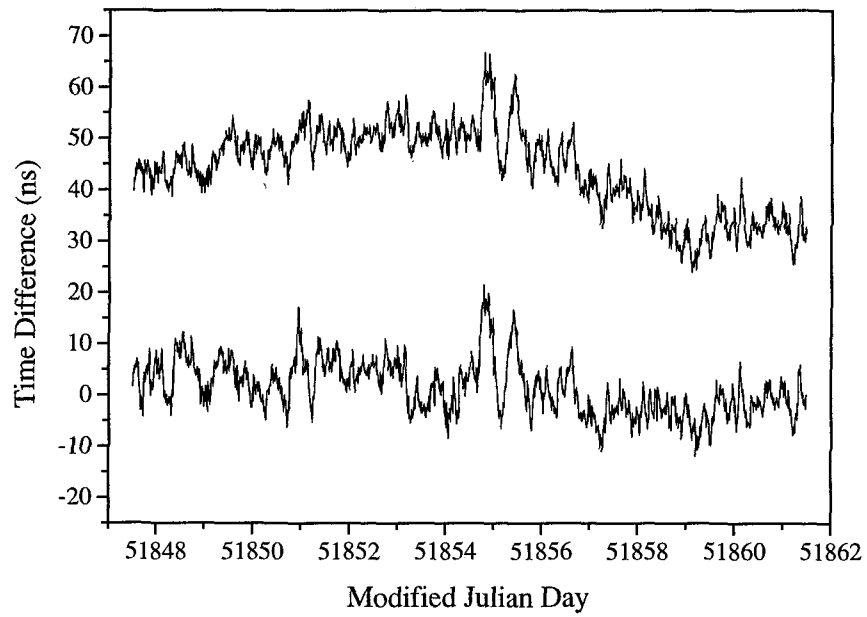


Figure 4. Time differences between the corrected local time-scale and the 1 PPS outputs of two receivers compensated using the real-time ionosphere estimation technique. The magnitude of the compensation has been enhanced by a factor of 1.10, as discussed in the text. Upper curve: UTC/GPS correction disabled. (Data shifted up 40 ns for clarity.) Lower curve: UTC/GPS correction enabled. The data are composed of 10-minute averages, and the absolute values of the time differences are not significant.

Questions and Answers

THOMAS CLARK (NASA Goddard Space Flight Center): What was the receiver and firmware?

ROBIN GIFFARD: Motorola Oncore VP. Of course, I'm just using standard pseudo-range on carrier phase. So it could be done by another receiver.

CLARK: I was going to ask which firmware did you use?

GIFFARD: It's 8.9 or 10, I'm not sure. It is important to get beyond 8.9.

BOYD MOORE (ITT Industries): Because solar flux affects ephemeris drastically, right? For lower orbits, I don't know about that height. I wonder if there is a correlation between solar flux affecting your TEV and ephemeris. Could you comment on that?

GIFFARD: I don't think I can comment on that. I'm sort of focused on producing a real-time answer, so I don't have time with this equipment. I can't calculate autonomous orbits or anything like that. So if there were such an effect, that would certainly spoil the result.

PROGRESS ON A NEW GPS COMMON-VIEW RECEIVER*

Marc A. Weiss

National Institute of Standards and Technology
Time and Frequency Division, 847
325 Broadway, Boulder, CO 80305-3328, USA
e-mail: mweiss@boulder.nist.gov

Abstract

We are developing a new GPS common-view time transfer receiver to support both International Atomic Time (TAI) and comparison of frequency standards. Our goal is to realize a time-transfer accuracy of one ns or below, and time-transfer stabilities of 0.5 ns out to 1 year. Having obtained consistent stabilities at 100 ps or below with common-clock experiments out to 1 month with three laboratory prototype systems, we are now building a unit that can be moved among different timing labs. We show studies of three different time-interval counter cards considered for this project, revealing stabilities as a function of temperature and supplied voltage.

INTRODUCTION

We have developed a common-view time transfer receiver using a commercial GPS engine [1]. We have stabilized the time delay through the receiver by controlling receiver temperature, and supply voltage, and by minimizing reflected power through the downlink antenna cable [2]. Three prototype units have obtained pair-wise common-clock Time Deviation (TDEV) stabilities below 100 ps for periods from 1 d to 10 d and longer. This can be seen in Figures 1 and 2. Figure 1 shows data from MJD 51600 (January 7, 2000) to MJD 51835 (October 8, 2000) for the common-clock common-view difference between two units, N3 and N2, whose antennas are separated about 10 m. Figure 2 shows the TDEV of the data from Figure 1. Figure 3 shows the outdoor temperature for this period. While there are large changes in temperature, the data do not visibly exhibit a correlation. Nor do the TDEV data show evidence of a +1 slope in long term. This would occur if parabolic behavior appeared due to a measurable annual variation. We are now interested in building a portable system which can be moved to different sites, to determine its capabilities for common-view time transfer over longer baselines.

Common-view time transfer is one of the two main systems for measuring clock differences as input for the generation of International Atomic Time (TAI) [3]. A receiver was developed in 1980 at NIST (then NBS) that has been used since then as the most popular receiver for this purpose. There is a need to replace it with newer technology. While there has been significant research in developing new

*Contribution of U. S. Government, not subject to copyright

common-view systems, the goal of receiver stability below 1 ns for time periods of 1 year still remains a challenge. The prototype systems we have built may be able to achieve this.

We are packaging the system in a design which can be moved to other labs. This includes a rack mounted PC, a temperature-controlled receiver, and a choke-ring mounted antenna, with electronics underneath it. The PC will contain a time-interval counter on a card that plugs into the PC bus. We discuss the design of this system here, and report tests of some of the components. In particular, we studied the stability and accuracy of various counter cards with variations in temperature and voltage. We also have stability measurements using the antenna system for the new unit. Here we have duplicated the design that terminates the antenna cable with 50 ohms at both the antenna and the receiver.

A STUDY OF THREE COUNTERS

The receiver needs a counter that plugs into the PC bus. Our three existing systems use counter cards that were built at NIST by D. Davis [4] some years ago in support of a project to build a two-way time transfer modem. These have been shown to be accurate to better than 100 ps. Since we don't have any more of these, we needed to find an alternative counter that is accurate to 100 ps or better. We studied three time-interval counters for this purpose: two made under contract especially for NIST, and one manufactured commercially. We refer to the two counters built for NIST as DD and BD, and the commercial counter as GT. The BD counter has been studied in [5].

We studied the variations of the three counters' time-interval measurements with voltage and with temperature. We did this by placing a PC in a temperature-controlled chamber. We then altered a PC bus extension card so we could supply the +/- 5 V and the +/- 12 V from an external power supply. This allowed us to control the counters and collect the data using the PC, while independently controlling and monitoring the power supply voltages.

When counters showed a dependence of the measurement on voltage, it was only on the +5 volts. The results are summarized in Table 1 below.

Table 1

	+5 Volt Dependence ps/V	Temperature Dependence ps/°C
DD Counter	negligible	15.6
BD Counter	800.7	3.2
GT Counter	-2704.4	21.2

We decided to use the DD counter both because of availability and because of the above results. The various counters can be calibrated against a more accurate counter, and the result of this calibration used in the receiver software. This will change with the instability of the counter and its internal calibration. It appears that all the counters studied can be calibrated to an internal consistency of 100 ps.

STABILITY OF ANTENNA AND CABLING SYSTEM

We have shown that the long-term stability of a common-view GPS receiver can be significantly improved by reducing coherently reflected signals in the antenna cable [2]. We have duplicated the systems we used previously for this purpose. We provide a temperature-stable 25 dB amplifier after the antenna, followed by a DC-pass 10 dB attenuator, then a temperature-stable antenna cable down to the lab, then another 10 dB DC-pass attenuator. The stability of this system has reproduced previous results. Figure 4 shows common-clock common-view difference between the N01 receiver with the new antenna system, and another, N03, from MJD 51803 to 51862, September 15-November 13, 2000. Figure 5 shows the TDEV of these data. We obtain TDEV stabilities of under 100 ps from 1 d on, independent of temperature or rain. Snow, on the other hand, causes delay shifts, presumably because of effects from covering the antenna.

FUTURE WORK

We are planning to build a temperature controller around the GPS engine, and a precise power supply. We also plan to package the counter in a rack-mountable PC that will control both the counter and the GPS receiver. This is functionally equivalent to what we have done in our three prototype systems, but this operational system will use more compact than the prototype.

REFERENCES

-
- [1] We used a Motorola VP ONCORE receiver for our commercial engine. We mention the trade name for completeness. No endorsement by NIST is implied. We are aware that these receivers are discontinued, yet we have a number of them available which we can use.
 - [2] M. A. Weiss 2001, "*Long-term effects of antenna cables on GPS timing receivers,*" Proceedings of the 2001 IEEE International Frequency Control Symposium, 6-8 June 2001, Seattle, Washington, USA (in press).
 - [3] C. Thomas 1997, "*The accuracy of International Atomic Time TAI,*" Proceedings of the 11th European Forum on Time and Frequency, 1997, pp. 283-289.
 - [4] V. S. Zhang, D. D. Davis, and M. A. Lombardi 1995, "*High resolution time interval counter,*" Proceedings of the 26th Annual Precise Time and Time Interval (PTTI) Applications and Planning Meeting, 6-8 December 1994, Reston, Virginia, USA, pp. 191-200.
 - [5] A. N. Novick, M. A. Lombardi, V. S. Zhang, and A. Carpentier 2000, "*A high performance multi-channel time-interval counter with an integrated GPS receiver,*" Proceedings of the 31st Annual Precise Time and Time Interval (PTTI) Systems and Applications Meeting, 7-9 December 1999, Dana Point, California, USA, pp. 561-567.

N3 - N2, Common-Clock Common-View
1 Point/Hour

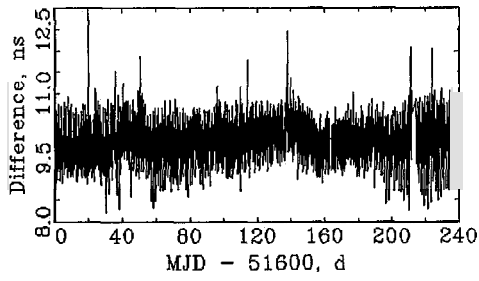


Figure 1 235 days of common-view common-clock differences between two prototype receivers. The data are 1-hour averages.

N03 - N02
MJD 51600 to 51835

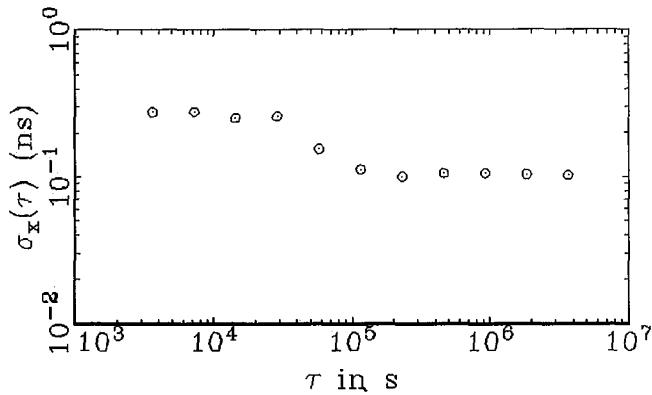


Figure 2 TDEV of the data in Figure 1, showing a flicker PM floor of about 100 ps.

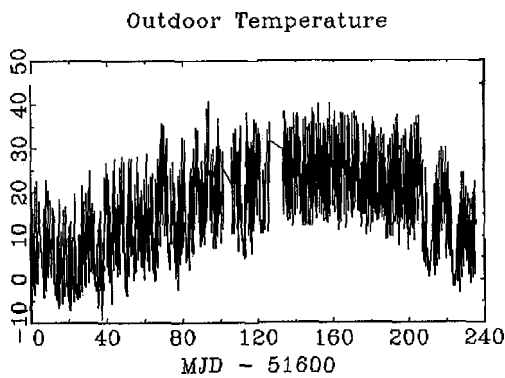


Figure 3 Outdoor temperature for the antennas during the periods shown in Figures 1 and 2.

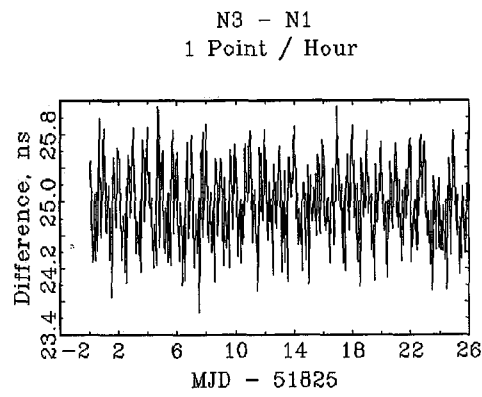


Figure 4 N3-N1 common-view common-clock difference with 1-hour averages, for the antenna system of the new receiver.

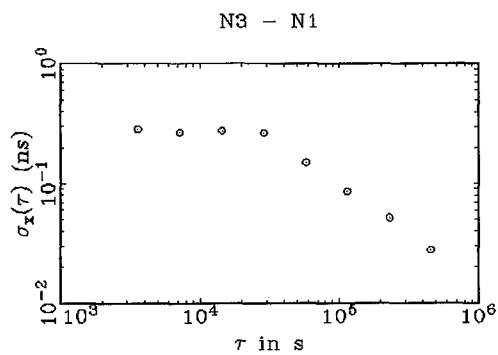


Figure 5 TDEV of data of Figure 4.

THE INFUSION OF MCS KALMAN FILTER DATA INTO GPS BLOCK II/IIA FREQUENCY STANDARD ANALYSIS TECHNIQUES

Gary L. Dieter, Gregory E. Hatten, and Jack Taylor
Boeing Space and Communication Services

440 Discover Avenue, Suite 38

Schriever Air Force Base, CO 80912-4438, USA

Tel: (719) 567-3176, (719) 567-2943, (719) 567-5953

E-mail: Gary.L.Dieter@Boeing.com, Gregory.E.Hatten@Boeing.com,
Jack.Taylor2@Boeing.com

Abstract

Recent advances have allowed Boeing GPS navigation payload analysts the ability to transfer, archive, and manipulate Master Control Station (MCS) Kalman filter data. Previously, access to these data was cumbersome and restricted to a limited timespan. The new data retrieval process has proven to be useful in many areas of GPS analysis, including frequency standard performance characterization. Both routine and anomalous frequency standard performance analysis techniques are enhanced by considering the characteristics and trends of key MCS filter variables.

This paper describes the methodology by which the MCS Kalman filter data is attained. It also examines situations in which MCS Kalman filter clock state estimates and navigation performance metrics have proven to be useful in analyzing frequency standard performance. Examples include routine examination of frequency standard stability using MCS phase offset estimates, analysis of MCS frequency offset estimates before and after a "clock q-bump," and comparison of MCS clock state estimates versus those of the National Imagery and Mapping Agency (NIMA). Conclusions reveal that new, valuable insight is gained by considering MCS Kalman filter data when performing frequency standard analysis.

MCS KALMAN FILTER DATA TRANSFER METHODOLOGY

Until the summer of 1999, analysis of GPS Kalman filter data was limited to on-line tools. Because of security constraints and the awkwardness of the Jovial-based architecture, the ability to move data off-line and employ COTS analysis tools was labor-intensive and, in practice, rarely done. Instead, most analysis was done on-line and in real-time. The on-line tools are relatively effective in spotting and analyzing anomalies as they occur, but any additional analysis often has to be performed by outside agencies.

Beginning in the summer of 1999, Boeing personnel working at the MCS began retrieving selected MCS data from the on-line system and archiving it off-line. This method of archiving data allowed much greater flexibility for analysis. COTS tools such as Stable32 and MS Excel could be used to analyze and graphically display the data. Also, time spans are limited only by the beginning of this archive. Many on-line tools are restricted to accessing data from the last 48 - 72 hours. Even MCS tapes containing stored data are erased within 6 months.

The data retrieval activity is a three-step process. First, one or more batch scripts are run on the standby mission package. The standby mission package is identical to the active mission package, and is kept in a

state of readiness in case there is a need to switch-over. The batch jobs are run on the standby package to prevent any slow-downs of the various processes required to run the MCS mission package. Once the batch jobs have created the files containing the various GPS performance data, the files are transferred to a classified PC. This is a relatively slow process; 1 day's worth of data takes approximately one hour to transfer. Once the files are on the classified PC, they are transferred to a zip drive by secure means. Finally, the files on the zip disk are moved to an unclassified PC and archived on the Schriever AFB LAN.

This rather tedious, labor-intensive process is performed every weekday to ensure that the archives have the most up-to-date information available. The information is in ASCII format and can be read by most COTS analysis tools.

Clearly, the process would be improved by automation. Boeing personnel, in conjunction with the Air Force and other GPS contractors, are trying to streamline the process. Several issues remain to be addressed. Security is a major issue. Several aspects of the GPS mission package are classified. Any scheme to remove data (even unclassified data) from a classified system requires extensive security reviews. Several means of removing the data from the system have been rejected for security reasons. Our ultimate goal is to have the additional MCS data automatically downloaded to the Integrated Mission Operations Support Center (IMOSC) terminals, where an ensemble of Windows-based analysis tools will reside.

The advanced age and complexity of the MCS Legacy system is another difficult issue. The Air Force is trying to move MCS operations to a newer, more advanced system. This makes it very difficult to commit resources to upgrading the older, Legacy system. Although the new system is not expected to be delivered for several years, few MCS Operational Control System (OCS) resources are devoted to the outgoing Legacy system. Despite these challenges, the authors believe that the data retrieval and archival process can be streamlined and that this valuable effort will continue.

Currently, 18 files are transferred on a daily basis. This list of files contains the following data: Kalman state estimates (including backup and KF maintenance activities); reference trajectory data and coordinate system (ECI-ECEF) transformation data; GPS-UTC steering activity; smoothed measurements and residuals; navigation message upload data; and performance monitoring data (Estimated Range Deviations (ERDs), Observed Range Deviations (ORDs); and navigation solution (NAVSOL) data).

ROUTINE DATA ANALYSIS

Transferred MCS data, along with downloaded NIMA ephemeris and clock data, and published Notice Advisories to NAVSTAR Users (NANUs), are combined to generate 3 groups of periodic reports: weekly, monthly, and quarterly.

The weekly report consists of an upload count plot (see Figure 1), which shows the number of navigation uploads transmitted to each SV over the previous week. A health scan is also done, and only those uploads transmitted while the SV was healthy are counted. This report grew out of a contingency upload list which formerly was manually transcribed from crew Payload Systems Operator (PSO) log records. Reasons for excessive uploads are listed on the chart. Typical reasons for additional uploads include AFS instability, momentum dumps, and eclipse season operations.

Weekly ERD plots (see Figure 2) are used to investigate reasons for extra uploads. These charts are compiled weekly, but not distributed due to their large file size.

Monthly reports include a constellation ERD summary, an upload count summary, an upload aging summary, and a NIMA vs. MCS clock stability comparison chart. The ERD summary chart (Figure 3) lists an average daily RMS value for the constellation (both with and without GPS IIR SVs included), along with a monthly average daily RMS summary by SV. Finally, notes describe the poorest and best performers in the GPS constellation.

The monthly upload summary (Figure 4) shows the average number of uploads per day (while SVs are healthy) for the entire constellation for the past 6 months. Also included in this report are the daily upload statistics for each SV for the current and previous months. A table at the bottom lists SV outages.

Monthly upload aging plots (Figure 5) are compiled each month for each SV over a two-week and 60-day duration for the period 2 months prior to the current month. In these reports, every upload built for each SV for the month is reconstructed and compared to NIMA precise ephemeris and clock data. Mean uploads for each SV are plotted. Over 6,000,000 data points are processed each month to generate the upload aging report. [1]

The NIMA vs. MCS comparison report is also accomplished on a monthly basis. This report compares the stability (Hadamard deviation) of the MCS Kalman clock phase estimates with the phase estimates derived through NIMA post-processing. This check is accomplished on a Windows-PC platform using Stable32 developed Hamilton Technical Services. Three examples are discussed in more detail in the next section.

In addition to weekly and monthly reports, the quarterly reports contain a 90-day ERD summary for each SV (average and RMS daily statistics), and an overall ERD summary (see Figures 6 & 7).

RESULTS OF DATA ANALYSIS

NIMA Vs. Kalman Comparison

Figure 8 is an example of a "good" stability comparison between NIMA and MCS Kalman data. In this case, the Hadamard deviation plots line up on top of each other for $\tau > 2000$ s. For $\tau < 2000$ s, there is some divergence, but as this occurs for every satellite in the GPS constellation, it is assumed that this is due to processing differences between the MCS and NIMA.

Figure 9 is an example of a "poor" comparison between NIMA and MCS Kalman data. In this case, the phase data supplied by the MCS Kalman filter indicates a more stable clock than NIMA's phase data. This is due to the process noise values (Q's) that are specific to that particular clock. As a clock's characteristics change over time, the process noise values are periodically updated. Since new process noise values are derived approximately once per quarter, it is possible that a frequency standard's current performance characteristics can be different than the performance characteristics as measured several months ago.

Figure 10 is an example of intentional clock-ephemeris "cross corruption" of MCS Kalman filter states. In this case, the frequency standard has known, time-dependent, periodic behavior. Since the MCS Kalman filter can not model periodic behavior in the clock states, the process noise values (Q's) are set artificially tight. In this manner, periodic behavior in the clock states is transferred to the ephemeris states. Although this results in the separate ephemeris and clock states being modeled improperly, the combination results in a more accurate navigation solution.

SVN 19 Frequency Step Analysis

On May 25, 2000, SVN 19's Cesium Frequency Standard #3 experienced a frequency offset shift of approximately 2E-12 s/s. Frequency jumps, although not common, are on-orbit anomalies that 2 SOPS operators expect from time to time. Although there is nothing that 2 SOPS can do from a hardware perspective to minimize the effect of such perturbations, proper MCS Kalman filter maintenance can ensure a minimal impact on navigation signal accuracy, as well as on the MCS crew workload.

Each satellite's process noise values (Q's) are optimized for day-to-day operations, and do not take anomalous behavior such as frequency steps into consideration. In the case just described, it is the job of 2 SOPS analysts to adjust the filter to allow for the frequency step. This is accomplished by re-initializing the clock process noise to a database value. This procedure is known as a clock "Q-bump."

The transferred Kalman data, along with a set of "truth" data (in this case post-processed NIMA data), provides valuable insight into this anomaly, its effects, and the 2 SOPS corrective action taken. Figure 11 shows a plot of the phase-derived NIMA frequency offset estimates for SVN 19 during the timeframe of the frequency step. As seen in the figure, the frequency offset shifted at approximately 18:00 Z on 5/25/00. Also seen in this figure is the MCS Kalman filter frequency offset estimate before any filter maintenance was performed (Pre-Q-Bump). It is seen that the MCS filter frequency offset estimate did not react instantaneously to the frequency step (as discussed, the filter is designed for prediction purposes, and nominally does not expect a sudden shift in frequency). Once MCS operators observed the problem, a clock state Q-bump was performed. The figure shows how the filter adjusted its frequency offset estimate to fall in line with what actually occurred on the spacecraft.

Figure 12 shows not only the NIMA (non-phase-derived, in this case) and MCS frequency offset estimates, but also how the MCS mismodeling affected the navigation signal. It is clearly seen that SVN 19's navigation signal accuracy was degraded during the period of misestimation, and the MCS crews were kept busy re-uploading the navigation message. (New uploads appear as downward spikes in ERD data.) However, it is also seen that once the clock Q-bump was performed and the spacecraft was uploaded with an adjusted navigation message, the ERD runoff was much less severe, and eventually performance returned to normal. This careful post-anomaly analysis allows us to refine operational recommendations and procedures to minimize navigation signal accuracy and GPS crew impacts.

SVN 22 C-Field Tune Analysis

The current operational method of changing a GPS frequency standard's output frequency is to tune its C-field. After a C-field tune is commanded, the previous MCS Kalman filter estimate of the clock frequency is incorrect, and a ranging error runoff will occur. To correct this error, 2 SOPS operators use navigation signal data collected at the MCS monitor stations to calculate the new clock frequency and update the Kalman filter's state estimates.

Figure 13 shows data from a C-field tune which occurred on SVN 22's Rubidium Frequency Standard #1 on 6/15/00. As is typical in the case of a C-field tune, the spacecraft was set unhealthy to users (this timeframe can be seen as the shaded area in the figure). In this case, one can observe from comparing NIMA frequency offset estimates to MCS Kalman filter estimates that the MCS estimate was not optimal at the conclusion of the C-field tune and associated filter maintenance. Although the MCS estimate was close enough that the spacecraft could be set healthy, several additional navigation message updates were necessary during the first couple days following the event. ERD levels did not stay consistently low until the MCS estimate caught up with the actual frequency offset.

CONCLUSION

The ability to transfer Kalman filter data from the MCS to an offline system has proven to be extremely valuable to Boeing navigation payload analysts. This capability has provided insight into many aspects of GPS navigation payload analysis, including frequency standard trending and anomaly resolution. Although the transfer process is currently fairly cumbersome, plans for the future include an emphasis on ease of use and automation. It is hoped that the continued utilization and refinement of this data transfer process will assist Boeing in not only improving frequency standard analysis techniques, but in continuing to provide 2 SOPS and the user community the best overall GPS support possible.

ACKNOWLEDGMENTS

The authors would like to gratefully thank the following individuals and organizations for their assistance with this paper and for their contributions to the GPS Program:

*Dr. John Berg, The Aerospace Corporation
The Boeing GPS Operations Team at Schriever AFB, CO
The Men and Women of 2 SOPS*

REFERENCES

- [1] G. E. Hatten, and J. V. Taylor "Navigation Upload Performance," Proceedings of ION GPS-00, September 2000.

Weekly Upload Count for Week 40, 2000

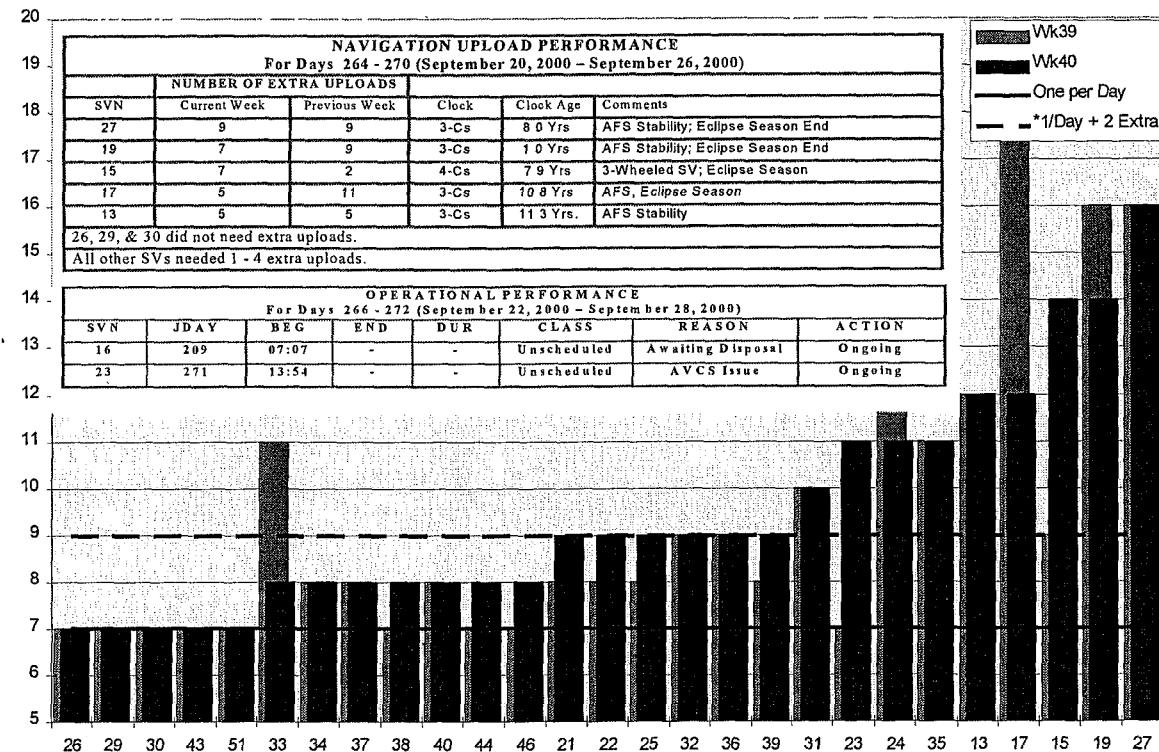


Figure 1. Weekly Upload Count Chart.

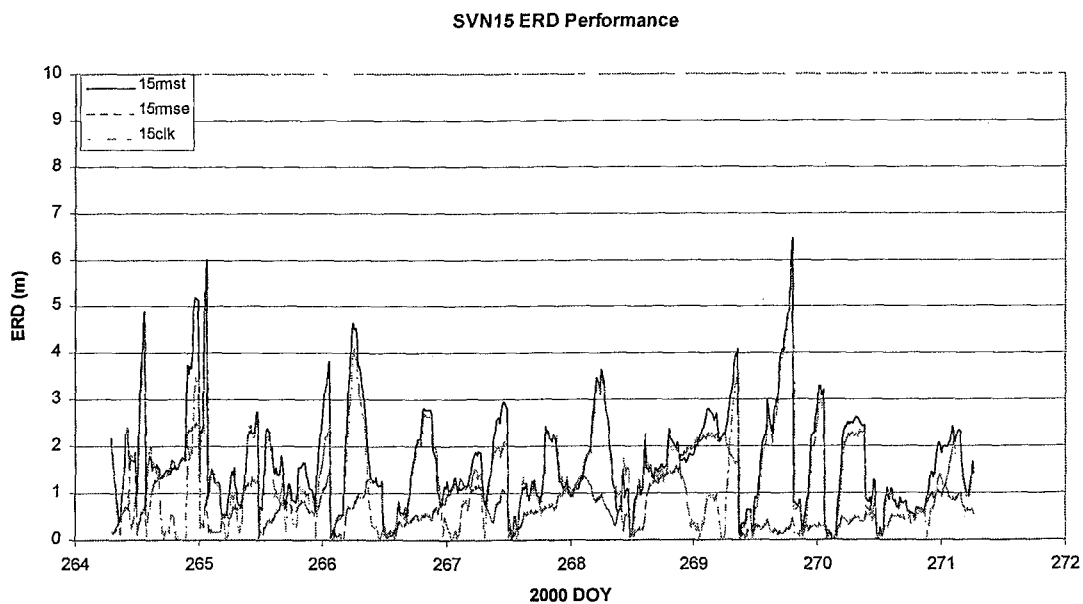


Figure 2. Weekly ERD Performance Chart (SVN15).

GPS Navigation Performance

(As exhibited by Estimated Range Deviation)

August 2000 - 1 Year Performance

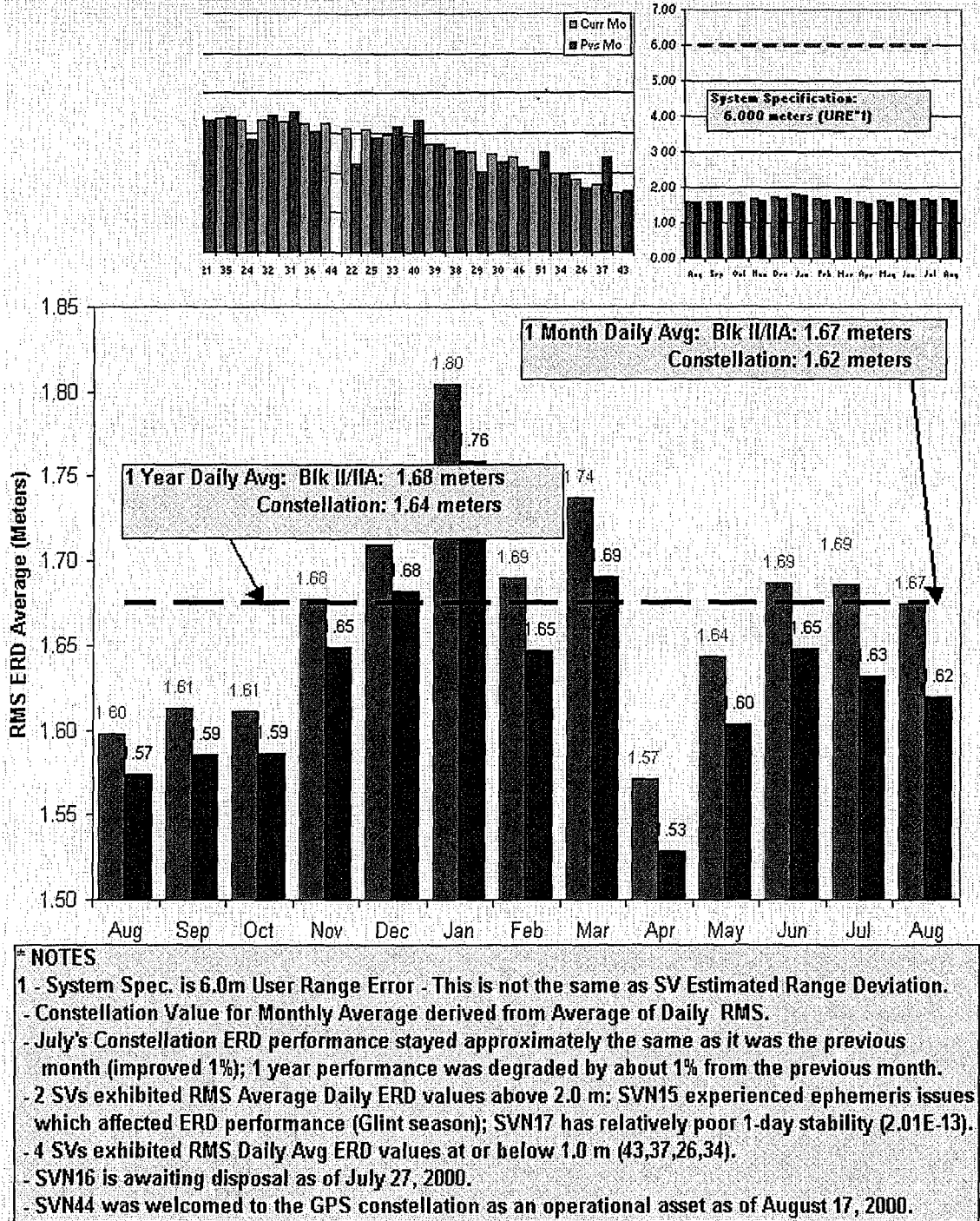


Figure 3. Monthly Navigation Performance Chart.

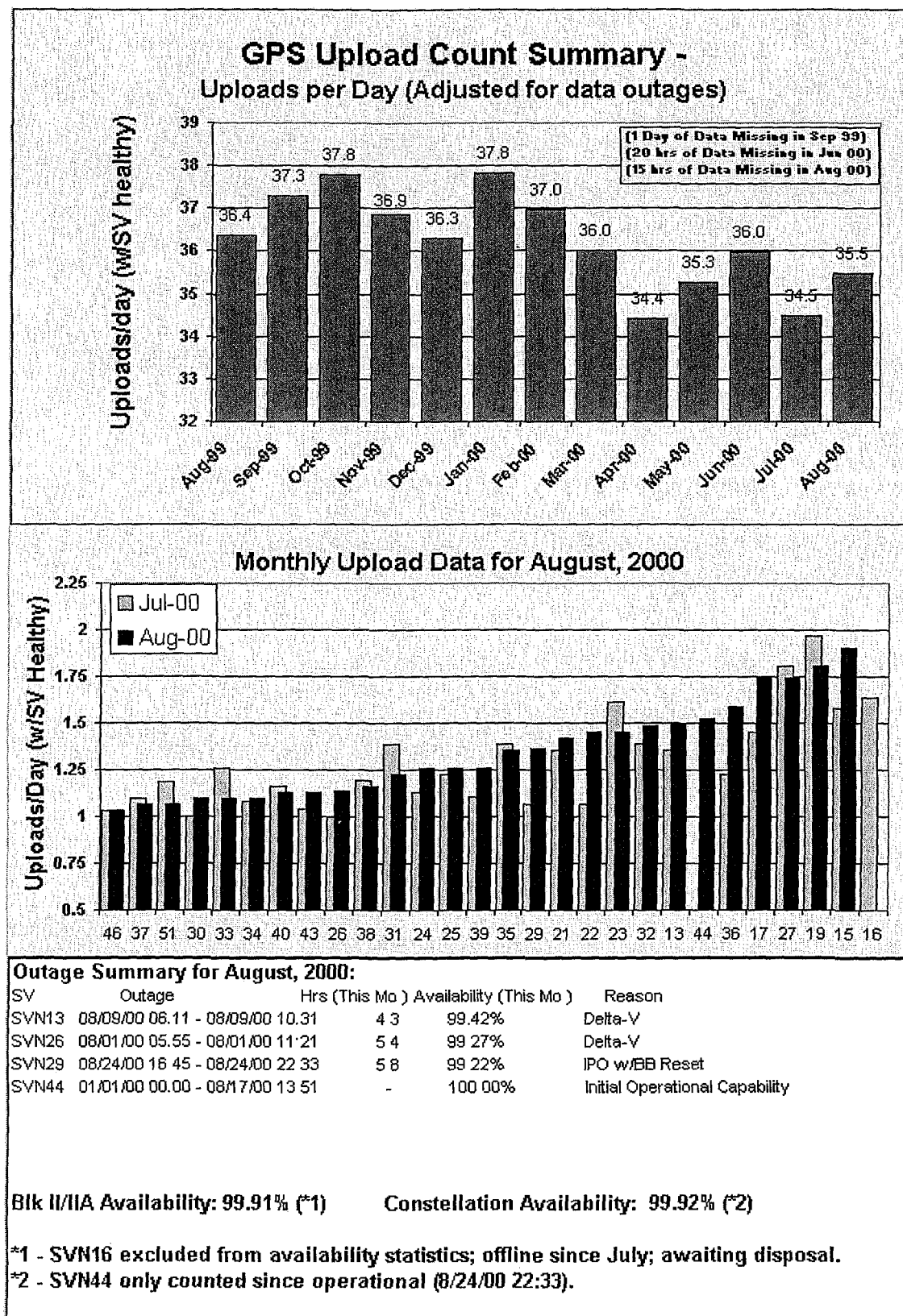
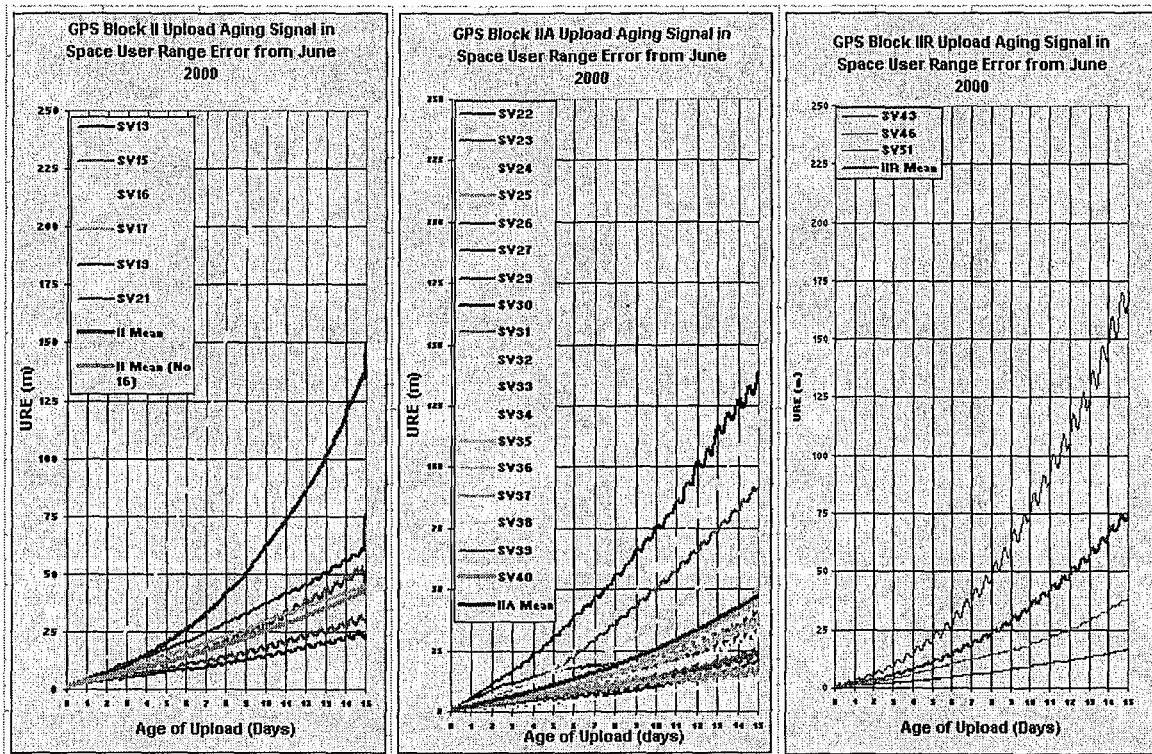


Figure 4. Monthly Upload Count Chart.



NOTES:

SVN16 Upload June 2000 UREs varied at 15 days from below 75 meters to over 1500 meters.

SVN18 was decommissioned during June 2000.

Bad upload data from SVN32 was edited out.

Figure 5. Upload Aging Chart (15 Days).

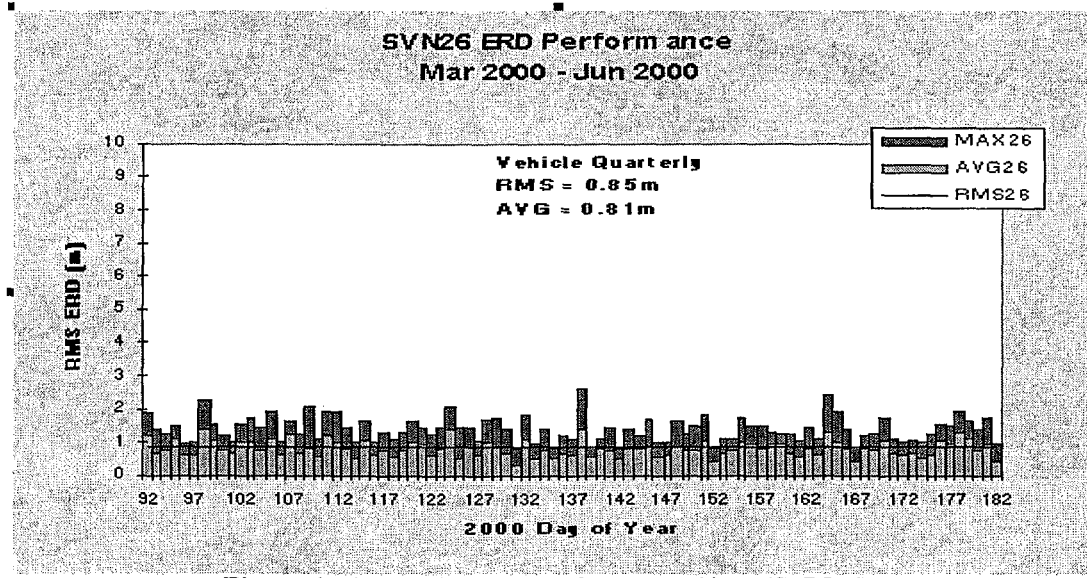


Figure 6. Quarterly ERD Performance Chart (SVN26).

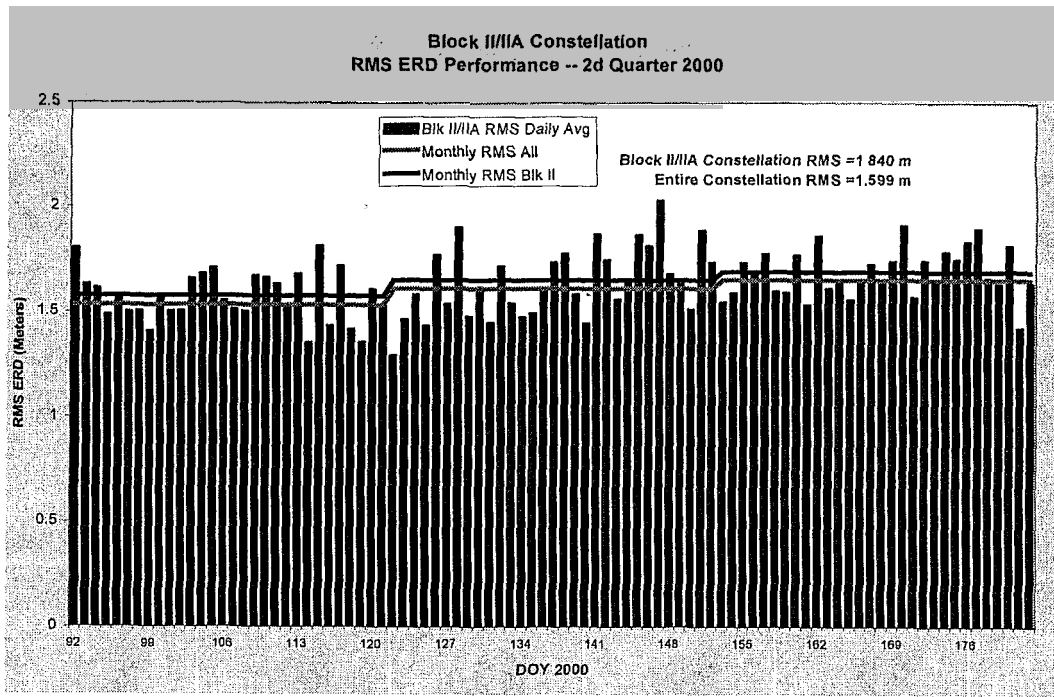


Figure 7. Quarterly ERD Constellation Performance Chart.

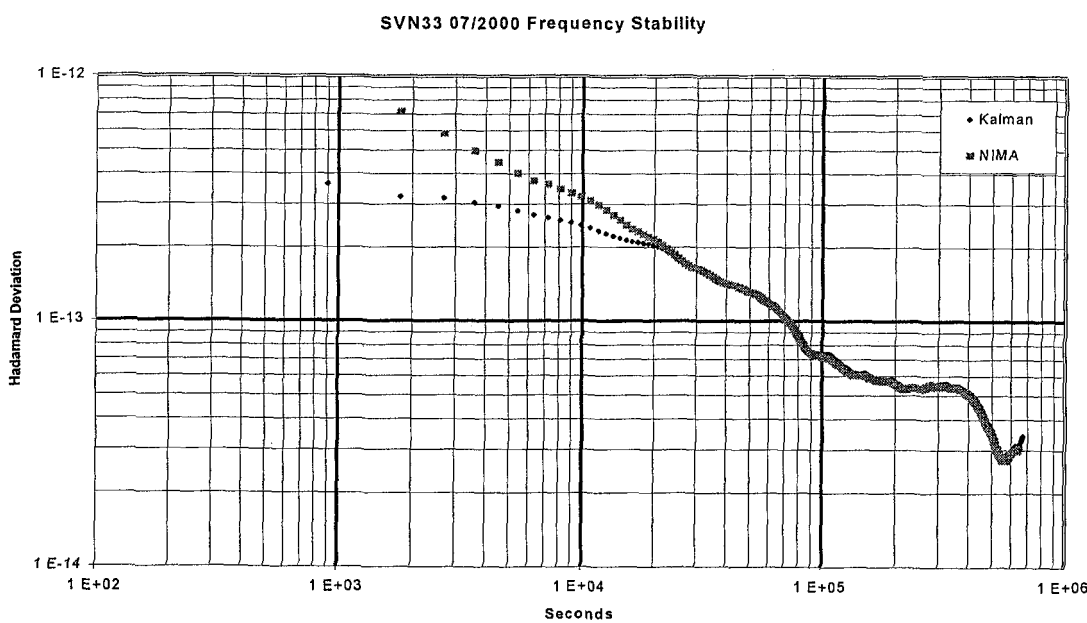


Figure 8. Example of “good” NIMA vs. MCS stability comparison.

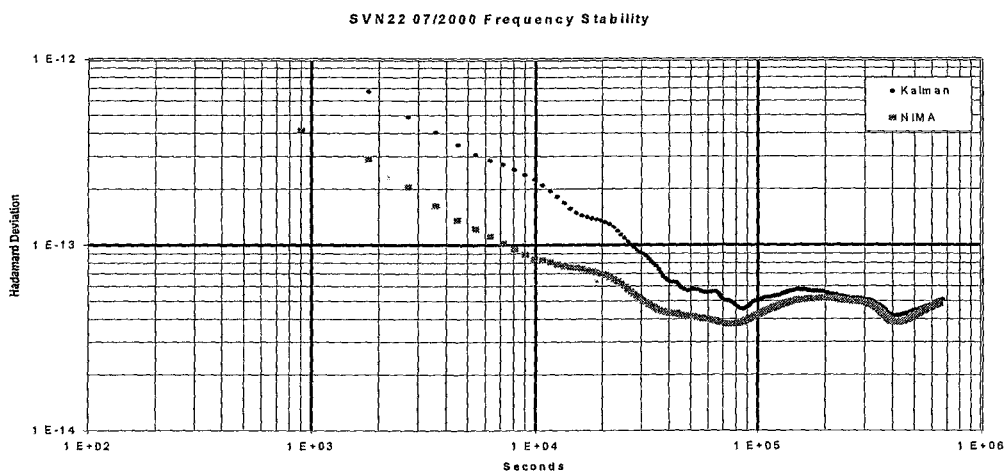


Figure 9. Example of “poor” NIMA vs. MCS stability comparison.

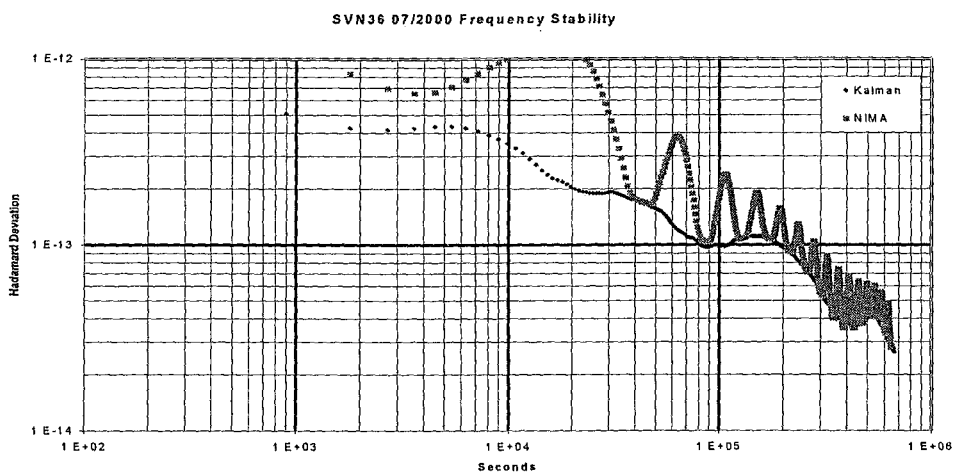


Figure 10. Example of MCS “cross-corruption”.

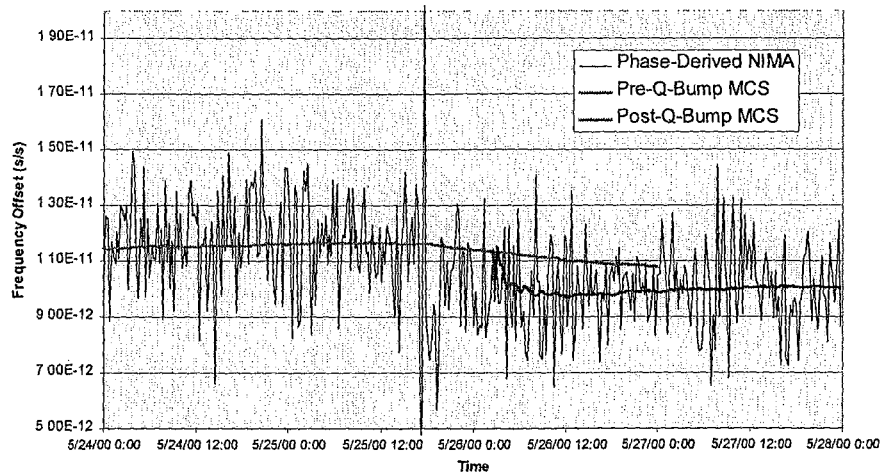


Figure 11. NIMA & MCS SVN 19 Frequency Offset Estimates.

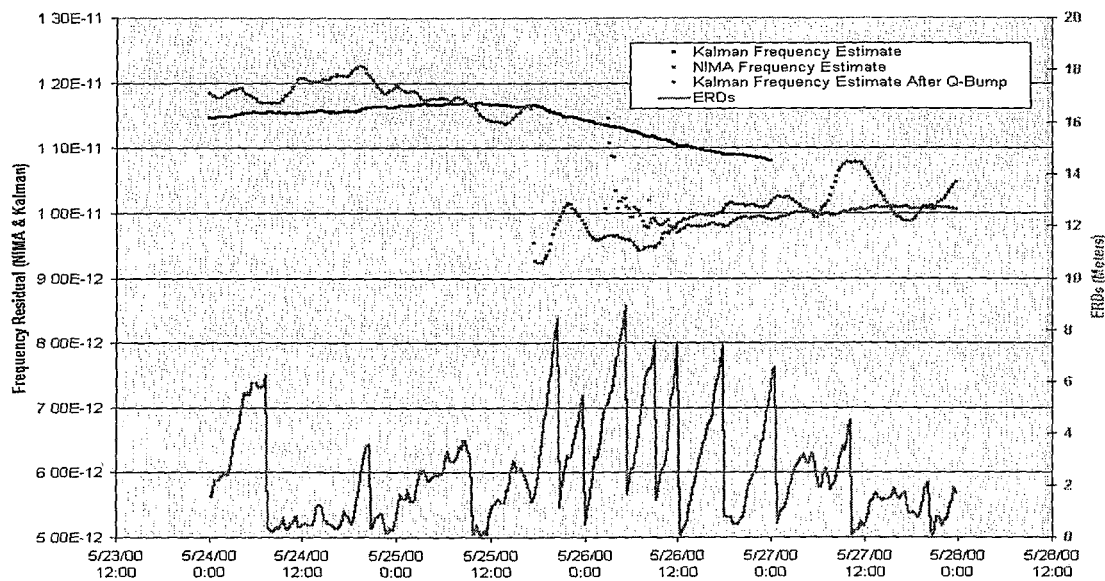


Figure 12. SVN 19 Frequency Step Impacts.

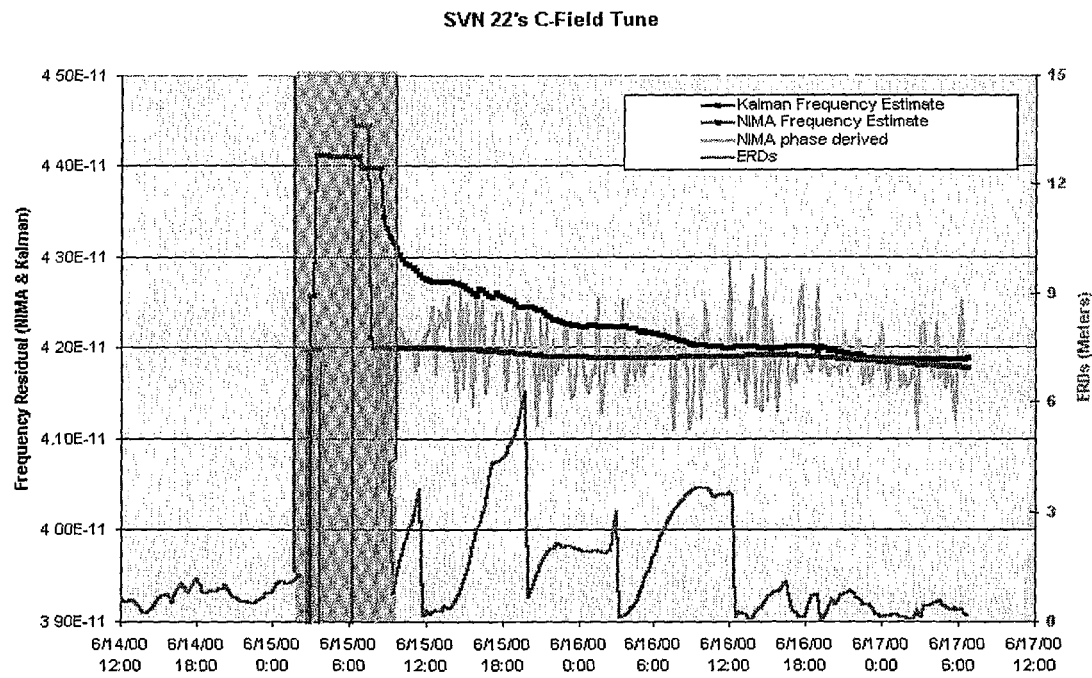


Figure 13. SVN 22 C-Field Tune Impacts.

THE DEVELOPMENT OF MULTI-CHANNEL GPS RECEIVERS AT THE CSIR — NATIONAL METROLOGY LABORATORY

E. L. Marais

CSIR-NML, P.O. Box 395, Pretoria, 0001, South Africa

Tel: +27 12 841 3013; Fax: +27 12 841 2131

E-mail: elmarais@csir.co.za

Abstract

The primary responsibility of the Time and Frequency laboratory of the CSIR-National Metrology Laboratory (CSIR-NML) is the maintenance of the South African time scale. To perform this duty, the highest level of accuracy in time transfer is required. To this end a multi-channel GPS receiver was developed in the Time and Frequency Laboratory, as a replacement for the NBS-type single-channel receivers. This paper discusses the development of this Motorola-based GPS receiver.

INTRODUCTION

In 1998 the Time and Frequency laboratory of the CSIR - National Metrology Laboratory (CSIR-NML) had to decide on its replacement strategy for the NBS type Allan Osborne and Associates (AOA) TTR5 and TTR5A single-channel Global Positioning System (GPS) timing receivers. These receivers would have stopped working at the GPS week rollover, which occurred on 22 August 1999 at 0h Coordinated Universal Time (UTC). It was extremely important to replace these receivers, as they formed the primary traceability link for time in South Africa at that time.

Several options were available to the CSIR-NML. These included replacing the firmware of the AOA receivers, purchasing new timing receivers and designing and building receivers in-house. The replacement of the firmware of the AOA receivers was ruled out due to cost and the age of the receivers. The purchase of new timing receivers was ruled out due to cost.

The most cost-effective solution to this problem was the development of new GPS timing receivers at the CSIR-NML. An additional benefit of this solution is the development of expertise in the operation of GPS receivers, generation of Consultative Committee on Time and Frequency (CCTF) Sub-group on GPS and GLONASS Time Transfer Standards (CGGTTS) GPS data format files, and interpretation of GPS timing results. Utilizing this solution also means that the GPS receiver could be upgraded with relative ease as new hardware becomes available, providing that the software interface remains compatible. An additional

motivation for choosing this solution is that several other laboratories around the world have decided to follow this route [1,2].

HARDWARE

Motorola has developed a GPS module specifically for use in timing applications, the model Oncore UT+. This module forms the basis for the GPS timing receivers designed and operating at the CSIR-NML. Most of the other timing centers use the older (and now discontinued) Motorola Oncore VP module.

In addition to these modules, each receiver consists of a power supply, data interface, and a Pentium-class computer for downloading data and computing results. A counter in time-interval mode is used for measuring the offset between the GPS One Pulse Per Second (1PPS) and the reference clock 1PPS (see Fig. 1).

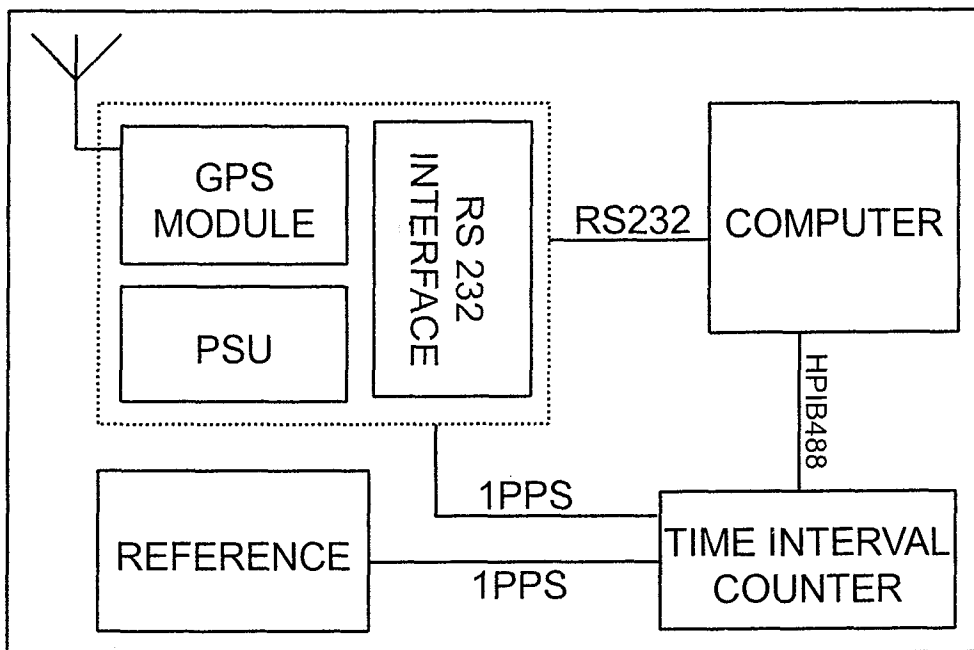


Fig. 1: Block diagram of GPS receiver.

The computers used are Pentium class machines, running either the Windows NT4 or the Windows 95 operating system. The software development language used was Borland (now Inprise) Delphi 4, with serial communication components by Turbo Power Software.

The counters used are Hewlett-Packard (now Agilent Technologies) model 53131A counters. These were the lowest cost counters with sub-nanosecond resolution and remote programmability available on the market at the time.

SOFTWARE

The software developed had to generate data files in the CGGTTS GPS data format [3]. For this to be possible, the contribution of each satellite to the timing solution generated by the receiver, had to be extracted. In addition, the offset between the reference and the receiver had to be corrected for the granularity of the receiver output.

Both this correction (known as the negative saw-tooth error) and the individual corrections for each satellite are extracted from the Motorola receiver using the '*En*' firmware command [4]. According to the CGGTTS directives, a Common View (CV) track is 780 seconds long, and has 52 data points, to which a least-squares linear fit is made. Each data point is the mid-way value of a fit to 15 consecutive readings (15 seconds) to which a quadratic least-squares fit is made.

At present the software developed for the receiver only calculates the average Elevation, Azimuth, and Time Transfer values (Mid-point value, slope, and delta-sigma values). The UT+ module does not provide a raw data output, which means that the internally generated values of the receiver must be used to report the calculated values. The atmospheric corrections used are not available, although the module does have a feature to turn the modeled ionospheric and tropospheric corrections on or off individually. Future versions of the receiver (most probably with new hardware providing raw data output) will include the modeled atmospheric corrections.

The computer software downloads several of the binary protocol messages from the GPS module. It also receives the time-interval measurement from the time-interval counter. During initialization the offset between the reference and the GPS receiver is adjusted through a Motorola firmware command to be within a 200 microsecond wide window, centered at 300 microseconds. This window is maintained continuously, although it should never be exceeded during normal operation. This feature ensures that proper timing is maintained for the signals. The offset introduced is subtracted from the result in software.

The first step is to correct the time-interval measurement for the negative saw-tooth error. This produces the corrected offset between the GPS receiver 1PPS and the reference 1PPS. The individual satellite contributions to the average 1PPS output by the receiver is then extracted and each observed satellite offset is calculated. These values are calculated every second.

If the receiver is within a common-view track, the calculated values for each satellite is stored and the relevant values, calculated according to the technical directives in [3], is computed and stored. In addition to the CGGTTS data, a 5-second average value is also stored in a separate data file.

The Motorola Oncore UT+ cannot be forced to track only one satellite, or set to track a specific satellite using a specified hardware channel. If a tracked satellite switches hardware channels during a track, that measurement is flagged as "bad." A comment is added after each recorded data track in the data file, stating which channel was used to perform the measurement.

PRELIMINARY RESULTS

More than a year of data is now available from each of the receivers, which were installed in the TF clock room in the week preceding the GPS week rollover. The calculated drift rates using the 5-second average

values and the GGTTS data files agree very well with the results calculated using the 3S Navigation R100/30T multi-channel receiver (reference receiver) CGGTTS data.

An offset has been noted between the Motorola and the reference receiver results, but it is not possible to determine the source of this offset at this time, as none of the CSIR-NML GPS receivers have been absolutely calibrated. A calibration receiver from the Bureau International des Poids et Mesures (BIPM) visited the CSIR-NML during 1999, and the results of this calibration are expected soon. Once the results are available, it will be possible to calibrate all the other GPS receivers of the CSIR-NML.

In Fig. 2 and 3 below the results for one of the Motorola GPS receivers are shown for a week and a month. In Fig. 4 and 5 the results for the reference receiver is shown for the same period.

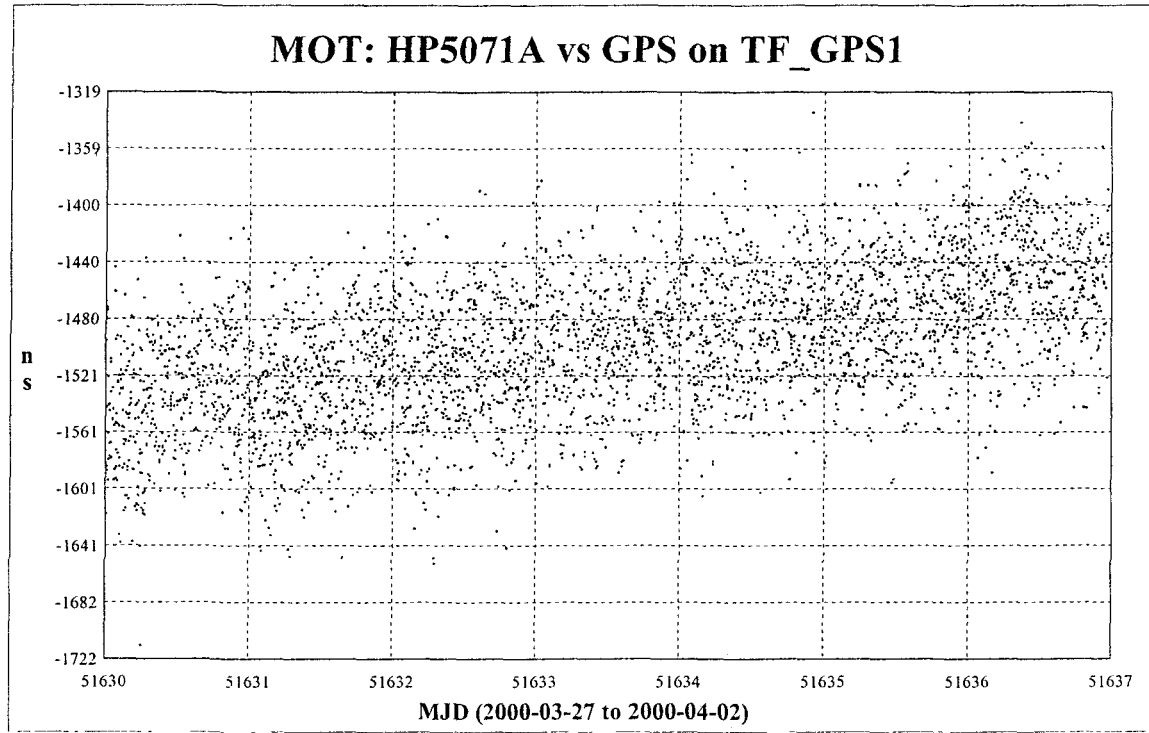


Fig. 2: Motorola data for MJD 51630 to 51636.

The weekly data plot is generated using all full (duration of 780 seconds) tracks for the observation period, with the full dataset being filtered using a 3-sigma filter. An additional constraint is placed on the 3-sigma filter, that being a maximum allowable standard deviation of 1 microsecond (at present).

The monthly data plot is computed using all full (duration of 780 seconds) tracks for the observation period, with the daily average and standard deviation being computed from a 3-sigma filtered subset of the data (each subset is 1 day's data). The 3-sigma filter has an additional constraint, this being a maximum allowable standard deviation set at 1 microsecond (at present).

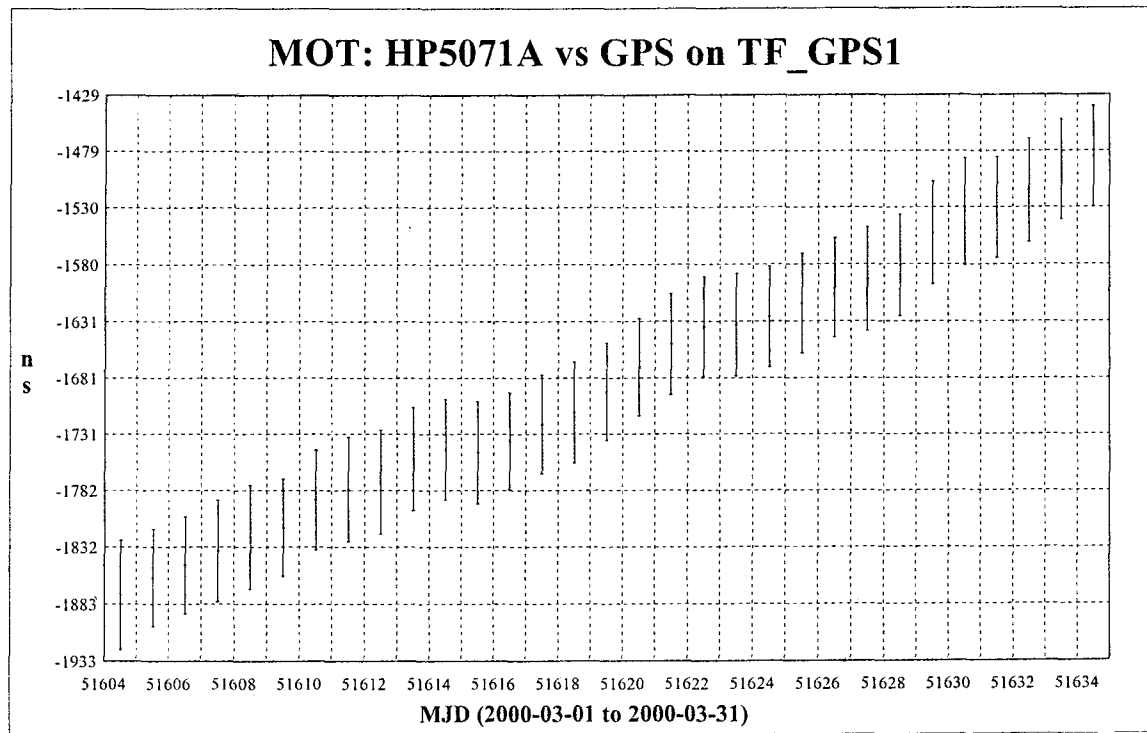


Fig. 3: Motorola data for March 2000.

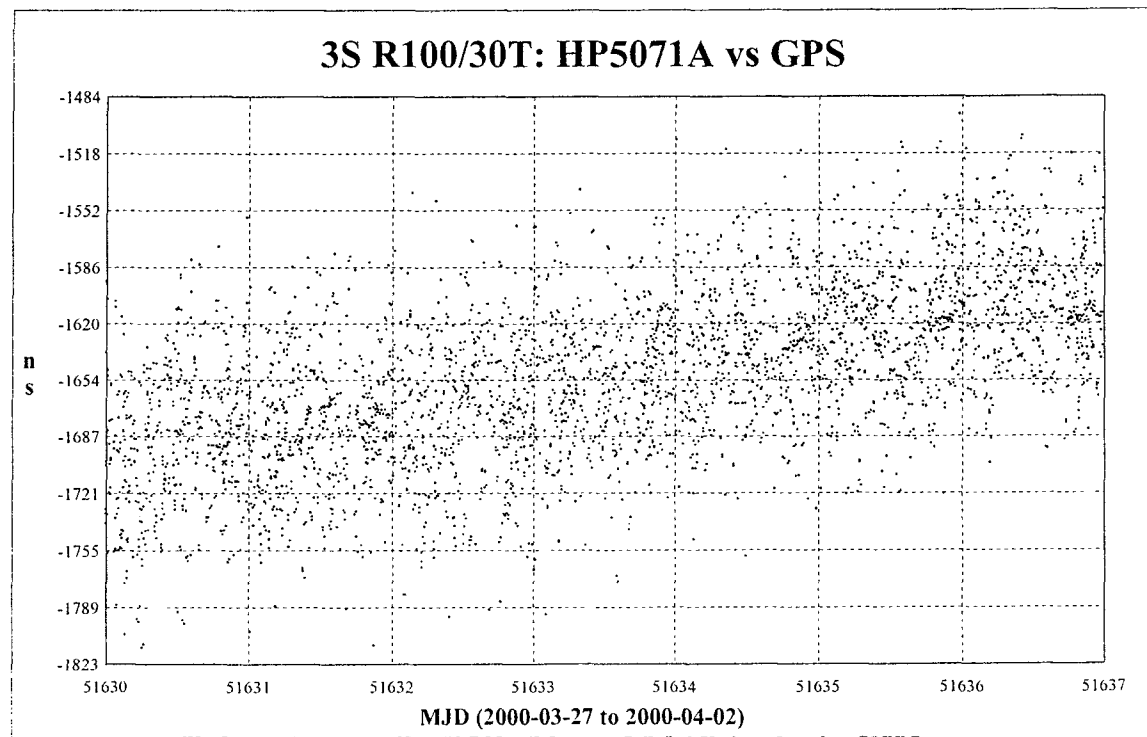


Fig. 4: 3S Navigation R100/30T data for MJD 51630 to 51636.

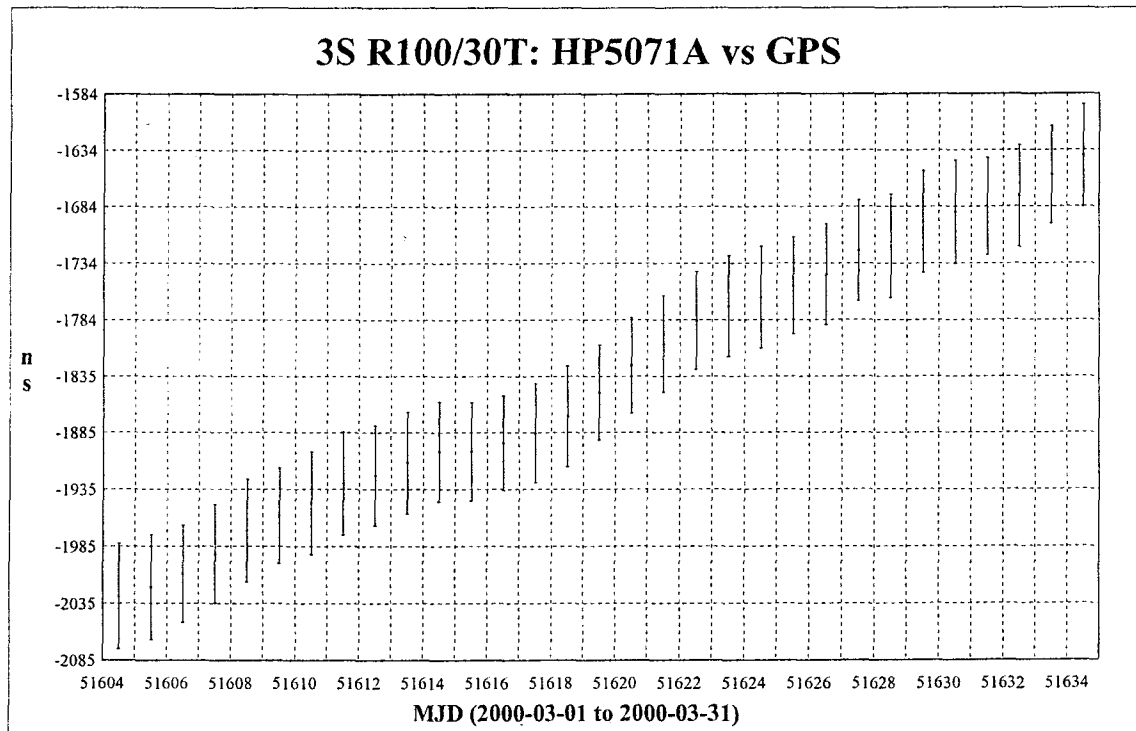


Fig. 5: 3S Navigation R100/30T data for March 2000.

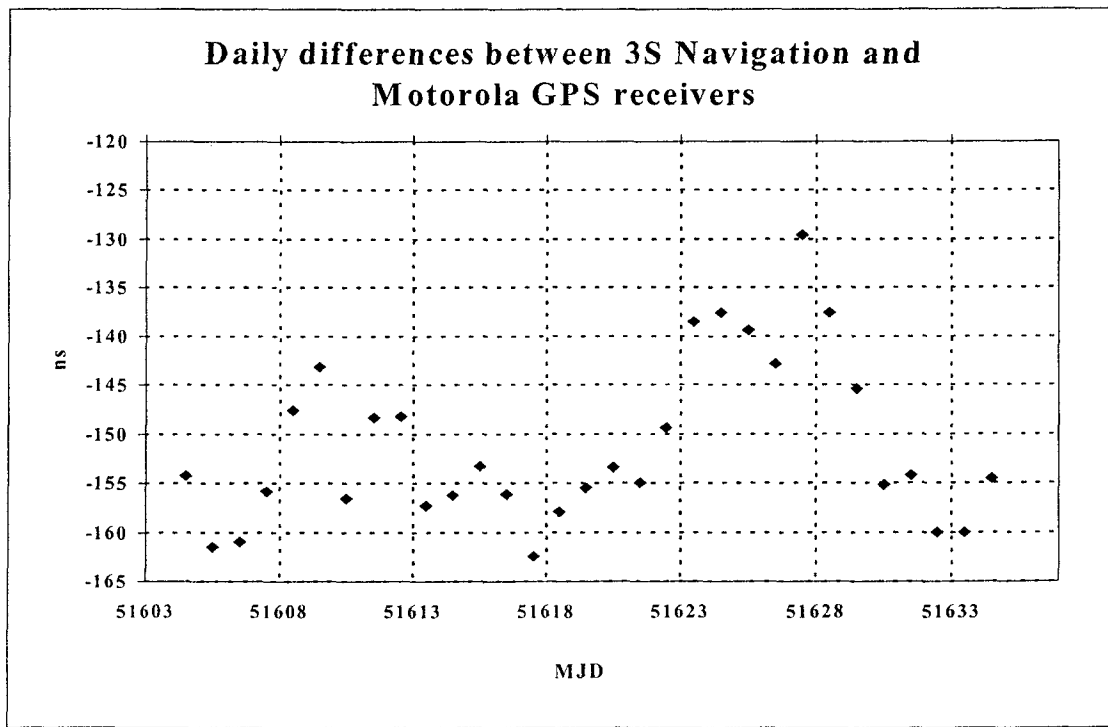


Fig. 6: Daily averages of offset between 3S Navigation R100/30T and Motorola receiver.

The offset between the two receivers for March 2000, as shown in Fig. 6, was found to be -151.2 ns, with an uncertainty of 63.6 ns. The uncertainty was calculated using the average uncertainty for each receiver, combined in a root-sum-square fashion with the uncertainty for the offset, which was 8.4 ns. This is not the best method for determining the offset, as the values are most probably not statistically independent.

The relative high noise on the results obtained can be attributed to a number of effects. Since no detail study of these differences have been made, it is not possible to pinpoint the sources of these differences. One or more of the following can contribute to these differences: Motorola antenna not temperature compensated, cables exposed to direct sunlight in daytime, position of Motorola antennas not known with very high accuracy, inaccuracy of ionosphere and troposphere correction models in one or both receivers, and perhaps some others.

FUTURE WORK

Further development of the Motorola-based GPS receivers are underway. The new M12 Oncore receiver from Motorola is being evaluated at present. This module may be a worthwhile replacement for the discontinued VP Oncore receiver, used in many parts of the world as the engine for GPS timing receivers. It is hoped that the M12 will overcome some drawbacks of the UT+ Oncore.

In parallel to the Motorola Oncore M12 evaluation, an investigation of the capabilities of the u-Blox MS-1 receiver module is underway. This receiver uses the SiRF chipset, and can output raw GPS data. A project is also underway to build a low cost temperature-stabilized antenna (TSA), based on the patch antennas available from Motorola, as these TSAs reduce time transfer uncertainties considerably [5].

DISCLAIMER

Certain trade names and company products are mentioned in text of this paper. In no case does such mention imply recommendation or endorsement by the CSIR - National Metrology Laboratory, or the CSIR, nor does it imply that the products are necessarily the best available for the purpose.

REFERENCES

- [1] J. B. Bullock, T. M. King, H. L. Kennedy, E. D Berry, and G. Zanfino 1997, "*Test results and analysis of a low cost GPS receiver for time transfer applications*," IEEE Publication 97CH36016, Proceedings of the 1997 IEEE International Frequency Control Symposium, Orlando, Florida, USA, pp. 314-322.
- [2] J. Levine 1999, "*Time transfer using multi-channel GPS receivers*," IEEE Transactions on Ultrasonics, Ferroelectrics, and Frequency Control, UFCC-46, 392-398.
- [3] D. W. Allan and C. Thomas 1994, "*Technical directives for standardization of GPS time receiver software*," Metrologia, 31, 69-79.
- [4] "*Oncore User's Guide*," Revision 3.2, Motorola, 1997.
- [5] W. Lewandowski, P. Moussay, J. Danaher, R. Gerlach, and E. Levasseur 1997, "*Temperature-protected antennas for satellite time transfer receivers*," Proceedings of the 11th European Frequency and Time Forum (EFTF), March 1997, Neuchâtel, Switzerland, pp. 498-503.

ONE-WAY GPS TIME TRANSFER 2000

Al Gifford

**National Institute of Standards and Technology
325 Broadway, Boulder, CO 80303, USA**

Scott Pace
Rand Corporation

Jules McNeff
SAIC

Abstract

On 1 May 2000, the White House issued a Presidential directive for the Global Positioning System (GPS) to turn off Selective Availability (SA) on 2 May 2000. For nearly a decade, authorized user performance of one-way synchronization via GPS has improved every single year. This paper provides an annual assessment of how well the Global Positioning System can predict and disseminate UTC (USNO) to these specified users, based on data generated and processed by the United States Naval Observatory (USNO). And, because the recent Presidential directive now permits civilian timing users to exploit nearly the same, impressive time transfer accuracy of GPS, these annual metrics now offer a fairly representative performance assessment for both military and civilian timing users.

INTRODUCTION

Many worldwide users of precise time utilize “one-way” GPS time transfer, also known as “direct-access” GPS time transfer. In the direct-access GPS technique, a user can access a globally available common time reference, UTC(GPS) [1], by employing only one receiver and taking advantage of the available information in the broadcast GPS navigation message [2]. UTC(GPS) is GPS’s real-time prediction of UTC as maintained by USNO, known as UTC(USNO), and UTC(GPS) is traceable to UTC(USNO). Empirically, this traceability has recently been at the 6-7 ns (1 sigma) level. The worldwide availability of UTC(GPS) satisfies the intent of both Presidential and congressional mandates to actively promote GPS as a global standard [3,4].

Direct-access GPS time transfer is mandated by the Master Positioning, Navigation and Timing Plan, [CJCSI 6130.01b] as the primary means for all Department of Defense (DoD) systems to access precise time [5]. Direct-access offers advantages over point-to-point time transfer techniques (GPS common view and Two-Way Satellite Time Transfer) that are most useful for military or military-related systems. Though point-to-point techniques are suitable for high accuracy applications, direct-access GPS time transfer doesn’t require station-to-station communications between users and other ground receiver systems. Thus, direct-access GPS users can operate autonomously, in anonymity. Direct-access GPS

¹The terminology “UTC(GPS)” is inconsistent with internationally accepted timing nomenclature in which the abbreviation in parentheses following “UTC” is meant to refer to a timing laboratory that contributes clock data to the formation of the international standard UTC(BIPM) and is steered to UTC(BIPM). The clocks used to create the independent GPS time scale are not used in the formation of UTC(BIPM) and GPS timing information is steered to UTC(USNO). The terminology “UTC(GPS)” used by the authors does not appear in U.S. Air Force documentation. –the Editor

time transfer has become a significant service for a diverse array of both military and civilian applications.

The United States Naval Observatory (USNO) performs around-the-clock monitoring of the GPS broadcast of time. USNO monitors three main time scales/references: 1) individual satellite time, 2) GPS ensemble time (the GPS Composite Clock), and 3) UTC(GPS). USNO currently employs keyed dual-frequency (L1 and L2) receivers, capable of tracking P(Y)-Code, to perform this monitoring function. USNO forwards daily time transfer information, gathered and processed from these receivers, to the GPS control segment, which is operated by the 2d Space Operations Squadron (2 SOPS). 2 SOPS, in turn, uses these USNO data to, among other purposes, keep UTC(GPS) aligned with, and traceable to, UTC(USNO).

As many know, not all GPS time transfer receivers are key-able, and therefore, not all GPS receivers can track P(Y)-Code. These civilian, or “unauthorized” receivers may not realize the same performance that keyed, or “authorized” sets benefit from. In particular, since the granularity of the civilian C/A-Code is a factor of ten worse than P(Y)-Code, some civilian users may experience slightly less accuracy than military users; however, some manufacturers have, for the most part, overcome this accuracy reduction with digital tracking algorithms. Also, the inability to track P(Y)-Code can translate into the unavailability of dual-frequency ionosphere measurements; however, techniques, such as codeless dual-frequency, exist to produce ionospheric measurements that are almost as good as those produced by pure dual-frequency code tracking.

Additionally, users who choose to augment GPS receiver systems with atomic frequency standards and all-in-view processing techniques can realize even further improved performance. This paper exclusively reviews the recent performance of direct-access GPS time transfer for *authorized* users in a fixed [surveyed] location scenario.

CURRENT TIME TRANSFER PERFORMANCE

Figure 1 shows a plot of the daily UTC(GPS)-UTC(USNO) time transfer root-mean-square (RMS) and average (AVGERR) errors for January 1999 through September 2000. This metric essentially indicates how well GPS is predicting and delivering precise time for the DoD. During this period, the time transfer was 6.32 ns RMS. That is, a fixed-location authorized user, tracking one satellite at a time, typically obtained DoD precise time with an accuracy of about 6.32 ns, 1 sigma. These numbers will not necessarily represent typical error figures for all users, particularly if certain users operate unauthorized receivers, have significant surveyed location biases or calibration errors, or experience unusual problems with multipath, troposphere modeling, or environmental stability.

Numerous enhancements at both the GPS Master Control Station (MCS) and USNO have contributed to this level of performance, well below the UTC(GPS)-UTC(USNO) budget total of 28 ns (1 sigma), listed in the USNO/2 SOPS interface control document, ICD-GPS-202 [6]. The GPS Program Office is currently reviewing documentation related to this error budget. Recently, USNO agreed to reduce its Measurement calibration uncertainty allocation from 12 ns (1 sigma) down to 3 ns (1 sigma) [7]. Assuming the other contributing error budget components remain unchanged, this USNO change would drop the overall error budget from 28 ns (1 sigma) to 25.5 ns (1 sigma) [8]. See Figure 2.

GPS-UTC(USNO) PERFORMANCE

A critical element in the delivery of UTC(GPS) to users is the GPS timescale, called the GPS Composite Clock, labeled herein simply as GPS. Typically, direct-access GPS time transfer users obtain satellite time by locking onto a broadcasting GPS vehicle, subsequently obtain GPS time by correcting for satellite clock offsets in subframe 1 of the navigation message, and finally obtain UTC(GPS) by applying GPS-UTC(USNO) corrections in subframe 4, page 18 of the navigation message. [2].

The stability of GPS-UTC(USNO) significantly affects the performance of UTC(GPS)-UTC(USNO), and usually serves as a second indication of how well GPS is delivering precise time. The daily GPS-UTC(USNO) offsets, corrected for leap seconds, for January 1999 through September 2000, are displayed in Figure 3. GPS remains well within ICD-GPS-200's specification for $|GPS-UTC(USNO)|$, 1000 ns, corrected for leap seconds [2].

It is important to note that, contrary to popular opinion, GPS time *was never designed* to represent the DoD's precise time source, UTC(USNO). Rather, GPS time serves as a stable timescale *internal* to GPS. For this reason, GPS time is not tightly synchronized to UTC(USNO). Instead, the MCS steers GPS time only to keep its offset from UTC(USNO), corrected for leap seconds, within the limits of the 1000 ns specification. GPS time steering is currently significantly below the noise level of GPS time itself, over satellite upload prediction spans. With this level of steering, the MCS is easily able to meet the 1000 ns specification without significantly degrading the stability of GPS time. By the way, users who want GPS's closest prediction of UTC(USNO) should make use of UTC(GPS), obtained by using the timing information in subframe 4, page 18.

GPS TIMESCALE STABILITY

The stability of $|GPS-UTC(USNO)|$, based on daily GPS-UTC(USNO) data points provided by USNO from October 1999 through September 2000, is presented in Figure 4. The 1-day stability for 2000, 1.53×10^{-14} , is consistent with typical performance demonstrated in recent years.

Note how the Allan deviation slope gradually changes to -1 at a tau value of around 10 days, indicating the finite bounding of GPS-UTC(USNO). Additionally, note that the effective instability caused by GPS steering, at most, *never* approaches the inherent noise level of GPS-UTC(USNO) for $\tau = 1$ day. One-day stability is especially important, since 1 day is the nominal GPS navigation upload prediction span. These indicators again demonstrate the effectiveness of GPS's time steering algorithm—long-term synchronization at a very small sacrifice to short-term stability.

Also shown within the same figure is a plot of the stability of UTC(GPS)-UTC(USNO), showing the superior long-term ($\tau > 1$ day) stability of UTC(GPS) as compared to GPS time, highlighting a difference between the purposes of GPS time and UTC(GPS). GPS time is designed for stability over nominal satellite upload prediction spans (0-24 hours); UTC(GPS) is designed to deliver a prediction of UTC(USNO). The superior long-term stability of UTC(GPS) as compared to GPS time is a byproduct of

this design. However, UTC(GPS) does exhibits inferior short-term ($\tau < 1$ day) stability as a result, because of the additional uncertainty of the subframe 4, page 18 time transfer parameters.

NEAR-TERM ENHANCEMENTS

Under current operations, 2 SOPS downloads USNO-generated time transfer information once per day, shortly after 1500 UTC. 2 SOPS utilizes a 486-based computer, connected to a voice phone configured as a modem, and software written in-house. This current setup is not officially integrated into the MCS architecture, and therefore has no maintenance support or configuration control/management. Given the criticality of GPS's time transfer mission to the world, the community is currently pursuing the establishment of a more formal interface between USNO and the MCS.

Several agencies, including the GPS Program Office, the Aerospace Corporation, 2 SOPS, USNO, and the National Imagery and Mapping Agency (NIMA) have recently participated in technical discussions of possibilities for formalizing a USNO-MCS data transfer interface. The discussions have covered possibilities that would make use of the SIPRNET secure network and/or existing communication lines between USNO, NIMA, and the MCS, to pipe USNO data into the MCS in near-real time.

The establishment of a near-real-time data interface between USNO and the MCS opens up possibilities for optimizing GPS-UTC(USNO) predictions in the MCS. Under current operations, the MCS predicts GPS-UTC(USNO) using the two most recent daily estimates of GPS-UTC(USNO), generated by USNO using a least-squares fit on a 37-hour batch of individual satellite tracks based on broadcast parameters.

Were the MCS, in the future, to obtain the individual tracks in near-real time, the MCS would experience major benefits. In particular, near-real-time transfer of these satellite tracks would permit the MCS the ability to apply corrections for known observables in MCS files, which are, in particular, the MCS Estimated Range Deviations (ERDs). Applying these corrections would refine the quality of individual satellite tracks by removing known broadcast errors. The MCS would, in turn, send these refined tracks into a two-state Kalman filter designed to optimize estimation and prediction, tailored for the noise types and levels inherent to the system. In essence, optimized estimation and prediction of GPS-UTC(USNO) means that each satellite upload would have the most current, and accurate parameters in subframe 4, page 18 of the navigation message. Translation—an optimization of GPS's delivered prediction of UTC(USNO). See Figures 5 and 6.

Additionally, near-real time data availability would permit around-the-clock direct access GPS time transfer performance monitoring. The MCS monitors satellite ranging performance around the clock, it does not currently have the ability to similarly monitor time transfer or GPS timescale stability. A formalized, near-real time data interface between USNO and the MCS would change this.

The security, documentation, programmatic, and support issues associated with the establishment of a formalized data interface are not insignificant. Ultimately, the community's realization of the critical dependence of GPS time transfer mission on the USNO-MCS interface will dictate the priority of establishing formality to this data interface.

LONG-TERM GOALS

In order to satisfy the intent of both Presidential and Congressional mandates to actively promote GPS as a global time standard [3,4], a change in the GPS time transfer paradigm must occur. The perception that GPS is a noisy transponder of UTC(USNO) must change. In reality, GPS provides an independent time scale [GPS time] and a prediction of the offset between GPS time and the DoD Master Clock. Because direct-access GPS time transfer users apply this predicted offset, broadcast in subframe 4, page 18, these users are, in effect, realizing UTC(GPS). The operational and hardware changes required to realize the vision of GPS as a distributed space-based clock are minimal. These changes will be documented in a follow-on paper which will be offered to the PTTI Manager, the GPS Joint Program Office, the Interagency GPS Executive Board and the National and International timing communities for their consideration. The goal of this dialog is to reach consensus on the roadmap and technical end states for GPS Time Transfer. These actions will be a part of on-going implementation of the GPS Presidential and Congressional direction to make GPS useful to civilian users around the world.

CONCLUSION

Worldwide civil and military applications are just beginning to realize the power and utility of GPS as a space-based common time reference. 2 SOPS and USNO, along with other agencies, have sustained the outstanding performance of UTC(GPS) and remain committed to improving GPS time transfer in the future. In the near term, the formalization and automation of the USNO-MCS data interface to an around-the-clock operation will enhance the integrity and performance of UTC(GPS). In the long term, many in the community anticipate that the Global Positioning System will gain acceptance worldwide as an independent, space-based distributed clock.

ACKNOWLEDGMENTS

The authors wish to thank:

Captain Michael Rivers and Captain Ronald Chernak of 2 SOPS, for their data and consultation.
Steven Hutsell, for his support of the GPS time transfer mission over the years.
Captain Curtis Hay, GPS JPO, for his initiative in improving the USNO-MCS interface.

REFERENCES

- [1] The terminology "UTC(GPS)" is nontraditional in that the term in parentheses normally refers to a timing laboratory which contributes to the formation of international standard time UTC(BIPM). However, in the opinion of the authors, "UTC(GPS)" accurately reflects the fact that large numbers of users around the world are taking UTC time directly from GPS and this is leading to the use of GPS time as a convenient and distinct standard. In addition, promoting the use of GPS as a global standard for positioning, navigation, and timing is required by presidential policy, U.S. legislation, and international statements such as the U.S.-Japan Joint Statement on GPS.
- [2] ICD-GPS-200, Revision C, 10 October 1993, IRN-200C-002, 25 September 1997.

- [3] White House Fact Sheet, “*U.S. Global Positioning System Policy*,” from the Office of Science and Technology Policy, National Security Council, 29 March 1996.
- [4] United States Code, Title 10, Subtitle A, Part IV, Chapter 136, Section 2281, “Global Positioning System”, 27 January 1998.
- [5] CJCSI 6130.01 b, “*2000 CJCSI Master Positioning, Navigation and Timing Plan*,” 15 June 2000.
- [6] ICD-GPS-202, Revision A, 13 December 1996.
- [7] USNO-MCS Time Transfer Memorandum of Agreement, 2000.
- [8] S. Hutsell, “*A Statistical Analysis Of The GPS Time Transfer Error Budget*,” Proceedings of the 51st ION Annual Meeting, Colorado Springs, CO, 5-7 June 1995, pp. 421-428.

Actual Performance

*UTC(GPS) - UTC(USNO), Keyed Receiver
Based on 24 hours of 13-minute tracks*

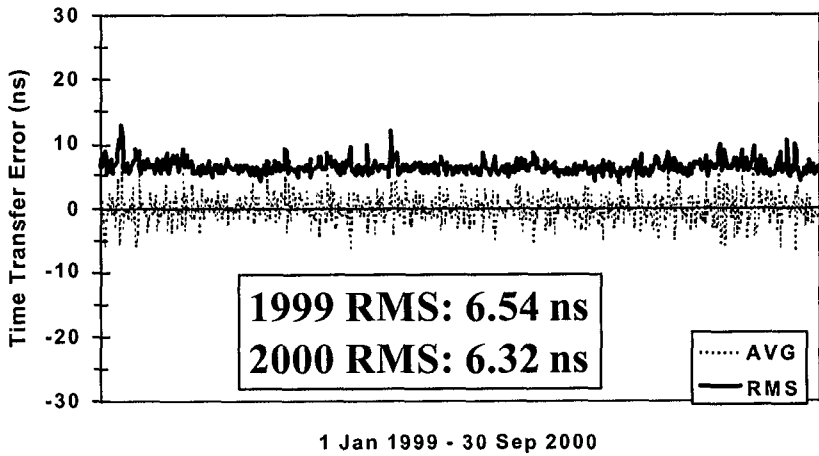


Figure 1. UTC(GPS) – UTC(USNO) Root Mean Square and Average Error

Time Transfer Error Budget

Fixed Location User (ns)

■ Component	Spec	PPS (Typical)
■ <u>USNO Measurement</u>	<u>3</u>	2-3
■ GPS Prediction	9.7	2-4
■ SV Component	20	5-7
■ User Component	12	2-5
■ Totals (RSS)	25.5	6-10

Figure 2. 2000 GPS Time Transfer Error Budget

GPS-UTC(USNO)

Corrected for Leap Seconds
Specification: +/- 1000 ns

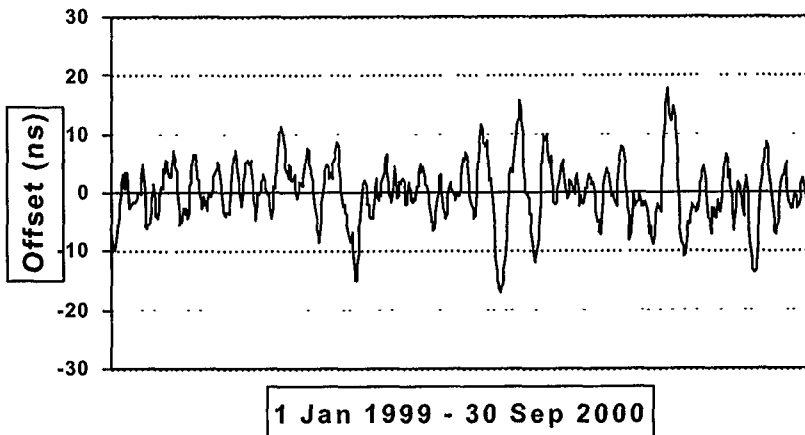


Figure 3. Daily GPS – UTC(USNO) Offset

Timescale Stability

1 Oct 1999 - 30 Sep 2000

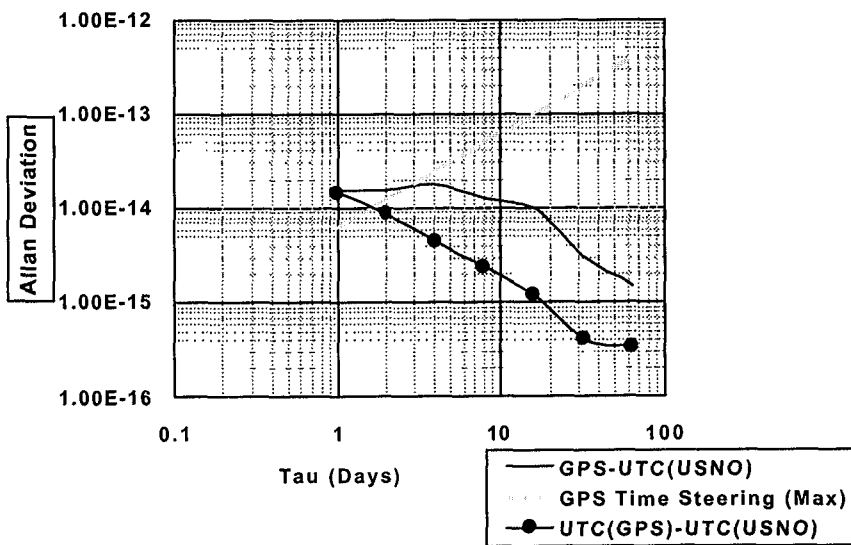


Figure 4. Timescale Stability: GPS Time vs. UTC(GPS)

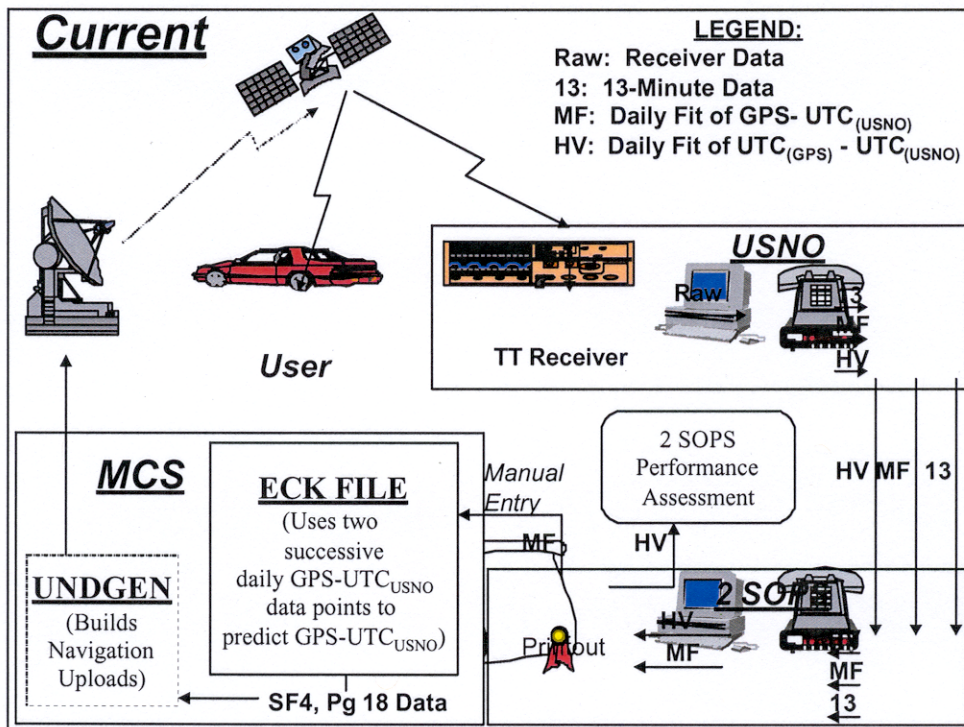


Figure 5. Current USNO – MCS Time Transfer Data Interface

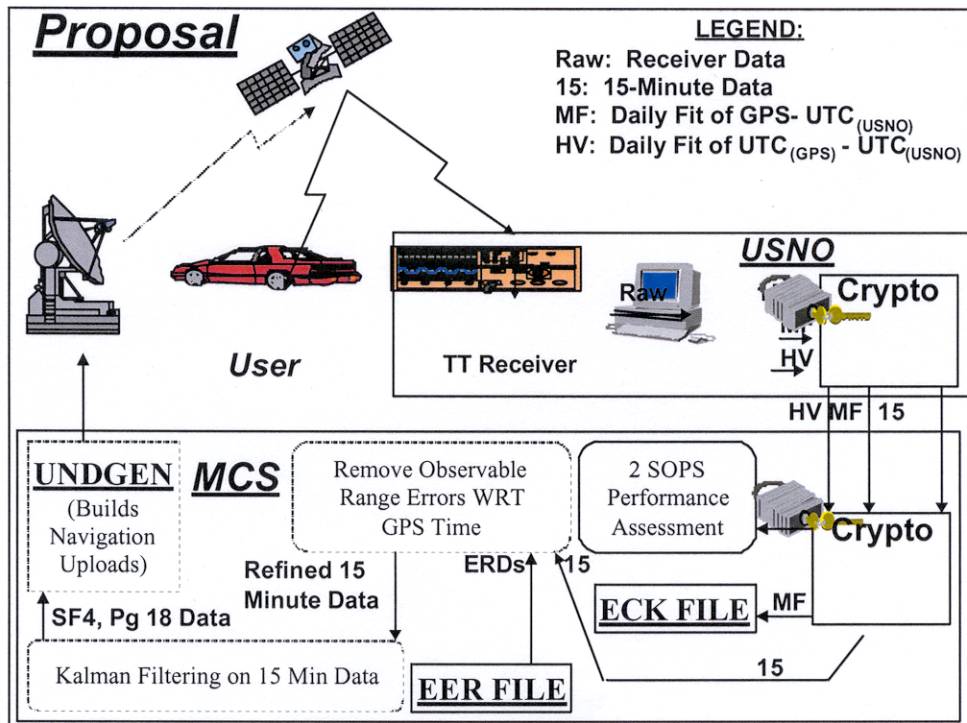


Figure 6. Proposed USNO – MCS Time Transfer Data Interface

COMMON-VIEW AND MELTING-POT GPS TIME TRANSFER WITH THE UT+

F. Meyer

Laboratoire d'Astrophysique de l'Observatoire de Besançon (LAOB)
UPRES-A CNRS 6091, Observatoire de Besançon
41 bis avenue de l'Observatoire, BP 1615, 25010 Besançon Cedex, France
E-mail: fmeyer@obs-besancon.fr

Abstract

I report results of GPS time transfer realized in France between the BNM-LPTF (Bureau National de Métrologie-Laboratoire Primaire du Temps et des Fréquences) at the Paris Observatory (OP) and Besançon Observatory (OB) using an Oncore UT+ receiver, Motorola's last evolution of precise-time-capable GPS receivers. So-called "melting pot" measurement sessions, where all visible satellites are tracked to produce one average time measurement, were conducted and are reported on. A solution to overcome the poor set of controlling commands of the early versions of the UT+ to lead single-satellite common-view is presented, together with experimental data. The performance reached by the two methods is discussed against their respective constraints. Performance is evaluated by comparisons with data acquired through classical time dedicated GPS receivers (Sercel NRT2 and AO TTR5). An operational solution allowing frequency comparisons to the French national standards at the level of a few 10^{-14} over a 1-day averaging time, based on UT+ melting-pot measurements, is presented.

INTRODUCTION

For several years now, the Observatory of Besançon has been operating GPS links to national time standards, for both academic and industrial laboratories. Two different categories of hardware are involved in the realizations of these links :

- time dedicated "classical" receivers;
- all-purpose, small format, cheap receivers, but with comparable metrological performances.

Among the last category, Motorola's Oncore receivers have been shown to exhibit surprising metrological qualities [1] that have triggered the interest of the time & frequency community. The VP oncore has been the most achieved realization and it has been tested and utilized by a certain number of teams throughout the world for the past years.

One of the reasons for its success was, apart from its good time capabilities, a very complete internal software command set offering a wide control over the behavior of the receiver, and the availability of raw navigation and timing data allowing for example multichannel operations [2], testing of ionospheric models [3], or quality time services [4].

Unfortunately, the VP has been discontinued and replaced by the UT+. If the intrinsic timing capabilities of the UT+ seem to be at least as good as the VP's, the same cannot be said about the internal software. Only a reduced command set is available and it excludes all raw navigation and timing data ; with the early released units (internal software version prior to 3.0, July 1998) it was even impossible to assign a given satellite to a given channel; thus, following a schedule as BIPM's was impossible. So before 3.0 units appear, a method to overcome these weaknesses has been developed and is presented here.

COMMON-VIEW TIME TRANSFER

Workarounds to UT+ Reduced Command Set

Receiver with a software version 3.0 and on

Common-view time transfer with the UT+ looks impossible, since this unit lacks the commands controlling satellite ID-to-channel assignment. Fortunately, latest versions of the receiver internal software (software version 3.0 and on) have support for an "ignore satellite" command that allows the user to set an ignore list; ignoring all but the desired SV allow easy following of a standard common-view schedule.

Receivers with a software version prior to 3.0

Even receivers with an older software version can be under certain conditions used in common-view conditions: in this case, it is possible to achieve these kind of measurements between two stations by using one of the rare feature provided by the unit, that is to set a satellite elevation mask angle that allows only those satellites with an elevation above this mask angle to be tracked. By choosing an appropriate mask angle, it is sometimes possible to have the receiver track only one satellite (the highest satellite in view, of course). Provided the second station is not too far away, there are some periods of time during which one and the same satellite is the highest visible satellite at both sites and then can be tracked in common-view at both locations.

Scheduling in this case implies that each site has the ability to predict satellite elevations with a precision below 1 degree. This can be achieved using the satellite ephemeris set contained in the almanac data, that the UT+ can provide on demand.

Of course there are a number of situations where such scheduling gives no solutions, the constraints on the scheduling process are the following:

- The granularity of the mask angle that can be specified to the UT+ is 1 degree
- The satellite elevation output by the receiver (and that serves to decide whether or not a satellite is above the mask angle and, hence, whether or not it will be tracked) can eventually show a somewhat bizarre behavior (for example for a rising satellite, the elevation output may happen to be successively 29, 30, 29, 30, 31,.. degrees) that can lead to no satellite being tracked if the mask angle has been set at 30 degrees.
- The duration of a common-view session (which has been set to a standard 13 minutes); this duration is the time during which the highest satellite in view must remain the same at both sites. Of course, the probability that this condition can be fulfilled decreases as the length of the session increases.

From these constraints, I elaborated the scheduling algorithm whose description follows.

The goal of the algorithm is to output a series of dates representing the beginning of tracking sessions, associated to a pair of mask angles, one for the local site, one for the remote site; the algorithm may be run periodically, e.g. each day at both sites.

The algorithm examines for each minute the constellation of visible satellites and makes some tests to see:

1. Is there a satellite whose elevation is 'really'¹ above the other satellites'

- (a) if yes, is it the same situation at the remote location ?

- i. if yes, will this situation have at least a duration greater than the scheduled track length (i.e. examine what the configuration will be in, say 13 minutes if we adopt that track length) ?

- A. if yes, add the selected date to the schedule.

- B. if no, examine next minute.

- ii. if no, examine next minute.

- (b) if no, examine next minute.

Here is a sample of the output of the algorithm for a given MJD: stations are OP (Observatoire de Paris) and OB (Observatoire de Besançon) 324 km southeast from Paris.

```
SchedBuildSchedule: (SCV) 14 22 09 41 42
SchedBuildSchedule: (SCV) 14 36 09 42 43
SchedBuildSchedule: (SCV) 14 51 09 43 44
...
SchedBuildSchedule: (SCV) 22 38 03 66 44
SchedBuildSchedule: (SCV) 22 53 03 67 44
SchedBuildSchedule: (SCV) 23 07 03 68 44
```

First 2 numbers are the time UTC of the beginning of the track; next is the satellite PRN, then an index, and finally the index of the next scheduled track. The index shows that 68 tracks can be scheduled in 1 day (this number does not significantly change over time for a given pair of stations).

Other tests have given similar results between

1. OP and a station located 700 km south (average of 56 daily tracks);
2. OP and a station located 500 km west (average of 61 daily tracks).

Single common view experimental results

Figure 1 shows 2 sets of data: one acquired with classical GPS receivers (AO TTR5

¹By really, I mean without ambiguity considering the constraints mentioned above about the 'granularity' of the mask and the uncertainty on the satellite elevation as output by the receiver. In practice, 'really' means that the elevation difference between the highest satellite and the one whose elevation is immediately below is at least 2 degrees.

at OP and Sercel NRT2 at OB) following BIPM's standard schedule; the second set of data was acquired using 2 UT+ units following the above described common-view schedule. Each point represent a 13-minute tracking processed as recommended by the CCDS. All the UT+ receivers that were used have a software version 2.2, and do not support the "satellite ignore" command, making standard common-view scheduling impossible. Of course, the acquisition dates have no reason to match between the 2 sets. The two sets are in good agreement. The average slope is -2.35 ns/day with the TTR5/NRT2 receivers and -2.42 ns/day with the UT+ receivers. The latter are a little bit more noisy, with an rms of 7.8 ns versus 5.6 ns for the TTR5/NRT2. These data have been recorded before removal of the SA, but it has negligible influence on such short baseline links when operating in common-view. These results confirm that the UT+ timing capabilities are very similar to those of the VP oncore unit [3].

MELTING-POT TIME TRANSFER

Receiver Setup

The different receivers used where:

- at the BNM-LPTF (OP): 1 Allen Osborne TTR5 GPS receiver (ttr5op), 1 motorola UT+ GPS receiver (ut+op)
- at Observatory of Besançon (OB): 1 Sercel NRT2 GPS receiver (nrt2ob) and 3 motorola GPS receivers (ut+ob1, ut+ob2, ut+ob3)

The time reference at the BNM-LPTF is UTC(OP), realized by a HP5071A, and Cs172(OB) at OB, both being realized by HP5071A-001 cesium clocks. Data acquisition with the ttr5op, nrt2ob receivers of course follow the BIPM standard common-view schedule, extended to 86 daily tracks. On the UT+, data acquisition was scheduled at the same dates in order to provide simultaneous measurement results, thus simplifying postprocessing.

Melting-Pot Experimental Results

Figure 2 allows comparisons between UT+ melting-pot time transfer and common-view data obtained with classical time-dedicated GPS receivers. Figure 2 shows three sets of data, all being measurements of the difference between UTC(OP) and Cs172(OB) (HP5071A-001); data from the upper plot have been obtained through the pair of receivers (ut+op, ut+ob1), while the lower plot was obtained with (ut+op, ut+ob3); the third plot has been derived from data obtained via (ttr5op, nrt2ob).

For each set of data the standard deviation is indicated for each period of 24 hours. It ranges from roughly 4 to 6 ns for (ut+op, ut+ob1); it is a little lower for (ut+op, ut+ob3) around 4 ns and still lower around 2.5 ns for the time dedicated receivers. The next 2 figures show the Allan deviation (together with a multivariate fit and the associated confidence interval) for (ut+op, ut+ob1) and (ttr5op, nrt2ob); the lesson of these plots is that the UT+ is suitable to perform frequency transfer at the level of 10^{-13} or better for an averaging time of 1 day.

OPERATIONAL CONSIDERATIONS

A system based on common-view GPS measurements with low-cost receivers has been

operational at the Observatory of Besançon since 1998: laboratories can link their frequency reference to the national standards at the BNM-LPTF, under the control of the french standards authority BNM (Bureau National de Metrologie) and COFRAC (COmite FRAncais d'accréditation). The original system (still in operation) uses the VP oncore and the BIPM common-view schedule. In the new version, the VP is replaced by the UT+ and melting pot operations where data acquisition are synchronized to the BIPM schedule, simplifying possible comparisons with other common-view data sets. The supporting operating system MSDOS has been replaced by a Linux platform, (see annex for details), which provides much more flexible operations. From the final user point of view, operations can now be virtually completely automated. Data can be sent to the reference laboratory on a regular basis (a periodicity of one week seems reasonable) either through a direct modem line or through (permanent or on-demand) IP connectivity. Data are then processed and linked to the national standards and results can then be downloaded by the user using the same link. An official certificate is then issued on a monthly basis.

CONCLUSION

We have shown that the UT+ can be used to compare frequencies at the level of a few 10^{-14} for a one day averaging time. Common-view and melting-pot operations have been shown to have roughly the same performances. In the latter case, the BIPM schedule can be discarded, even if, for compatibility considerations, tracking times are still derived from it. A way of linking one's frequency to the French national standards has been built around this hardware and requesting laboratories will install the first operational systems in December 2000. Important software evolutions and new opportunities have permitted to offer to the final user highly simplified procedures ensuring proper data processing and a more user-friendly graphic interface together with enhanced monitoring capabilities.

ACKNOWLEDGMENTS

This work is supported by the Bureau National de Métrologie.

REFERENCES

- [1] R. Giffard 2000, "Estimation of GPS ionospheric delay using L1 code and carrier-phase observables," Proceedings of the 31st Precise Time and Time Interval (PTTI) Systems and Applications Meeting, 7-9 December 1999, Dana Point, California, USA, pp. 405-417.
- [2] J. Nawrocki, W. Lewandowski, and J. Azoubib 1998, "GPS multi-channel common-view time transfer using Motorola Oncore receiver with CCDS standards," Proceedings of the 12th European Time and Frequency Forum (EFTF), 10-12 March 1998, Warsaw, Poland, pp. 510-515.
- [3] W. Lewandowski, P. Moussay, P. Guerin, F. Meyer, and M. Vincent 1997, "Testing Motorola Oncore GPS receiver for time metrology," Proceedings of the 11th European Time and Frequency Forum (EFTF), 4-7 March 1997, Neuchâtel, Switzerland, pp. 493-497.
- [4] P. T. H. Fisk, R. B. Washington, M. A. Lawn, and M. J. Wouters 2000, "Time and frequency activities at the CSIRO National Measurement Laboratory, Sydney, Australia," Proceedings of the 31st Precise Time and Time Interval (PTTI) Systems and Applications Meeting, 7-9 December 1999, Dana Point, California, USA, pp. 211-218.

ANNEX Some considerations about software solutions to operate one (or more) UT+ and a GPIB board under Linux

Operating system and language

As mentioned in the paper, the early version of the system runs under MSDOS. MSDOS is reliable for what it can do, but is now kind of a Jurassic OS: not multitask, not multiuser and all the consequences. From MSWindows and Linux, we choose the latter for reliability, flexibility, and free access. Programming language is C.

User interface

The graphic user interface was developed using *glade* (<http://glade.pn.org>); glade is basically a graphic frontend to ease graphic interfaces creation. It outputs a bunch of boring C code, that it is still possible to manually modify in case of problems.

The controlling software that was obtained allow remote control of the unit, provided IP connectivity exists to the remote unit. This is a very valuable and time sparing option when testing units at different sites.

Figure 5 shows a screenshot of the user interface; gnuplot, a free plotting software, can be used to continuously and graphically monitors the data being taken, allowing a quick detection of problems.

Time interval counter, GPIB operations

Controlling the time-interval counter often involves the use of the GPIB bus. Unfortunately until recently, GPIB board manufacturers did not offer GPIB drivers for the Linux platform. The only known possibility was the driver developped as part of the Linux Lab project; still it is limited to 2.0 kernel versions and seems to be no longer supported. National Instruments has started the development of a Linux driver for its PCI GPIB card. This driver was used for this experiment. It showed no problem except for the IRQ processing; further tests are needed to check whether or not the driver is the cause of the problem. Anyway, this is not a real concern as far as only one measurement has to be acquired each second.

For now, our software supports Stanford Research SR620 (serial port) and Hewlett-Packard HP53132A time-interval counters, but alternate counter support could be added very easily.

Contact the author for further details.

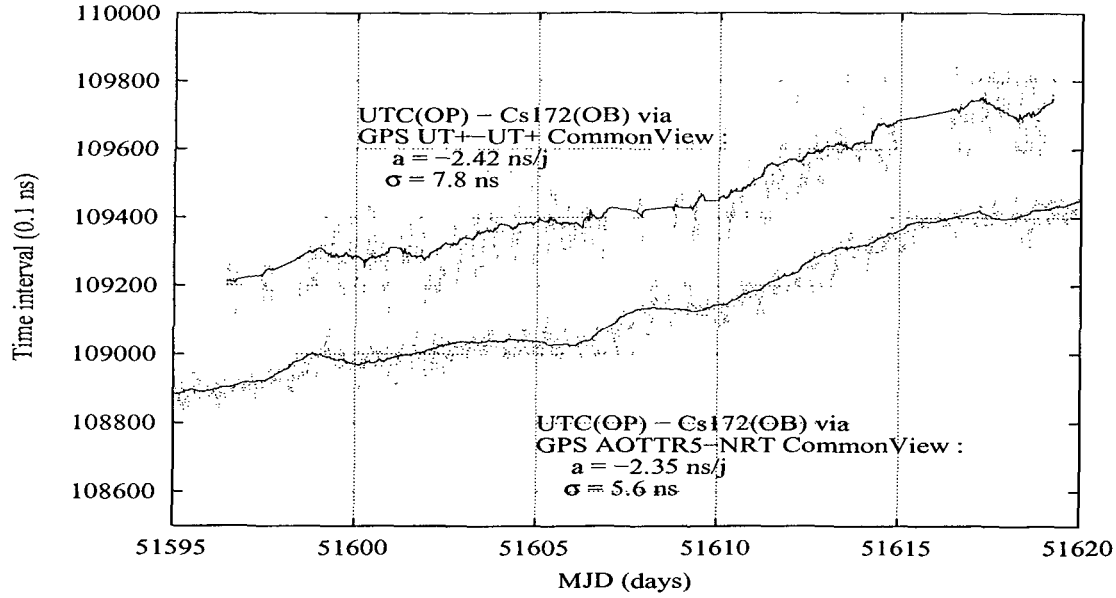


Figure 1: Common-view UT+ measurements compared to common-view NRT2/AOTTR5:
plot of UTC(OP) - GPS(ttr5op) - (Cs172(OB) - GPS(nrt2ob))
and UTC(OP) - GPS(ut+op) - (Cs172(OB) - GPS(ut+ob))

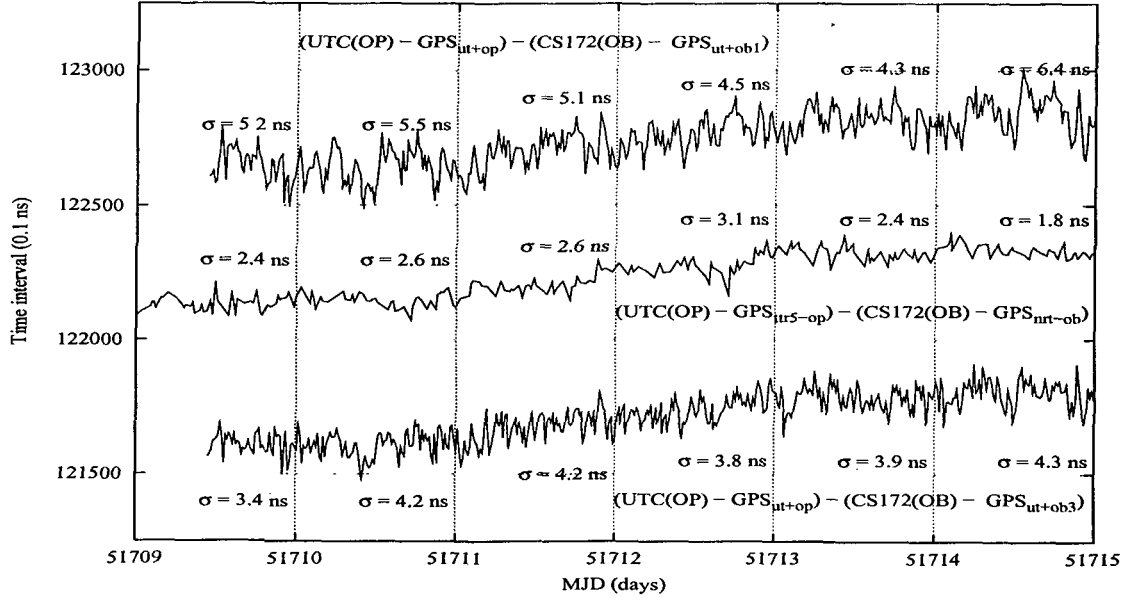


Figure 2: Melting-pot UT+ measurements compared to common-view NRT2/AOTTR5:
(2 different UT+ units were used at OB)
plot of UTC(OP) - GPS(ttr5op) - (Cs172(OB) - GPS(nrt2ob))
UTC(OP) - GPS(ut+op) - (Cs172(OB) - GPS(ut+ob1))
UTC(OP) - GPS(ut+op) - (Cs172(OB) - GPS(ut+ob3))

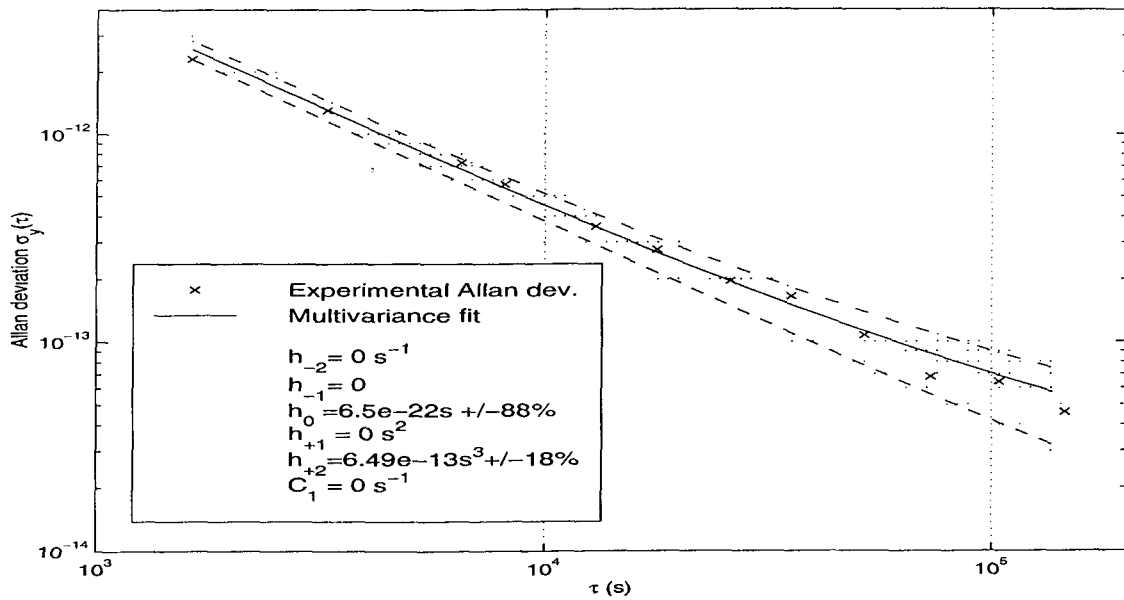


Figure 3: Allan deviation of UTC(OP) - GPS(ttr5op) - (Cs172(OB) - GPS(nrt2ob))

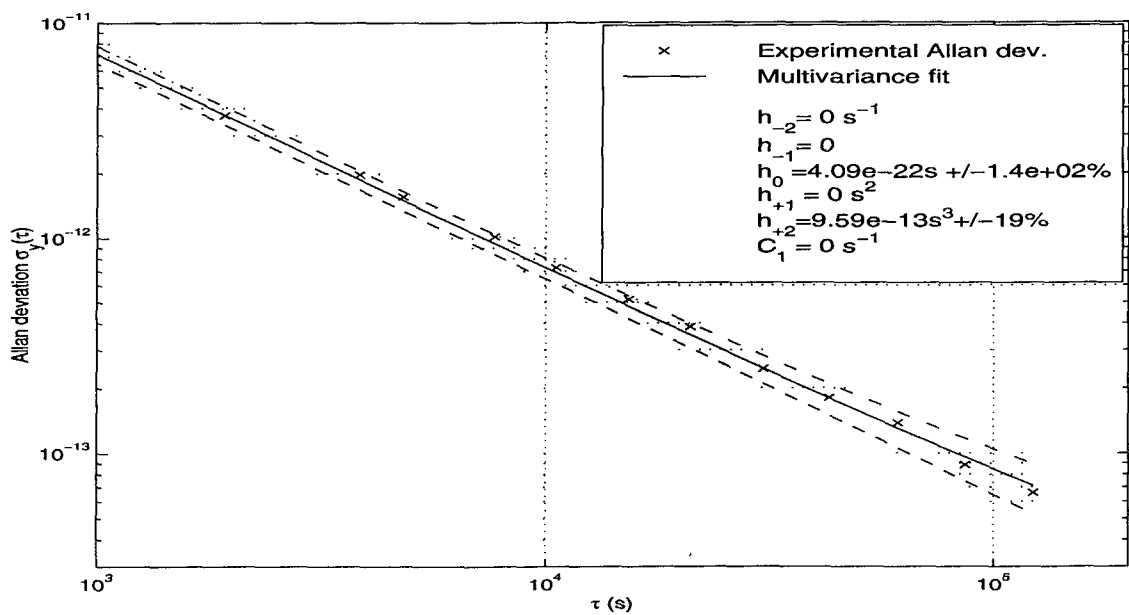
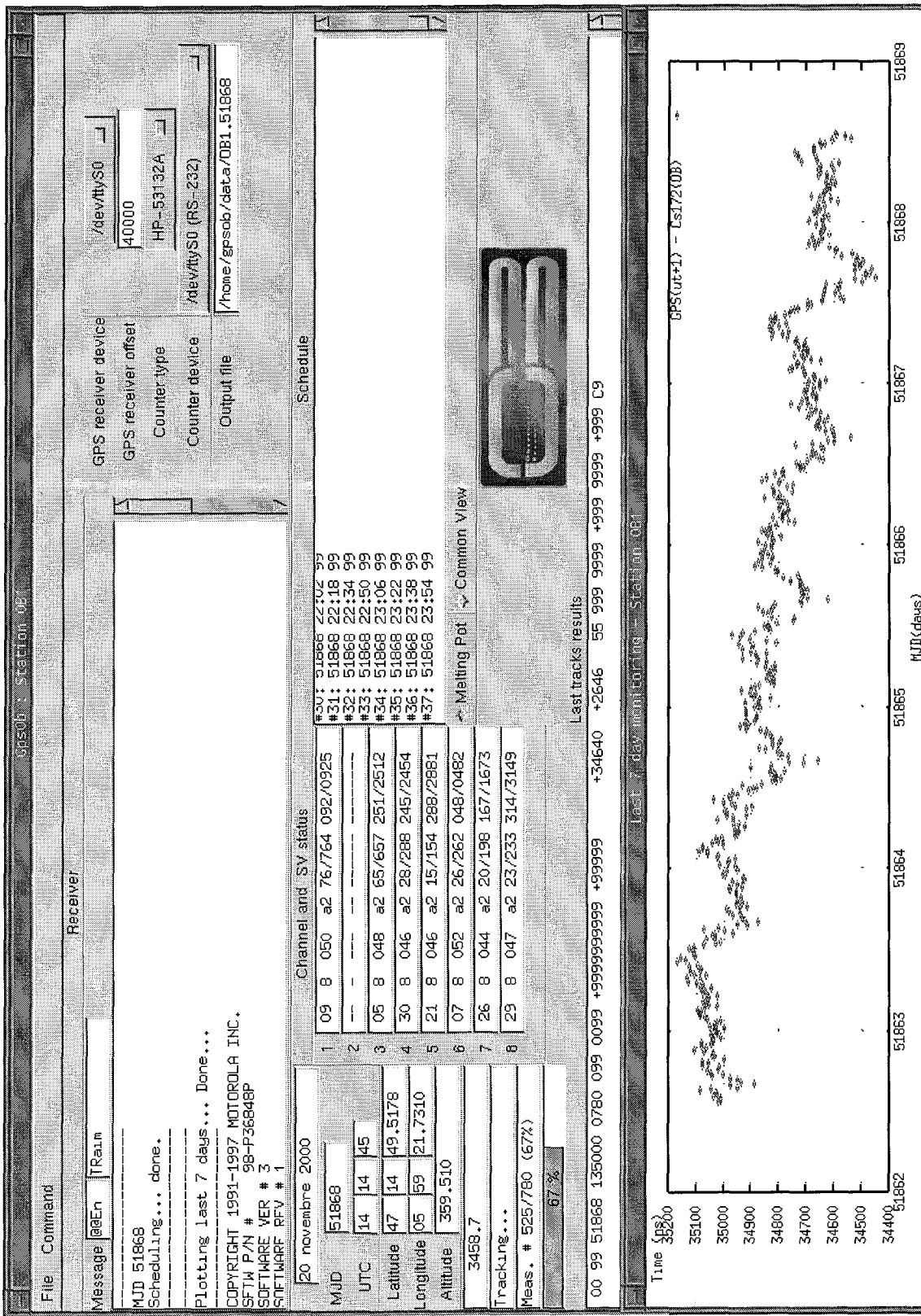


Figure 4: Allan deviation of UTC(OP) - GPS(ut+op) - (Cs172(OB) - GPS(ut+ob3))



GPS-BASED TIME ERROR ESTIMATES PROVIDED BY SMOOTHING, WIENER, AND KALMAN FILTERS: A COMPARATIVE STUDY

Y. S. Shmaliy*, A. V. Marienko**,

M. Torres-Cisneros*, and O. Ibarra-Manzano*

*Electronics Dept., Guanajuato University, Salamanca, 36730, Mexico

**“Sichron” Center, 4 Skrypniaka St., Kharkiv, 310057, Ukraine

E-mail: shmaliy@salamanca.ugto.mx

Abstract

GPS timing plays a critical role in modern practice of time errors estimate and synchronization. Big noise of the GPS-based measured data and inherent non-stationarity of a time error cause major difficulties here. In spite of theoretical separation of the application fields for the filters (stationary and non-stationary signals), GPS-based time error processes require more explicit practical answer. Indeed, what process may be practically treated as a stationary one and, to opposite, how to recognize a non-stationary case? In this report we answer these questions by numerically and show that for the same transient time the following filter should be used to get the best accuracy for the known initial fractional frequency offset y_0 (time error rate) of oscillator, namely an average smoother for $|y_0| < r_1$, the Wiener filter for $r_1 \leq |y_0| \leq r_2$, and the Kalman filter for $r_2 < |y_0|$, where r_1 and r_2 are coordinates dependent on the required accuracy. We prove this conclusion by the example of a time error estimate of the rubidium standard based on the reference timing signals of the Motorola GPS UT+ Oncore Timing receiver.

INTRODUCTION

GPS timing plays a critical role in modern practice of time errors “on-line” estimate and synchronization. Major difficulties here are caused mainly by big noise of the measured data provided by GPS receiver and inherent non-stationarity of a time error. Statistically, once a random signal exhibits stationary nature, then the optimal Kolmogorov-Wiener approach (Wiener filter [1]) is efficiently used and, conversely, the Kalman-Bucy technique (Kalman filter [2]) yields the best estimator for the non-stationary random signals. In spite of both approaches evidently covering all cases, test and measurement still use an average smoother [3] owing to its transparency and small variance, and despite of an estimate bias caused inevitably by non-stationarity.

Modern timekeeping systems employ all three filters. Observing them even in the past Proceeding of PTTI'99, we realize that, for instance, to detect the failure of a single satellite clock three different space-

segment timekeeping subsystems are designed [4]. Two subsystems use a direct average and the three-state Kalman filter is implemented in the third case, yielding the most accurate estimate as compared to the average filters. In the synchronization algorithm for the WAAS network they are based on the two-state Kalman filter [5], providing a control error of 50ns. The same two-state filter was used in the new steering strategy for the USNO Master Clock[6]. Contrarily, while steering the cesium-based primary clock of the Geo Uplink Subsystem they employ an average smoother [7]. Finally, to estimate a time error of the master clock for the WAAS test transmissions the algorithm was designed based on the IIR digital filter of the 2nd order [8], which may be considered as a non-optimal Wiener filter.

The result is following, for rather the same quality master clocks and time errors the different estimators are used, and it seems obvious that aiming to obtain the smallest estimate and synchronization error, one must follow the rules to select the filter in the optimal way. To work the rules out for the GPS-based time error processes, first, we must realize what process may be practically considered as a stationary one and, conversely, how to recognize a non-stationary case? Finally, what type of the digital filters should be used to be the most accurate in practice for the certain transient time and known rate of change of a time error caused by the crystal oscillator, rubidium standard, cesium standard, or even hydrogen maser?

In this report we answer the questions in the following way. We numerically study all three filtering algorithms based on an average smoother, the Wiener and Kalman filters for the same common transient time t_n taken as an average time of a smoother. We then simulate the GPS-based time error random process with a constant initial fractional frequency offset y_0 between reference and local oscillators and study the filtering errors for the proper y_0 . In this way we determine the ranges for y_0 , in which each filter exhibits a minimal either total (RMS variance plus mean bias) or a maximum error. We show that for the same t_n the following filter should be used to get the best accuracy, depending on y_0 :

- *Average smoother is for the range of $|y_0| < r_1$,*
- *Wiener filter is for $r_1 \leq |y_0| \leq r_2$, and*
- *Three-state Kalman filter is for $r_2 < |y_0|$,*

where r_1 and r_2 are determined for the total error as r_{1t} and r_{2t} , and for the maximal error as r_{1m} and r_{2m} , respectively. Because processing time influences the error strongly then we study the errors for the different t_n , finding out correspondent dependencies $r_{1,2}(t_n)$ and presenting the simple approximation function $r_i = a_i t_n^{-1/5}$, where $i \equiv 1t, 2t, 1m, 2m$, and a_i is a constant.

We, finally, consider the example of the filter selection to get the most accurate estimate of the time error of the rubidium standard with known y_0 employing the Motorola UT+ Oncore receiver. First, through the equality $y_0 = a_i t_n^{-1/5}$ we establish the critical transients for the total and maximal errors, t_{n1t} , t_{n2t} and t_{n1m} , t_{n1m} , respectively, and expect that an average smoother will give the smallest error for $t_n < t_{n1t}$ or $t_n < t_{n1m}$, the Wiener filter should be the most accurate for $t_{n1t} < t_n < t_{n2t}$ or $t_{n1m} < t_n < t_{n2m}$, and, finally, the Kalman filter must be the best for $t_{n2t} < t_n$ or $t_{n2m} < t_n$. As a matter of the fact we conclude that the methodology holds true at least for the considered case.

MATHEMATICAL MODELS OF THE SIGNALS

Consider mathematical presentation of a timing signal of local oscillator and a noisy time error.

An Oscillator Timing Signal

A model of total instantaneous phase $\Phi(t)$ of oscillator is truly legalized in [9] as

$$\Phi(t) = \Phi_0 + 2\pi\nu_{nom}(1 + y_0)t + \pi D\nu_{nom}t^2 + \phi(t), \quad (1)$$

where: Φ_0 is initial phase offset,

y_0 is the fractional frequency offset from the nominal frequency ν_{nom} (mainly due to finite frequency setability of the clock), y_0 [in ns/hour] = $3.6 \times y_0$ [in parts of 10^{-12}],

D is the linear fractional frequency drift rate (basically representing oscillator aging effects),

$\phi(t)$ is the random phase deviation component.

While subtracting from (1) the same type phase model of a reference source and then dividing the result by $2\pi\nu_{nom}$, one comes to the time error error model

$$x(t) = x_0 + (y_0 - y_{0ref})t + \frac{D - D_{ref}}{2}t^2 + \frac{\phi(t) - \phi_{ref}(t)}{2\pi\nu_{nom}}. \quad (2)$$

In (2) one can also take that all the degradation sources y_{0ref} , D_{ref} , and $\phi_{ref}(t)$ of the reference source are negligible as compared to those of the clock under test. As a result, the $x(t)$ model reduces to the practical form of a time error of local oscillator

$$x(t) = x_0 + y_0 t + \frac{D}{2}t^2 + \frac{\phi(t)}{2\pi\nu_{nom}}. \quad (3)$$

A Noisy Time Error

Basically, we measure a time error $x(t)$ in discrete time, providing values x_v for discrete time points t_v for the constant time interval $\Delta = t_v - t_{v-1}$, where $v = 0, 1, 2, \dots$. GPS-based measurements add a noise to a time error, which has a normal histogram, thus, may be modeled as a Gaussian noise. Both a time error and a noise are summed (3) allowing presentation of a measured noisy time error (observation) and a clock state with respect to (3) in the matrix form as follows

$$\xi_v = \mathbf{H}_v \lambda_v + n_{0v}, \quad (4)$$

$$\lambda_v = \mathbf{A}_{v-1} \lambda_{v-1} + \mathbf{n}_{\lambda v}, \quad (5)$$

where ξ_v is a measured noisy time error (observation), λ_v is 3-dimensional oscillator (clock) state vector (time error, frequency, and aging), \mathbf{H}_v is 1×3 dimensional measurement matrix, \mathbf{A}_v is 3×3 dimensional clock state transition matrix, n_{0v} and $\mathbf{n}_{\lambda v}$ are jointly independent white noises with zero expectations and covariances V_v and Ψ_v of 3×3 dimension, respectively,

$$V_v = E\{n_{0v} n_{0v}^T\}, \quad (6)$$

$$\Psi_v = E\{\mathbf{n}_{\lambda v} \mathbf{n}_{\lambda v}^T\}. \quad (7)$$

In discrete time the model (3) is transferred to the form of

$$x_v = x_{v-1} + y_{v-1}\Delta + \frac{D_{v-1}}{2}\Delta^2 + n_{xv}, \quad (8)$$

where $y_v = y_{v-1} + D_{v-1}\Delta + n_{yv}$; $D_v = D_{v-1} + n_{Dv}$; and n_{xv} , n_{yv} , and n_{Dv} are correspondent discrete noises.

Correspondingly, (8) allows writing all the matrixes for (4) and (5) as

$$\boldsymbol{\lambda}_v = \begin{bmatrix} x_v \\ y_v \\ D_v \end{bmatrix}, \quad \mathbf{A}_v = \begin{bmatrix} 1 & \Delta & \Delta^2/2 \\ 0 & 1 & \Delta \\ 0 & 0 & 1 \end{bmatrix}, \quad \mathbf{n}_{\lambda v} = \begin{bmatrix} n_{xv} \\ n_{yv} \\ n_{Dv} \end{bmatrix}, \text{ and } \mathbf{H}_v = [1 \ 0 \ 0], \quad (9)$$

present (4) in a form of

$$\xi_v = x_v + n_{ov}, \quad (10)$$

and describe the noise matrix (7) as

$$\boldsymbol{\Psi}_v = E\{\mathbf{n}_{\lambda v} \mathbf{n}_{\lambda v}^T\} \cong S_{Dv} \Delta \begin{bmatrix} 0 & 0 & 0 \\ 0 & 0 & 0 \\ 0 & 0 & 1 \end{bmatrix}, \quad (11)$$

where S_{Dv} is two-side spectral density of a continuous white noise of aging depending on Δ [10] and expressed through the time error noise straightforward.

ESTIMATION OF A TIME ERROR

Consider the three statistical algorithms, namely an average smoothing, Wiener's, and Kalman's.

Average Smoother

Average smoother allows a non-optimal estimate \hat{x}_v of a time error x_v (in a sense of a minimal RMS error) based on an observation ξ_v (10). The algorithm does not require any a priori knowledge about an oscillator state model, time error, and even an observation and is straightforward

$$\hat{x}_v = \frac{1}{N} \sum_{i=v-N+1}^v \xi_i, \quad (12)$$

where $\xi_v = 0$ if $v < 0$, N is number of average points. According to (12), the first estimate appears with delay on N points of the process, thus, a filter transient time equals $t_{tr} = \Delta(N-1)$.

Wiener Filter

In discrete time domain the realizable Wiener filter provides estimate through a convolution of its impulse response h_v and an observation (10)

$$\hat{x}_v = \sum_{i=v-M+1}^v \xi_i h_{v-i}, \quad (13)$$

where $\xi_v = 0$ if $v < 0$, M determines the length of h_v that is taken to be equal zero apart the time interval $0, \dots, (M-1)\Delta$. To get a minimal RMS error for estimate, first, in the tradition of Wiener define an optimal unrealizable response $H_{0k} = S_{xk} / (S_{xk} + S_{n0})$, where S_{xk} is discrete power spectral density of a time error (oscillator phase) that in spirit of Leeson [11] is taken here as $S_{xk} = \alpha f_k^{-2}$, where f_k is Fourier frequency; α is a constant; S_{n0} is constant power spectral density of a white noise; $k = 0, \dots, K-1$, and K limits the length of the time error sequence taken at the early stage to estimate the spectral densities with enough accuracy. Then use a proper approximating filter with response $H_k \exp(j\phi_k)$ and come through the inverse discrete Fourier transform to the optimal impulse response h_{ov} of a realizable filter

$$h_{ov} = B \mathcal{D}^{-1} \{ H_k e^{j\phi_k} \}, \quad (14)$$

where B is a constant. In our experiment we increase (reduce) the level of S_{n0} , increasing (reducing) in this way a filter transient time.

Kalman Filter

The three-state Kalman filter is matched with a clock model (3) [12], allowing the following algorithm for (4) and (5) to get estimates in discrete time

$$\hat{\lambda}_v = \mathbf{A}_{v-1} \hat{\lambda}_{v-1} + \mathbf{K}_v (\xi_v - \mathbf{H}_v \mathbf{A}_{v-1} \hat{\lambda}_{v-1}), \quad (15)$$

where a filter gain is defined as

$$\mathbf{K}_v = \tilde{\mathbf{R}}_v \mathbf{H}_v^T (\mathbf{H}_v \tilde{\mathbf{R}}_v \mathbf{H}_v^T + V_v)^{-1}, \quad (16)$$

where $\tilde{\mathbf{R}}_v = \mathbf{A}_{v-1} \mathbf{R}_{v-1} \mathbf{A}_{v-1}^T + \Psi_v$ is a matrix of predicted errors, and the filtering errors are calculated as

$$\mathbf{R}_v = (\mathbf{I} - \mathbf{K}_v \mathbf{H}_v) \tilde{\mathbf{R}}_v, \quad (17)$$

where \mathbf{I} is a unit matrix. Transient of the on-line operating Kalman filter is due to time expended to get estimate (17). It may be varied around the optimal value by changing S_{Dv} in (11), so that since S_{Dv} rises then t_h decreases, and vice versa. The total filtering error rises once transient is a non-optimal.

NUMERICAL STUDIES OF THE FILTER ERRORS

All three filters, namely an average smoother (12), Wiener's (13), and Kalman's (15), are examined here for the same time error process. To show the effect, the noisy process (3) is simulated with variance $\sigma = 40\text{ns}$ and with both a stationary part of a deterministic function ($0 \leq t < 25$ hours), in which case $x_0 = y_0 = D = 0$ in (3), and a non-stationary part ($25 \leq t$ hours) with $y_0 = -2 \cdot 10^{-12} = -7.2 \text{ ns}/\text{hour}$ and $D = 0$. Because we consider a transient time as a principal performance of a filter, then, to know trade-off, we obtain the same $t_h = 10\text{hours}$ for all three filters. While providing, the transient of a smoother was evaluated by its average time $t_h = \Delta(N-1)$ and that of the Wiener and Kalman filter finished at the level of 0.9. Figure 1 shows the simulated processes and estimates extracted by the filters. Figure 2 gives correspondent errors calculated as difference between estimated and simulated functions

$$\epsilon_v = \hat{x}_v - x_v. \quad (18)$$

Just as it had been expected based on the filter strategies for the dynamic range ($25\text{hours} < t$), the Kalman filter showed the smallest error, the Wiener filter was less accurate, and, the smoother stayed hors-concours with its biggest error. Conversely, for the range of a stationary noisy error ($t < 25\text{hours}$), the smoother was the best, the Wiener filter exhibited more big error, and the Kalman filter looked like the worst. Nevertheless, it is obviously speaks in favor of the Kalman filter that its error remains say rather the same for the both stationary and non-stationary ranges (Figure 2).

Excited by the curiosity of the different filtering errors for the stationary and non-stationary processes with the constant transient, we come to another experiment, while simulating only a non-stationary process and evaluating (18) for $t_{tr} = \text{const}$ and various y_0 by the total filtering error

$$\sigma_t = \langle |\epsilon_v| \rangle + \sqrt{\langle [\epsilon_v - \langle \epsilon_v \rangle]^2 \rangle} \quad (19)$$

and the maximal filtering error

$$\epsilon_{\max} = \max |\epsilon_v|. \quad (20)$$

Before going on to analyze the results, let us study Figure 3, which shows the total (*a*) and maximal (*b*) errors as functions of y_0 for $t_{tr} = 6$ hours for all three filters. There an average smoother yields the smallest total error for $y_0 < r_{1t} = 1.57 \times 10^{-13}$, the Wiener filter is the most accurate for $r_{1t} = 1.57 \times 10^{-13} < y_0 < r_{2t} = 4.035 \times 10^{-13}$, and the Kalman filter is for $r_{2t} = 4.035 \times 10^{-13} < y_0$. The same filters provide the smallest maximal error for the ranges of $y_0 < r_{1m} = 7.59 \times 10^{-13}$, $r_{1m} = 7.59 \times 10^{-13} < y_0 < r_{2m} = 9.22 \times 10^{-13}$, and $r_{2m} = 9.22 \times 10^{-13} < y_0$, respectively. We then estimate coordinates r_{1t} , r_{2t} , r_{1m} , and r_{2m} by changing t_{tr} , and come to the correspondent dependences (Table 1).

Table 1
DEPENDENCIES OF THE COORDINATES (FIGURE 3) ON THE FILTER TRANSIENT

Transient, hours	Measure	Total error coordinates		Maximal error coordinates	
		r_{1t}	r_{2t}	r_{1m}	r_{2m}
1.5	y_0 , ns/hour	4.032	11.376	20.844	32.782
		1.12×10^{-12}	3.16×10^{-12}	5.79×10^{-12}	9.106×10^{-12}
3.0	y_0	1.804	4.054	8.28	11.376
		5.01×10^{-13}	1.126×10^{-12}	2.3×10^{-12}	3.16×10^{-12}
4.5	y_0	0.984	2.07	3.996	6.091
		2.733×10^{-13}	5.748×10^{-13}	1.11×10^{-12}	1.692×10^{-12}
6.0	y_0	0.565	1.453	2.733	3.318
		1.57×10^{-13}	4.035×10^{-13}	7.593×10^{-13}	9.217×10^{-13}
7.5	y_0	0.3636	1.1506	1.878	2.107
		1.01×10^{-13}	3.196×10^{-13}	5.217×10^{-13}	5.854×10^{-13}
9.0	y_0	0.3	0.8028	1.1088	1.5329
		8.36×10^{-14}	2.23×10^{-13}	3.08×10^{-13}	4.258×10^{-13}
10.5	y_0	0.2578	0.703	1.036	1.272
		7.16×10^{-14}	1.952×10^{-13}	2.878×10^{-13}	3.533×10^{-13}
12.0	y_0	0.2542	0.4896	1.1614	1.6718
		7.06×10^{-14}	1.36×10^{-13}	3.226×10^{-13}	4.644×10^{-13}
13.5	y_0	0.2031	0.4913	0.7423	0.9086
		5.643×10^{-14}	1.3647×10^{-13}	2.062×10^{-13}	2.524×10^{-13}
15.0	y_0	-	0.398	0.7636	0.7758
		-	1.106×10^{-13}	2.121×10^{-13}	2.155×10^{-13}
16.5	y_0	0.0295	0.3207	0.583	0.6548
		3.19×10^{-14}	8.91×10^{-14}	1.619×10^{-13}	1.819×10^{-13}
18.0	y_0	-	0.2497	0.5526	0.6073
		-	6.937×10^{-14}	1.54×10^{-13}	1.69×10^{-13}

The curves provided in this way (Figure 4) were noisy because of different length-limited samples of the simulated random process. Nevertheless, it seems obvious that the following approximating function $G \times t_{tr}^{-1.5}$ is accurate enough to be used in practical calculations for each coordinate. We approximate those as follows

$$r_{1t} \cong 2.3 \times t_{tr}^{-1.5}, r_{2t} \cong 6.0 \times t_{tr}^{-1.5}, r_{1m} \cong 11 \times t_{tr}^{-1.5}, \text{ and } r_{2m} \cong 15 \times t_{tr}^{-1.5}, \quad (21)$$

and use (21), while considering the below-given example of the filter selection for the GPS-based time error process generated by the rubidium standard.

EXAMPLE: FILTER SELECTION FOR THE GPS-BASED TIME ERROR OF A RUBIDIUM STANDARD

Measurement of the time error of the rubidium standard had been carried out based on the Motorola GPS Timing Receiver Oncore UT+ with average time $\Delta = 100\text{s}$ for about 30 hours with the initial error of $x_0 \cong 2.1\text{ns}$ and offset $y_0 \cong -4.7\text{ ns/hour} = -1.3 \times 10^{-12}$. To separate the ranges for each filter, substitute the known y_0 for each coordinate in (21) and come to the following prediction:

For the total error (19)

If $t_n < 1.455\text{hours}$ then **an average smoother** should be the most accurate

If $1.455\text{hours} < t_n < 2.757\text{hours}$ then **the Wiener filter** should be the most accurate

If $2.757\text{hours} < t_n$ then **the three-state Kalman filter** should be the most accurate

For the maximal error (20)

If $t_n < 4.129\text{hours}$ then **an average smoother** should be the most accurate

If $4.129\text{hours} < t_n < 5.078\text{hours}$ then **the Wiener filter** should be the most accurate

If $5.078\text{hours} < t_n$ then **the three-state Kalman filter** should be the most accurate

Then tune the filters step by step for several transients to satisfy the above-determined conditions and estimate total (19) and maximal (20) errors (Table 2).

Table 2
TOTAL AND MAXIMAL ERRORS OF THE FILTERS FOR THE DIFFERENT TRANSIENT TIMES

t_n , hours	Total error, ns			Maximal error, ns		
	Smoothen	Wiener	Kalman	Smoothen	Wiener	Kalman
1.0	8.367	8.210	10.83	17.204	16.626	36.363
2.2	9.429	8.225	9.446	14.447	14.842	18.088
3.0	10.447	8.677	8.279	15.536	14.763	16.850
4.5	13.363	10.25	6.622	19.021	14.486	13.805
6.0	16.942	12.376	5.306	26.099	16.204	12.759

An analysis of Table 2 shows that just as it had been predicted the three-state Kalman filter allows the smallest both total error for $3.0\text{hours} \leq t_n$ and maximal error for $4.5\text{hours} \leq t_n$. The Wiener filter exhibits the smallest those errors for $2.2\text{hours} = t_n$ and $3.0\text{hours} = t_n$, respectively. An average smoother gives the smallest both those errors for $t_n \leq 1.0\text{hours}$ and $t_n \leq 2.2\text{hours}$, respectively. In the range of $t_n \leq 1.0\text{hour}$ we watched also for the small error of the Wiener filter. This is because of the limited processing sequence available with small average time. Thus, we have proved in this way the above-given methodology generalized by Figure 4, except the case of $t_n = 1.0\text{hour}$, and, finally, to illustrate the real filtering process, we bring Figures 5—8, those show four cases of a time error estimate provided by all three filters.

CONCLUDING REMARKS

We have numerically examined in this report the errors of the three filtering approaches, namely an average smoothing, Wiener's, and Kalman's once they are employed to get "on-line" time error estimate in the modern timekeeping systems. As a major result we present Figure 4, which, at first, practically answer the question "What are stationary and non-stationary time error processes?" separating space for them left and right, respectively, by correspondent curves. And, it is the most important, Figure 4 allows selection of the filter type for the initial frequency offset y_0 (rate of change of a time error) and the filter transient t_{tr} . Based on this, once interesting of the maximal filtering error, we conclude that the following filter seems to be the most accurate depending on y_0 and t_{tr} , namely

- For $y_0 \approx 10^{-11}$ (crystal) the three-state Kalman filter is the most accurate once $t_{tr} > 1\text{ hour}$
- Once $y_0 \approx 10^{-12}$ (crystal or rubidium) then an average smoother is accurate for $t_{tr} < 5\text{ hours}$, the Wiener filter is for $5\text{ hours} < t_{tr} < 6\text{ hours}$, and the three-state Kalman filter is for $6\text{ hours} < t_{tr}$
- For $y_0 \leq 10^{-13}$ (cesium and hydrogen) an average smoother is accurate for $t_{tr} < 24\text{ hours}$

The results are readily extended to the general case, including aging. Just account the maximally possible frequency offset of your oscillator for the measurement (observation) and follow the above-given methodology, for which more satisfactory justification we plan to revise the results further analytically.

REFERENCES

- [1] N. Wiener 1949, *Extrapolation, Interpolation, and Smoothing of Stationary Time Series*, John Wiley & Sons, New York.
- [2] R. E. Kalman 1960, "*A new approach to linear filtering and prediction problems*," Transactions ASME, Ser. D, *Journal of Basic Engineering*, 82, pp. 35-45.
- [3] S. K. Mitra, and J. F. Kaiser (eds.) 1993, *Handbook for Digital Signal Processing*, John Wiley & Sons, New York, 1268 p.
- [4] Y. C. Chan, J. C. Camparo, and R. P. Frueholz 2000, "*Space-segment timekeeping for next generation satcom*," Proceedings of the 31st Annual Precise Time and Time Interval (PTTI) Systems and Applications Meeting, 7-9 December 1999, Dana Point, California, USA, pp. 121-132.
- [5] C. Griffith, S. Peck, and P. Diamond 2000, "*WAAS network time performance using WRS data*," Proceedings of the 31st Annual Precise Time and Time Interval (PTTI) Systems and Applications Meeting, 7-9 December 1999, Dana Point, California, USA, pp. 161-172.
- [6] P. A. Koppang, and D. N. Matsakis 2000, "*New steering strategies for the USNO Master Clocks*," Proceedings of the 31st Annual Precise Time and Time Interval (PTTI) Systems and Applications Meeting, 7-9 December 1999, Dana Point, California, USA, pp. 277-284.
- [7] M. S. Grewal, W. Brown, R. Lucy, and P. Hsu 2000, "*Geo Uplink System (GUS) clock steering algorithms performance, validation, and results*," Proceedings of the 31st Annual Precise Time and Time Interval (PTTI) Systems and Applications Meeting, 7-9 December 1999, Dana Point, California, USA, pp. 173-180.

- [8] P. Fenton, E. Powers, W. Klepczynski, and R. Douglas 2000, “*Time transfer using WAAS: an initial attempt*,” Proceedings of the 31st Annual Precise Time and Time Interval (PTTI) Systems and Applications Meeting, 7-9 December 1999, Dana Point, California, USA, pp. 191-202.
- [9] G.810, “*Definitions and terminology for synchronization networks*,” ITU-T, Geneva, August 199.
- [10] O. E. Rudnev, Y. S. Shmaliy, et al. 1999, “*Kalman filtering of a frequency instability based on Motorola Oncore UT GPS timing signals*,” Proceedings of the 1999 Joint Meeting of the European Frequency and Time Forum and the IEEE International Frequency Control Symposium, IEEE Publication 99CH36313, 13-16 April 1999, Besançon, France, pp. 251-254.
- [11] D. B. Leeson 1966, “*A simple feedback oscillator noise spectrum*,” Proceedings of the IEEE, 54, 329-330.
- [12] Y. S. Shmaliy, A. V. Marienko, and S. V. Savchuk 2000, “*GPS-based optimal Kalman estimation of time error, frequency, and aging*,” Proceedings of the 31st Annual Precise Time and Time Interval (PTTI) Systems and Applications Meeting, 7-9 December 1999, Dana Point, California, USA, pp. 431-440.

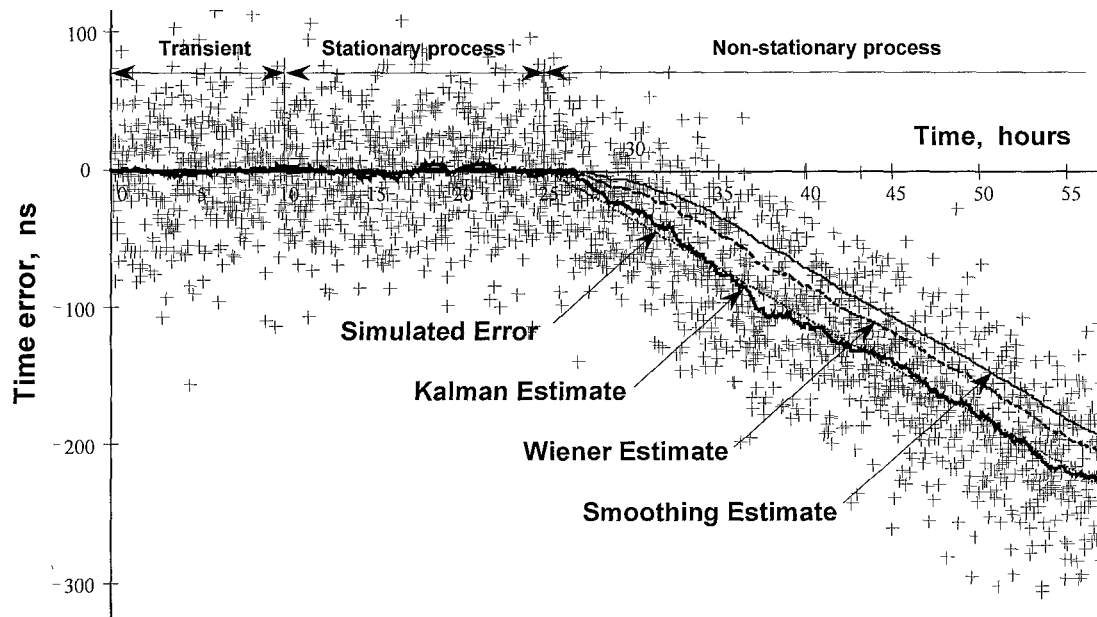


Figure 1. Simulated error, noisy observation, and estimates provided by the average smoothing, Wiener, and three-state Kalman filters for the stationary and non-stationary processes

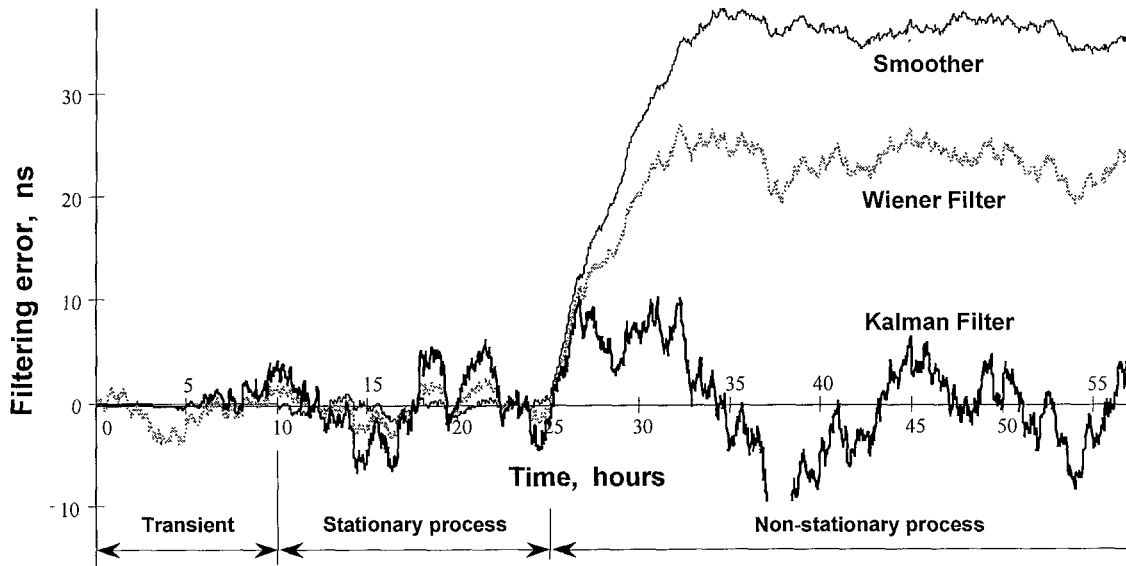


Figure 2. Errors of the average smoothing, Wiener, and three-state Kalman filters in the stationary and non-stationary ranges (see Fig.1)

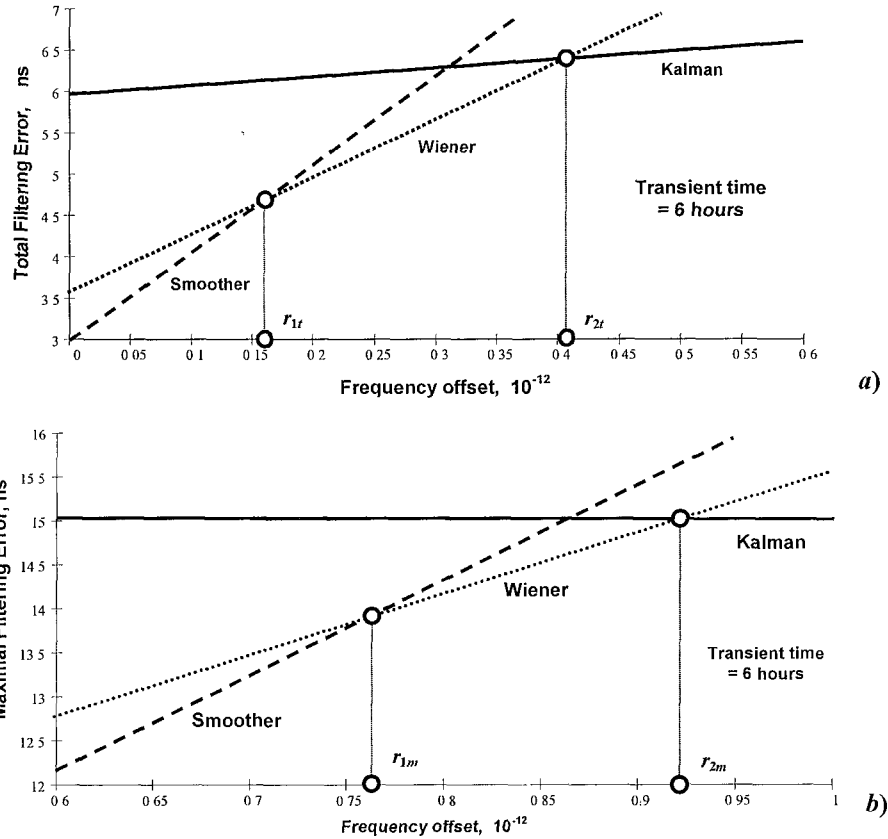


Figure 3. The total (a) and maximal (b) errors of the average smoothing, Wiener, and three-state Kalman filters as functions of the initial frequency offset y_0

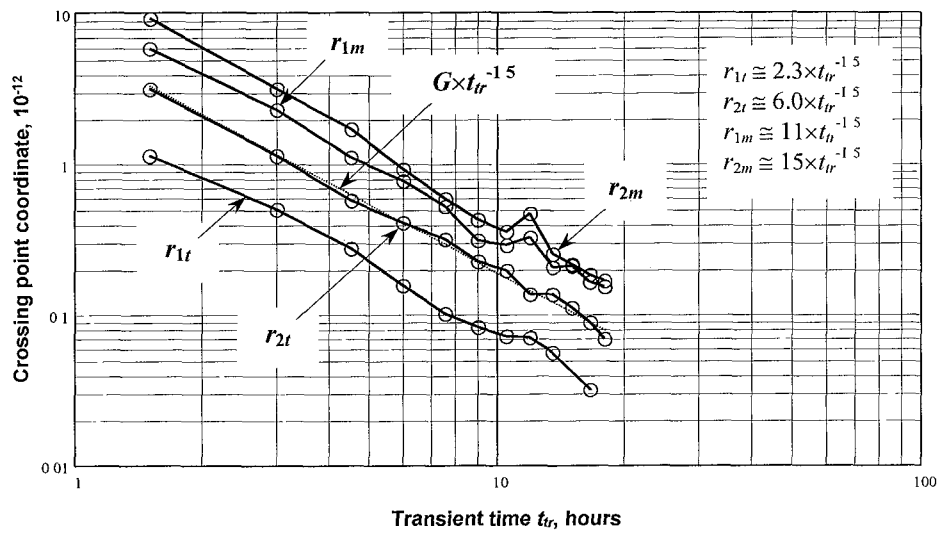


Figure 4. Coordinates r_{1t} , r_{2t} , r_{1m} , and r_{2m} as functions of the filters transient time t_{tr} , and correspondent approximating functions

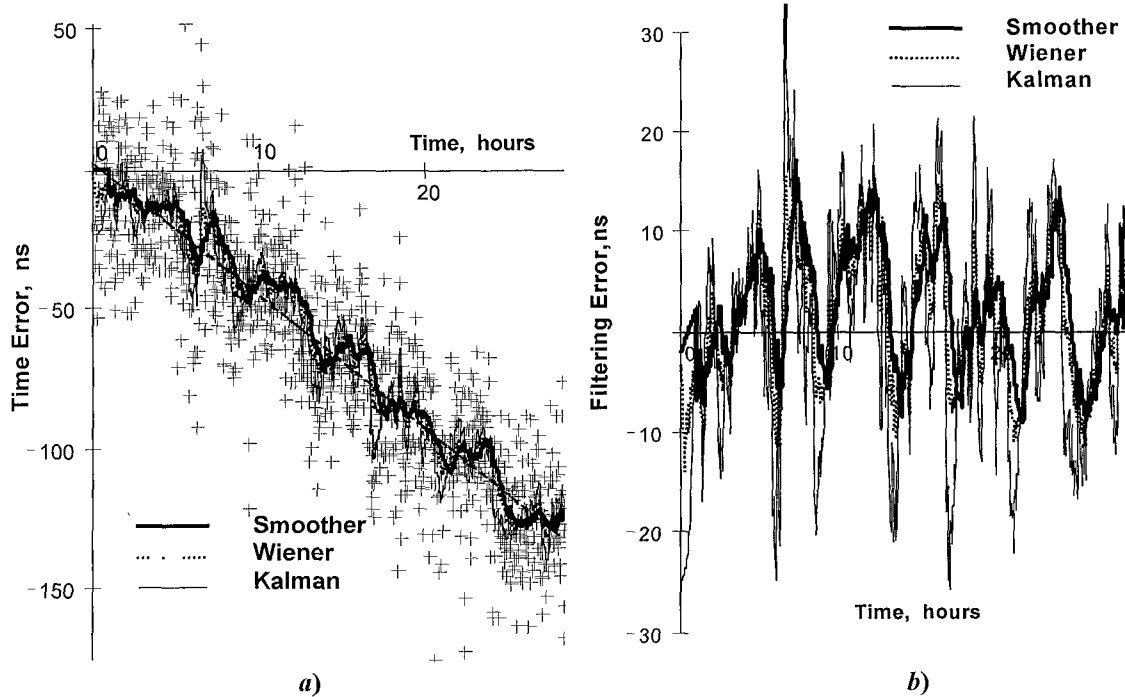


Figure 5. Estimates for $t_{tr} = 1.0$ hour (a) and filtering errors (b): the average smoother is the most accurate

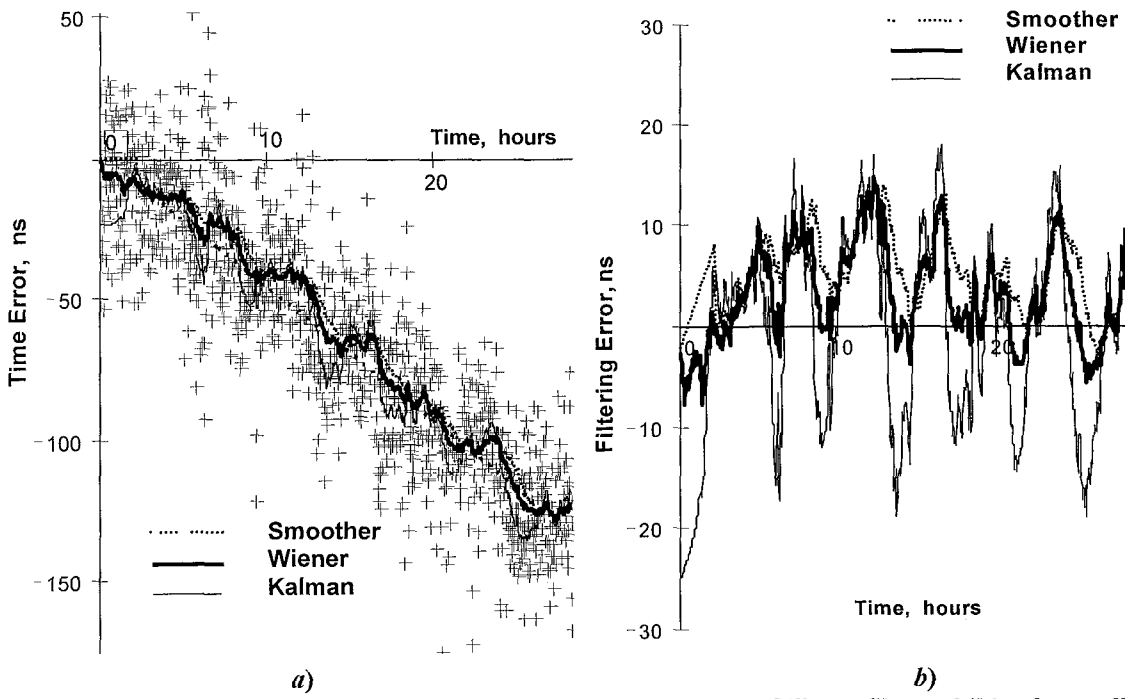


Figure 6. Estimates for $t_{tr} = 2.2$ hours (a) and filtering errors (b): the Wiener filter exhibits the smallest error

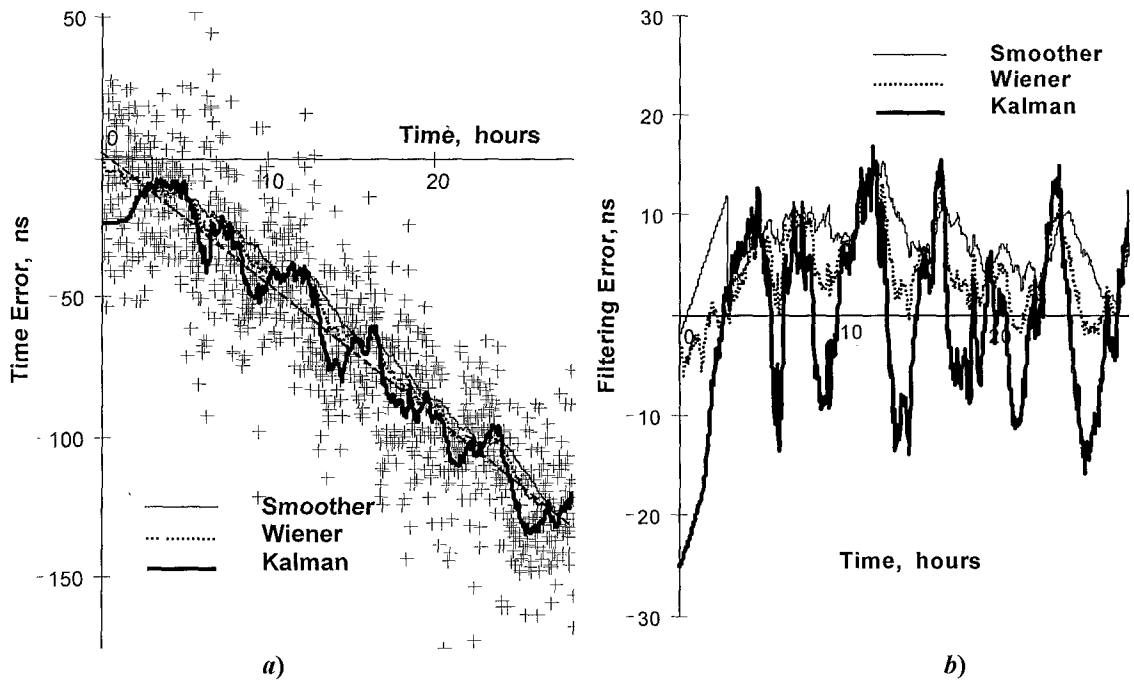


Figure 7. Estimates for $t_{tr} = 3.0$ hours (a) and filtering errors (b): the Kalman filter is the most accurate

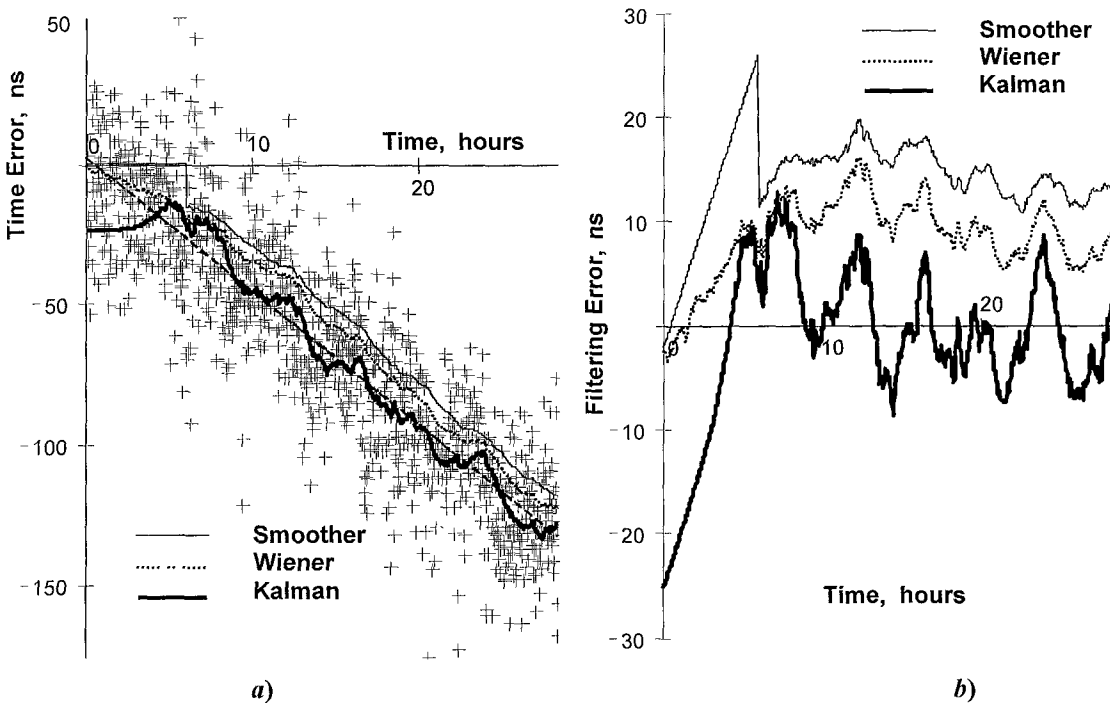


Figure 8. Estimates for $t_{tr} = 6.0$ hours (a) and filtering errors (b): the Kalman filter seems obviously like the best estimator

CLOCK SYNCHRONIZATION USING GPS/GLONASS CARRIER PHASE

K. Y. Tu¹, H. M. Peng¹, C. S. Liao²

National Standard Time & Frequency Lab.,
TL, Chunghwa Telecom Co., Ltd., Taiwan

F. R. Chang³

Dept. of Electrical Engineering, National Taiwan University, Taiwan

¹Associate Researcher

²Senior Researcher

³Professor

Abstract

Clock synchronization by means of GPS/GLONASS is proposed. The GPS/GLONASS receivers with the external frequency input interface are used in our system. While the remote OCXO (Oven-Controlled Crystal Oscillator) clock and the primary H-maser clock are connected to the receivers, the frequency offset of the remote clock with respect to the primary clock can be estimated by performing the linear-least-square fit on carrier-phase single-difference observables. The proportional controller is adopted in our system for tuning the remote clock in real time. Through the D/A converter, the remote clock is then steered to synchronism with the primary clock. For averaging times of 1 day under the configuration of about a 30-meter baseline, our experimental results show that the accuracy of the remote clock can be improved from about 2×10^{-9} to about 6×10^{-14} , and the stability of the remote clock can be improved from about 2×10^{-10} to about a few parts in 10^{14} . Based on the proposed architecture, the frequency traceability can be achieved. The potential applications include a frequency source system for calibration laboratories, telecommunication networks, and power transmission systems.

INTRODUCTION

The capability of using GPS carrier phase to transfer precise time and frequency has been recognized and described by many researchers [6-10]. Because the frequency of the carrier is roughly 1000 times higher than that of C/A code, time and frequency dissemination using carrier phase has much greater resolution, in principle. When combined with Russia's GLONASS constellation, which provides similar capabilities, the potential precision of the system becomes even greater. Recent development in time and frequency applications have led the timekeeping community to focus on using both these systems for time metrology.

In this paper, we propose a scheme for clock synchronization by using GPS/GLONASS carrier phase. The basic architecture of the system is shown in Figure 1. With all-in-view observations, the frequency offset of the remote clock with respect to the primary clock is estimated in real time by performing the linear-least-square fit on carrier-phase single-difference observables over observation period. In the process, the errors and biases that affect the measurements are substantially reduced. In our system, the carrier-phase data and other observation messages are passed between both stations through PSTN (Public Switched-Telephone Network). The frequency offset is then fed into a proportional controller, which automatically issues commands

to steer the remote clock to synchronize with the primary clock. On the other hand, the master station can also monitor the performance of the remote clock in real time.

With the above-mentioned method, the accuracy of the remote OCXO clock could be improved from about 2×10^{-9} to about 6×10^{-14} for average times of one day. The stability of the remote OCXO clock could be improved from about 3×10^{-10} to about 2×10^{-14} . The potential roles of our system include the PRSs for telecommunication networks and the FSs for calibration laboratories, power systems, navigation systems, instrument calibration, and others.

THE MODEL OF CARRIER PHASE OBSERVABLES

In order to combine GPS and GLONASS, a unique time scale for all observations and satellite ephemerides and a unique reference system for all satellite and receiver positions are required. In our approach, all computations is based on GPS time as reference time and referred to the reference frame WGS-84. Therefore, the epochs of the GLONASS ephemerides are approximately corrected to GPS time by applying the leap seconds between GPS time and UTC. The GLONASS satellite positions are transformed from the frame PZ-90 to WGS-84 by applying the transformation parameters given in [3]. The observation equations for both GPS and GLONASS systems may also be modeled as Equation (1) [1-2], provided the corresponding carrier frequencies are introduced. In the processing of combined GLONASS/GPS observations, the differences between GPS and GLONASS frequencies and the wavelengths for GPS/GLONASS satellite pairs need to be considered, however.

$$\Phi_A^j = \rho_A^j + c(dt^j - dT_A) + \lambda^j N_A^j - d_{ion}^j + d_{trop}^j + \varepsilon_A^j, \quad (1)$$

where Φ_A^j is the carrier-phase measurement of the receiver A from the satellite j in meter; ρ_A^j is the true distance between the receiver A and the satellite j ; c is the speed of light; dt^j is the clock bias of the satellite j ; dT_A represents the clock difference between the satellite system time and receiver A clock; λ^j is nominal wavelength of the signal from satellite j ; N_A^j denotes the unknown integer number of cycles (ambiguity); and d_{ion}^j and d_{trop}^j are the ionospheric delay and the tropospheric delay, respectively; ε_A^j is the unmodeled errors primarily due to multipath, temperature variation, physical factors, etc.

To study the clock synchronization, we would like to first examine the behavior of the oscillator. Hence, both of the remote clock and primary clock are connected to the GNSS receivers, respectively. Under this arrangement, the term dT_A in (1) represents the time difference between the satellite clock and the external clock A . Denoting the two receivers by A and B and the satellite by j , respectively, the single-difference equation is

$$\Delta\phi_{AB}^j = \Delta\rho_{AB}^j - c\Delta dT_{AB} + \lambda^j \Delta N_{AB}^j + \Delta\varepsilon_{AB}^j, \quad (2)$$

where $\Delta(\cdot)$ represents the operator for differences between receivers with the same satellite. Due to the strong correlation between the unmodeled ionospheric and tropospheric delays of the

two receivers over a short baseline, the terms d_{ion}^j and d_{hop}^j in (1) are then eliminated. Since dT_A and dT_B are both referring to the same satellite system clock, their difference ΔdT_{AB} in (2) is nothing but the phase difference between external clock A and external clock B .

SYSTEM ARCHITECTURE

Figure 3 shows the functional block diagram of our system. It consists of the master station and the remote station. The master station contains the hydrogen-maser clock, GNSS receiver, and PC. The remote station includes the low-cost OCXO, GNSS receiver, D/A converter and industrial PC. Through the wired or wireless data links, the carrier-phase data and other observation messages can be sent between both stations. The positions of the antennae are predetermined by IGS (International GPS Service), and the j -th GPS and GLONASS satellite positions are obtained from the broadcasting navigation messages.

By performing the linear-least-square fit on the carrier-phase single-difference model (2) over observation interval τ , we can estimate the frequency offset y_τ of the remote clock with respect to the primary clock. With all-in-view GPS/GLONASS observations, the integrated frequency offset \bar{y}_τ then can be obtained by weighted averaging y_τ .

In general, the fine frequency tuning can be performed on the inexpensive oscillator through voltage control. Because of environmental effects such as vibration, temperature, pressure, and humidity, the desired frequency output is not always under a constant voltage. In our system, the frequency offset \bar{y}_τ is chosen as the input variables of the controllers. An incremental voltage $\Delta V(t_i)$ will be generated to update the voltage for steering the oscillator.

$$V_{i+1} = V_i + \Delta V. \quad (3)$$

In our system, we considered the proportional control [4] in the remote clock. The block diagram for the controller used in our experiment is shown in Figure 3. The control signal is proportional to the frequency offset \bar{y}_τ with gain K being adjustable. To design a particular control loop for the clock synchronization applications, we merely have to adjust the constants K in Figure 3 to achieve an acceptable level of performance. With some trial and error, the gain K is determined.

EXPERIMENTAL RESULTS

The basic experimental structure for tests is shown in Figure 2. In the master station, the 5 MHz of the hydrogen clock used as primary clock was connected to a Ashtech™ GG-24 receiver. The OCXO manufactured by Datum™, Model FTS 1130, was used as the remote clock. The carrier-phase data and other observation messages were passed between both stations through the PSTN interface.

In our experiment, the software, including the proportional controller, communication interface, and data collection, were programmed in C++ on Windows® 2000 and executed on an industrial

PC manufactured by ADVANTECHTM. The data used for the frequency accuracy and stability analysis were measured every 1 second by a TIC (Time Interval Counter) manufactured by SRSTM, model SR620.

For the stability analysis of frequency source under tests, we made use of the IEEE recommended MDEV (Modified Allan Deviation) [11], which is a standard practice in the time and frequency community. In our experiment, the confidence intervals applied to the frequency stability analysis were set to $\pm 68\%$.

We examined the performance of free-running OCXO used in our system and the OCXO under control. These frequency analyses are shown in Figure 4. The OCXO line in Figure 4 shows the frequency instability. The OCXO-C line shows the typical results of frequency stability analyses of the remote OCXO clock under control. These results reveal the high frequency stability of the remote clock not only over the short term, but also over the long term. The frequency stability of the OCXO clock could be improved from about 3×10^{-10} to about 2×10^{-14} for average times of 1 day.

In addition, to assess the limitations of our system regarding clock synchronization, we conducted an experiment by connecting a common hydrogen-maser clock to GNSS receivers in both stations over about a 30-meter baseline. The results of the frequency stability analyses are shown in Figure 5. These results show that our system has a very high frequency stability of about 2×10^{-15} for averaging times of one day.

Figure 6 shows the phase differences between the free-running OCXO clock and the primary clock. The accuracy of this OCXO is about 2.3×10^{-9} for average times of 1 day. Over the approximately 30-meter baseline, the remote OCXO clock is automatically steered to approach synchronization with the primary clock. The accuracy of the remote OCXO clock can be improved from about 2.3×10^{-9} to 5.49×10^{-14} for averaging times of 1 day.

CONCLUSIONS

A new scheme for clock synchronization by using GPS/GLONASS carrier phase is presented. Experimental results show that combining GPS and GLONASS carrier phase seems to provide definite additional value for frequency dissemination. In the experiments, the low-cost OCXO clock could be automatically steered to obtain the very high frequency accuracy and stability in the short term as well as in the long term. In addition, the proposed architecture can achieve the traceability of frequency dissemination. At present, we are trying to establish the frequency source for calibration laboratories and telecommunication networks based on the proposed scheme in Taiwan.

ACKNOWLEDGMENT

We gratefully acknowledge the NBS (National Bureau of Standards) of the R.O.C. for supporting this project.

REFERENCES

- [1] B. Hofmann-Wellenhof, H. Lichtenegger, and J. Collins, *Global Positioning System Theory and Practice*, Springer-Verlag Wien, New York, USA, 1994.
- [2] D. Wells, *Guide to GPS Positioning*, Canadian GPS Associates, 1996.
- [3] von H. Habrich, *Geodetic Applications of the Global Navigation Satellite System (GLONASS) and of GLONASS/GPS Combinations*, 2000
- [4] G. F. Franklin, J. D. Powell and A. Emami-Naeini, *Feedback Control of Dynamic Systems*, 3rd ed. MA: Addison-Wesley, 1994.
- [5] J. A. Davis and J. M. Furlong, *Report on the study to determine the suitability of GPS disciplined oscillators as time and frequency standards traceable to the UK national time scale UTC(NPL)*, Centre for Time Metrology, National Physical Laboratory, UK, 1997.
- [6] G. Petit and C. Thomas, "GPS frequency transfer using carrier-phase measurements," *Proc IEEE Freq. Contr Symp.*, pp. 1151-1159, 1996.
- [7] K. Larson, and J. Levine, "Time-transfer using GPS Carrier Phase Methods", *Proc 29th the Precise Time and Time Interval Meeting*, Long Beach, California, 1997.
- [8] C. Bruyninx, P. Defraigne, J. M. Sleewaegen, and P. Paquet, "Frequency transfer using GPS: comparative study of code and carrier phase analysis results," *Proc 30th Precise Time and Time Interval Meeting*, 1998.
- [9] D. Jefferson, S. Linchten, and L. Young, "A test of precision GPS clock synchronization," *Proc IEEE Freq. Contr Symp.*, pp. 1206-1210, 1996.
- [10] D. Allan and M. Weiss, "Accurate time and frequency transfer using common-view of a GPS satellite," *Proc IEEE Freq. Contr Symp.*, pp. 334-356, 1998.
- [11] International Telecommunication Union Telecommunication Standardization Sector (ITU-T), G. 810, "Definitions and terminology for synchronization," Aug. 1996.
- [12] International Telecommunication Union Telecommunication Standardization Sector (ITU-T), G.811, "Timing characteristics of primary reference clocks," Sept. 1997.

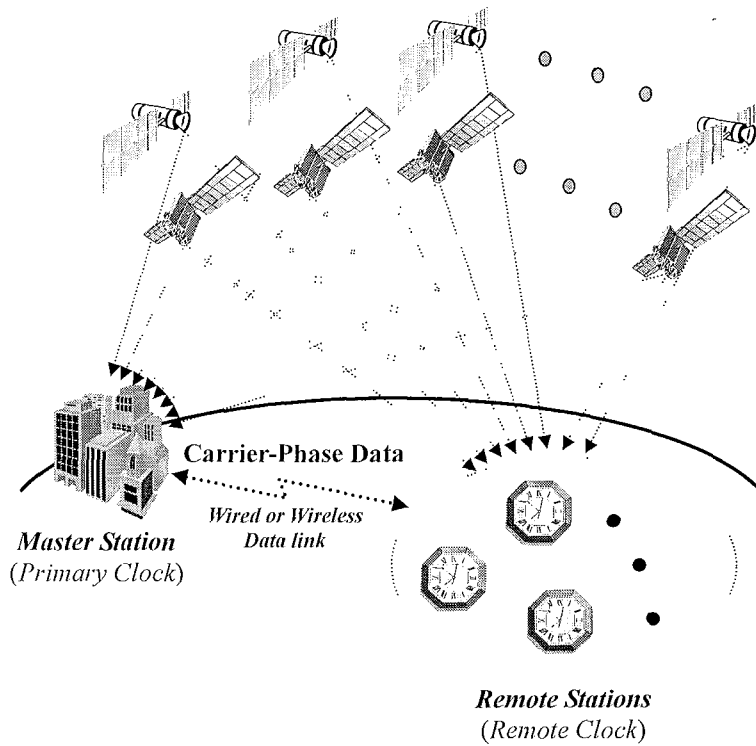


Figure 1. The system architecture for the clock synchronization by using GPS/GLONASS carrier-phase measurements.

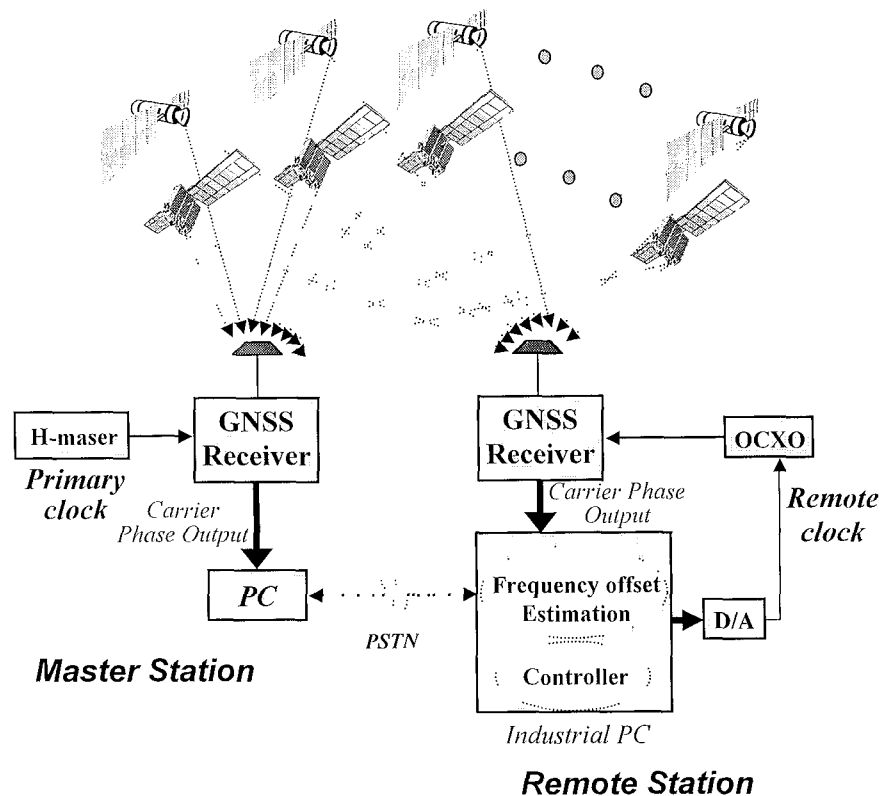


Figure 2. The functional block diagram for the clock synchronization by using GPS/GLONASS carrier-phase measurements.

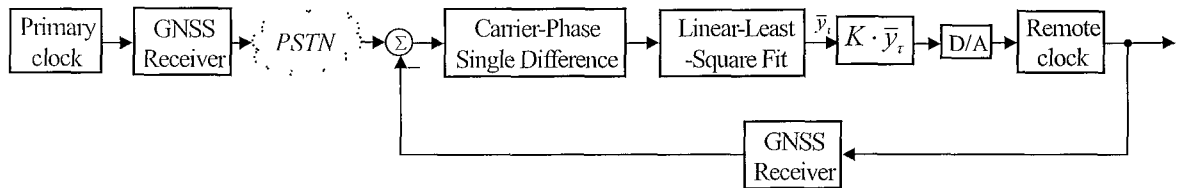


Figure 3. Control block diagram.

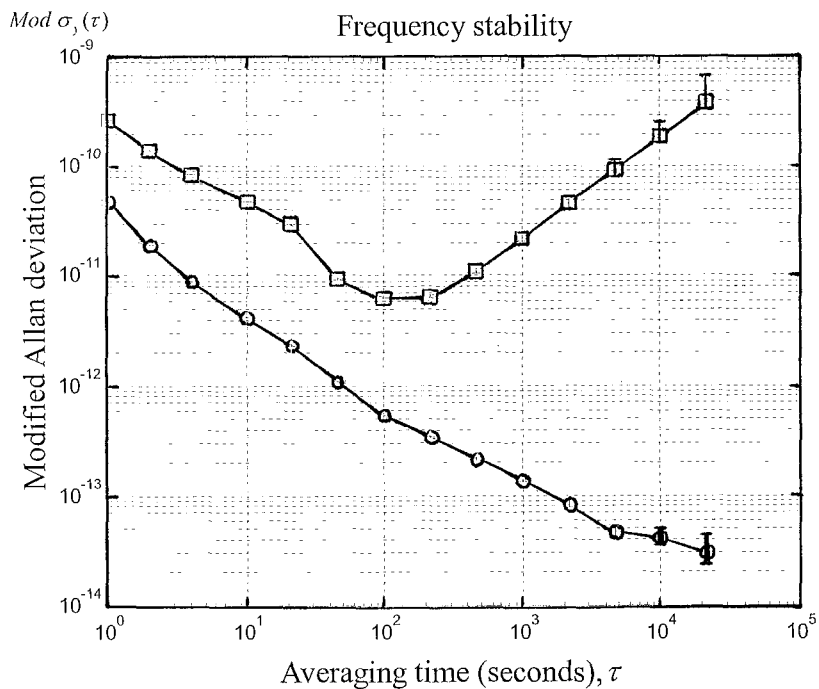


Figure 4. The frequency stability analysis of the free running OCXO (OCXO line) and the OCXO under control (OCXO-C line).

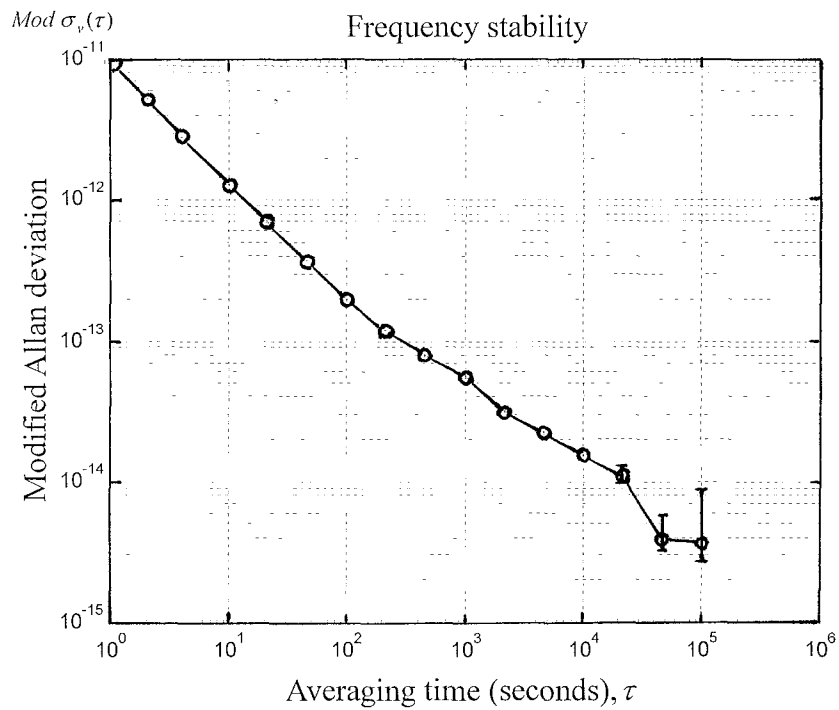


Figure 5. The frequency stability analysis of our system by using the common H-maser clock over short baseline.

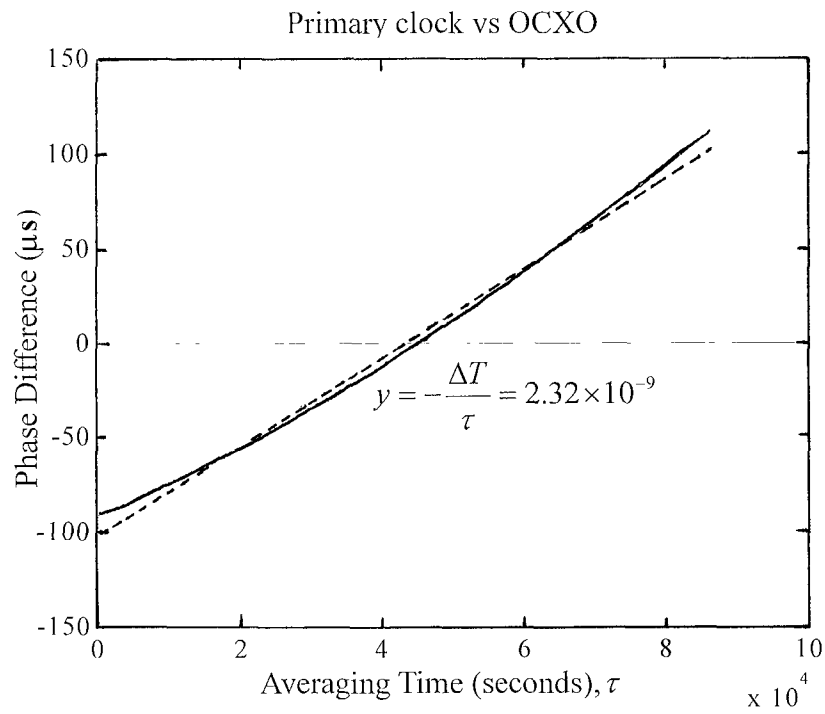


Figure 6 Phase difference between free-running OCXO and primary clock with linear-fit line.

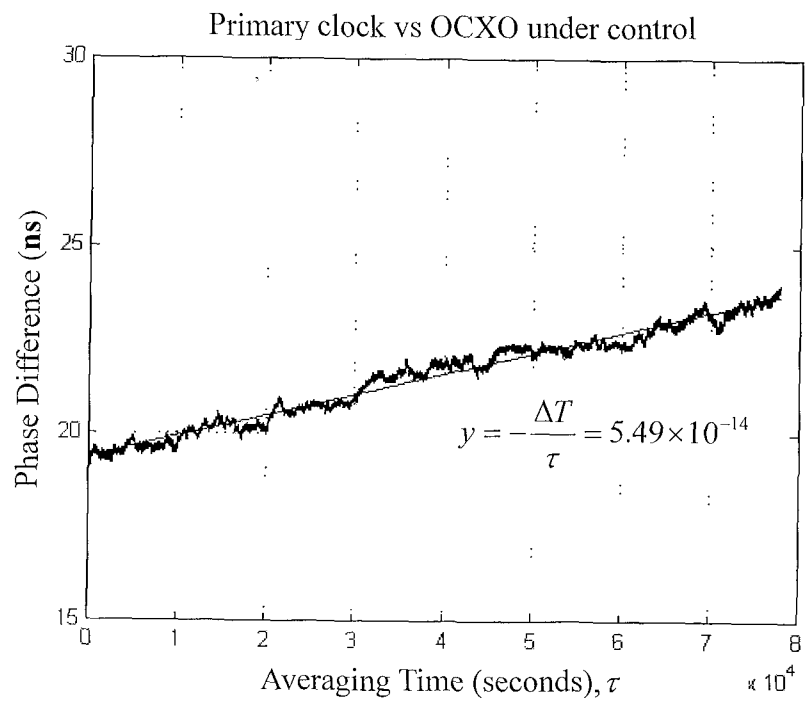


Figure 7. Phase difference between primary clock and remote OCXO clock under control with linear-fit line.

TIME LINKS FOR THE CONSTRUCTION OF TAI

J. Azoubib and W. Lewandowski
Bureau International des Poids et Mesures
Pavillon de Breteuil, F-92312 Sèvres, France

Abstract

The American Global Positioning System (GPS) has served the principal needs of national timing laboratories for regular comparisons of remote atomic clocks for the last two decades. Single-channel GPS C/A-code common-view time transfer is, however, barely sufficient for comparison of today's atomic clocks within a few days, and certainly not sufficient for comparison of clocks currently being designed. For this reason the timing community is engaged in the development of new approaches to time and frequency comparisons, including techniques based on multi-channel GPS and the Russian Global Navigation Satellite System (GLONASS) C/A-code measurements, GLONASS P-code measurements, GPS carrier-phase measurements, temperature-stabilized antennas, standardization of receiver software, and two-way satellite time and frequency transfer through telecommunication satellites. This paper describes how the above-mentioned techniques can be used to meet TAI needs. Some of the techniques are already operational, and the others are expected to be introduced to meet the requirements of future higher accuracy clocks.

INTRODUCTION

The American Global Positioning System (GPS) has served the principal needs of national timing laboratories for regular comparisons of remote atomic clocks for the last two decades [1]. In the pre-GPS era the technology of atomic clocks was always ahead of that of time transfer. The uncertainties of long-distance time comparisons, carried out using the LORAN-C system, were some hundreds of nanoseconds and large areas of the Earth were not covered. This resulted in an annual term in International Atomic Time (TAI). The introduction of GPS has led to a major improvement of world-wide time metrology in precision, accuracy, and coverage. With GPS operated in single-channel common-view C/A-code mode, time comparisons can be performed with an uncertainty of a few nanoseconds, which corresponds to 1 part in 10^{14} for averaging times of a few days. For periods of about one month, the stability of TAI after removal of GPS noise is currently about 2 parts in 10^{15} . Single-channel GPS C/A-code common-view time transfer is, however, barely sufficient for comparison of today's atomic clocks within a few days, and certainly not sufficient for comparison of clocks currently being designed. For this reason the timing community is engaged in the development of new approaches to time and frequency comparisons, including techniques based on multi-channel GPS and the Russian Global Navigation Satellite System (GLONASS) C/A-code measurements, GLONASS P-code measurements, GPS carrier-phase measurements, temperature-stabilized antennas (TSAs), standardization of receiver software, and two-way satellite time and frequency transfer (TWSTFT) through telecommunication satellites.

The performances of various methods of time transfer are illustrated in Figure 1. It has been shown that the stability of time and frequency transfer is improved by a factor of about 3 when GPS common-view time transfer is carried out in multi-channel mode. The use of GLONASS P-code shows a reduction in noise level by a factor of 5 in comparison with GPS C/A-code. It is now well documented that satellite-receiving equipment is subject to significant systematic effects due to environmental conditions; the use of TSA antennas and better cables reduces these effects and improves the accuracy of time transfer. The GPS carrier-phase technique allows frequency comparisons at a level of 1 part in 10^{15} and should soon be a useful tool for the comparison of primary frequency standards. Difficulties in calibration of GPS carrier-phase equipment remain unresolved, however, and this technique can not yet be used for operational time transfer. The TWSTFT technique, which has a similar performance to that of carrier phase, is already operational and used in TAI for several time links.

This paper reviews the above-mentioned techniques and assesses their potential impact on TAI.

EVOLUTION OF CLOCKS AND TIME LINKS CONTRIBUTING TO TAI

The international time scales computed at the Bureau International des Poids et Mesures (BIPM) – TAI and UTC – are based on data from some 220 atomic clocks located in about 50 time laboratories around the world. The number of clocks fluctuates a little, but remains roughly constant. The quality of the clocks, however, has been improving dramatically. In 1992 the first HP* 5071A caesium clocks with high-performance tubes were introduced into the TAI computation (see Figure 2), and the number of hydrogen masers has also been increasing steadily. In 1999 about 65 % of the participating clocks were HP 5071A with a high-performance tube and about 17 % were hydrogen masers [2]. Other commercial cesium clocks (including HP 5071A clocks with a low-performance tube, and continuously operating primary frequency standards) account for only 18 %. This progress has of course contributed to a significant improvement in the stability of TAI.

The quality of the clocks, although an important issue, is not the only factor contributing to the stability of TAI. Another important factor is the quality of the time links used to compare the clocks. Prior to 1981 only LORAN-C and TV links were used to compare clocks contributing to TAI. In 1981 the first GPS common-view single-channel C/A-code links were introduced. These allowed, for the first time, comparison of the stability of remote atomic clocks within an averaging time of several days. The proportion of GPS common-view links has increased steadily over the years and reached almost 100% in 1999 (see Figure 3). A new technique was then entered into TAI: that of Two-Way Satellite Time and Frequency Transfer (TWSTFT). As of June 2000 five TWSTFT links are used for TAI, and several others are in preparation.

* Acronyms are listed and defined at the end of the article.

To illustrate the impact of the improved quality of the time links on the frequency stability of TAI, we have analysed the period mid-1986-1993, during which the number of GPS links steadily increase, but there was no dramatic change in the nature of the participating clocks. The frequency stability of EAL (the échelle atomic libre) against the primary frequency standard PTB CS2 is indicated in Figure 4 for the three periods mid-1986-mid-1988, 1988-1989 and 1992-1993. EAL is the free atomic time scale from which TAI is derived using steering corrections. We observe a significant improvement in the frequency stability of EAL for each consecutive period for averaging times up to a few tens of days (for these averaging times the white phase noise due to the time-transfer methods by which EAL was affected is drastically reduced). The evaluation of the frequency stability of EAL is here limited by the frequency stability of PTB CS2.

A more recent evaluation of the stability of the frequency of EAL is illustrated in Figure 5. This time, the *N*-cornered-hat method was employed using the best independent atomic time scales (maintained at the OP, the NIST, the PTB, and the USNO).

ORGANIZATION OF TAI LINKS

Until recently the TAI GPS common-view time links were organized in three major stars centered on the CRL, the NIST and the OP. Only two very long-baseline links, NIST/OP and OP/CRL, were corrected for IGS precise ephemerides [3] and ionospheric measurements [4] (see Figure 6). Since the first use of IGS ionospheric maps for international time transfer in July 1999 [5], these corrections are now applied to all TAI GPS common-view links.

In July 1999 the first TWSTFT link, PTB/TUG, was introduced into the computation of TAI. In January 2000 other TWSTFT links followed. At the time of writing there are three TWSTFT links directly used for TAI: USNO/NPL, VSL/PTB, and NPL/PTB (see Figure 7). These three links are backed-up by GPS common-view data. Further TWSTFT links are expected to be introduced in 2001. There is also a backup TWSTFT link used to check the GPS common-view NIST/PTB link. The AMC/USNO TWSTFT link is an internal link between the USNO headquarters in Washington DC and their Alternate Master Clock (AMC) in Colorado Springs.

Two transatlantic links are being used for the first time for the construction of TAI. In addition each of these links is performed by two independent techniques. This very new situation increases the robustness of the construction of TAI, which no longer relies on a single technique. These changes modify the shape of the TAI network in Europe, with TWSTFT links acting as main shore and new pivots. The first three GPS multi-channel GPS common-view links were introduced into TAI at the beginning of 2000, with NPL as pivot.

CALIBRATION OF TAI LINKS

Differential calibration of remote GPS time equipment is the basic technique for the calibration of TAI GPS common-view time links. The stated uncertainty of such a differential calibration is about 3 ns under ideal conditions.

Over the last fifteen years a number of differential calibrations have been performed by the BIPM [5], including about half of the TAI GPS links. The GPS time equipment located at the NIST in Boulder, Colorado, and the Paris Observatory (OP) have been compared about 10 times; differential time corrections determined during these calibrations differ by no more than a few nanoseconds. This gives an indication of the reproducibility that can be obtained when calibrations are performed under ideal conditions in laboratories where the GPS time equipment, including cables, is carefully maintained. It also gives some idea of the long-term stability of GPS time equipment.

Consistency between repeated calibrations is not found for all sites, however. Where discrepancies of 10 ns are found, these may be attributed to different responses of the receivers being compared, to seasonal changes of temperature, or to an unrecognized multipath effect. Other repeated calibrations have shown large discrepancies, sometimes of tens of nanoseconds; such changes probably arise from unrecorded changes, intended or not, in the GPS receiving hardware.

All TWSTFT links currently used for TAI have been calibrated: the PTB/TUG link by a portable TWSTFT station, all the others by *Circular T* (in other words, by GPS). Future GPS calibration trips will improve the calibration of the TWSTFT links. However, only repeated calibrations by portable TWSTFT equipment will allow the TWSTFT technique to be exploited to the full extent. In May 2000 the USNO undertook the calibration of the PTB/USNO TWSTFT link using a portable station. The NPL/USNO link will be calibrated by the same very shortly. These calibrations are of particular interest, because they use a geostationary satellite with a footprint covering the Eastern United States, South America, and large parts of Europe and Africa. This allows the use of the same transponder for transatlantic links and, consequently, the differential calibration of transatlantic TWSTFT links.

NEW TIME-TRANSFER TECHNIQUES

In this section we briefly review latest developments in time-transfer techniques. These are already benefitting TAI, or expected to do so in the near future.

GPS and GLONASS Multi-Channel Observations and TSA

In a field trial of time transfer over a baseline of several hundred kilometers the number of daily standard 13-minute common views increased from 40 for GPS single-channel observations to 585 for GPS+GLONASS multi-channel observations [7]. In the case of white phase noise, the

corresponding gain in stability is predicted to be $(585/40)^{1/2} = 3.8$, and a value close to this was observed. Additional systematic effects were observed for averaging times of about 1 day; these are probably linked to the environmental sensitivity of the antennas and receivers.

In a one-site comparison (two separate antennas on a single site), a similar systematic effect was observed until both antennas were temperature-stabilized (TSA). Full advantage could then be taken of the improved stability offered by multi-channel time transfer [7].

There are currently about 15 TSA antennas operating at time laboratories contributing to TAI, and there are three multi-channel GPS common-view links used for TAI.

GLONASS P-Code Common View

Unlike GPS, GLONASS P-code signal is available to civil users as it is not subject to Anti-Spoofing (AS) or other encryption. GLONASS P-code has two main advantages for precise time synchronization. First, its chip-length is one-tenth that of GLONASS C/A-code and about one-fifth that of GPS C/A-code. Thus GLONASS P-code pseudo-range measurements are considerably more precise than comparable GPS or GLONASS C/A-code measurements [8]. Second, GLONASS P-code is transmitted on both L1 and L2 frequencies, so it allows high-precision measurements to be made of ionospheric delays.

GPS Carrier Phase

Locking on the carrier phase reduces multipath effects. With the multi-channel receivers now available and using the common-view double-differencing techniques typical in geodesy, two sites may well be able to maintain a common carrier phase. If measured ionospheric delays were used in combination with nominally compensated tropospheric corrections, a frequency stability of 1 part in 10^{15} might be attainable with integration times of about 1 day [10]. This performance is about what is required for the comparison of current primary frequency standards. Continuous measurements, rather than measurements taken once a day, are necessary to achieve this performance. Several trials have already demonstrated the advantages of using carrier-phase measurements for time and frequency comparisons [11].

Time metrologists have recently joined forces with geodesists in an important initiative known as the "IGS/BIPM Pilot Project to Study Accurate Time and Frequency Comparisons Using GPS Carrier Phase and Code Measurements". An important issue is the calibration of carrier-phase timing equipment, which limits the performance of the technique.

It is important to note that carrier phase is also affected by hardware delay instabilities. Here also, to take full advantage of this promising technology, the delays of various parts of the receiving equipment must be stabilized and measured.

In the near future the carrier-phase technique is likely to be used for frequency comparisons of primary standards.

Two-Way Satellite Time and Frequency Transfer

TWSTFT is a technique that utilizes geostationary telecommunications satellites to provide time transfer with a theoretical precision of several hundred picoseconds [12]. At present the TWSTFT technique is operational in eight European, three US and two Japanese time laboratories. Some other laboratories have reached pre-operational status. The technique has been contributed to TAI since July 1999, following recommendations of the Consultative Committee for Time and Frequency (CCTF). The number of such links used for TAI is likely to increase from the present five.

In May 1999 the BIPM started publishing Monthly TWSTFT Reports. Some selected TWSTFT links through INTELSAT 307° E are computed and compared with GPS at the time of preparation of *Circular T*. An example of such a comparison is given in Figure 8.

Modified Allan variance analysis of TWSTFT and GPS links shows better behavior of TWSTFT for all analysed links up to 10 days. This is particularly striking for the USNO/NPL link where TWSTFT is showing the behavior of clocks already for averaging time of 5 days (see Figure 9). Using a GPS link we have to wait 20 days to smooth out white-phase noise due to time transfer.

SUMMARY

The construction of TAI requires time-transfer techniques that allow participating clocks to be compared at their full level of performance for intervals at which TAI is computed. In the pre-GPS era this was impossible because the technology of atomic clocks was always ahead of that of time transfer. This resulted in an annual term in TAI. The replacement of LORAN-C links by GPS C/A-code common-view links during the years 1981-1998 has progressively reduced the impact of white phase noise on TAI, improving its stability up to about 80 days. During the 1980s, GPS allowed for the first time the comparison of remote atomic clocks at their full level of performance for averaging times of just a few days, fully satisfying needs of TAI, computed at this epoch at intervals of 10 days.

However, with the improvements in clock technology made during the 1980s and the resulting dramatic increase in the quality of the clocks contributing to TAI in the 1990s, intercontinental GPS C/A-code common-view measurements now need to be averaged over up to 20 days in order to smooth out measurement noise. This is no longer sufficient for TAI, computed at 5-day intervals from 1 January 1996.

The first analysis of the performance of TWSTFT, which is now in use for several TAI links, shows that clocks located on different continents can be compared by this technique at 5-day intervals at their full level of performance, without being affected by time-transfer measurement noise. Thus, if TWSTFT were used for all TAI links, the stability of TAI would be improved for periods of up to 20 days.

The introduction of TWSTFT into TAI has brought about another important change for the better; TAI is no longer reliant on a single technique, because TWSTFT links are backed up by GPS links and vice versa. Also, for the first time, two transatlantic links are used for its construction,

and each of these links is performed by two independent techniques. This very new situation increases the robustness of TAI construction.

Another important issue is the accuracy of TAI time links. These determine the accuracy with which laboratories have access to UTC. Significant proportion of GPS links were never calibrated and their accuracy is limited to several tens of nanoseconds. The other GPS links and all but one of the TWSTFT links have been calibrated by a differential technique using a portable GPS receiver. The uncertainty of such a calibration is limited to several nanoseconds, mainly due to the environmental instability of GPS time-receiving equipment. This could be reduced by using TSAs, keeping receivers in air-conditioned rooms, and, if possible, using GLONASS P-code observations.

One TWSTFT link, PTB/TUG, has been calibrated by a portable TWSTFT station. The uncertainty of this calibration is believed to be 1 ns or better. Other TWSTFT calibrations are planned, and it is expected that use of TWSTFT will bring a substantial improvement to the accuracy of TAI time links.

For better monitoring of the accuracy of time links, repeated calibrations are required, either by GPS or by TWSTFT.

ACRONYMS

- AMC – Alternate Master Clock
- BIPM – Bureau International des Poids et Mesures
- CCTF – Consultative Committee for Time and Frequency
- CRL – Communications Research Laboratory
- CV – Common View
- EAL – Echelle atomic libre
- GLONASS – Global Navigation Satellite System
- GPS – Global Positioning System
- HP – Hewlett-Packard
- IGS – International GPS Service
- IGEX – International GLONASS Experiment
- IGLOS-PP – International GLONASS Service Pilot Project
- MJD – Modified Julian Day
- NIST – National Institute of Standards and Technology
- NPL – National Physical Laboratory
- OP – Observatoire de Paris
- PTB – Physikalisch-Technische Bundesanstalt
- TAI – Temps atomic international
- TUG - Technical University of Graz
- TWSTFT – Two-Way Satellite Time and Frequency Transfer
- USNO – United States Naval observatory
- UTC - Coordinated Universal Time

REFERENCES

- [1] D. W. Allan, and M. A. Weiss 1980, "Accurate time and frequency transfer during common-view of a GPS satellite," Proceedings of the 34th Annual Symposium on Frequency Control, 28-30 May 1980, Philadelphia, Pennsylvania, pp. 334-336.
- [2] W. Lewandowski, and J. Azoubib 2000, "Time transfer and TAI," Proceedings of the 2000 IEEE/EIA International Frequency Control Symposium and Exhibition, 7-9 June 2000, Kansas City, Missouri, USA, IEEE 00CH37052, pp. 586-597.
- [3] W. Lewandowski, and M. A. Weiss 1990, "Precise ephemerides for GPS time transfer," Proceedings of the 21st Annual Precise Time and Time Interval (PTTI) Applications and Planning Meeting, 28-30 November 1989, Redondo Beach, California, USA, pp. 95-106.
- [4] M. Imae, W. Lewandowski, C. Thomas, and C. Miki 1989, "A dual frequency GPS receiver measuring ionospheric effects without code demodulation and its application to time comparisons," Proceedings of the 20th Annual Precise Time and Time Interval (PTTI) Applications and Planning Meeting, 29 November-1 December 1988, Tysons Corner/Vienna, Virginia, USA, pp. 77-86.
- [5] P. Wolf, and G. Petit 2000, "Use of IGS ionosphere products in TAI," Proceedings of the 31st Annual Precise Time and Time Interval (PTTI) Systems and Applications Meeting, 7-9 December 1999, Dana Point, California, USA, pp. 419-429.
- [6] J. Azoubib, W. Lewandowski, and J. Nawocki 2001, "First calibration trip of GPS+GLONASS receivers," BIPM Report (in preparation).
- [7] W. Lewandowski, J. Azoubib, G. de Jong, J. Nawrocki, and J. Danaher 1997, "A new approach to international time and frequency comparisons: "all-in-view" multi-channel GPS+GLONASS observations," Proceedings of the ION GPS-97, pp. 1085-1091.
- [8] J. Azoubib and W. Lewandowski 2000, "Test of GLONASS precise-code time transfer," *Metrologia*, 37, 55-59.
- [9] W. Lewandowski, J. Nawrocki, and J. Azoubib 2000, "First use of IGEX precise ephemerides for international GLONASS P-code time transfer," *Journal of Geodesy* (in press).
- [10] T. Schildknecht, G. Beutler, W. Gurtner, and M. Rothacher 1990, "Towards subnanosecond GPS time transfer using geodetic GPS processing techniques," Proceedings of the 4th European Frequency and Time Forum (EFTF), 13-15 March 1990, Neuchâtel, Switzerland, pp. 335-346.
- [11] S. L. Shemar, J. D. Clarke, J. A. Davis, A. J. Lowe, and P. J. Chapman 2000, "Comparisons of the two-way, GPS carrier-phase and GPS common-view time transfer methods," Proceedings of the 14th European Frequency and Time Forum (EFTF), 14-16 March 2000, Torino, Italy (in press).
- [12] D. Kirchner, H. Ressler, P. Grudler, F. Baumont, C. Veillet, W. Lewandowski, W. Hanson, W. J. Klepczynski, and P. Uhrich 1993, "Comparison of GPS common-view and two-way satellite time transfer over a baseline of 800 km," *Metrologia*, 30, 183-192.

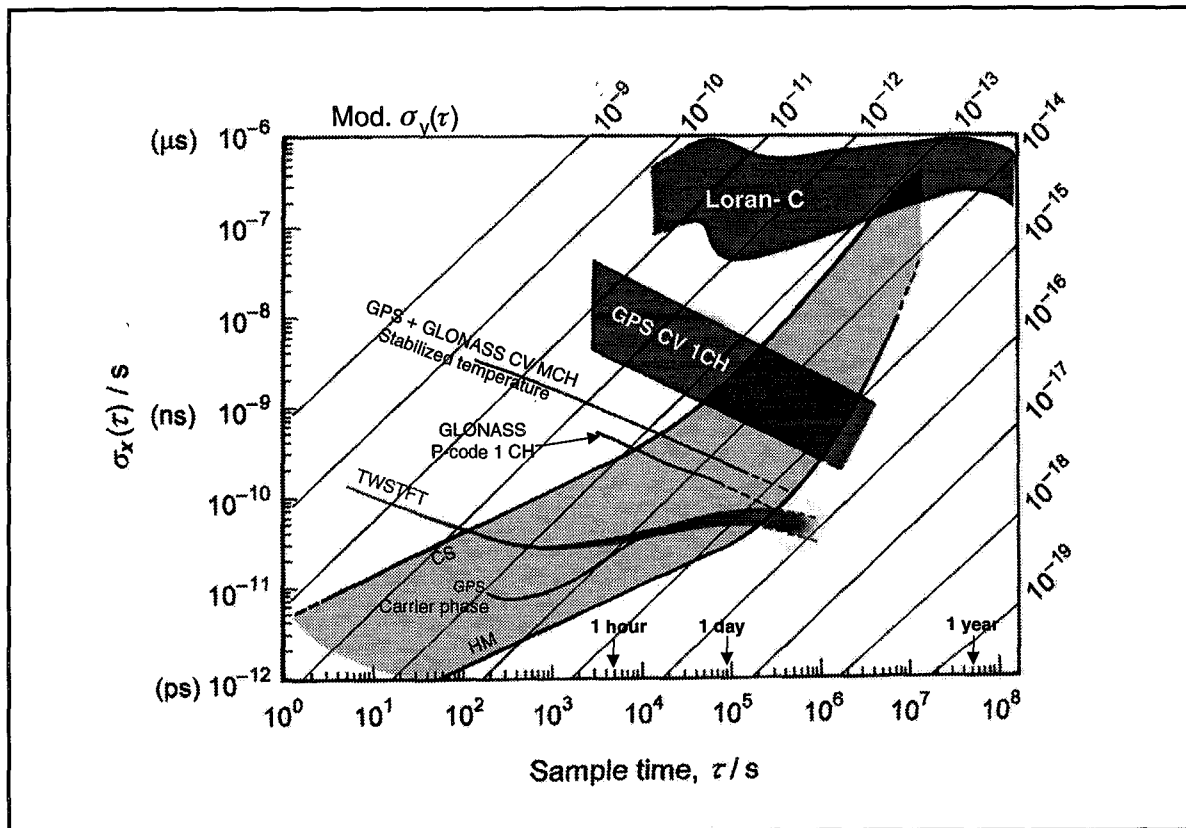


Figure 1. Comparison of some newer techniques with classical GPS single-channel common-view time transfer. Also indicated are typical clock performances.

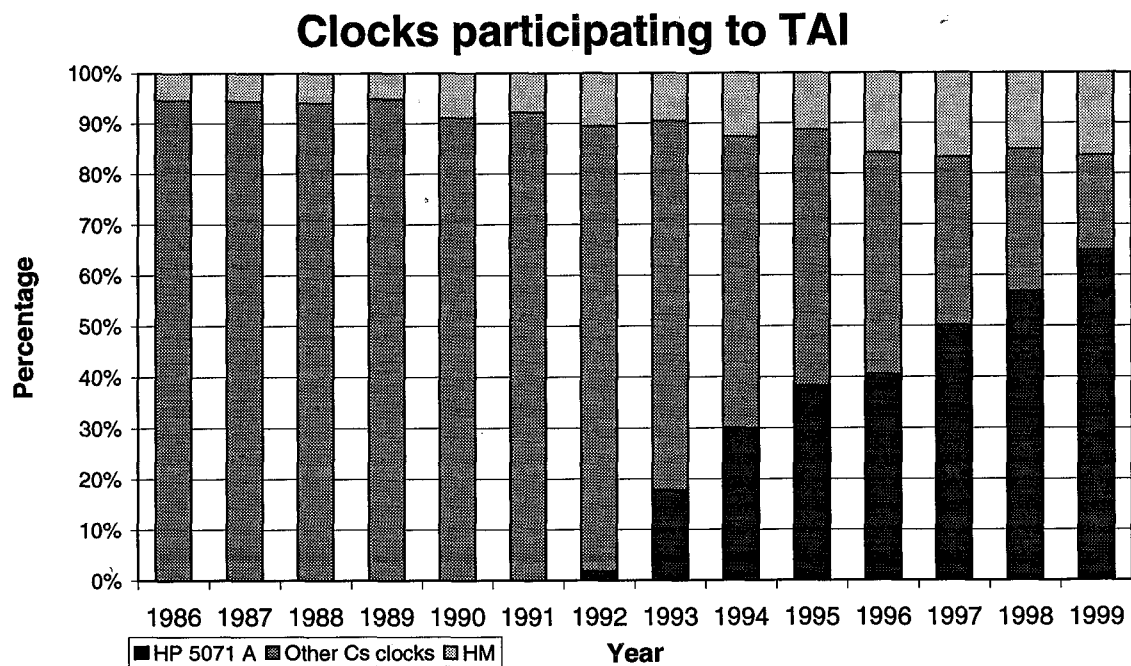


Figure 2. Clocks participating in TAI.

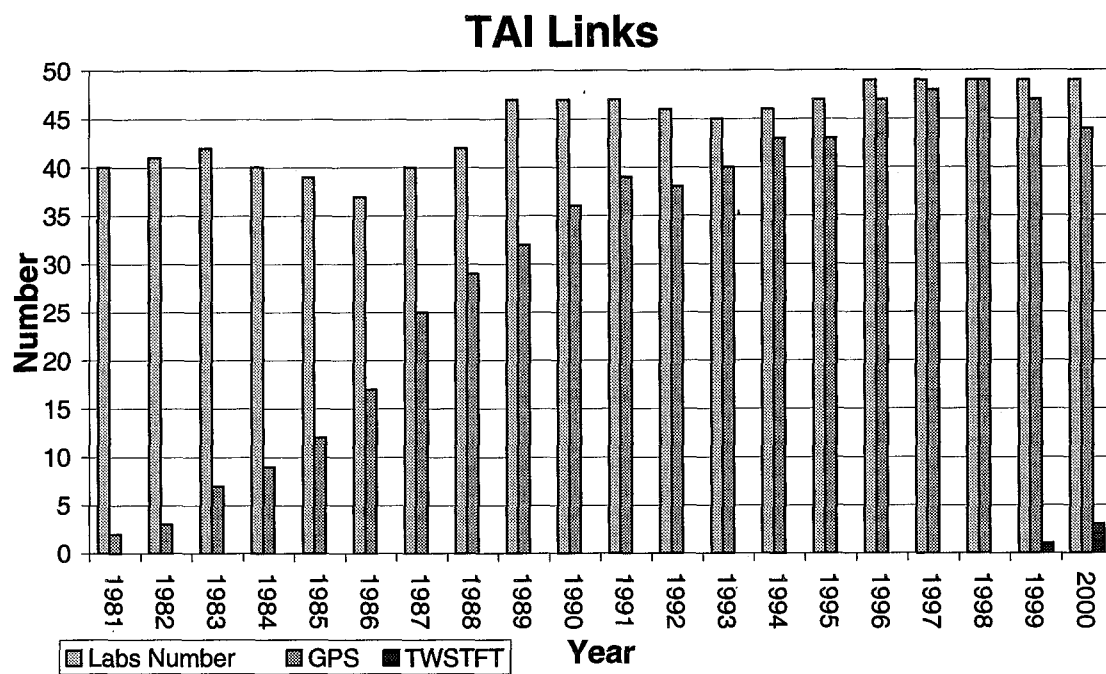


Figure 3. TAI time links.

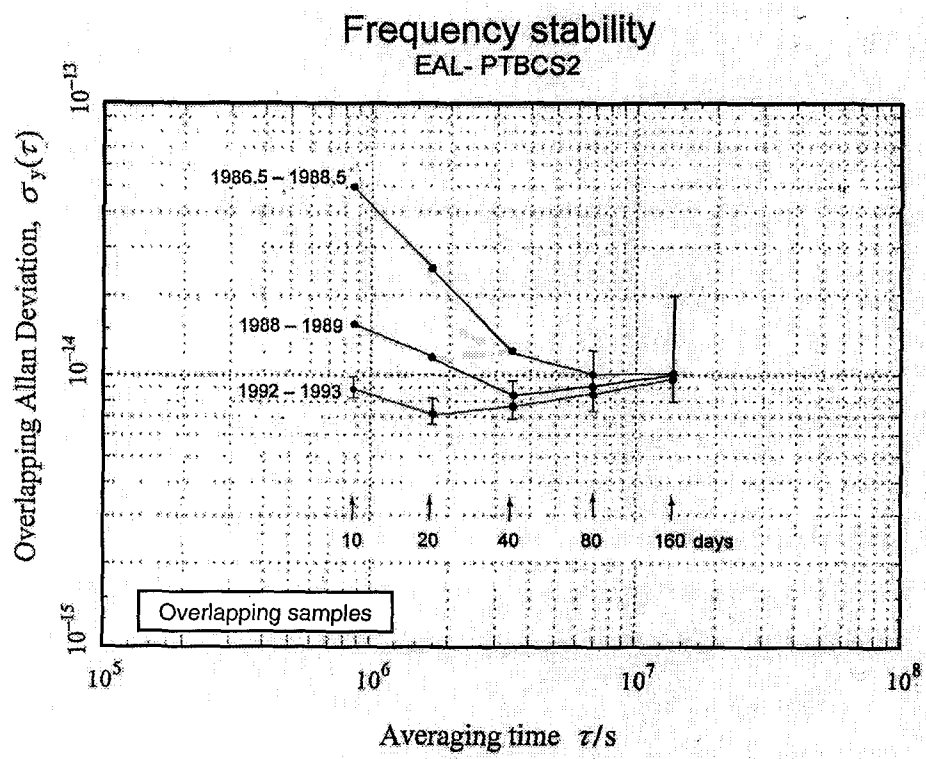


Figure 4. Frequency stability of [EAL – PTB Cs2].

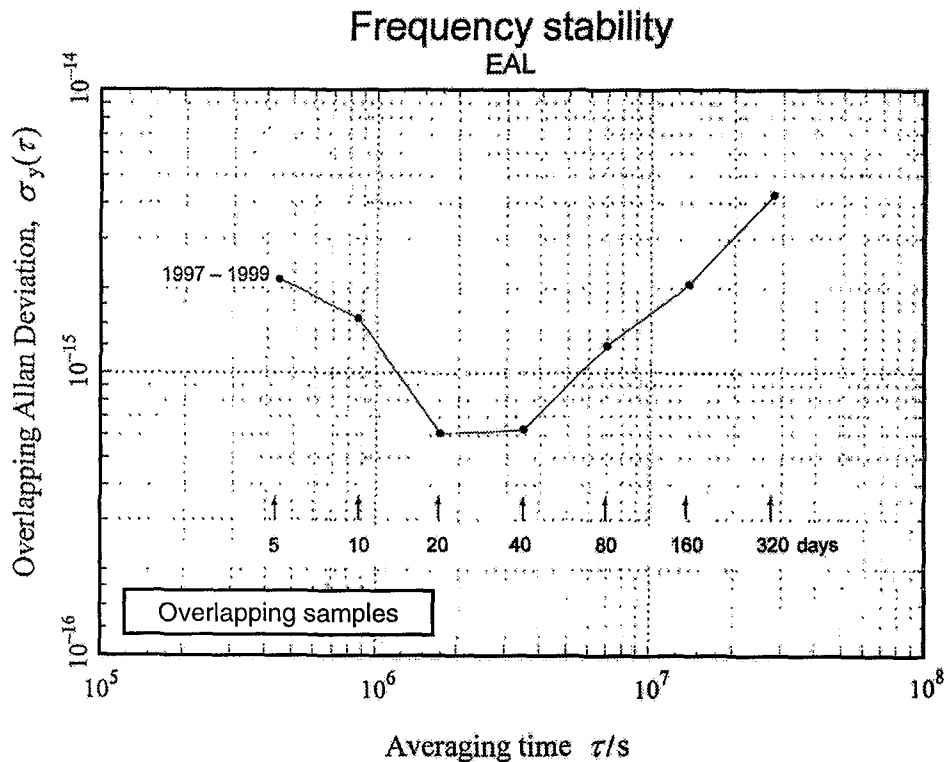
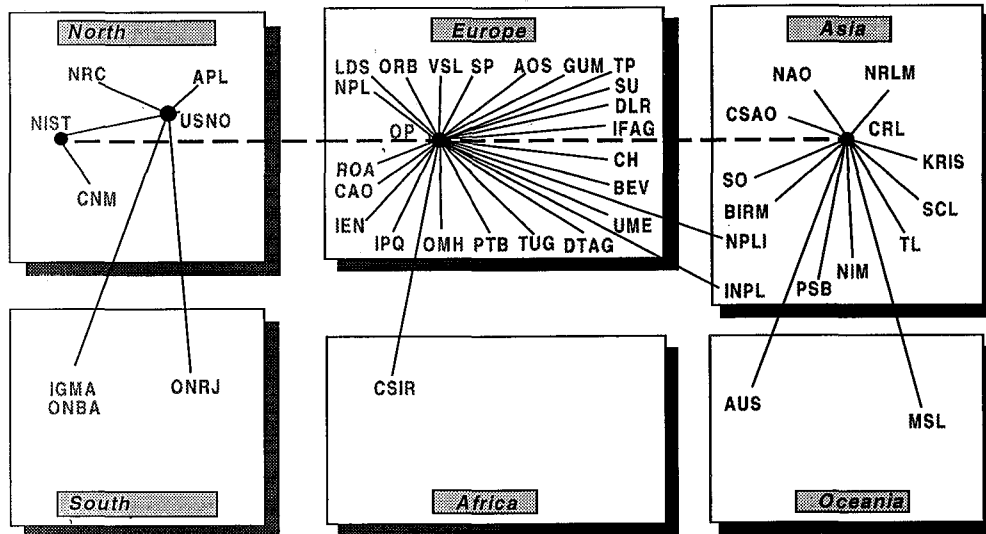


Figure 5. Frequency stability of EAL obtained by N -cornered-hat method using independent atomic time scales maintained at the OP, the NIST, the PTB and the USNO.



June 1999

ORGANIZATION OF THE INTERNATIONAL TIME

- GPS common view
- - - GPS common view (corrected with IGS precise ephemerides and ionospheric maps).

Figure 6. Organization of international time links in June 1999.

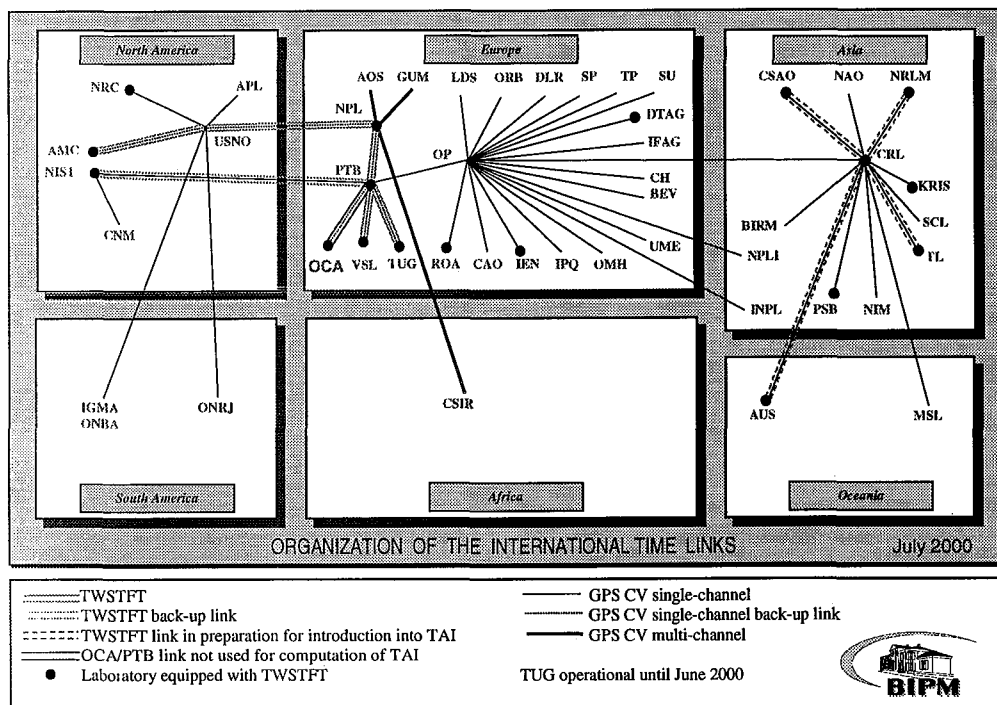


Figure 7. Organization of international time links in November 2000.

$$Y = [UTC(USNO)-UTC(NPL)] \text{ twstft-gps}$$

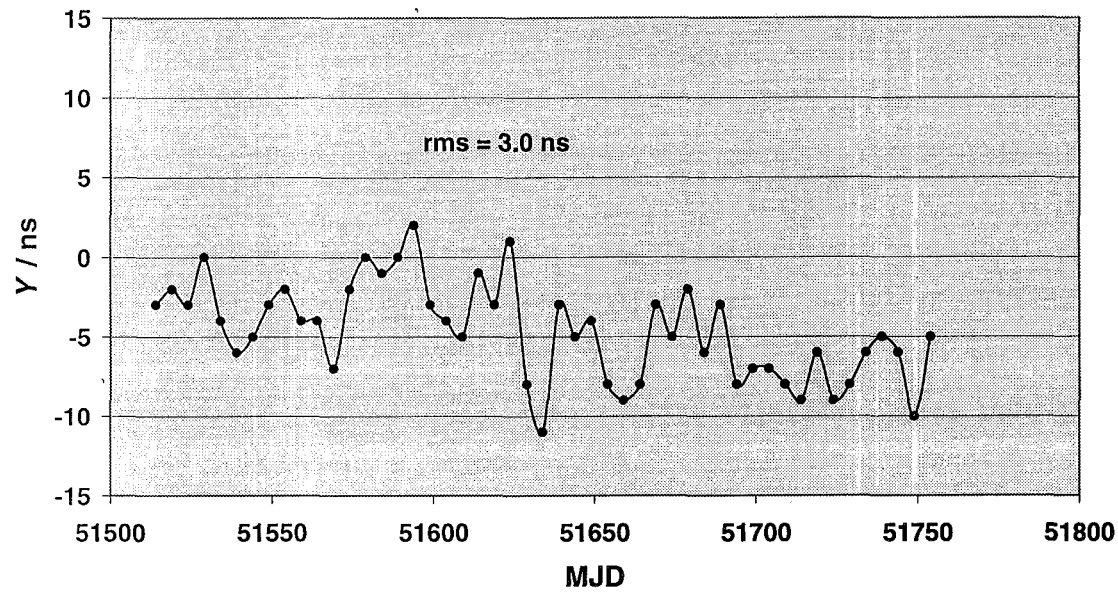


Figure 8. Differences between TWSTFT and GPS common-view for USNO/NPL link.

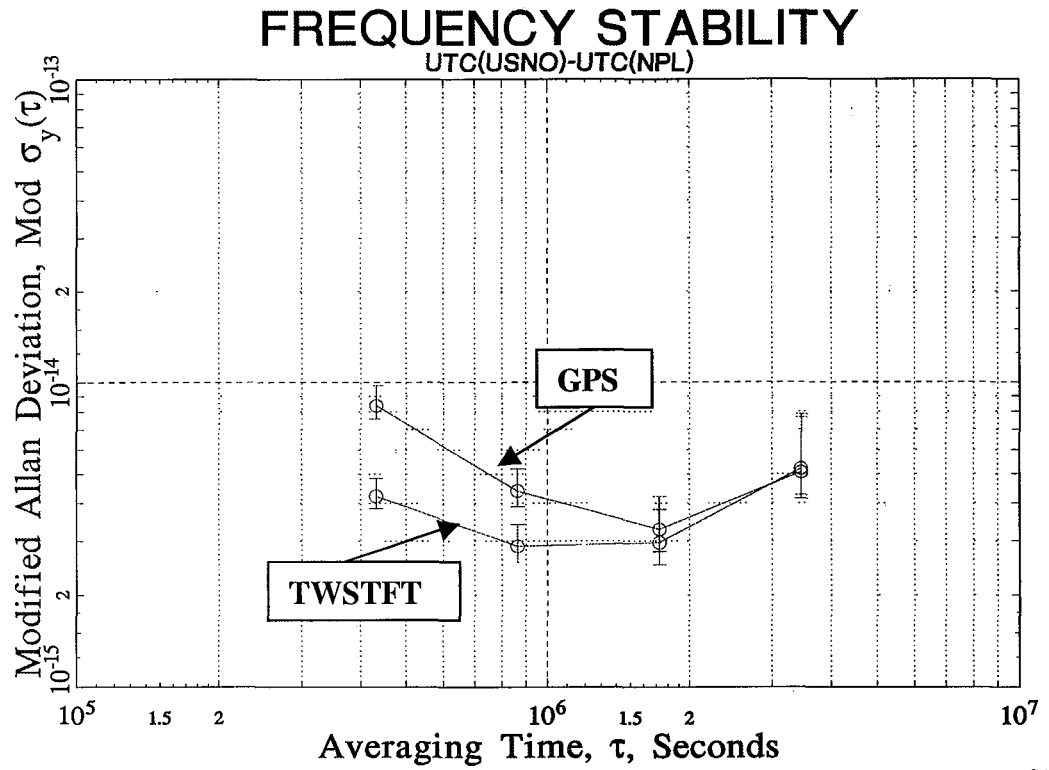


Figure 9. Frequency stability of $[UTC(USNO) - UTC(NPL)]$ by GPS and by TWSTFT.

Questions and Answers

DEMETRIOS MATSAKIS (USNO): Let me ask a loaded question. Is there any activity going on to look at the difference between northern and southern hemispheres to find any kind of seasonal variations that way?

WLODZIMIERZ LEWANDOWSKI: You mean in time links?

MATSAKIS: Time or frequency.

LEWANDOWSKI: Well, in Japan there were some studies about the correlation between clocks. Right now, I don't see any studies done. It could be that we should provide something. For example, for the seasonal changes between two-way and GPS common-view, where we have a seasonal change, we would look in the hemisphere. But, we do not have two-way links. We may have a link between Tokyo and Australia and in the future we could be looking at that.

A REVISED WAY OF FIXING AN UPPER LIMIT TO CLOCK WEIGHTS IN TAI COMPUTATION

J. Azoubib

Bureau International des Poids et Mesures
Pavillon de Breteuil, F-92312 Sèvres Cedex, France
Jazoubib@bipm.org

Abstract

The free atomic time scale Échelle Atomique Libre (EAL), from which International Atomic Time (TAI) is derived by frequency steering, is obtained as a weighted average of a large number of free-running and independent atomic clocks spread worldwide, using the algorithm ALGOS which is optimized for long-term stability. Since January 1998, a new procedure for implementing an upper limit of clock weights has been used. The use of an absolute maximum weight p_{MAX} , was replaced by the choice of a relative maximum weight, ω_{MAX} . This new technique is more robust than the former one and it optimizes the stability of the time scale at the expense of a more complicated computation. The chosen value $\omega_{MAX} = 7.00 \times 10^{-3}$ corresponded to the value of the maximum relative weight assigned to clocks in the EAL computation, with $p_{MAX} = 2500$, in the 60-day interval November/December 1997. In this paper, we show that $\omega_{MAX} = 7.00 \times 10^{-3}$ is no longer appropriate. No efficient discrimination is made between the HP 5071A units: more than 80% of such clocks reach the maximum relative weight. The value of ω_{MAX} really needs to be updated from time to time in order to obtain an efficient discrimination between the HP 5071A units and to improve the stability of EAL. To avoid frequent redefinition of ω_{MAX} , we suggest here making ω_{MAX} a function of the number, N , of clocks that participate in TAI. A relation such as $\omega_{MAX} = A/N$, where A is an empirical constant, could be used. Such a relation has been tested using ALGOS with values 3.0, 2.5, and 2.0 for A . The resulting computed time scales (over 2.5 years) using real data show that all the HP 5071A units are not equivalent. We also obtain an improved stability for the computed time scales, which is the underlying aim of this study.

1 INTRODUCTION

The free atomic time scale EAL (échelle atomique libre), from which TAI is derived by frequency steering, is obtained as a weighted average of a large number of free-running and independent atomic clocks spread worldwide. The computation uses the algorithm ALGOS, which is optimized for long-term stability.

Since January 1998, a modified form of the algorithm has been used for the calculation of TAI. This algorithm is based on the same defining equations as ALGOS [1], but includes two changes:

- reduction of the time interval T of the computation from two months to one month [2];
- application of an upper limit to the relative weights, ω_{MAX} , instead of to the absolute weights, p_{MAX} , attributed to the contributing clocks [3, 4].

These changes are described in more detail in [5] and [6].

The value $\omega_{\text{MAX}} = 7.00 \times 10^{-3}$ was fixed at the time of the first computation (January 1998) to ensure continuity of the time scale. It corresponds to the value of the maximum relative weight assigned to clocks in the EAL computation (with $p_{\text{MAX}} = 2500$) in the 60-day interval November/December 1997. Our analysis of the distribution of the relative weights attributed to clocks shows, however, that this value is no longer appropriate.

The underlying aim of this study is to improve the stability of EAL and, hence, of TAI. To achieve this we need to take best advantage from the HP 5071A clocks and also from the hydrogen masers, by discriminating efficiently between them. Fixing an appropriate upper limit to the clocks weights in the EAL computation can ensure this.

As the choice of ω_{MAX} is empirical, we could simply update its value, but, as we demonstrate that fixing ω_{MAX} to a constant could lead to a situation where the weights ω_i attributed to clocks are not normalized.

To avoid such a situation, we suggest making ω_{MAX} a function of the number, N , of clocks participating in TAI. A relation such as $\omega_{\text{MAX}} = A/N$ is proposed, where A is an empirical constant.

Three test time scales (E2, E25 and E3) have been established over 2.5 years using real clock data. They are based on the algorithm ALGOS and use the values 2.0, 2.5 and 3.0, respectively, for the constant A . By comparing the distributions of the resulting relative weights attributed, we show that E2, E25, and E3 allow a much better discrimination between clocks than does EAL. As they rely more heavily on the very best clocks, the time scales E2, E25, and E3, are thus more stable than EAL. We conclude that the stability of EAL, and hence that of TAI, can be improved.

2 THE UPPER LIMIT OF RELATIVE WEIGHTS IN EAL COMPUTATION

The computational process used to apply an upper limit to relative weights in ALGOS is described in [4]. The most important feature of this process is that it does not independently assign a weight to each clock; instead, the set of clocks is treated globally.

The classical variance of the frequency of clock H_i relative to EAL [$\sigma_i^2(12,T)$, computed from 12 consecutive 30-day samples] plays an important part in the computation of its relative weight, ω_i , and therefore has an effect on the stability of EAL. This variance $\sigma_i^2(12,T)$ (calculated over twelve consecutive samples of duration T) is an estimate of the zero-dead-time sample variance $\sigma_i^2(12,T,T)$ [7, 8] of the frequencies of clock H_i relative to EAL, and is linked to the usual Allan variance $\sigma_{y_i}^2(T)$ by the relation:

$$\sigma_i^2(12,T,T) = B_1 \sigma_{y_i}^2(T) \quad (1)$$

where $B_1 = 1.924$ in the case of flicker-frequency noise modulation over averaging times $T = 30$ d.

When EAL is computed, $\sigma_i^2(12,T)$ values of the clocks reaching ω_{MAX} , differ significantly. We define σ_{MIN}^2 to be the largest of these variances, corresponding to the least stable clock attributed ω_{MAX} .

Figure 1 shows the distribution of relative weights, $\{\omega_i, i = 1, N\}$, attributed to clocks in the EAL computation. The given values are the means calculated over 2.5 years (from January 1998 until June 2000). The number of clocks reaching $\omega_{\text{MAX}} = 7.00 \times 10^{-3}$ and falling within five other classes of relative weight ω_i are presented. The classes are defined below:

class I	$80 \% \omega_{\text{MAX}} \leq \omega_i < \omega_{\text{MAX}}$
class II	$60 \% \omega_{\text{MAX}} \leq \omega_i < 80 \% \omega_{\text{MAX}}$
class III	$40 \% \omega_{\text{MAX}} \leq \omega_i < 60 \% \omega_{\text{MAX}}$
class IV	$20 \% \omega_{\text{MAX}} \leq \omega_i < 40 \% \omega_{\text{MAX}}$
class V	$\omega_i < 20 \% \omega_{\text{MAX}}$

We observe that 123 clocks reach ω_{MAX} and that there are less than 10 clocks within each class, apart from class V which includes 29 clocks. Fixing ω_{MAX} to 7.00×10^{-3} thus allows a large number of clocks (70 % of the total number) to reach this upper limit.

The clocks that contribute to the construction to EAL can be separated into three different clock types: hydrogen masers, HP 5071A clocks, and other caesium clocks. Figure 2 shows the distribution of relative weights for these three clock types. Again the same classes of relative weights are presented. For each clock type there are less than 5 units within each class, apart from class V which includes 3 HP 5071A clocks, 6 hydrogen masers and 20 other caesium clocks. Among the clocks reaching ω_{MAX} , we have: 93 HP 5071A clocks (83 % of the total number of such clocks), 17 hydrogen masers (60 % of the total number of hydrogen masers), and 31 % other cesium clocks (31 % of this group). These data are summarized in Table 1. It is clear that the discrimination is not efficient, especially for the HP 5071A clocks and the hydrogen masers.

3 NEED TO UPDATE ω_{MAX}

When attributing relative weights, efficient discrimination between clocks must be made in order that the resulting time scale relies most heavily upon a maximum number of the very best clocks. With $\omega_{\text{MAX}} = 7.00 \times 10^{-3}$, however, clocks with $\sigma_i(12, T) = 15.9 \times 10^{-15}$ are given the same relative weight as clocks with $\sigma_i(12, T)$ values many times less than this. Figure 3, a histogram of the $\sigma_i(12, T)$ data, clearly shows that $\omega_{\text{MAX}} = 7.00 \times 10^{-3}$ yields a value of σ_{MIN} that does not achieve the required discrimination. It is, therefore, necessary to update ω_{MAX} such that the corresponding σ_{MIN} value is small enough that such discrimination is possible.

Figures 4 and 5 show the relative frequency stabilities of some of the best HP 5071A clocks and hydrogen masers used in the establishment of TAI. On each figure, the indicated value of $\sigma_{y\text{MIN}}(30)$, computed from (1), differs significantly from the plotted $\sigma_{y_i}(30)$ values.

4 REVISED WAY OF FIXING AN UPPER LIMIT TO CLOCK WEIGHTS

We propose not to fix ω_{MAX} to a given value, but to make ω_{MAX} a function of the number, N , of clocks contributing to the construction of TAI. A relation such as $\omega_{\text{MAX}} = A/N$ is suggested, where A is an empirical constant. There is no fundamental difference between this function

and a fixed value; in both cases the choice of ω_{MAX} is empirical. Nevertheless, a fixed value of ω_{MAX} could lead, if N were small, to a situation where N_1 clocks reach ω_{MAX} , while the weights of the remaining $(N - N_1)$ clocks is zero. This situation is very unlikely to occur, but if it did, then the relative weights would not be normalized and the relation of definition of EAL would no longer be valid. Such a situation could not occur with the proposed alternative: if N decreased suddenly, then ω_{MAX} would increase so that discrimination among clocks would still be made and the normalization requirement fulfilled.

5 TESTS ON REAL DATA

In this section three time scales are considered and compared to EAL. Each is calculated by running the ALGOS algorithm on real clock data, using different values of $\omega_{\text{MAX}} = A/N$. These time scales are E2, E25, and E3, with values of 2.0, 2.5, and 3.0, respectively, for the constant A .

The results for our set of clocks over the period from January 1998 to June 2000 are summarized in Table 1, where they are compared with EAL, and the properties of the test time scales are described in more detail below.

Table 1. Summary of the results of the four time scales EAL, E2, E25, and E3 calculated over the period January 1998 to June 2000. The values of ω_{MAX} and σ_{MIN} are indicated, along with the fraction of clocks attributed the maximum weighting.

Time scale	$10^3 \times \omega_{\text{MAX}}$	$10^{15} \times \sigma_{\text{MIN}}$	100 × Fraction of clocks reaching ω_{MAX}			
			Total	HP 5071A	Hydrogen masers	Other Cs clocks
EAL	7.00	15.9	70	83	60	31
E2	9.51	7.8	41	50	41	12
E25	11.89	5.8	27	33	36	7
E3	14.27	4.9	18	20	3	1

5.1 TIME SCALE E2

Figures 6 and 7 show the distribution of relative weights attributed to clocks in the computation of E2. The results seem more satisfying than those obtained with EAL (cf. Fig. 1) in the following respects:

- it reduces reasonably the amount of clocks reaching this upper limit;
- it allows a given clock H_i , providing it does not show abnormal behavior, to reach ω_{MAX} if its $\sigma_{(12,30)}$ value is less than or equal to 7.8×10^{-15} ;
- it allows a reasonable discrimination between the clocks;
- it relies more heavily upon the best clocks.

5.2 TIME SCALE E25

Figure 8 shows the distribution of relative weights, attributed to clocks in the computation of E25. The value σ_{MIN} , corresponding to the least stable clock attributed ω_{MAX} , is nearly three times smaller than that obtained for EAL (Table 1). The conditions for a given clock to reach the upper limit of relative weights are more severe here than for EAL or E2.

The distribution of relative weights for the three clock types defined in Section 2 is presented in Figure 9. We observe that an efficient discrimination among the clocks is made, and that the number of clocks at ω_{MAX} is still great enough to ensure the reliability of the time scale. Figure 10 shows a histogram of the standard deviation $\sigma_i(12,30)$ and the position of σ_{MIN} .

For the group of clocks considered, the time scale E25 has the following advantages over EAL:

- it substantially reduces the number of clocks attributed ω_{MAX} ;
- it allows a given clock H_i , providing it does not show abnormal behavior, to reach ω_{MAX} when its $\sigma_i(12,30)$ value is less than or equal to 5.8×10^{-15} ;
- it allows efficient discrimination between the clocks;
- it relies more heavily upon the very best clocks.

5.3 TIME SCALE E3

Figures 11 shows the distribution of relative weights attributed to clocks in the computation of E3, and Figure 12 shows the distribution of relative weights for the three different clock types. Only 18 % of the clocks are attributed the maximum relative weight, and this fraction is not enough large to ensure the reliability of TAI. Here the conditions required for a clock to obtain the maximum relative weight are too severe. Figure 13 shows a histogram of the standard deviations $\sigma_i(12,30)$ and the position of σ_{MIN} .

With the considered clock ensemble, E3

- reduces excessively the number of clocks attributed ω_{MAX} ;
- allows a given clock H_i , providing it does not show abnormal behavior, to reach ω_{MAX} if its $\sigma_i(12,30)$ value is less than or equal to 4.9×10^{-15} ;
- provides severe discrimination between the clocks;
- relies more heavily upon a selection of the very best clocks than the other time scales considered here, but the small fraction selected is not large enough to ensure the reliability of the resulting time scale.

5.4 STABILITY OF TIME SCALES EAL, E2, E25, AND E3

The stabilities of the time scales EAL, E2, E25, and E3 have been compared to three of the best independent time scales in the world: those maintained at the NIST (Boulder, Colorado, USA), the BNM-LPTF (Paris, France), and the AMC (Colorado Spring, USA). Intrinsic values of $\sigma_y(\tau)$ computed using the N -cornered-hat technique are shown in Figure 14.

As expected, because the time scales E2, E25, and E3 allow more efficient discrimination between the clocks, they rely more heavily upon the very best units and are consequently more stable than EAL.

6 CONCLUSIONS AND PROPOSAL

The fixed value 7×10^{-3} for the upper limit of clock weights ω_{MAX} is no longer appropriate because it does not allow efficient discrimination between the clocks. It is suggested that this fixed value be replaced by a function $\omega_{\text{MAX}} = A / N$, where A is an empirical constant and N is the number of clocks participating in the construction of TAI. Such a function would avoid a possible problem described in Section 4 which could arise if an insufficient number of clocks were available.

The suggested function has been tested successfully, with $A = 2.0$, $A = 2.5$, and $A = 3.0$, using real clock data over 2.5 years, and the resulting time scales E2, E25, and E3 are more stable than EAL.

We, therefore, propose to adopt a function such as $\omega_{\text{MAX}} = A/N$ to define the upper limit for clock weights in the algorithm ALGOS used to calculate TAI. Regarding the choice of the constant A , among the three tested values, $A=3.0$ must be set aside because it causes an excessive reduction in the number of clocks reaching ω_{MAX} . A more appropriate value seems to be $A = 2.5$; the corresponding time scale E25 allows a more efficient discrimination between clocks and shows a better stability. Adoption of this value for TAI computation would, however, change ω_{MAX} from 7.00×10^{-3} to 11.89×10^{-3} . Such a discontinuity could influence the behavior of TAI and should be avoided. It would be preferable to move more gradually towards this value, for example by using $A = 2.0$ for one year and then moving to $A = 2.5$.

We, thus, propose to set $A = 2$ from January 2001 until December 2001, and to set $A=2.5$ from January 2002 onwards. In this way ω_{MAX} will change from 7.00×10^{-3} to 9.51×10^{-3} at the beginning of January 2001, and from 9.51×10^{-3} to 11.89×10^{-3} in January 2002. Based on the experience of the BIPM Time Section, such small changes will not perturb the behavior of TAI.

7 REFERENCES

- [1] B. Guinot, and C. Thomas 1988, "Establishment of International Atomic Time," Annual Report of the BIPM Time Section, 1, D1-D22.
- [2] J. Azoubib, and C. Thomas 1995, "Shortening of the definitive computation time of TAI," Report to the CCDS Working Group on TAI, GT-TAI/95-7, 28 p.
- [3] J. Azoubib, and C. Thomas 1995, "The upper limit of weight for clocks contributing to TAI," Report to the CCDS Working Group on TAI, GT-TAI/95-8, 26 p.
- [4] C. Thomas, and J. Azoubib 1996, "TAI computation: study of an alternative choice for implementing an upper limit of clock weights," Metrologia, 33, 227-240.
- [5] C. Thomas, and J. Azoubib 1995, "A modified version of the TAI algorithm under test," Report to the CCDS Working Group on TAI, GT-TAI/95-9, 15 p.
- [6] C. Thomas, and J. Azoubib 1998, "Proposals for updating TAI algorithm," Proceedings of the 29th Annual Precise Time and Time Interval (PTTI) Systems and Applications Meeting, 2-4 December 1997, Long Beach, California, USA, pp. 7-17.

- [7] J. A. Barnes 1969, "*Table of bias functions, B_1 and B_2 , for variances based on finite samples of processes with power law spectral densities,*" NBS Technical Note No. 375.
- [8] J. Rutman 1978, "*Characterization of phase and frequency instabilities in precision frequency sources: fifteen years of progress,*" *Proceedings of the IEEE*, **66**, 1048-1075.

Clocks weights distribution (scale EAL)

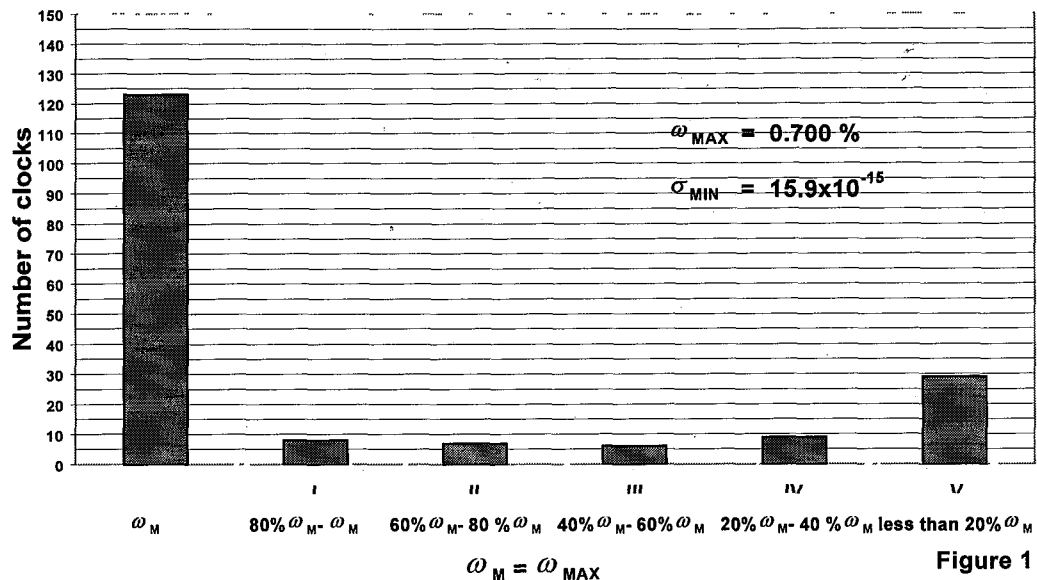


Figure 1

Weights distribution for various types of clocks (scale EAL)

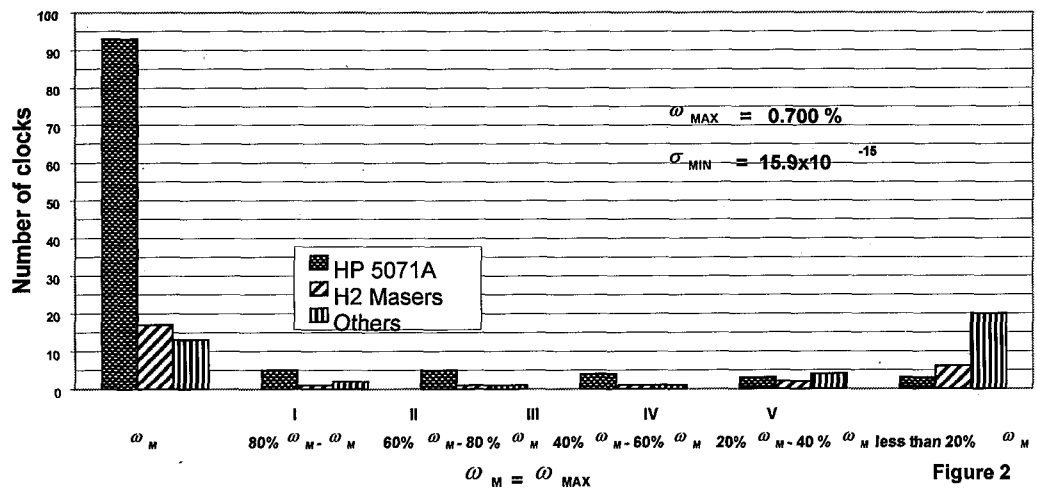
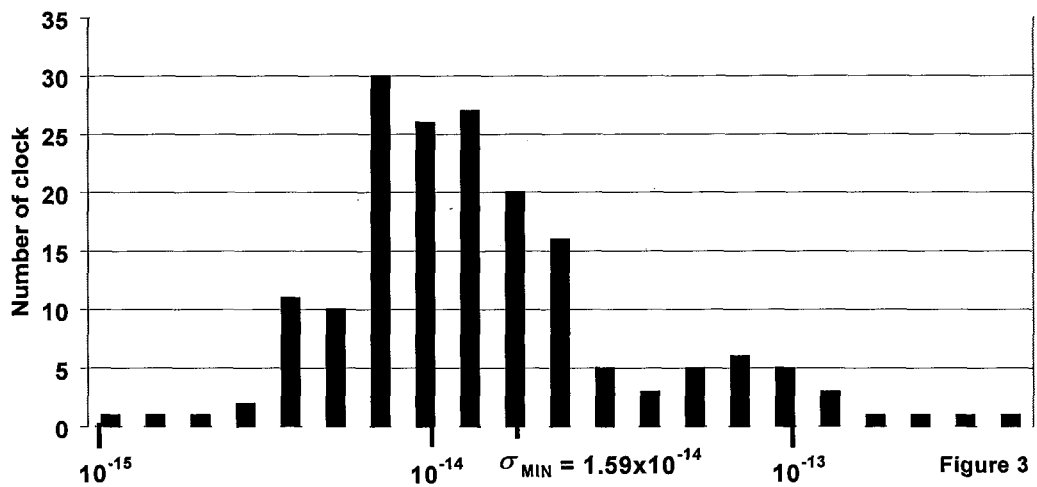


Figure 2

Histogram of $\sigma_i(12,30)$ (Scale EAL)



Relative frequency stability of the best HP 5071A used in TAI

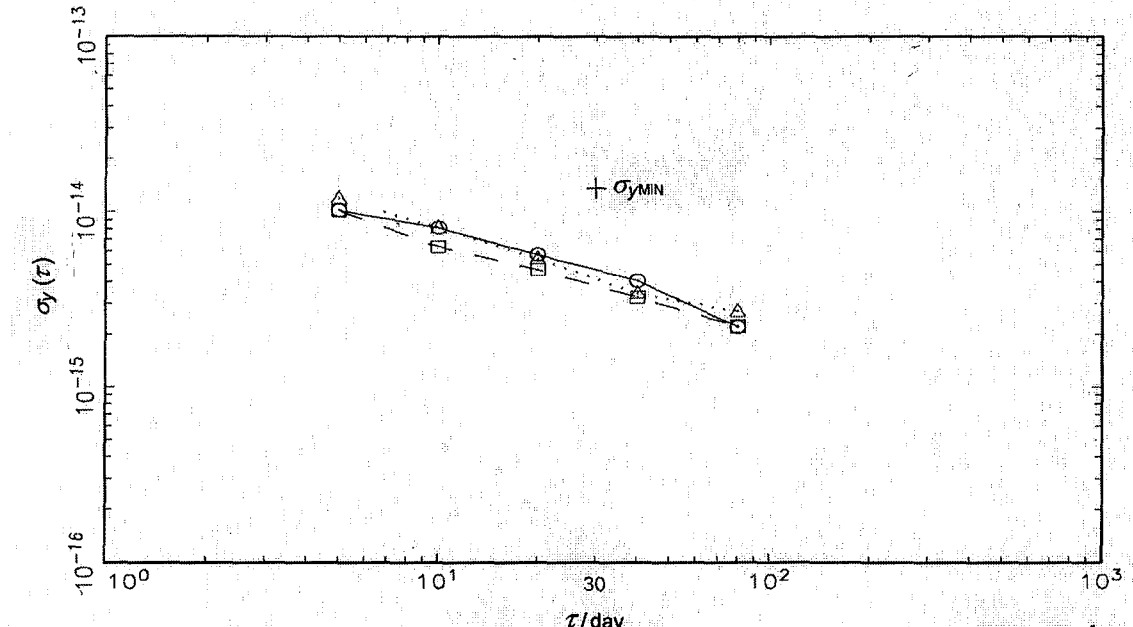


Figure 4

Relative frequency stability of the best H₂ masers used in TAI

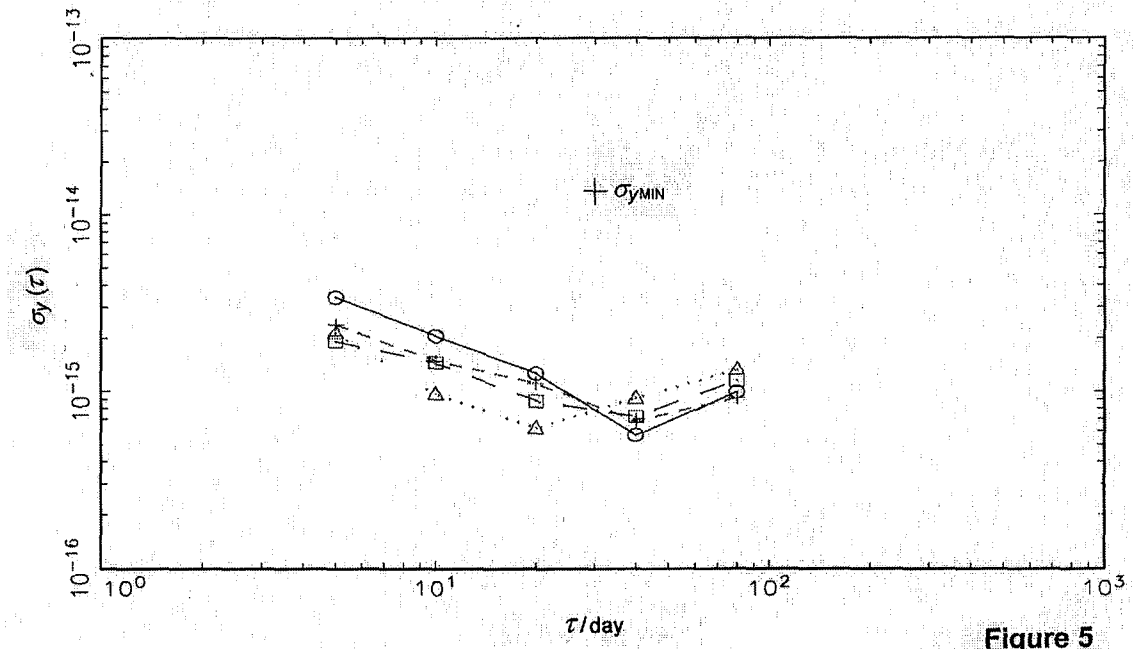


Figure 5

Clocks weights distribution (scale E2)

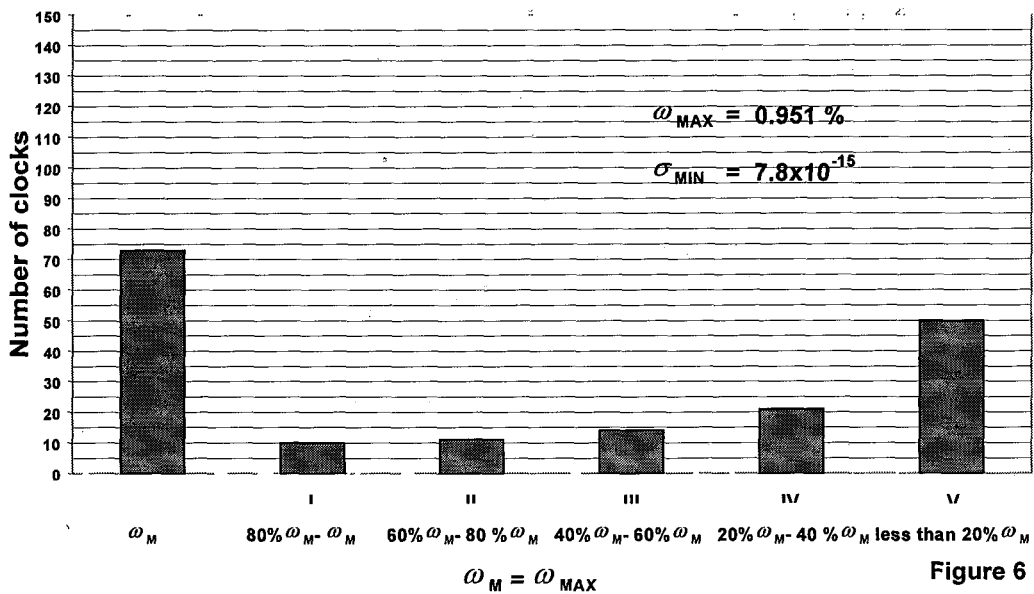


Figure 6

Weights distribution for various types of clocks (scale E2)

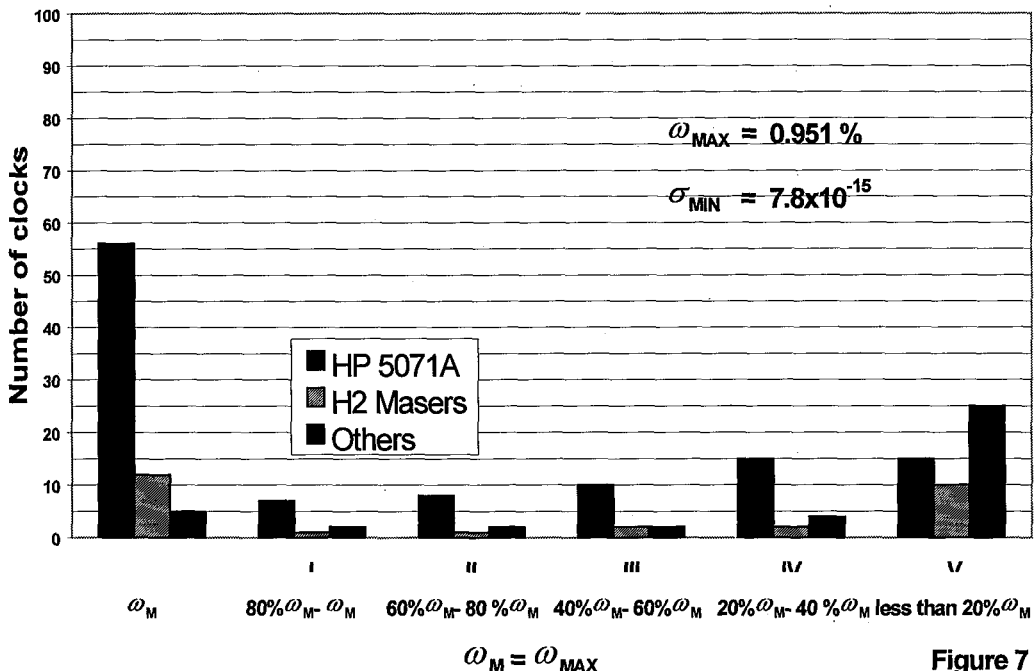


Figure 7

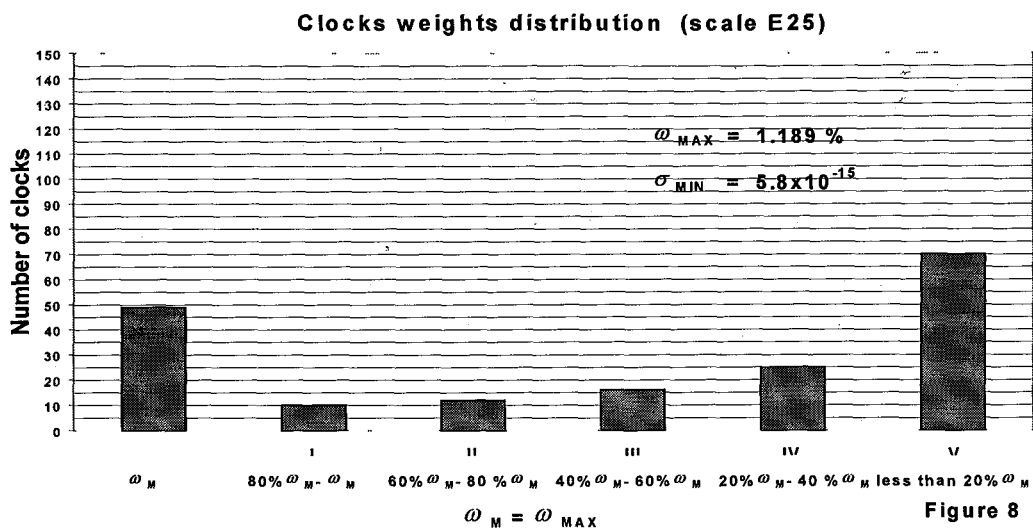


Figure 8

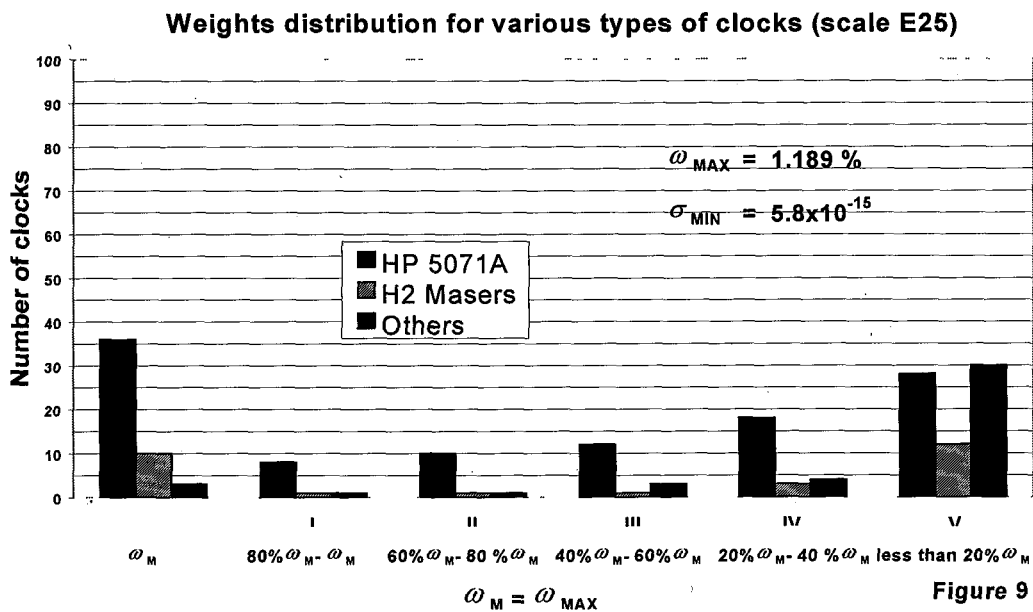


Figure 9

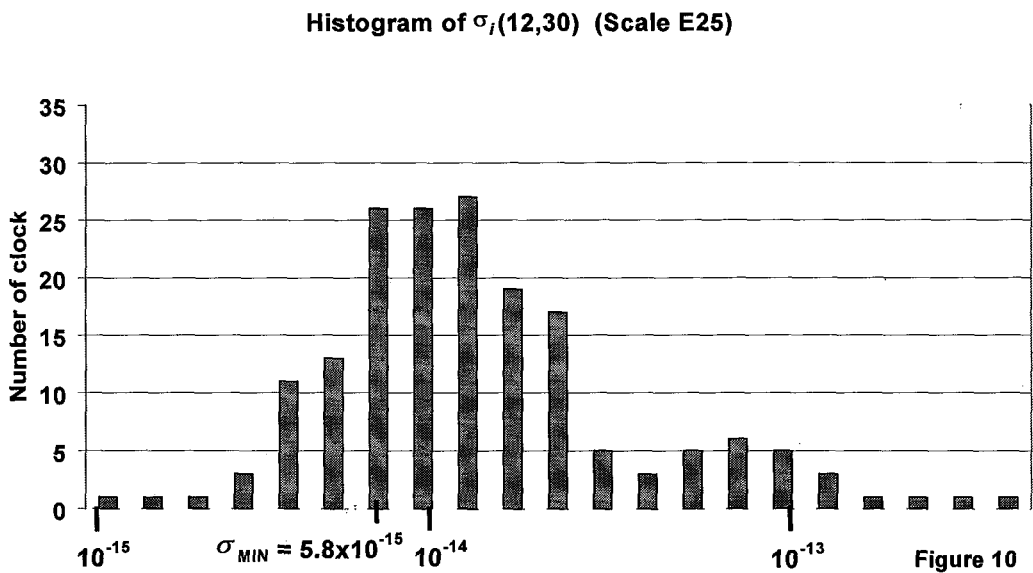


Figure 10

Clocks weights distribution (scale E3)

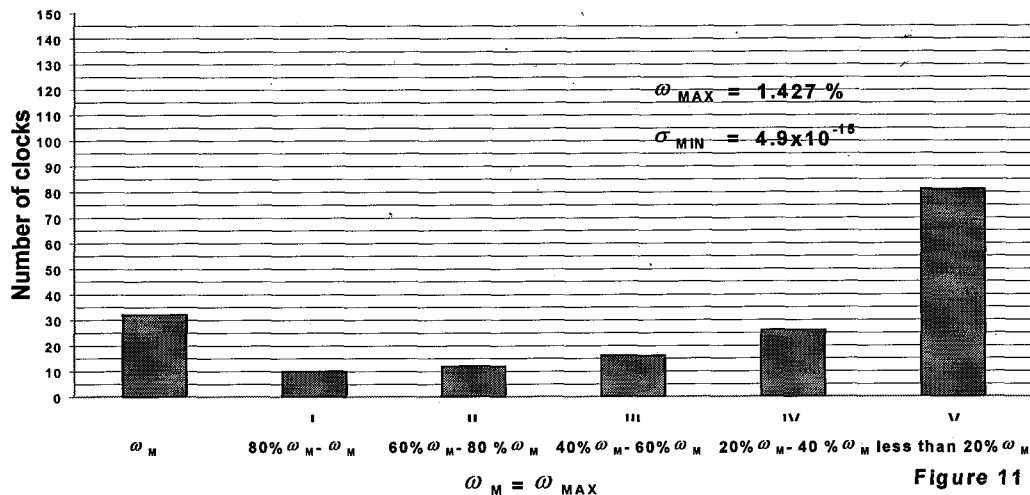


Figure 11

Weights distribution for various types of clocks (scale E3)

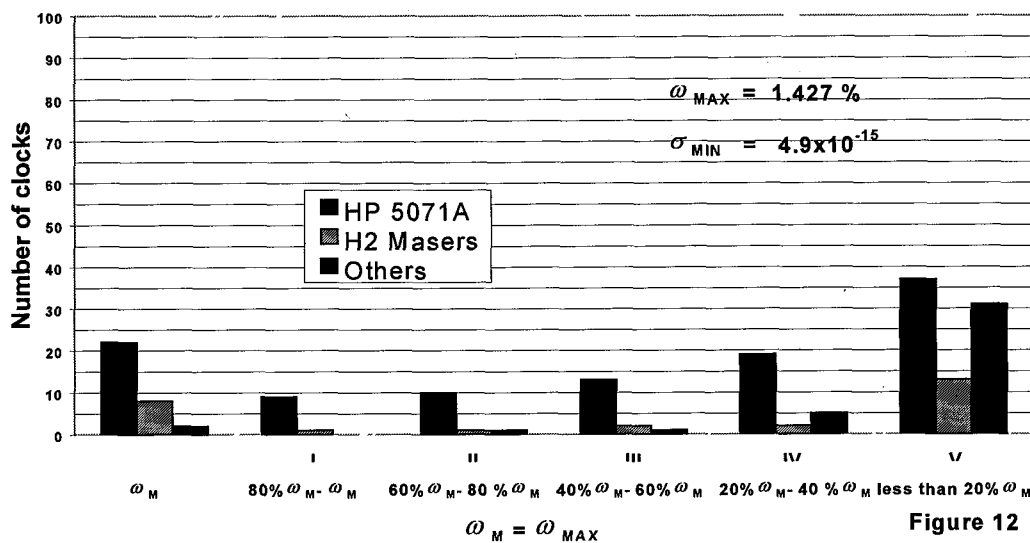


Figure 12

Histogram of $\sigma_i(12,30)$ (Scale E3)

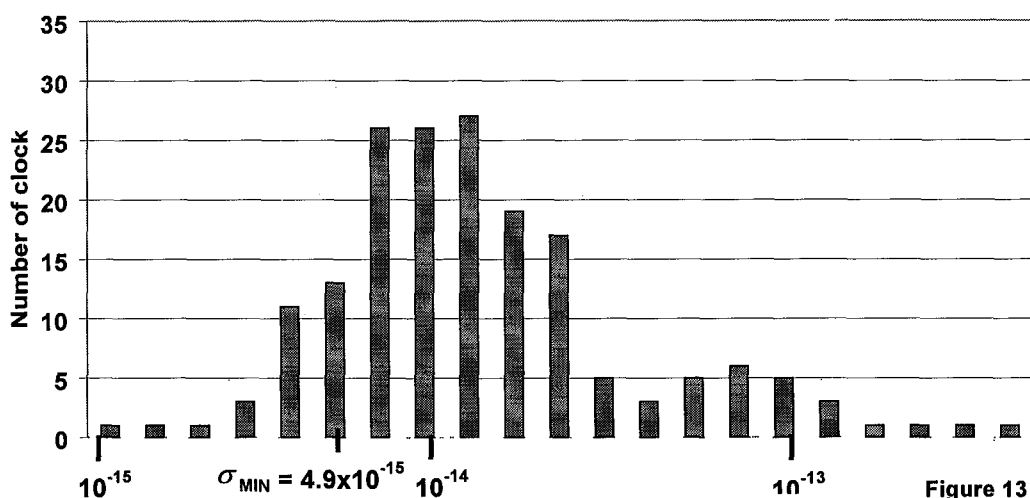
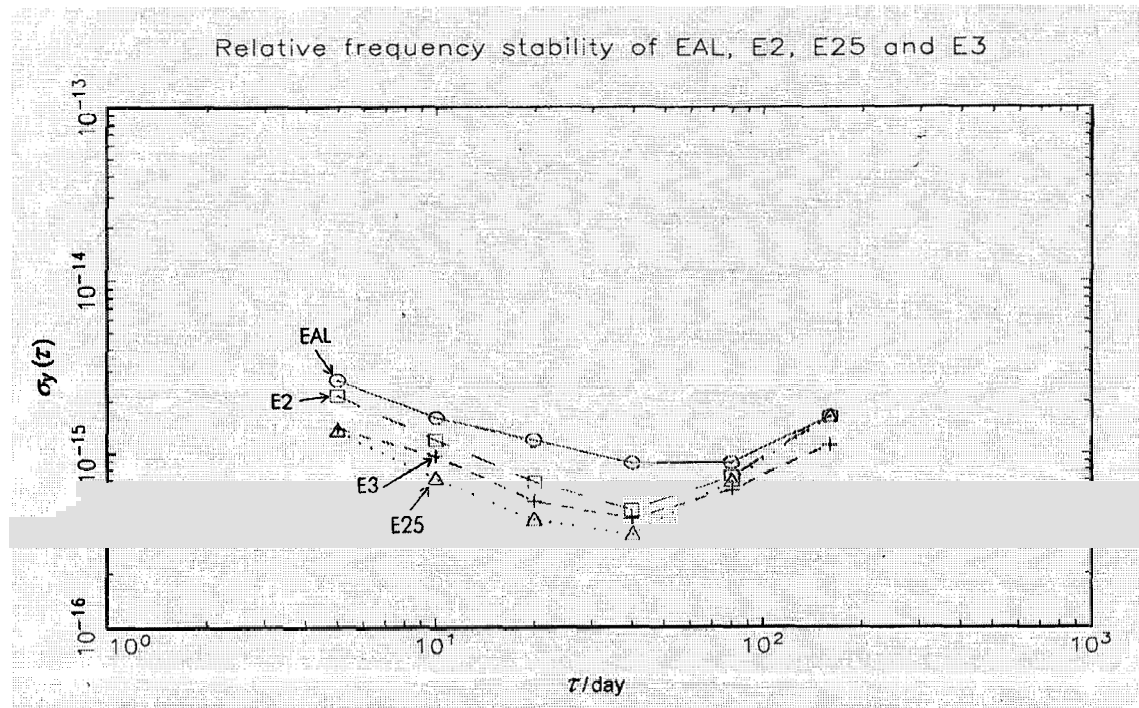


Figure 13



Fi 11

Questions and Answers

JUDAH LEVINE (NIST): I think that's a good idea. One of the things that you will have to be concerned about is as you raise the maximum weight that a clock can have, the hydrogen masers will begin to take over, because in short term, they are much more stable than anything else. But that will introduce frequency drift into TAI, because almost all the hydrogen masers drift. That will mean that you may need more steering to TAI as the hydrogen masers begin to pull the scale. As you make the weight larger and larger, that will become an effect that you will begin to see. I mean, we have that effect on our hydrogen masers; they drift.

JACQUES AZOUBIB: The drift of hydrogen masers is not taken into account in the algorithm because we have a test that analyzes if a clock shows an abnormal behavior. And if a hydrogen maser shows a frequency drift, its weight is set to zero.

LEVINE: The drift would be too small for you to see. It will be like 10^{-16} /day. In short term, it will look much, much better than a cesium.

AZOUAIB: Yes, in short term, yes.

WLODZIMIERZ LEWANDOWSKI (BIPM, France): Just a comment on what was said. What Jacques is suggesting, if I understand, it will not increase the number of masers used, but it will take into account the best masers. So there will be a big increase of the use of masers, but it will be an increase of the best, taking advantage of the best masers. There will be a better discrimination between masers, but not an increase of the number of masers used for TAI. The idea is a better discrimination between the best clocks and not to increase. So the best masers will have bigger impact on TAI. There will be no more masers.

AZOUAIB: You can see on this scale that the maximum weight will have 10 hydrogen masers, exactly. It is 36% of the number of hydrogen masers. In EAL with omega maximum at 0.7%, we have 60% of the total number of hydrogen masers. That means that here only the very, very best hydrogen masers are selected.

DEMETRIOS MATSAKIS (USNO): I'll just mention my prediction which I made in print, and you've heard before. I wonder if you would comment on my comment. I made a prediction that 10 years from now the BIPM will be using the improved time transfer, probably two-way, but maybe GPS carrier-phase, to view EAL much more closely spaced, and they will be using masers completely for the short term; and they'll be steering it to cesiums in the long term. Which would answer Judah's comment. And I see this as a step in that direction.

AZOUAIB: Yes, we are working in that direction.

MATSAKIS: Let me ask you a question also. I just wondered when you computed your sigmas, you did it by N-cornered hats and, you know, that they are very—

AZOUAIB: Yes, of course, and I used the best time scales in the world, but not USNO's. Not because it's a bad time scale, but it is too much correlated with the scales. USNO has too many clocks. I used NIST, the AMC, and LPTF.

MATSAKIS: And they all agreed.

AZOUAIB: Yes, because the correlation is very small. For instance, for NIST, we have 9% percent of the total weight, so the correlation is small enough to use it.

MATSAKIS: You could also make a prediction based on elementary Gaussian statistics.

AZOUAIB: Yes.

MATSAKIS: Did that agree with the other thing?

AZOUBIB: Our way to work with this is, for each computation make a diagram and to fix sigma squared so that one clock of the three reaches the maximum weight. But it is far too complicated to do now. We work step by step, you know.

MATSAKIS: You need Judah's computers.

RESULTS OF A CONTINUOUS TRANSATLANTIC TWO-WAY TIME TRANSFER TEST USING COMMERCIAL SATELLITE MODEMS

T. P. Celano, Timing Solutions Corporation

S. P. Francis, Zeta Associates

G. A. Gifford, National Institute of Standards and Technology

B. J. Ramsey and T. L. Erickson, Timing Solutions Corporation

Abstract

This paper is the second in a two-part series that introduces the concepts of two-way time transfer using commercial satellite modems. The first paper [1] presented the concept of time-based communication and detailed multiple implementations using satellite channels. This paper presents the results of a transatlantic proof-of-concept demonstration of the technology. A short review of time-based communications is presented, followed by a detailed description of the test. Results are presented and data examined for consistency over time and temperature.

1.0 TIME-BASED COMMUNICATION

Time-based communication is a technology in which an active data communications channel is utilized as a vehicle for two-way time transfer. The impetus for the development of this technology is the existence of users with stringent timing requirements and existing or planned communications infrastructures. Time-based communication provides very precise time transfer capability in the background of a data transfer channel. This allows two ends of a communications link to be precisely synchronized without fielding an independent timing system.

Time-based communication is a generic technology with a few basic requirements [1]. The data channel must be duplex using a medium that has uniform delay characteristics over the time of the measurement. Implementation of these concepts has been accomplished over fiber [2] and satellite channels [1]. In this paper, an over-the-air (OTA) system is evaluated using commercial satellite modems between Europe and the United States.

The different tasks performed by the modem in the OTA system are seen in Figure 1. The top (darker shade) section contains the typical communications tasks. These tasks, from the administration of the link to the actual transfer of data, are performed in order to transfer data from one end of the link to the other. The bottom section (lighter shade) shows the timing tasks that are performed in the background of the data link. These tasks, detailed in reference 1, include injecting a pattern to measure, measuring the pattern at each end of the link, and exchanging measurement data.

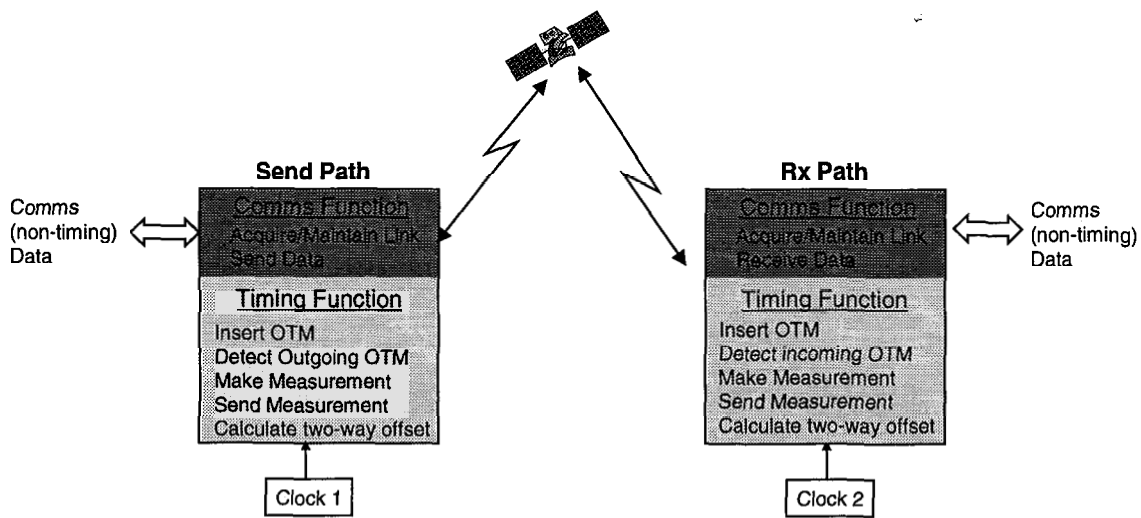


Figure 1: OTA Modem Responsibilities

2.0 HARDWARE CONFIGURATION

Figure 2 depicts the hardware implementation used for the demonstration. The OTA system was fielded between a site in Europe and a site in the United States. The two sites use identical GPS-based systems (darkly shaded elements in Figure 2) for timing recovery where passive GPS data are processed to steer a local cesium. Cross-site time synchrony is achieved by virtue of the fact that each site steers to a common reference, UTC(GPS). The OTA system (lightly shaded elements in Figure 2) was connected to the on-time point at each site. The OTA system produced a measurement of the cross-site time offset.

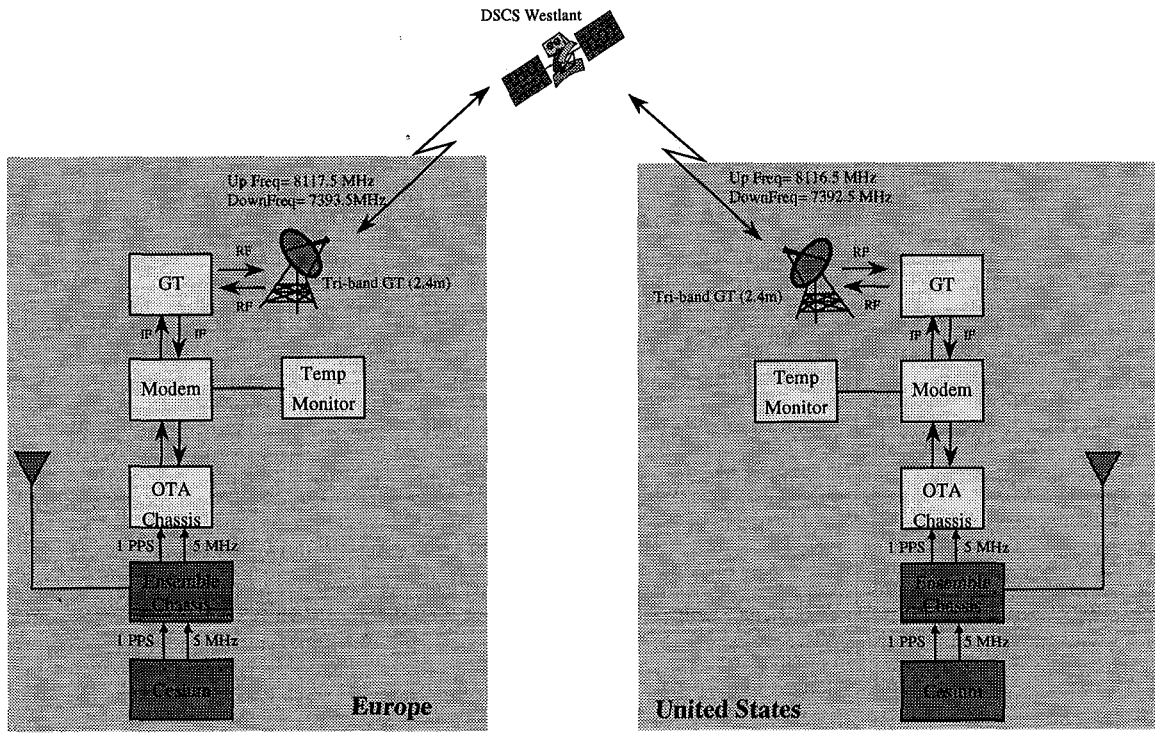


Figure 2: Demonstration Hardware Configuration

The OTA hardware consists of three significant pieces: the ground terminal, the modem, and the measurement hardware. An additional chassis for temperature measurements was also included (temperature compensation is discussed in Section 4.2). The ground terminal used for this test was a mobile 2.4 meter, tri-band dish. The dish (seen deployed in Figure 3) is owned and operated by the US Air Force Mobile Communications Unit (MOCOMM). The modem is a commercially available satellite communications modem manufactured by Radyne/Comstream. The measurement equipment consisted of a Timing Solutions chassis with precision timers run from a pentium controller.

The satellite channel for the test was a 256 kbs duplex link using the DSCS Westlant satellite. X-Band frequencies were used for uplinks and downlinks to/from the sites. The system was calibrated using identical frequencies and transponders after the test. This was possible due to the use of mobile terminals that could be fielded as two ends of a link and then co-located after the test for calibration.

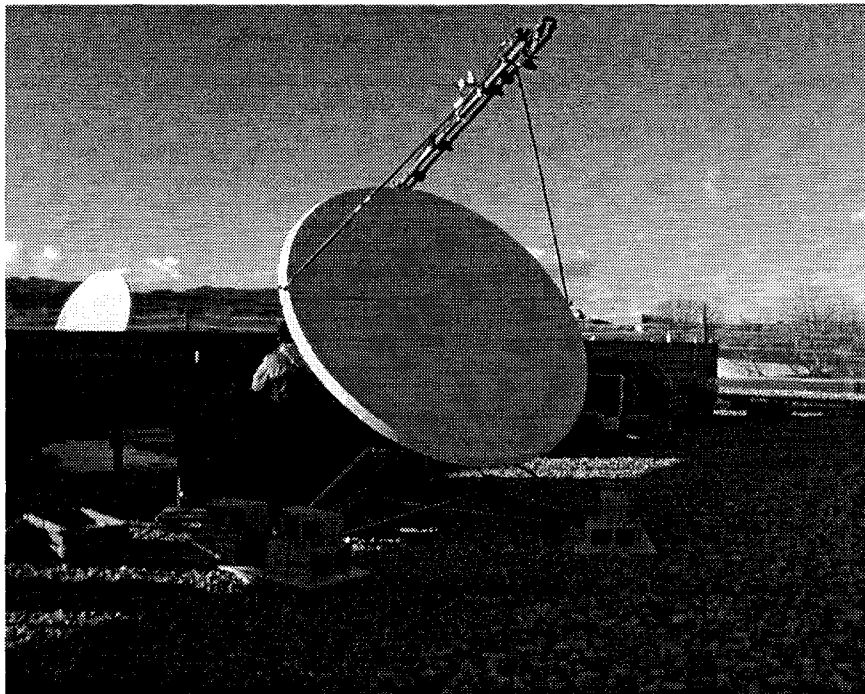


Figure 3: MOCOMM Tri-Band Ground Terminal

3.0 TEST RESULTS

Data were collected over a 9-day period for this test. The resulting measurement is seen in Figure 4. The blue curve is the post-processed OTA data. The raw 1-second data were processed using a running 900-second average to produce the continuous plot in Figure 4. The data have been corrected for Sagnac effect (239 ns), temperature differences, and absolute delay differences in the modems. The standard deviation of the data set is below 1 ns and the quality of the data is sufficient to see the motion of the clocks at the two ends of the link (each system is actively steering).

The data in Figure 4 provide a continuous record of the cross-site timing performance over the demonstration period. The first 5 days show steady-state operation of the systems. On mjd 51853, the cesium at one end reached end-of-life and its performance began to degrade. This is evident in the data set by the increased noise level and 25ns movement in the plot. The cesium was removed and replaced on mjd 51855. The plot in Figure 4 shows the system recovery as the GPS filter learns the frequency of the new clock after the cesium was replaced.

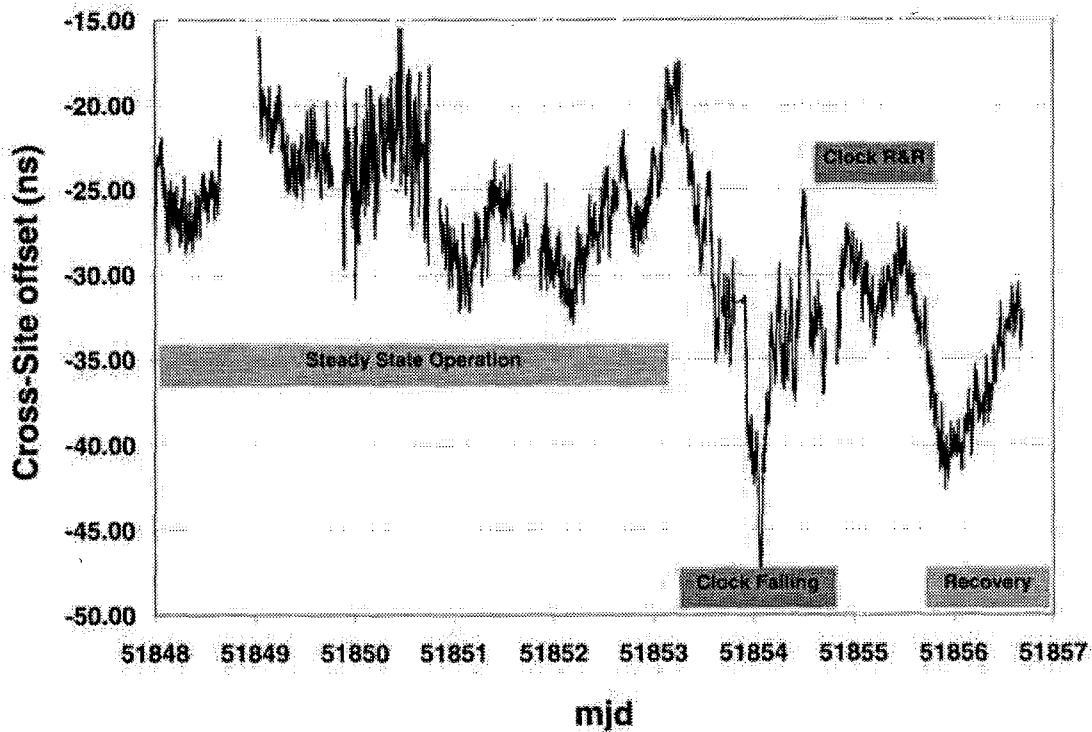


Figure 4: OTA Data

4.0 DATA CORRECTIONS

The use of commercial modems for timing becomes challenging as the precision level required gets better. Commercial satellite modems are not designed or manufactured with time-transfer requirements in mind. Although bit synchronization at higher bit rates requires better clock recovery, the absolute delay stability is not an issue. There are two primary effects that have been observed while using commercial satellite modems for time transfer. The first effect is a direct correlation between bit rate and timing stability. The second effect is the dependence of modem propagation delay on temperature. These two effects are discussed in detail below.

4.1 Bit Rate

Commercial satellite modems are typically manufactured to operate over a large range of data rates. The Radyne/Comstream modem used for the transatlantic demo has been tested at rates ranging from 128 kbps to 1.544 Mbps. The jitter on the received signal is directly relatable to the bit rate. Figure 5 shows the dependence of the two-way RMS on the achieved bit rate and how it relates to averaging time. The RMS stability of the raw data is seen in the blue curve. The raw data stability ranges from 5ns at 1.536 Mbps to 50 ns at 128 kbps. The goal of this measurement is 1-ns RMS and averaging times are chosen accordingly. Figure 5 shows that 100-second averages are sufficient to achieve sub-nanosecond performance at bit rates over 512 kbps and below 512 kbps it is necessary to use a longer average.

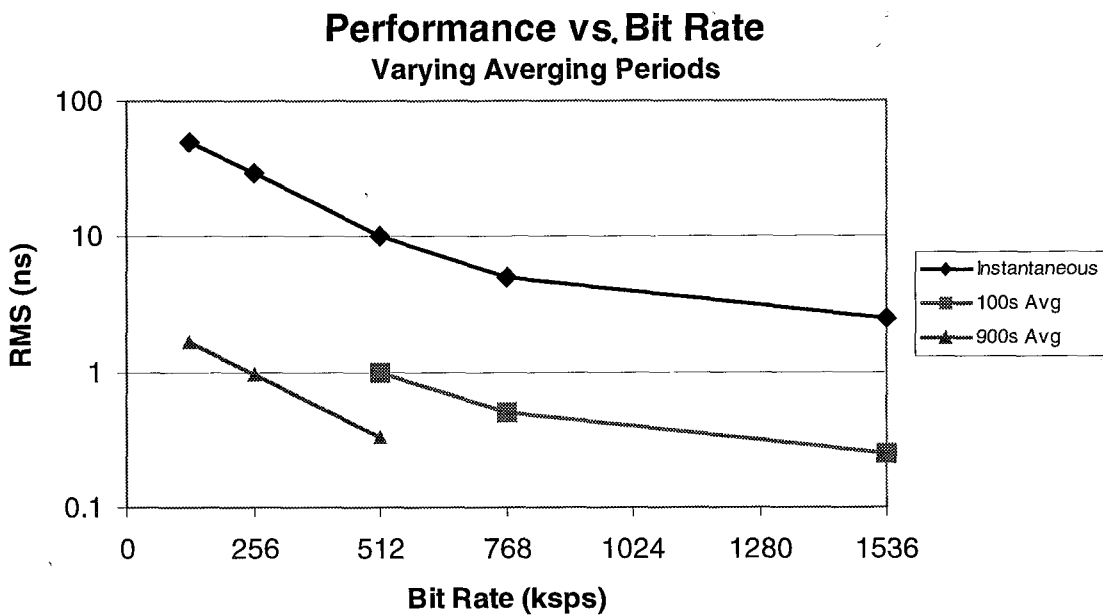


Figure 5: Performance vs. Bit Rate

For the transatlantic demonstration, a data rate of 256 kbps (before coding) was used. Although a higher rate would have allowed shorter averaging times, the link rate choice was driven by the power limitations of the DSCS satellite. The actual channel bit rate was higher than 256 kbps due to the use of Viterbi 7/8 and Reed Solomon coding. The data rate was changed to 128 kbps for a day to show the higher noise level. This is highlighted in Figure 6.

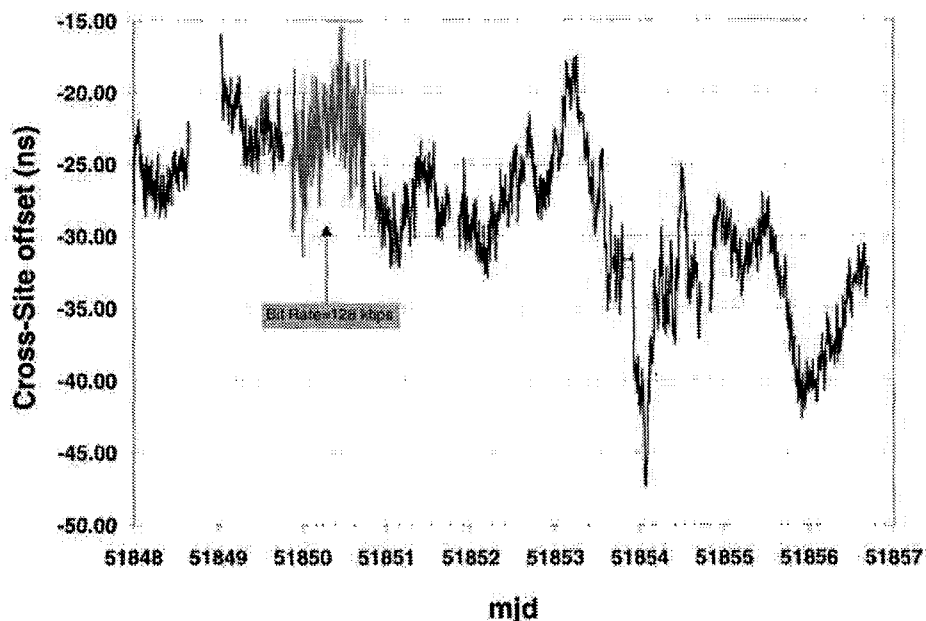


Figure 6: Elevated Noise due to Lower Bandwidth

4.2 Temperature

Commercial modems have temperature dependencies that must be measured and removed. Due to the requirement to support a wide range of bit rates, the modem design includes a bank of filters between switches where the filter choice is driven by the selected bit rate. These filters have group delay characteristics that vary with temperature. The modems were calibrated in dual temperature chambers prior to the experiment. Temperature coefficients of 1.5 ns/deg F were determined. Temperature sensors were added to the modems to log data during the test. The data were corrected using the temperature information to remove the effect. In order to verify that the correction was being done properly, the temperature was raised in one modem for a 2-day period during the test. Figure 7 shows the temperature record for each side of the link and highlights the two-way data during the period where the temperature was raised at one side. The data do not show any bias due to the change in temperature. This provides confidence that the effects of varying temperature were properly removed.

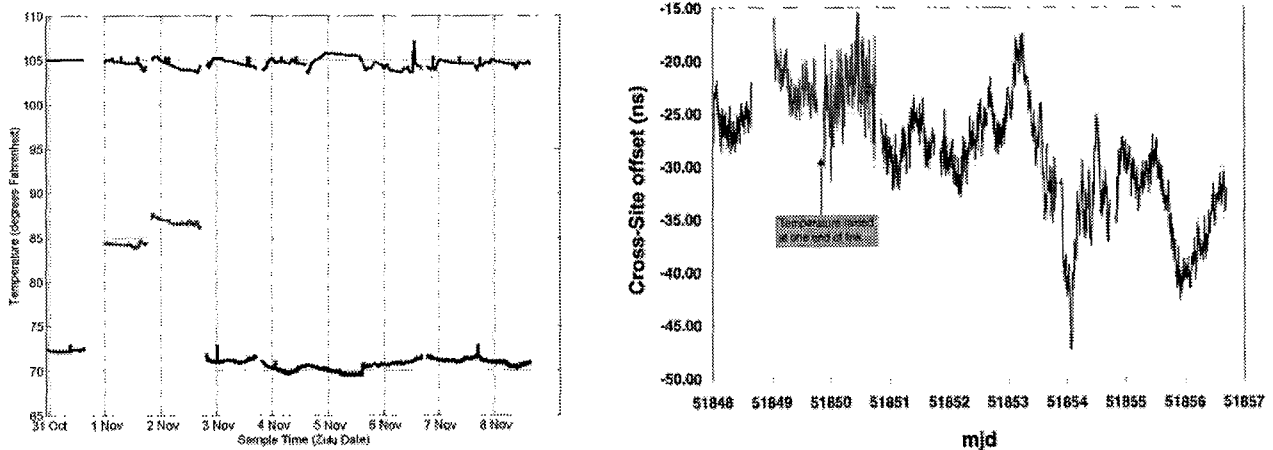


Figure 7: Performance vs. Temperature

5.0 CONCLUSIONS

This paper provides final proof-of-concept for conducting time-based communications over satellite links. The concepts of time-based communications were implemented using a commercial satellite modem. Timing was performed in the background of an active data channel. Data were processed to provide a sub-nanosecond (RMS) continuous estimate of the relative performance of two GPS timing systems. The performance of the system was sufficient to see the steering of the clocks and to detect the failure of a cesium clock in the system. The prototype hardware used for this demonstration had bit-rate and temperature-related performance dependencies that were accommodated and documented during the test.

Time-based communication is a viable option for users who require precision time synchrony and have a communications infrastructure. Timing can be performed in the background with no impact to data users (negligible bandwidth is used). The concepts of time-based communications extend to any two-way communications channel and have been demonstrated at the 20 picosecond level over fiber.

6.0 REFERENCES

- [1] T. P. Celano, S. P. Francis, and G. A. Gifford 2000, "*Continuous two-way time transfer using commercial modems,*" Proceedings of the 2000 IEEE/EIA International Frequency Control Symposium and Exhibition, 7-9 June 2000, Kansas City, Missouri, USA, pp. 607-611.
- [2] M. Calhoun, P. Kuhnle, R. Sydnor, S. Stein, and G. A. Gifford 1997, "*Precision time and frequency transfer utilizing SONET OC-3,*" Proceedings of the 28th Annual Precise Time and Time Interval (PTTI) Applications and Planning Meeting, 3-5 December 1996, Reston, Virginia, USA, pp. 339-348.

Questions and Answers

HUGO FRUEHAUF (Zyfer, Inc.): Can you do this during normal communications? And, how much overhead would you require to practically make this happen?

THOMAS CELANO: In the case that I just showed you, we were doing normal communications throughout. In order to show that we were not affecting the bit error rate of the link, we were conducting normal communications. And yes, this is intended to be conducted in the background. In this particular case, on a 256 kilobit per second channel, we were taking 9600 bits per second. We were taking an engineering service channel, so it's really minimal to what they were doing. They didn't notice we were doing it.

TWSTFT NETWORK STATUS IN THE PACIFIC RIM REGION AND DEVELOPMENT OF A NEW TIME TRANSFER MODEM FOR TWSTFT

M. Imae¹, M. Hosokawa¹, Y. Hanado¹, Z. Li²,
P. Fisk³, Y. Nakadan⁴, and C. S. Liao⁵

¹Communications Research Laboratory (CRL), Japan

²Shaanxi Astronomical Observatory (CSAO), China

³National Measurement Laboratory (NML), Australia

⁴National Research Institute of Metrology (NRLM), Japan

⁵Telecommunication Laboratories (TL), Taipei, Taiwan

Abstract

Two-Way Satellite Time and Frequency Transfer (TWSTFT) is one of the most precise and accurate time transfer techniques. Recently TWSTFT results among the European and North American time and frequency institutes have been started applying to the TAI calculation. A TWSTFT network in the Pacific Rim region is also being developed rapidly. CRL and NRLM in Japan, NML in Australia, CSAO in China, and TL in Taiwan have been doing TWSTFT time transfer on a regular basis. Some other institutes, such as KRISS in South Korea and PSB in Singapore, are also planning to join this network within 1 year. By performing TWSTFT time transfer it became obvious that several problems in TWSTFT should be solved for practical use and contribution to TAI with the full performance of TWSTFT. We have been developing a new time transfer modem to solve or reduce most of these problems with TWSTFT. It has three PRN code modulator units for transmission and eight PRN code demodulator and time-interval measurement units for receiving. It realizes simultaneous time transfer among up to eight stations.

INTRODUCTION

Research and development of the atomic clocks and primary frequency standards realize improvement of the stability and accuracy of the International Atomic Time (TAI) and Coordinated Universal Time (UTC). The stability of TAI and UTC is currently about 2×10^{-15} over a few weeks. It is also predicted that the stability of TAI and UTC will reach a few parts in 10^{-16} within 10 years. Thus, the new precise time and frequency transfer methods are being investigated in the time and frequency community. They are based on GPS carrier-phase measurements, GPS/GLONASS multi-channel C/A code measurements [1], and Two-Way Satellite Time and Frequency Transfer (TWSTFT). This paper relates to the TWSTFT method.

The concept of TWSTFT is very old. TWSTFT experiments were made around 1970; these experiments showed very high time transfer precision [2-3]. However the TWSTFT method

was not used as a regular time transfer method until 1990's. One of the main reasons is that the TWSTFT method has very high capabilities for precise and accurate time transfer, but it needs expensive facilities and has a high running cost compared with the one-way method, such as GPS common-view.

But the progress of atomic clocks and primary frequency standards require more precise time transfer techniques, so the TWSTFT method has been widely investigated in time and frequency standard institutes [4-8]. Especially in Europe and North American area, the regular TWSTFT has been performed to contribute to the TAI calculation [9]. As we reported at PTTI'98 [10], major T&F institutes in this region are making effort to construct a TWSTFT network there.

TWSTFT NETWORK IN THE PACIFIC RIM REGION

The history of the construction of TWSTFT network in the Pacific Rim region and its present status are shown in Table 1. Due to several problems for each time transfer link, such as failure of the earth station and change of the transponder of the satellite, some of them were interrupted after the start of the operation. But as shown in Fig. 1, the time transfer links shown by black solid lines are operating or going to re-start in the very near future. In addition these links, PSB in Singapore and KRISS in South Korea, will join to this network around the middle of 2001.

Table 1 History and present status of the TWSTFT network in the Pacific Rim region

Link	Start epoch	Satellite	Frequency band	Status
CRL-NML	October 1997	INTELSAT 702, 176° E	Ku-band	Interrupted
CRL-CSAO	October 1998	JCSAT-1B, 150° E	Ku-band	Operating
CRL-NRLM	March 1999	JCSAT-1B, 150° E	Ku-band	Operating
CRL-TL	June 2000	JCSAT-1B, 150° E	Ku-band	Interrupted
NML-NIST	July 1999	INTELSAT 701, 180° E	C-band	Operating

DRAWBACKS OF TWSTFT

TWSTFT has big advantages compared with the one-way methods, such as GPS common-view, but it also has several drawbacks:

- (1) difficulty of full automatic operation due to radio signal transmission to the satellite,
- (2) expensive cost of the satellite links,
- (3) difficulty of performing time transfer among more than three stations simultaneously using conventional time transfer modems, and
- (4) accurate evaluation of internal delays and delay variations in earth stations.

Due mainly to item (1), it is difficult to perform the time transfer just on TAI's calculation reference epoch, which is at 0:00 UTC every 5 days. In the case of GPS common-view, we have more than 30 common-view tracks between long-distance cases for each TAI's calculation epoch, but in the case of TWSTFT, we have only two or three time transfer results per week. So the estimation error for the reference epoch of TAI's calculation from the observed database is much larger than the precision of the each observation. Even in this case, the TWSTFT results have almost the same stability as GPS common-view.

DEVELOPMENT OF A NEW TIME TRANSFER MODEM

To compensate for or minimize the drawbacks described in previous section, a new time transfer modem for TWSTFT is now under construction at CRL. Table 2 shows the main specifications of the new modem. As described in the table, the new modem uses a multi-channel method to perform time transfer experiments among more than three stations simultaneously.

Table 2 Specifications of the new time transfer modem

Modulation	Direct-sequence spread-spectrum method using PRN code
Modulation Channels	3 one for time transfer two for Earth station delay calibration
Demodulation or Receiving Channels	8 six for time transfer two for Earth station delay calibration
Clock rate of PRN code	2.04775 MHz or 2.0455 MHz
Bit length of PRN code	8191 bits (13 stage FSR) or 4091 bits (12 stage FSR)
Communication function	Communication function for data transmission among the participating stations
Remote control function	the modems on the slave stations can be controlled from the master station via Internet

MULTI-POINT SIMULTANEOUS TIME TRANSFER USING THE NEW TIME TRANSFER MODEM

The time transfer concept using this new modem with four stations is shown in Fig. 3. Each station transmits a time transfer signal that is modulated using the spread-spectrum method. The pseudo-random noise code for the modulation used at each station is different. All of the received signals at the satellite are combined and retransmitted back to the ground. The multi-channel receiving section at each station demodulates the signals from the satellite and makes arrival time measurements using the station reference clock. The time differences for all the pairs of participating stations can be calculated by exchanging the measured data. Thus, the time transfer of all pairs of participating stations can be performed simultaneously.

The following equations explain the above principle. As shown in Fig. 3, we assume that four stations are participating the TWSTFT, and T_a , T_b , T_c , and T_d denote the time of the reference clock at each station. T_{a1} , T_{a2} , and T_{a3} are the measured values at "station a" for the received signal from station b, c, and d, and they are expressed by the equations (1), (2), and (3), respectively.

$$T_{a1} = \Delta T_{ab} + T_{Ub} + \Delta T_s + T_{Da} \quad (1)$$

$$T_{a2} = \Delta T_{ac} + T_{Uc} + \Delta T_s + T_{Da} \quad (2)$$

$$T_{a3} = \Delta T_{ad} + T_{Ud} + \Delta T_s + T_{Da} \quad (3)$$

where $\Delta T_{ij} = T_i - T_j$, T_{Ui} is the up-link signal propagation delay from the station j to the satellite, T_{Di} is the down-link signal propagation delay from the satellite to the station i, and ΔT_s is internal signal delay in the satellite.

Equations (4), (5), and (6) are measured values at "station b."

$$T_{b1} = \Delta T_{ba} + T_{Ua} + \Delta T_s + T_{Db} \quad (4)$$

$$T_{b2} = \Delta T_{bc} + T_{Uc} + \Delta T_s + T_{Db} \quad (5)$$

$$T_{b3} = \Delta T_{bd} + T_{Ud} + \Delta T_s + T_{Db} \quad (6)$$

Equations (7), (8), and (9) are measured values at “station c.”

$$T_{c1} = \Delta T_{ca} + T_{Ua} + \Delta T_s + T_{Dc} \quad (7)$$

$$T_{c2} = \Delta T_{cb} + T_{Ub} + \Delta T_s + T_{Dc} \quad (8)$$

$$T_{c3} = \Delta T_{cd} + T_{Ud} + \Delta T_s + T_{Dc} \quad (9)$$

Equations (10), (11), and (12) are measured values at “station d,”

$$T_{d1} = \Delta T_{da} + T_{Ua} + \Delta T_s + T_{Dd} \quad (10)$$

$$T_{d2} = \Delta T_{db} + T_{Ub} + \Delta T_s + T_{Dd} \quad (11)$$

$$T_{d3} = \Delta T_{dc} + T_{Uc} + \Delta T_s + T_{Dd} \quad (12)$$

The time difference between clock i and clock j is expressed by equation (13).

$$\Delta T_{ij} = T_i - T_j = -(T_j - T_i) = -\Delta T_{ji} \quad (i,j=a,b,c,d) \quad (13)$$

The up-link and down link propagation delay between the earth station and the satellite are almost same, so they can be assumed as equations (14).

$$T_{Ui} = T_{Di} \quad (i=a,b,c,d) \quad (14)$$

By using above equations, we can easily obtain the all pairs of the time difference between the participating stations shown as equations (15) to (20):

$$\Delta T_{ab} = (T_{a1} - T_{b1})/2 \quad (15)$$

$$\Delta T_{ac} = (T_{a1} - T_{c1})/2 \quad (16)$$

$$\Delta T_{ad} = (T_{a1} - T_{d1})/2 \quad (17)$$

$$\Delta T_{bc} = (T_{a1} - T_{b1})/2 \quad (18)$$

$$\Delta T_{bd} = (T_{a1} - T_{c1})/2 \quad (19)$$

$$\Delta T_{cd} = (T_{a1} - T_{d1})/2 \quad (20)$$

These equations show the simultaneous time transfer between all pairs of the participating stations can be performed using the new modem.

CONCEPT OF AUTOMATIC OPERATION

The new modem has the function to be controlled from the master station using the Internet. Table 3 shows the sequence to perform the TWSTFT session among the participating stations.

Table 3 Sequence of TWSTFF using the new modem

-
1. The operator at the master station makes the arrangement to the satellite management organization,
 2. Distribution of time transfer parameters from master station to the slave stations,
 3. Wait until the start time,
 4. Start the carrier signal transmission from all of the participating stations,
 5. Automatically measure the received power level, frequency and C/No at each station,
 6. Control the transmission power at the slave station according to the command from the master station,
 7. Exchange the status of all of the channels used at each station,
 8. Wait the start epoch of the time transfer,
 9. Make time transfer operation and exchange the measured data among the participating stations,
 9. Finish the time transfer operation at each station.
-

To do item 1, at least one person at the master station should make the communication with the satellite management organization, but no manpower is needed at the slave stations; this function realizes a large reduction in manpower and the performance of the time transfer exactly at TAI's reference time. It can reduce the initial synchronization time of the PRN code modulation signal by using the frequency information of the carrier signal from each station measured in item 5.

MEASUREMENTS OF DELAY VARIATION OF THE EARTH STATION

The delay and delay variation in the earth station is one of the most significant error sources in the TWSTFT method. The new modem is able to monitor and compensate the transmission path and receiving path in the earth station. Fig. 4 shows the schematic diagram of the measurement of the internal delays of the earth station. A small portion of the transmission signal is transferred from the front end of the earth station to the modem. The calibration signal for the receiving path is transferred from the modem to the front end part of the earth station. These signals are transferred using same cable to cancel the delay and the delay variation due to the cable length change. After the frequency conversion, the transmission signal, and the calibration signal are fed to the new modem. Thus, delay and delay variation of the transmission path and the receiving path of the earth station are measured by the modem simultaneously performing the time transfer among the other stations.

CONCLUSIONS

We described the present situation of the TWSTFT network in the Pacific Rim region. The number of the participating stations is increasing steadily. The TWSTFT has many advantages compared with the one-way methods, such as the GPS common-view, the GPS carrier phase, and the GPS/GLONASS multi-channel, but it also has several disadvantages. It is expected that the new type of the time transfer modem described in this paper is one of the solutions to eliminate or reduce the problems of TWSTFT.

By using this new time transfer modem, we can realize the following improvements in TWSTFT experiments:

- (1) shortened use of satellite time and reduced satellite link charges,
- (2) simultaneous time transfer among participating stations, and
- (3) lower manpower requirements.

Thus, it can be said that items (2) and (3) allow TWSTFT to be performed at the exact same time as TAI's calculation reference epoch.

ACKNOWLEDGMENTS

We wish to thank all participants of the Pacific Rim TWSTFT network institutes for doing the time transfer on a regular basis. We also thank to the STA for the financial support for the development of the new time transfer modem.

REFERENCES

- [1] W. Lewandowski, and C. Thomas 1991, "GPS time transfer," Proceedings of the IEEE, 79, 991-1000.
- [2] W. Markowitz, C. A. Lidback, H. Uyeda, and K. Muramatsu 1966, "Clock synchronization via Relay II satellite," IEEE Trans. Instrum. Meas., IM-16.
- [3] Y. Saburi, M. Yamamoto, and K. Harada 1976, "High-precision time comparison via satellite and observed discrepancy of synchronization," IEEE Trans. Instrum. Meas., IM-25.
- [4] D. Kirchner 1991, "Two-way time transfer via communication satellites," Proceedings of the IEEE, 79, 983-990.
- [5] D. Kirchner, 1999 "Two way satellite time and frequency transfer (TWSTFT): principle, implementation, and current performance," in Review of Radio Science, Oxford University Press, pp. 27-44.
- [6] Report of the 12th CCDS Meeting, BIPM, 1993.
- [7] G. de Jong 1998, "Delay stability of the TWSTFT earth station at VSL," in Proceedings of the 29th Annual Precise Time and Time Interval (PTTI) Systems and Applications Meeting, 2-4 December 1997, Long Beach, California, USA, pp. 241-252.
- [8] D. Kirchner, H. Ressler, P. Hetzel, A. Soring, and W. Lewandowski 1999, "Calibration of three European TWSTFT stations using a portable station and comparison of TWSTFT and GPS common-view measurement results," in Proceedings of the 30th Annual Precise Time and Time Interval (PTTI) Systems and Applications Meeting, 1-3 December 1998, Reston, Virginia, USA, pp. 365-376.
- [9] J. Azoubib, D. Kirchner, W. Lewandowski, et al. 1999, "Two-way satellite time transfer using INTELSAT 706 on a regular basis: status and data evaluation," in Proceedings of the 30th Annual Precise Time and Time Interval (PTTI) Systems and Applications Meeting, 1-3 December 1998, Reston, Virginia, USA, pp. 393-404.
- [10] M. Imae, M. Hosokawa, et al. 1999, "Two-way satellite time transfer activities in Asian-Pacific Region," in Proceedings of the 30th Annual Precise Time and Time Interval (PTTI) Systems and Applications Meeting, 1-3 December 1998, Reston, Virginia, USA, pp. 355-363.

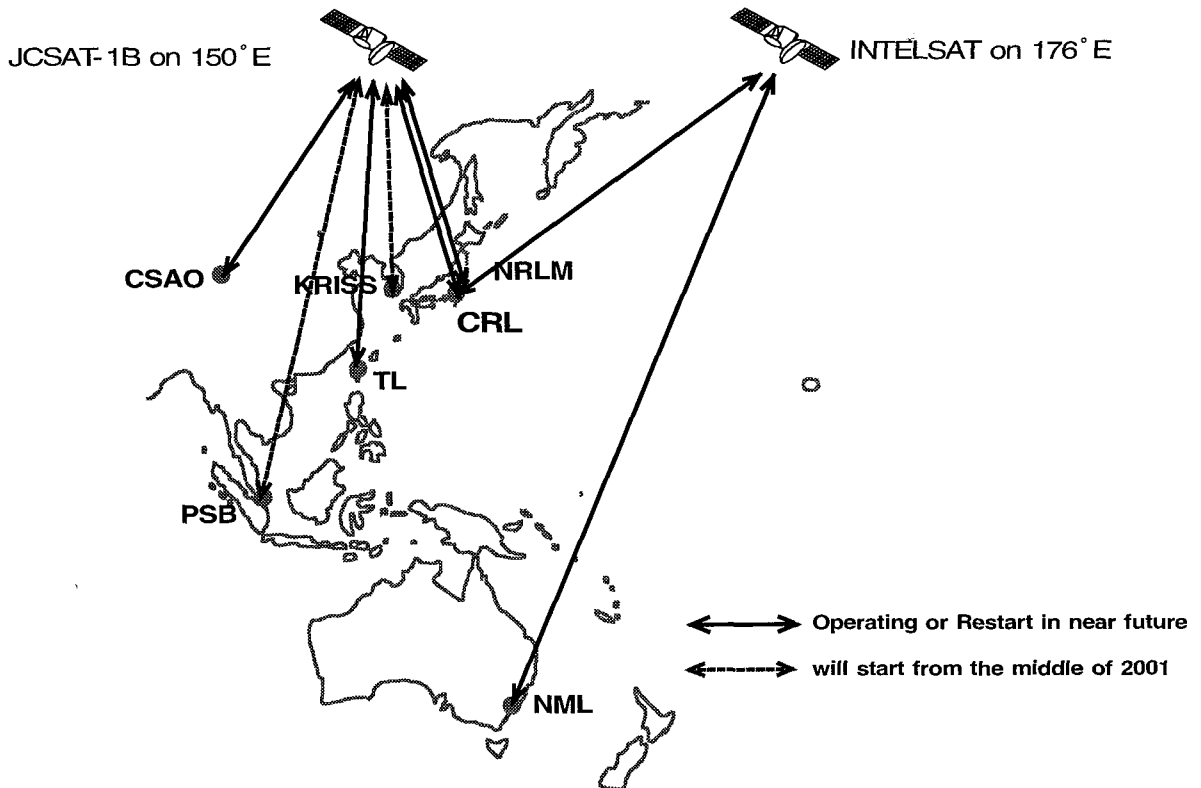


Fig. 1: The TWSTFT network in the Pacific Rim region.

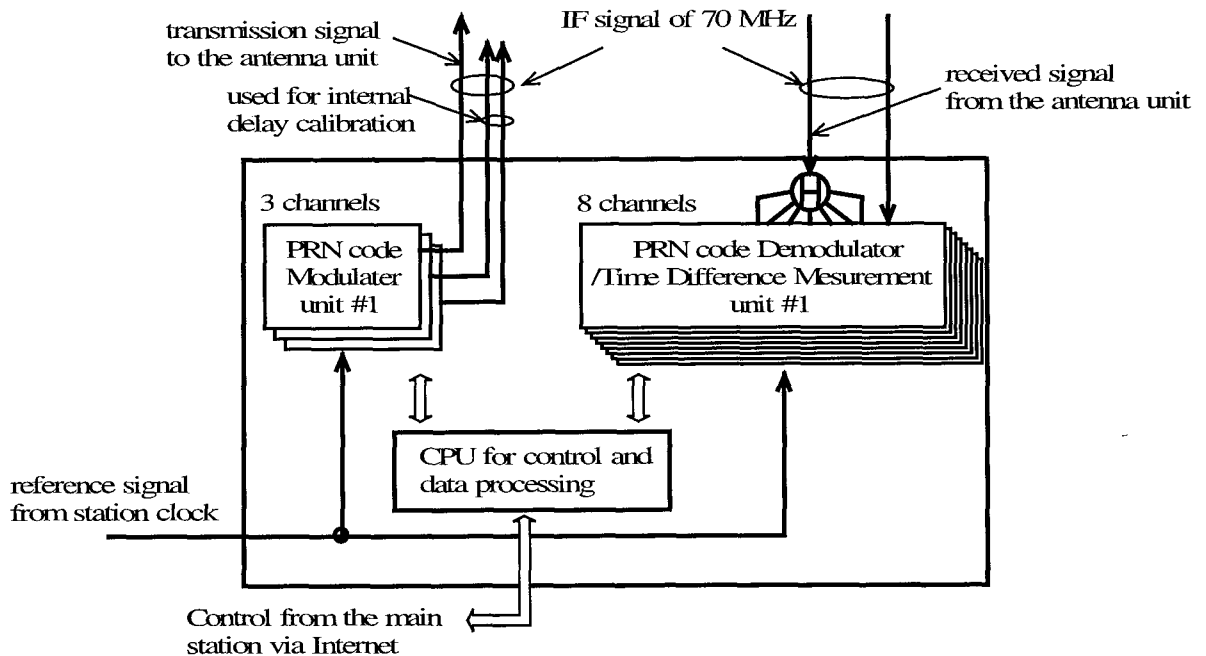


Fig.2: A block diagram of the new modem for the TWSFTF.

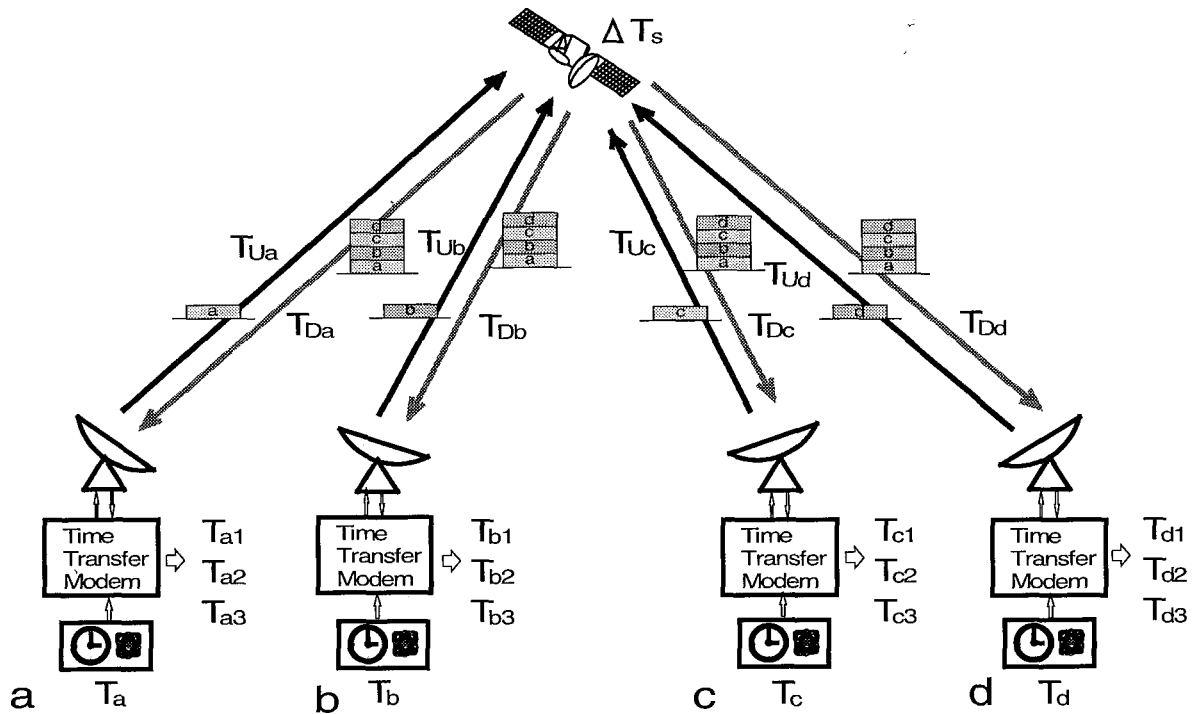


Fig. 3: A concept Multi-points simultaneous time transfer using the new modem.

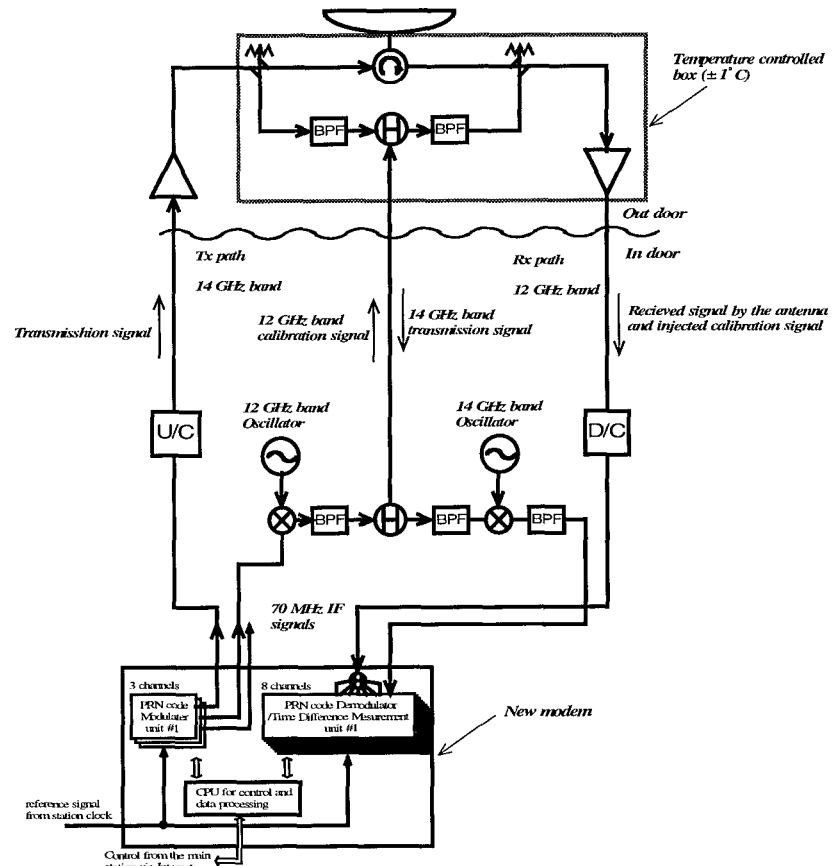


Fig. 4: A concept of the measurement of the internal delays in the earth station for TWSTFT.

REPORT ON THE 8TH MEETING OF THE CCTF WORKING GROUP ON TWO-WAY SATELLITE TIME AND FREQUENCY TRANSFER

W. Lewandowski
Secretary of the CCTF WG on TWSTFT
Bureau International des Poids et Mesures
Pavillon de Breteuil, F-92312 Sèvres Cedex, France
Tel: +33 1 45 07 70 63; wlewandowski@bipm.org

Abstract

The 8th Meeting of the BIPM Working Group on Two-Way Satellite Time and Frequency Transfer (TWSTFT) took place on October 5-6, 2000. It was hosted by the Time and Frequency Division of the BIPM at Sèvres, France. This paper reports on highlights of the meeting as well as covers the latest developments in the area of Two-Way Satellite Time Transfer (TWSTT).

INTRODUCTION

The 8th meeting of the Consultative Committee for Time and Frequency (CCTF) Working Group (WG) on Two-Way Satellite Time and Frequency Transfer (TWSTFT) was held on 5 and 6 October 2000 at the Bureau International des Poids et Mesures (BIPM), Sèvres near Paris. An additional session of the participating stations was held on 5 October at the end of the general session. The meeting was organized by the Time Section of the BIPM and was chaired by Dr W.J. Klepczynski of ISI, Inc. The list of participants is given in the Appendix to this report. Dr T.J. Quinn, Director of the BIPM, welcomed participants with an opening address. Other contributions to the meeting are available on the http://www.bipm.fr/pdf/cctf/wg_twstft.html

SUMMARY OF THE MEETING

The meeting was devoted to an overview of current TWSTFT operations, studies of uncertainties of TWSTFT links, the possible extension of TWSTFT observations to 5 or 7 days per week, calibrations of TWSTFT stations, expansion of TWSTFT links to the Pacific Rim region including links with Europe and North America, and the introduction of further TWSTFT links into TAI. Electronic versions of all reports/presentations are available at the BIPM website (see above).

REPORTS

Reports from Participating Stations. The participating stations presented reports on their work. The ROA TWSTFT station is now operational and will soon start to send data to the BIPM on a regular

basis. The IEN TWSTFT station is completely automated, and INTELSAT approval of the IEN VSAT antenna was obtained in May 2000. In July 2000 the NIST undertook the first TWSTFT comparison of the NIST and PTB cesium fountains. It plans to continue to use TWSTFT for comparisons of NIST and PTB caesium fountains when they are operating simultaneously. The NIST will use TWSTFT as its main link to TAI as soon as some issues concerning reliability are resolved. The NPL's primary station NPL01 is almost completely automated, and the back-up station NPL02 provides a secondary TWSTFT link with the USNO. The OCA TWSTFT data are now sent to the BIPM on a regular basis and this station is expected to be fully automated before the end of 2000. In the Pacific Rim region the CSAO and TL stations should soon be operational.

BIPM TWSTFT Monthly Reports. J. Azoubib highlighted that the variances of all the studied links show that TWSTFT has a clear advantage over GPS common-view for averaging times of up to a few tens of days. He noted that at some stations the GPS equipment is subject to systematic errors. He stressed that the use of TWSTFT significantly improves transatlantic links because, unlike GPS, TWSTFT is unaffected by ionospheric delays. This is particularly important during the present period of high solar activity.

Analyses of the current performance of TWSTFT show that clocks located on different continents can be compared at their full level of performance within 5-day intervals, without being affected by time-transfer measurement noise. Thus, if TWSTFT were used for all TAI links, the stability of TAI would be improved for periods of up to 10 days. The introduction of a number of TWSTFT links into TAI has already increased robustness of TAI construction: TAI no longer relies on a single technique, because TWSTFT links are backed-up by GPS links and vice versa, and for the first time two transatlantic links are included, each of which being performed by two independent techniques.

USNO Time Transfer Monthly Reports. On behalf of K. Senior, D. Matsakis presented a summary of the USNO Time Transfer Reports. The USNO is carrying out comparisons of the TWSTFT, GPS common-view, and GPS carrier-phase (CP) techniques. Although recognizing the qualities and future potential of GPS CP, he said that for the time being TWSTFT gives the best performance.

Comparisons with other techniques. Several participants presented the results of comparisons of the TWSTFT, GPS common-view, and GPS CP techniques (refer in particular to the presentations from the NIST, USNO, and BIPM).

Study of uncertainty of TWSTFT links. Several detailed studies on uncertainties were presented during the meeting. Of particular interest were the presentations by D. Kirchner and T. Parker.

Calibration of TWSTFT link with a portable X-band station. In May 2000 USNO carried out a calibration of the PTB-USNO link using a portable X-band station. Simultaneous X- and Ku-band sessions were recorded on 2 days. The data are being evaluated at the USNO, and calibrations of other links with this X-band station are planned.

Calibration of TWSTFT link with GPS. It was stressed that frequent calibration of TWSTFT equipment using GPS should be organized. In addition each calibration of TWSTFT equipment by a portable TWSTFT station should be confirmed by GPS. G. de Jong has recently discovered that AOA TTR6 receivers use a trigger level of 1.4 V instead the 0.5 V used by older models. This may complicate GPS calibrations and must be taken into account.

Relocation of NPL station. In March or April 2001, the NPL Time Section will move to a new building. A procedure will be put in place to ensure the continuity of time operations. The BIPM and WG will be kept informed.

Future of TWSTFT. D. Kirchner shared his views on possible future developments of TWSTFT. Among them are: more frequent, fully automated measurements, higher chip rate (20 MHz; SATRE modem is ready), exchange of 1 s data via satellite (SATRE and other modems are available), use of carrier phase for TWSTFT (SATRE is available), development of a small and self-contained (hardware, software) station that is simple to operate.

New modems at NRL. R. Beard reported that new modem has been developed at the NRL and will be adapted for use in mobile applications, for example for a ship to use as a back-up system for GPS. The possible implementation of MITREX code is considered too costly.

IGS Analysis Center Workshop 2000. F. Arias reported that this workshop took place during 25-29 September at the USNO. Three main themes dominated the meeting: the IGS/BIPM Timing Pilot Project; the IGS near-real-time products and their applications; and potential interactions between the IGS and various GNSS systems (GPS, Galileo, GLONASS).

ACTIONS

The WG decided the following actions:

- **Extension of the number of weekly TWSTFT sessions.** A group comprising J. Davis, B. Klepczynski, T. Parker, and S. Shemar under the leadership of G. de Jong will investigate if the TWSTFT acquisition time can be reduced from 60 s to 30 s and TWSTFT sessions can be reduced from 120 s to 60 s to allow seven sessions a week. A report will be prepared for the PTI meeting of participating stations.
- **Payment of INTELSAT.** G. de Jong will coordinate payment of INTELSAT, addressing related issues concerning INTELSAT's privatization in April 2001.
- **Pacific Rim/Europe TWSTFT link.** A working group on this issue was set up, with Z. Li as chairman and M. Imae, G. de Jong, B. Klepczynski, T. Parker, and S. Shemar as members. A short report will be prepared for the PTI meeting of participating stations.
- **Filtering of outliers.** It was decided that during treatment of TWSTFT 1 s data, observations that deviate by more than 3σ from the quadratic fit to the data will be eliminated, but only one at a time.
- **GPS calibrations.** Frequent (thrice yearly) GPS calibrations of TWSTFT equipment should be organized. The involvement of regional organizations such as EUROMET is welcomed.
- **TWSTFT calibrations.** The TWSTFT community should dedicate a portable TWSTFT station for frequent calibrations. A de-Jong-type satellite simulator should also be used more frequently for calibration. TWSTFT calibrations should always be confirmed by GPS calibrations.

- ***Log files.*** It is recommended that log files be implemented on ftp sites to record the evolution of TWSTFT stations.
- ***Empty data files.*** Because an empty TWSTFT file is ambiguous it is recommended that an entry such as “no measurements” be made.
- ***E-mail dispatching software.*** The USNO plans to equip the TWSTFT community with software allowing the distribution of e-mail to the community. The software would also allow consultation of all exchanged messages.
- ***Theoretical uncertainty of TWSTFT.*** A draft table showing a theoretical estimation of different sources of uncertainties in TWSTFT will be prepared by J. Davis and W. Lewandowski for the PTTI meeting of participating stations.
- ***Studies of TWSTFT.*** Further investigations should be carried out to study the improvements brought into TAI by the use of TWSTFT. These studies should be completed in advance of the next meeting of the CCTF.
- ***USNO TWSTFT calibrations using US X-band satellite.*** The continuation of the calibrations by the USNO, including TAI TWSTFT links, is most encouraged.
- ***Introduction of new TWSTFT links into TAI.*** The WG recommends the introduction of further TWSTFT links, including Pacific Rim links, into TAI.

DIETER KIRCHNER

The WG expressed its gratitude to Dr. Dieter Kirchner, scientist and engineer. Dr. Kirchner is one of the pioneers of the TWSTFT technique and remains one of the main contributors to its development. The WG expressed the hope that the TWSTFT community will continue to benefit from his expertise, despite the TUG ceasing operation.

FORTHCOMING MEETING

It was agreed that the next meeting of participating stations will be held during the PTTI'2000 conference at the end of November 2000. The next full meeting of the Working Group will be held at the CSAO, Lintong, China, at the end of October 2001.

APPENDIX

List of participants

F.E. Arias, BIPM,
J. Azoubib, BIPM,
F. Baumont, OCA/CERGA,
R. Beard, NRL,
J.A. Davis, NPL,
G. de Jong, NMi VSL,
W. Hanson, NIST,
P. Hetzel, PTB,
Z. Jiang, BIPM,
D. Kirchner, TUG,
W.J. Klepczynski, ISI, Inc.,
H. Konate, BIPM,
W. Lewandowski, BIPM,
Z. Li, CSAO,
S.Y. Lin, TL,
D. Matsakis, USNO,
P. Moussay, BIPM,
J. Palacio, ROA,

T. Parker, NIST,
G. Petit, BIPM,
Z. Piwowarczyk, GUM,
T. J. Quinn, BIPM,
S. Shemar, NPL,
P. Uhrich, BNM-LPTF,
B. Yujing, CSAO.

Excused:

F. Cordara, IEN,
M. Imae, CRL,
V. Pettiti, IEN,
W. Schaefer, TimeTech.

LEAPSECONDS: PANEL DISCUSSION

**Dennis D. McCarthy, Chairman
U.S. Naval Observatory**

This session is designed to be a little different in what we have had in the last few days. So I will call on the panel members, if they're here, and that would be Steve Malys and Ron Beard.

What we are attempting to do here is to get out some discussion on the leap second. The session itself is meant to be a discussion session, so we invite your questions, opinions, the good points, and bad points about leap seconds. We'd like to bring out some of the considerations that we need to think about.

The format for this will be that Harold Chadsey is going to give a brief historical introduction as to how we got into the situation where we are today. I'm going to talk about some of the considerations for doing something about leap seconds that is different from what we are doing today. Steve Malys is going to talk about some of the reasons to keep the current situation, why we need to consider doing that. Ron Beard is going to talk about the reaction to the International Telecommunications Union to recent suggestions about changes in the process. And then we would like to invite some discussion on what we would like to see in the future about this. We will also talk about some of the other activities that are going on in this business right now. With that, we'll start off with Harold's presentation on the historical background of the current situation.

RELATING TIME TO THE EARTH'S VARIABLE ROTATION

H. Chadsey and D. McCarthy
U.S. Naval Observatory
Washington, DC 20392, USA

Abstract

With the beginning of the 21st Century, the timing community finds itself again facing a decades-old problem of how to synchronize a uniform time scale with time derived from the Earth's rotation. Atomic time is the basis for most everyday timing applications. However, time astronomically determined from the Earth's rotation is essential for other applications including navigation. The history of relating atomic time to the Earth's rotation is presented, including background information related to the current synchronization method of leap seconds.

INTRODUCTION

The technological advances of the 20th Century are causing the timing community to examine once again the decision to synchronize atomic time with the Earth's rotation using leap seconds. Historically, time scales in common use have been maintained to within at least 1 second of time derived from the Earth's rotation. The current practice is to insert 1-second adjustments, called leap seconds, into the atomic-based time scale to bring the two types of time to within 0.9 seconds of one another. These adjustments are made internationally, preferably at 23h 59m 59s on 30 June or 31 December depending on the varying rotation of the Earth. However, as technology advances, the time steps required to maintain that level of synchronization become more inconvenient for some users to implement. Before going into the details of leap second implementation, we should first look at the history of the second and leap seconds.

RECENT HISTORY OF THE DEFINITION OF THE SECOND

Two concepts for the definition of the second have been used in modern times. The first is the definition of a second based on the Earth's rotation with respect to the Sun. The second is based on the Earth's revolution about the Sun and is realized in practice by the frequency of an atomic transition in the cesium atom.

ROTATIONAL SECOND

Throughout history, the definition of time has traditionally been related to repetition of solar phenomena such as successive sunrises, sunsets or transits of the local meridian. In modern times, the astronomical second was defined conventionally as 1/86400 of the time required for

an average rotation of the Earth on its axis with respect to the Mean Sun (the mean solar day). Although the variability of the Earth's rotational speed had been established in the 1930s [1,2], this definition of the second was generally accurate enough for the technology and time applications of the day. However, by 1956, the need for a more uniform time scale was recognized.

ATOMIC SECOND

The need for a second that was not dependent on the variable rotation of the Earth prompted the definition of a new "ephemeris second" determined by astronomical means. It was defined as $1/31,556,925.9747$ of the tropical year at 12:00 hours Ephemeris Time on 0 January 1900 (i.e., 31 December 1899) [3,4]. The numerical value of the defining fraction was obtained from Simon Newcomb's equation for the apparent motion of the Sun. However, operational measurement of the ephemeris second was available only retrospectively as an average of several years' continuous observations of the Moon's position. One major drawback to the ephemeris definition was that only astronomers could measure it directly.

The development of atomic clocks made it possible to access this ephemeris second more easily. Observations of the position of the Moon with respect to the stars made it possible to calibrate an atomic transition in the cesium atom in terms of the ephemeris second. The atomic second was adopted in October 1964 by the International Committee of Weights and Measures. They "declared that the transition to be used is that between the hyperfine levels $F = 4, m_F = 0$ and $F = 3, m_F = 0$ of the ground state $2S1/2$ of the atom of cesium, unperturbed by external fields, that the value $9,192,631,770$ Hz is assigned to the frequency of this transition." [5] This has been the definition of the SI (Système International) second since 1967.

TIME SCALES

Having defined the length of 1 second, we can now examine the different time scales that have been formed using these seconds.

ROTATIONAL TIME SCALES

Rotational time scales are based on the astronomical observations of the Earth's rotation angle with respect to a quasi-inertial reference frame and related to mean solar time through an adopted mathematical expression. Greenwich Mean Time (GMT) was used to designate the local mean solar time along the Greenwich meridian. Before 1925 mean solar time was measured from noon. Beginning on 1 January 1925, however, by international agreement, mean solar time was measured from midnight. To distinguish between the two means of reckoning GMT, the terminology "Greenwich Civil Time" (GCT) was employed by some to refer to the measurement of mean solar time from midnight [6]. Eventually the name "Universal Time" (UT) was accepted to replace both GMT as a rotational time scale and GCT. GMT is still used in the United Kingdom to refer to the local civil time.

Improving accuracy in the measurement of UT made it desirable to distinguish among different versions of UT. UT0 is the time directly observed locally from star observations. It does not provide an accurate description of the Earth's rotation angle, since it is corrupted with local effects such as the motion of the vertical and the effects of the motion of the rotational pole

over the surface of the Earth (called polar motion). UT1 is UT0 corrected for polar motion as specified by data furnished by astronomical observations. UT1 is a true representation of the rotation of the Earth free from local effects. UT2 is UT1 corrected for annual and seasonal variations by means of a conventional formula. Neither UT0 nor UT2 are in common use today by the non-specialist. Coordinated Universal Time (UTC) was originally defined as the piecewise uniform scale that approximates UT2. It is currently used as a “stepped offset” scale and is derived by making leap second adjustments [7].

ATOMIC TIME SCALES

With the advent of atomic clocks, a number of time scales, making use of the second defined by the frequency of cesium, came into use. The A.1 time scale of the U.S. Naval Observatory, established officially on 1 January 1959 [8], was defined by setting A.1 equal to UT2 on 1 January 1958 at 00:00 GMT (UTC). It was derived from clock information from nine laboratories and eventually made available back to 15 June 1955. Contributors to the A.1 time scale sometimes referred to the output of their clocks as A.1. The A.1 time scale is now derived solely from USNO clocks. Similarly, other timing laboratories created atomic scales based on their atomic clocks. In 1971, the international community accepted the A.3 Bureau International de l'Heure (BIH) atomic time scale as the standard and this came to be known as International Atomic Time (TAI). The BIH atomic time scale, determined between July 1955 and 1971, may also be referred to as TAI [9].

EAL (Echelle Atomique Libre) is a free atomic time scale produced by an iterative algorithm using the weighted average of clock readings from laboratories spread around the world. The processing is currently done in deferred-time and in whole 1-month data blocks. TAI (International Atomic Time) is derived from EAL by adding a linear function of time with a convenient slope to ensure the accuracy of the TAI scale interval as determined from primary cesium frequency standards. (The length of a second is calibrated in TAI where it is not in EAL.) The frequency offset between EAL and TAI may be changed to maintain the accuracy of the length of the second [10].

COORDINATED UNIVERSAL TIME

Because the rotational second is variable in length, atomic time and rotational time got out of step with each other. As a result, time scales were created that steered atomic clocks to the astronomical time. Some of these never gained widespread acceptance for practical use. Universal Atomic Time (UAT) [11] was used to designate a piecewise uniform scale that approximates UT2 to within about 0.1 second. It is a “stepped offset” scale and is derived by making adjustments in offset and epoch from the uniform atomic time scale. Stepped Atomic time (SA) [11] was used to designate the piecewise uniform scale that approximates UT2 to within about 0.1 second. It is a “stepped offset” scale and is derived by making adjustments in offset.

In August, 1959, national agencies in the United States (U.S. Naval Observatory, Naval Research Laboratory, and National Bureau of Standards) and the United Kingdom (Royal Greenwich Observatory, National Physical Laboratory, General Post Office) along with radio stations that provided precise time in those countries (NBA, Canal Zone; WWV, Beltsville; WWVH, Hawaii; GBR and MSF, Rugby) agreed to coordinate time so that broadcast time signals would be synchronized to 1 millisecond (ms) [12]. Time pulses were to remain within 50 ms

of UT2. This was accomplished by coordinated fractional offsets in the frequency of cesium and occasional adjustments in epoch if required. As more agencies and broadcasting stations began to participate, the time emitted by the participating radio stations came to be known as Coordinated Universal Time (UTC) [9]. However, UTC was not strictly defined until 1965 when the Bureau International de l'Heure (BIH) defined it with respect to its atomic time scale.

Prior to 1960, clocks had been steered by individual observatories and laboratories to match the time determined from the Earth's rotation. In the United States, the USNO rotational time scale called "N2" was used as the scale to which clocks were steered from 1 April 1953 until 1 January 1956 [13]. After 1 January 1956, the USNO determination of UT2 was used as the time scale to which U.S. clocks were steered [14]. These steers were in the form of steps of the order of tens of milliseconds inserted occasionally through 1959. Beginning in 1960, a combination of frequency and step offsets was made to steer UTC to UT2. From 1969 on, no time steps were employed until UTC was redefined as of 1 January 1972 to be the time scale that uses leap seconds to keep UTC within 0.9 s of UT1.

Dr. Gernot Winkler and Dr. Louis Essen proposed the concept of leap seconds independently in 1968 at a meeting at the International Bureau of Weights and Measures (BIPM) [15]. Winkler proposed that integer steps of seconds replace the steps of 200 milliseconds used to keep UT2 within 100 milliseconds of astronomical time. The 200-millisecond steps were occurring too often and were too small to be entered into most systems. He drew an analogy to the concept of leap years in the Julian Calendar. Interestingly, in his original proposal, Winkler stated that the leap seconds could be introduced either whenever necessary or "on a fixed day, such as the 29th of February" [16].

The transition from adjusting the length of a second to using a second of uniform length and inserting leap seconds to account for the time difference was made on 1 January 1972. It was made in such a way that the start of the rotational second and the atomic second would coincide at 0h 0m 0s on 1 January 1972. Figure 1 displays the history of TAI-UTC showing the step changes in epoch as well as the adjustments in frequency.

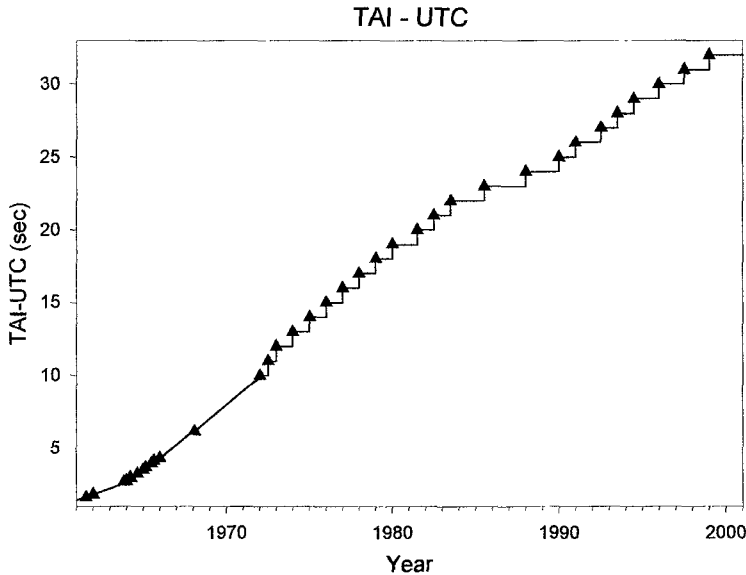


Figure 1. History of TAI-UTC showing the step changes in epoch as well as the adjustments in frequency.

CONSIDERATIONS REGARDING LEAP SECONDS

Naturally, the first consideration for keeping a uniform time synchronized to the Earth's rotation is navigation. The original reason for needing precise time was navigation at sea. Longitude determination requires one to know the correct time at a known location and at the location in question simultaneously. This was such an important issue in the early 1700s that the British government offered substantial rewards for anyone able to build a clock with a specified precision. Today, with GPS, GLONASS, LORAN, and other electronic navigation systems, celestial navigation is not as common. However, keeping the atomic time and Earth rotation synchronized is important to astronomers and others working with non-electronic-based navigation.

Another important consideration is the growing use of computers. In these applications time is independent of the Earth's orientation and problems can occur whenever a leap second is introduced into time systems. In today's world of high-speed inter-computer communications that time-stamp messages at the sub-second level, 1 second can be a significant length of time. In addition, clocks normally count from 59 seconds to 0 seconds of the next minute. Leap seconds require that the count is 59 seconds, 60 seconds, and then 00 seconds of the next minute. Many computer systems have a problem introducing the second labeled "60."

A third consideration is the legal definition of time. For example, legal time in the United States is based on mean solar time. UTC suitably adjusted for time zones is considered to be an adequate representation. Should the definition of UTC be revised, the effect on legal codes may need to be investigated.

Another concern that is sometimes raised is the effect on religious observances that are related to time synchronized to Earth rotation. Generally religions base make use of tables suited for their general location to coordinate observances. Those tables are produced with 1-minute accuracy. Some believers may choose to play it safe by waiting an extra 4 or 5 minutes to account for any irregularities in the tables and refraction of light.

Although there may not be a leap second in the next year, the Earth's deceleration is well documented and will not stop. It is due to the tides and change in the Earth's figure. Figure 2 shows the difference between UT1 and a uniform time scale. We can clearly see that the difference will continue to grow in the future with a rate larger than the current rate. Because the Earth will continue to decelerate, the frequency of leap seconds will increase producing increasing public annoyance. The insertion of leap seconds will also remain essentially unpredictable requiring continuous time counting systems such as computers to handle 86,401-second days and to time stamp a second labeled "60" without large amounts of pre-scheduling notice.

OPTIONS

Several options are available. Some proposed solutions are presented here.

Status Quo

The status quo would require no changes to most operations and would provide a minimum of concerns to celestial navigators. On the other hand, as noted earlier, the frequency of the leap seconds will increase causing problems for communications and software. It may lead to the growth of systems based on independent time scales.

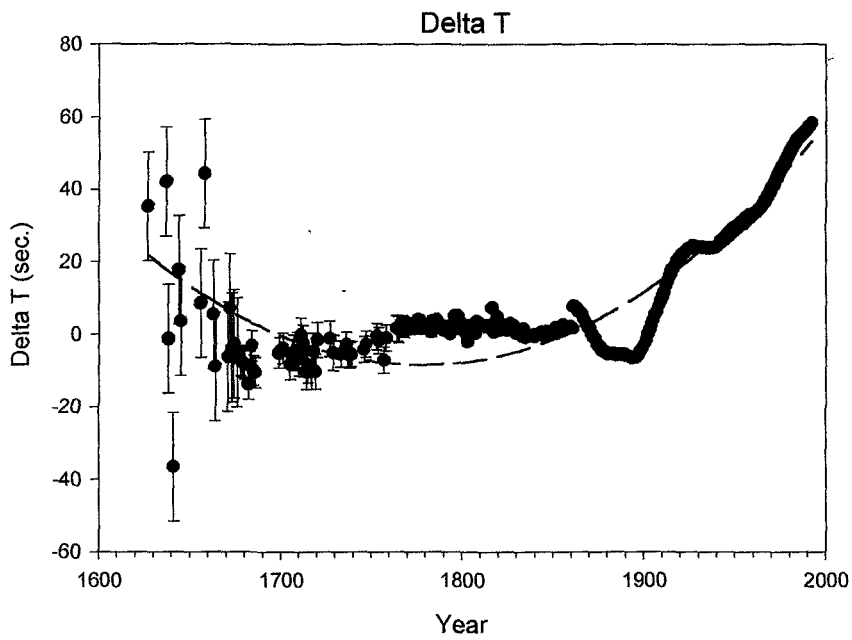


Figure 2. Observations of Delta T (UT1-Uniform Time) versus time. The thin broken line is a parabola fit to the observational data

Discontinue Leap Seconds

Leap seconds could be discontinued eliminating the cause for concern. However, there would be an unlimited growth in the difference between atomic and astronomical time ($|UTC - UT1|$). This could lead to major problems with civil law and the legal definitions of time.

Wider Use of International Atomic Time

Those needing a uniform time scale could use TAI instead of UT1. This would eliminate the concern, but TAI would have to be made much more accessible to users. Also, more of the general population would have to be educated about the existence of TAI and its use.

Redefine the Second

The length of the second could be redefined. This is a fundamental solution, but if it were done, it would require the redefinition of other physical units (e.g., length, force, and energy). Because the rotation of the Earth is decelerating, however, it would be necessary to continue to redefine the second periodically in the future.

Smoothing the Leap Second Occurrence

This option would require the length of seconds in the immediate neighborhood of the occurrence of a leap second to be changed so that there would be no "extra" second needed to adjust the uniform time by 1 second. This would, in effect, redefine the length of a second over a short period of time so the leap second would not appear. It would require seconds of different lengths, whose implementation process would have to be very clearly defined. The date of implementation would be unpredictable just as the insertion of leap seconds is currently.

Increase the Tolerance

The tolerance for $|UTC - UT1|$ could be increased. This would be easy to accomplish. However, the size of the discontinuities (currently 1 second) would increase and possibly cause more serious problems than the present leap second system. The DUT1 codes have limitations and the magnitude of the difference would have to be considered. The date of adjustment would be as unpredictable, and the acceptable limit may be difficult to establish.

Periodic Predictable Adjustments

UTC could be periodically adjusted by an unpredictable number of leap seconds on predictable dates based on an adopted deceleration model. The number of leap seconds inserted though could be unpredictable and large discontinuities would be possible. An extension of this possibility is that a known number of leap seconds could be inserted at predictable intervals. The date and number of leap seconds would be known. However, large discontinuities would be possible and $|UTC - UT1|$ would be likely to be much greater than 1 second. Figure 3 shows a simulation of possible predictable adjustments. The simulation is based on the past observational history of TAI - UTC and shows that differences ($UTC - UT1$) on the order of 10 seconds would be expected if a plan were implemented in which periodic predicted adjustments were made to UTC based on the parabolic fit to the past history of $UT1 - TAI$.

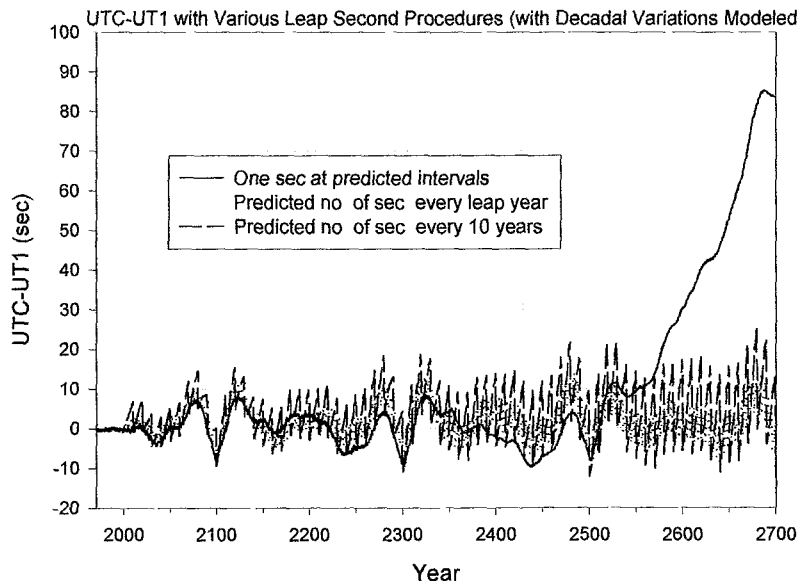


Figure 3. Simulation of expected UTC-UT1 showing the effects of different leap second insertion schemes.

CURRENT STUDY GROUPS

The International Union of Radio Science (URSI), the International Astronomical Union (IAU) and the International Telecommunications Union Radiocommunications Sector (ITU-R) are currently studying this topic. The ITU-R is expected to take the lead in formulating any possible changes to the current procedure.

REFERENCES

- [1] H. Spencer Jones 1939, *Monthly Notices of the Royal Astronomical Society*, **99**, 541-558.
- [2] N. Stoyko 1937, "Sur la periodicite dans l'irregularite de la rotation de la terra," *Comptes Rendues de l'Académie des Sciences*, **205**, 79.
- [3] *Transactions of the International Astronomical Union*, IX, Proceedings of the Ninth General Assembly, Dublin, Ireland, 1955, edited by P. Oosterhoff, Cambridge University Press, New York, New York, USA, 1956.
- [4] "The international system of units (SI)," 7th edition, Bureau International des Poids et Mesures, Sèvres, France, 1998, p. 119.
- [5] W. Markowitz, R. Hall, L. Essen, and J. Parry 1958, "Frequency of cesium in terms of Ephemeris Time," *Physical Review Letters*, **1**, 105-107.
- [6] *Transactions of the International Astronomical Union*, III, Third General Assembly, Leiden, Netherlands, 1928, edited by F. Stratton, Cambridge University Press, New York, New York, USA, 1929, p. 300.
- [7] *Transactions of the International Astronomical Union*, **10**, 1961, p. 489.
- [8] "Time Service notice no. 6," U.S. Naval Observatory, Washington, D.C., USA, 1959.
- [9] B. Guinot 2000, "History of the BIH," in *Polar Motion, Historical and Scientific Problems*, IAU Colloquium No. 178, edited by S. Dick, D. McCarthy, and B. Luzum, Astronomical Society of the Pacific Conference Series, **208**, pp. 175-184.
- [10] P. Seidelmann (editor) 1992, *Explanatory Supplement to the Astronomical Almanac*, revised edition, University Science Books, Mill Valley, California, USA, p. 85.
- [11] G. Hudson 1972, "Some characteristics of commonly used time scales," NBS Special Publication 300, Vol. 5, pp. 224-230.
- [12] *Transactions of the International Astronomical Union*, XIA-Reports, edited by D. Sadler, Academic Press, New York, New York, USA, 1962, p. 363.
- [13] Reference [10], p. 87.
- [14] "Time Service notice no. 4," U.S. Naval Observatory, Washington, D.C., USA, 1956.
- [15] G. Winkler 2000, private communication.
- [16] G. Winkler 1968, "The future of international standards of frequency and time," memorandum submitted to the Ad Hoc Group meeting at the International Bureau of Weights and Measures (BIPM).

Discussion

RONALD BEARD (NRL): Good morning. As many of you are aware, the ITU is the international organization that regulates many of the things that relate across the different countries and organizations that require coordination. Such things as radio spectrum, telecommunication standards, and many of these things that are required for nations, companies, organizations, and systems to work together. You may also be aware that time and frequency broadcast services in the nations are also based on recommendations of the ITU-R. Within the ITU-R, Study Group VII, Science Services has established a working party, 7A, which looks at and recommends time and frequency services in relationships to time that are broadcasted by these services and their relationships to different time scales.

Many of the things that Dennis has talked about earlier are based on ITU-R recommendations on time and frequency broadcasts and their relationship to time scales. The tolerance between the UT and UTC are based primarily on recommendation ITU-R, TF460-5, which was established first in 1970 and modified in '74, '82, '86, and '97—we do a lot of modifications sometimes, to the 0.9 second difference between UT1 and UTC. These recommendations, opinions, and other things that the ITU establishes become ultimately established in legal facts in the various member states. These also regulate international treaties and other things relating to frequency spectrum and services used internationally. Consequently, UTC is in a number of other recommendations relating to the use of UTC frequency; the use of the term "UTC," what does it mean, and how do you establish that internationally; how do you compare these international time scales and other time scale notations; and a lot of other things that are looked at recommended by the ITU-R.

The way the procedures work within the ITU-R is they first establish a question to change, regulate, modify, or add some type of recommendation that may affect a number of these different treaties and things that are related to the ITU-R. Once these are studied and the questions are answered, these may end up in recommendations. These types of recommendations were first studied, agreed to, and looked at by many people before they were established. The recommendations and changes to them are also based on different studies that may last a number of years and examined by a number of different people.

From last year's result of many of these questions that are being asked that Dennis just went through, a new question was established on the future of the UTC time scale. If you were to consider going through a different time scale, that might affect time and frequency coordination and broadcast worldwide. These need to be accommodated in these types of recommendations. So a question was established last year as to what are the requirements if we change these recommendations. Whom does it impact? Does it make any difference? What are the present and future requirements for this tolerance? Do some of these changes make sense in the terms of the different systems, organizations, and legal bodies that may use them? Does the current procedure essentially satisfy everybody or should an alternative approach be adopted? These kind of general questions were asked last year.

After this occurred or around that time, the issue also raised in the consulting committee for time and frequency and other scientific bodies resulted in the Director of the BIPM writing a letter to the Secretary General of the ITU, who presides over the ITU-T and the ITU-R. The letter said that if these types of changes were to be contemplated, the ITU would need to take them up, actually incorporate them, and put them into effect. So as a result of this, the issue seemed to be a little bit more urgent than the normal method of studying the question for several years and ultimately coming to a conclusion. So this year, a special repertoire working group, by correspondence, on the UTC question was established. These are members:

I am fortunate enough to be the chairman of this group which is going to work this issue. We have adopted a plan of action of how to attack this. Since we are not exactly sure how much of an impact this is going to have and how much reaction we are going to get from the telecommunications, radio industry, and the scientific communities, this is a preliminary plan to at least assess the situation, see what might be necessary in order to fully address this issue, and establish a new recommendation or lack of recommendation.

The first step is that the Director of ITU-R will be sending a letter to the member states and section members within the ITU saying that this group has been established, what the basic plan of action is going to be, and what we are going to be doing. This is the usual formal step for the ITU to establish these types of groups and study plans. We had hoped that would have been out by the end of this month, but it is still not out yet, so it is still in the first step. Once that is done, then the participating organizations of sector members or member states would be then be identifying points of contact who would work with this special group to address the issues and assess the impact, or lack of impact, or changes that might be necessary to coordinate. We would then provide additional material on the question, distribute that, and begin the process of actually doing the study.

We're now in the fourth step, and the first step really hasn't occurred yet of introducing this question and our intentions to study this problem and address it with the various member states and organizations involved at this meeting. So we have accomplished one of our tasks already. During the time after the letter comes out and this discussion here, we will be collecting statements, comments, and studies that may have occurred already from the various agencies to incorporate those into a database or a library of information to base the studies on.

The next step would be to conduct a coordination meeting with the various member states or organizations and participants at the EFTF that will occur in France in March. Hopefully, we will be able to get enough information by that time to at least try to size the magnitude of the problem. It could be that nobody cares and nothing happens. Or it could be that everybody cares and we are covered up in information. We really don't know yet. So we would be able to assess the impact agencies that want to participate in the study and in the study group. Then we can discuss and try to coordinate what really should be what I anticipate to be the final plan of action to be formulated at that time. Exactly what we need to do, do we need to do certain studies? Do we need to do simulations? Do we need to coordinate with different agencies? Or exactly what needs to be done? We would hope to compile the results of that at that time and report back to the next working party 7A meeting, which will occur in May in Geneva next year, so that we may either finalize the issue or formulate a new plan of action and try to determine how long it's going to take to resolve this issue and come to closure on it.

So basically that is what we are working to right now. The working method for this is still being established as well. We would hope to establish a contact point at the ITU for e-mail or providing of material through their e-mail server that they have there. That has not been established yet. So at this time, I would offer up—I hesitate to do this—my e-mail address at the ITU. Any material sent to me by participants who would be participating in this, or representatives of member states, sector members, or scientific organizations could contact me. We would like to limit participation in the study group itself to representatives of agencies so that we can try to maintain a reasonably sized body. They could act as the focal point for their respective organizations and provide that to the study group.

Once the e-mail reflector is actually established, and hopefully that will occur within the next month or so, you may either send e-mails to me directly and I will distribute it to the rest of the working group, or later on you can subscribe to the e-mail. You can get involved and see what is going on in the formulation of the plan or submit inputs that you have representing

your organization. So basically, that is what we are up to. Thank you.

DENNIS McCARTHY: Thanks, Ron. The next member of the panel that we have here is Steve Malys from the National Imagery and Mapping Agency. And he's here to point out some of the concerns about making any changes in the definition of UTC. So Steve is here to argue for the status quo—just to more or less leave it alone.

STEVEN MALYS (NIMA): Thank you, Dennis. As we heard from Harold earlier, on the surface of the earth for a ship or any other navigator, 1 second of time is about a quarter mile. But if you think about a satellite in low-earth orbit, 1 second of time corresponds to about 7 kilometers of movement. So it's obviously very important that we account for 1 second very accurately. At the GPS altitude, which is higher than low-earth orbit, at that altitude a GPS satellite moves about 3 kilometers in 1 second. So leap seconds become very important, and procedures have been developed over the years to take leap seconds into account when they do occur. Keep in mind that over the last few decades we saw the evolution of time. Satellite systems have become operational over those last few decades and they are no longer experiments. GPS is obviously a very good example of operational system that we wouldn't want to have an interruption of service for any reason. There are other operation systems, particularly in the DoD, that the DoD depends upon very heavily. A good example of another satellite system would be something like the Defense Support Program, which looks at the earth for missile launches. You don't want to have an interruption of service to a system like that.

Another example is the operation that takes place in Cheyenne Mountain out in Colorado, the space surveillance operation that keeps track of more than 8,000 objects in orbit. It's a very operational system. There are strict procedures setup to handle things like leap seconds, and they have evolved over the years. Certainly, mistakes were made in the past and procedures have been refined. It is my experience that things have improved significantly. People have come to understand much better how to handle leap seconds to prevent the problem. We know, of course, that the Russian GLONASS systems has some difficulty dealing with that kind of operational system. It is my experience that within the U.S. DoD, we have become much better at dealing with leap seconds when they do occur.

So if there were changes to be proposed, and I'm just thinking of one of the cases that Dennis pointed out, if we were to allow the tolerance between UT1 and UTC to grow more than 0.9 seconds, what would happen? What would we actually have to do within the U.S.—DoD and other U.S. Government systems—to accommodate that? Keep in mind, for all of these satellites that are in orbit, we're doing orbit determination for these satellites in an inertial reference frame. We integrate the equations of motion in the inertial reference frame, but our tracking stations typically are on the ground. So our tracking stations are rotating with the earth, which means we need very precise knowledge of UT1. We routinely account for the difference between UT1 and UTC. That parameter is predicted on a routine basis. That is a very important piece of that transformation from the earth-fixed reference frame—it is the inertial reference frame.

So no matter what happens to time scales in the future, we need to account for the earth rotation rate because the tracking stations are most likely going to remain on the ground—at least, some of them will. The earth rotation is not going to go away from the perspective of doing orbit determination. So if we were to change current procedures, systems like GPS and other DoD systems would require some modification to the software. Remember these are operational systems, so a change of UT1 minus UTC graded on 1 second would mean there would have to be some effort initiated within each of these systems by somebody in the government who runs them. Most satellite systems are operated within the U.S. by the

government. Of course, there are commercial systems evolving now. You may have heard of the commercial imaging systems like ICONOS, which is operational. There are other commercial systems as well. I'm mostly referring to government-operated systems here. But there would have to be some initiation of software changes, documentation changes, other changes to the procedures that train personnel, and a significant amount of testing. It wasn't that long ago that Y2K was the big deal, and there was a lot of testing that went on. Even with all the testing that went on, there were still minor problems that occurred. But it's that type of thing that costs a lot of money to do, and there are strict interfaces set up among different satellite systems within the DoD. Those interfaces would have to be carefully looked at and analyzed.

Those are some of things that would have to start off if we were to make a change to the current procedure. Keep in mind that the original definition UT1 minus UTC, as we know it today, cannot exceed this 0.9 seconds. Well, many software systems were designed with that piece of information in mind. There are lots of software packages that treat that as a tolerance. The software will not allow UT1 minus UTC to be bigger than 1 second or it declares that there is a problem of some kind. There is a lot of range checking on parameters that go across different interfaces. Well, today these interfaces have this limit imposed in it. So it is similar to the problem that Dennis mentioned where many systems that broadcast UTC parameters have a limit of 1 second. This is another manifestation of that same kind of problem. These interfaces would have to be changed to accommodate something greater than 1 second.

So really, this is really a practical argument for keeping things the same. If we wanted to make changes, it is going to cost money. Like any good government institution, it is tough to change something once it gets institutionalized and operational. There would be money involved to the U.S. taxpayers, and other countries that run systems like this would have to allocate resources to make changes. Of course, experimental systems or systems that are just being designed now would be easier to change. That is mostly the operational system that I am talking about here today.

The typical procedure to change an operational system is to first obtain a rough order of magnitude from the contractors who are working with these systems. People who are involved in those systems will present a request for change to some configuration management board. If it is approved, there would have to be funds identified to go and change it. Believe it or not, even for a little thing like changing a tolerance from 0.9 seconds to something greater, you need to go through this whole process for an operational system. We would do all of that for no identifiable benefit. It would just be another way to handle the difference between earth rotation rates and some atomic time scale. There would be no improvement in accuracy that I have been able to identify. It would be just be another way of handling a procedure different from what we do today. That would be difficult to sell. If you are going to argue for making a change to one of these systems, you have to explain to the people who manage the funds for those system why they should do this. That would not be an easy argument to make because there is no identifiable benefit to any of these operational systems. It's just a different way of handling it. That is really the practical side that I am here to talk about today.

McCARTHY: Thanks, Steve. That is a real concern, one of the big issues.

Now I would like to open this for discussion. Wlodek, did you have something that you would like to say?

WLODZIMIERZ LEWANDOWSKI (BIPM, France): What I would like to say about this issue is that the BIPM does not have an official position on this issue. We are just taking calculations, computing UTC. We do not have a specific point of view or expertise to express ourselves on the issue because we do not have touch with the users and so on.

But I would like to make some comments about the possible use of TAI, because during CCTF, there was some discussion in Europe on this issue and some exchanges on this matter. After the last CCTF, about 2 years ago, our director wrote a letter to the operators of Global Navigation Systems informing them that if they have any troubles with UTC because of leap seconds, the suggested alternative is TAI. That is fine. If they use TAI for internal time scale systems, I argue with this.

But what worries me is that this letter is maybe not expressing as clearly as it should that the use should be limited only to such internal applications. I also saw in another document of ITU somewhere that TAI was suggested as an alternative to UTC for much broader applications. That worries me because this means, already having UTC, a legal time scale, we are suggesting introduction into civil life another time scale, TAI, which does not have legal meaning. But because of this discussion about leap seconds, some people begin to say—and this happened at the last CCTF—we in fact have a time scale that does not have leap seconds, so let's use it. But this is a problem. Because if people begin to use TAI for civil applications, which will be apparent and visible to the public, that will be a problem because we will be going to two time scales and that will lead to mistakes and possible disasters even. Because now the difference between two time scales is 32 seconds.

For example, on BIPM's Web site, we can see making two time scales, UTC and TAI. That worries me a little bit, because many people go into this Web site and they ask what the matter is and what time is it. What should I put my watch on, UTC or TAI? Which is the right time? In fact, the right time is not UT1, it is UTC. We should not make mistakes with TAI time. TAI is something else. In fact, TAI, I should say, is a UTC system time. It is an internal time scale to generate the final, official, legal time scale for the world which is UTC. So what I would like to point out, in summary, we should not go too quickly to TAI as an alternative because we would go into some big trouble. When I spoke about this issue with some people, they said that GPS time does not have leap seconds and people are getting GPS time. In fact, what I know of this, according to my experiments, GPS users don't use GPS time. GPS time is an internal time scale to the system. GPS users are using UTC(USNO) as broadcast by GPS so they use the right second.

McCARTHY: We often have that question about GPS time. People often think they're using GPS when they are not really using what is strictly defined as GPS time. They are using UTC, but they call it GPS time. Demetrios, if you could just briefly say something about URSI. Demetrios conducted a survey of an URSI group to give its opinions. If you could just say briefly what the results of that survey were.

DEMETRIOS MATSAKIS (USNO): You probably know this too. A lot of times, people turn their GPS receiver the wrong way and we get a phone call on why their receiver is 13 seconds off. That's an easy problem to fix. We did a survey—I actually talked about this a little bit at the last PTTI when the survey was in progress. It was under the auspices of URSI, but I tried to send it everywhere. I asked people to distribute it around, and I got several hundred replies. The committee prepared a final report, which we sent to everybody who sent us a reply. If any of you want it, we can send it to you. We set up a chat group to talk about the problem after the report went out. The computer got wiped out by a virus, we believe, about 2 weeks ago, and unfortunately, it was not correctly backed up. We recovered most of what we had, and I want to give it to Ron Beard. I'll give him all of the comments that people made about the report and after the report.

BEARD: If you look at the international community and the people who might be involved in this, it would get extremely large and complicated.

MATSAKIS: I made some notes and but did not come prepared to talk. Typically, the majority was against the change. Most of the people I got were complainers who didn't like the change. That's typical: when you say you want to do something, those who are in favor don't say much about it. When you look at why they were opposed to it, most of the people were opposed to it for reasons that were not related to money or anything practical. Steve was one of two people who came in with a practical objection. They both were the same, having to do with the expense of going over codes for large, expensive systems.

But the greater tone was a lot of very strong, sometimes emotional, people who said, "don't mess up our clocks." But there was nothing religious that I got, which was a bit of a surprise. I didn't go out of my way to contact religious leaders. I got one opposition from Saudi Arabia, and I asked him why; and the answer was he was concerned about amateur astronomers. And that was one class of user, amateur astronomers who cannot get the number of leap seconds or want to know how they can point their telescopes.

That was along with the other people who were giving reasons why you just don't want to have time going off. There was a problem with the NIST WWVB. When they broadcast the difference between UT1 and UTC, they only have a fixed area in their format. So that will eventually fail, and quite quickly. Any user who is getting that correction off of WWVB series will run into troubles. They don't know how many people, if any, are using that system, but they may find out if this thing happens.

So those are all the comments I can make just now concerning the notes I made on this.

THOMAS CLARK (NASA Goddard Space Flight Center): A couple of things that I want to make comments on relate to Dennis's comments earlier. First of all, just so you all are aware, of course, UT1 is an astronomical definition of time. The current arbiter of astronomical time is VLBI observation techniques. That comes through programs in this country from NASA, namely my program and Dennis's at USNO.

One of the things in talking about the parabolic type of tidal model that was not included in that, which is one of the things that concerns me, is that in addition to the predictable tidal terms there are a series of essentially random-walk phenomena. The recent El Niño that happened, the transition from El Niño to La Niña caused a sundial error of about 5 milliseconds. It happened to be about 3.5 milliseconds on one side and then 1.5 milliseconds as it recovered into the other. So the peak-to-peak range was about 5 milliseconds. So there was this random-walk curve of 5 milliseconds due to one discrete, albeit couple-year-long weather events on relatively short times. Those happened and it essentially has to be treated as a chaotic, stochastic noise process in terms of the clocks.

In addition, Dennis alluded to the decadal scale variations. Most of that comes from essentially climatological variations in our atmosphere and, more important than that, climatological variations in terms of the circulation of fluids inside the earth. Those have to be considered in all of this. They are not really predictive quantities, at least at our current level of knowledge. They have to be treated as a random-walk term. So I just wanted to make sure that people realize that it is not just the soli/lunar tidal drag of the earth that cause these effects.

I tend to come down on the side of let's not make changes based on the "it ain't broke, don't fix it" model. The current scheme keeps the attention of the populace. In many cases, the population, the human experience lives by astronomical events. I'm surprised at Demetrios's comments that he didn't get more in the way of religious types of input. I think it could be that URSI did not really solicit the opinions of religious and civil communities. They were soliciting scientific communities. Certainly, several faiths have events that are scheduled by

either solar or lunar events. Many of the fundamentalists that have those beliefs are also potential hostile enemies of more technologically advanced who don't want to have the feeling that Americocentric ideas are being crammed down their throat. So I would offer the caution that if changes are made, it could be viewed politically/religiously as being a very negative thing. I think that does have to be factored into all of this. We really need to think about it.

Ron Beard talked in terms of the ITU events. A couple of us were talking back here, and we are a little surprised that the ITU views this as a crisis event that is putting it into a fast-track status. I'm not sure that it is a crisis event. The civilization is certainly living with the current situation. Until the year 2600, when we hit a definition problem that the tidal effects make it so that it drags us into a 6-month refresh interval, not being adequate to maintain the current definition, there really is not a serious problem with the status quo. I hardly believe that making a decision that doesn't have an effect until approximately 2600 puts us into a crisis condition. So I guess I argue for maintaining the status quo.

McCARTHY: I would just like to offer one thing there. The decadal variations are what you saw in that simulation, so that's where that comes in. But it's not just 2600, because those decadal variations could force us to go to more than every 6 months insertions within the next 100 years. The crisis comment still stands.

BEARD: A crisis in the ITU—you are not familiar with the ITU time scale, obviously. ITU time and whatnot are very much governed by a lot of bureaucratic procedures. Putting it on the fast track means it will happen before the next decade happens, more than likely. So I did not mean to say that we were going to general quarters to address this by next month, certainly not. The issue was significant enough—perhaps I should have said—to put special focus on it. Perhaps shorten some of the time. But help focus the study and the highlighting of it to assess the full impact. As Steve pointed out, there is a significant impact on various section members, on costs of doing changes. Certainly, the status quo minimizes these types of status change cost.

However, some of the other issues are—let me say, many systems are using internal time scales rather than the official time scales in order to avoid leap seconds. GPS time, I think, is a classic example. Many other systems are doing this so that they can have a continuous time scale and do a lot of automatic processing that a discontinuous time scale does not permit. So if you look at the other systems that are coming on, the relationships and trying to bring all of these systems onto a common time scale have a significant problem by having a discontinuous time scale. One of the more significant decisions that is going to be made in the next year or so is the Galileo time scale. Its relationship to the other satellite systems, GPS, GLONASS, possibly other telecommunication systems on the ground that all these things need to be seeing this with, what time will they use? Will they use another internal time or will they use international standards? So that is part of the reason.

JUDAH LEVINE (NIST): I have just a few comments. First of all, David Mills and I are presenting a paper on the idea of simultaneously transmitting UTC and TAI over the Internet with the idea of addressing one of the solutions that you proposed of making TAI more available. That way you have both UTC and TAI sort of simultaneously. That doesn't take a position on the question, it kind of provides a solution that is available today without having to wait for the ITU to go into crisis mode. I think that is the first issue.

The second issue is that I have written to Demetrios about the finite resolution of our time services which would be broken if UT1 minus UTC were allowed to become bigger than a second. I don't think that is a big issue. We could redefine the time service transmissions to have a different resolution. I don't see that as a real issue.

When I was involved with Demetrios's questionnaire – I live in an astrophysical and astronomical institute, and so, of course, I had a long line of folks out the door discussing the astronomical and astrophysical religious fervor of "you mustn't change the time" and so on. But one of the things that emerged from that discussion is that there already is, of course, an annual term, because, when you talk about mean solar time, that is not a physical time. That's an average over a year. There is an annual variation in the time, which is like 15 minutes. Those folks have managed to cope with that 15-minute time without any difficulty at all. Of course, the whole leap second effect is a perturbation on this 15 minutes, and will remain a perturbation on this 15 minutes for quite some time to come. So I don't think it is really such a big issue as has been made, in a sense that you don't have to deal with this 15-minute question.

I guess the final comment I have is that I have been involved on and off in the definition of the Jewish religious calendar, which is locked to sunrise and sunset as defined locally. And we just use the tables from the Naval Observatory; there is no issue. We just define sunset, we look up what time it is, we print it on the calendar; and that is the end of it. It is just not a question.

WILLIAM KLEPCZYNSKI (Innovative Solutions International): I have a comment to make about UTC and GPS time. A lot of papers I've seen at some of the conferences, especially the ION conferences, are now referring to UTC(GPS). But really, they are referring to GPS time. So GPS time is neither UTC nor TAI, or even close to it because it's off by about 12, 13 seconds or so. So that is the problem that Włodzimierz was referring to when the difference between TAI and UTC is a whole integral number of seconds. The difference between GPS time and UTC is also still a whole number of seconds, and it has to be really kept in mind by the users.

THOMAS CELANO (Timing Solutions Corporation): I'd like to address a point that Steve made and I believe something that was missing in the previous talk. I think cost to the user community is an issue that is going to drive a lot of this. But I think that you missed a point in that there is a cost associated with how we do it now. You made a point of all the systems know how to deal with it now. But we install timing systems in a lot of places that literally shut down when the leap second happens. There is a cost associated with that that needs to be taken into account and if we're going to consider making the change. Because that cost would go away if we could become operationally continuous over these intervals. I don't think that we should use the changes in RFC that are going to be required to do all this stuff, but I don't think we should use the process of change as a reason not to do it. I think we need to be able to recoup the operational cost that we're spending now in testing and the loss of time during the steps in a more continuous fashion.

One thing that I think was missing in all of the options that you guys provided for how we deal with this is the cost associated with each one. I think Steve made that point very well. Different ideas are going to have different implications cost-wise, and one thing that produces cost is predictability. You had a couple options that had predictability, and if you have that, it really simplifies a lot of things operationally and it does reduce cost.

MALYS: One comment to that that I would like to add. Speaking of shutting down, one little anecdote I wanted to share: About 15 years ago, I was doing orbit determination on the Navy's Transit satellites. There was a gentleman working with me who did the prediction of earth orientation, including UT1. Well, every time there was a prediction of leap second, he would go on vacation because it was too stressful for him to handle. So I took over his job, and I owe him a thanks for introducing me to leap seconds.

HUGO FRUEHAUF (Zyfer, Inc.): I'm dressed in black to represent all the religions of the

world today. The three major high-profile religions that deal with time. First of all, in Judaism, as Judah has already mentioned, it is a matter of sunset, and that's taken care of, as he mentioned. In Catholicism, I know of no particular issues with respect to time, so I think that part of it is okay. In Islam, we're dealing with pointing to Mecca, and that can certainly be done without the leap second consideration. So there you have it, no mystery.

CHADSEY: One issue about the leap second and the timing for the religious community was from the people we've been able to talk to and get the information from. Most of them base it on the tables produced by USNO, or you can look them up in several books. Those are general tables, and it changes by a minute for about every 9 miles that you move in position, so there is a little bit of leeway there.

The people who are very orthodox believers say "Well, we need to worry about the refraction of the sun around the earth, and what about the mountains and things like this?" So a lot of those folks, through their religious upbringing and their training, have come to realize, "well, let's adjust it by 4 or 5 minutes," whatever their leaders have instructed them on. So they can account for these small variations of not only their location, but also the scientific fact of refraction of the sun and things like that.

So they're handling it and it is a minor problem for them. The major problem is more for the scientific and the communications industry. The costs of it are going to be ridiculous whichever way we go.

ROBERT NELSON (Satellite Engineering Research Corporation): The principal difficulty with the leap second is the operational problem that it presents to complex timing equipment. So, therefore, I would speak to eliminating the need for the leap second and continuing a time scale such as UTC, which means continuity with the present civil time scale. The difference between UTC and UT1 can be applied mathematically by those people who are best equipped to understand it, who are the celestial navigators.

I think history can provide us with a guide. What we are facing today with the atomic clock technology is that we have a paradigm shift. In the 14th century, when mechanical clocks first became possible with the invention of the escapement, they were used to ring church bells. It introduced to the public perception of time, for the first time, the notion of an equal hour rather than an unequal hour.

In the early part of the 19th century, astronomical ephemerides were constructed with apparent time as the argument, instead of mean solar time. But when pendulum clocks advanced to the state that they could reliably provide a direct measure of mean solar time, then the equation of time, as Judah alluded to, with the maximum difference of 16 minutes between apparent and mean, was used in reverse. Instead of being used to determine mean solar time from apparent time, which was directly measured by the altitude of a star or the sun, it was being used to determine apparent time from the measured mean solar time as given directly by a clock. So I think the time has come in the 21st century, in modern society, to break the tie with the sun all together. After all, in a given time zone, the clock reading can be off from apparent time by as much as half an hour. We use the difference between Daylight Time and Standard Time regularly, which is a difference of a whole hour.

One of the options mentioned was the possible use of TAI. I think that was already addressed by the fact that it is different from UTC by 32 seconds. So if we went to TAI, we would have to change our clocks by 32 seconds. It is much like the calendar had to be changed by 10 days in 1582 when the Gregorian Calendar was adopted.

So I would propose then that instead, UTC be maintained continuously without leap seconds

and that, if necessary, a new time scale, which one could call "UT1C," could be provided, much as UTC is used today to provide the means of celestial navigation. Those people will need a direct measure of UT1. The difference between these two could be provided, for example, by coded signals, much as D-UT1 is provided now to give the difference to the nearest tenth of a second.

A TOTAL ESTIMATOR OF THE HADAMARD FUNCTION USED FOR GPS OPERATIONS *

Dave Howe

Time and Frequency Division, National Institute of Standards and Technology
325 Broadway, Boulder, CO 80305, USA

Tel: 303-497-3277; Fax: 303-497-5996

E-mail: *dhowe@nist.gov*

Ron Beard

U.S. Naval Research Laboratory

4555 Overlook Ave. S.W., Washington, D.C. 20375-5354, USA

Tel: 202-404-7054; Fax: 202-767-2845

E-mail: *beard@juno.nrl.navy.mil*

Chuck Greenhall

Jet Propulsion Laboratory

4800 Oak Grove Dr., 298-100, Pasadena, CA 91109, USA

Tel: 818-393-6944; Fax: 818-393-6773

E-mail: *charles.greenhall@jpl.nasa.gov*

Francois Vernotte

Observatoire de Besançon

41 bis, avenue de l'Observatoire, Besançon Cédex, France

E-mail: *francois@obs-besancon.fr*

Bill Riley

Datum – Timing, Test & Measurement

34 Tozer Road, Beverly, MA 01915-5510, USA

E-mail: *wriley@datum.com*

Abstract

We describe a method based on the Total deviation approach whereby we improve the confidence of the estimation of the Hadamard deviation that is used primarily in GPS operations. The Hadamard-total deviation described in this paper provides a significant improvement in confidence indicated by

*Contribution of the U.S. Government, not subject to copyright. Sponsored by the Colorado Springs detachment of the GPS Joint Program Office. Portions of this work were carried out by the Jet Propulsion Laboratory, California Institute of Technology, under a contract with the National Aeronautics and Space Administration.

an increase of 1.3 to 3.4 times the one degree of freedom of the plain Hadamard deviation at the longest averaging time. The new Hadamard-total deviation is slightly negatively biased with respect to the usual Hadamard deviation, and τ values are restricted to less than or equal to $T/3$, to be consistent with the usual Hadamard's definition. We give a method of automatically removing bias by a power-law detection scheme. We review the relationship between Kalman filter parameters and the Hadamard and Allan variances, illustrate the operational problems associated with estimating these parameters, and discuss how the Hadamard-total variance can improve management of present and future GPS satellite clocks.

1 INTRODUCTION

Using a type of Hadamard variance, the goal of this paper is to reduce the uncertainty of long-term estimates of frequency stability without increasing the length of a data run. For measurements of frequency stability, the two-sample frequency variance known as the Allan variance was generalized to an N -sample variance weighted with binomial coefficients by R. A. Baugh [1]. The case of the three-sample frequency variance that is used here is the Picinbono variance [2] times $\frac{3}{2}$. However, in this paper, it will be called a Hadamard variance (following Baugh's work) that is defined as follows. Given a finite sequence of frequency deviates $\{y_n, n = 1, \dots, N_{y_{max}}\}$, presumed to be the measured part of a longer noise sequence and with a sampling period between adjacent observations given by τ_0 , define the $\tau = m\tau_0$ -average frequency deviate as

$$\bar{y}_n(m) \equiv \frac{1}{m} \sum_{j=0}^{m-1} y_{n+j}. \quad (1)$$

Let $H_n(m) = \bar{y}_n(m) - 2\bar{y}_{n+m}(m) + \bar{y}_{n+2m}(m)$ be the second difference of the time-averaged frequencies over three successive and adjacent time intervals of length τ . Define the Hadamard variance as

$${}_{H\sigma_y}^2(\tau) = \frac{1}{6} \langle H_n^2(m) \rangle, \quad (2)$$

where $\langle \cdot \rangle$ denotes an infinite time average over n , and ${}_{H\sigma_y}^2$ depends on m .

The GPS program office uses this particular time-series statistic for estimating Kalman algorithm coefficients according to [3], which coefficients will be discussed in a later section. The Hadamard deviation ${}_{H\sigma_y}(\tau)$ is a function that can be interpreted like the more efficient Allan deviation as a frequency instability *vs.* averaging time τ for a range of frequency noises that cause different slopes on ${}_{H\sigma_y}(\tau)$. This is shown in figure 1. For estimating Kalman drift noise coefficients, ${}_{H\sigma_y}(\tau)$ is inherently insensitive to linear frequency drift and reports a residual "noise on drift" as a $\tau^{\frac{3}{2}}$ slope, or what is commonly called random run FM (RRFM). This is in contrast to the Allan deviation, which is sensitive to drift and causes a τ^{+1} slope. If the level of drift is relatively high, it masks the underlying random noise. It is customary to estimate and remove overall frequency drift. Depending on the method of drift removal, this procedure can significantly alter the Allan deviation in the longest term τ region of interest, so estimating underlying noise can be a formidable task for any given data span. On the other hand, the Hadamard deviation is unaffected by removing overall frequency drift. For this reason, it is the preferred statistic in situations in which the frequency drift may be above the random noise effects, which is the case with the use of Rb clocks in the GPS Block II satellite program. We do not imply that systematics such as frequency drift can be ignored. Indeed, satellite clocks are changed and these systematics must be learned as quickly as possible to ensure a smooth changeover.

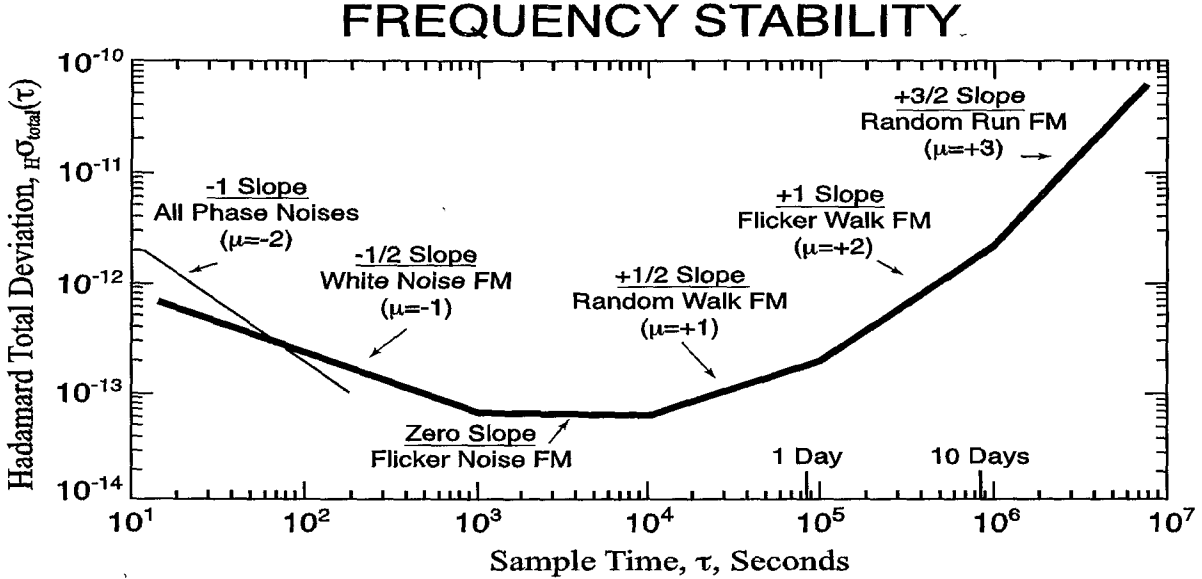


Figure 1: The Hadamard deviation (root Hvar) shows FM power-law noises as straight lines in addition to PM sources of noise for τ -domain power-law exponent μ (that is, $H\sigma_y^2(\tau) \propto \tau^\mu$) range of $-2 \leq \mu \leq 3$. We define a new estimator that can be interpreted identically called Hadamard-total deviation (root TotHvar) and that has significantly improved confidence at long term. The Hadamard-total deviation is insensitive to linear frequency drift that can mask characteristic random noise typically encountered here in the region where τ = one-week and longer. The goal is to identify μ even-integer power-law noises and accurately estimate their levels in order to set system parameters associated with the GPS Kalman filter.

Throughout this writing, we will make comparisons using the traditional best statistical estimators, denoted by “Hvar” and “Avar” referring to the maximum-overlap estimators of the Hadamard and Allan variances. Section 2 reviews the “total” approach to improving statistical estimation. Sections 3 and 4 give two methods of computing total Hadamard variance, designated as TotHvar, using measurements first of fractional frequency deviations and then of time deviations. Then we quantify the advantage of TotHvar over Hvar in Section 5, giving formulae for computing bias and equivalent degrees of freedom (edf) of TotHvar. Section 6 gives a method for efficiently determining the noise type at a given τ -value for automatically correcting the bias and determining confidence intervals for the range of noises considered by TotHvar. Section 7 reviews how an estimate of τ -domain frequency stability is used to set Kalman filter parameters (or q 's) used in GPS operations, problems associated with the application of either the traditional Allan variance or Hvar to the Kalman filter, and how TotHvar serves as a unifying solution. Finally, Section 8 discusses a past scenario in GPS operations in which TotHvar is applied to real data showing the benefit of improved estimation of long-term frequency stability.

2 THE “TOTAL” APPROACH

The total estimator approach has been developed to improve confidence of major statistical tools used in analyzing and characterizing instabilities in phase and frequency of oscillators and synchronization systems [4–9]. Making a “total” estimator of eqn. (2) involves joining each real data

subsequence, namely the subsequence of y_i that goes into each $H_n(m)$ term, at both its endpoints by the same original data subsequence so that it repeats. This creates a new extended version of each y_i subsequence that may be extended by a forward or backward repetition, with or without sign inversion, thus with four possible ways to extend. From numerous simulation studies, we have determined that an extension by even (uninverted) mirror reflection of linear-frequency-detrended $H_n(m)$ subsequences yields the largest edf gain and least bias for the range of noise types identified by standard Hvar.

3 COMPUTATION USING y_n -SERIES

$H_n(m)$ is computed from a $3m$ -point data segment or *subsequence* $\{y_i\}_n = \{y_i, i = n, \dots, n+3m-1\}$. Before applying any data extensions, we must remove a linear frequency trend (drift) from each subsequence by making

$${}^{\circ}y_i = y_i - c_1 i,$$

where c_1 is a frequency offset that is removed to minimize $\sum_{i=n}^{n+3m-1} ({}^{\circ}y_i - \overline{{}^{\circ}y_i})^2$, to satisfy a least-squared-error criterion for the subsequence. In practice, it is sufficient to compute this background linear frequency slope by averaging the first and last halves of the subsequence divided by half the interval and subsequently subtracting the value. Now extend the “drift-removed” subsequence $\{{}^{\circ}y_i\}_n$ at both ends by an uninverted, even reflection. Utility index l serves to construct the extensions as follows. For $1 \leq l \leq 3m$, let

$${}^{\circ}y_{n-l}^{\#} = {}^{\circ}y_{n+l-1}, \quad {}^{\circ}y_{n+3m+l-1}^{\#} = {}^{\circ}y_{n+3m-l}, \quad (3)$$

to form a new data subsequence denoted as $\{{}^{\circ}y_i^{\#}\}_n$ consisting of the drift-removed data in its center portion, plus the two extensions, and thus having a tripled range of $n-3m \leq i \leq n+6m-1$ with $9m$ points. To be clear, we now have *extended subsequence* $\{{}^{\circ}y_i^{\#}\}_n = \{{}^{\circ}y_i^{\#}, i = n-3m, \dots, n+6m-1\}$.

Define

$$\text{Total}_H \sigma_y^2(m, \tau_0, N_{y_{max}}) = \frac{1}{6(N_{y_{max}} - 3m + 1)} \sum_{n=1}^{N_{y_{max}} - 3m + 1} \left(\frac{1}{6m} \sum_{i=n-3m}^{n+3m-1} ({}^{\circ}H_i^{\#}(m))^2 \right), \quad (4)$$

for $1 \leq m \leq \left\lfloor \frac{N_{y_{max}}}{3} \right\rfloor$, where $[c]$ means the integer part of c and notation ${}^{\circ}H_i^{\#}(m)$ means that $H_n(m)$ above is derived from the new triply-extended subsequence $\{{}^{\circ}y_i^{\#}\}$. The symmetries of the extension and the Hvar filter allow the computational effort to be halved. Let $k = [3m/2]$. We need to calculate ${}^{\circ}H_i^{\#}$ only for $n-k \leq i \leq n+k+3m-1$, and ${}^{\circ}H_i^{\#}(m)$ only for $n-k \leq i \leq n+k$. Then

$$\begin{aligned} \sum_{i=n-3m}^{n+3m-1} ({}^{\circ}H_i^{\#}(m))^2 &= 2 \sum_{i=n-k+1}^{n+k-1} ({}^{\circ}H_i^{\#}(m))^2 + ({}^{\circ}H_{n-k}^{\#}(m))^2 + ({}^{\circ}H_{n+k}^{\#}(m))^2, \quad m \text{ even}, \\ &= 2 \sum_{i=n-k}^{n+k} ({}^{\circ}H_i^{\#}(m))^2, \quad m \text{ odd}. \end{aligned} \quad (5)$$

4 COMPUTATION USING x_n -SERIES

The methodology described above can be written in terms of calculations on residual time differences between clocks, namely an x_i -series (to adhere to usual notation), recalling that

$$\bar{y}_i(m) = (x_{i+m} - x_i) / (m\tau_0).$$

Thus in the total approach applied to x_i -series, the data extensions on subsequences of x_i will be constructed in such a way that

$${}^{\circ}y_i^{\#} = \left({}^{\circ}x_{i+1}^{\#} - {}^{\circ}x_i^{\#} \right) / \tau_0,$$

in agreement with section 3 above. This has the effect of requiring an *odd* mirror extension and a *third-difference* operator when considering subsequences of x_i . The Hadamard variance discussed in section 3 as a second-difference operator on τ -averaged y_n values can now be re-expressed in terms of a third-difference operator on time-error x_i -values. The sample variance (or mean square) of these third differences falls neatly into a class of structure functions, namely the variance produced by a difference operator of order three [10]. The modified Allan variance can also be treated as a third-difference variance [11].

The x_i -subsequence that corresponds to the y_i -subsequence starting at n is $\{x_i, n \leq i \leq n + 3m\}$, which has $3m + 1$ terms. Compute the detrended subsequence ${}^{\circ}x_i$ according to

$$k = \left\lfloor \frac{3m}{2} \right\rfloor, \quad c_2 = \frac{x_n - x_{n+k} - x_{n+3m-k} + x_{n+3m}}{k(3m-k)},$$

$${}^{\circ}x_i = x_i - \frac{1}{2}c_2(i-n)(i-n-3m), \quad n \leq i \leq n + 3m.$$

Define the extended subsequence $\{{}^{\circ}x_i^{\#}, n-3m \leq i \leq n+6m\}$ by

$$\begin{aligned} {}^{\circ}x_i^{\#} &= {}^{\circ}x_i, \quad n \leq i \leq n + 3m, \\ {}^{\circ}x_{n-l}^{\#} &= 2({}^{\circ}x_n) - {}^{\circ}x_{n+l}, \quad 1 \leq l \leq 3m, \\ {}^{\circ}x_{n+3m+l}^{\#} &= 2({}^{\circ}x_{n+3m}) - {}^{\circ}x_{n+3m+l}, \quad 1 \leq l \leq 3m. \end{aligned}$$

Then

$$m\tau_0 \left({}^{\circ}H_i^{\#}(m) \right) = -{}^{\circ}x_i^{\#} + 3 \left({}^{\circ}x_{i+m}^{\#} \right) - 3 \left({}^{\circ}x_{i+2m}^{\#} \right) + {}^{\circ}x_{i+3m}^{\#}, \quad n-3m \leq i \leq n+3m-1,$$

where ${}^{\circ}H_i^{\#}(m)$ has the same meaning as in Section 3. Now the Hadamard-total variance is computed from (4) as before with $N_{y_{max}} = N_{x_{max}} - 1$. Because of symmetry we need ${}^{\#}x_i^{\circ}$ only for $n-k \leq i \leq n+k+3m$, and (5) applies.

5 BIAS AND EQUIVALENT DEGREES OF FREEDOM

We consider the random frequency-modulation (FM) noises since these dominate at long-term averaging times where we can capitalize on the improved confidence of using the total approach. To analyze phase-modulation (PM) noises, one would usually use Total TDEV [6] rather than the Hadamard deviation. For brevity, let $\text{Total}_H \sigma_y^2(m, \tau_0, N_{y_{max}})$ be $\text{TotHvar}(\tau, T)$, where $\tau = m\tau_0$, $T = N_{y_{max}}\tau_0$. The normalized bias and edf for TotHvar are given by

$$\text{nbias}(\tau) = \left[\frac{E\{\text{TotHvar}(\tau, T)\}}{E\{\text{Hvar}(\tau, T)\}} - 1 \right] = a, \quad (6)$$

$$\text{edf}(\tau) = \text{edf}[\text{TotHvar}(\tau, T)] = \frac{T/\tau}{b_0 + b_1\tau/T}, \quad (7)$$

where $E\{\cdot\}$ is expectation of $\{\cdot\}$, $0 < \tau \leq \frac{T}{3}$, $\tau \geq 16\tau_0$ (to be explained), and a , b_0 , and b_1 are given in Table 1 for the five FM noise types considered by the Hadamard variance. α is the corresponding power-law exponent of the fractional-frequency noise spectrum $S_y(f) \propto f^\alpha$. In the context here, its valid range is $-4 \leq \alpha \leq 2$. $E\{\text{TotHvar}(\tau, T)\}$ relative to $E\{\text{Hvar}(\tau, T)\}$ in (6) is independent of τ and T , dependent on noise type, and biased low, giving a the negative sign in Table 1. The edf formula (7) is a convenient, empirical or “fitted” approximation with an observed error below 10% of numerically computed exact values derived from Monte-Carlo simulation method using the b_0 and b_1 coefficients of Table 1 and with the error decreasing with averaging factor $m = \tau/\tau_0$ increasing. In fact, (7) should be used only if data-sampling period τ_0 is sufficiently short compared to the averaging time τ by $\tau/\tau_0 \geq 16$. Otherwise, there are not enough points for the data-extension procedure in the total estimator to have significant advantage over the plain Hadamard estimator. In other words, the τ_0 -dependence of the total estimator of (4) plays a significant role, whereas the weaker τ_0 -dependence of the maximum-overlap estimator of plain $H\sigma_y^2(\tau)$ given by (2) is generally suppressed as in (2). It is well known that maximum-overlap statistical estimators will increase edf, hence confidence, and the degree of data overlap is dependent on sampling interval τ_0 relative to τ [12, 13]. Real data should be sampled as fast as practical for a given averaging time. This is especially true in order for the data extension of each subsequence to be effective in the total approach.

Assuming chi-square distribution properties and edf computed by (7) and the values of Table 1, confidence intervals will be conservative since the distribution is actually narrower than chi-square. Although not quantitatively investigated, the narrowing of the distribution is proportional to increasing averaging factor $m = \tau/\tau_0$. Fortunately with real data runs, m is, of course, always largest at longest-term. Depending on the noise type, we have seen narrowing by as much as 15% for $m \approx 100,000$.

To show the improvement in estimating the Hadamard function, Table 2 lists the exact values of edf from theory for computations using TotHvar *vs.* plain Hvar for the longest averaging factor in which $\tau = T/3$. This point is the last point in the estimate, and the improvement in confidence using

Table 1: Coefficients for computing (6) and (7), normalized bias and edf of TotHvar.

Noise	Abbrev.	α	a	b_0	b_1
White FM	WHFM	0	-0.005	0.559	1.004
Flicker FM	FLFM	-1	-0.149	0.868	1.140
Random Walk FM	RWFM	-2	-0.229	0.938	1.696
Flicker Walk FM	FWFM	-3	-0.283	0.974	2.554
Random Run FM	RRFM	-4	-0.321	1.276	3.149

TotHvar is substantial, particularly for the general case of WHFM noise. TotHvar is a significantly improved estimator that offsets much of the criticized inefficiency in using the sample Hadamard deviation as opposed to the sample Allan deviation in the presence of common WHFM noise in frequency standards.

Table 2: Exact $\frac{\text{edf}\{\text{TotHvar}(T/3, T)\}}{\text{edf}\{\text{Hvar}(T/3, T)\}}$ gain for $\tau_{max} = T/3$.

Noise	edf gain of TotHvar ($T/3, T$)
WHPM	3.447
FLFM	2.448
RWFM	2.044
FWFM	1.676
RRFM	1.313

6 POWER LAW DETECTION

It is important to be able to determine which power-law noise type is present for a given τ -value in the range $-4 \leq \alpha \leq 0$ so that TotHvar's bias can be removed automatically. Similarly, before the edf can be determined to establish confidence intervals and set error bars for a stability measurement, it is necessary to identify the dominant noise process. This section describes a noise-identification (noise-ID) algorithm that has been found effective in actual practice, and that works for a single τ -point over the full range of $-4 \leq \alpha \leq 2$. It is based on the Barnes B1 function [14], which is the ratio of the N -sample (standard) variance to the two-sample (Allan) variance, supplemented by applying this function to frequency data, and the R(n) function [15], which is the ratio of the modified Allan to the normal Allan variances.

The B1 function has as arguments the number of frequency data points N , the dead time ratio r (which is set to 1), and the power-law τ -domain exponent μ . The B1 dependence on μ is used to determine the power-law noise type for $-2 \leq \mu \leq 2$ (WHPM and FLPF to FWFM). For a B1 that is consistent with a $\mu = -2$ result, the $\alpha = 1$ or 2 (FLPM or WHPM noise) ambiguity can be resolved with the R(n) ratio using the modified Allan variance.

For the Hadamard variance, the noise determination must be extended to $\mu = 3$ (or $\alpha = -4$, RRFM). This can be done by applying the B1 ratio to *frequency* (instead of the usual phase) data and *adding 2* to the resulting μ . This procedure is called “*B1” herein. Since the *B1 procedure simply applies the Barnes B1 ratio to frequency data instead of phase data, its use is as before, but now its range is effective from WHFM to RRFM noise. (This is analogous to simulation of RRFM data by treating RWFM phase data as frequency data.)

The overall noise identification process is as follows:

- calculate the standard and Allan variances for the applicable τ averaging factor,
- calculate B1, $B1(N, r = 1, \mu) = \frac{N(1-N^\mu)}{2(N-1)(1-2^\mu)}$,
- determine the expected B1 ratios for $\alpha = -3$ through 1 or 2,
- set boundaries between them and find the best power-law noise match,
- resolve an $\alpha = 1$ or 2 ambiguity with the modified Allan variance and R(n), or
- resolve an $\alpha = -3$ or -4 ambiguity with *B1.

Table 3: Formulae for $B1(N, r = 1, \mu)$. Substituting frequency data into the usual phase-data measurement of B1 ratio will shift these formulae to the $\mu + 2$ range, thus covering RRFM.

Noise	μ	$B1 =$
FWFM	2	$\frac{(N)(N+1)}{6}$
RWFM	1	$N/2$
FLFM	0	$\frac{N \ln N}{2(N-1) \ln 2}$
WHFM	-1	1
WH or FL PM	-2	$\frac{N^2 - 1}{1.5(N)(N-1)}$

For a data run of length N , Table 3 gives five specific formulae for $B1$ corresponding to $\mu = -2, -1, 0, 1$, and 2 . Table 4 summarizes the power-law detection scheme and gives the boundaries for demarcating each noise type. The boundaries between the $B1$, $*B1$, and $R(n)$ functions are, in general, set as the geometric means of their expected values, and the actual measured ratio is tested against those values *downward* from the largest applicable μ . For example, if, during the testing, the measured $B1$ ratio is greater than the square root of the product of the expected $B1$ values for RWFM and FLM noise, it is determined to be the former ($\alpha = -2$, RWFM).

High levels of frequency drift should be removed to best identify the underlying noise process by this method. Also, the $R(n)$ ratio cannot, of course, be used for $\tau = \tau_0$ averaging factor (in which case it is 1 for all noise types). Finally, at the very longest averaging factor or last τ -point, it is better to use the previous or $\tau - \tau_0$ point to estimate the noise type. This algorithm has been used in commercial frequency-stability software [16] for the past decade with good success. It allows bias corrections and error bars to be calculated automatically during an analysis for all of the common time-domain stability statistics (including the new Hadamard total variance here) over the full range of noise types and for essentially all τ averaging times.

7 THE KALMAN NOISE MODEL AND THE GPS OPERATIONS PROBLEM

The time update of clock states in the Master Control Station (MCS) Kalman prediction algorithm is based on an average of the most recent measurement of these states for each individual clock, modeled simply by random noise acting on phase $x(t)$, frequency $y(t)$, and frequency drift $z(t)$. With this model, the measured power-law α exponents of the frequency-fluctuation noise spectrum take on only the values 0, -2, and -4, corresponding to WHFM, RWFM, and RRFM, or $\mu = -1, 1$, and 3 in the τ -domain. Hence, we want to precisely extract the level of these noises for each clock using the most efficient method possible, which heretofore has been the sample Allan variance with drift removed from the data run, and more recently the sample Hadamard variance, because of its logical link to the model. If white PM (WHPM) is a significant noise component, and for completeness, the $\alpha = 2, \mu = -2$ case corresponding to WHPM is included as a separate error.

The parameters used by the MCS within GPS system operations are denoted as Kalman filter q 's. By convention, each filter parameter $q_i, i = 0, 1, 2, 3$ corresponds respectively to τ -domain power law exponents $\mu = -2, -1, 1, 3$. For the Hadamard variance, the relationship is [3]

$$\begin{aligned} {}_{\text{H}}\sigma_y^2(\tau) &= \sigma_{WHPM}^2 + \sigma_{WHFM}^2 + \sigma_{RWFM}^2 + \sigma_{RRFM}^2 \\ &= \frac{10}{3}q_0\tau^{-2} + q_1\tau^{-1} + \frac{1}{6}q_2\tau + \frac{11}{120}q_3\tau^3. \end{aligned} \quad (8)$$

For the Allan variance, the relationship is [17]

$$\sigma_y^2(\tau) = 3q_0\tau^{-2} + q_1\tau^{-1} + \frac{1}{3}q_2\tau + \left[+ \frac{1}{20}q_3\tau^3 \right], \quad (9)$$

where the inclusion of the RRFM noise term as $\left[+ \frac{1}{20}q_3\tau^3 \right]$ is a point of contention for two reasons.

Table 4: Power-Law Noise Identification.

Noise	α	μ	ID by	Remarks
RRFM	-4	3	B1&*B1	Use *B1 to resolve $\alpha = -3$ or -4 ambiguity Decision boundary: $\{B1(FWFM) + B1(RWFM)\} / 2$
FWFM	-3	2	B1&*B1	Use *B1 to resolve $\alpha = -3$ or -4 ambiguity Decision boundary: $\{B1(FWFM) + B1(RWFM)\} / 2$
RWFM	-2	1	B1	Decision boundary: $\sqrt{\{B1(RWFM) \times B1(FLFM)\}}$
FLFM	-1	0	B1	Decision boundary: $\sqrt{\{B1(FLFM) \times B1(WHFM)\}}$
WHFM	0	-1	B1	Decision boundary: $\sqrt{\{B1(WHFM) \times B1(FLPM)\}}$
FLPM	1	-2	B1&R(n)	Use R(n) to resolve $\alpha = 1$ or 2 ambiguity Decision boundary: $\sqrt{\{B1(FLPM) \times B1(WHPM)\}}$
WHPM	2	-2	B1&R(n)	Noise ID Methods: $B1 = \text{Barnes } B1(N, r, m)$ bias function with $r = 1$ [14]. *B1 = B1 applied to frequency data as phase data with $\mu = \mu + 2$. $R(n) = \text{ratio, mod Allan variance/Allan variance}$. [15].

First, estimating q_3 by (9) using real data is unreliable because RRFM is inconsistent by the definition of the Allan variance. Second, ref. [17], from which the term derives, does not compute the Allan variance; instead, it computes the optimal mean-square prediction error variance of $\bar{y}(t_0, t_0 + \tau)$ based on $\{x(t), t \leq t_0\}$, for frequency noise spectra with $\alpha = 0, -2$, and -4. For these reasons, we advise omitting the RRFM term entirely from (9). The other terms of (9) happen to be correct for Allan variance.

The GPS Hadamard variance is defined to be equivalent to the Allan variance for WHFM, which is confirmed in comparing (8) and (9); however the variances differ by a factor of two for RWFM, therefore they cannot be used interchangeably under normal circumstances and involving drift-free stochastic processes.

Tuning the Kalman filter depends on the ability to “ q ” each individual clock according to estimates of its noise. The GPS Block IIR satellite program incorporates Rb atomic oscillators that are characterized by a mix of various levels and types of random noise and with frequency drift that may be significantly above noise. This kind of oscillator mix is difficult to manage using Avar and (9), which must be used based on drift-removed frequency *residuals*. However, reverting to using “frequency-drift insensitive” Hvar and using (8), the confidence becomes a factor of about $\frac{1}{3}$ less near the last and crucial long-term $\tau_{max} = T/3$ value owing to the plain sample Hadamard’s edf of one less as compared to Allan’s edf. For the proper perspective, note that we are in the one-week averaging τ -region with a last real-time data run of about one month, thus edf $\approx 1-2$; so estimating filter q ’s is somewhat subjective. Figure 2 illustrates a summary of estimates of frequency stability for each GPS satellite clock as published in reports issued by the Naval Research Laboratory [18].

Table 2 shows that the new TotHvar ($T/3, T$) edf is multiplied by a factor of 1.3 to 3.4 over

plain Hvar ($T/3, T$). TotHvar can be applied directly and reliably, while retaining the efficiency of the sample Allan variance without the difficulty associated with real-time drift removal.

The work of this paper has impact on two GPS operational issues. The first is that the time needed to estimate the Hadamard variance is substantially reduced. For example, to obtain a $\tau =$ one-week estimate of the Hadamard variance with, say, the last 40 days of measured data, the Total approach using TotHvar obtains a one-week estimate with the same or better confidence in about 26 to 34 days of measured data. The second issue is that satellite data are obtained by the linked common-view method [19], and the delay in receiving the monitor station tracking data is currently at 2 to 3 days. Thus, it is important to extract maximum information from data at hand.

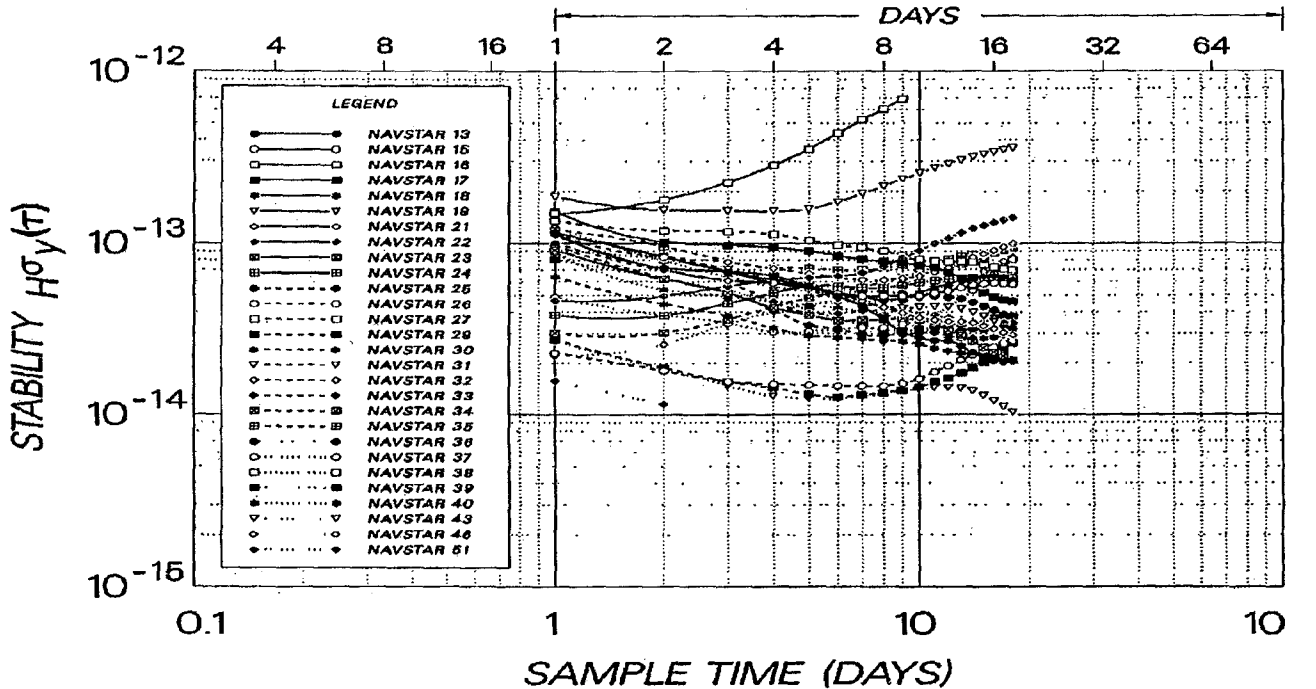


Figure 2: Hadamard-deviation frequency stability of individual GPS satellite clocks *vs.* USNO Master Clock for the period 1 January to 1 July, 2000 [18].

8 EXAMPLE

Figure 3 is data of SV24, a Block IIA GPS satellite. Total Hadamard deviation, plain Hadamard deviation, and Allan deviation are compared with increasing data spans starting at 7 days and extending to 28 days and shows how each of these statistics behaves as it evolves. As is generally the case, TotHdev performs better at estimating the longest-term noise level than plain Hdev for measured data spans as indicated by estimated levels from later (longer) data spans.

9 CONCLUSION

We have developed a significantly improved estimator of the three-sample Hadamard frequency variance based on the so-called “total” approach and denoted as TotHvar, for use in GPS operations and analysis. Practically speaking, we have reduced the long-term estimation uncertainty in terms of edf by a factor of 1.3 to 3.4, depending on the noise type, and we have presented a way to

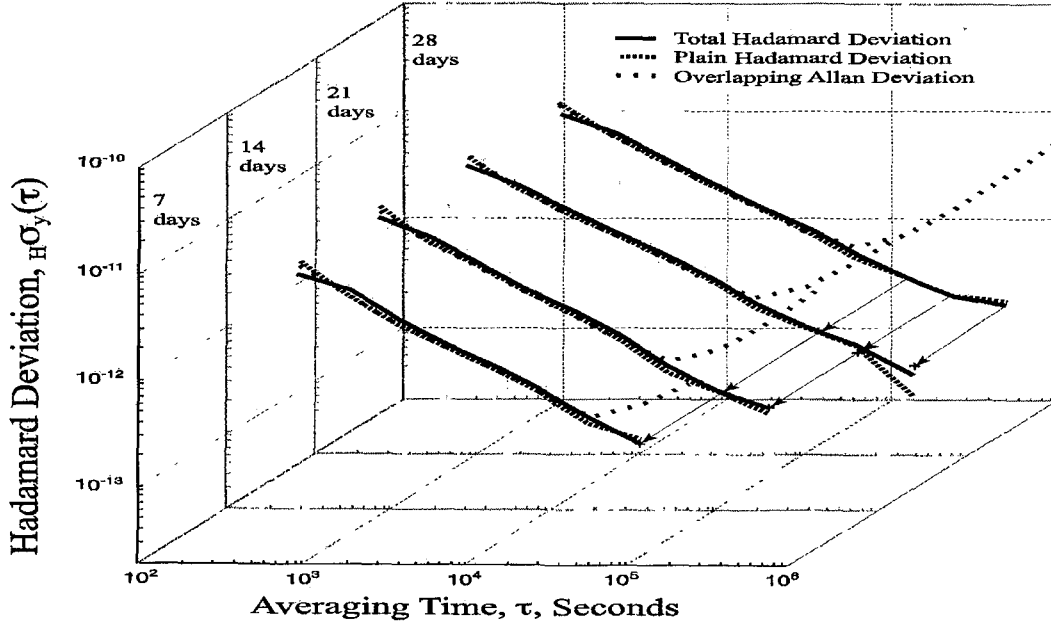


Figure 3: Total Hadamard deviation, plain Hadamard deviation, and Allan deviation for SV24 satellite clock data as the data run increases from 7 days (front plot) to 28 days (rear plot). The last (rightmost) values of TotHdev for shorter data runs anticipates the underlying noise level of longer runs compared to plain Hdev (arrowed lines are projected off 28-day data run). The Allan deviation's response to frequency drift masks the long-term noise level.

automatically remove the moderate negative bias of TotHvar by a power-law detection algorithm. Having confidence greater than plain Hvar and even equal to or greater than Avar, TotHvar is a statistic that permits tuning of the MCS Kalman filter with more accurately chosen clock-estimation parameters (or q 's) that are linked to the most recent measurements of frequency stability of each clock. The increased confidence from TotHvar and shorter data processing delays will play significant roles in adequately managing future GPS system events.

ACKNOWLEDGMENTS

We thank Capt. Curtis Hay of the GPS Joint Program Office and Steven Hutsell for valuable discussions leading to this work.

REFERENCES

- [1] R. A. Baugh 1971, in "Frequency modulation analysis with the Hadamard variance," Proceedings of the 25th Annual Frequency Control Symposium, 26-28 April 1971, Ft. Monmouth, New Jersey, USA, pp. 222-225.
- [2] E. Boileau and B. Picinbono 1976, "Statistical study of phase fluctuations and oscillator stability," IEEE Transactions on Instrumentation and Measurement, IM-25, 66-75.

- [3] S. T. Hutsell 1996, "Relating the Hadamard variance to MCS Kalman filter clock estimation," Proceedings of the 27th Annual Precise Time and Time Interval (PTTI) Systems and Applications Meeting, 29 November-1 December 1995, San Diego, California, USA, pp. 291-301.
- [4] D. A. Howe and C. A. Greenhall 1998, "Total variance: a progress report on a new frequency stability characterization," Proceedings of the 29th Annual Precise Time and Time Interval (PTTI) Systems and Applications Meeting, 2-4 December 1997, Long Beach, California, USA, pp. 39-48.
- [5] D. B. Percival and D. A. Howe 1998, "Total variance as an exact analysis of the sample variance," Proceedings of the 29th Annual Precise Time and Time (PTTI) Systems and Applications Meeting, 2-4 December 1997, Long Beach, California, USA, pp. 97-105.
- [6] M. A. Weiss and D. A. Howe 1998, "Total TDEV," Proceedings of the 1998 IEEE International Frequency Control Symposium, 27-29 May 1998, Pasadena, California, USA, pp. 192-198. Total TDEV has subsequently been redefined by using [8] below to be published in D. A. Howe and T. K. Pepple, "Definitions of total estimators of common time-domain variances," Proceedings of the 2001 IEEE International Frequency Control Symposium, 6-8 June 2001, Seattle, Washington, USA.
- [7] C. A. Greenhall, D. A. Howe and D. B. Percival 1999, "Total Variance, an estimator of long-term frequency stability," IEEE Transactions on Ultrasonics, Ferroelectrics, and Frequency Control, UFFC-46, 1183-1191.
- [8] D. A. Howe and F. Vernotte 2000, "Generalization of the Total variance approach to the modified Allan variance," Proceedings of the 31st Annual Precise Time and Time Interval (PTTI) Systems and Applications Meeting, 7-9 December 1999, Dana Point, California, USA, pp. 267-276.
- [9] D. A. Howe 2000, "The Total deviation approach to long-term characterization of frequency stability," IEEE Transactions on Ultrasonics, Ferroelectrics, and Frequency Control, UFFC-47, 1102-1110.
- [10] F. Vernotte and D. A. Howe 2000, "Generalization of the Total variance approach to the different classes of structure functions," Proceedings of the 14th European Frequency and Time Forum (EFTF), March 2000, Torino, Italy.
- [11] C. A. Greenhall 1997, "The third-difference approach to modified Allan variance," IEEE Transactions on Instrumentation and Measurement, IM-46, 696-703.
- [12] D. A. Howe, D. W. Allan, and J. A. Barnes 1981, "Properties of Signal Sources and Measurement Methods," Proceedings of the 35th Frequency Control Symposium, 27-29 May 1981, Philadelphia, Pennsylvania, USA, pp. A1-A47, and reprinted in [15].
- [13] C. A. Greenhall 1991, "Recipes for Degrees of Freedom of Frequency Stability Estimators," IEEE Transactions on Instrumentation and Measurement, IM-40, 994-999.
- [14] J. A. Barnes 1969, *Tables of Bias Functions, B1 and B2, for Variances Based on Finite Samples of Processes with Power Law Spectral Densities*, National Bureau of Standards Technical Note NBS-375.

- [15] D. B. Sullivan, D. W. Allan, D. A. Howe, and F. L. Walls (editors) 1990, "*Characterization of Clocks and Oscillators*," National Institute of Standards and Technology Technical Note 1337, Sec. A-6.
- [16] Stable, Frequency Stability Analysis Software, Hamilton Technical Services, 195 Woodbury Street, S. Hamilton, MA 01982, USA, phone (978)-468-3703, <http://people.ne.mediaone.net/rile>.
- [17] J. W. Chaffee 1987, "*Relating the Allan variance to the diffusion coefficients of a linear stochastic differential equation model for precision oscillators*," *IEEE Transactions on Ultrasonics, Ferroelectrics, and Frequency Control*, UFFC-34, 655-658.
- [18] Navstar Quarterly Report 00-3, Space Application Branch, U.S. Naval Research Laboratory, Washington, DC, USA, 20 July 2000.
- [19] W. G. Reid, "*Continuous observation of Navstar clock offset from the DoD Master Clock using linked common-view time transfer*," Proceedings of the 28th Annual Precise Time and Time Interval (PTTI) Applications and Planning Meeting, 3-5 December, 1996, Reston, Virginia, USA, pp. 397-408.

Questions and Answers

MASSIMO TINTO (JPL): I have a quick question. The Hadamard function, in a sense, can be seen as the Allan variance of the Allan variance because you're taking the difference of the difference. From your definition, you have $Y(T)$ minus $Y(T + \tau)$, minus the shift of 1 by τ . So have you thought about doing the Hadamard of the Hadamard, so going to the third order? So going a step further from what you have done and see if that will also give you some extra—

DAVID HOWE: I haven't. The problem with going to higher differences is that the efficiency goes down for the kinds of noise processes which are characteristic of the clocks, because you lose degrees of freedom as you have to use longer data lengths to estimate averaging times.

TINTO: Oh, I see.

STEVE HUTSELL (USNO AMC): Dave, I was wondering if you could comment on the increase of the effective degrees of freedom. How much of it was due to the overlapping technique and how much of it was due to the extension in the total technique?

HOWE: All of this was due to the extension. That gain was due to the extension entirely because the numbers were taken at the last point. There is not overlapping at the last point.

Now, that does raise the point that, as a practical matter, total and overlapping estimators rely heavily on sampling as fast as practical. You understand that you take estimates and you shift by τ_0 , your sampling interval. Total takes advantage of that more fully than overlapping, but that has been true for quite a while.

PERFORMANCE AND CHARACTERIZATION OF U.S. NAVAL OBSERVATORY CLOCKS

Lee A. Breakiron and Demetrios N. Matsakis
Time Service Department
U.S. Naval Observatory
Washington, DC 20392, USA

Abstract

Six years of U.S. Naval Observatory clock data are analyzed to determine the optimal data filter length and the amplitude and frequency of occurrence of statistically significant changes in the frequencies and frequency drifts of cesium-beam frequency standards and hydrogen masers by means of relative and correlation-corrected N-cornered-hat analyses of the frequency stabilities of postprocessed mean timescales. The effects of temperature and humidity on cesium and maser frequencies and drifts are also investigated.

1 INTRODUCTION

The U.S. Naval Observatory (USNO) maintains an ensemble of about 50 HP5071 cesium-beam frequency standards and a dozen Datum-Sigma Tau hydrogen masers at its Washington, DC site, which are kept in environmentally controlled conditions. Since each of these clocks has been acquired, time (phase) differences between them and the Master Clock have been recorded once per hour, using a Data Acquisition System (DAS) of coaxial cables, multiplexed switches, time-interval counters, and computers.

One motivation for this work is simply to use our available data to determine the long-term, observed, statistical behavior of all the clocks in our ensemble. Although the lack of an absolute frequency reference makes it technically impossible to determine the absolute stability of any individual clock or ensemble, a considerable body of literature [e.g. 1-6] has provided some tools that allow mathematically precise "N-cornered-hat" estimates, subject to specific limitations. In this work we have chosen to use the tools of Torcaso et al. [3,4] because they were available for use in a form that allows simple batch processing of hundreds of clock combinations. The maser stabilities derived from this N-cornered hat analysis are shown to be a few tenths of a dB higher than stabilities derived from simpler analyses comparing individual clocks to USNO unsteered cesium and maser averages, EAL [7], and TT99 [8,9]. The reasons for this are discussed below.

A second motivation for this work has to do with the operational issues concerning the generation of USNO mean timescales. These timescales are actually integrated frequency scales, created by averaging clock frequencies that have been detrended by removing clock-specific rates (frequencies) and drifts (linear change of rates with time). The timescales differ in how they weight clocks, but all clocks are currently characterized through comparison with an unsteered cesium mean timescale [10,11]. Since all frequency standards exhibit nonwhite

noise over long enough periods, a problem develops because there is no optimal manner to average nonwhitened noise. In practice, USNO has taken advantage of the large number of clocks in its ensemble by using the timescale itself as a reference with which to determine epochs of significant changes in clock rates and drifts. The epochs of these "clock breaks" are chosen by inspection of the whiteness of the frequency data and linearity of the phase data.

These breaks may occur at any time due to changes in environmental conditions or spontaneous changes within the clock. Such breaks are checked for during each hourly measurement and computation of the real-time mean timescale, and the clocks involved are deweighted. The clocks are later reweighted after sufficient data have accumulated to accurately model the clocks' rates and (if any) drifts. Clocks are also checked for, and deweighted in the event of, general degradations in stability.

Cesiums are weighted equally in the timescale computation due to lack of evidence that any other procedure is optimal, at least using weights based on Allan variances [11,12] or rate solution variances. This is probably due to the deweighting of any clocks showing changes in performance or character. In the combined cesium-maser timescale toward which the Master Clock is steered, masers are deweighted relative to cesiums in a manner varying with time since the latest measurement [10]. Clock parameter recharacterization is done prior to weighting and is relative to the mean of the other, weighted clocks. The number of clocks recharacterized at any one time is limited to a small fraction of the weighted ensemble, lest the stability of the whole timescale be afflicted by errors associated with indeterminacy because of the lack of an absolute reference.

How well the rates and drifts of the individual clocks are modelled and how quickly any changes therein are recognized and allowed for have definite effects on the stability of the mean timescales, both those that are used diagnostically in postprocessing and those that are used in real time as a target toward which to steer the USNO Master Clock. The stability of the Master Clock is, however, not strongly affected by the rate of clock recharacterization, since even the most aggressive recharacterization studied herein does not result in any significant destabilization over the monthly intervals between steers of the mean timescale toward TAI. This study is the first of several different empirical and theoretical attempts at USNO to quantify the costs and benefits of different levels of precision in clock characterization. Another objective is the determination of the average size of and average interval between clock breaks, i.e. the temporal stability of these frequency standards.

CLOCK DATA AND ANALYSIS

Data reported here were taken from MJD 49532-51857 (29 Jun 94-9 Nov 00), using a DAS which each hour switches each clock's 5 MHz signal to a time-interval counter for a phase measurement against the Master Clock. These measurements have an hourly precision of about 50 ps rms, but the very long-term accuracy is 1 ns peak to peak. Although recently experimental, lower-noise measurement systems are being used in parallel [13], DAS switch data are used throughout this analysis.

The physical environment of the USNO clocks are usually maintained to an rms of 0.1°C and 1% relative humidity through the use of temperature-stabilized chambers inside of temperature-controlled rooms. However, there are short-term fluctuations in any given chamber of a degree or more, due to equipment failure about once a year. Also, each clock can experience long-term temperature changes when nearby equipment is relocated or when components of the environmental control system are replaced through normal maintenance. Humidity variations

are usually associated with temperature variations, but no significant clock variations have been ascribed purely to humidity variations. Temperature variations, however, can noticeably affect maser frequencies, whose temperature dependence has been reported to be up to $9 \cdot 10^{-15}/^\circ\text{C}$ [14] in absolute value. As part of this work, we have also examined available "health and status" information from the RS-232 ports of the masers and cesiums, which are used here as diagnostic tools [15,16]. We have found, as did Chadsey [17] for cesiums, that neither maser nor cesium frequency variations correlate well with the health and status information, except for hardware (e.g. power supply) failures and maser temperature variations.

Rates are determined by averaging the first differences of the hourly phase measurements, unless there appears to be significant drift, in which case rate and drift are derived from a linear least-squares fit to the first differences. This procedure has been found to be optimal for our data [18], because a sampling time of 1 hour is in the white FM noise region of both the cesiums and our DAS measurement system (hence, the masers as well). While rate can be inferred from initial and final phase measurements, the above procedure permits data editing and confidence level determination.

The least precise aspect of USNO clock characterization is the determination of the clock breaks. In practice, the methods have varied considerably over the years. In an on-line situation, it has not been unusual for the data analysts to remove a clock from the averaging simply because a few hours' data show a trend that could, over a weekend, affect the mean timescale significantly. This is often a prudent decision, because the loss of just one good clock affects stability by the square root of N, while a mischaracterized clock affects the average by $1/N$, and because in general robustness is more critical than stability. Another reason to err on the side of caution is because USNO Master Clock steering strategies are designed to protect against short-term mean instabilities, but long-term trends are removed only by the steers to UTC (BIPM) [19,20].

Even in postprocessed work such as this, the difference between a time series characterized by clock breaks and one characterized by flicker noise can be as much philosophy as substance [21]. For this work, clock breaks were determined by four different sets of criteria, characterized by different levels of increasingly strict modelling. All methods discarded obviously bad data, and inserted clock breaks at times of disturbances and repairs, such as clock moves and beam tube replacements. To these, all methods added additional clock breaks of a number proportional to the level of significance adopted. These criteria are summarized in Table 1. The strictest criteria (Set #4) are those currently used in day-to-day timescale operations, though these are approximate; the actual values varied with the empirical philosophy of the data analyst at the

Table 1. Minimum Clock Break Levels (Absolute Values)

Set #	Cesiums		Masers	
	Rate Change	Drift Change	Rate Change	Drift Change
1	$5.0 \cdot 10^{-14}$	$5.0 \cdot 10^{-16}/\text{day}$	$3.0 \cdot 10^{-14}$	$1.0 \cdot 10^{-16}/\text{day}$
2	$1.5 \cdot 10^{-14}$	$2.5 \cdot 10^{-16}/\text{day}$	$4.0 \cdot 10^{-15}$	$1.5 \cdot 10^{-17}/\text{day}$
3	$4.6 \cdot 10^{-15}$	$1.0 \cdot 10^{-16}/\text{day}$	$9.3 \cdot 10^{-16}$	$4.6 \cdot 10^{-18}/\text{day}$
4	$3.5 \cdot 10^{-15}$	$5.8 \cdot 10^{-17}/\text{day}$	$4.6 \cdot 10^{-16}$	$3.5 \cdot 10^{-18}/\text{day}$

time the data were current. Moreover, the tabulated values do not reflect the entire story, since there is some variation with effective filter size. For criteria Sets #1-3, clock breaks would be assumed if changes smaller than the tabulated values occur over long periods of time.

By way of illustration, Figure 1 shows how two different cesium clocks (serial numbers 114 and 1097) were broken into clock breaks by the four different sets of criteria. Also, Table 2 summarizes the total number of clock breaks detected.

Table 2. Number of Clock Breaks Detected

Set #	Cesiums	Masers	Totals
1	150	39	189
2	260	90	350
3	312	92	404
4	577	155	732

POSTPROCESSED TIME SCALES

In order to compare the four different clock-characterization methods, postprocessed timescales were generated using a modified form of Percival's [22] algorithm through the in-house least-squares program SuperP [12]. Figure 2 compares cesium-only mean timescales, generated by SuperP with TT99 as the reference. Similar results are found with maser-only mean timescales or using the EAL as a reference. It appears that the USNO data have in the past been over-aggressively characterized, although the least aggressive set of criteria was also suboptimal. This conclusion is supported by analysis of timescales generated using SuperP on different halves and thirds of the USNO ensemble by performing N-cornered-hat frequency stability analyses upon the independent thirds and computing the Hadamard deviations [6].

For the rest of this work, clock characterizations will be determined using Set #3. It should be noted that Set #2 may be equally valid, and would result in slightly higher stability measures, because it has clock breaks at fewer positions where the data begin to look nonwhite. No matter which criteria set was used, the clocks on the whole had indistinguishable stability measures for sampling times τ of < 10 days, because the clock weighting and clock-break determinations were made on a longer scale than this. For $\tau > 10$ days, the computed cesium and maser stabilities tended to be about 0.1 and 2 dB higher, respectively, for Set #1 compared with the other sets.

STATISTICAL MEASURES AND REFERENCE TIMESCALES

The stability characteristics of individual clocks were compared to the following four available references: USNO's unsteered maser mean timescale (MM), USNO's unsteered cesium mean timescale (CM), EAL, and TT99. Figure 3 compares Allan deviations [1] of the MM with each of the other three references using data corrected for drift. Note that the MM is considerably more stable than the CM in the short term, and its stability approaches that of the CM in the long term because both cesiums and masers are detrended against the same standard.

Figure 4 shows the Allan and Hadamard deviations for the median of the masers and cesiums relative to the MM, and for the mean of the best third of the masers and cesiums relative to the maser mean. The stabilities are consistent with similar analyses wherein the reference was the cesium mean, EAL, or TT99. Figure 4 implies that at least 30 days of data are required to determine a clock's frequency to within 4 parts in 10^{15} , and that at least 60 days of data are required to determine a clock's drift to within a part in $10^{16}/\text{day}$. This is consistent with established USNO practice to not weight a clock until it has at least 30 days of data that are stable in rate and display no significant drift, or 60 days of data that are stable in drift and, aside from that, rate.

Figure 5 plots the N-cornered-hat stabilities for all the aforementioned combinations, as well as drift removal, derived using the methods of Torcaso et al. [3,4]. The derived stabilities agree for the Hadamard deviations of the masers and for both Allan and Hadamard deviations of the cesiums. The high values for the Allan deviations of our masers are due to the sensitivity of the N-cornered-hat method of Torcaso et al. to noisy clocks, such as masers with large drifts. Such high values do not appear in our plots of Allan deviation for drift-corrected data. We note also that the technique failed to give reasonable values for masers in hybrid (maser and cesium) ensembles.

Note that the manufacturer's rating for a typical USNO maser's time deviation (TDEV) is 100 ps over a day. Since this is comparable to the noise in the measurement system that produced the data reported here, we do not report maser Allan deviations for $\tau < 2$ days or Hadamard variances for $\tau < 4$ days.

CESIUM-BEAM CLOCK PERFORMANCE

High-performance HP5071A cesium-beam frequency standards have been in general use at USNO since 1993 and were the basis of a stability analysis in 1994 [23]. The lifetime of a typical high-performance tube, warranted for 3 years, has been found to range from 5 to 7 years [17,24]. An initial "burn-in" phase of instability ranges from 0 to about 90 days, an example of which is shown in Figure 6a (relative to the MM). Figure 7 plots the length of each burn-in period, in days, vs. the MJD the tube was received at USNO.

An end-of-life period of high instability generally ranges from about 1 day up to about a year during which the instability is significantly higher or more nonwhite than normal. Figure 6b shows a typical tube demise, which is first signaled by a sharp rise in the electron multiplier voltage to its maximum voltage (2553 V), followed by a rise of the signal gain to its maximum (100%) [15]. A very slight increase in noise is observed up to 300 days before tube failures in about a quarter of the cases (e.g. Figure 6c). This is roughly consistent with Allan and Hadamard deviation statistics computed over each 160-day interval, and which show a very small degradation in the average stability as a function of the age of tube (perhaps 1 dB over the tube life).

Examining Set #3 of times of rate and drift changes, it was noted that significant changes in rate (more than about 3 parts in 10^{15}) occur on the average of once every 312 ± 15 days, the absolute value of the average rate change being 1.7 ± 0.17 parts in 10^{14} . Despite the occurrence of very transient temperature excursions of about 10°C and changes of a few degrees over several hours in the environmental chambers, not a single significant frequent step could be unequivocally attributed to temperature or humidity change. This is consistent with the specifications and test results for these clocks [25].

Figure 8 plots the observed cesium drifts as a function of MJD, for Set #2 data. The increase in

drift scatter at the plot's extremities may be due, in whole or part, to insufficient measurement time.

As noted in the previous section, 60 days appears to be the minimum length of an optimal filter for the determination of cesium rates. But 60 days also approximates the maximum length, as is evident in Figures 2-5 and 9. The improvement in rate accuracy slows down after 2 months because of nonwhite noise. Thus, increasing the filter length much beyond 2 months would subject the rate determinations to random walk FM.

HYDROGEN MASER PERFORMANCE

The frequency performance of six of our earlier Datum-Sigma Tau auto-tuned masers has been published in [23]. The relative sizes of our masers' drifts, as well as their associated errors, are plotted in Figure 10. As it is for the rates of cesiums, 60 days also appears to be the approximate upper limit on the optimal filter length for the drifts of masers (see Figures 3-5 and 11).

Examining Set #3 of times of rate and drift changes, it was noted that significant changes in drift ($> 5 \cdot 10^{18}/\text{day}$) occur on the average of once every 209 ± 16 days, the absolute value of the average drift change being $7.3 \pm 1.7 \cdot 10^{17}/\text{day}$. About a fifth of the rate changes could be attributed to temperature excursions in the environmental chambers. Regarding drift, the three correlations found all concerned the same maser (NAV8). Spikes greater than 3°C or variations of 0.5°C prolonged over several hours could cause rate changes, though excursions as large as 8°C could have no effect, and only about fifth of temperature changes $> 3^\circ\text{C}$ caused rate changes.

Determination of reliable temperature coefficients from these data is problematic because it is based on failures or adjustments of the environmental chambers, rather than on controlled experiments. Separate determination of the relative or absolute humidity coefficients is further complicated by the high correlation between relative humidity and temperature, and the fact that both tend to vary when an environmental chamber fails.

Temperature-induced frequency variations were not always consistent for the same maser. Short-term correlations were observed ranging from approximately -1.8 to +1.5 parts in $10^{14}/^\circ\text{C}$. Figure 12 shows long-term variations for maser NAV3 indicative of a temperature coefficient on the order of $-1 \cdot 10^{-14}/^\circ\text{C}$. Parker [14] found long-term coefficients ranging from -9 to +1.3 parts in $10^{15}/^\circ\text{C}$.

As stated, we also found probable effects on drift. Figure 13 displays a long-term variation for maser NAV8 consistent with a temperature coefficient of $+0.81 \cdot 10^{-17}/\text{day}^\circ\text{C}$. Short-term correlations were found ranging from -0.7 to +5.8 parts in $10^{17}/\text{day}^\circ\text{C}$.

Frequency variations in the masers often correspond to fluctuations in the maser health and status information, particularly the "top plate heater" voltage, the changes in which are related both to chamber temperature and temperature gradients within the maser. Moreover, the measured temperatures are dependent on the placement of the sensors within the chamber. Hence, the aforementioned temperature coefficients are not necessarily reflective of the temperature experienced by the maser.

CONCLUSIONS

Allan and Hadamard deviations of the USNO ensemble of HP5071 cesium standards and hydrogen masers were computed several different ways. Sixty days appears to be the optimal length for a filter on hourly first differences in the determination of clock rates and drifts. Thus, less aggressive recharacterization than is presently used operationally will improve USNO timescale stability, although it will not necessarily affect the short-term stability of the Master Clock over periods of less than 60 days.

Comparison of postprocessed timescales indicate that cesium rates and drifts should be recharacterized after changes of about 5 parts in 10^{15} and 1 part in $10^{16}/\text{day}$ respectively. Such changes occur about every 312 days, averaging 1.7 parts in 10^{14} . There appears to be an increase in the drift of new cesium tubes, but this may be due to insufficient averaging time.

Similar comparisons indicate that maser rates and drifts should be recharacterized after changes of about 1 part in 10^{15} and 5 parts in $10^{18}/\text{day}$ respectively. Such changes occur about every 209 days, averaging 7.3 parts in $10^{17}/\text{day}$.

While no frequency dependence on temperature or humidity could be ascertained for the cesium standards, the masers evinced frequency dependences of 1 or 2 parts in $10^{14}/^\circ\text{C}$ in absolute value and drift dependences of about 1 to a few parts in $10^{17}/\text{day}^\circ\text{C}$ in absolute value.

DISCLAIMER

References to specific commercial products do not imply an endorsement by the U.S. Naval Observatory. Although the analysis of clock stabilities is believed to be accurate with regard to the actual experience of the USNO, it should not be construed that this would be characteristic of clocks maintained at other laboratories at the same period, nor of clocks currently marketed by any manufacturer.

ACKNOWLEDGMENTS

We would like to thank the past and current staff of the USNO Time Service Department for their dedicated efforts on behalf of the Master Clock, and in particular Harold Chadsey, Randy Clarke, and Tony Kubik. We also thank Fred Torcaso for advice on N-cornered-hat solutions, and Bill Riley (Datum) for his computer program Stable used to check in-house statistical software, and Ken Senior for assistance with the figures.

REFERENCES

- [1] D. Allan 1987, "*Time and frequency (time-domain) characterization, estimation, and prediction of precision clocks and oscillators*," IEEE Transactions on Ultrasonics, Ferroelectrics, and Frequency Control, UFFC-34, 647-654.
- [2] P. Tavella, and A. Premoli 1993/1994, "*Estimating the instabilities of N clocks by measuring differences of their readings*," Metrologia, 479-486.
- [3] F. Torcaso, C. R. Ekstrom, E. A. Burt, and D. N. Matsakis 1999, "*Estimating frequency stability and cross-correlations*," Proceedings of the 30th Annual Precise Time and

Time Interval (PTTI) Systems and Applications Meeting, 1-3 December 1998, Reston, Virginia, USA, pp. 69-81.

- [4] C. R. Ekstrom, F. Torcaso, E. A. Burt, and D. N. Matsakis 1999, "*Estimating the stability of N clocks with correlations*," Proceedings of the 1999 Joint Meeting of the European Frequency and Time Forum (EFTF) and the IEEE International Frequency Control Symposium, IEEE Publication 99CH36313, 13-16 April 1999, Besançon, France, pp. 168-172.
- [5] F. J. Galindo, and J. Palacio 2000, "*Estimating the instabilities of N correlated clocks*," Proceedings of the 31st Annual Precise Time and Time Interval (PTTI) Systems and Applications Meeting, 7-9 December 1999, Dana Point, California, USA, pp. 285-296.
- [6] S. T. Hutsell 1996, "*Relating the Hadamard variance to MCS Kalman filter clock estimation*," Proceedings of the 27th Annual Precise Time and Time Interval (PTTI) Applications and Planning Meeting, 29 November-1 December 1995, San Diego, California, USA, pp. 291-301.
- [7] C. Thomas, P. Wolf, and P. Tavella 1994, "*Time scales*," BIPM Monograph 94/1.
- [8] B. Guinot 1995, *Scales of time*, Metrologia, 31, 431-440.
- [9] TT99 from BIPM by anonymous ftp at 62.161.69.5/pub/tai/scale/ttbipm.99
- [10] L. A. Breakiron 1992, "*Timescale algorithms combining cesium clocks and hydrogen masers*," Proceedings of the 23rd Annual Precise Time and Time Interval (PTTI) Applications and Planning Meeting, 3-5 December 1991, Pasadena, California, USA, pp. 297-305.
- [11] L. A. Breakiron 1989, "*The effects of data processing and environmental conditions on the accuracy of the USNO timescale*," Proceedings of the 20th Annual Precise Time and Time Interval (PTTI) Applications and Planning Meeting, 29 November-1 December 1988, Tysons Corner/Vienna, Virginia, USA, pp. 221-235 (see errata in [10], p. 302).
- [12] D. Matsakis, and L. A. Breakiron 1999, "*Postprocessed timescales at the U. S. Naval Observatory*," Proceedings of the 30th Annual Precise Time and Time Interval (PTTI) Systems and Applications Meeting, 1-3 December 1998, Reston, Virginia, USA, pp. 19-33.
- [13] D. N. Matsakis 2000, "*Recent and pending improvements at the U.S. Naval Observatory*," Proceedings of the 31st Annual Precise Time and Time Interval (PTTI) Systems and Applications Meeting, 7-9 December 1999, Dana Point, California, USA, pp. 257-265.
- [14] Parker, T. E. 1998, "*Influence of environmental factors on hydrogen maser frequency stability*," Proceedings of the 12th European Frequency and Time Forum (EFTF), 10-12 March 1998, Warsaw, Poland, pp. 126-131.
- [15] H. Chadsey, and A. Kubik 1998, "*Maintenance of HP 5071A primary frequency standards at USNO*," Proceedings of the 29th Annual Precise Time and Time Interval (PTTI) Systems and Applications Meeting, 2-4 December 1997, Long Beach, California, USA, pp. 49-59.
- [16] A. Kubik 2000, private communication

- [17] H. Chadsey 2000, “*An automated alarm program for HP5071A frequency standards*,” Proceedings of the 31st Annual Precise Time and Time Interval (PTTI) Systems and Applications Meeting, 7-9 December 1999, Dana Point, California, USA, pp. 649-655.
- [18] L. A. Breakiron 1994, “*A comparative study of clock rate and drift estimation*,” Proceedings of the 25th Annual Precise Time and Time Interval (PTTI) Applications and Planning Meeting, 29 November-2 December 1993, Marina del Rey, California, USA, pp. 401-411.
- [19] L. A. Breakiron 1996, “*Frequency steering of hydrogen masers*,” Proceedings of the 1996 IEEE International Frequency Control Symposium, IEEE Publication 96CH35935, 5-7 June 1996, Honolulu, Hawaii, USA, pp. 1113-1122.
- [20] P. A. Koppang, and D. N. Matsakis 2000, “*New steering strategies for the USNO Master Clock*,” Proceedings of the 31st Annual Precise Time and Time Interval (PTTI) Systems and Applications Meeting, 7-9 December 1999, Dana Point, California, USA, pp. 277-284.
- [21] G. J. Dick, and C. A. Greenhall, “*L.O. limited frequency stability for passive atomic frequency standards using “square wave” frequency modulation*,” Proceedings of the 1998 IEEE International Frequency Control Symposium, IEEE Publication 98CH36165, 27-29 May 1998, Pasadena, California, USA, pp. 99-103.
- [22] D. B. Percival 1978, “*The U.S. Naval Observatory clock time scales*,” IEEE Transactions on Instrumentation and Measurement, IM-27, 376-385.
- [23] L. A. Breakiron 1995, “*The effect of clock errors on timescale stability*,” Proceedings of the 26th Annual Precise Time and Time Interval (PTTI) Applications and Planning Meeting, 6-8 December 1994, Reston, Virginia, USA, pp. 369-380 (see Errata vol. #2 for figures).
- [24] J. A. Kusters, L. S. Cutler, and E. D. Powers 1999, “*Long-term experience with cesium beam frequency standards*,”, IEEE Publication 99CH36313, Proceedings of the 1999 Joint Meeting of the European Time and Frequency Forum (EFTF) and the IEEE International Frequency Control Symposium, 13-16 April 1999, Besançon, France, pp. 159-163.
- [25] J. A. Kusters and J. L. Johnson 1992, “*A new cesium beam frequency standard performance data*,” IEEE Publication 92CH3083-3, Proceedings of the 1992 IEEE Frequency Control Symposium, 27-29 May 1992, Hershey, Pennsylvania, USA, pp. 143-156.

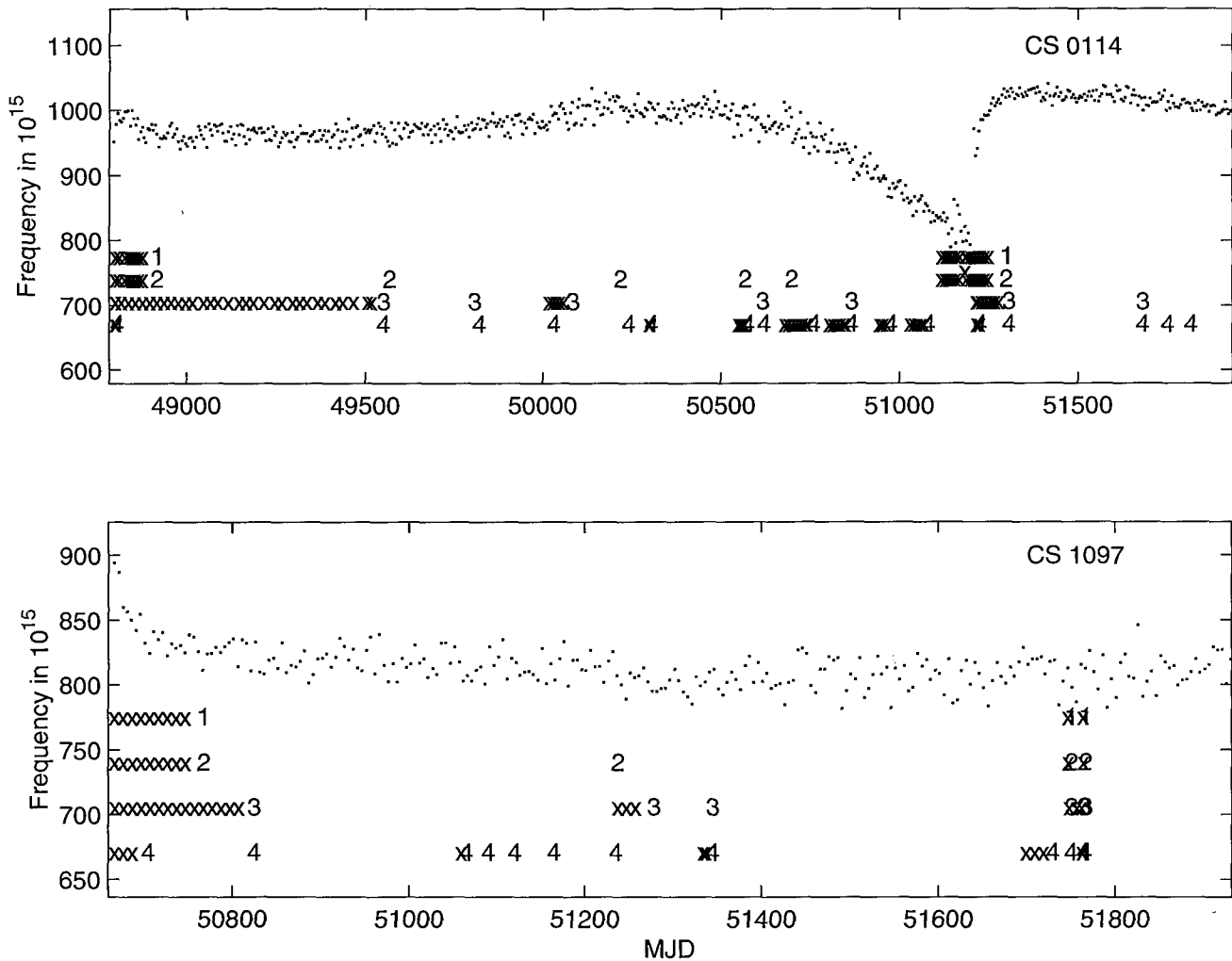


Figure 1. The frequencies of two cesium standards referenced to the cesium mean timescale, with the times of clock breaks determined by the four different sets of criteria indicated by "1," "2," "3," or "4." "x"'s in the row dedicated to a particular criteria set indicates that data were deweighted from that point on until the next clock break.

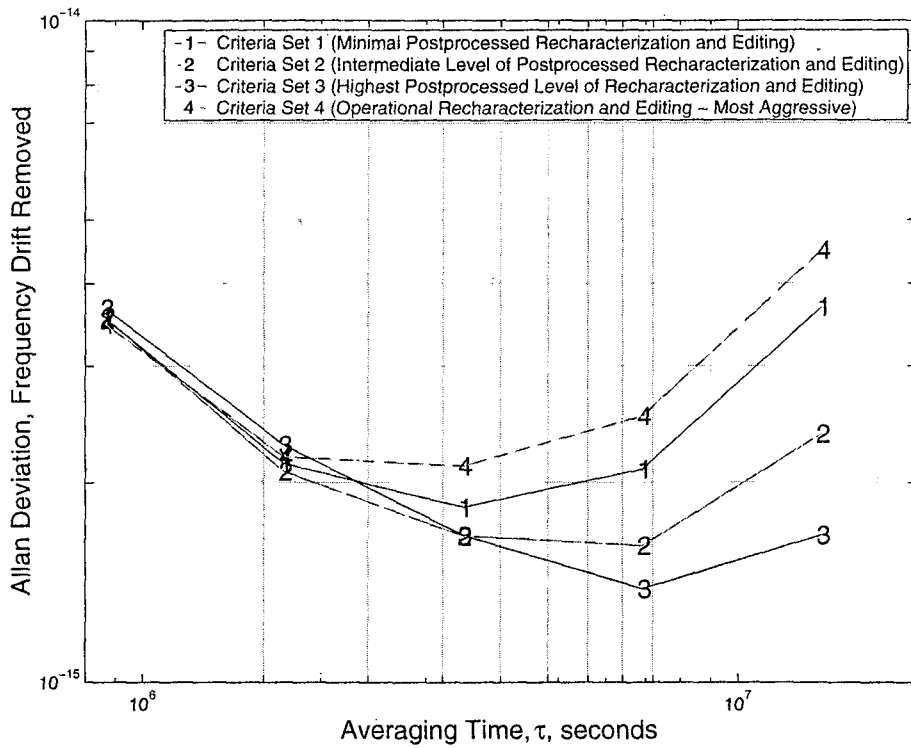


Figure 2. USNO unsteered cesium mean timescale frequency stabilities referenced to TT99.

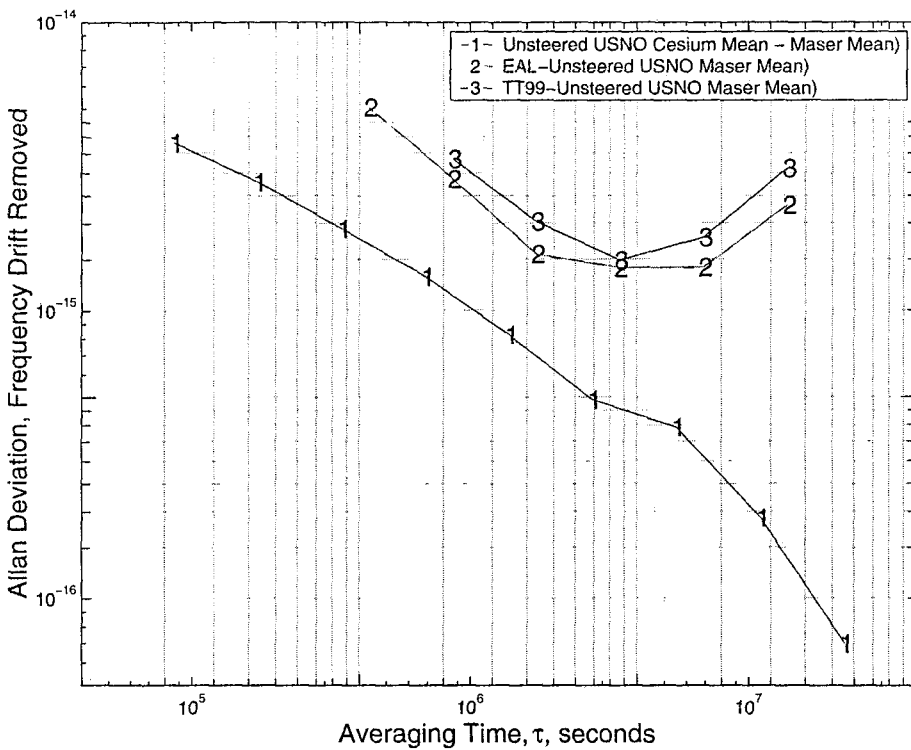


Figure 3. Timescale frequency stabilities referenced to the unsteered USNO maser mean timescale.

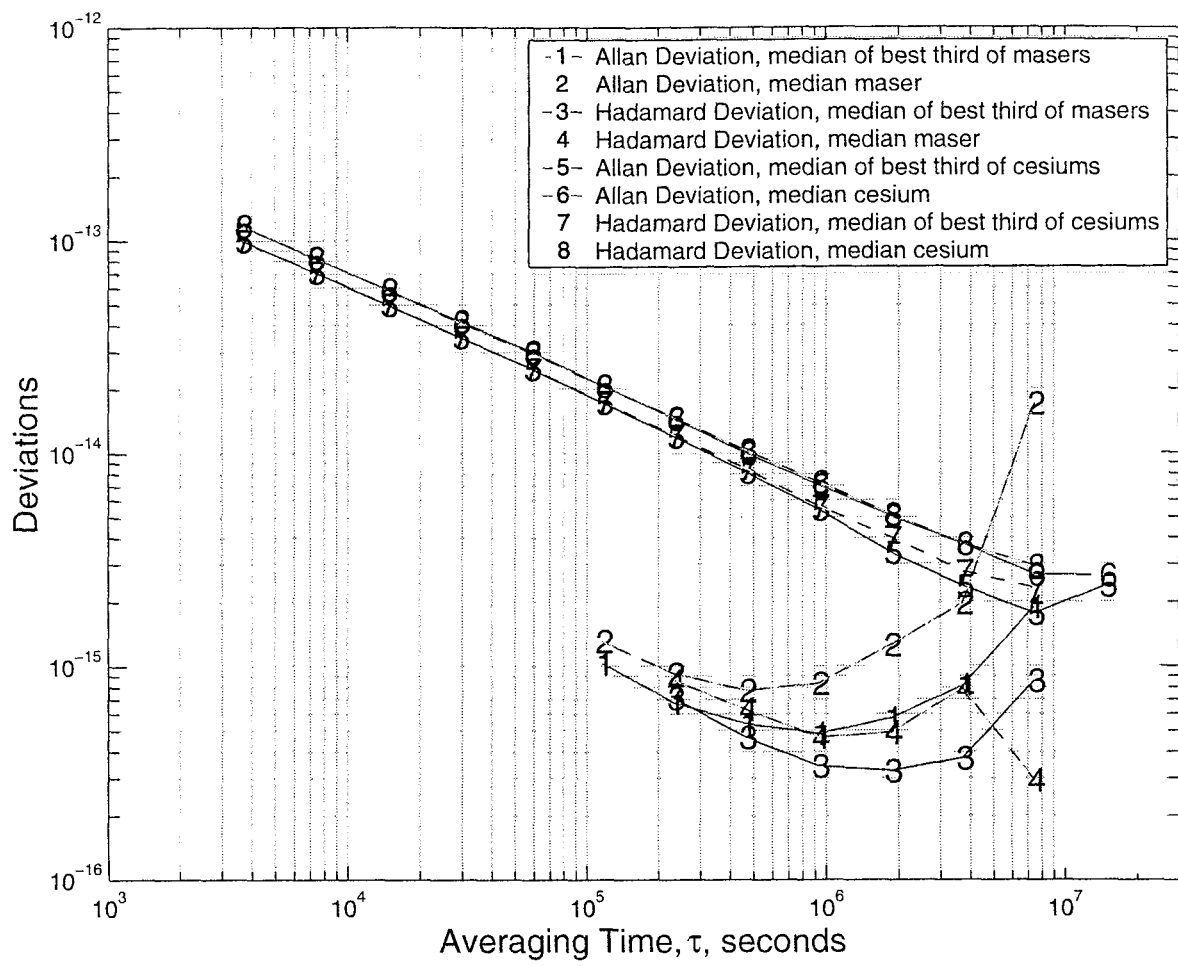


Figure 4. Postprocessed timescale frequency stabilities referenced to the unsteered USNO maser mean timescale using editing criteria Set #3.

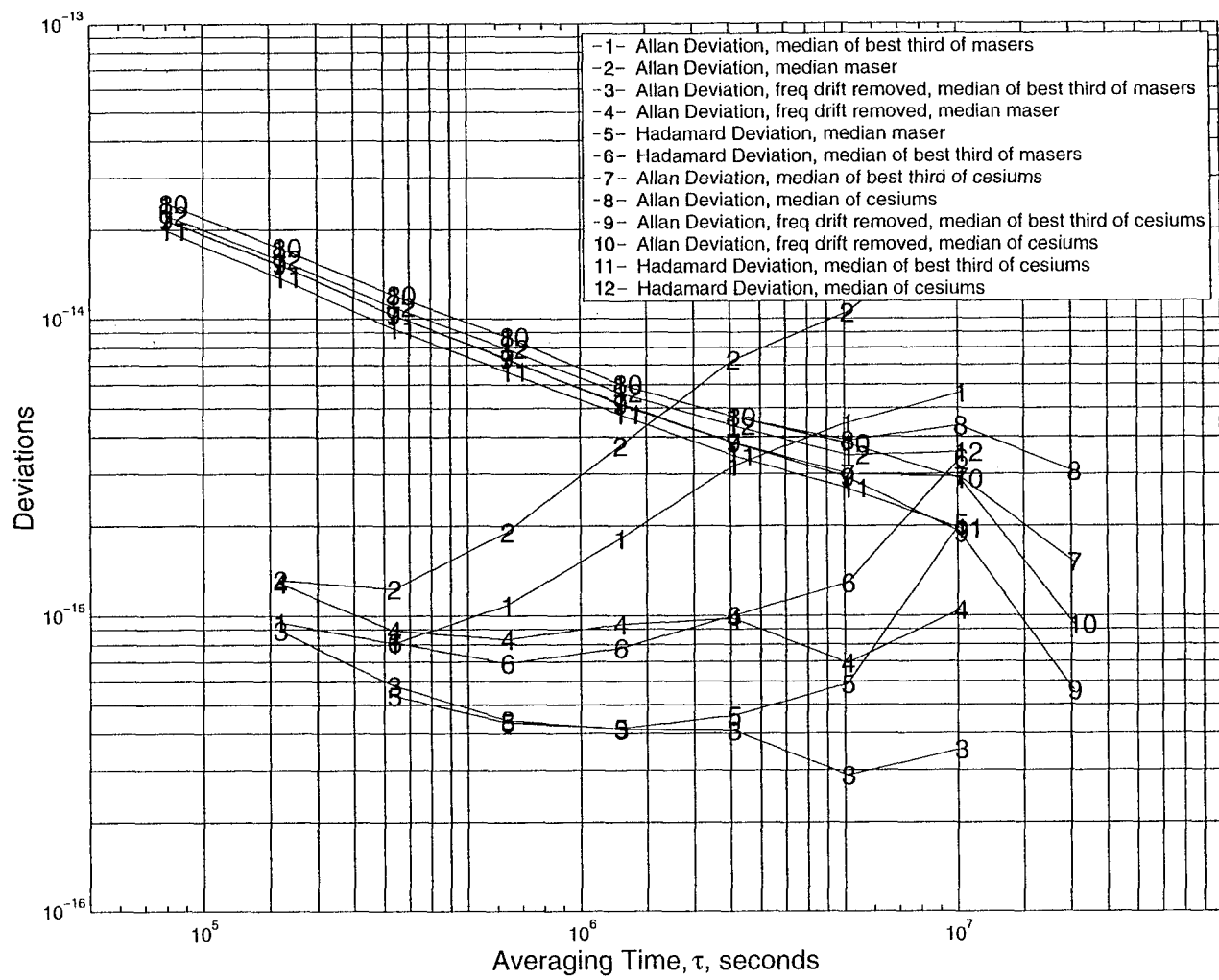


Figure 5. Postprocessed timescale frequency stabilities from N-cornered-hat analyses using editing criteria Set #3. The high values for curves "1" and "2" are due to the analyses systematically overstating the uncertainties of the lower-sigma clocks.

Fractional Frequency

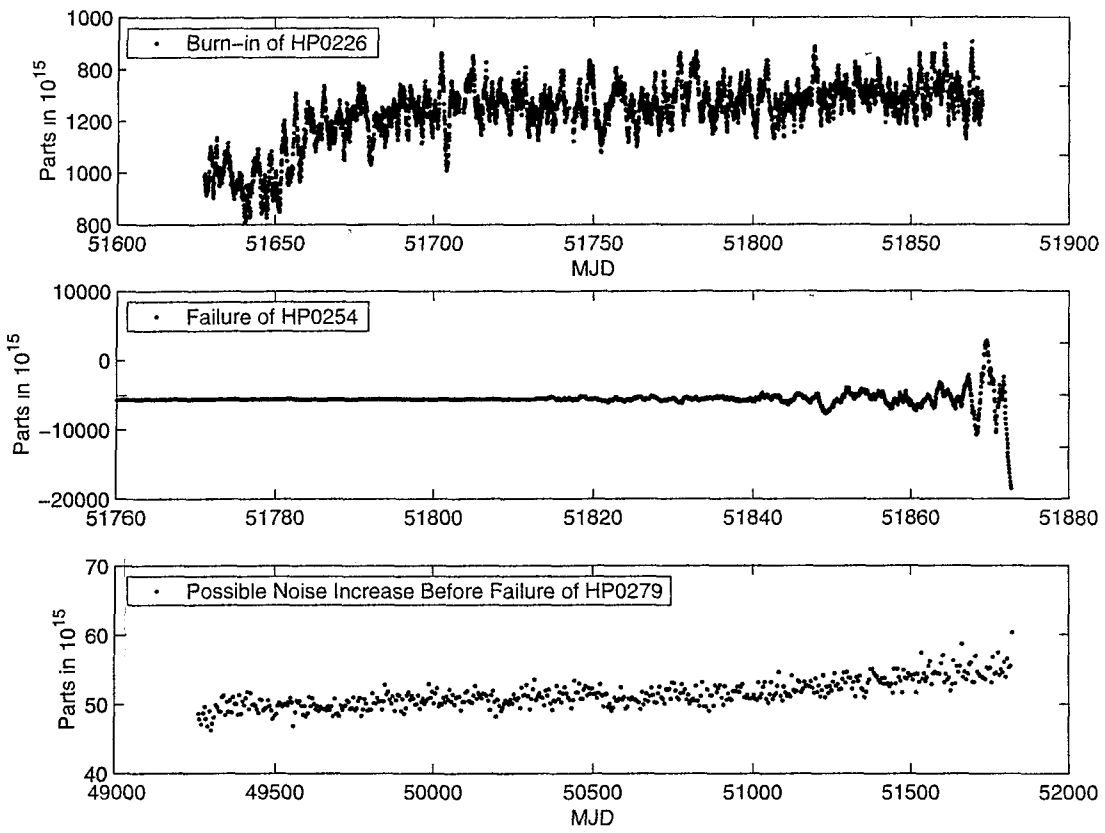


Figure 6. Samples of cesium beam tube burn-in and failure modes.

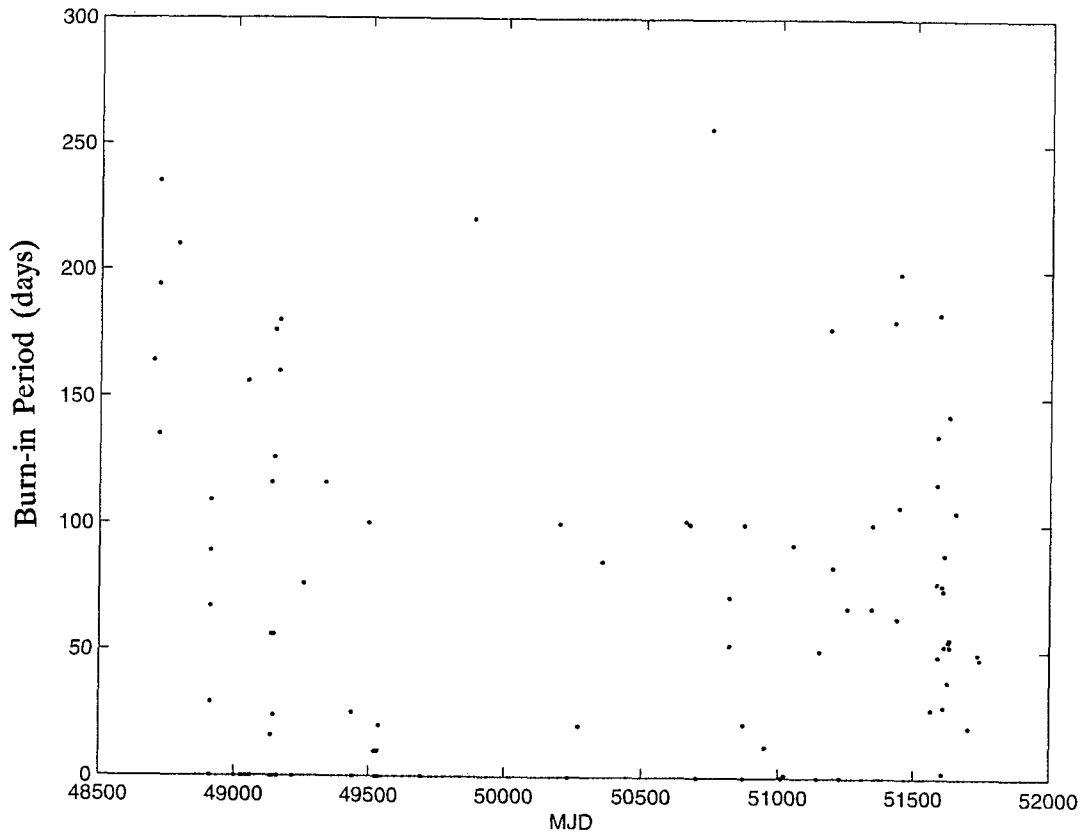


Figure 7. Length of cesium tube burn-in as a function of MJD.

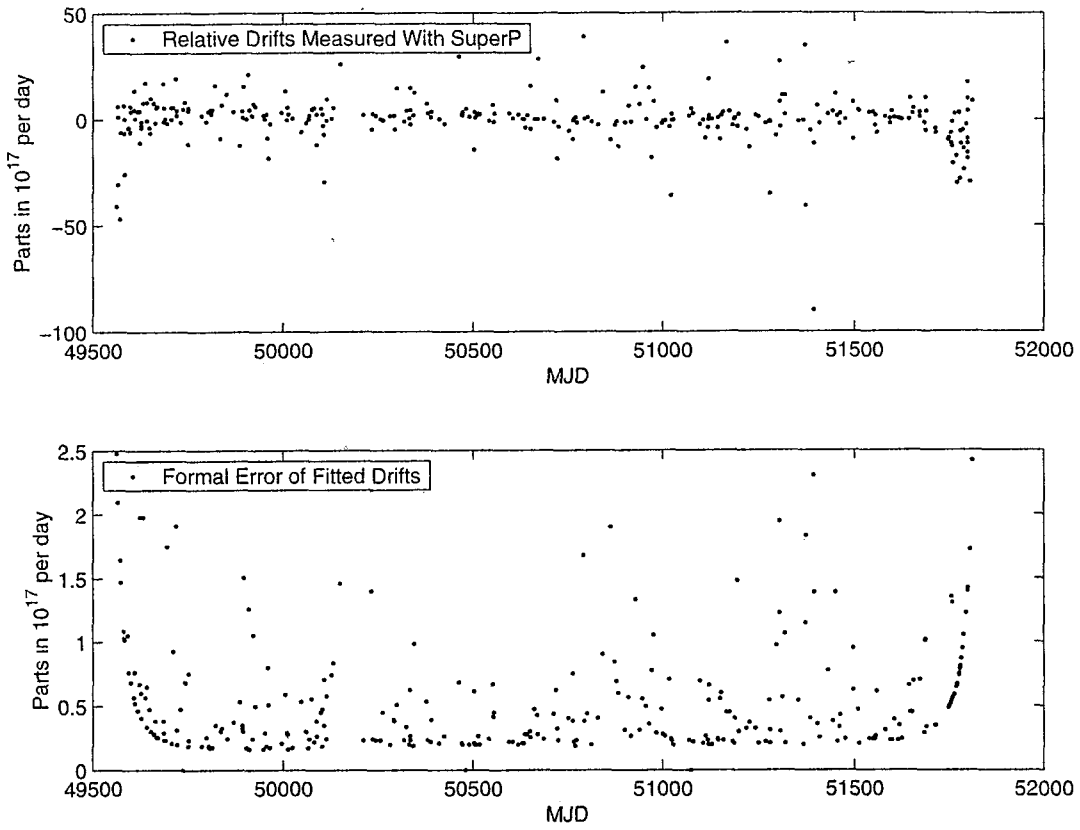


Figure 8. Fitted cesium clock drifts and associated standard errors as a function of characterization date.

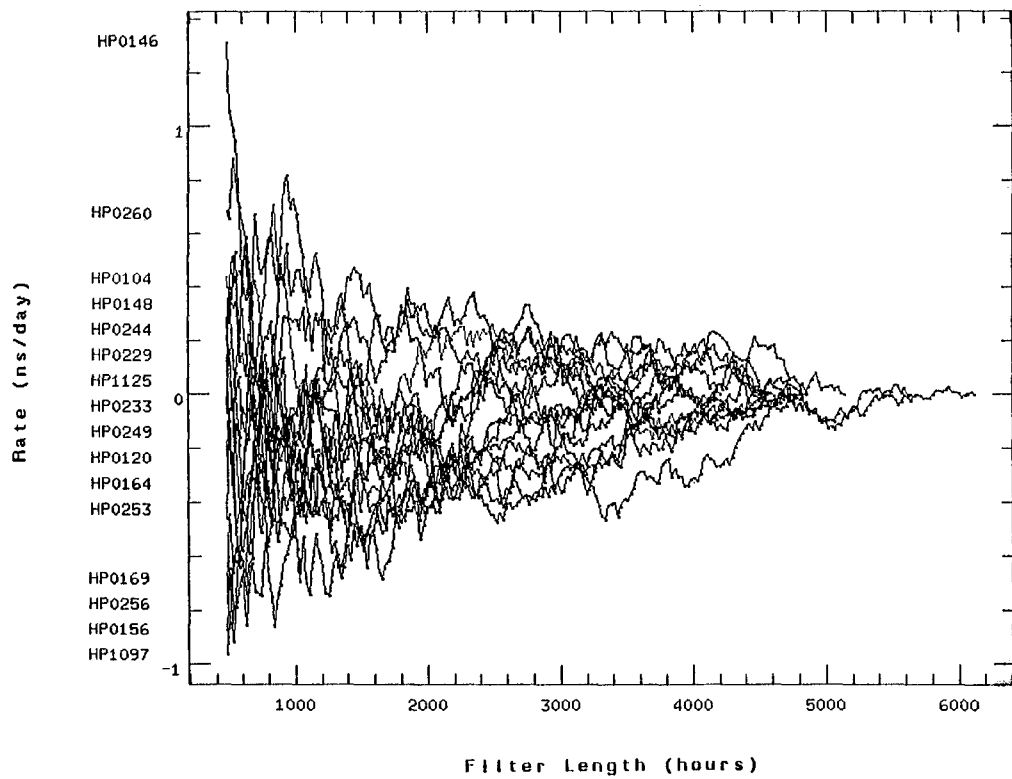


Figure 9. The decrease in the change of mean rate as data accumulate with time (converging toward zero at the final adopted rate) for a selection of 16 cesiums.

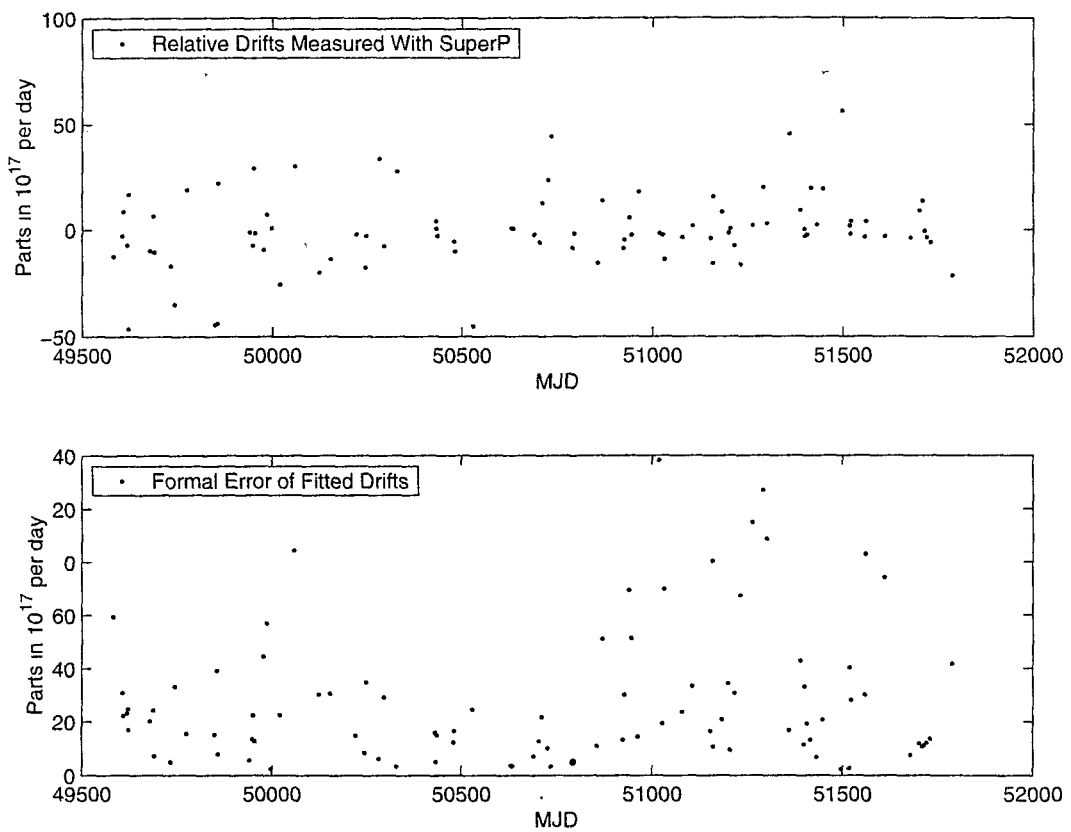


Figure 10. Fitted maser drifts and associated standard errors as a function of characterization date.

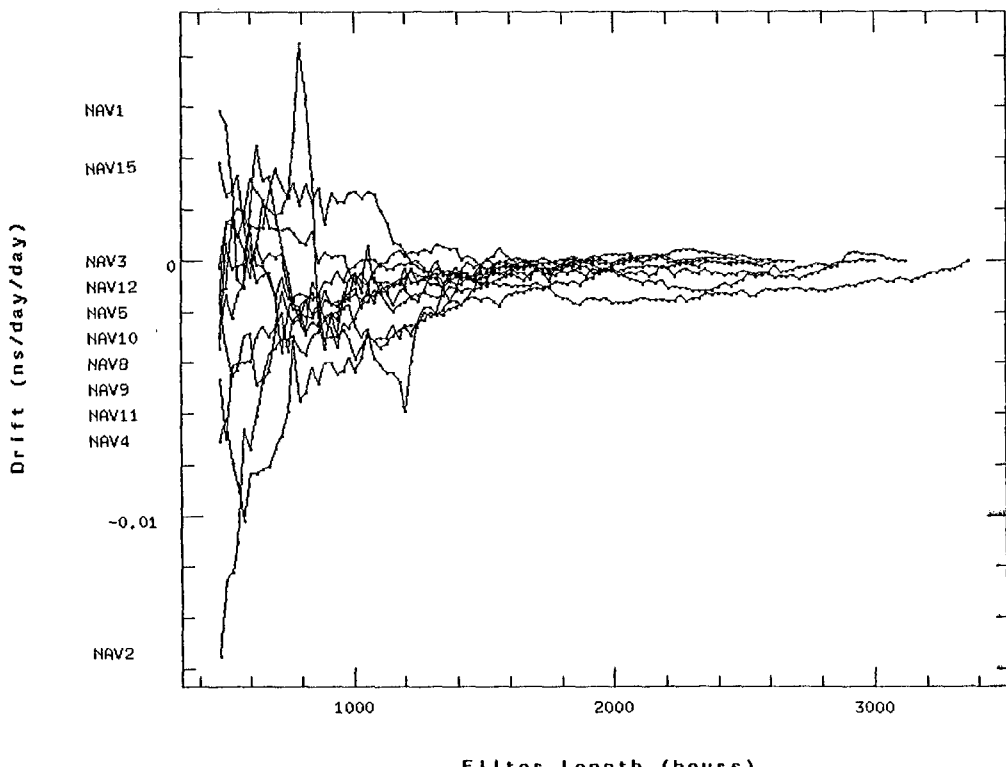


Figure 11. The decrease in the change of mean drift as data accumulate with time (converging toward zero at the final adopted drift) for 11 masers.

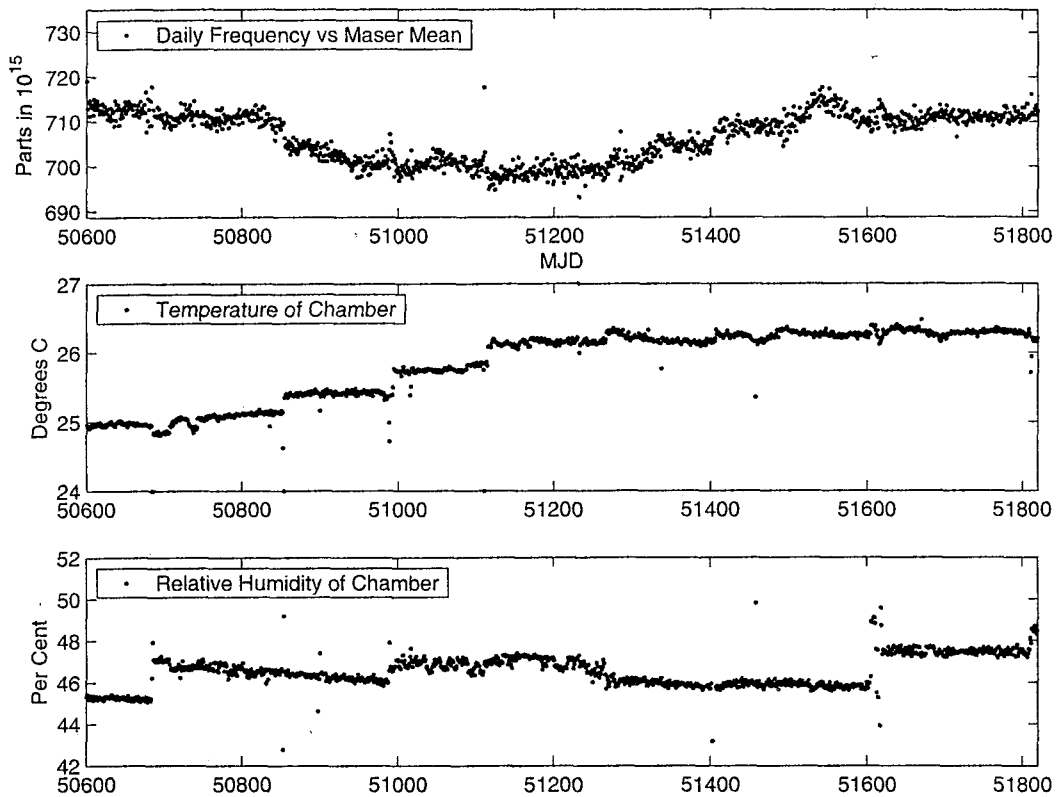


Figure 12. Observed frequency dependence of maser NAV3 on temperature and humidity as measured at the chamber ceiling.

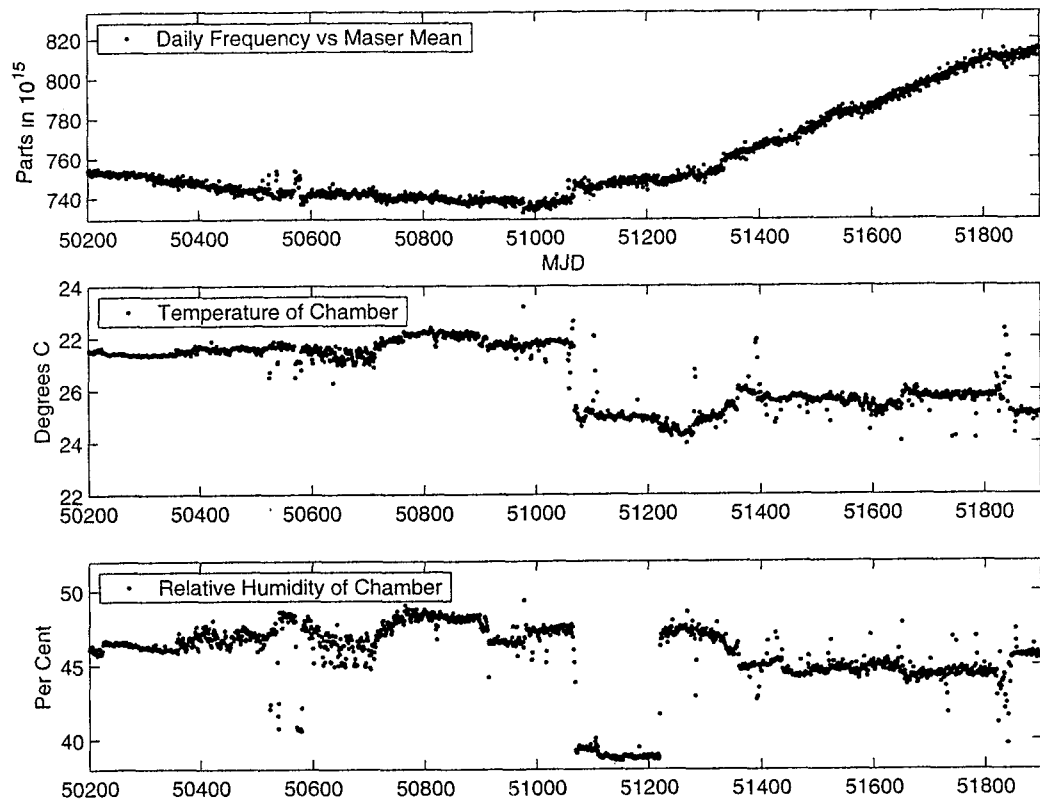


Figure 13. Observed frequency drift dependence of maser NAV8 on temperature and humidity as measured at the chamber ceiling.

Questions and Answers

DAVID HOWE (NIST): One of the comments you made, Lee, was that you take 60 days worth of data to get an estimate of the drift and correct for that drift. Yet, at the same time, you admit that the drift changes in those hydrogen masers for shorter intervals.

LEE BREAKIRON: Shorter than 60 days? No.

HOWE: You commented that you could make corrections more frequently, but that would raise the level of random walk. Do I understand that correctly?

BREAKIRON: Yes.

DAVE HOWE: Okay, then what I would comment about is that as your administered effort to reduce the random walk invariably will result in an increase in the noise on the drift in longer term. In other words, you will stretch the instabilities out farther. Now, we've observed this at NIST. One of the reasons why it is a dangerous business to have hydrogen masers without sufficiently periodic frequency evaluations is that you cannot predict an event in hydrogen maser reliably in terms of its drift. The drift is high. I believe that the Hadamard will report numbers that are significantly higher than one would expect.

HAROLD CHADSEY (USNO): I am interested, Lee, in two items. First of all, you said you did this analysis over 6 years, and you said using our current method of data analysis. As a person doing the real-time analysis, I am curious to know what standards you used, because we have changed them over the past 3e years. In fact, we have changed them over the past 6 months as to what we are evaluating as being good, bad, and mediocre clocks. I am also interested in knowing in your paper, are you going to have the specific criteria for Set #1, #2, #3, and #4 so we can figure out exactly what is the best and see if we can do that in real time versus the postprocessing that you did?

BREAKIRON: Certainly the latter we can do. I quoted the numbers for the cesium masers for Set #3, which was 5 parts in 10^{15} for a significant rate change for a cesium, and a change of 5 parts in $10^{18}/\text{day}$ for the drift of a maser.

As far as the change in the operational criteria over time, I found those to be much less significant than the rate and drift changes and the differences between the different sets of criteria. So I don't think that will be an important effect. But we will publish those numbers.

THOMAS CLARK (NASA Goddard Space Flight Center): I'm interested, since you have sort of the longest span and operation on the largest number of clocks of both types, that you now have talked more definitively in statistics. Certainly, from the masers that we run in VLBI, I have some feeling for the answer to this question. That is, in VLBI, in the masers, we find that vac ion pumps are the most common failure and that tends to be about 3 to 4 years that we see vac ion pump problems. Can you comment on what your experiences are on how long standards will keep running before the experience of a problem. And then the other question I was going to ask, which is unrelated, are you starting to include any fountain data in these ensembles and how is it performing?

BREAKIRON: Well, we've done only minimal adjustments to our masers, changes of heating plates and batteries, I think. But no large items, though that will presumably become a problem at some point. And perhaps one of our engineers here can tell you more.

As far as the fountain data, no that is still an experimental device. Bu, we certainly look forward to using the data when they become available.

CHADSEY: To answer your question, Tom, it depends on the manufacturer of the maser as to what pressures they are running and things like that as to when we are seeing failures. The Sigma Tau masers that we are running have been running very well, with minor things such as battery replacements. The SAO masers are running at higher pressures. We were doing plates and glassware on them. About 3 to 4 years was what we're getting out of them. But they are running significantly higher pressures in the chambers, so you would expect that.

DEMETRIOS MATSAKIS (USNO): Let me add another comment. A lot of the errors that we see with the masers are not necessarily intrinsic to the masers. We keep them in chambers that nominally are good to a 0.1°C . But every now and then, there is an adjustment to the chambers for one reason or another. The whole chamber can vary by half a degree, or on that level, and reach a new set point because of things we have done. We see that in the frequency of the masers. So part of the errors in the masers would not be there if they had been in a pristine, really perfect temperature-controlled environment. They are, however, in the best that we can do.

USNO ALTERNATE MASTER CLOCK STEERING

Steven T. Hutsell
U.S. Naval Observatory Alternate Master Clock
400 O'Malley Avenue, Suite 44
Schriever AFB, CO 80912-4044, USA

Paul A. Koppang
Datum – Timing, Test & Measurement
34 Tozer Road
Beverly, MA 01915, USA

Abstract

The primary mission of the U.S. Naval Observatory (USNO) Alternate Master Clock (AMC) facility, located at Schriever AFB, is to back up the critical functions of the USNO Time Service Department in Washington, D.C. The USNO AMC operates two Master Clocks, AMC #1 and AMC #2. Each one of these [Alternate] Master Clocks is ready to function as the nation's source for precise time, UTC(USNO), should the need arise.

This paper summarizes the current status of, and strategies used for, the steering of these Alternate Master Clocks. The various USNO AMC steering strategies utilize clock comparisons from Two-Way Satellite Time Transfer (TWSTT), GPS Common View (CV), and USNO AMC Timescale data. All current Alternate Master Clock steering strategies employ a combination of Kalman filtering and second-order control, first introduced into USNO operations in 1995. The respective designs for these steering strategies are based on several factors, including goals for synchronization and stability, as well as the desire for robustness and simplicity of operation. This paper analyzes the performance of these respective designs.

INTRODUCTION

As the criticality of precise timing to the security and economy of the United States increases, so does the need for robustness in the quality and availability of precise time. The United States Naval Observatory (USNO) must ensure its ability to provide a stable, continuous source of precise time for the nation. Key to ensuring the continuity of such operations is the USNO Alternate Master Clock (AMC), located in Colorado at Schriever Air Force Base (AFB). The AMC is ready, as necessary, to assume responsibility for the critical functions performed by the USNO Time Service department in Washington, D.C., for the Department of Defense and other United States customers.

During normal standby operations, the AMC provides various time and frequency signals to several users co-located at Schriever AFB. These users include the Air Force Technical Applications Center (AFTAC), Army and Air Force Defense Satellite Communications System (DSCS) stations and other communication modules, and Network Time Protocol (NTP) customers, as well as telephone modem and voice users. Additionally, the AMC provides an extremely stable 5 MHz reference to the GPS monitor station in Colorado Springs, as well as technical consultation on timing issues to the GPS community at Schriever AFB [1].

For clarity this paper will refer to the USNO facility located in Washington, D.C. as USNO, and the Alternate Master Clock facility as AMC.

AMC CLOCKS/TIMESCALES

As part of fulfilling the above missions, the AMC operates two Master Clock systems, AMC#1 and AMC#2. Each system uses an input 5 MHz signal from independent hydrogen maser frequency standards, and receives digital frequency steering commands. The current primary Alternate Master Clock is AMC#1, which is steered to UTC(USNO) in Washington, D.C. using hourly Two-Way Satellite Time Transfer (TWSTT) measurements (when available).

The AMC also maintains and operates various mean timescales, based on phase measurements from up to three hydrogen masers and up to 12 cesium frequency standards. Many of the AMC mean timescales are analogous to those residing at USNO, though with substantially less contributing frequency standards. In particular, the AMC maintains a cesium-only mean (#203), a maser-only mean (#198), and a “dynamic” mean that weights masers higher in short-term, and cesiums higher in long-term, through continuous, hourly recomputation (#200) [2]. The AMC also maintains steered versions of these means, (#204, #199, #202, respectively) which are synchronized to the USNO counterpart means monthly.

INTERMEDIATE MEANS

Since March 1997, the AMC has also maintained separate versions of the unsteered AMC mean timescales, which the AMC can steer towards selected references. Currently, these intermediate means include hourly-steered copies of #200 (200S), and #203 (203S). 200S acts as a buffer timescale for AMC#2 disciplining, and 203S contributes to the AMC Phase Monitoring system, described later.

Since the standard AMC timescales (#198, #199, #200, #202, #203, #204), like their USNO counterparts, are designed for retroactive recomputation, they often experience phase steps in real time. Phase steps, by themselves, can potentially impact monitoring and steering functions. The AMC has designed two available remedies for this phenomenon: 1) A program to bookkeep and counter-correct such steps in the Intermediate Means 200S and 203S (in use since 1997), and 2) Operational restrictions on retroactive recomputation (in use since 1999). Both have ensured that steps in the AMC means do not impact Alternate Master Clock steering or monitoring.

STEERING CONFIGURATIONS

USNO has two current operational techniques of performing time comparisons between USNO and the AMC: TWSTT and GPS Common View (CV). With these available synchronization sources, the two Alternate Master Clock systems, and the AMC Intermediate Means, the AMC can operate under several different steering configurations.

Primary Configuration

The primary measurement for synchronizing the AMC with USNO is TWSTT. Accordingly, AMC#1 is steered to UTC(USNO) via TWSTT. AMC#2 is steered to 200S, which is, in turn, steered to AMC#1.

The Intermediate Mean 200S acts as a stable buffer between AMC#2 and AMC#1, to a) keep AMC#2 close in time and frequency to AMC#1 in a “hot backup” sense, yet b) simultaneously protect AMC#2 from overly aggressive steering in the event of a runoff in AMC#1. See Figure 1.

The AMC has operated under this Primary Configuration for the majority of time since October 1998.

Secondary Configuration

Were the AMC to lose TWSTT measurements for an extended period of time, the AMC could begin steering 200S to UTC(USNO) using CV data, and simultaneously begin steering AMC#1 to 200S. Switching from Primary to Secondary Configuration incurs no change on AMC#2’s steering target—AMC#2 is steered to 200S in both configurations. See Figure 2.

The AMC does not normally operate under this configuration for two reasons. For one, USNO’s TWSTT system currently offers superior calibration stability over USNO’s current GPS CV receiver system [3]. Secondly, since GPS is an extremely important USNO customer, using GPS CV poses a potential, though unlikely, issue of operational fidelity. One could argue that USNO should never become dependent on the service provided by one of their own customers, in order to maintain service provided *to* that customer and other customers. Were GPS to malfunction in some very unlikely fashion, the AMC would lose GPS CV, and thus, the ability to use this described configuration. For this reason and others, USNO may benefit by continuing to maintain and utilize a synchronization source independent of the GPS system, as it does today with TWSTT.

Hybrid Configuration

The Hybrid Configuration makes use of both available synchronization sources. In the Hybrid, AMC#1 is steered to UTC(USNO) using TWSTT, as in the Primary Configuration, yet 200S is steered to UTC(USNO) using GPS CV, as in the Secondary Configuration. In the Hybrid Configuration, AMC#1 and 200S are compared, but neither one is steered towards the other. See Figure 3.

The AMC operated under this configuration for the full month of August 2000. This configuration permitted a comparison between the two synchronization methods. Performance numbers are presented later in this paper, but overall the Hybrid Configuration demonstrated the inherent calibration instability USNO experiences with its current operational authorized GPS receivers. USNO is currently testing new receivers that promise improved calibration stability.

Contingency Configuration

In the unlikely event of a catastrophic or temporary loss of the Department of Defense (DoD) Master Clock at USNO, the AMC must assume responsibility for maintaining time for the nation. Additionally, in the event that the AMC loses all synchronization measurements from USNO for an extended period of time, the AMC must freewheel. Under such scenarios, the AMC can operate in the Contingency Configuration.

The Contingency Configuration steers both AMC#1 and AMC#2 to 200S, which freewheels on the available hydrogen maser and cesium frequency standards. See Figure 4.

To date the AMC has not needed to operate under the Contingency Configuration.

AMC PHASE MONITORING

The AMC Phase Monitoring system, in operation since November 1997, compares both Alternate Master Clocks to a semi-independent AMC mean timescale, namely 203S. To independently monitor two hydrogen-maser-referenced Alternate Master Clock systems using a mean timescale, the AMC must use a mean that consists of only frequency standards independent of the Master Clock systems. A suitable choice for this task is a cesium-only mean. However, since any two independent clocks systems will eventually walk off from each other, a straight comparison between the unsteered AMC cesium mean and the Master Clocks would produce differences that would be unbounded over time.

Since GPS depends greatly on stability over time spans ≤ 1 day, the AMC phase monitoring system must detect significant, short-term excursions in the Master Clocks, as opposed to absolute long-term differences between independent timescales. To facilitate the monitoring of short-term excursions, the AMC gently steers 203S to AMC#1 hourly, with a magnitude limit of, currently, 2.7×10^{-16} s/s. The AMC then intercompares AMC#1, AMC#2, and 203S, using majority logic, to detect if a significant excursion in one of the three is occurring. The comparisons between AMC#1 and AMC#2 utilize two independent measurement systems.

As mentioned earlier, AMC#1 currently provides an extremely stable frequency signal to the GPS monitor station in Colorado Springs. If $|AMC\#1 - AMC\#2|$ and $|AMC\#1 - 203S|$ both exceed 5 ns, the AMC Phase Monitoring system will generate a “NOGO” flag for GPS operators to discontinue use of AMC#1. This system is also designed to work analogously for AMC#2, during times when AMC#2 provides the 5 MHz source to the GPS monitor station. See Figure 5.

AMC#1, since it first offered service to the GPS monitor station in September 1996, has operated without disruption. As such, the AMC Phase Monitoring System has not yet needed to produce a “NOGO” flag.

STEERING-RELATED MATHEMATICS

All of the above steering and monitoring systems make use of Kalman filter state estimation, and second-order control using two-state gain vectors, derived using Linear Quadratic Gaussian (LQG) control theory. This combination first appeared operationally in a program that steered AMC#1 to UTC(USNO) using TWSTT data, in 1995. The basic second-order steering function used is as follows [4]:

$$u(k) = -G_0x(k) \quad (1)$$

where $u(k)$ is the calculated steer command at Kalman time k , $G_0 = [g_\mu \ g_\lambda]$ is the 1×2 gain vector, and $x(k)$ is the 2×1 state estimate of phase and frequency. In essence, for each Kalman epoch k , a program multiplies the time/phase offset by g_μ and the rate/frequency offset by g_λ , and sums the results to produce a single frequency steering command for that control system, in units of seconds/second.

The matrix algebra involved in the derivation of these gains is covered in [4]. In short, designers input selected weighting matrices W_R and W_Q , into a steady-state Riccati equation to solve for G_0 , in order to satisfy a cost function:

$$J = \sum_k [(x(k)^T W_Q x(k) + u(k)^T W_R u(k))] \quad (2)$$

The message conveyed by the above cost equation is as follows: the goals of synchronization, syntonization, and stability are not mutually exclusive. That is, the desire for minimizing phase offsets, frequency offsets, and the amount of steering control used can, at best, only be *balanced*.

A rule of thumb from Applied Optimal Control [5] relates selected designer requirements/goals for phase and frequency offsets as well as steering values, to the derivation of optimal coefficients within the gain vector. This rule of thumb examines the diagonal elements of the weighting matrices used in the cost function equation:

$$W_R = [w_r] \quad (3)$$

$$W_Q = \begin{bmatrix} w_{q1} & 0 \\ 0 & w_{q2} \end{bmatrix} \quad (4)$$

Using the Applied Optimal Control approach, the authors set:

w_r = the inverse of the square of the steering magnitude goal

w_{q1} = the inverse of the square of the phase offset goal

w_{q2} = the inverse of the square of the frequency offset goal

The use of the word “goal” above is in the sense of relative maximum allowed offsets. Since continuously and simultaneously achieving zero phase offsets, zero frequency offsets, and zero use of steering is unachievable in our systems, the designer can, at best, only balance the relative, respective goals. As long as the relative “goals” are proportionate, the cost function will produce optimal gains intended to balance the respective input goals. Of course, empirical demonstration, either through simulation or safe off-line demonstration, is prudent for confirming how well the resultant gains do, in fact, achieve their respective goals. The designer must analyze the step and ramp responses of the system to ensure that the goals used have generated control gains with the desired damping characteristics and time constants.

Below is a table of the designer goals used in the respective steering algorithms described in this paper, as well as the gain coefficients produced by solving a steady-state Riccati equation. The below goals, and resultant gains, are current as of 1 October 2000. These goals are not fixed values, but rather are subject to change based on operational factors at the AMC:

STEERING SYSTEM	Update Interval	Phase Goal	Frequency Goal	Steering Goal	Gain Matrix [1/s (unitless)]
AMC#1 to UTC(USNO) via TWSTT	3600 s	1.90 ns	4.00 E-15 s/s	6.00 E-17 s/s	[3.135 E-08 0.0210]
200S to AMC#1	3600 s	1.50 ns	3.00 E-15 s/s	8.33 E-17 s/s	[5.446 E-08 0.0335]
AMC#2 to 200S	3600 s	0.90 ns	2.00 E-15 s/s	8.33E-17 s/s	[9.010 E-08 0.0477]
203S to AMC#1	3600 s	2.84 ns	6.00 E-15 s/s	9.00 E-17 s/s	[3.135 E-08 0.0210]
200S to UTC(USNO) via CV	86400 s	3.00 ns	6.00 E-15 s/s	2.00 E-15 s/s	[5.260 E-07 0.3780]

An important fact to note is that the AMC has, at its disposal, multiple configurations for steering AMC clocks. Often, the chosen configuration will steer clocks in a chainlike fashion. For example, currently AMC#2 is steered to 200S, which is steered to AMC#1, which is, in turn, steered to UTC(USNO). The primary advantage of the chainlike system is the inherent robustness in the event of an anomaly in one part of the chain. Impact down the chain is kept to a minimum by limiting hourly steers and by permitting the ability to freewheel if the system detects that a reference is either performing poorly or unavailable. The primary disadvantage of this chainlike approach is the potential for lesser quality steady-state performance. The tradeoff between minimizing worst-day errors vs. minimizing steady-state errors is ultimately up to the designer. The steering systems implemented at the AMC are designed around the principle, "A timing system is only as good as its worst day."

STEERING OPERATIONS

All of the above steering designs are currently either in use, or on standby ready for use, at the AMC. The respective Kalman filters in each of the above systems employ 3-sigma outlier detection, steering limiters, and a robust advisory system that notifies operators when less-than-desired performance is detected.

Figure 6 presents AMC#1 and AMC#2 steering performance, by plotting Kalman filter estimates of AMC#1 – UTC(USNO) [TWSTT], AMC#1 – 200S, and AMC#2 – 200S. Figure 7 presents AMC Phase Monitoring performance by plotting AMC#1 – 203S and AMC#2 – 203S.

The performance of all of the above systems can potentially experience some degradation in the absence of measurements, be the measurements in the form of TWSTT, CV, or on-site measurement systems. Thanks in large part to the superb stability offered by the on-site cesium and hydrogen maser frequency standards, such degradation will usually be below the noise level required by users, during reasonable outage intervals. Figure 8 compares linear residuals of the accumulation in frequency due to the steering of UTC(USNO), AMC#1, and AMC#2, during a continuous 10-month period in 1999. The figure shows how AMC#1 and AMC#2 track the steering of the USNO Master Clock.

CONCLUSIONS

The current AMC steering programs are designed to optimally balance the goals of minimizing phase offsets, frequency offsets, and instability due to steering. Empirical performance supports the success of this design.

TWSTT is important for good USNO-AMC synchronization, though GPS CV offers an acceptable secondary source for USNO-AMC synchronization, during extensive temporary absences of TWSTT measurements.

The AMC mean timescales, like their analogous counterparts at USNO, perform excellently. The AMC intermediate mean timescales, as a result, serve very well for the functions of Alternate Master Clock disciplining, and AMC Phase Monitoring.

The steering and monitoring systems described in this paper are robust, operate automatically, and usually require no operator intervention, except when database values, such as Kalman filter noise parameter and gain coefficients, require updates.

ACKNOWLEDGMENTS

The authors wish to thank:

All USNO Time Service co-workers who contribute to the successful operation of the USNO Alternate Master Clock.

GPS, for the experience of Kalman filtering in practice.

Sam Stein, Timing Solutions Corp., for his experience and guidance through the years.

REFERENCES

- [1] W. Bollwerk, "*The Alternate Master Clock And Precise Time Requirements: Why An Alternate Master Clock?*," Proceedings of the 28th Precise Time and Time Interval (PTTI) Applications and Planning Meeting, Reston, VA, 3-5 December 1996, pp. 141-150.
- [2] L. Breakiron, "*Timescale Algorithms Combining Cesium Clocks And Hydrogen Masers,*" Proceedings of the 23rd Annual Precise Time and Time Interval (PTTI) Applications and Planning Meeting, Pasadena, CA, 3-5 December 1991, pp. 297-305.
- [3] J. DeYoung, F. Vannicola, and A. McKinley, "*A Comparison Of The Highest Precision Commonly Available Time Transfer Methods: TWSTT and GPS CV,*" Proceedings of the 28th Annual Precise Time and Time Interval (PTTI) Applications and Planning Meeting, Reston, VA, 3-5 December 1996, pp. 349-356.
- [4] P. Koppang and R. Leland, "*Steering Of Frequency Standards By The Use Of Linear Quadratic Gaussian Control Theory,*" Proceedings of the 27th Precise Time and Time Interval (PTTI) Applications and Planning Meeting, San Diego, CA, 29 November – 1 December 1995, pp. 257-267.
- [5] A. Bryson, Jr., and Y. Ho, "*Applied Optimal Control,*" 1975, Hemisphere Publishing Corporation, pp. 148-176.

Primary Configuration

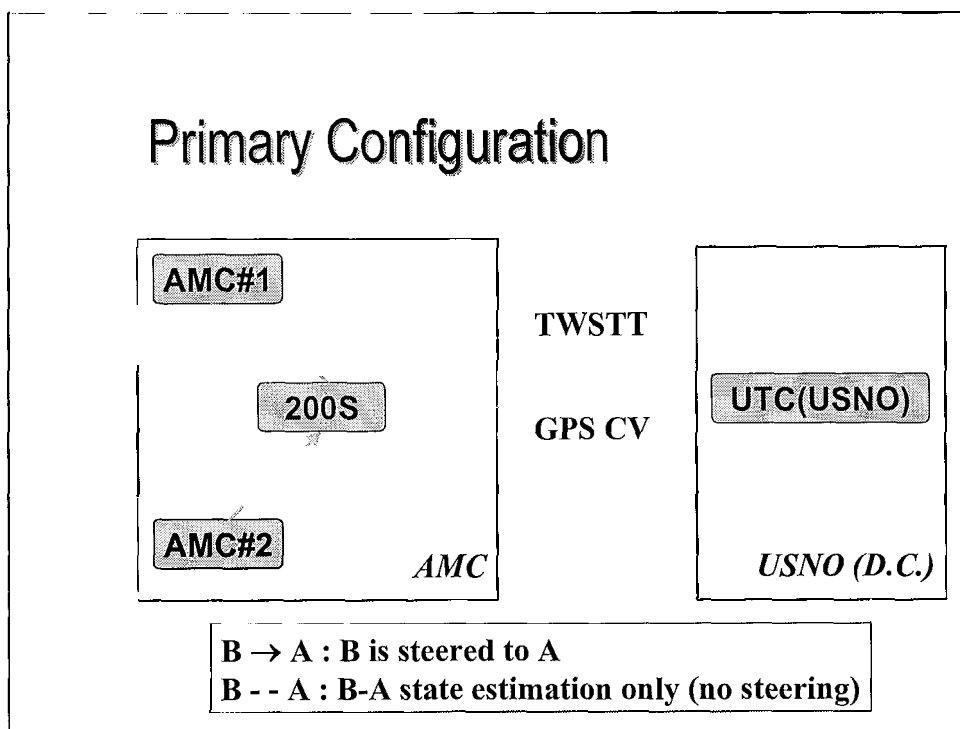


Figure 1. Primary AMC Steering Configuration

Secondary Configuration

(In absence of TWSTT)

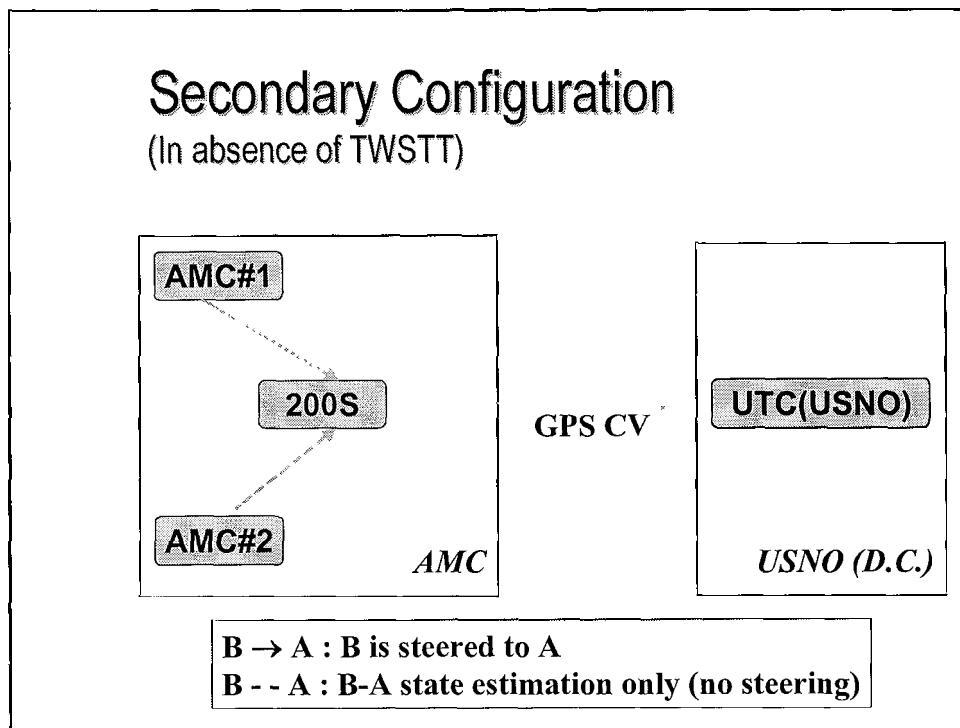


Figure 2. Secondary AMC Steering Configuration

Hybrid Configuration

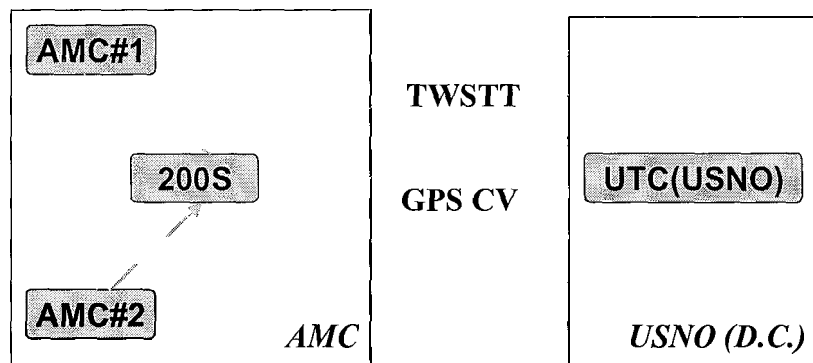


Figure 3. Hybrid AMC Steering Configuration

Contingency Configuration

(Catastrophic or temporary loss of USNO D.C.)

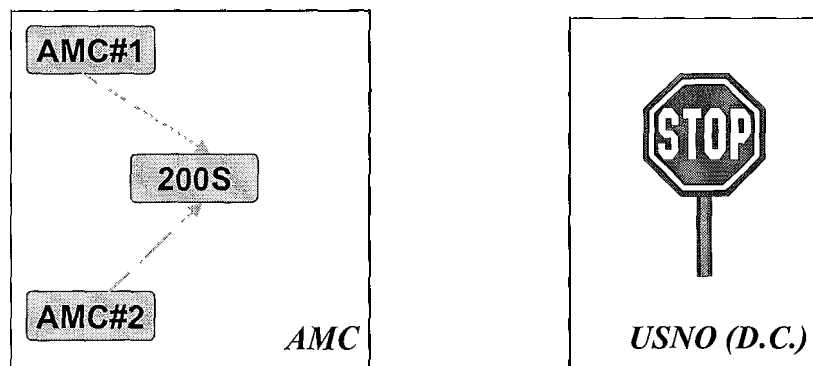


Figure 4. Contingency AMC Steering Configuration

AMC Phase Monitoring (Current Configuration)

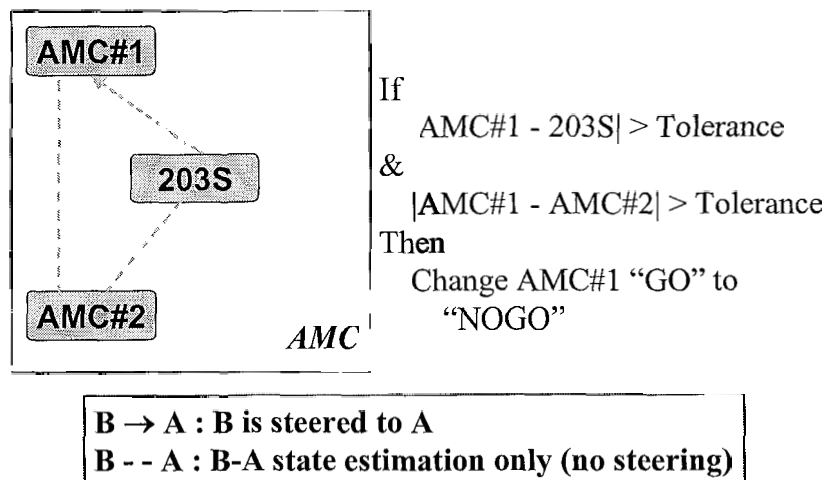


Figure 5. AMC Phase Monitoring

AMC Steering Performance

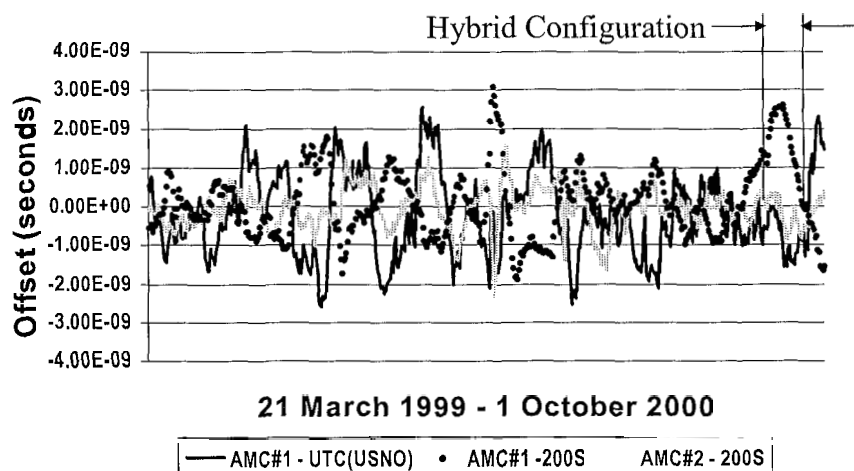


Figure 6. AMC Steering Performance

AMC Phase Monitoring System

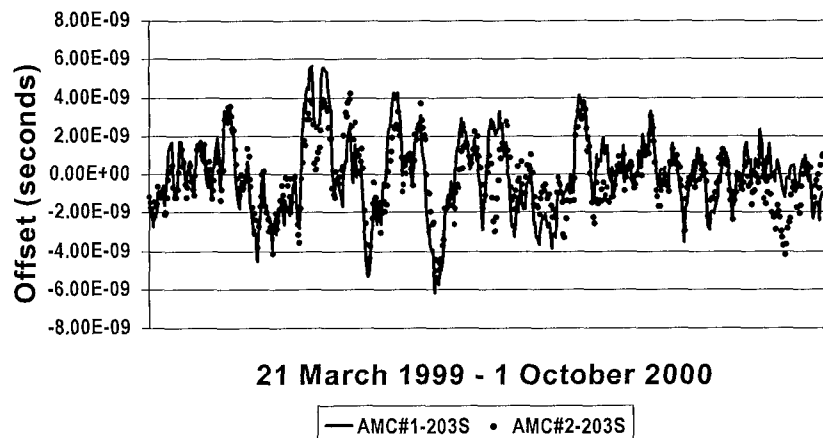


Figure 7. AMC Phase Monitoring Performance

Steering Comparison

Accumulated frequency due to steering (linear residuals)

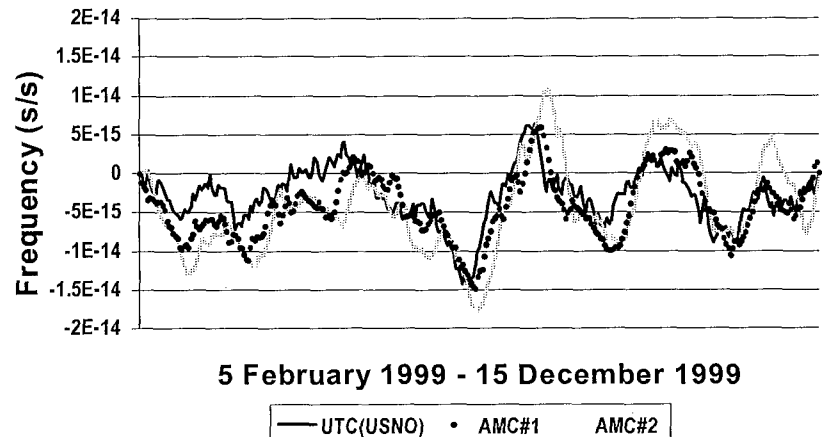


Figure 8. Clock Steering Comparison

OBSERVING A GRAVITATIONAL WAVE BACKGROUND WITH LISA

M. Tinto, J. Armstrong, and F. Estabrook
NASA Jet Propulsion Laboratory, California Institute of Technology
Pasadena, CA 91109, USA

Abstract

LISA (Laser Interferometer Space Antenna) is a proposed space mission which will use coherent laser beams exchanged between three remote spacecraft, to detect and study low-frequency cosmic gravitational radiation.^[1] The multiple Doppler readouts available with LISA, which incorporate frequency standards for measuring phase differences between the received and transmitted laser beams, permit simultaneous formation of several observables.^[2,3,4] All are independent of lasers and frequency standard phase fluctuations, but have different couplings to gravitational waves and to the various LISA instrumental noises. Comparison of the conventional Michelson interferometer observable with the fully-symmetric Sagnac data-type allows unambiguous discrimination between a gravitational wave background and instrumental noise. The method presented here can be used to detect a confusion-limited gravitational wave background.

INTRODUCTION

The Laser Interferometer Space Antenna (LISA) is a space mission, jointly proposed by NASA and ESA, aimed to detect and study gravitational radiation in the millihertz frequency band. With its three spacecraft, each carrying lasers, beam splitters, photodetectors and drag-free proof masses on each of their two optical benches, LISA will have the capability of measuring six time series of Doppler shifts of the one-way laser beams between spacecraft pairs, and six shifts between adjacent optical benches on each spacecraft. By linearly combining, with suitable time delays, these twelve data sets, it will be possible to cancel the otherwise overwhelming phase noise of the lasers ($\Delta\nu/\nu \simeq 10^{-13}$) to a level $h \simeq \Delta\nu/c \simeq 10^{-23}$. This level is set by the buffeting of the drag-free proof masses inside each optical bench, and by the shot noise at the photodetectors^[4].

LISA is expected to detect monochromatic radiation emitted by galactic binary systems. Particularly at low Fourier frequencies (say 0.1 – 8 mHz), however, there will be many galactic binaries radiating within each Fourier resolution bin^[1]. These latter signals will not be detectable individually, forming a continuum which could be confused with instrumental

noise. The level of this stochastic background is uncertain, but could be in the range $10^{-20} - 10^{-23}$. Since these galactic binary populations are virtually guaranteed, the detection of their signals could be the first direct detection of gravitational waves.

For this measurement it is very desirable that competing proof-mass and other instrumental noises be both characterized and calibrated before flight, and measured in the actual flight configuration while data are being taken. In contrast to Earth-based, equal-arm interferometer detectors of gravitational radiation, LISA will have multiple readouts, and the Doppler data they generate can be combined differently to give measurements not only insensitive to laser phase fluctuations and optical bench motions, but also with different sensitivities to gravitational waves and to the remaining system noise^[3,4].

In this article we discuss two laser-and-optical-bench-noise-free combinations of the LISA readouts, previously denoted ζ (Sagnac) and X (Michelson), that have very different responses to the gravitational wave background but comparable responses to instrumental noise sources^[4,5].

THE SAGNAC AND MICHELSON INTERFEROMETERS

The six Doppler beams exchanged between the LISA spacecraft imply the six Doppler readouts y_{ij} ($i, j = 1, 2, 3$) recorded when each transmitted beam is mixed with the laser light at the receiving optical bench. Delay times for light travel between the spacecraft must be carefully accounted for when combining these data. Six further data streams, denoted z_{ij} ($i, j = 1, 2, 3$), are generated internally to monitor both lack of rigidity and laser synchronization between the independent optical benches at each spacecraft. The combination ζ uses all the Doppler data symmetrically^[4,5]

$$\begin{aligned}\zeta = & y_{32,2} - y_{23,3} + y_{13,3} - y_{31,1} + y_{21,1} - y_{12,2} \\ & + \frac{1}{2}(-z_{13,21} + z_{23,12} - z_{21,23} + z_{31,23} - z_{32,13} + z_{12,13}) \\ & + \frac{1}{2}(-z_{32,2} + z_{12,2} - z_{13,3} + z_{23,3} - z_{21,1} + z_{31,1}) .\end{aligned}\quad (1)$$

The comma notation indicates time-delays along the arms of the 3-spacecraft configuration

$$y_{32,2} \equiv y_{32}(t - L_2) , \quad (2)$$

and so forth (units in which $c = 1$).

The transfer functions of ζ to instrumental noises and to gravitational waves were calculated in references [3, 4]. The resulting instrumental noise power spectrum for ζ is shown in Figure 1. Also shown there is the computed power spectrum of ζ , averaged over the sky

and elliptical polarization states, that would result from a stochastic background originated by an ensemble of galactic binary systems^[1].

The laser-and optical-bench-noise-free combination, X , only requires four data streams. This combination is equivalent to an (unequal arm) Michelson interferometer. Its expression is equal to^[4,5]

$$\begin{aligned} X = & y_{32,322} - y_{23,233} + y_{31,22} - y_{21,33} + y_{23,2} - y_{32,3} + y_{21} - y_{31} \\ & + \frac{1}{2}(-z_{21,2233} + z_{21,33} + z_{21,22} - z_{21}) \\ & + \frac{1}{2}(+z_{31,2233} - z_{31,33} - z_{31,22} + z_{31}) . \end{aligned} \quad (3)$$

The expected instrumental noise power spectrum in X is shown in Figure 1. Also shown is the anticipated galactic binary confusion spectrum^[1], which would be observed in X . Comparison of X and ζ allows the background to be discriminated from instrumental noise.

DETECTING THE GALACTIC STOCHASTIC BACKGROUND

The flight configuration of the three spacecraft forming LISA will be essentially equilateral, with $L_1 = L_2 = L_3 = L = 16.67$ sec. In the frequency band of interest ($0.1 - 8$ mHz), the expressions for the Fourier transforms of the gravitational wave signals $\tilde{X}^{gw}(f)$, $\tilde{\zeta}^{gw}(f)$ and the power spectral densities of the system noises in X and ζ , $S_{X^{noise}}(f)$, $S_{\zeta^{noise}}(f)$, can be Taylor-expanded in the dimensionless quantity fL . The first non-zero terms are equal to

$$\tilde{X}^{gw}(f) \simeq 2(2\pi ifL)^2 \left[\hat{n}_3 \cdot \tilde{\mathbf{h}}(f) \cdot \hat{n}_3 - \hat{n}_2 \cdot \tilde{\mathbf{h}}(f) \cdot \hat{n}_2 \right] , \quad (4)$$

$$\begin{aligned} \tilde{\zeta}^{gw}(f) \simeq & \frac{1}{12}(2\pi ifL)^3 \left[(\hat{k} \cdot \hat{n}_1)(\hat{n}_1 \cdot \tilde{\mathbf{h}}(f) \cdot \hat{n}_1) + (\hat{k} \cdot \hat{n}_2)(\hat{n}_2 \cdot \tilde{\mathbf{h}}(f) \cdot \hat{n}_2) \right. \\ & \left. + (\hat{k} \cdot \hat{n}_3)(\hat{n}_3 \cdot \tilde{\mathbf{h}}(f) \cdot \hat{n}_3) \right] , \end{aligned} \quad (5)$$

$$\begin{aligned} S_{X^{noise}}(f) \equiv & S_{X^{proofmass}}(f) + S_{X^{opticalpath}}(f) \\ \simeq & 16[S_1(f) + S_{1^*}(f) + S_3(f) + S_{2^*}(f)] (2\pi fL)^2 \\ & + 4[S_{32}(f) + S_{23}(f) + S_{31}(f) + S_{21}(f)] (2\pi fL)^2 \end{aligned} \quad (6)$$

$$\begin{aligned} S_{\zeta^{noise}}(f) \simeq & [S_1(f) + S_2(f) + S_3(f) + S_{1^*}(f) + S_{2^*}(f) + S_{3^*}(f)] (2\pi fL)^2 \\ & + [S_{32}(f) + S_{23}(f) + S_{31}(f) + S_{21}(f) + S_{13}(f) + S_{12}(f)] , \end{aligned} \quad (7)$$

where we have denoted by $S_{X^{proofmass}}(f)$, and $S_{X^{opticalpath}}(f)$ the aggregate contributions to the power spectrum of the noise in the response X from the proof mass and optical path noises respectively. The expressions in square brackets in Equations (4, 5) incorporate LISA

antenna responses^[3,4], and are of the same order of magnitude. The proof mass Doppler noise spectra $S_i(f)$, $S_{i*}(f)$ ($i = 1, 2, 3$) will be designed to a nominal power spectral level^[4] $S^0(f) = 2.5 \times 10^{-48}[f/1\text{Hz}]^{-2} \text{ Hz}^{-1}$, while the optical path noise spectra $S_{ij}(f)$, ($i, j = 1, 2, 3, i \neq j$), which include shot noises at the photo detectors and beam pointing noise^[1], are expected to be equal to a nominal spectrum $S^1(f) = 1.8 \times 10^{-37}[f/1\text{Hz}]^2$. Both these noise sources will be estimated before launch, but could be larger when the in-orbit data will be taken.

First consider the responses to the gravitational wave signal, given in Equations (4, 5). At $f = 10^{-3} \text{ Hz}$, for instance, (where $2\pi f L \simeq 10^{-1}$) the absolute value of the coefficient in front of the squared-bracket in the ζ response (Eq. 5) is about three orders of magnitudes smaller than the corresponding coefficient given in the expression for X (Eq. 4). The power spectral densities of the noises due to the proof masses and the optical-path noise (Eqs. 6, 7) will only differ at most by an order of magnitude. We conclude that in this lower frequency range the LISA Sagnac response, ζ , can be used as a *gravitational wave shield*. In what follows we will ignore the gravitational wave background contribution to ζ .

To take quantitative advantage of this property of ζ , consider the observed power spectral densities of X and ζ

$$S_X^{obs}(f) = S_{X^{gw}}(f) + S_{X^{proofmass}}(f) + S_{X^{opticalpath}}(f) \quad (8)$$

$$\begin{aligned} S_\zeta^{obs}(f) &= \frac{1}{16} \left[S_{X^{proofmass}}(f) + \frac{S_{X^{opticalpath}}(f)}{(\pi f L)^2} \right] + [S_{13}(f) + S_{12}(f)] \\ &\quad + [S_2(f) + S_{3*}(f)] (2\pi f L)^2, \end{aligned} \quad (9)$$

where in Equation (9) we have written the power spectra of the noises in ζ in terms of the power spectra of the noises in X and of some remaining terms that are not present in X , to emphasize commonality of some noise sources. We suppose that the noise contributed by any one of the proof masses and optical-path noise sources will be greater than or equal to the design values, $S^0(f)$ and $S^1(f)$ respectively. From Equation (9), if the magnitude of the measured power spectral density of the response ζ is at its anticipated level $S_\zeta^{obs}(f) = 6 S^0(f)(2\pi f L)^2 + 6 S^1(f)$, then the level of the power spectral density of the noise entering into X is known. The spectrum

$$S_{X^{gw}}(f) = S_X^{obs}(f) - 64 S^0(f)(2\pi f L)^2 - 16 S^1(f)(2\pi f L)^2, \quad (10)$$

should then be attributed to a galactic binary background of gravitational radiation. In any event, the RHS of Equation (10) is an upper bound to $S_{X^{gw}}$.

On the other hand, if the measured spectrum of ζ is above its anticipated design level, consider the following combination of the measured spectra

$$\begin{aligned}
S_X^{obs}(f) - 16 S_\zeta^{obs}(f) = & \quad S_{X^{gw}} - 16 [S_2(f) + S_{3^*}(f)] (2\pi f L)^2 \\
& - 16 [S_{13}(f) + S_{12}(f)] \\
& - 16 [S_{32}(f) + S_{23}(f) + S_{31}(f) + S_{21}(f)] \times \\
& \times [1 - (\pi f L)^2].
\end{aligned} \tag{11}$$

The coefficient of S_ζ^{obs} has been chosen so that the noise terms on the right hand side are all now negative-definite and can thus be bounded from above by their design, or nominal, values $S^0(f)$ and $S^1(f)$ respectively. The result is a lower bound for observational discrimination of the gravitational wave background spectrum

$$\begin{aligned}
S_{X^{gw}}(f) \geq & \quad S_X^{obs}(f) - 16 S_\zeta^{obs}(f) + 32 (2\pi f L)^2 S^0(f) \\
& + 16 [6 - (2\pi f L)^2] S^1(f).
\end{aligned} \tag{12}$$

Equations similar to (11) and (12) can be written for the other two interferometer combinations, Y and Z^[4]. In those equations, there will be different mixes of canceled and bounded noise sources, resulting, in general, in different gravitational wave spectrum lower bounds.

CONCLUSIONS

The response of the Sagnac interferometer to a gravitational wave signal is several orders of magnitudes smaller than that of the Michelson interferometer. In the frequency band of interests (0.1 – 8) mHz, however, the Sagnac response to the noise sources is of the same order of magnitude as that of the Michelson interferometer. As a consequence of these facts we have shown that it is possible to estimate the magnitude of the noise sources affecting the Michelson interferometer response in the low-frequency region of the accessible band by using the Sagnac interferometer. This in turn allows us to discriminate a gravitational wave background of galactic origin from instrumental noise affecting the Michelson interferometer response.

ACKNOWLEDGMENTS

This work was performed at the Jet Propulsion Laboratory, California Institute of Technology, under a contract with the National Aeronautics and Space Administration.

REFERENCES

- [1] P. Bender, and K. Danzmann 1998, “*Laser Interferometer Space Antenna for the detection of gravitational waves, pre-Phase A report,*” MPQ233, Max-Planck-Institüt für Quantenoptik, Garching, Germany, July 1998.
- [2] M. Tinto, and J. W. Armstrong 1999, *Physical Review D*, **59**, 102003.
- [3] J. W. Armstrong, F. B. Estabrook, and M. Tinto 1999, *Astrophysical Journal*, **527**, 814.
- [4] F. B. Estabrook, M. Tinto, and J. W. Armstrong 2000, *Physical Review D*, **62**, 42002.
- [5] M. Tinto, J. W. Armstrong, and F. B. Estabrook 2000, *Physical Review D Rapid Communications*, in press.

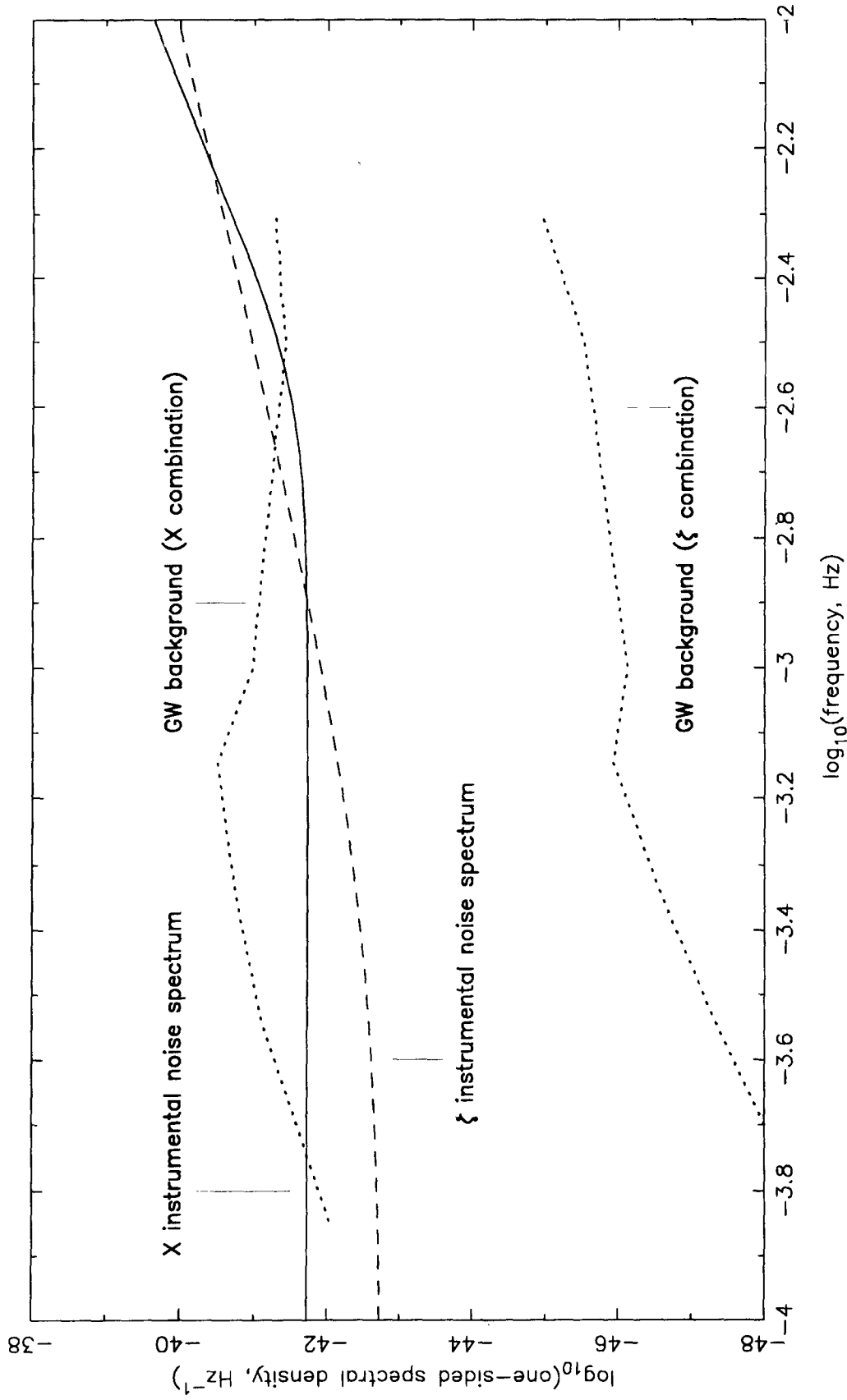


Figure 1. Fractional Doppler frequency instrumental noise power spectra for data combinations X (solid line) and ζ (dashed line). These are derived from the transfer functions for X and ζ to instrumental noises and the nominal LISA spectra for individual proof mass noise [$3 \times 10^{-15} (m/sec^2)/\sqrt{Hz}$] and one-way optical path noise [$20 \times 10^{-12} m/\sqrt{Hz}$], converted to fractional Doppler spectra. Also plotted are the spectral responses of X and ζ to the expected stochastic gravitational wave background, as discussed by Bender and Hils [3] and Hils [4]. Using ζ to measure on-orbit instrumental noise allows a gravitational wave background in X to be either uniquely determined or bounded.

Questions and Answers

ROBERT NELSON (Satellite Engineering Research Corporation): It might be appropriate to note that Dr. Joseph Webber of the University of Maryland passed away this past September. Dr. Webber founded the whole subject of experimental gravitational wave detection at the University of Maryland. In addition, in the late 1940s, he published one of the first papers on the notion of a population inversion concept that was the foundation for the invention of the maser.

Over the last decade or so, Dr. Webber did analyses that indicate some evidence of gravitational wave detection by VAR detectors at the University of Maryland and in Rome which were correlated to observations of neutrinos that were associated with the supernova, I believe it was 1985. One of the things that you might consider in the future is, in light of that type of analysis, is to correlate your own gravitational wave measurements with other sources such as neutrinos which, according to theory, are produced in gravitational collapse events.

MASSINO TINTO: Yes, I would like to add and I should have said it earlier, this particular instrument will work in the millihertz frequency band. So we are expecting to observe sources that will not be in the kilohertz frequency band where less detectors were operating. So supernova light is frozen and will not very likely be in this span of observations. Usually supernova explosions are accompanied by neutrino emissions.

The reason for this analysis, in a sense, is really trying to assess where the sensitivity is without relying on other instruments. In a sense, it would corroborate your observation. So once you know what the sensitivity curve is, anything that is above it, you know, sort of classifies as other sources.

DEMETRIOS MATSAKIS (USNO): Is there any timing requirements that you could talk about with this system?

TINTO: Yes, and I am getting to that. You see, when you actually phase for the phase differences from these Doppler measurements, you have to take into account that the spacecraft are moving relative to each other and is not stationary. So at 10^{-14} hertz, which is the frequency of the laser, the relative speed of 10 meters per second introduces big nodes of several megahertz. You have to track that bit node in your phase measurement. To do that, we rely on USOs, so we have a timing system aboard this spacecraft that allows us to measure the phase and then, on the other hand, introduce noise. It is so noisy, and we want to remove that noise. There are techniques to eventually remove this noise measurement introduced by the USOs which are incorporated into this interferometric technique that we have. So the system is certainly has on-board timing systems and timing requirements. In fact, we rely on state-of-art USOs in order to do these measurements. We need parts in 10^{15} or better USO performances.

But I didn't want to present all the details of the timing system on board the spacecraft.

MATSAKIS: It is covered in your published paper though.

TINTO: Yes, this is published and will be in the Proceedings anyway.

THOMAS CLARK (NASA Goddard Space Flight Center): I had looked at a similar type interferometer at one time, and maybe I don't understand the measurement. If you are talking about the laser measuring carrier phase of the laser—if I did the calculations you are talking about, travel times of about 16 seconds—that means that you have to have an intrinsic oscillator stability at the laser frequency to something better than one sixteenth of a hertz. Probably more like 10 millihertz at 10^{14} hertz. So that says you are expecting a laser to have an intrinsic

frequency stability over the Allan variance at the travel time, 16 seconds, of something like a part in 10^{16} .

TINTO: No, no, we don't need that. Even parts in 10^{13} you have to know accuracy of the uplink. The separation of the spacecraft is only 50 meters or so. If you know the uplink, then you can combine to six measurements in such a way as to remove the fluctuations of the laser to the level that you want to.

CLARK: The other question I was going to ask has to do with the background noise, which is a different one. I will have to think about your comment on that one. When we had thought about this in terms of a slightly different program, rather than the gravitational wave background noise, the gravity field background noise looked to me to be a serious problem. For instance, the gravity field changes at this interferometer location due to Venus orbiting around Mars are many times the effect of the signal that you are seeing. The gravity noise due to essentially all of the undetected and unmodeled asteroids looked to me like they would give so much position noise across the interferometer that gravity field could not be detectable. Have you thought in terms of just the solar system gravity noise?

TINTO: I think that has been included in the Phase A report, which you will find at that Web site that I gave. I believe the conclusion was that that was not a problem. Also, you have to take into account the time scales that you are talking about. LISA will be 1,000 to 10,000 seconds or so up to 1 second integration time. Most of the facts we're concerned about is the time scale completely outside the band. It will not be affecting the performance of the instrument. Other things have been analyzed and found not to be significant. To get the details, I can point out the references.

But I think the key point here for LISA is that you can actually synthesize an interferometer, which means you can remove the fluctuations of the laser. It requires a knowledge of the uplink. So going to your first question, if you know the uplink with an aperture of 30 meters or something, then you can combine these six Doppler measurements in such a way as to remove those fluctuations. So you need the laser at part in the 10^{13} or so. Even worse, if your knowledge of the uplink is better.

THEORETICAL AND EXPERIMENTAL STUDY OF LIGHT SHIFT IN A CPT-BASED RB VAPOR CELL FREQUENCY STANDARD

M. Zhu and L. S. Cutler
Agilent Laboratories
3500 Deer Creek Rd., Palo Alto, CA 94304, USA

Abstract

One of the important subjects in coherent-population-trapping-based (CPT-based) vapor cell frequency standards is the light shift (ac Stark shift). We calculate the light shift using a numerical method and perturbation approximation. Experimentally, we measure light shift using a pair of phase-locked diode lasers as well as a frequency-modulated diode laser. There is good agreement between theory and experiment. A method of controlling light shift in CPT-based frequency standards is proposed and implemented in Agilent Laboratories. The short-term stability of our CPT-based rubidium vapor cell frequency standard is measured as $1.3 \times 10^{-12} \tau^{-1/2}$, which is limited by the phase noise of the reference local oscillator used.

I. INTRODUCTION

Since it was observed^[1] and explained theoretically,^[2, 3] coherent population trapping (CPT) has been found in many applications.^[4 – 10] Its application in atomic frequency standards has also attracted a lot of attention.^[5, 11 – 13] In a CPT-based vapor cell atomic frequency standard, the potential elimination of the microwave excitation^[4, 5] promises a smaller and less expensive device. However, the light shift (ac Stark shift) in CPT-based atomic frequency standards is of great importance. Here we present our calculations and experimental measurements of the light shift in a CPT-based ⁸⁷Rb vapor cell frequency standard. Based on the calculations, we also show that the light shift in CPT-based atomic frequency standards can be controlled, or ultimately eliminated.

II. REVIEW OF THE CONCEPTS

The light shift (ac Stark shift) is the energy level shift that originates from the interaction between the atom and the applied ac electromagnetic field.^[14] Fig. 1(a) shows a two-energy-level atom interacting with a single frequency laser field with a Rabi frequency Ω , and a detuning $\Delta \equiv \omega_L - \omega_0$. This resembles part of a simple optical pumping scheme used in atomic frequency standards. Since the Rabi frequency Ω is usually much less than the spontaneous decay rate of the upper state $|e\rangle$, the light shift can be calculated using perturbation approximation.^[15, 16] The perturbation approximation can be readily expanded to include the case involving multiple atomic energy levels and multiple laser frequency components. Alternatively, the light shift can be obtained using the concept of the dressed state,^[14, 17] which gives a more intuitive physical explanation. The energy level shift (light shift) of the lower state $|g\rangle$ is given by

$$\delta E_g = \frac{\hbar}{4} \frac{|\Omega|^2 \Delta}{\Delta^2 + \gamma^2} \quad (1)$$

where γ is the decay rate of the excited state $|e\rangle$. The light shift in Eq. (1) has a dispersion line shape, the magnitude of which decreases inversely proportional to the detuning Δ when the detuning is large.

Coherent population trapping can happen in a three-energy-level atom interacting with a dual-frequency laser field as shown in Fig. 1(b). The two transitions from $|g_i\rangle$ to $|e\rangle$ driven by laser frequency ω_{Li} ($i = 1, 2$) are essential for CPT generation, so we call them CPT-generating interactions. In Fig. 1(b), we temporarily exclude the interaction of the frequency component with frequency ω_{L1} (ω_{L2}) and induced electric dipole moment between the upper state $|e\rangle$ and the lower state $|g_2\rangle$ ($|g_1\rangle$) in order to keep the following analysis simple. Using the rotating wave approximation (RWA), one can write the interaction Hamiltonian as

$$\hat{H}_I = \frac{1}{2} \hbar \Omega_1 e^{-i\omega_{L1}t} |e\rangle\langle g_1| + \frac{1}{2} \hbar \Omega_1^* e^{i\omega_{L1}t} |g_1\rangle\langle e| + \frac{1}{2} \hbar \Omega_2 e^{-i\omega_{L2}t} |e\rangle\langle g_2| + \frac{1}{2} \hbar \Omega_2^* e^{i\omega_{L2}t} |g_2\rangle\langle e| \quad (2)$$

where Ω_1 and Ω_2 are the Rabi frequencies of the corresponding transitions. When the resonance condition $\Delta_1 = \Delta_2$ is approximately satisfied, coherent population trapping (CPT) occurs, i.e., a specific coherence between the two lower states $|g_1\rangle$ and $|g_2\rangle$ forms a *dark state* given by

$$|\text{dark state}\rangle = \frac{\Omega_2}{\sqrt{|\Omega_1|^2 + |\Omega_2|^2}} e^{i\omega_{L1}t} |g_1\rangle - \frac{\Omega_1}{\sqrt{|\Omega_1|^2 + |\Omega_2|^2}} e^{i\omega_{L2}t} |g_2\rangle. \quad (3)$$

The dark state satisfies the condition

$$\langle e | \hat{H}_I | \text{dark state} \rangle = 0 \quad , \quad (4)$$

i.e., the dark state does not interact with the applied laser field. Hence, CPT lasts until the relaxation process between the two lower states destroys the coherence described by Eq. (3). For a given detuning, $\Delta \equiv \Delta_1 - \Delta_2$, the probability of finding the atom in the dark state is determined by the optical Rabi frequencies and relaxation rate between the lower states, γ_g . If there is an energy level shift, due to the interaction with external electromagnetic fields, in one or both lower states, the difference of the shifts can be measured in the laser frequency difference $\omega_{L1} - \omega_{L2}$, when the resonance condition, $\Delta \equiv \Delta_1 - \Delta_2 = 0$ is satisfied. The resonance condition for CPT generation can be detected using any combination of fluorescence, transmission, and microwave emission (by the magnetic dipole associated with the dark state). When the optical signal is detected, no microwave cavity is required for implementation of the CPT-based atomic frequency standards. Fig. 2 shows the detected optical signals associated with the CPT-generation in a small ^{87}Rb vapor cell.

III. LIGHT SHIFT IN CPT-BASED FREQUENCY STANDARDS

In a practical atomic frequency standard, the choice of the lower states, e.g., the sub-states $|F=L\pm 1/2, m_F=0\rangle$ in an alkaline atom's ground state, allows more transitions than the ones shown in Fig. 1(b) according to selection rules. The frequency component with frequency ω_{L1} (ω_{L2}) can also interact with induced electric dipole moment between the states $|e\rangle$ and $|g_2\rangle$ ($|g_1\rangle$) although it is detuned from resonance. When a single laser with frequency modulation (FM) is used for CPT-generation, every frequency component interacts with the induced electric dipole moment between the states $|e\rangle$ and $|g_1\rangle$ and the one between the states $|e\rangle$ and $|g_2\rangle$. The calculation has to take all these interactions into account. Typically, all the non-CPT-generating interactions have large detunings and low Rabi frequencies, so that they do not affect the CPT-generation process significantly. Therefore, it is justified that we consider the effects of the two CPT-generating interactions first, and treat the non-CPT-generating interactions as the perturbations. We will show that these non-CPT-generating interactions dominate the contributions to the light shift of the two lower states, $|g_1\rangle$ and $|g_2\rangle$, which are used to define the frequency standard. Based on these calculations, we propose a method to control or to ultimately eliminate the light shift.

III.1 LIGHT SHIFT FROM THE CPT-GENERATING INTERACTIONS

To calculate the effects of the two CPT-generating interactions we use the simplified system in Fig. 1(b). The density matrix equation for this system is

$$i\hbar \frac{d}{dt} \hat{\rho} = [\hat{H}_0 + \hat{H}_I, \hat{\rho}] - \frac{1}{2} i\hbar [\hat{\Gamma}\hat{\rho} + \hat{\rho}\hat{\Gamma}] \quad (5)$$

where \hat{H}_0 is the Hamiltonian for the internal atomic states, \hat{H}_I is given by Eq. (2), and $\hat{\Gamma}$ describes all the relaxation processes. Although the analytical solution for the steady state of this equation was given in the literature,^[18] it is not trivial to interpret the physical meaning of the solution. The perturbation approximation was also used to solve this equation.^[13] The results showed that the light shifts of the two lower states are the same for the dark state (with coherence shown in Eq. (3)) and for the case where there is no coherence between the lower states.

Here we solve Eq. (5) for a steady state solution in a closed form without further approximations. First the result is used for calculating the CPT under different parameter settings. Then this closed form result is used for the numerical calculation of the light shift difference between the lower states $|g_1\rangle$ and $|g_2\rangle$, which is the physical quantity measured in a frequency standard. We find out that the light shift difference between the lower states is much smaller in comparison with the one obtained without considering the coherence in Eq. (3). Fig. 3 shows an example of the light shift difference in the dark state vs. detuning with $2\Omega_1 = \Omega_2$. The result from the calculation without the presence of coherence is also shown in Fig. 3 for comparison. This small light shift is not a surprising result because the lack of the interaction between the dark state and the applied laser field, shown in Eq. (4), removes the light shift, at least to the lowest order. Therefore, we conclude that the light shift difference between the lower states from the two CPT-generating interactions is small enough, at least for the vapor cell type atomic frequency standards. However, the light shift from the non-CPT-generating interactions could be significant, and will be calculated in the next sub-section.

III.2 LIGHT SHIFT FROM THE NON-CPT-GENERATING INTERACTIONS

We start with the density matrix equation shown in Eq. (5) for the calculation of the light shift from the non-CPT-generating interactions. Here the interaction Hamiltonian only includes the non-CPT-generating interactions. Using perturbation approximations, one can eliminate the excited states in Eq. (5).^[16] The equivalent density matrix equation for the ground states can be written as

$$i\hbar \frac{d}{dt} \hat{\rho}^G = \left[\left(\hat{H}_0^G + \delta \hat{H}^G \right), \hat{\rho}^G \right] - \frac{1}{2} i\hbar \left[\left(\hat{\Gamma}^G + \delta \hat{\Gamma}^G \right) \hat{\rho}^G + \hat{\rho}^G \left(\hat{\Gamma}^G + \delta \hat{\Gamma}^G \right) \right] \quad (6)$$

where the superscript G designates the operators to the ground states. Due to the existence of the non-CPT-generating interactions, in Eq. (6), the equivalent operators $\delta \hat{H}^G$ and $\delta \hat{\Gamma}^G$ represent the extra interactions and relaxations, respectively, among all the ground states. For each laser frequency component with an amplitude \vec{E}_j and an angular frequency ω_{Lj} , we define the generalized Rabi frequency $\Omega_{m\mu}^j$ and detuning $\Delta_{m\mu}^j$ as

$$\Omega_{m\mu}^j \equiv \frac{1}{\hbar} \vec{E}_j \cdot \langle m | \hat{d} | \mu \rangle \quad (7a)$$

$$\Delta_{m\mu}^j \equiv \omega_{Lj} - \frac{1}{\hbar} (E_m - E_\mu) \quad (7b)$$

where $\langle m | \hat{d} | \mu \rangle$ is the induced electric dipole moment between the excited state $|m\rangle$ and ground state $|\mu\rangle$. Then corresponding matrix elements of operators $\delta \hat{H}^G$ and $\delta \hat{\Gamma}^G$ are given by

$$\langle v | \delta H^G | \mu \rangle = \frac{\hbar}{4} \sum_j \sum_m \frac{\Omega_{vm}^j \Omega_{m\mu}^j \Delta_{m\mu}^j}{\Delta_{m\mu}^{j^2} + \gamma_m^2} + \frac{\hbar}{4} \sum_j \sum_{k \neq j} \sum_m \frac{\Omega_{vm}^k \Omega_{m\mu}^j \cos(\omega_{jk} t + \theta_{m\mu}^j)}{\sqrt{\Delta_{m\mu}^{j^2} + \gamma_m^2}} \quad (8a)$$

$$\langle v | \delta \Gamma^G | \mu \rangle = \frac{1}{2} \sum_j \sum_m \frac{\Omega_{vm}^j \Omega_{m\mu}^j \gamma_m}{\Delta_{m\mu}^{j^2} + \gamma_m^2} + \frac{1}{2} \sum_j \sum_{k \neq j} \sum_m \frac{\Omega_{vm}^k \Omega_{m\mu}^j \sin(\omega_{jk} t + \theta_{m\mu}^j)}{\sqrt{\Delta_{m\mu}^{j^2} + \gamma_m^2}} \quad (8b)$$

$$\theta_{m\mu}^j \equiv \tan^{-1} \frac{\gamma_m}{\Delta_{m\mu}^j} \quad (8c)$$

where the sum of m is for all the excited states; sums of j and k are for all the frequency components. We write the non-oscillating terms and oscillating terms (with a frequency on the order of hyperfine splitting) separately in Eq. (8) because they have different effects on the ground states. In a typical vapor cell atomic frequency standard, the interaction strength, which is equivalent to the Rabi frequency, for each term in Eq. (8a) is much smaller than the relaxation rate among the ground states. Similarly, the rate of each term in Eq. (8b) is much smaller than the relaxation rate among the ground states. Therefore, the most important effect from Eq. (8) is the light shift, which is represented by the diagonal matrix element $\langle v | \delta H^G | v \rangle$. The

effect of the oscillating term in $\langle v | \delta H^G | v \rangle$ is averaged to zero while the non-oscillating term gives the light shift of state $|v\rangle$, which is similar to the one in Eq. (1). Although some of the oscillating terms in the off-diagonal matrix element $\langle v | \delta H^G | \mu \rangle$ can be in resonance with the transition used for frequency standards, their effects are still small due to the small interaction strength.

III.3 METHODS TO CONTROL OR ELIMINATE LIGHT SHIFT

From the above analysis, we demonstrate that one is able to control the total light shift in the CPT-based frequency standards by controlling the intensities and/or the frequencies of the non-CPT-generating frequency components.^[19] For example, one can add one or more non-CPT-generating interactions by introducing extra frequency components with desired intensities and frequencies to suppress the total light shift in the system. When a single FM laser is used for CPT generation, it is very convenient to control the total light shift using the frequency modulation index. Fig. 4 shows the total light shifts vs. frequency modulation index with a single FM laser. The residual amplitude modulation (AM) could change the modulation index for zero total light shift slightly. Fig. 5 shows the light shifts vs. detuning with different frequency modulation indices.

All the above light shifts in Fig. 4 and Fig. 5 are calculated in an optically thin absorption medium. In a practical vapor cell atomic frequency standard, the absorption in the vapor is significant. If the vapor cell is filled with buffer gas, the atoms are localized due to the collision with the buffer gas molecules. Therefore, the light shift in the vapor cell varies with the position due to the absorption of different frequency components. The contribution to the detected signal also varies with the position in the vapor cell. Furthermore, these variations depend on the input laser beam intensity due to the balance between the CPT-generating process and the relaxation process among the ground states. The saturation effect is usually small. To compare the calculation with experimental results, we have to take all these factors into account. The possible exception is the case where one uses an FM laser with a small modulation index. The dominating contribution of the light shift in this case is from the laser carrier frequency that is not absorbed significantly within the vapor cell.

IV. EXPERIMENTAL RESULTS

We use a ^{87}Rb vapor cell in our experimental study of the light shift in the CPT-based frequency standard. We use the D₁-line for CPT-generation, as shown in Fig. 1(c). The laser source consists of either a pair of phase-locked diode lasers or a single diode laser with frequency modulation at 3.4 GHz. In the case of using an FM laser, the ± 1 st order sidebands are used for CPT-generation. The optical power ratio of these two sidebands is measured as $|J_{+1}/J_{-1}|^2 \approx 1.2$ for most of our measurements due to residual amplitude modulation. The averaged power in the ± 1 st order sidebands is used to estimate the frequency modulation index, which can readily reach 3. The laser beam is collimated and truncated just before it enters the vapor cell. The intensity variation across the beam is less than 10%, so that in the calculation we only consider the intensity variation in the vapor cell along the propagation direction of the laser beam.

Fig. 6 shows the measured light shift with a pair of phase-locked diode lasers. The laser frequencies are locked to the peak absorption corresponding to the excited state $|F'=2\rangle$. Using the results in sub-section

III.2, we expect the positive light shift. To compare the experimental results with the calculation, the transmitted laser beam power is also measured to determine the absorption in the cell. By integrating the signal and the light shift along the absorption cell, the calculation of the total light shift is also shown in Fig. 6. The discrepancy between the calculation and the measurements is less than 5%.

Fig. 7 shows the measured light shifts using a single FM diode laser. We attribute the curvature of the light shift with a fixed modulation index to the factors discussed in sub-section III.3. It is clear from Fig. 7 that the light shift can be reduced or eliminated in the CPT-based vapor cell frequency standard by choosing the proper modulation index. The measured light shift can be used in a slow servo system to control the modulation index dynamically. Fig. (8) shows the light shift is suppressed using such a servo system with an incorrect initial modulation index setting.

We use a single FM diode laser to study the frequency stability of our CPT-based Rb vapor cell frequency standard. The frequency modulation index is either set or controlled to minimize the total light shift. The frequency stability is measured in comparison with an in-house ensemble consisting of two Agilent 5071A cesium-beam frequency standards. Fig. 9 shows the measured Allan deviations. Fig. 9 also shows the short-term frequency stability measurement ($1\text{s} \leq \tau \leq 4000\text{s}$) using a diode laser pumped Rb vapor cell frequency standard (not CPT-based) as a frequency reference. In this measurement, the frequency/phase noise from both the CPT-based Rb frequency standard and the reference contribute to the short-term stability $\sim 1.3 \times 10^{-12} \tau^{-1/2}$ and the flicker noise floor $\sim 1.4 \times 10^{-13}$. From the individual signal-to-noise measurements, we determine that the short-term stability is about the same for both the CPT-based Rb frequency standard and the reference. Removing the noise contribution from the reference, we expect the short-term stability to be $1 \times 10^{-12} \tau^{-1/2}$ and the flicker noise floor at $\sim 1 \times 10^{-13}$ for the CPT-based Rb frequency standard. The frequency drift of our CPT-based frequency standard is shown in Fig. 10. Apparently there is a frequency change with a period of 24 hours in our preliminary setup, especially during the weekends, when the temperature control of the building works in a different mode. This frequency change determines the Allan deviation for $\tau \approx 10,000\text{s}$, as shown in Fig. 9.

V. CONCLUSION

The calculation and measurement of light shift in CPT-based vapor cell frequency standards are presented. Our results show that the light shift could be significant. We present a general method^[19] to suppress the light shift in CPT-based vapor cell frequency standards. We also present the short-term frequency stability measurement of our CPT-based rubidium vapor cell frequency standard using a single FM diode laser. By implementing the light shift control method, it is feasible to make a compact, moderately inexpensive CPT-based vapor cell frequency standard with good performance.

VI. ACKNOWLEDGMENTS

We are greatly indebted to Robin Giffard for beneficial discussions. We also gratefully acknowledge Jim Johnson and Ray Wong for their help in the project.

VII. REFERENCES

- [1] G. Alzetta, A. Gozzini, L. Moi, and G. Orriols, *Nuovo Cimento B* **36**, 5 (1976).
- [2] E. Arimondo and G. Orriols, *Lett. Nuovo Cimento* **17**, 333 (1976).
- [3] G. Orriols, *Nuovo Cimento* **53**, 1 (1979).
- [4] J. Thomas, S. Ezekiel, C. Leiby, R. Picard, and C. Willis, *Opt. Lett.* **6**, 298 (1981).
- [5] J. Thomas, P. Hemmer, S. Ezekiel, C. Leiby, R. Picard, and C. Willis, *Phys. Rev. Lett.* **48**, 867 (1982).
- [6] A. Aspect, E. Arimondo, R. Kaiser, N. Vansteenkiste, and C. Cohen-Tannoudji, *Phys. Lett.* **61**, 826 (1988).
- [7] M. O. Scully, *Phys. Rev. Lett.* **67**, 1855 (1991).
- [8] M. O. Scully, *Phys. Rep.* **219**, 191 (1992).
- [9] E. Arimondo, *Prog. Opt.* **XXXV**, 257 (1996), and the references therein.
- [10] S. Brandt, A. Nagel, R. Wynands, and D. Meschede, *Phys. Rev. A* **56**, R1063 (1997).
- [11] P. Hemmer, V. Natoli, M. Shahriar, B. Bernacki, H. Lamela-Rivera, S. Smith, and S. Ezekiel, in *Proceedings of the 1987 IEEE International Frequency Control Symposium*, p. 42.
- [12] N. Cyr, M. Tetu, and M. Breton, *IEEE Trans. Instrum. Meas.* **42**, 640 (1993).
- [13] J. Vanier, A. Godone, and F. Levi, *Phys. Rev. A* **58**, 2345 (1998).
- [14] See, for example, C. Cohen-Tannoudji, J. Dupont-Roc, and G. Grynberg, *Atom-Photon Interactions*, (John Wiley & Sons, New York 1992).
- [15] See, for example, L. Schiff, *Quantum Mechanics*, (McGraw-Hill Book Company, New York 1968).
- [16] See, for example, W. Happer, *Rev. of Mod. Phys.* **44**, 169 (1972), and the references therein.
- [17] C. Cohen-Tannoudji, in *Frontiers of Laser Spectroscopy*, R. Balian, S. Haroche, and S. Liberman, eds. (North-Holland Publishing Company, Amsterdam 1977).
- [18] See, for example, R. Brewer and E. Hahn, *Phys. Rev. A* **11**, 1641 (1975).
- [19] U. S. Patent pending.

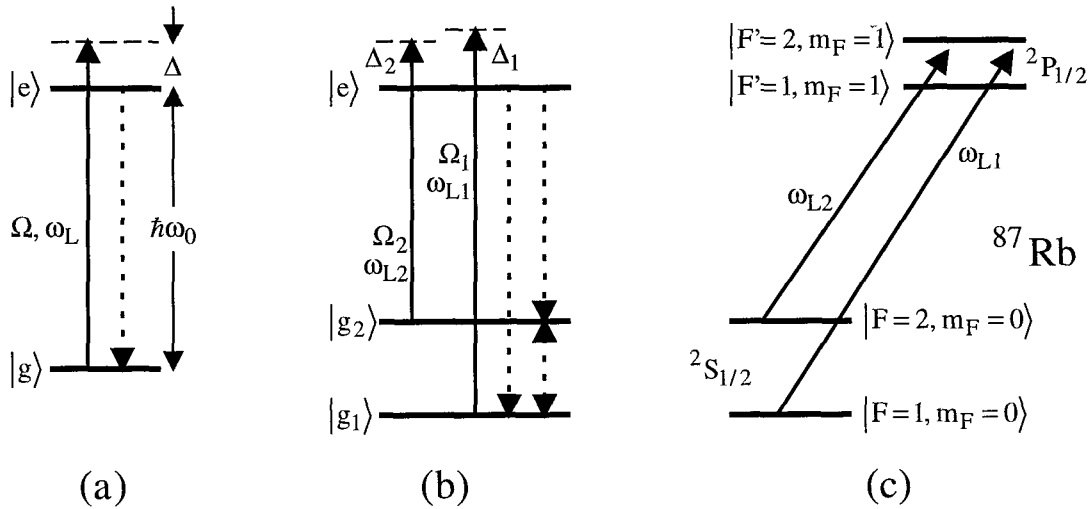


Figure 1. (a) A two-energy-level atom interacting with a single frequency laser field for calculation of light shift. (b) A three-energy-level atom interacting with a dual-frequency laser field for CPT-generation. (c) Part of the energy levels in a ^{87}Rb atom for implementing a CPT-based frequency standard. Only two laser frequency components driving the CPT-generating interactions are shown explicitly. Relaxation processes are presented by dashed lines in (a) and (b), but are not shown in (c) explicitly.

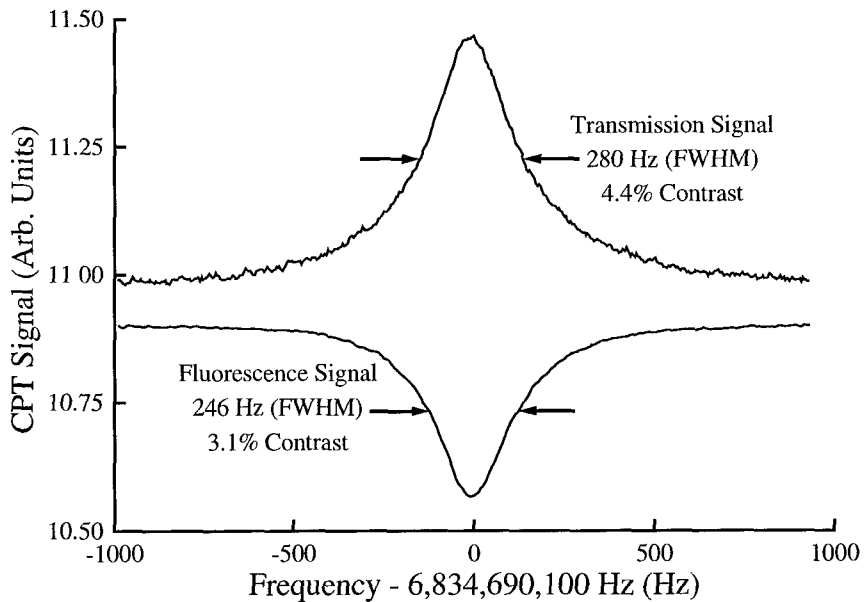


Figure 2. Transmission and fluorescence signals of coherent population trapping in a ^{87}Rb vapor cell. A single FM laser is used with frequency modulation index about 2.2. A solid angle of ~ 1.2 steradian is covered by the photo-detector for fluorescence detection.

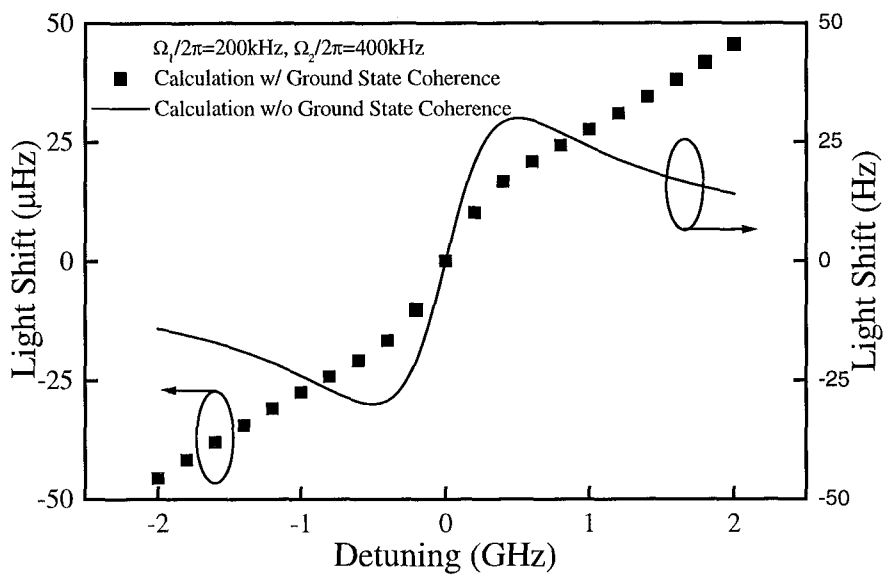


Figure 3. Calculated light shifts from CPT-generating interactions.

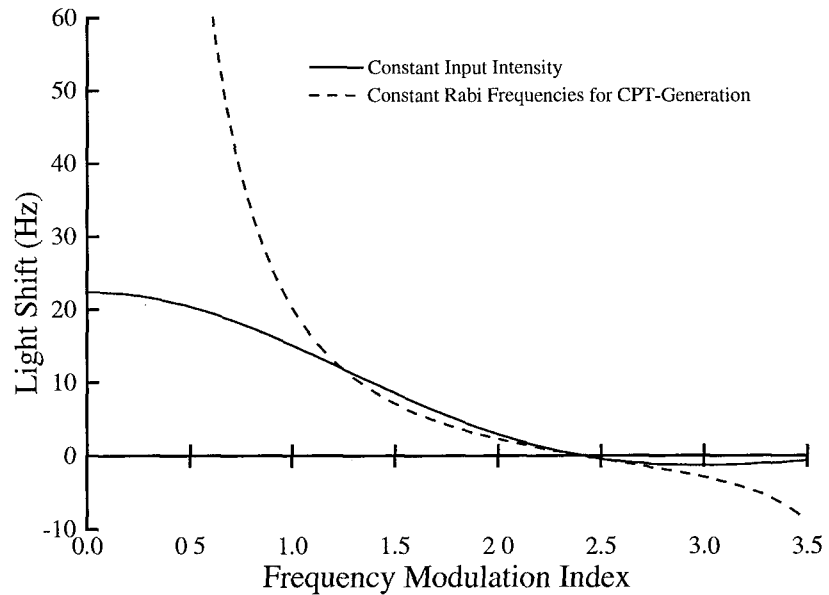


Figure 4. Calculated light shifts vs. frequency modulation index. The Rabi frequencies for both CPT-generating interactions are 200 kHz when FM index equals to 2.45.

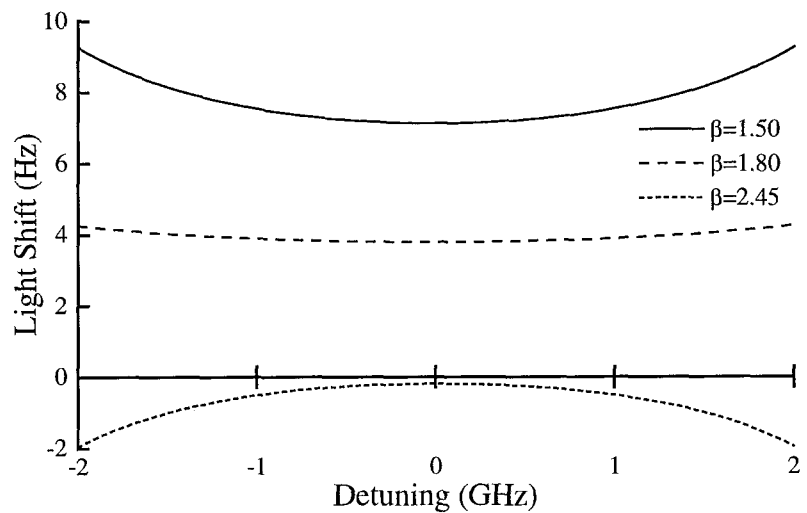


Figure 5. Calculated light shifts vs. detuning. The Rabi frequencies are 200 kHz for both CPT-generating interactions.

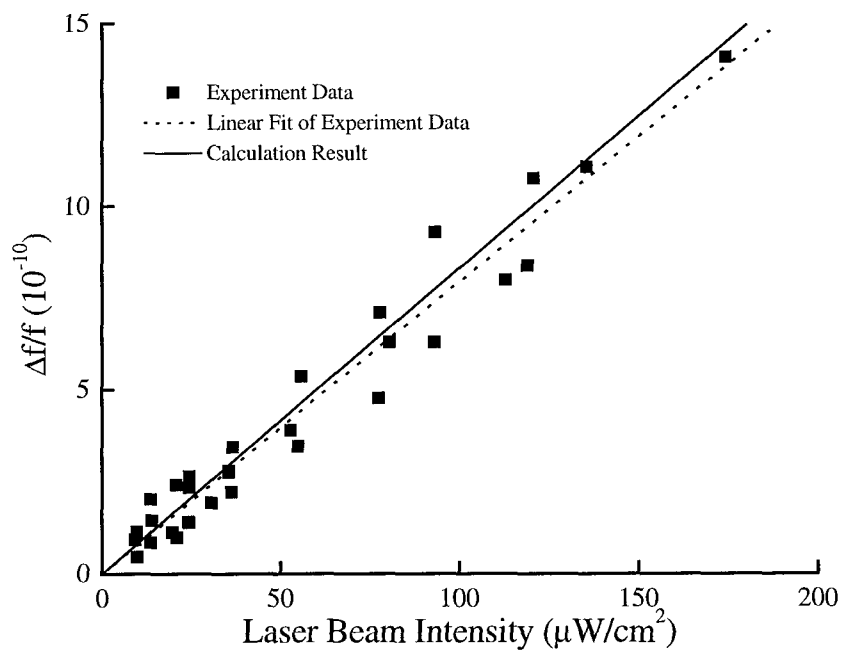


Figure 6. Light shifts in a CPT-based ^{87}Rb vapor cell frequency standard using a pair of phase-locked diode lasers.

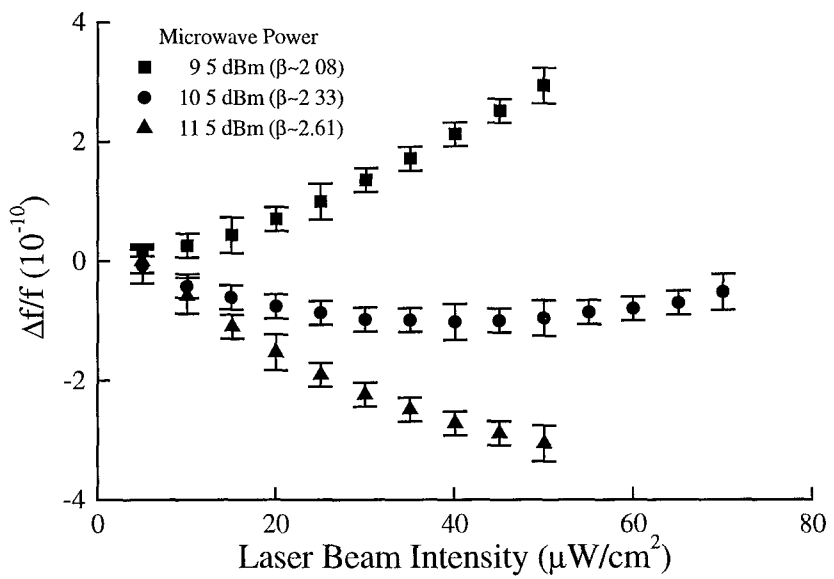


Figure 7. Light shifts in a CPT-based ^{87}Rb vapor cell frequency standard with an FM laser.

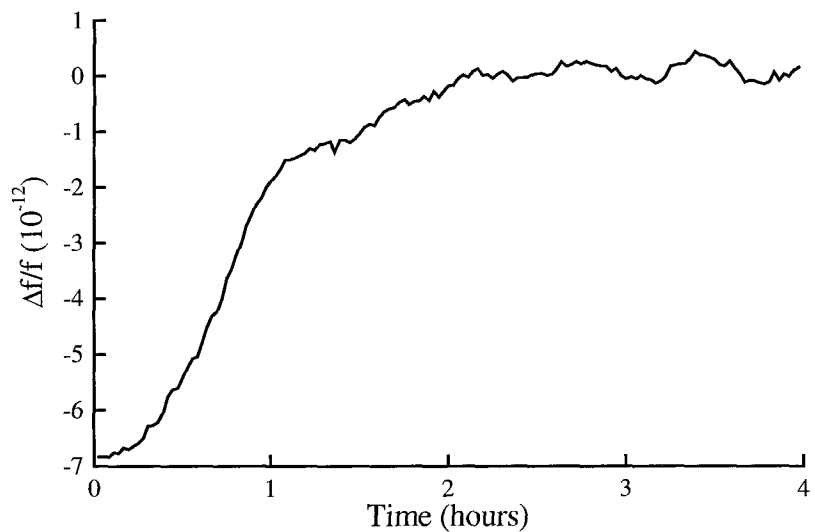


Figure 8. Correction of the initial offset of frequency modulation index.

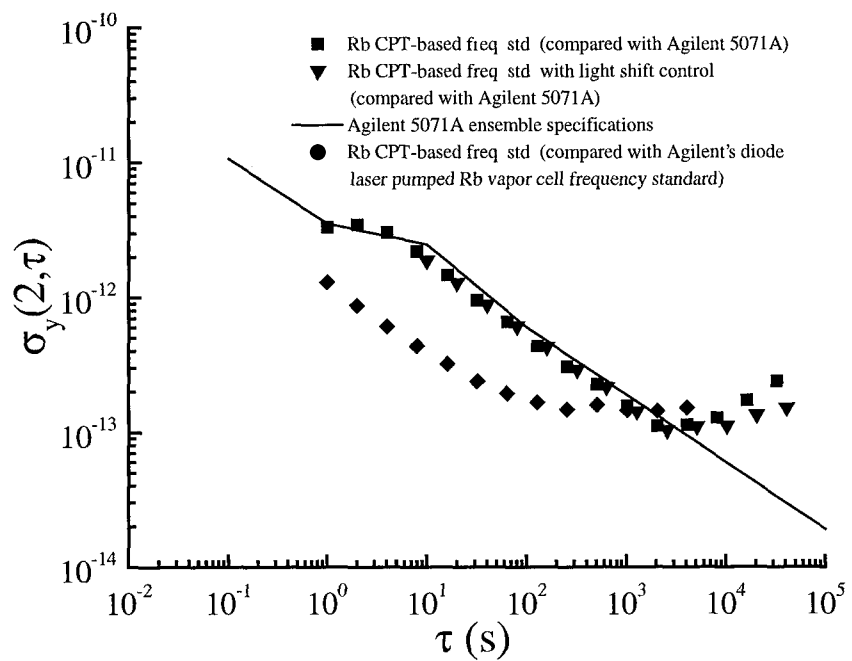


Figure 9. Short-term stability measurements of a CPT-based ^{87}Rb vapor cell frequency standard.

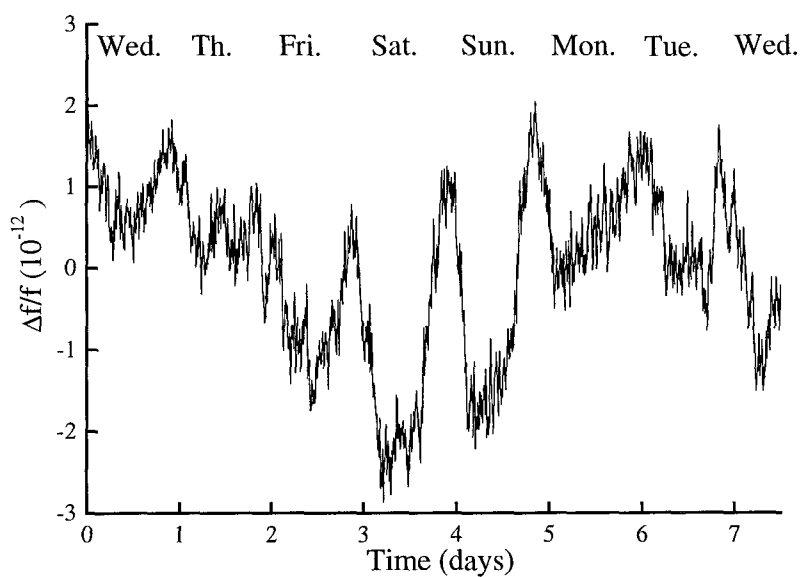


Figure 10. Relative frequency drift of a CPT-based ^{87}Rb vapor cell frequency standard.

Questions and Answers

ROBERT LUTWAK (Datum): When you servo the microwave power to eliminate the light shift, what do you servo to? To what are you leveling that signal?

MIAO ZHU: Do you mean what I servo to or where did I do the servo?

LUTWAK: What is the error signal that determines the TR microwave modulation as causing a non-zero light shift?

ZHU: You can modulate it or have it at a low frequency and that can drive that signal from there.

PRELIMINARY RESULTS FROM THE USNO ATOMIC FOUNTAIN DEVELOPMENT PROJECT

Thomas B. Swanson, Eric A. Burt, and Christopher R. Ekstrom
U.S. Naval Observatory
Washington, DC 20392, USA

Abstract

Atomic fountain clocks are emerging as an important new technology for the realization of extremely precise passive atomic standards. The U.S. Naval Observatory (USNO) has undertaken a project to develop atomic fountains for eventual incorporation into the USNO Master Clock.

We have recently demonstrated short-term stability of 2×10^{-13} at 1 second with white frequency behavior into the mid 10^{-15} 's in our first cesium R&D device. We report on these results and hope to have frequency measurements relative to internal timescales at the USNO. We also discuss plans for more heavily engineered operational devices and their incorporation into the USNO Master Clock.

INTRODUCTION

The last decade has seen advances in laser cooling and trapping that have allowed the practical construction of atomic fountain frequency standards. These devices are now producing results at several national standards institutions [1].

We have undertaken a program to integrate atomic fountain clocks into the timing ensemble at the USNO. The mission of the Observatory does not require that any of our standards be accurate realizations of the second, only that they be stable and run continuously. In support of that mission, the observatory maintains an ensemble of atomic clocks that consists of approximately 60 commercial cesium-beam standards and 14 hydrogen masers. These standards are used to compute and produce several timescales, most importantly UTC(USNO). Our goal is to have several atomic fountain standards running with a short-term stability of $1 - 2 \times 10^{-13} \tau^{-1/2}$ and a statistical floor of $1 - 3 \times 10^{-16}$ to improve the medium- and long-term stability of the ensemble.

Because our goal is precision rather than accuracy, we are primarily interested in minimizing fluctuations in systematic contributions. Also, although this fountain uses cesium, future devices will use rubidium in order to take advantage of the smaller cold-collision shift [2].

EXPERIMENTAL LAYOUT

The physical layout of our cesium fountain is shown in Figure 1. In addition to the small optical table that houses the vacuum chamber, there is a larger table that houses all of the lasers, with optical fiber coupling of all light onto the table with the vacuum chamber. All background pressures in the vacuum chamber are below 4×10^{-8} Pa.

LASERS

We collect atoms in either a magneto-optic trap (MOT) or molasses and then cool and launch them in an optical lattice with a (1,1,1) geometry. The laser light for the upward- and downward-directed laser beams originates with a low-power diode laser which is frequency stabilized and injection-locks a second diode laser. The 100 mW output from this second laser separately injection-seeds two tapered amplifiers with independent frequency control, and also provides the detection light. The collection and launching light from the tapered amplifiers and the detection light are transported to the vacuum chamber with optical fibers. All of these beams have power servos closed around the fiber path to reduce amplitude noise at the atoms. Collection and launching beams are expanded to 22 mm in diameter, with up to 30 mW of power per beam.

LAUNCHING

The atoms are launched in two phases. The first phase applies a violent acceleration for 1.4 milliseconds with an average detuning from resonance of 6 MHz. A second phase follows immediately with an average detuning of 40 MHz for 0.8 milliseconds, half the laser intensity, and a linear ramp of the intensity to zero at the end of the launch. We measure launch temperatures of $1.6 \pm 0.2 \mu\text{K}$ by monitoring the vertical width of the launched cloud when it passes the detection region both on the way up and on the way down, which allows us to remove the effects of initial cloud size.

STATE SELECTION

Immediately after launch, the atoms are pumped into the $F=4$ hyperfine levels with a vertical repumping beam tuned to the $F=3$ to $F'=4$ transition. The atoms are state-selected at the detection zone. They are exposed to a 3 millisecond long, shaped pulse of 9.2 GHz microwaves from an axial loop antenna inside the vacuum chamber. This pulse transfers the $F=4$, $m_F=0$ atoms to the $F=3$, $m_F=0$ state. The remaining $F=4$ atoms are removed from the atomic sample by radiation pressure from a laser beam in the lower detection zone.

CAVITY, SHIELDS, AND DRIFT REGION

The microwave cavity and drift regions are temperature-stabilized to 0.1 °C and enclosed in a set of three magnetic shields. The shields are made from 1.6 mm thick moly permalloy (MIL-N-14411B, “comp 1”) and have an axial shielding factor of 35,000, measured by observing the Rabi pedestal shift of atoms launched through the cavity with an known external field perturbation. Details of the construction of the shields have been provided previously [3]. An axial solenoid provides a 225 nT magnetic field for the cavity and free precession regions.

DETECTION

After making two transits of the microwave cavity the atoms return to the detection region. The upper detection zone monitors the $F=4$ population and the laser beam removes these atoms from the sample due to an imbalance in the radiation pressure. The radiation pressure is exerted by an imbalance in the retroreflected intensity of the laser and by detuning 2 MHz to the blue of resonance. The remaining $F=3$ atoms are then optically pumped into the $F=4$ state by a thin sheet of light tuned to the $F=3$ to $F'=4$ transition. The lower detection zone monitors the $F=3$ population by detecting these optically pumped atoms. The signals are collected, background levels are subtracted from each signal, and the $F=4$ signal is normalized by the sum of the $F=3$ and $F=4$ signals.

We run the fountain with a total cycle time between 1.1 and 1.9 seconds.

RESULTS

Data were taken for experiments involving both the clock transition and a magnetic field sensitive transition. The local oscillator for these experiments is an active hydrogen maser from our clock ensemble. The microwave frequency chain is locked to a 100 MHz output of the maser. As the maser is separated from the fountain by a ~100 meter cable, we plan to move a maser into the same room as the atomic fountain in the near future.

CLOCK TRANSITION

Figure 2 shows a microwave Ramsey resonance pattern on the $F=3, m_F=0$ to $F=4, m_F=0$ clock transition from our fountain.

We have collected stability data by iteratively jumping between the half-height points on either side of the central fringe. The transition probability can be easily converted to a fractional frequency stability measurement of the local oscillator. Figure 3 shows the Allan deviation from a typical data set. The maser is more stable than the fountain on all time scales for this data set.

Because the maser is also monitored by our measurement systems, we can reference our frequency measurement of the maser to any other clock or average within our ensemble. This will also allow us to easily reference the long-term stability of our fountain to any other time scale, such as TAI or local realizations of UTC, which we monitor with our time transfer efforts.

MAGNETIC FIELD SENSITIVE TRANSITION

The fountain can also be run as a "flop-out" experiment, in which the atoms are not state-selected prior to their transit of the microwave cavity, so all magnetic sublevels of the $F=4$ state are populated. The cavity is tuned to the $F=4, m_F=-1$ to $F=3, m_F=-1$ transition. The atoms then make the transition to the $F=3, m_F=-1$ state as the cavity is tuned through the resonance. A stability plot generated by iteratively jumping between the half-height points on either side of a central fringe for this transition shows results that are consistent with a magnetic field fluctuation of less than 2 pT over $\sim 10^5$ seconds. This corresponds to a systematic fluctuation of $\sim 5 \times 10^{-18}$ on the field-insensitive clock transition. Figure 4 shows the Allan deviation on the field-sensitive transition.

During these experiments the MOT coils were turned off only for the launch and state selection phases, a duration of ~ 50 ms, in order to minimize the magnetic field fluctuations from shield relaxation.

SYSTEMATIC FLUCTUATIONS

The magnetic field fluctuations measured on the $m_F = -1$ transition correspond to a field fluctuation in the lab of ~ 50 nT, consistent with the expected variation in the earth's field. At this level these fluctuations would contribute less than 5×10^{-18} to our systematic floor, and the system could tolerate fluctuations several times larger, without the need for active cancellation of the external field. This would still be an acceptably small contribution to our systematic floor.

Temperature fluctuations contribute via the blackbody shift and the temperature-dependent cavity shift. Fluctuations of the cavity and drift region have been limited to 0.1 °C, which limit the combined systematic fluctuation below 5×10^{-17} .

OPERATIONAL POSSIBILITIES

We are considering several possible ways of running our fountain as a continuous clock. The first is to directly steer a high quality quartz crystal. The short-term stability of our best crystal will require us to close our steering control loop in 2 to 4 seconds. The steering interval also sets the time scale over which the fountain can be allowed to not steer the local oscillator.

We are planning on using a different method of producing a steered, continuous output that employs an active hydrogen maser as a local oscillator. This would allow a steering time of roughly 1 hour for the class of masers at our disposal. The steered output would be monitored by our local measurement systems and would be introduced into our timescales in an identical manner to all other classes of clocks at the USNO. We anticipate that with our expected fountain performance and the measured drift rates of the masers in our ensemble, that the fountain should be steering out the maser drift starting at 1 to 20 days. The longer steering interval greatly reduces the stress on the operating duty cycle of the underlying atomic fountain at the addition of considerable cost for the maser and steering generator. In addition, the medium-term stability of the unsteered maser is much better than that of an unsteered crystal.

It is our intention to build one more research device with rubidium atoms and to then produce up to five atomic fountains for operational use at the USNO and our alternate master clock facility in Colorado. We will use rubidium-based devices due to the dramatically smaller cold collision frequency shift [2].

CONCLUSIONS

In conclusion, we have observed reasonably high signal-to-noise microwave fringes in our atomic fountain with a preliminary stability of $2.0 \times 10^{-13} \tau^{-1/2}$ relative to an active hydrogen maser from our clock ensemble, meeting our short-term stability goal.

We have measured the magnetic field fluctuation contribution to our systematic floor and estimated the contributions from temperature fluctuations. These appear to be consistent with meeting our systematic floor goal of $1 - 3 \times 10^{-16}$.

We have also outlined potential strategies for moving this class of device into continuous operation at the USNO.

REFERENCES

- [1] A. Clairon, *et al.*, "Preliminary Accuracy Evaluation of a Cesium Fountain Frequency Standard," in *Proceedings of the Fifth Symposium on Frequency Standards and Metrology*, 1995, pp. 49-59; S. Bize, *et al.* "Interrogation Oscillator Noise Rejection in the Comparison of Atomic Fountains," pp. 9-11; S. R. Jefferts, *et al.*, "Preliminary Accuracy Evaluation of a Cesium Fountain Primary Frequency Standard at NIST," pp. 12-15; S. Weyers, *et al.*, "First Results of PTB's Atomic Caesium Fountain," pp. 16-19; P. B. Whibberly, "Development of a Caesium Fountain Primary Frequency Standard at the NPL," pp. 24-26, all in *Proceedings of the Conference EFTF and IEEE FCS*, 1999.
- [2] Y. Sortais, *et al.*, "An Evaluation of the Collisional Frequency Shift in a ^{87}Rb Cold Atom Fountain," pp. 34-38; C. Fertig, *et al.*, "Laser-Cooled Rb Fountain Clocks," pp. 39-42, both in *Proceedings of the Conference EFTF and IEEE FCS*, 1999.
- [3] E. Burt, *et al.*, "Cesium Fountain Development at USNO," in *Proceedings of the Conference EFTF and IEEE FCS*, 1999, pp. 20-23.

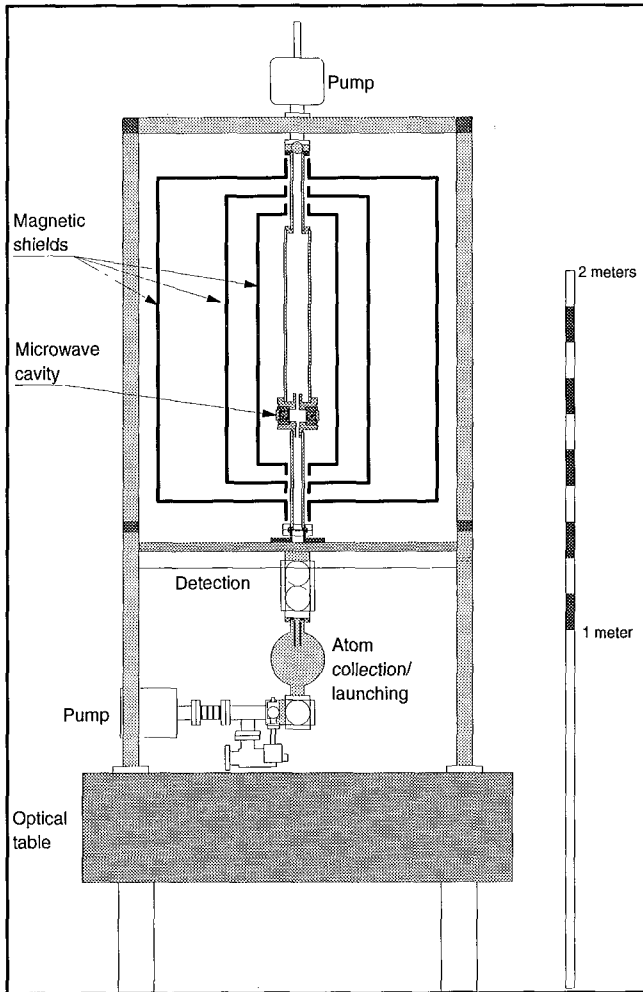


Figure 1: Cutaway mechanical view of the fountain.

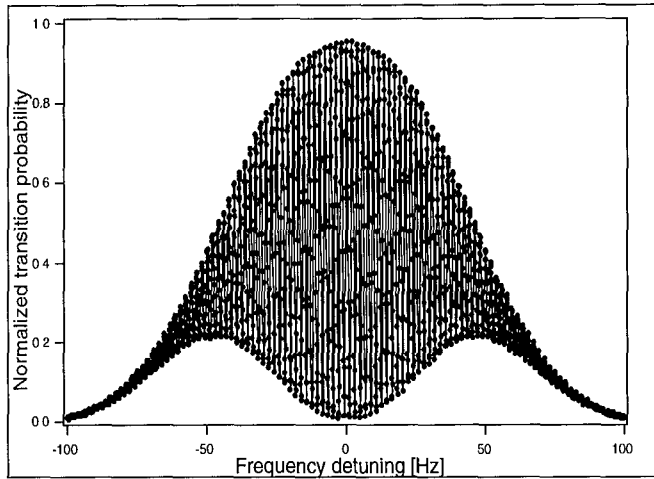


Figure 2: Normalized microwave resonance pattern on the $F=3, m_F=0$ to $F=4, m_F=0$ transition with no averaging. Cycle time is 1.9 seconds and the FWHM fringe width is 0.94 Hz. Lines connect data points only.

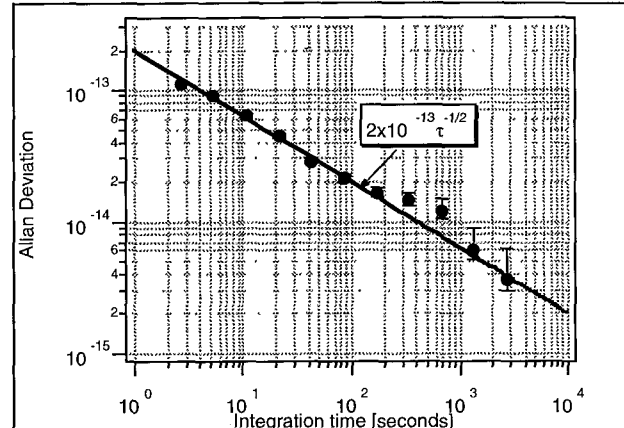


Figure 3: Stability of the fountain measured relative to an active hydrogen maser. The solid line is $2.0 \times 10^{-13} \tau^{-1/2}$ and is intended for reference only.

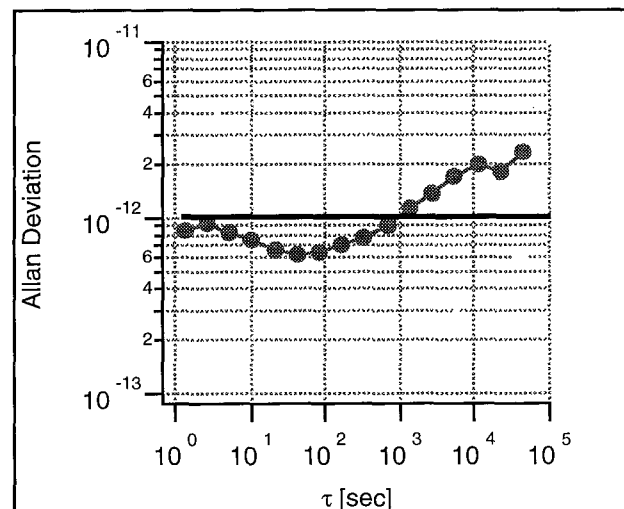


Figure 4. Stability of the fountain on the $F=4, m_F=-1$ to $F=3, m_F=-1$ transition. The solid line is 1.0×10^{-12} and intended for reference only.

Questions and Answers

ROBERT TJOELKER (JPL): I have one on that Allan variance performance curve you showed. There was a small perturbation from the longer time frames. Do you have any indication what made the times that way?

THOMAS SWANSON: At this point, we think that was environmental in the lab. At the time we were taking this, we had some issues with temperature stabilization. There were components that were not well insulated and some issues with the temperature in the labs from air handler system.

TJOELKER: Was it temperature sensitivity to some of the electronics?

SWANSON: We think so. We are still looking at that, but there are some things that we have corrected and some things still to be addressed.

STABILIZED REFERENCE FREQUENCY DISTRIBUTION FOR RADIO SCIENCE WITH THE CASSINI SPACECRAFT AND THE DEEP SPACE NETWORK

M. Calhoun, R. Wang, A. Kirk, W. Diener, G. J. Dick, and R. L. Tjoelker
NASA Jet Propulsion Laboratory, California Institute of Technology
MS 298-100, 4800 Oak Grove Drive, Pasadena, CA 91109, USA

Abstract

A high-performance frequency distribution system which includes two key technologies, the Stabilized Fiber-Optic Distribution Assembly (SFODA) and the Compensated Sapphire Oscillator (CSO), has been developed to provide state-of-the-art frequency reference in the NASA Deep Space Network (DSN). This frequency distribution system was developed to enable sensitive gravity wave searches and occultation experiments between earth-based antennas in the DSN and the Cassini spacecraft. The experiments, to be conducted at S, X, and Ka band, require the highest possible frequency stability over observation times from 1 second to 1 day. The DSN frequency and timing subsystem generates and distributes coherent signals to multiple antennas up to 30 km away. The SFODA measures and compensates for distribution-related phase perturbations, and the CSO provides short-term stability cleanup and low phase noise at the antenna.

This paper provides an overview and update of the end-to-end performance frequency and timing subsystem. Focus is given to the final SFODA design and test results using a 16-km optical fiber under controlled test conditions. Test data show a factor of 1000 improvement in long-term stability when the active phase compensator is used, thus enabling degradation-free distribution from the highest performing atomic frequency standards. Recent measurements between two CSO standards are also presented.

INTRODUCTION

A series of ambitious radio science experiments are planned between the NASA Deep Space Network(DSN) and the Cassini spacecraft both in the spacecraft cruise phase and when in orbit around Saturn [1]. For maximum sensitivity these experiments, which include gravity wave searches on a two-way Ka band Doppler link and one-way occultation experiments with the spacecraft ultra-stable oscillator, require the highest stability frequency references and distribution available. In the DSN, the source of the frequency reference signal is typically a hydrogen maser or a mercury Linear Ion Trap Frequency Standard (LITS) [2]. Although the atomic frequency standards operate in an environmentally controlled room at the Signal Processing Center (SPC) the low-noise, high-stability signals are needed at the spacecraft tracking antennas, which may be thousands of meters from the frequency standard. Frequency distribution systems which carry signals to the antennas can be subject to temperature extremes, electromagnetic and radio frequency interference, and vibration. The distribution challenge is to preserve atomic frequency standard long-term stability to all antennas and, for the case of the Cassini occultation experiments, improve close in phase noise.

NEED FOR FIBER STABILIZATION

For antennas located near the Signal Processing Center (SPC) the reference frequency stability is distributed through a special optical fiber with a low thermal coefficient of delay (LTCD). The thermal coefficient of delay is typically less than 1 ppm/ $^{\circ}$ C for temperatures below 35 $^{\circ}$ C, and near 0.1 ppm/ $^{\circ}$ C over the range 10 $^{\circ}$ C to 25 $^{\circ}$. This cable is not suitable for direct burial applications and its cost limits implementation to antennas close to the SPC. Remote antennas, up to 30 km from the central SPC, are serviced by direct burial fiber optic cables. Since the remote antennas are not equipped with the LTCD fiber, they do not meet the very stringent radio science stability requirements. The 34-meter antenna DSS-25, selected for Ka band support of the Cassini radio science mission, is 16 km from the central SPC. The thermal coefficient of the distribution optical fiber is approximately 7 ppm/ $^{\circ}$ C and exposed to a number of temperature variations.

The ground temperature profile at the California DSN site is shown in Figure 2 [3]. These ground temperature profiles were measured with thermocouples at depths of 2 feet, 3 feet, 4 feet, 5 feet, and 6 feet between the months of January and June. The line in Figure 2 with the larger variations from day to day is the surface temperature averaged over a 24-hour period. The existing fiber-optic cable from the SPC to DSS-25 is buried at a depth of approximately 1.5 meters. At this depth the fiber is sufficiently insulated from short-term and daily thermal perturbations. Unfortunately, regions of the fiber are exposed along the 16-km path. There are 4 access vaults, each of which hold approximately 10 m of coiled cable. These vaults have steel covers and are exposed to large air temperature variations, as great as 50 $^{\circ}$ C peak-to-peak. Additionally, the fiber cables pass through an air plenum at the SPC, the plenum at the remote station, and the antenna pedestal at DSS-25. Temperature cycling in the air plenums and pedestal varies and has been observed to be as great as 2 $^{\circ}$ C peak-to-peak with varying periods, typically in the 2000-to 4000-second range. All of these factors can contribute to phase delay variations measured at the user end of the distribution system. Figure 3 shows the measured Allan deviation of the distribution at antenna DSS-25 when the phase delays are uncompensated.

FREQUENCY REFERENCE SYSTEM

Early prototype development of the two key technologies, the Stabilized Fiber Optic Distribution Assembly (SFODA) and the Compensated Sapphire Oscillator (CSO) have been previously discussed [4]. Figure 1 shows the block diagram of the reference frequency distribution system to the remote Beam Wave Guide (BWG) antenna, DSS-25. The driving force for the development of the SFODA was temperature-induced phase delay variations in optical distribution links. The design of the actively stabilized reference frequency distribution system is based on optical closed-loop feedback. A reference frequency signal at 1 GHz is transmitted over the fiber link and the SFODA utilizes active feedback with a temperature-compensating fiber-optic reel to compensate for thermally induced phase variations over the 16-km fiber cable. The optical transmitter is a commercial, single-mode distributed feedback laser diode with an integral optical isolator. The companion optical receiver with a phase-lock loop and distribution amplifiers are located at the remote antenna. The distribution can deliver 100 MHz or 1 GHz to steer the CSO or to supply other users as needed. The CSO and SFODA receiver are both located in a special environmentally controlled building near the base of the antenna DSS-25. The temperature within this building is controlled to ± 50 millidegrees C.

The planetary occultation and gravity wave radio science measurements place stability requirements on the frequency distribution system of 1.5×10^{-16} between 1000 and 3600 second averaging times. The short-term stability requirement is 3×10^{-15} at 1 second. The SFODA has sufficient signal-to-noise to preserve atomic frequency standard stability at distances up to 30 km, providing the long-term stability to meet Cassini sensitivity goals for gravity wave detection. The SFODA short-term stability is approximately 1.5×10^{-14} at one second, which falls short of the frequency reference requirements for occultation measurements. These occultation experiments measure phase and amplitude fluctuations of the S, X, and Ka band carriers resulting

from transit through intervening media, such as the rings of Saturn or the atmosphere of Titan. For these measurements the CSO is phase-locked to the 100 MHz SFODA output providing a short-term reference stability of 3×10^{-15} from 1 second to 100 seconds. The CSO was developed to provide practical, continuous operation for a year at a time using a closed-cycle refrigerator [5]. If desired, the CSO can also serve as a local oscillator to achieve the highest performance possible with passive atomic frequency standards [6].

STABILIZED FIBER-OPTIC DISTRIBUTION ASSEMBLY

The atomic frequency standard located at the SPC is used as the source of a highly stable signal, typically 100 MHz, and distributed to users of the Deep Space Network tracking stations. Local distribution (internal to the SPC) of these stable signals is through high-quality coaxial cables. Reference frequencies to nearby 34m and 70m antennas are distributed via fiber-optic links utilizing the LTCD fiber previously discussed. For the remote antenna locations, direct burial optical fiber is the preferred medium of distribution. Optical fibers offer the advantages of low loss, EMI/RFI immunity, and broad bandwidth.

A detailed block diagram of the SFODA is shown in Figure 4. The SFODA utilizes active feedback and a thermally controlled reel of fiber to offset the thermal variations in the 16-km fiber cable between the stations. The major components at the SPC are the power supply , master controller, a bipolar power supply to both heat and cool the compensating reel, and the compensating reel. The electronics package in the master controller is mounted on a thermally controlled plate. The signal input to the master controller is 100 MHz from the on-line frequency standard. This signal is split and multiplied to 1 GHz for transmission over the fiber link. The X10 multiplier is a phase-locked cavity oscillator with low phase noise. The second output of the splitter is used as a reference to a phase detector, which produces the phase error signal. The reference signal modulates the 1310-nm laser diode with the 1-GHz carrier. The optical output utilizes an optical isolator and an optical circulator, allowing two-way transmission on a single-channel fiber. The channel fiber, one of a 96-fiber cable, is standard SMF 28, single mode with a temperature coefficient of delay of 7 ppm/ $^{\circ}\text{C}$.

At the remote antenna site, the optical signal goes into a receiver where the 1 GHz modulation is detected and amplified for distribution. The 1-GHz signal phase-locks a 100 MHz low-noise voltage-controlled oscillator (VCO). The output of the 100 MHz VCO is coherent with the signal from the on-line frequency standard and is available for distribution. The CSO, when steered to the 100-MHz input provides the required short-term stability at the antenna.

Figure 5 illustrates the Allan deviation achieved with the SFODA and Figure 6 shows the system stability performance with and without compensation while in a environmental chamber programmed to generate 1 $^{\circ}\text{C}$ temperature swings once every 24 hours. Tests in the laboratory as well as preliminary in-situ tests indicate a factor of 1000 improvement in the long-term stability of the reference frequency distribution over a distance of 16 km.

COMPENSATED SAPPHIRE OSCILLATOR

Cryogenic oscillators operating below about 10K offer the highest possible short-term stability of any frequency sources. However, their use has so far been restricted to research environments due to the limited operating periods associated with liquid helium consumption. The Compensated Sapphire Oscillator (CSO) has been developed for ultra-high short-term stability and low phase noise [5,6]. With cooling provided by a commercial cryocooler instead of liquid helium, this standard is designed to operate continuously for periods of a year or more.

This development was enabled in part by a new generation of two-stage Giffard-McMahon cryocoolers, which allow operation at temperatures down to 4.2K. Previously, such temperatures could only be achieved by the use of an additional Joule-Thompson expansion stage, with increased complication and cost, and with

reduced reliability. Any cryocooler generates vibration which, if coupled to a high-Q electromagnetic resonator will degrade frequency stability. Sufficient vibration isolation is accomplished by using turbulent convection in a gravitationally stratified helium gas.

Cryogenic standards have used both superconducting and sapphire resonators to achieve the $Q > 10^9$ required for 1×10^{-15} frequency stability. Superconducting resonator Q's degrade to unacceptable values above about 2K. Q's of a billion have been previously measured in whispering gallery sapphire resonators at temperatures up to 10K. However, the temperature sensitivity of sapphire resonators is so large that high stability can only be attained near a preferred turnover temperature where the slope of frequency versus temperature approaches zero. The actual value of the turnover for any given resonator depends on the concentration of incidental paramagnetic impurities, as well as the properties of the electromagnetic mode that is being excited. The CSO resonator design compensates the frequency variation of a whispering-gallery sapphire resonator by means of a thermally attached ruby element. The high chromium concentration in the ruby provides a means for adjustable external compensation by varying its position with respect to the sapphire element. With this ruby element, sapphire turnover temperatures are raised from typical as-supplied values of 5-6K to a reproducible 8-10K, resulting in a practical continuously operating standard at the 10^{-15} level.

The CSO provides low phase noise at 10 GHz and continuous operation for up to 1 year. Phase noise tests between two independent CSO's (Figure 7) show a 24-28 dB improvement over hydrogen masers in the frequency range of 1 Hz to 40 Hz. Figure 7 also shows some harmonics of the 2.4Hz refrigerator cycle which were previously masked by maser noise. Figure 8 shows a direct high stability measurement against a hydrogen maser of 2.5×10^{-15} between 300 and 600 seconds. Also shown is direct pair data between two CSO's. Currently three CSOs are operational. A total of four will reside in the DSN, one at each complex (Goldstone, California USA; Madrid, Spain; and Canberra, Australia) to act as low noise reference for the antennas close to the Signal Processing Centers. A fourth will operate at the end of the SFODA distribution link (Figure 1) at the remote antenna DSS-25 to clean up the limiting phase noise and short-term stability of the atomic standard distribution link.

CONCLUSIONS

Stability measurements indicate that the 100-MHz reference frequency signal for radio science experiments meets or exceeds needed performance. This will enable a new generation of low frequency gravity wave searches using a two-way Ka-band Doppler link between the NASA Deep Space Network and the Cassini Spacecraft. Environmental temperature effects on the distribution fiber to the DSN Ka-band antenna, DSS-15, have been reduced by measuring and actively stabilizing the 16-km optical fiber link. Short-term stability and phase noise requirements are met by use of a continuously operating Compensated Sapphire Oscillator.

Presently, two SFODAs are operational in the Deep Space Network at Goldstone, California. One is operating between the SPC and DSS 25 to support the Cassini Radio Science experiments and the second installed between the SPC and DSS 13, a distance of 28 km, also in support of Cassini-related experiments to calibrate the effect of the Earth's troposphere. Two CSOs are in preparation for delivery to Goldstone, which will take place upon completion of the environmental facility at DSS 25 in February 2001.

ACKNOWLEDGMENTS

This work was carried out at the Jet Propulsion Laboratory, California Institute of Technology, under a contract sponsored by the National Aeronautics and Space Administration.

REFERENCES

- [1] M. Tinto 1997, "Requirements," in Cassini Radio Science Ground System Cost and Schedule Review, JPL document, 19 June 1997.
- [2] R. L. Tjoelker, C. Bricker, W. Diener, R. L. Hamell, A. Kirk, P. Kuhnle, L. Maleki, J. D. Prestage, D. Santiago, D. Seidel, D. A. Stowers, R. L. Sydnor, and T. Tucker 1996, "A mercury ion frequency standard engineering prototype for the NASA Deep Space Network," Proceedings of the 1996 IEEE International Frequency Control Symposium, IEEE Publication 96CH35935, 5-7 June 1996, Honolulu, Hawaii, USA, pp. 1073-1081.
- [3] M. Calhoun, J. C. Law, and P. F. Kuhnle 1993, "Environmental effects on optical fibers used for reference frequency distribution," Proceedings of the Institute of Environmental Sciences Applications Meeting, May 1993, Las Vegas, Nevada, USA.
- [4] M. Calhoun, G. J. Dick, and R. T. Wang 1999, "A frequency transfer and cleanup system for ultra-high stability at both long and short times for the Cassini Ka-band experiment," Proceedings of the 30th Annual Precise Time and Time Interval (PTTI) Systems and Applications Meeting, 1-3 December 1998, Reston, Virginia, USA, pp. 405-412.
- [5] R. T. Wang, and G. J. Dick 2000, "Stability tests of three cryo-cooled sapphire oscillators," Proceedings of the Conference on Precision Electromagnetic Measurements 2000, pp. 190-191.
- [6] G. J. Dick, R. T. Wang, and R. L. Tjoelker 1998, "Cryo-cooled sapphire oscillator with ultra-high stability," Proceedings of the 1998 IEEE International Frequency Control Symposium, IEEE Publication 98CH36165, 27-29 May 1998, Pasadena, California, USA, pp. 528-533.

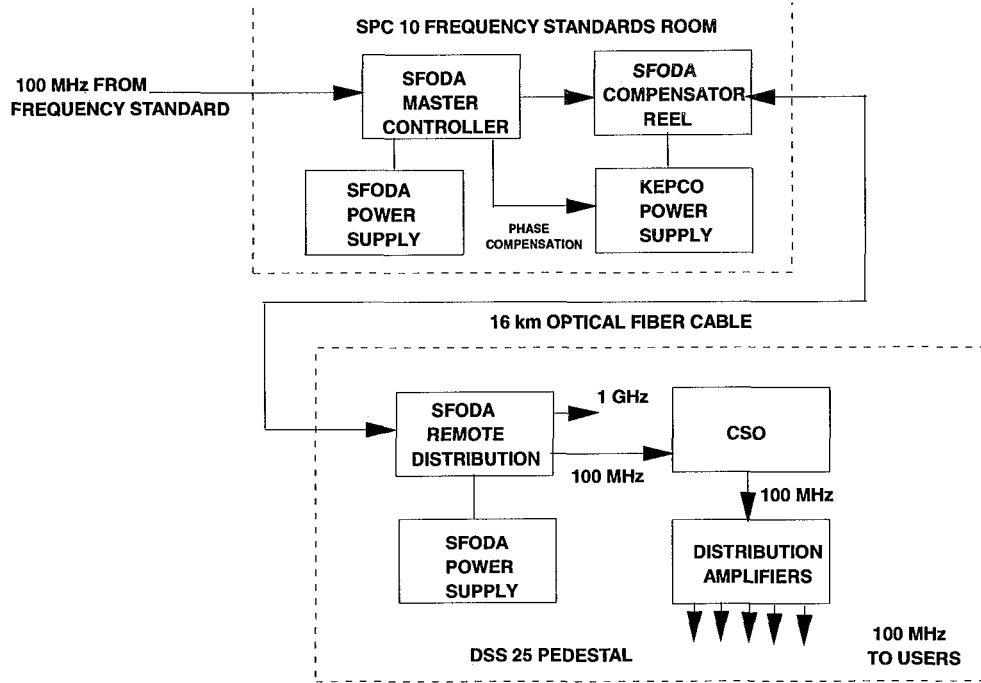


Figure 1. Block diagram of 100 MHz reference frequency distribution at the Deep Space Network tracking station (Goldstone, California) between the Signal Processing Center SPC-10 (location of the atomic frequency standard) and the Ka-band transmit/receive antenna DSS-25.

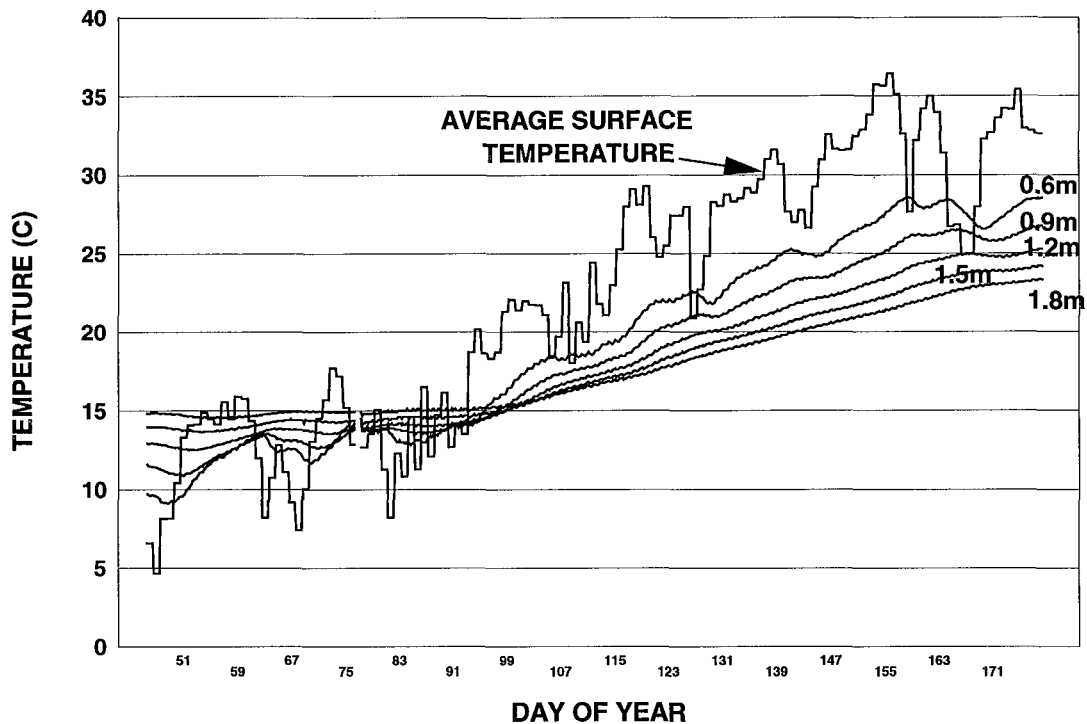


Figure 2. Ground temperature at Goldstone Deep Space Communications Complex at different depths over time.

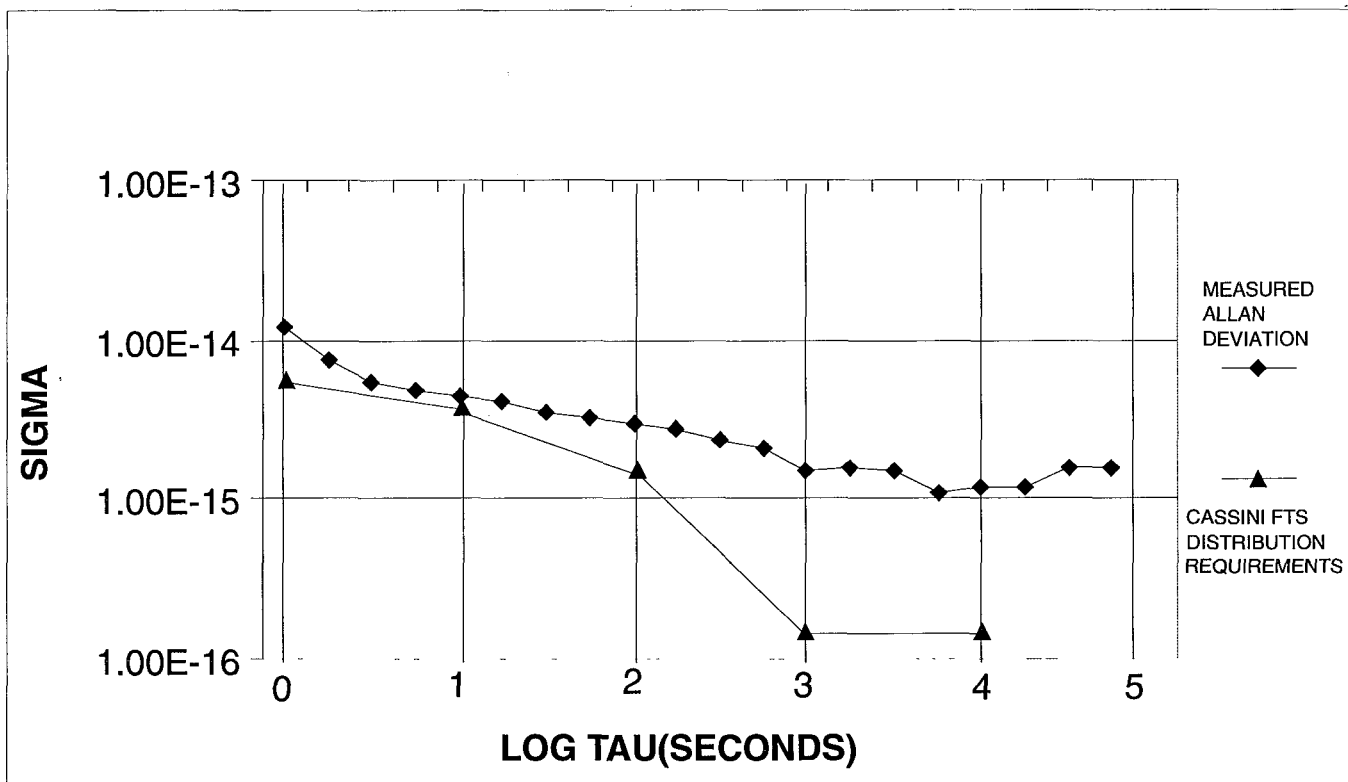


Figure 3. Allan deviation of the 100 MHz Reference frequency measured at the remote antenna DSS-25 before installation of the compensated fiber-optic distribution system.

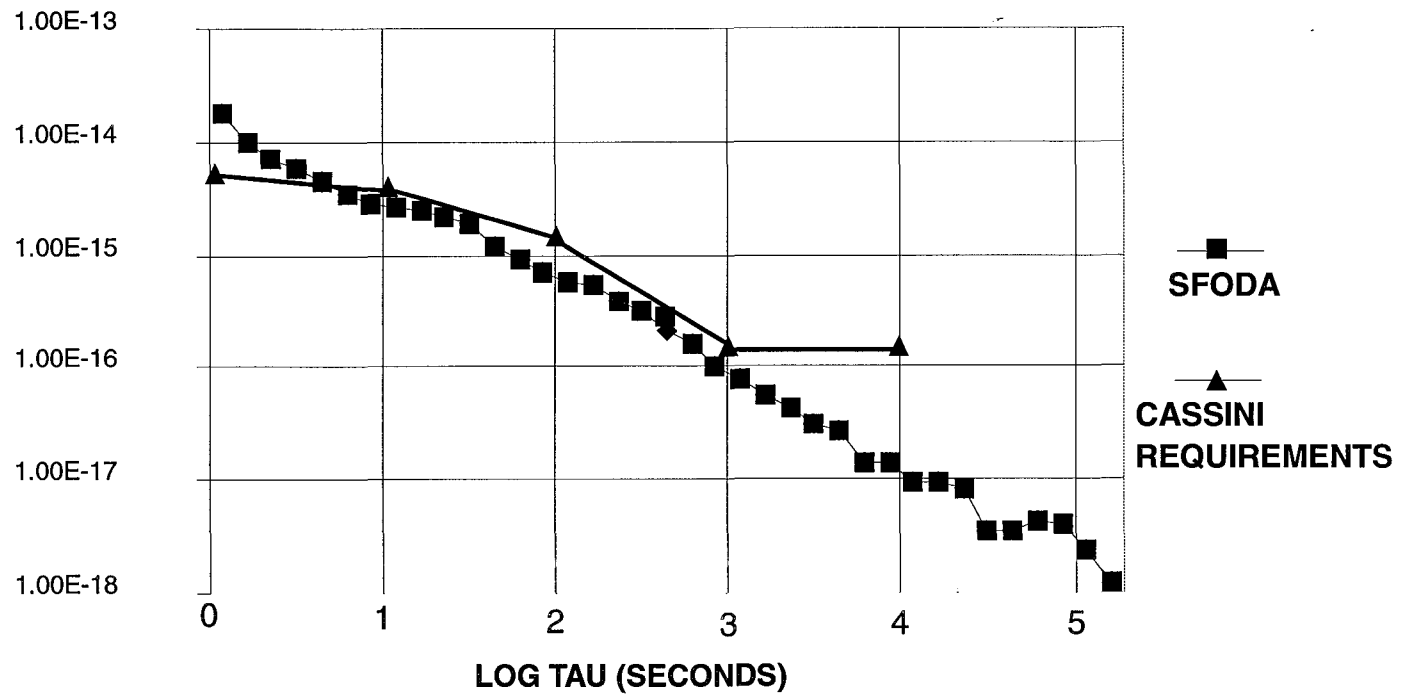


Figure 5. Allan deviation of SFODA 100 MHz reference frequency over 16 km fiber link during 1 degree C peak-to-peak thermal cycling in an environmental chamber.

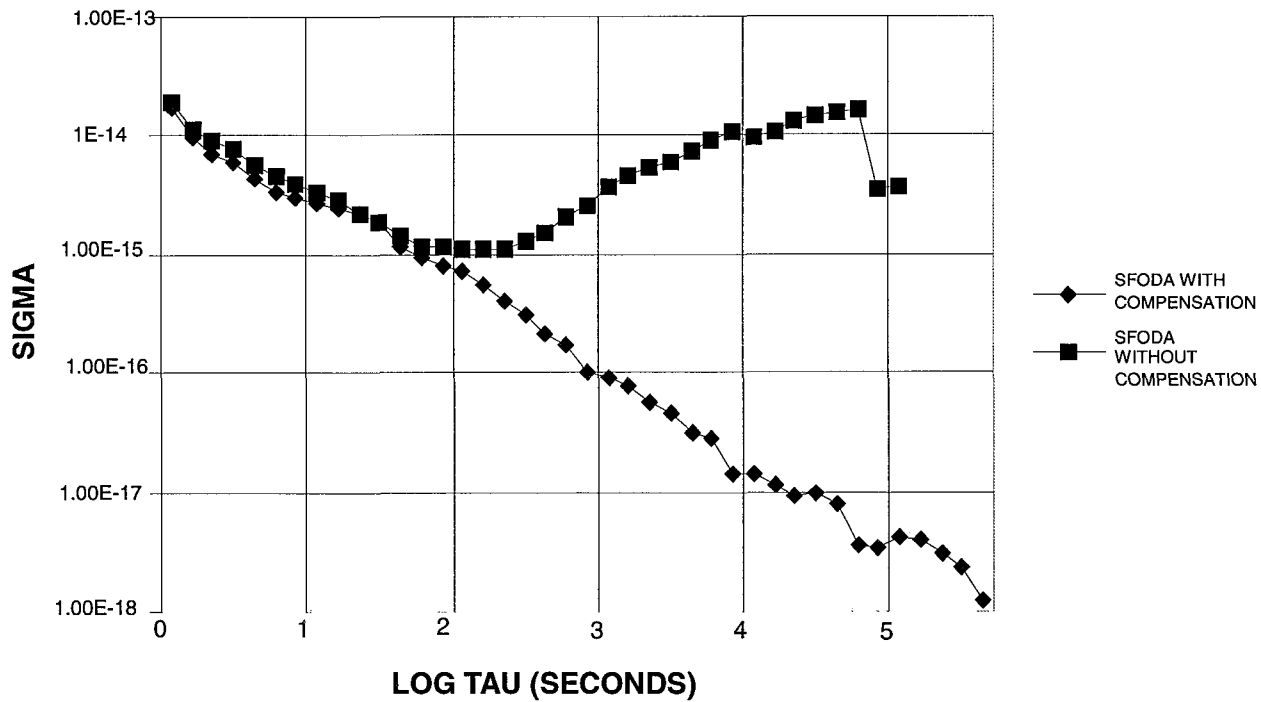


Figure 6. Allan deviation of the SFODA with and without active phase compensation during 1 degree C peak-to-peak thermal cycling in an environmental chamber at a period of 24 hours.

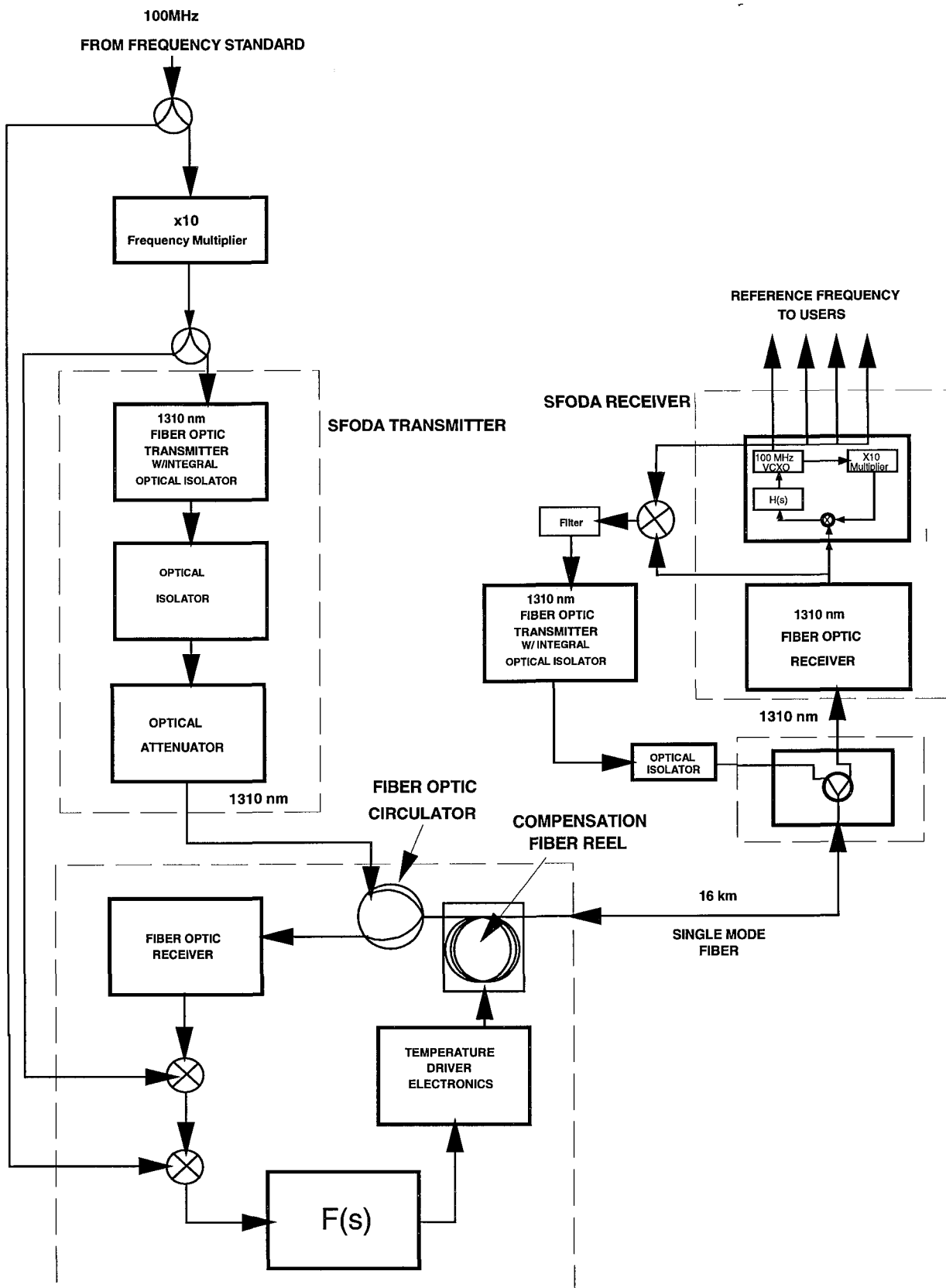


Figure 4. Block diagram of the Stabilized Fiber-Optic Distribution Assembly.

CSO Phase Noise Performance

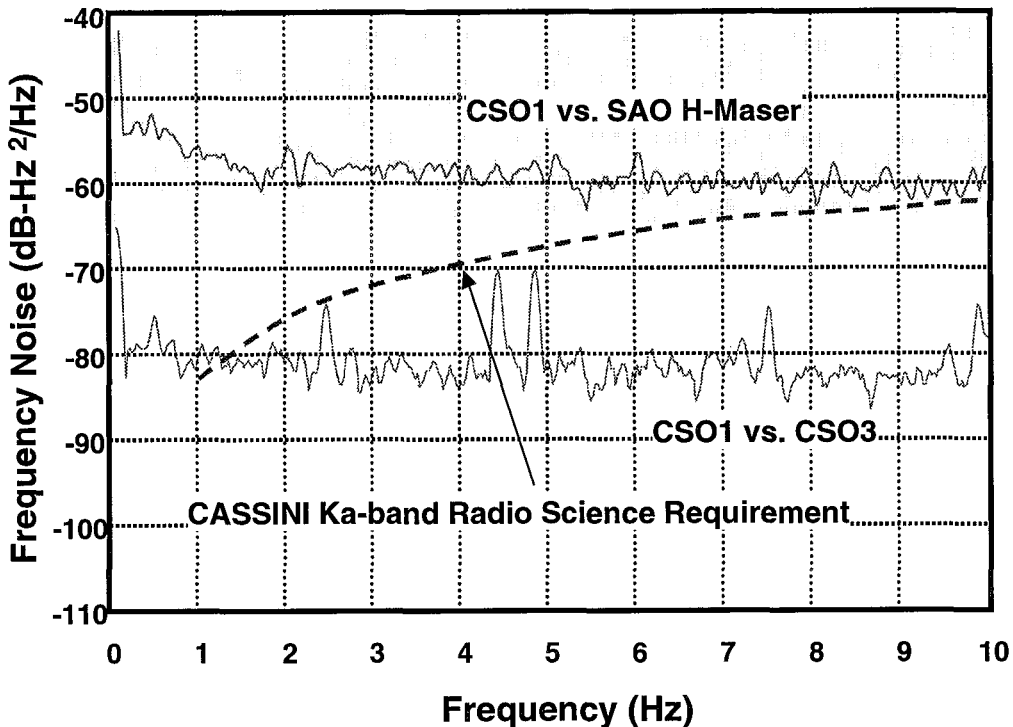


Figure 7. Compensated Sapphire Oscillator (CSO) Phase Noise Performance as measured a) against a hydrogen maser and b) a second CSO.

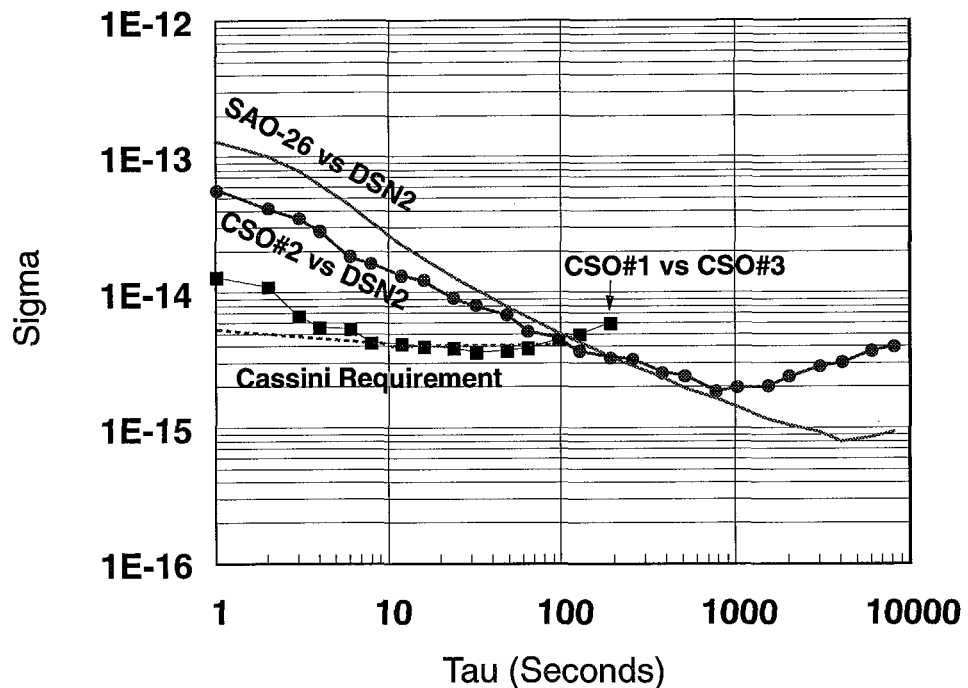


Figure 8. Compensated Sapphire Oscillator (CSO) Allan deviation as measured against a) the hydrogen maser DSN2 and b) against a second CSO.

MULTI-PURPOSE TIME ANALYZER AND MONITOR FOR DEEP SPACE NETWORK TIME SYNCHRONIZATION

J. Gonzalez, Jr., M. Calhoun, S. Cole, and R. L. Tjoelker
Jet Propulsion Laboratory, MS 298-100
4800 Oak Grove Dr., Pasadena, CA 91109, USA

Abstract

We report the development of a multi-purpose, automated, and continuously operating Time Analyzer to measure and monitor distributed 1 pps reference signals in the NASA Deep Space Network (DSN). The instrument reports the performance of each 1 pps signal relative to the station master clock and displays time offset and jitter (standard deviation) data for each measurement. The long-term stability of the primary and backup frequency standards are also monitored by measuring time offset data and analyzing over a 24-hour period. The instrument output includes alarms that alert the station operator of anomalies or an out-of-specification condition. All monitor and user displays are developed with Labview and use the LINUX operating system.

INTRODUCTION

NASA/JPL operates the Deep Space Network (DSN), a network of sensitive antennas that support interplanetary spacecraft missions and radio and radar astronomy observations. These antennas are located at three sites near Goldstone, California; Madrid, Spain; and Tidbinbilla, Australia. Time offsets between each station are measured against UTC using traditional GPS common-view techniques.

Each station operates an independent Frequency and Timing Subsystem (FTS) [1] and distributes timing signals to approximately 100 users. Since time users are scattered over several antennas up to 30 km away from the station master clock, distribution delays due to cable lengths must be accounted for. These delays are typically measured during initial installation, but there presently is no monitoring of the residual time offset or stability of the delivered signal. Consequently timing quality can be inadvertently compromised either by human error or equipment anomalies. The Time Analyzer instrument design described here measures time offsets and jitter of the timing output of more than 120 timing users and alerts the DSN operator of any anomalies or out of specification condition. The analyzer also tracks the long-term drift of primary and backup frequency standards and provides a generic test capability for any 1 pps signal. The analyzer provides station operators a snapshot view of the entire timing system integrity and performance. The instrument is networked to allow long-term data archiving or post-processing by DSN time analysts.

DEEP SPACE NETWORK FREQUENCY AND TIMING SUB-SYSTEM

The primary components of the FTS are multiple frequency standards, reference frequency synthesis and distribution, and master clock and time distribution. GPS time transfer is used for time synchronization and frequency synthonization between complexes.

The complement of frequency standards presently consists of four atomic clocks (Fig 1), two Hydrogen Masers, one Mercury Linear Ion Trap Standard (LITS), and one commercial cesium-beam standard. Each standard provides stable output frequencies at 0.1, 1, 5, 10, and 100 MHz with 140 dB isolation between channels. The four frequency standards are connected to the Coherent Reference Generator (CRG) for distribution (Fig 2). Relay switches select one of the frequency standard inputs to feed the driver amplifiers in the CRG. The output signals from the driver amplifiers are applied to frequency synthesizers for conversion and to further distribution amplification. There are 256 output ports provided to users with available frequencies at 0.1, 1, 5, 10, 10.1, 45, 50, 55, and 100 MHz. To minimize crosstalk the output signals have a 100 dB reverse isolation between them. One of the 5 MHz output ports from the CRG is sent to the Master Clock and Timing system to provide synchronized and very stable time.

The timing system consists of a triple redundant Master Clock (MCA), Time Insertion and Distribution Assembly (TID), and multiple Time Code Translators (TCTs) (Figure 3). The three time-code generators in the master clock are synchronized and driven by the single, online frequency standard. All three generators are voted on by majority vote logic that selects a minimum of two within limits as the correct time of day and pulse timing. The TID is a distribution assembly that generates a modified IRIG-G code for distribution to all the TCT's in the complex. The number of individually addressable TCTs is limited to 100 by the number of output ports. The distribution time code from the TIDS's contains real time (Universal Time Code or UTC) and Simulation (SIM) Time. The SIM time is used primarily for testing, training, or software exercises.

Time Code Translators (TCT) translate the TID time code and provide outputs to users in a variety of formats. The Master Clock provides the 5 MHz distribution, which originates from the online frequency standard. The TCT's provide timing pulses at 1 pps, 10 pps, 100 pps, and 1000 pps, time code on an RS-232 format, and a 1 pps monitor output. This 1 pps port is used by the time analyzer to measure time offset and jitter performance with respect to the master clock.

METHOD OF MONITORING TIME DISTRIBUTION

Presently, most of the 1 pps TCT monitor signals are routed back to a patch panel near the master clock. The patch panel contains over one hundred 1 pps signals from individual TCTs distributing time from the master clock, plus ten more ports for TCT's free running from distinct 5 MHz inputs from each frequency standard.

A small sample of the TCT's are manually measured daily by a technician who connects one TCT output, along with the Master Clock output, to a HP5370B Universal Time Interval Counter. The counter measures the start and stop time between the sampled TCT and the Master Clock. The samples are measured over a 100-second period to allow sufficient averaging to measure the timing jitter (typically 1- 2 ns level). All frequency standards are sampled in a similar manner providing a single data point to characterize time offset from the master clock.

The current monitoring method leaves most TCT's unmonitored. As a result, performance data are typically not available and the station operations must rely upon the timing user to detect any failure or out of specification condition. The Time Analyzer was developed to address these operational shortcomings.

TIME ANALYZER SYSTEM DESIGN

The Time Analyzer System (Figure 4) was designed for continuous, autonomous, monitoring of TCT performance and does not interfere with timing system functionality. The Time Analyzer program is written in Labview and is executed on a standard rack mount computer with LINUX operating system.

The instrument interfaces to the existing patch panel and multiplexes the 1 pps signals from individual TCT's to an HP E1420B Time-Interval Counter. The second 1 pps signal for the counter comes from the master clock. The counter, switching multiplexers, and the controller to run the measurement process all reside in a standard VXI card cage. The Time Analyzer samples each TCT by switching through the HP E1472/3 multiplexer modules.

Long-distance monitoring of remote TCTs is done through an RS-232 interface transmitted through fiber-optic line and converted to IEEE 488 standard at the receiver. A second, remotely located VXI card cage and command module controls the multiplexing of the remote TCTs. The multiplexed 1 pps signals at the remote site are routed back to the local time analyzer through a single fiber-optic link. To verify switching of the local and remote Multiplexer cards the command module switches to a time delayed reference signal between sampling. The delay signal at the local Time Analyzer is supplied by the master clock and by a custom-built time-delay circuit at the remote site. The switching is done between TCT sampling and is designed to give the operator confidence in the reliability of the sampled data.

TIME ANALYZER USER INTERFACE AND DISPLAYS

Front Panel

The primary program display "front panel" is shown in Figure 5. When the Time Analyzer Icon in the desk top is clicked the Time Analyzer begins executing using two default files. The two files provide information on TCTs and time standards to the program. The two buttons below the STOP button bring up editing windows. Using these editing windows, a TCT or standard can be removed or added to the program, the time offset can be adjusted, the location of the TCT or standard can be entered or changed, and the name of a time standard can be entered. The time offset in the data compensates for cable delay required to carry the one-pulse-per-second signal to the Time Analyzer Subsystem rack.

Below these buttons on the front panel is the STATUS light. This light will turn from green to orange to indicate a high level time analyzer alarm. There are three sources of errors: a TCT mean or standard deviation value outside the allowable range, an active time standard with no signal, and a mux error. The alarms are reported to station operators by the Status Summary Display Subsystem through an isolated relay switch closure. The switch is closed when one or more errors are active. Removal of all error conditions is required to return the light and the error status to the non-error (green) state.

The MUX STATUS light to the right, below the STATUS light, indicates a multiplexer error. After 100 measurements of the next TCT and after all time standards are measured, the multiplexer is switched to channel 111. There should be no signal on this channel. Data acquisition is then attempted. If the acquisition is successful (a signal is detected on the channel), the multiplexer is not functioning properly and an error will result. If the multiplexer does not switch from this channel, when the next TCT is to be measured, that TCT will flag an error. The two lights below the DATASET and MUX STATUS lights indicate whether a TCT or a standard is being measured at any point in time.

The histogram to the right of the lights and buttons discussed above indicates the time differences between all TCT's and the master clock. Each "bin" is 10 nanoseconds wide. The 21 bins in the center represent time differences from -105 nanoseconds to +105 nanoseconds. The two bins on either side of the center set of bins indicate time differences too large to fit into the center set. For these bins, the indicators are orange rather than blue. The height of each indicator displays the number of TCTs having time differences that fall within that bin's range.

The number matrix to the right of the histogram indicates the status of all local TCTs. The background color behind each TCT number is light blue when the TCT is not active. Green indicates that the TCT is present and no error has been detected. The background turns to orange when the TCT's time difference mean or standard deviation falls outside the acceptable range. Clicking directly on a TCT number will cause a detailed status window for that TCT to open. The window displays a histogram representing 100 one-second measurements to determine the mean offset and standard deviation (jitter) for that individual TCT. This feature allows the time analyzer user to override the default chronological TCT measurement sequence.

To the left of the main TCT status matrix, at the bottom of the front panel, is a second TCT matrix. This matrix provides the same functions as the local TCT matrix, for the remote TCTs. The location of the TCTs have no effect on the behavior of the program other than the size of the time offset required in the TCT data file.

Between the remote TCT status matrix and the histogram are a set of indicators that display information on the TCT currently being measured. Data displayed include the location (local or remote) and number of the TCT, the subsystem and rack where the TCT is located, the active measurement number (0 to 99), and the value of the previous measurement. When the last measurement is made, this set of measurements is used to calculate the mean and standard deviation for that TCT. Those values are then checked against the limits to determine whether or not an error has occurred.

The frequency standard display is in the lower left corner. At the far left is a set of lights that display the time standard status. When the time signal is present and the channel is active, the light is green. The light is light blue when the channel is not active (the time standard name field is blank). The light is orange when the one-pulse-per-second signal is not present on an active channel. Standard names are shown in the next column. If the standard name is blank, the channel is not active. The next column shows the mean of the previous 100 measurements. Since 100 TCT measurements are made between frequency standard measurements, the mean value will remain at zero for the first 4 hours and 10 minutes after the program is started. The

mean is not recorded in the log but the individual measurements of the dataset used to calculate the mean are saved in the log. The next column shows the measured drift per day of the frequency standards. The values in this column represent the difference between the current mean time offset reading and the mean time offset reading acquired 24 hours previous. This value is updated every 3 hours and is not recorded in the log. The final column in this area is a column of buttons. Clicking on a button will bring up the frequency standard detail window showing a histogram of the measurements that were used to calculate the mean value. The window functions in the same way as the TCT detailed window described above.

TCT Assignment List Window

The first column of the TCT Assignment List Window (Figure 6a) begins with an “L” or an “R” indicating whether the TCT is local or remote respectively. The location letter is followed by the TCT number. The next column is used to identify the subsystem to which the TCT is attached. If this parameter is blank, the TCT will be inactive and the background color for the status matrix in the front panel will be light blue. The next column is used to indicate the TCT location. The final column sets the time offset required for that TCT. This value should be the time required for the one-pulse-per-second signal to travel from the TCT to the Time Analyzer subsystem. Once set, this parameter should only require change when the TCT is moved.

Standard Assignment List Window

The Standard Assignment List Window is shown in Figure 6b. This window is similar to the TCT Assignment List Window, except that there is no index. Here, the first column is the standard name. If the name is blank, the channel is skipped during the measurement process. The second and third columns identify the location of each standard. As in the TCT Assignment List Window, the final column holds a time offset which should correspond to the time required for the one-pulse-per-second signal to travel to the Time Analyzer Subsystem.

TCT Detail Window

The TCT Detail Window (Figure 7a) appears when the user clicks on one of the TCT numbers in the local or remote TCT matrix on the front panel. The window overlays part of the front panel, but does not affect measurements being made by the Time Analyzer Subsystem, except as described below.

Indicators at the top of the window show the TCT number, Subsystem, and Rack for the selected TCT. The histogram in the center of the window functions in the same way as the histogram on the front panel. Here, however, the values being displayed represent the measurement to measurement jitter. Two indicators below the histogram display the precise mean and standard deviation values for the TCT.

Two buttons are displayed at the bottom of the window. Clicking the CONTINUE button will close the window. Clicking on the NEW ACQUIRE button forces the Time Analyzer Subsystem to sample the selected TCT as the next TCT in sequence. If a TCT is being sampled when the button is clicked, that set of samples is finished, the time standards are measured, and the selected TCT is sampled. When the sampling of the selected TCT starts, two more indicators

appear in the TCT Detail Window as shown in Figure 7b. The upper of the two new indicators displays the measurement count (from 0 to 99). The lower indicator displays the measurement values as measurements are made. In addition, the histogram registers each measurement in real time as it is made. When the measurement set is complete, the mean and standard deviation are re-calculated and the new values are displayed in the window. The TCT number and values are stored in the log, indicating out-of-sequence measurements. The time standards are read again before returning to the normal TCT sequence.

Frequency Standard Detail Window

Clicking on one of the buttons on the right of the frequency standard data display on the front panel will bring up a frequency standard detail window, as shown in Figure 7c. This window functions in the same way as the TCT detail window described above. The only difference, besides the source of the measurements, is that the frequency standard name appears in an indicator at the top of the window.

The histogram in the detail window reflects the previous 100 time-difference measurements of the selected frequency standard. The range of time differences covered by the time standard histogram is -10.5 microseconds to +10.5 microseconds. Each bin covers 1 microsecond. This dataset displayed in the histogram represents a time history of 4 hours and 10 minutes. Clicking on the NEW ACQUIRE button will cause the Time Analyzer VI to acquire a set of time measurements of the selected standard in the same way that TCT datasets are acquired, in 100 seconds. As with the TCT Detail Window, two new indicators appear when the measurement process begins. These new indicators show the measurement number and the previous measurement value. The mean and standard deviation are recalculated and the new values are displayed when the new dataset is complete. Data from the acquisition are stored in the log in the same way as TCT data.

CONCLUSION

We described the development of a multi-purpose, automated, and continuously operating time analyzer to measure and monitor distributed 1 pps signals in the NASA Deep Space Network. The instrument consists of a Labview based user interface on a LINUX OS and performs three major functions needed for operation of the DSN Frequency and Timing Subsystem.

- 1) Performance tests and monitor of timing offsets and jitter of 1 pps timing outputs of 120 TCT's relative to the station master clock. Time offset data from each TCT is summarized in histogram form. Additional test channels to monitor 1 pps from any other source (e.g., the GPS time sync receivers) against the master clock are also provided
- 2) Captures any anomalies and alerts station operators in event of performance or operational failure and archives timing configuration, station performance, and status.
- 3) Provides monitor of frequency offsets and long-term stability of backup frequency standards with respect to the online frequency-standard (which drives the master clock). Time and frequency offset data between online and backup frequency standards are analyzed over a 24-period and displayed numerically.

The user interface is designed to provide a high level summary of the entire timing system performance and to alert station operations in the event of an anomaly. Raw data are fully archived and network accessible if detailed analysis is warranted.

ACKNOWLEDGMENTS

This work was carried out at the Jet Propulsion Laboratory, California Institute of Technology, under a contract with the National Aeronautics and Space Administration.

REFERENCES

- [1] P. F. Kuhnle 1990, "*NASA/JPL Deep Space Network frequency and timing*," Proceedings of the 21st Annual Precise Time and Time Interval (PTTI) Applications and Planning Meeting, 28-30 November 1989, Redondo Beach, California, USA, pp. 479-489.

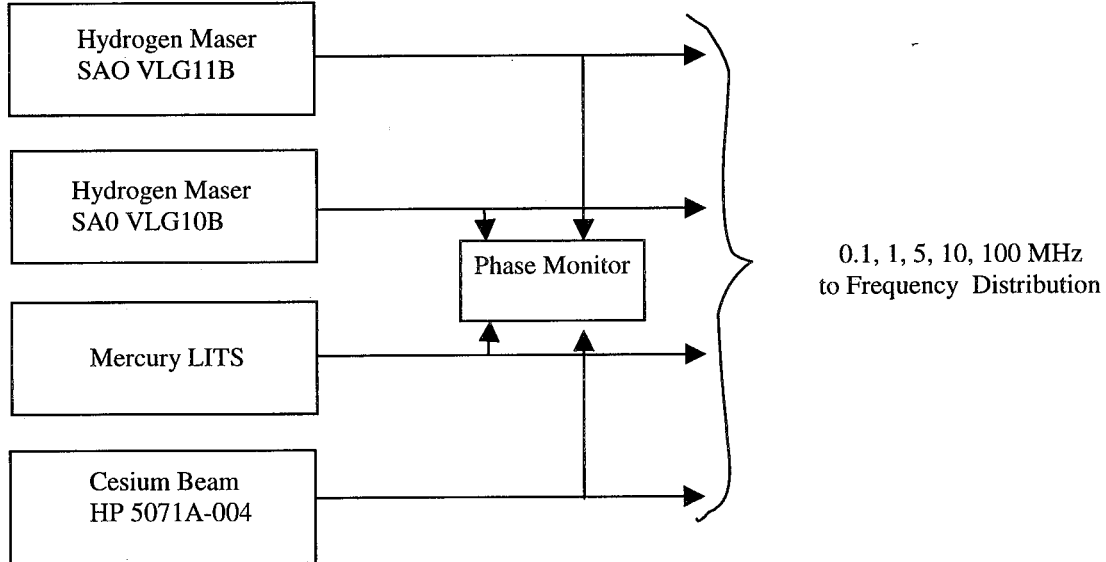


Figure 1. DSN Frequency Standards

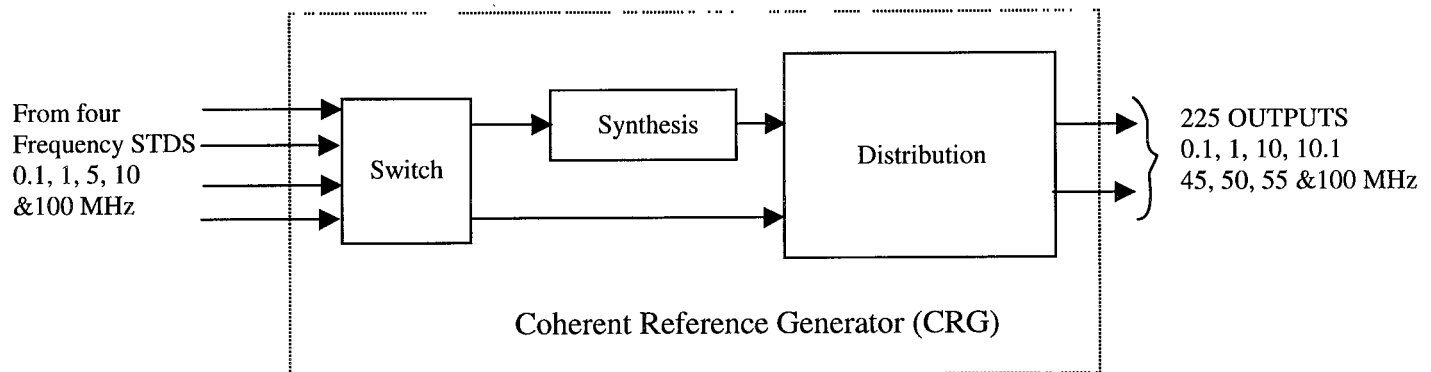


Figure 2. Reference Frequency Synthesis and Distribution

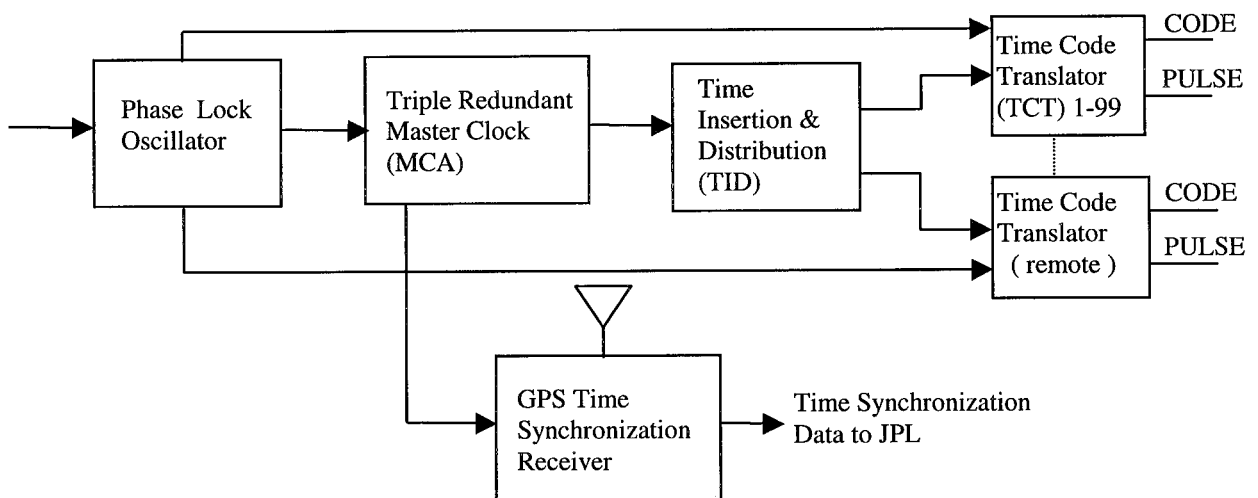


Figure 3. DSN Timing System

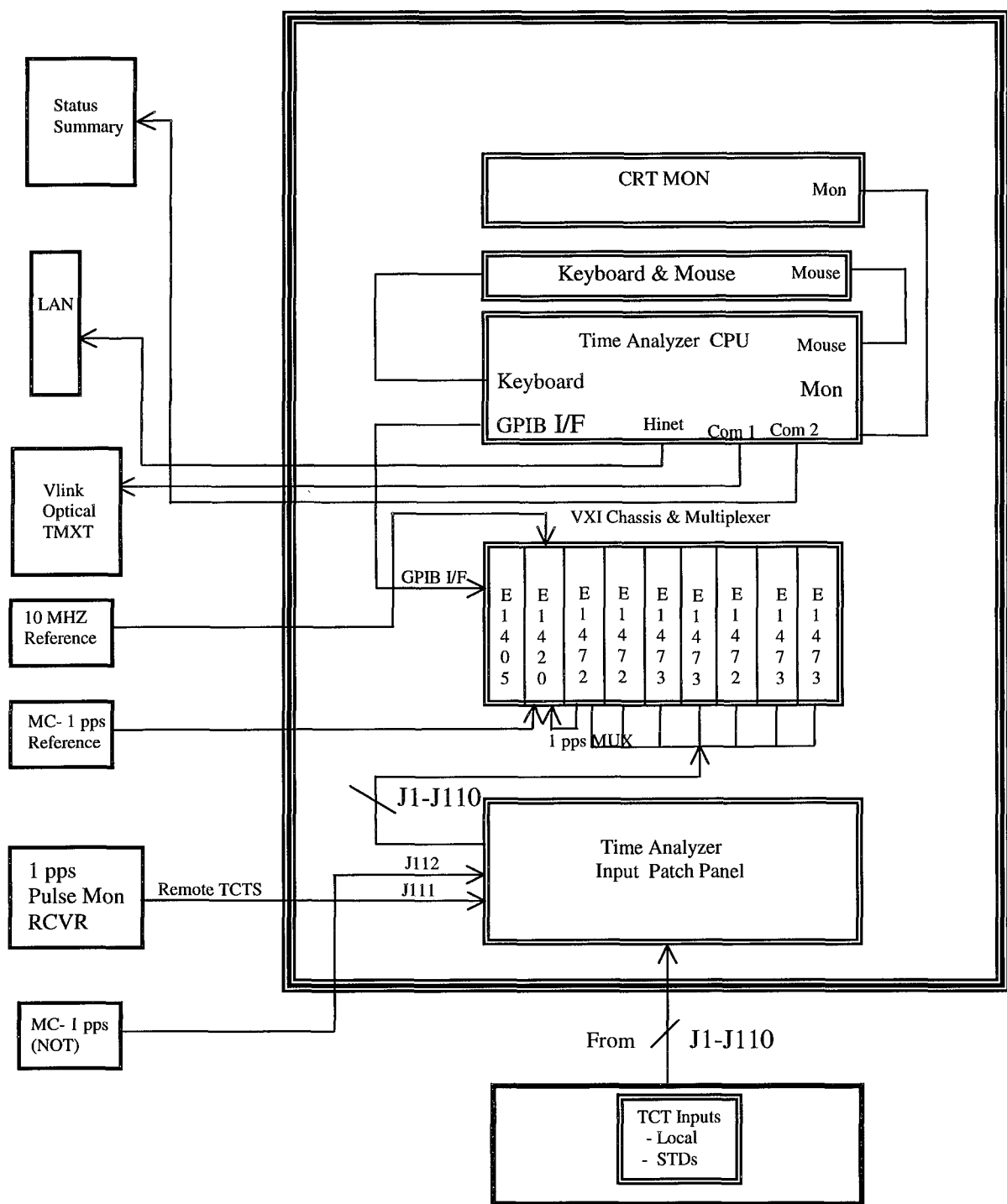


Figure 4: Time Analyzer Block Diagram

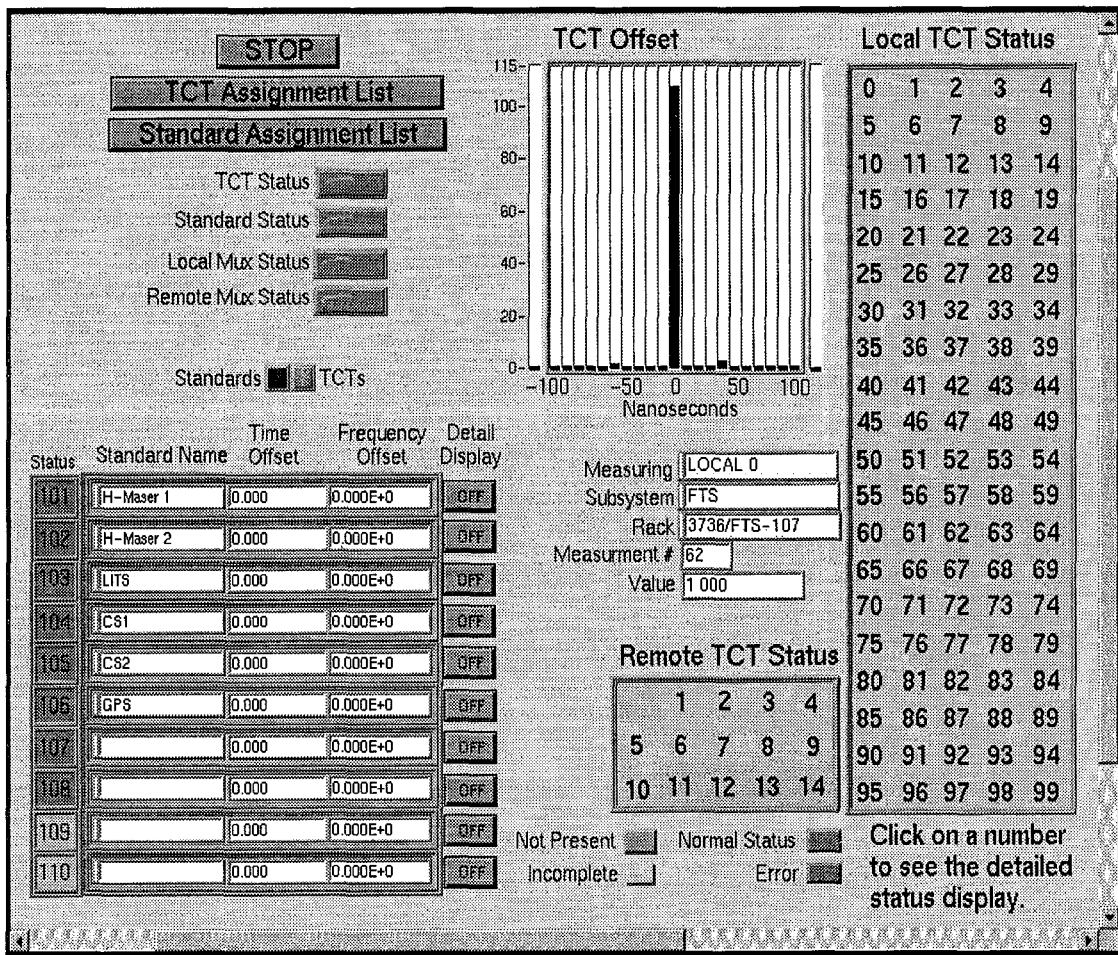


Figure 5. Time Analyzer Front Panel. The upper left shows summary alarm conditions to station operators. The right half displays individual TCT status and a summary histogram capturing synchronization of all TCT's to the master clock. The lower left provides a user configurable window for monitoring frequency standards and other 1 pps tests.

TCT Assignments

TCT #	SUBSYS	RACK	COMMENT	Delay (us)
L 98	DSS 34 # 2	5363/FTS 259	via o/fibre	21
L 99	DSS 34 # 1	5363/FTS 259	via o/fibre	21
R 0			do not use	0
R 1	FTS	3736/FTS-107	TIDS	4311159
R 2	FTS	3731/FTS 108		3254093

APPLY & CLOSE LOAD FROM FILE SAVE TO DEFAULT

Enter/Load/Save TCT Assignments.
Blank SUBSYS entry will mark TCT as not present.

(a)

Standard Assignments

STD NAME	SUBSYS	RACK	COMMENT	Delay (us)
H-Maser 1	FTS	3736/FTS-107	TIDS	0
H-Maser 2	FTS	3736/FTS-107	TIDS	0
UTS	FTS	3731/FTS-108		0
CS1	BLK IV	2601/RCV-402	DSS 43	0
CS2	SDE			0
GPS	RS 1	4705/RCV-123		0

APPLY & CLOSE LOAD FROM FILE SAVE TO DEFAULT

Enter/Load/Save Standard Assignments.
Blank STD NAME entry will mark standard as not present.

(b)

Figure 6: Assignment List Windows for a) TCT assignments and b) frequency standard and test input assignments.

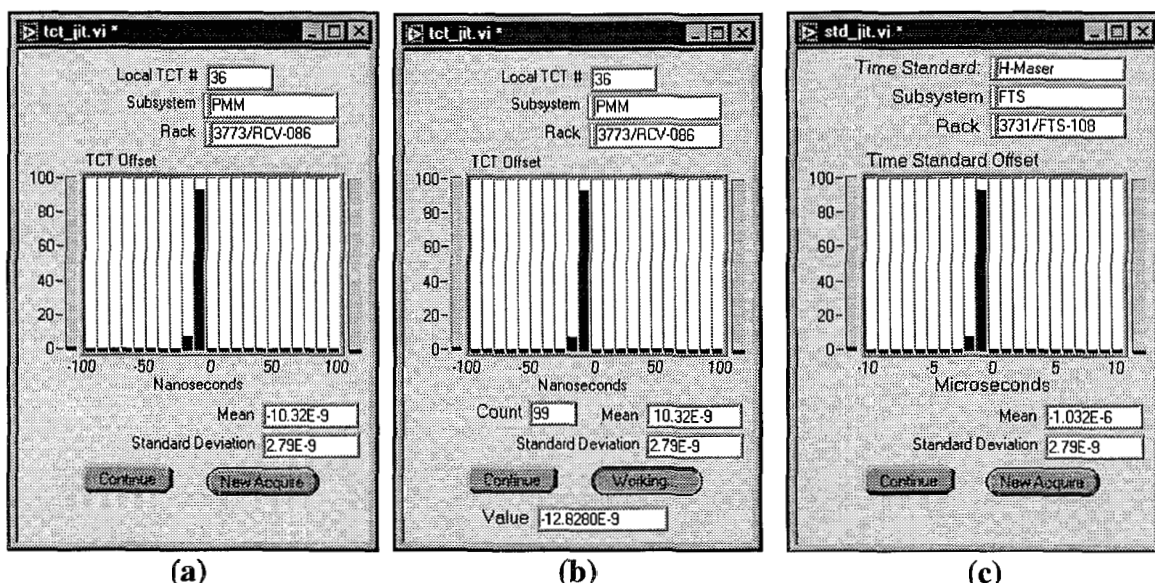


Figure 7: Time offset and jitter detail display windows.
a) b) for individual TCT, c) for frequency standards or 1 pps test input.

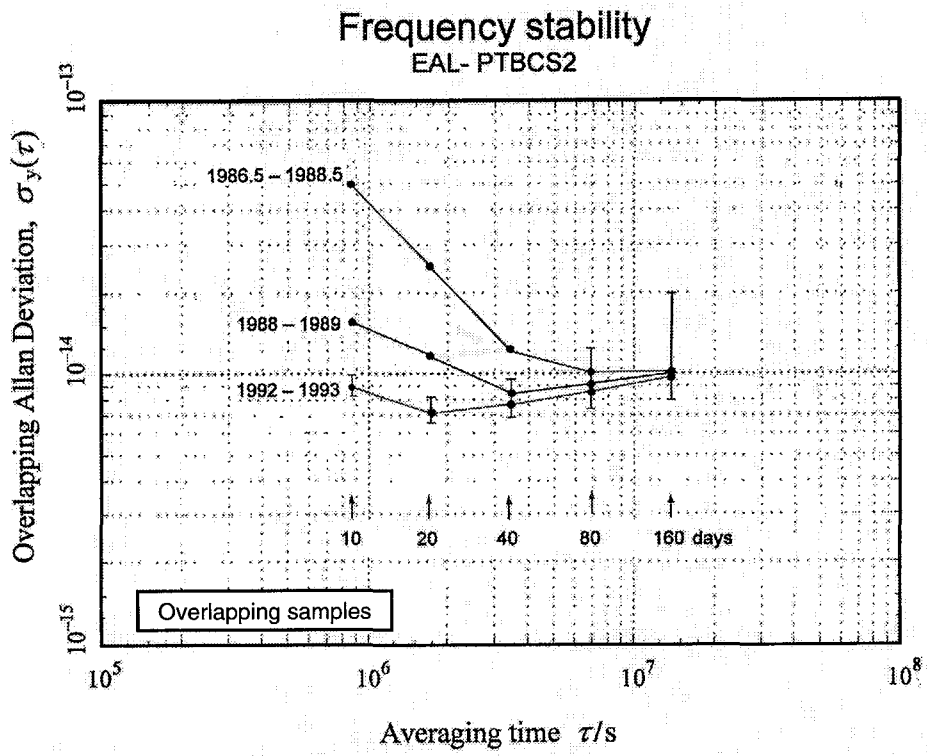


Figure 4. Frequency stability of [EAL – PTB Cs2].

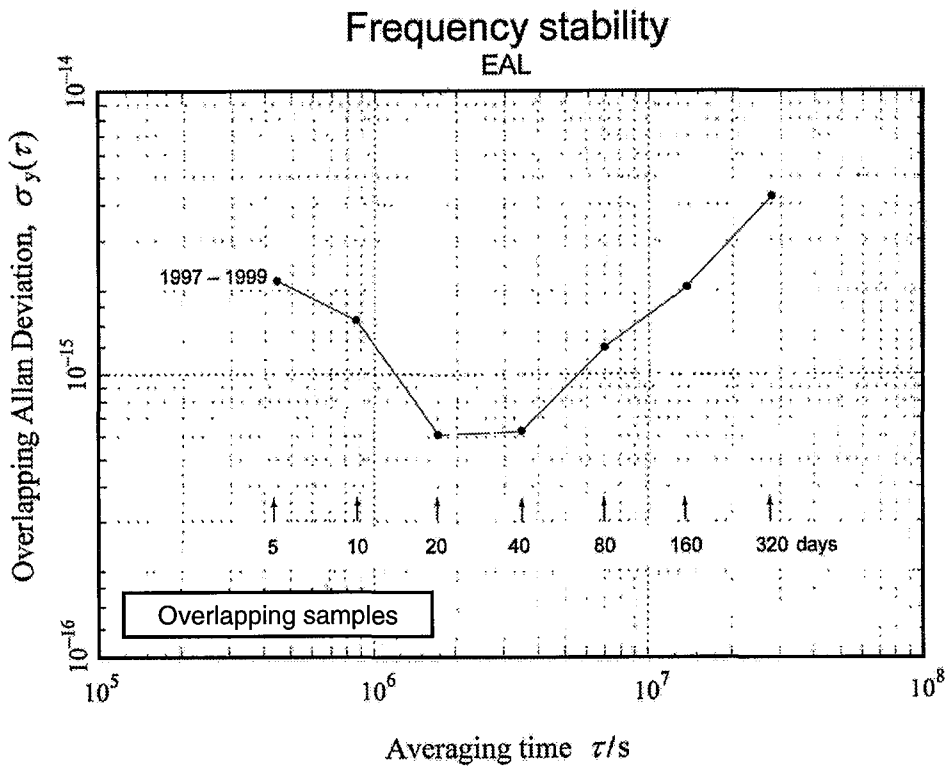
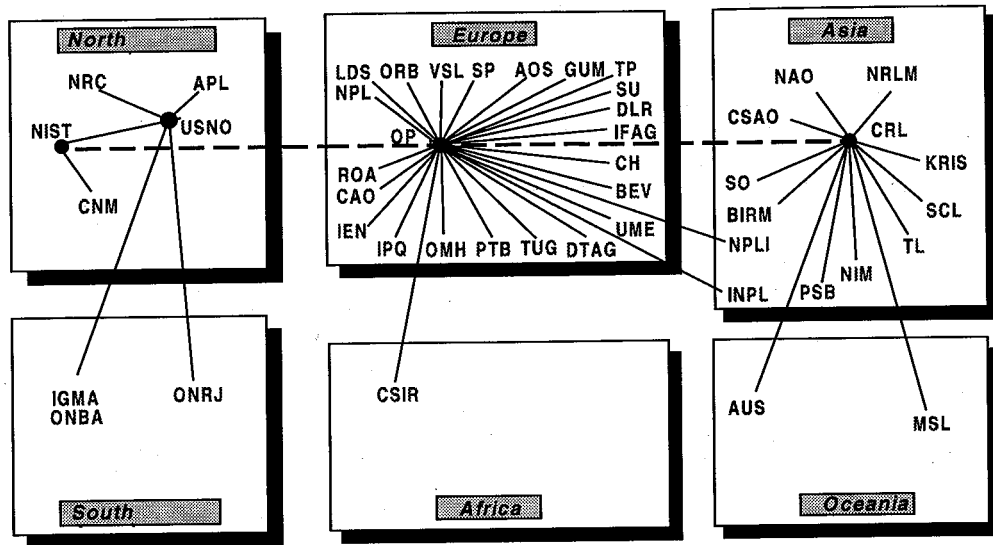


Figure 5. Frequency stability of EAL obtained by N -cornered-hat method using independent atomic time scales maintained at the OP, the NIST, the PTB, and the USNO.



June 1999

ORGANIZATION OF THE INTERNATIONAL TIME

— GPS common view

- - - GPS common view (corrected with IGS precise ephemerides and ionospheric maps).

Figure 6. Organization of international time links in June 1999.

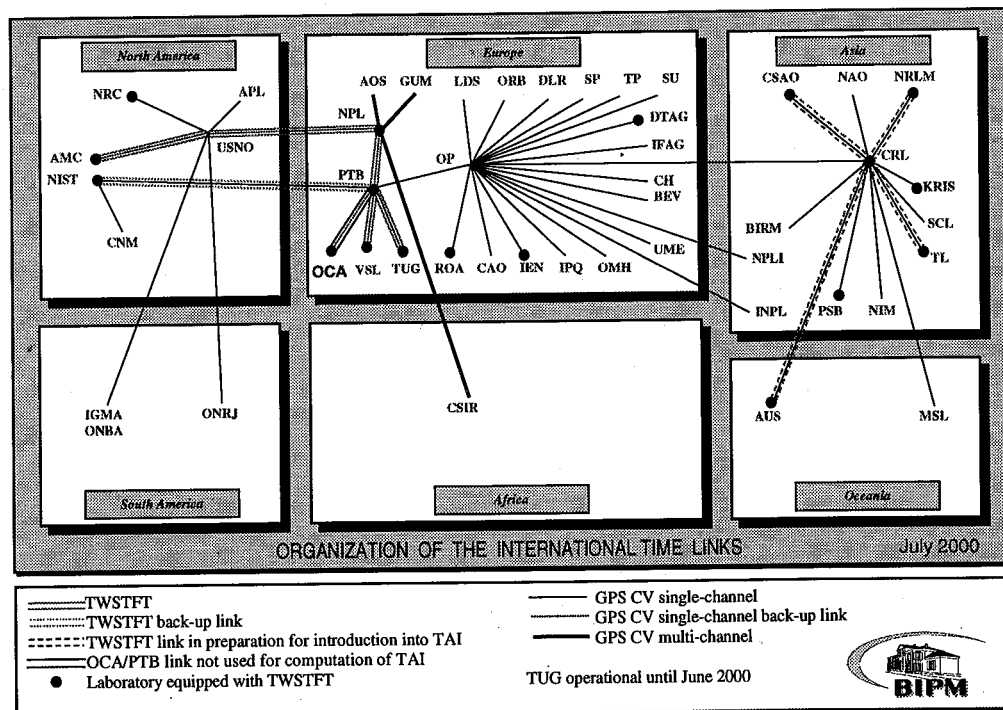


Figure 7. Organization of international time links in November 2000.

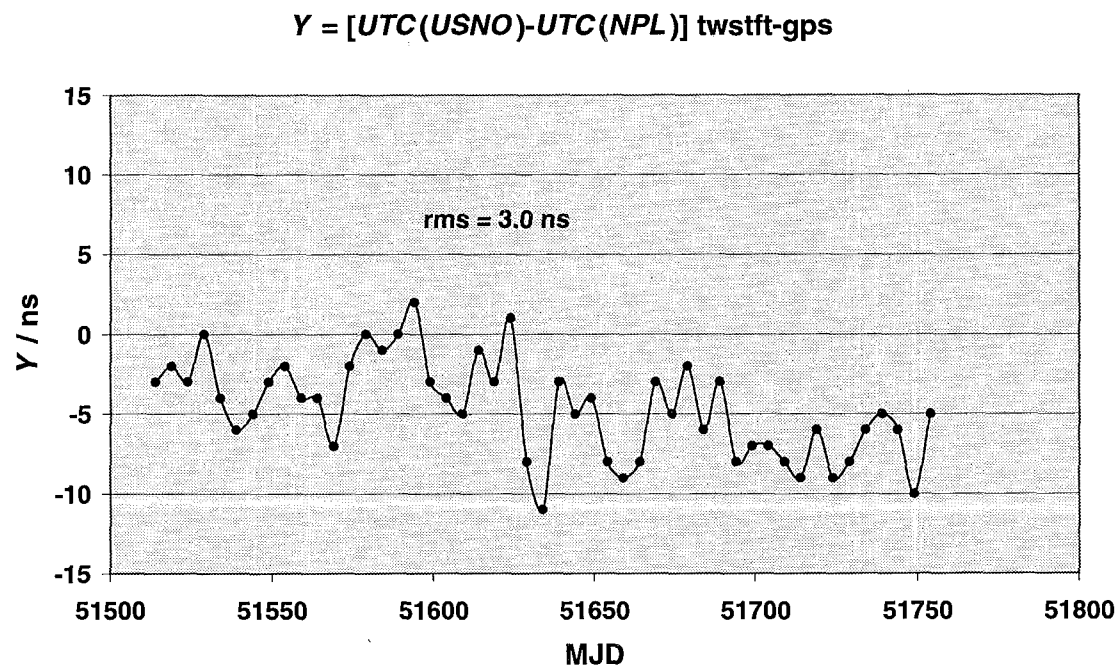


Figure 8. Differences between TWSTFT and GPS common-view for USNO/NPL link.

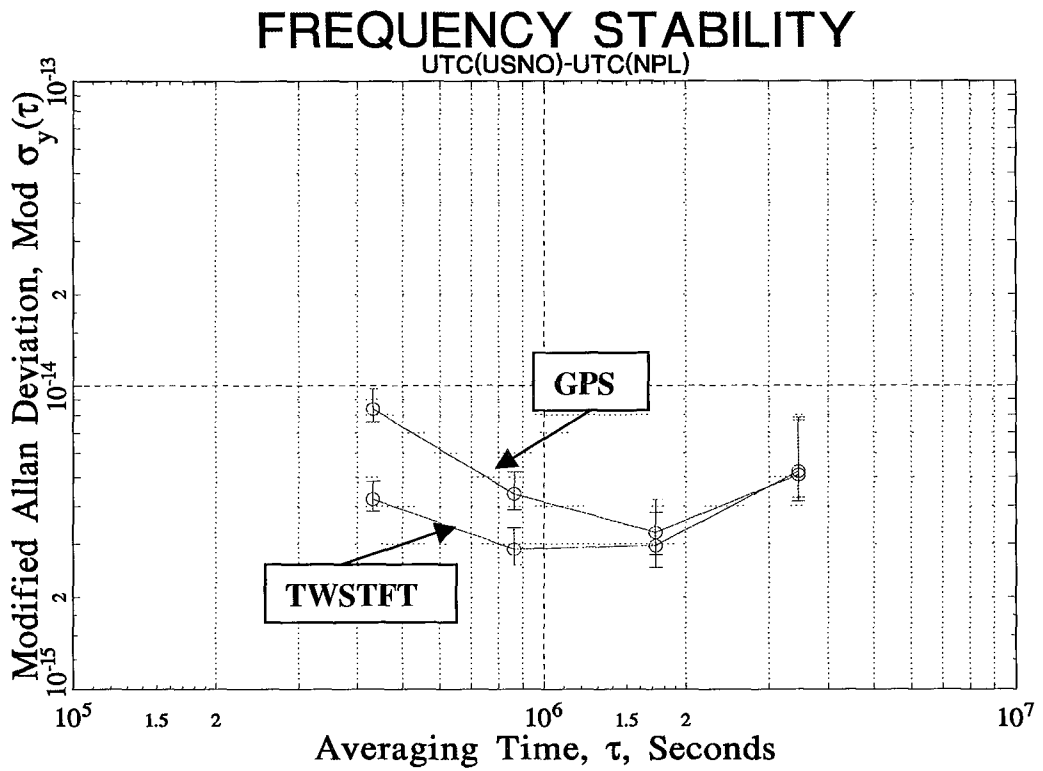


Figure 9. Frequency stability of $[UTC(USNO) - UTC(NPL)]$ by GPS and by TWSTFT.

DEVELOPMENT OF A PRIMARY REFERENCE CLOCK

Clive Green
Quartzlock (UK) Ltd.
Gothic, Plymouth Rd., Devon, TQ9 5LH, UK
Tel: +44 (0) 1803 862062; Fax: +44 (0) 1803 867962
E-mail: clivegreen@quartzlock.com; Website: www.quartzlock.com

Abstract

Quartzlock is engaged in research to improve the generation, measurement, and distribution of accurate frequency sources that are stable with environmental changes. The elements in this progress report are both active and passive masers, quartz frequency standards, measurement systems, GPS/Glonass receiver, GPS CVTT, and rubidium standards. Space-qualified passive hydrogen masers and rubidium oscillators are considered. A new measurement system is detailed and the first noise floor results are reported.

ACTIVE AND PASSIVE MASERS, GPS-GLONASS, AND GPS CVTT

NIST-traceable measurements have been made of a passive hydrogen maser with GPS, rubidium, and other elements for a new primary reference clock being developed with European Union assistance.

IEM Kvarz provided an ensemble of active hydrogen masers to measure the GPS carrier-phase tracking RX performance of 5×10^{-14} over 3 to 33 days. This figure was confirmed at PTB. The active maser performance has been significantly improved at 1 day to 3×10^{-16} for drift after 1 year of operation (5×10^{-16} in the first month).

The H masers used as a reference are CH1-75's. Results include the CH1-75 active hydrogen maser frequency stability measurement, which has an automatic cavity frequency control (ACFC) system. Two ACFC systems were investigated. The first system was non-autonomous, because another hydrogen maser was required for its operation; the second system was autonomous. The atom line quality modulation method was used in both systems.

The ACFC system is based on measurement of the frequency difference of masers at two atom-line quality values by means of a frequency comparator and a reversible counter and cavity frequency control versus the value and sign of this difference. In the non-autonomous system, a cavity autotuning was produced by cycles with a 2300-s duration (a count time of the reversible counter in one direction was 1000 s); atom-line quality was changed by beam intensity.

10 s was used. The modulation was performed by introduction of an inhomogeneous magnetic field into the storage bulb. The tuning was performed by cycles with 25-s duration (the count time of reversible counter was 10 s). An additional digital filter (the second reversible counter) was introduced after the first reversible counter.

The experimental frequency stability of the hydrogen maser with autonomous ACFC was 5×10^{-15} per day. Using a more stable crystal oscillator having a frequency stability of 1.5×10^{-13} at 1 s to 10 s will improve maser frequency stability approximately by 3 times and using a microprocessor or a personal computer as a digital filter improves dynamic performance of the ACFC loop.

The Autonomous Autotune (AAT) system employed enables close to Cavity Autotune (CAT) performance with two active hydrogen masers, which achieve Allan variances of 2×10^{-13} at 1 s, 3×10^{-14} at 10 s, and 2×10^{-15} at 1 d, but without the advantage of a redundant system needed for HiRel timing. IEM KVARZ is providing active H masers for qualification and specification analysis of a new passive maser, a GPS/Glonass RX measurement system, and GPS, CVTT, and rubidium elements. The passive H maser target performance meets the European Space Agency PM specification requirement.

GPS size, weight, and power reductions are significant. A new low-cost GPS element result is illustrated. It is not expected to be reproducible in production quantities as a product spec, but is a typical test result.

MEASUREMENT SYSTEM

The current measurement system A7 has the highest resolution available in the shortest measurement time: 1.5×10^{-15} in only 100 s and 1.5×10^{-16} in 1000 s. For the new passive maser this is the development tool used. However, in a system where the new PHM is the standard against which the DUT is measured, a low cost, smaller size, lighter weight module is required for it to be a component part in a complete system. The performance required is not as high as the current A7, but innovative solutions enabling substantial cost size and weight were required. A completely new approach was adopted that met the need of the Alpha project in all respects – the results achieved are plotted.

RUBIDIUM OSCILLATOR

The rubidium oscillator element has to be the most rugged because this link in the redundancy chain must survive longest, and telecom component applications in both civil and defense use have differing environmental requirements.

Current HSRO, LPRO, SRAFS, and LCRO specs are tabled below.

LABORATORY ENVIRONMENTAL DATA

Mechanical/physical environmental testing revealed the following results during tests of the rubidium element.

REFERENCES

V. A. Logachev 1999, in "The hydrogen maser cavity step autotuning: theoretical analysis and experimental results," Proceedings of the Joint Meeting of the 13th European Frequency and Time Forum and 1999 IEEE International Frequency Control Symposium, 13-16 April 1999, Besançon, France, pp. 129-132.

N. Demidov, private communication.

European Space Agency

Specifications	Active Hydrogen Maser CH1 - 75	Active Hydrogen Maser +AAT CH1 - 75A Autonomous Auto Tune Version	Active Hydrogen Maser +CAT CH1-75 (2 units) CH1-75B	Passive Hydrogen Maser CH1-76	S-PHM Space Qualified Passive Hydrogen Maser @10-s mBar	S-RAFS Space Qualified Rubidium Atomic Frequency Standards
Sine wave						
Frequency, MHz	5,100	5,100	5,100	5,100	10	10
Voltage at 50 Ohm load, V	1±0.2	1±0.2	1±0.2	1±0.2	7dBm±1	
Harmonic distortion dB	-30	-30	-30	-30	-60	-40
Non-harmonic distortion in 10 MHz – 10kHz range dBc	-120	-120	-120	-100	-84 & -60	-84 & -60
Phase noise dBc/Hz						
1 Hz	-110	-110	-110	-100	-124	-90
10 Hz	-130	-130	-130	-120	-146	-110
100 Hz	-140	-140	-140	-140	-155	-130
1000 Hz	-150	-150	-150	-150	-155	-150
10000 Hz	-150	-150	-150	-150	-155	
- pulse						
Frequency Hz	1	1	1	1		
Amplitude at 50 Ohm load V	>2.5	>2.5	>2.5	>2.5		
Width ns	10 – 20	10-20	10-20	10-20		
Rise time ns	15	15	15	30		
Jitter ns	0.1	0.1	0.1	0.1		
Frequency accuracy (within 1 year period)	±3.10 ⁻¹²	±1.10 ⁻¹²	±5.10 ⁻¹³	±1.5.10 ⁻¹²		1.0·10 ⁻¹⁰
1s	2.10 ⁻¹³	3.10 ⁻¹³	2.10 ⁻¹³	1·5.10 ⁻¹²	1.10 ⁻¹²	5·10 ⁻¹²
10s	3·10 ⁻¹⁴	1·10 ⁻¹³	3·10 ⁻¹⁴	5·10 ⁻¹³	3.2·10 ⁻¹³	1.5·10 ⁻¹²
100s	5·10 ⁻¹⁵	1·10 ⁻¹⁴	1·10 ⁻¹⁴	1.5·10 ⁻¹³	1·10 ⁻¹³	5·10 ⁻¹³
1000s	2.5·10 ⁻¹⁵	5·10 ⁻¹⁵	5·10 ⁻¹⁵	5·10 ⁻¹⁴	3.2·10 ⁻¹⁴	1.5·10 ⁻¹³
1h	1·10 ⁻¹⁵	3·10 ⁻¹⁵	3·10 ⁻¹⁵	3·10 ⁻¹⁴	1·10 ⁻¹⁴	7·10 ⁻¹⁴
1 day	1·10 ⁻¹⁵	3·10 ⁻¹⁵	2·10 ⁻¹⁵	1 10 ⁻¹⁴		5·10 ⁻¹⁴
Frequency drift per 1 day	3·10 ⁻¹⁵	5·10 ⁻¹⁵	2·10 ⁻¹⁵	1 10 ⁻¹⁴		
At launch	5·10 ⁻¹⁵	5·10 ⁻¹⁶	5 10 ⁻¹⁶	2·10 ⁻¹⁵		
After 1 year	3·10 ⁻¹⁵	3·10 ⁻¹⁶	3·10 ⁻¹⁶	2 10 ⁻¹⁵	3·10 ⁻¹²	3.0·10 ⁻¹¹
Temperature frequency coefficient 1/°C	2·10 ⁻¹⁵	2·10 ⁻¹⁵	1·10 ⁻¹⁵	2·10 ⁻¹⁴		1·10 ⁻¹³
External magnetic field effects, 1/Gauss	1·10 ⁻¹⁴	1·10 ⁻¹⁴	1·10 ⁻¹⁴	2.5·10 ⁻¹⁴	2·10 ⁻¹⁴	1·10 ⁻¹³
Frequency corrector resolution	1·10 ⁻¹⁵	1·10 ⁻¹⁵	1·10 ⁻¹⁵	1·10 ⁻¹⁴		

Fig.1 NIST traceability of A8-B

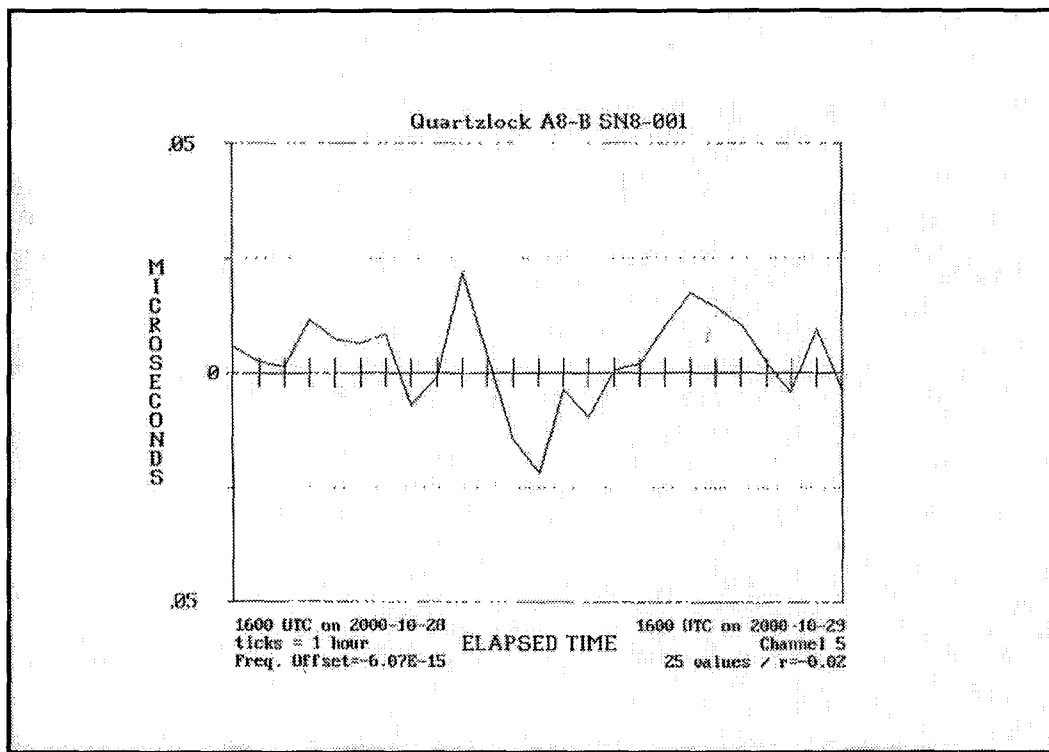


Fig.2 NIST traceability of Passive Hydrogen Maser

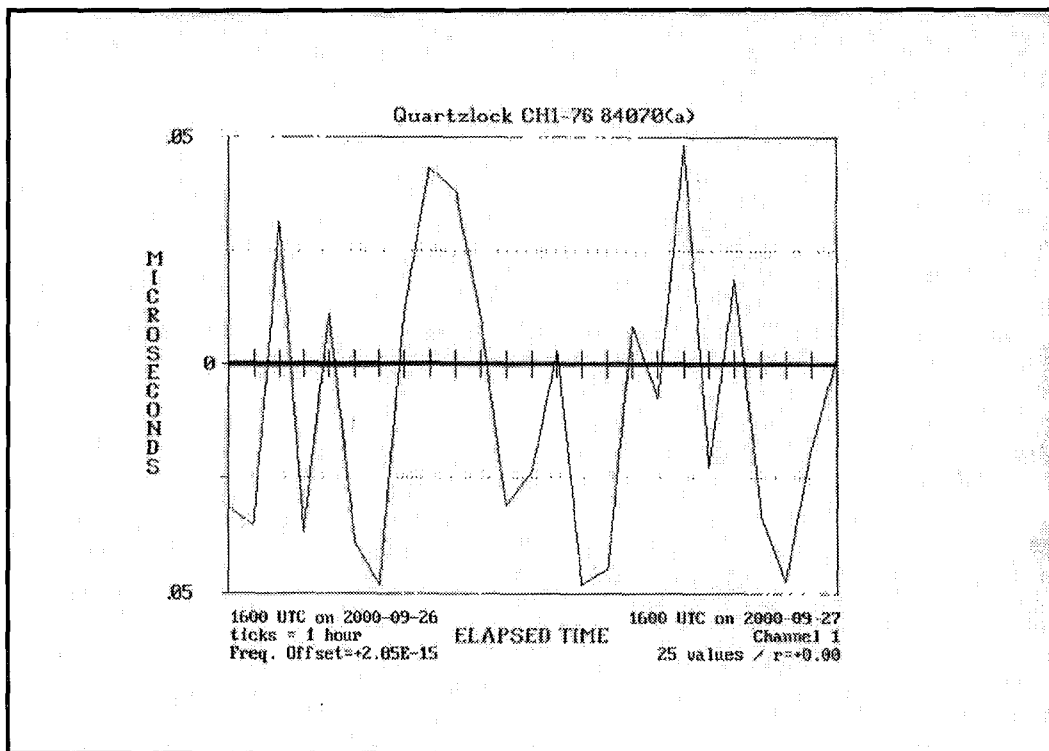


Fig.3:
Resonance Search - Axis 1.
Monitor Accelerometer on Rubidium Module.
Pre –Endurance Testing

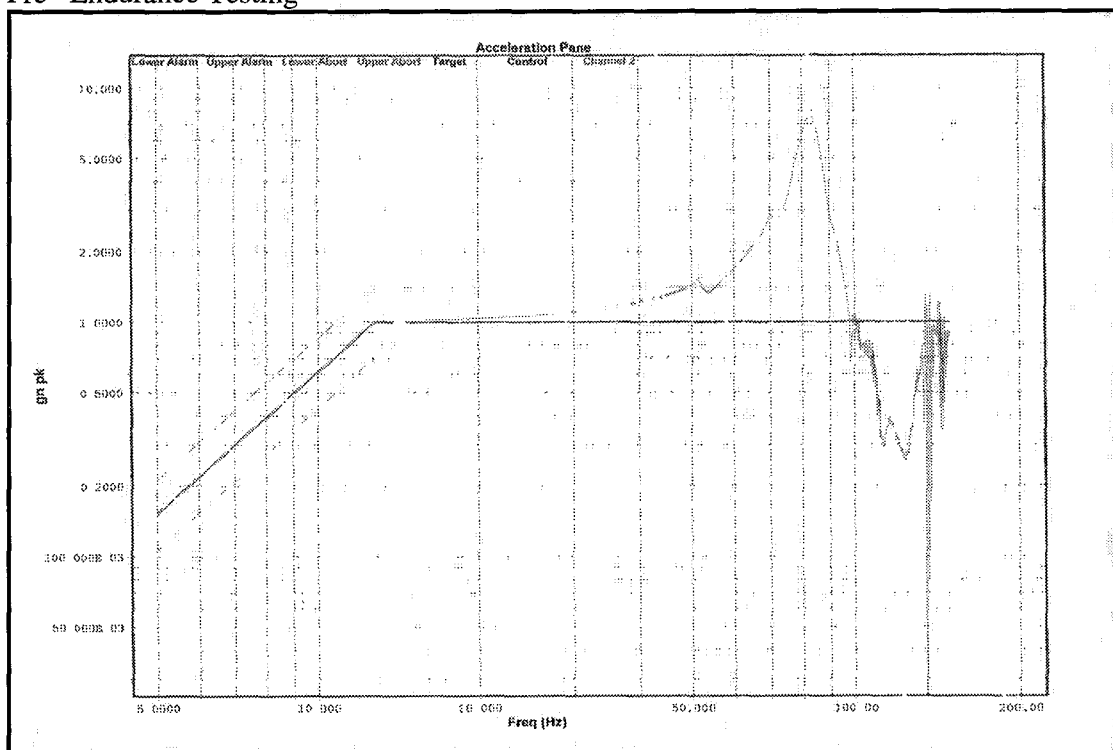


Fig.4 Applied Shock Pulse – 25gn for 6ns

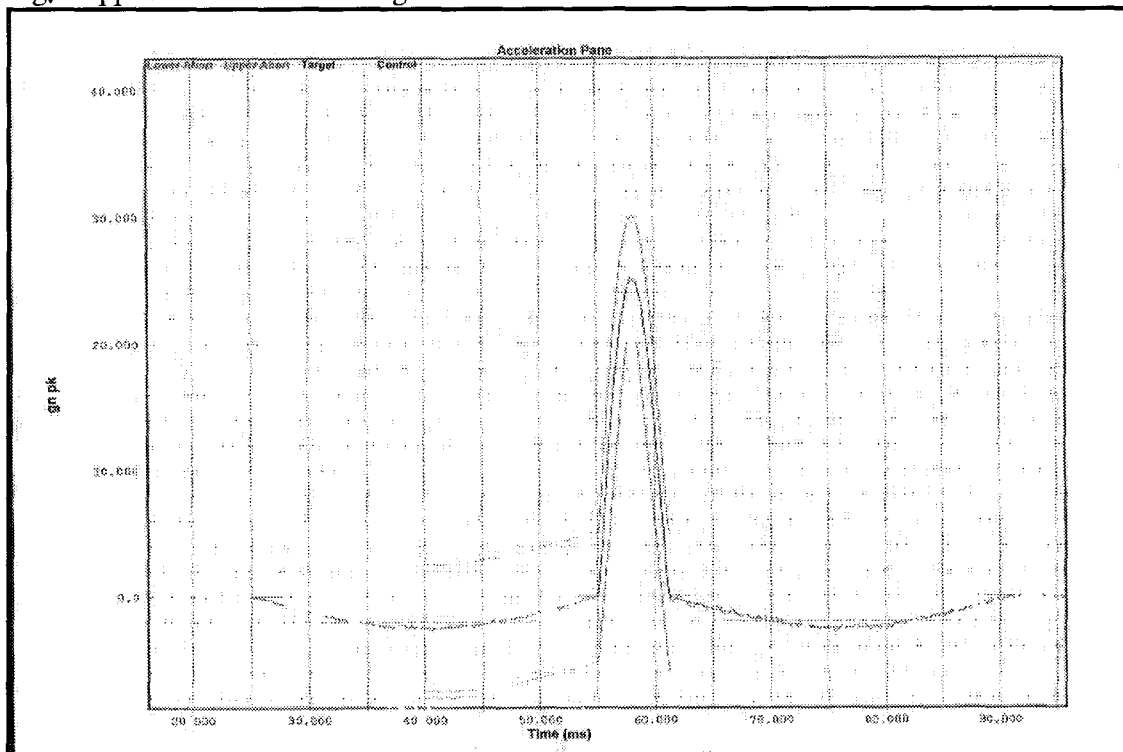


Fig.5

Report of Calibration
NIST Service ID Number 76100S - Frequency Measurement Service

Time and Frequency Division
National Institute of Standards and Technology
Boulder, CO 80303-3328

Customer: Quantock Gatton, Plymouth Road Tiverton Devon, UK TQ9 5H	Device Under Test (DUT): Quartzlock A1 Hydrogen Maser
	Description of DUT: Hydrogen Maser Frequency Standard
Contact: Lucy Martin	Period of Calibration: July 2000

1 Description of Calibration Procedure

The calibrations were performed at the customer's site using a computer-controlled data acquisition system. The calibrations are monitored from the NIST laboratories in Boulder, Colorado through a dedicated telephone line, and NIST personnel compile the data used in this report.

Traceability to NIST is established by using a Global Positioning System (GPS) satellite module as a frequency standard. A phase comparison between the customer's frequency standard and the GPS receiver is performed using the time interval method. A daily estimate for frequency offset is obtained by making continuous phase comparisons between the frequency standard and GPS signals over a 24-hour period, and fitting a linear least squares line to this phase data. The correlation coefficient (r) indicates the confidence level of the measurement.

Table 1 lists the daily frequency offset estimates and a status code for each calibration. A status code of 0 is used for a valid calibration. Other status codes are used to identify and explain situations when no data were collected, when measurement errors occurred, or when the DUT was out-of-tolerance.

Figure 1 is a graph of the daily frequency offset estimates. Table 2 is a statement of measurement uncertainty.

Measurement uncertainty ($k = 2$) is reported with respect to the national frequency standard for a 24-hour averaging period. Measurement uncertainty is contributed by the GPS receiver, by DUT aging and frequency drift, and by measurement system noise. The GPS receiver contributes an uncertainty of 12.5×10^{-15} . Measurement system noise contributes an uncertainty of $<2 \times 10^{-15}$.

2 General Information

NIST supplies the hardware, software, and calibration method used to perform the calibration. When measurement system components fail, NIST is responsible for replacing them. When possible, this is done using an overnight delivery service.

Since calibrations are made at the customer's site, maintaining an acceptable laboratory environment is the responsibility of the customer. The customer is also responsible for following the installation and operating procedures outlined in the Operator's Manual supplied with each measurement system.

Issue Date: August 02, 2000 NIST Customer Report #: 230007
NIST Service ID #: 76100S Page 1 of 3

Fig.6

Table 1 - Daily Frequency Offset Values, Confidence Levels, and Status Codes

Date	Frequency Offset	Confidence Level (%)	Status Code	Comments
2000-07-01	+0.305E-13	-0.07	0	
2000-07-02	+3.052E-14	+0.03	0	
2000-07-03	+1.385E-13	+0.10	0	
2000-07-04	-2.57E-14	-0.02	0	
2000-07-05	-7.81E-14	-0.08	0	
2000-07-06	12.34E-13	+0.03	0	
2000-07-07	-2.285E-13	-0.17	0	
2000-07-08	-2.785E-13	-0.24	0	
2000-07-09	+1.818E-13	+0.18	0	
2000-07-10	-1.005E-13	+0.09	0	
2000-07-11	+3.052E-14	+0.03	0	
2000-07-12	-2.77E-13	+0.42	0	
2000-07-13	+1.57E-13	+0.12	0	
2000-07-14	+1.47E-13	+0.12	0	
2000-07-15	-3.82E-13	-0.29	0	
2000-07-16	-4.00E-13	-0.30	0	
2000-07-17	-7.23E-14	-0.07	0	
2000-07-18	-5.87E-13	-0.48	0	
2000-07-19	-4.28E-13	-0.40	0	
2000-07-20	-6.53E-13	-0.45	0	
2000-07-21	-1.01E-12	-0.62	0	
2000-07-22	-1.02E-12	-0.62	0	
2000-07-23	-4.82E-14	-0.07	0	
2000-07-24	-5.28E-13	-0.54	0	
2000-07-25	-4.44E-13	-0.34	0	
2000-07-26	-1.452E-13	-0.12	0	
2000-07-27	-6.34E-14	-0.08	0	
2000-07-28	(*****)	(****)	1	System stopped, cause unknown
2000-07-29	(*****)	(****)	1	System stopped, cause unknown
2000-07-30	(*****)	(****)	1	System stopped, cause unknown
2000-07-31	-4.58E-12	-0.58	0	

Status Key: 0 - Valid Calibration, 1 - No Data, 2 - GPS Reception Error, 3 - GPS Broadcast Error,
4 - Measurement System Error, 5 - DUT Error, 6 - DUT Change

Issue Date: August 02, 2000 NIST Customer Report #: 230007
NIST Service ID #: 76100S Page 2 of 3

Fig.7

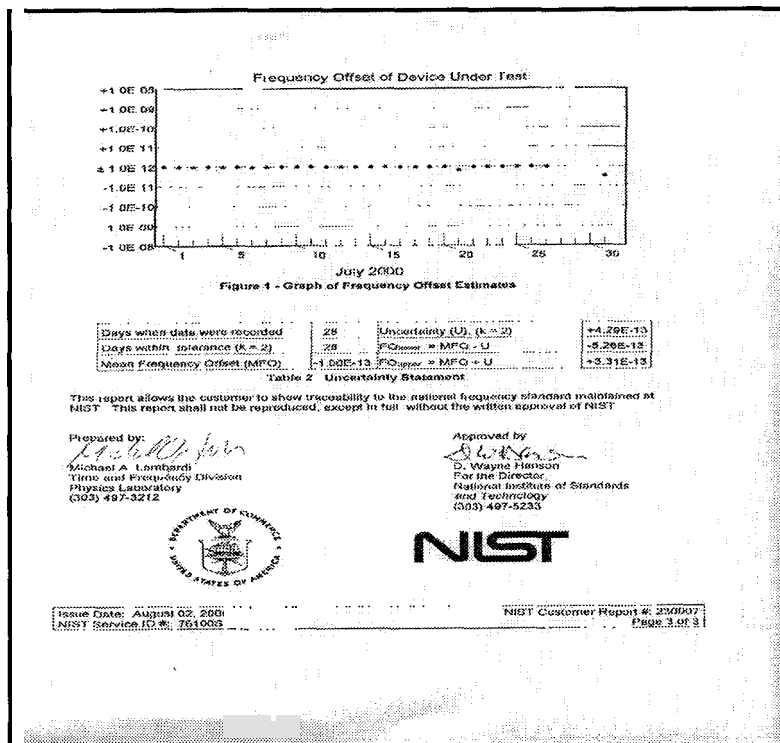


Fig.8

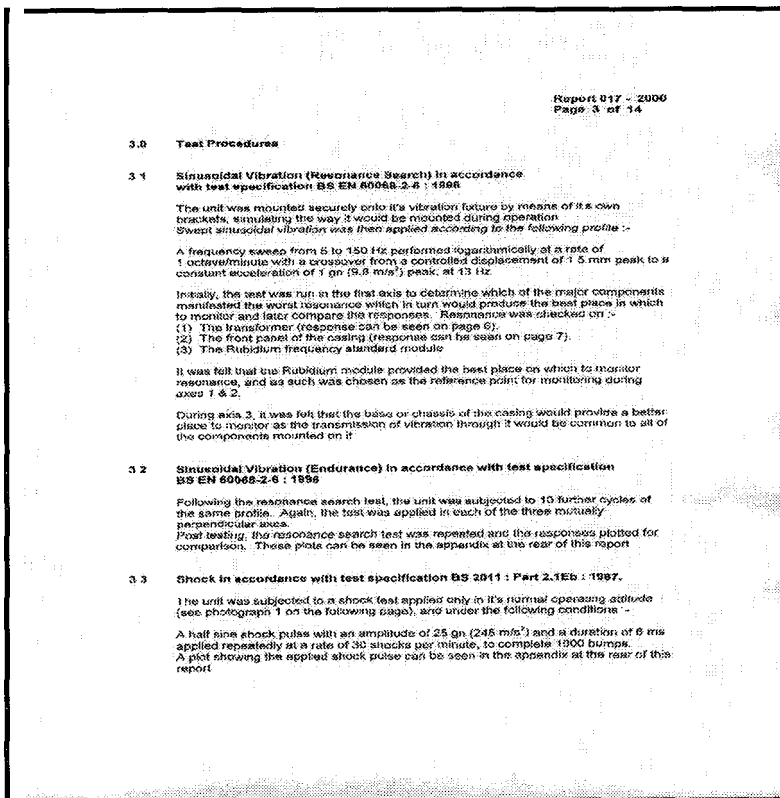


Fig.9

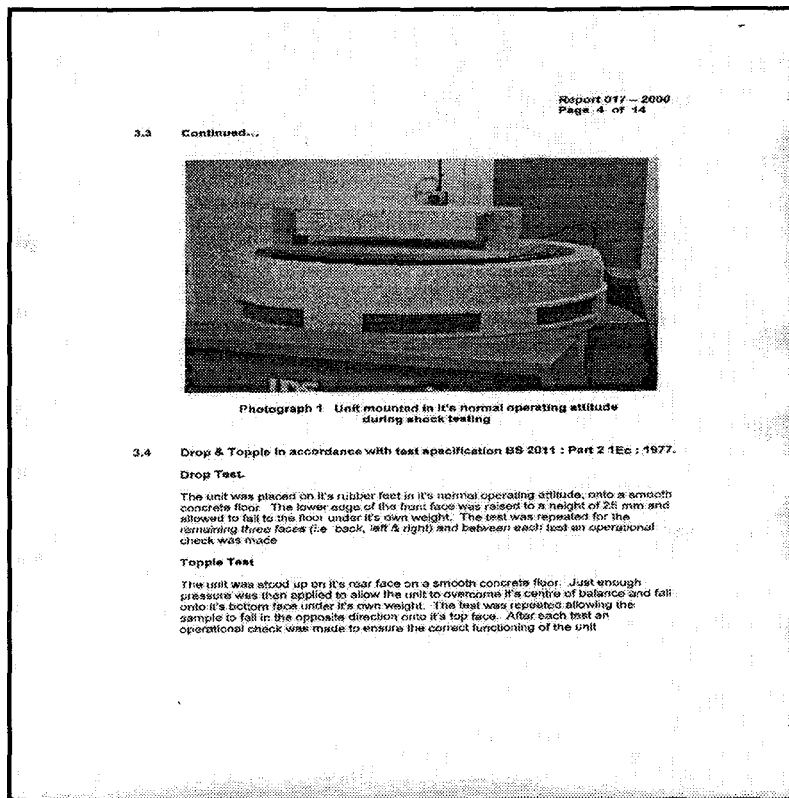


Fig.10

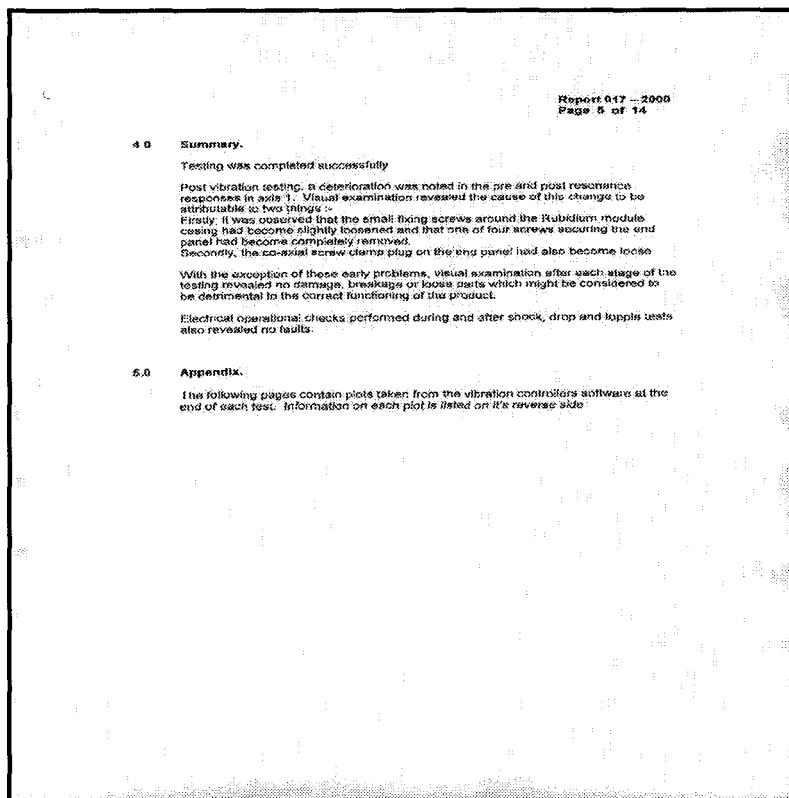
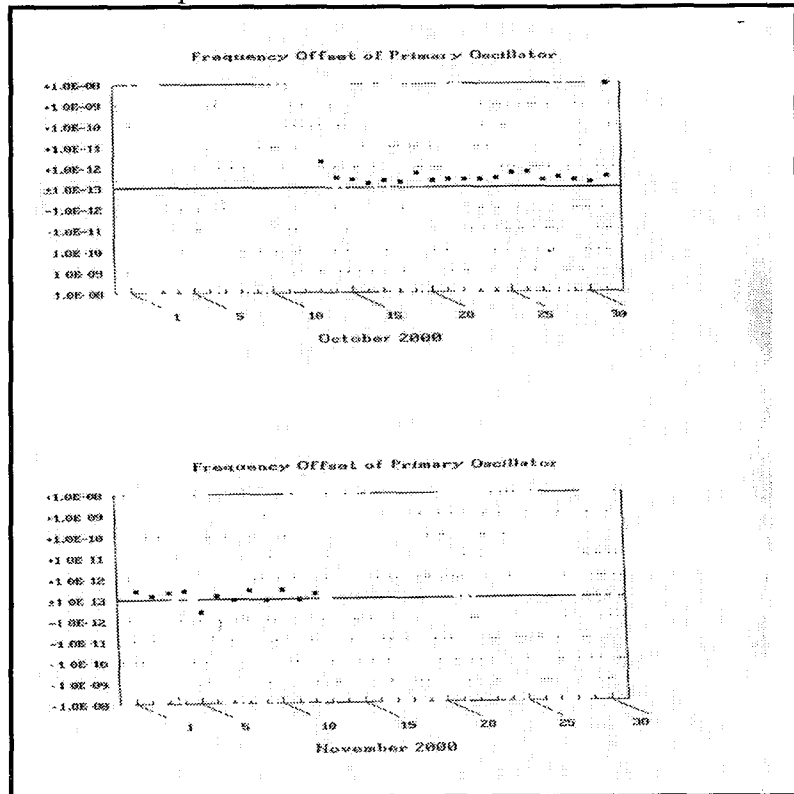


Fig.11 NIST-traceable passive maser offset



Synthesizer adjustment end Oct.

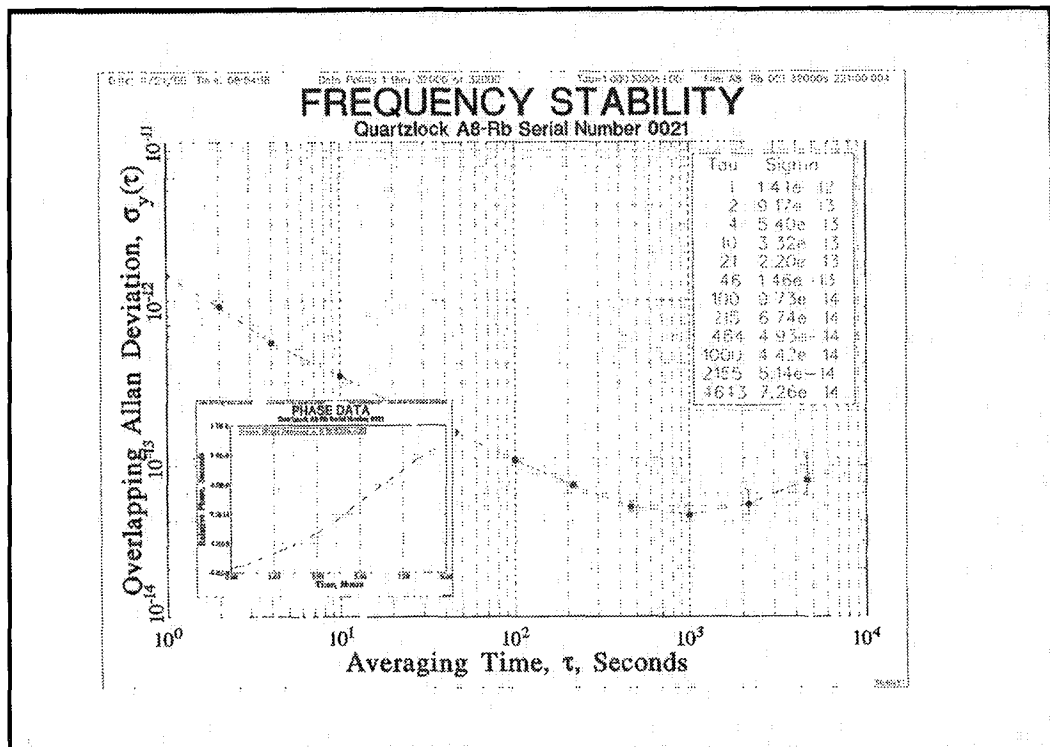


Fig12

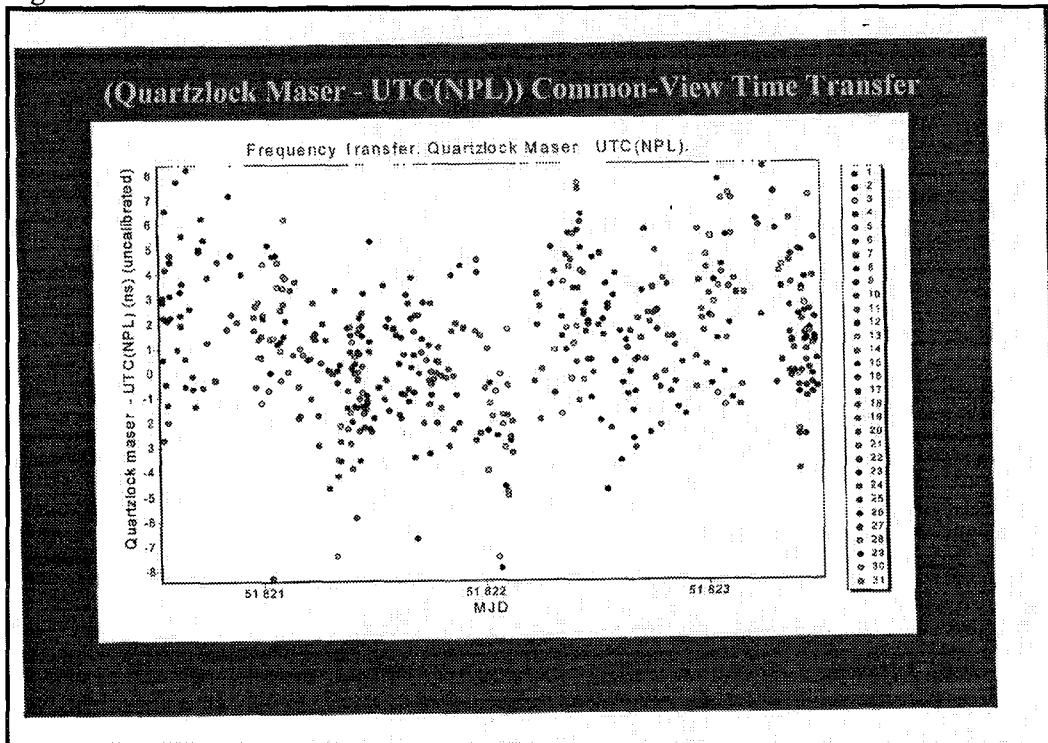
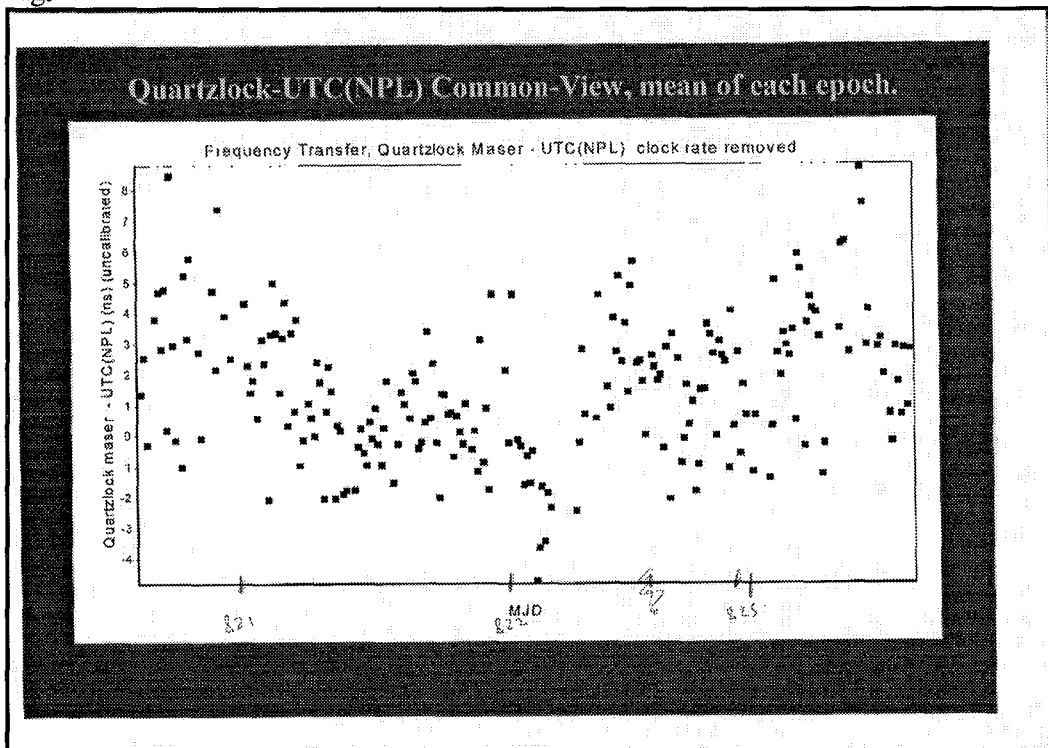


Fig.13



COMMON TIME REFERENCE TECHNOLOGY FOR SYSTEMS INTER-OPERABILITY

R. L. Beard and J. D. White
U.S. Naval Research Laboratory
Washington, D.C. 20375, USA

Abstract

The Global Positioning System has become the primary and most accurate means of disseminating time and frequency information. A growing and diverse mix of military positioning, communication, sensor, and data processing systems are using precise time and frequency from GPS. The precise accuracies required for their operation are also becoming more stringent. A new system architecture for providing a Common Time Reference to the operating forces and their related subsystems is being developed. This architecture is to provide a robust enhancement to implementations of GPS time and frequency subsystems. Through its implementation, inter-operability between systems is enabled by providing a Common Time Reference and the means for systems to operate synchronously as a foundation for common interfaces and data exchange.

The Common Time Reference approach and its relationship to present GPS time and frequency usage will be described to show the concept and approach of this architecture. A robust architecture utilizing distributed time standards and existing standards within individual systems is to provide new capabilities for existing fielded systems without the impact of requiring major retrofit. This combination of enabling existing and new resources to be utilized in a common reference will reduce the sensitivity to GPS anomalies and lack of continuous contact for precise updating. These systems would then be interconnected at the fundamental level of internal time and frequency generation, which would provide an inherent basis for functional inter-operability. The elements necessary for implementation of this architecture with generic systems will be discussed. Technical developments necessary for implementation of the concept and the impact on inter-operability will be discussed.

INTRODUCTION

The Global Positioning System (GPS) has become the primary dissemination system for Precise Time and Frequency (PT&F) for inter-operability of Naval and Department of Defense (DoD) systems. The move toward joint, diverse inter-operating systems that can gather raw data, process, communicate, and place weapons on target through a continuous stream of information moving from sensors to weapons carriers requires a level of synchronization not possible before GPS. This flow of information requires mobile platforms in the field, oceans, and sky to receive, maintain, and distribute PT&F data previously only available at major timing centers. Consequently, PT&F precision and accuracy are emerging in the utility to disseminate the reference time scale and maintain it throughout the operating forces. This utility and increasing dependence on GPS supplied PT&F is complicated by the vulnerability of GPS to electronic countermeasures.

The consideration of the vulnerability of GPS and its interaction with the various systems that use or need this capability has led to the development of a Common Time Reference (CTR)

Technical Architecture using Distributed Time Standards (DTS) to form a complementary capability working with GPS. The many systems using GPS previously often used precise atomic clocks and extensive supporting systems, which are being displaced by GPS timing receivers disciplining an internal oscillator. These receiver oscillators can be of low quality and still output the precise time provided from the spaceborne atomic clocks of the GPS system. As the use of GPS-disciplined, low quality clocks/oscillators increases, so does the dependence upon GPS as the time source. The increased use of GPS has created the demand for a profusion of receivers. To reduce the proliferation of GPS receivers, GPS-derived time signals are being consolidated and signals distributed to satisfy existing and new systems requirements. This situation is placing greater dependence upon continuous GPS contact.

Developments are being investigated to supply increased PT&F capabilities and reduce dependence upon continuous GPS contact by utilizing existing resources and unifying systems and interfaces. By providing the capability to maintain a coordinated local CTR within the operating forces, individual systems may approach the accuracy of that performed at timing centers. This complementary capability would decrease reliance upon GPS as a direct, continuous source of PT&F and provide the infrastructure for synchronizing the systems in the operating forces. A synchronous systems infrastructure requires accurate coordination and interchange of timing information between systems in order to achieve a network-centric environment for future military operations.

NETWORK-CENTRIC WARFARE

A concept for operating diverse military forces in localized theater areas is known as Network-Centric Warfare [1]. This concept relies upon inter-operable systems operating with closely coordinated precision across warfare areas, services, and weapons systems. Illustrated in Figure 1, joint forces in theater area operation require participating elements to inter-operate with

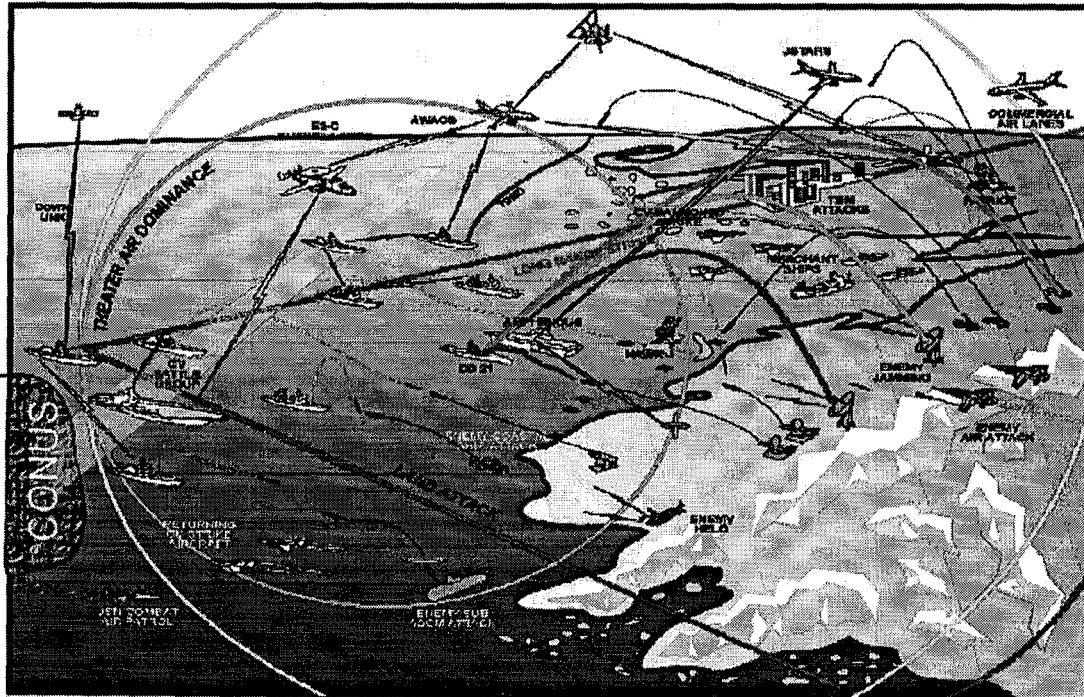


Figure 1. Network-Centric Theater Area Operation

a variety of centrally controlled, cooperative levels of deployment, surveillance, defensive, and offensive roles. Communications and data transfer are central to cooperative inter-operation. An example of this inter-operation is the need to dominate the airspace over the operating theater, which first requires a precise knowledge of everything within that airspace.

THEATER AIR SURVEILLANCE

To provide protection and enable air operations, the theater airspace must be controlled completely and continuously. For this to be possible, the operating forces must detect, identify, and monitor all aircraft within the theater. Data collection and transfer from the various sensors, platforms, and systems must be accurately referenced to common standards. The common positioning reference has become the World Geodetic System 84, now a global universal standard complementary with the International Terrestrial Reference System. The CTR is Universal Coordinated Time as maintained by the U.S. Naval Observatory, UTC (USNO) [2], which is a major contributor to and referenced with International Universal Coordinated Time.

An example of the possible joint surveillance forces in theater airspace is illustrated in Figure 2. In this example, surveillance and tracking functions of the different Naval and Air forces deployed for detecting and tracking hostile air forces or missiles are shown tracking an unknown aircraft. The times of observation by the different units are time-tagged with their local clock. Denoted T_{Ship} , T_{Air} , T_{E2} , and T_{Awacs} , the times of the radar or sensor measurement are measured and relayed to the ship in the case of the Naval Task Group.

These data are then processed onboard the ship for ship defense and formulating tactical response, as well as being relayed to the Theater Command and Control Center for inclusion in the overall surveillance picture. The data collected by the forces in the area would then be merged and processed to form a common picture. The common picture formed at the command center with these data from joint and coalition forces would need to be redistributed or identical to the ones formed by contributing task groups. Each step in this process may require updating the time-tagged measurements or processed results.

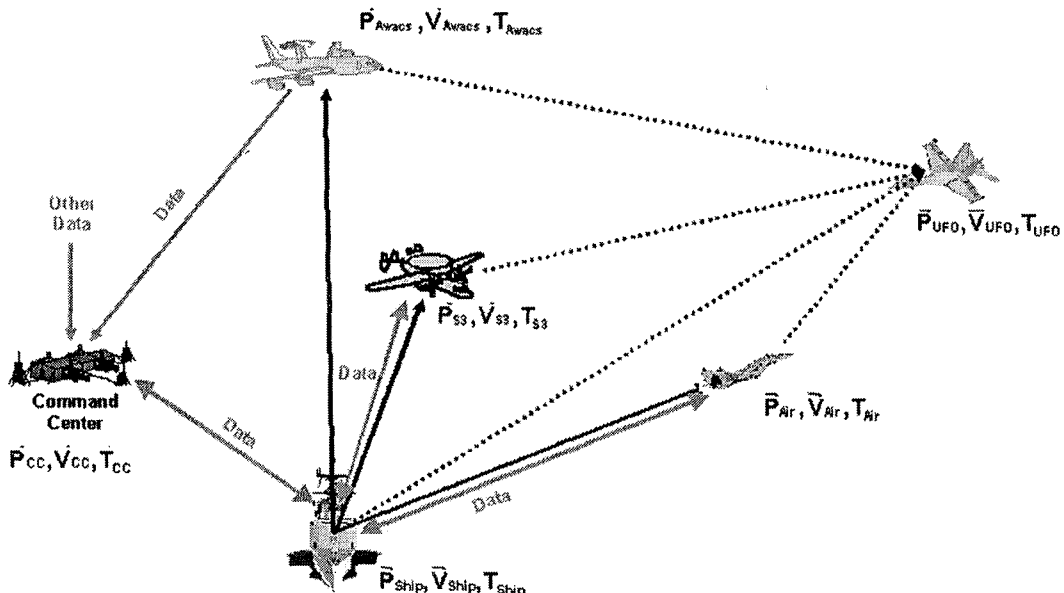


Figure 2. Theater Air Surveillance

So it can be seen in this operation, time has multiple influences from determining the time tags themselves to timing the transmission of the data messages through the various links. Processing of data is also dependent on the time and frequency capabilities of the various systems, which may be configured to be independent of the primary data being transferred. The integrity and accuracy of the time-tagged data passing through these systems is then a function of the systems infrastructure supporting its processing or transmission. The systems' infrastructure must then be configured for accurate synchronization that can be maintained, both internally and externally, to provide the accurate inter-operability necessary.

Timing in these surveillance units is generated from their local clock. How these clocks are used varies with the specific application, but they can be represented by the time maintained by the unit's local clock for sensor data. A simulated comparison of the different unit's local clocks compared to a common time is shown in Figure 3.

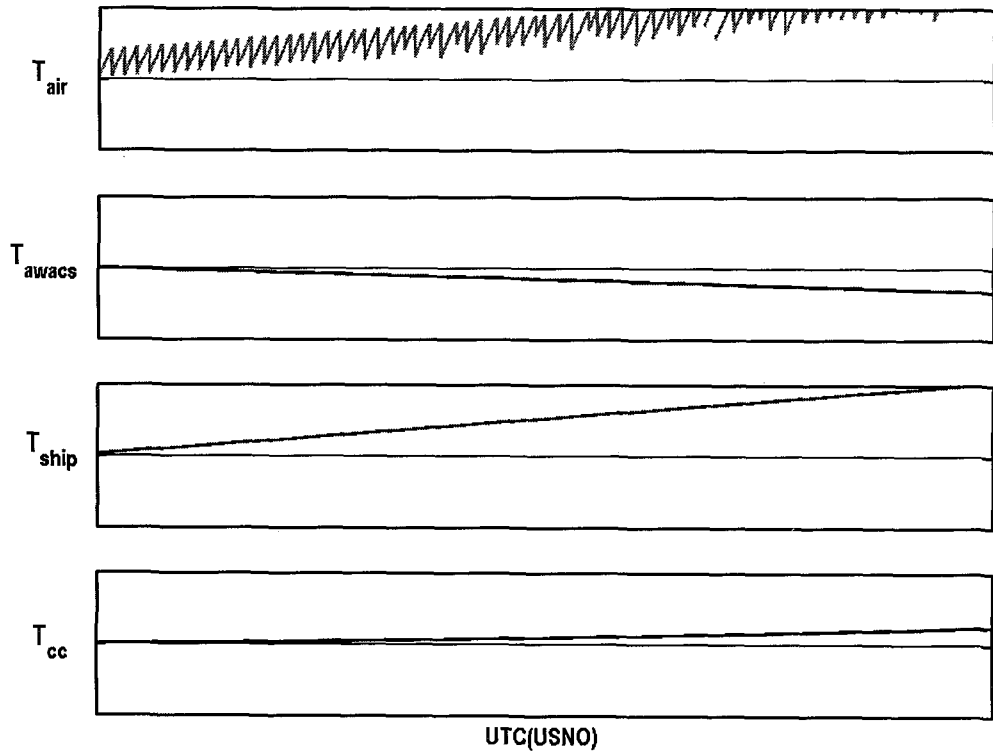


Figure 3. Unit Time Tag References

Each unit's time is represented by the clock Equation [3],

$$T(t) = T_0 + Rt + \frac{A}{2}t^2 + \int_0^t E(t)dt + t\sigma(t)$$

T_0 is the initial time setting,

R is the frequency or rate of time accumulation between time settings,

A is the frequency drift or aging.

These terms constitute the basic systematic performance of the clocks that may be modeled and monitored by each system to maintain synchronization. The last two terms represent those performance parameters more difficult to control. Environmental effects, denoted as

$$\int_0^t E(t) dt,$$

will integrate over operating time and environmental changes. Most notable among those effects are temperature effects. The preponderance of clocks throughout the systems are quartz oscillators of different qualities that are specified for their environments. However, the oscillator's performance within those limits or compensation for cumulative environmental effects are typically not monitored or accurately known in operation. The random noise component of performance, $t \cdot \sigma(t)$, determines the precision and ultimate accuracy possible with the specific clock involved with all other effects removed or compensated. The noise component is described as the product of the frequency stability, estimated by the Allan deviation and elapsed time from initialization or update [4].

The final performance of each system's timekeeping is then determined by the clocks used and methods to maintain them in synchronization. A variety of applications and techniques for maintaining synchronization within each system's overall design is used. The implications of this variety of techniques and methods are discussed in the following sections.

TIME UTILIZATION WITHIN SYSTEMS

Most DoD systems deployed in operational use today were designed 10 to 20 years ago. In designing these systems and determining PT&F requirements, the ability to maintain clocks remotely on board ships, for example, was very difficult. The precise means of time dissemination that were available had limited coverage and capabilities. Consequently, most systems were designed around local synchronization and relative operation that they would be independent of external inputs. Systems so designed would perform very well under independent, stand-alone conditions. Absolute common time was necessary for coordinating worldwide operation, but its accuracy did not impact operation of these relative systems. Therefore, absolute time was not viewed as a major operational issue and consequently not a system's requirement. The relationship in today's interactive systems has changed significantly.

Relative Networks

Relative time systems operate over a local area with a local network master time. Clocks and oscillators used in these networks needed precision in making time interval (frequency) measurements and relative time synchronization. Short periods of free-running performance are used between resynchronization with other local system elements [5]. Long-term free-running performance is necessary between widely dispersed strategic or worldwide systems, such as secure communications systems. For tactical systems within a theater of operations, quartz crystal oscillators, such as Temperature Compensated Crystal Oscillators (TCXOs) and more stable Ovenized Crystal Oscillators (OCXOs), are quite capable under these conditions [6]. Use in a relative tactical communication system is illustrated in Figure 4.

The Net Master controls system synchronization and participation of the user aircraft in the net. User clocks are set in synchronization by special acquisition preambles for net entry monitored in normal system operation and periodically updated through special communication signals. These updates would typically update the initial time difference of the clock in the user terminal, T_0 , and therefore maintain it within the system signal tracking and reception limits. This update technique is simulated in the data plotted in Figure 5. Changing the time offset introduces time steps small enough so that they do not seriously affect system operation and the integrity of the timing information. Consequently, if the Net Master Clock were compared to UTC (USNO), as in the bottom plot of Figure 5, it could be of almost any offset value and rate; the relative net would still work perfectly.

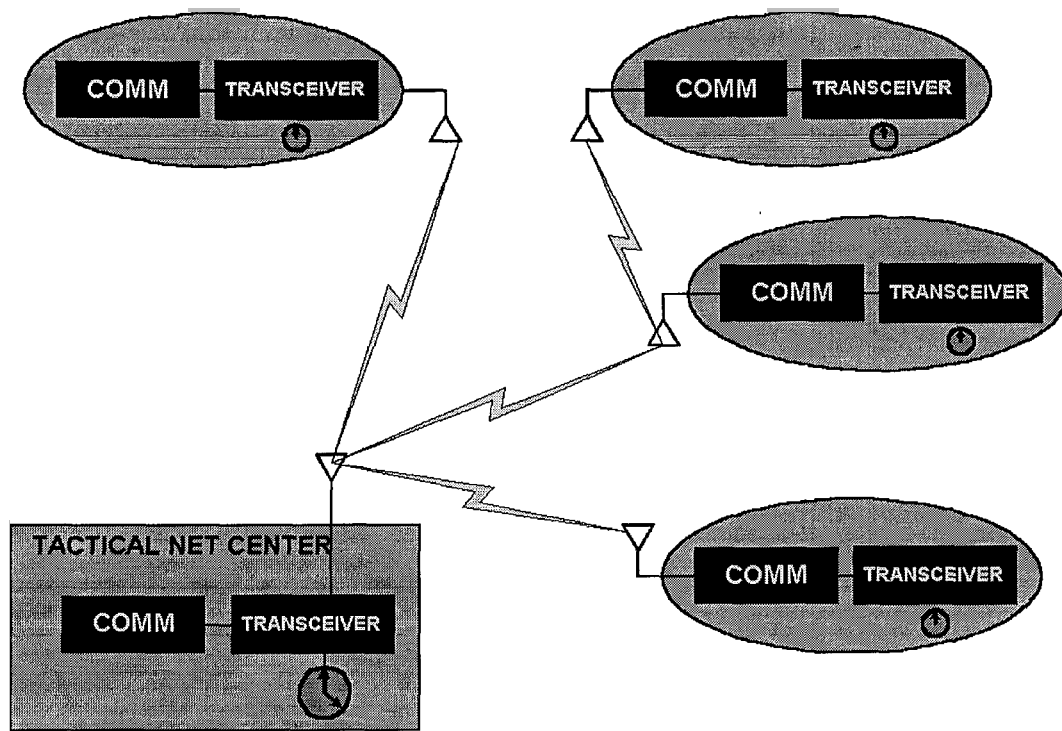


Figure 4, Tactical Communications Network

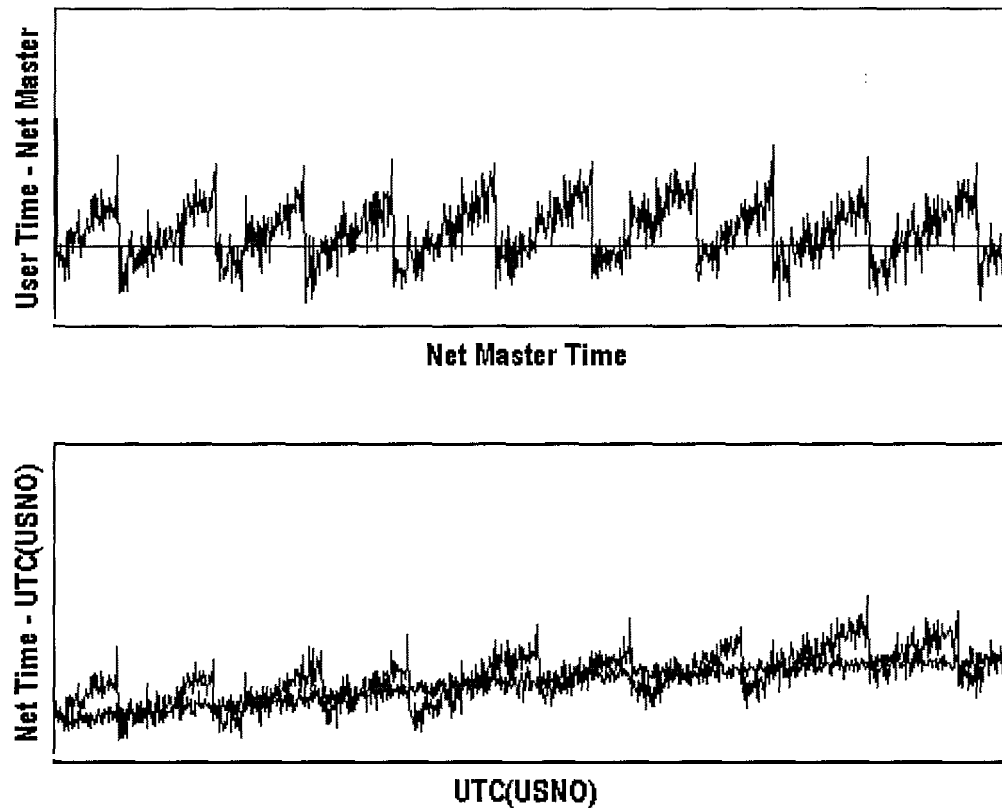


Figure 5. Network User Time Updates to Net Master

Referencing a relative net time to a remote absolute time scale has been quite difficult and inaccurate in the past. It is also unnecessary for independent operation. In today's environment of supporting joint operations, such as a common air picture with other systems or multiple relative networks, synchronization for data correlation becomes significant.

Clock synchronization within these relative networks was based on a hierarchy of accurate clocks. Clocks are configured in a hierarchy within the system design, from the most accurate to the least accurate. This system configuration arranges the more precise and accurate ones to update the lesser ones in a fixed arrangement to keep them all in synchronization. Performance accuracy is implicit within the hierarchy. Global absolute time dissemination systems were similarly arranged. For telecommunication networks in continuous operation, the fixed hierarchy is known as stratum levels [7]. Stratum 1 was the most accurate and stable of clocks, typically a cesium-beam standard. It would then maintain or update Stratum 2 level clocks, and so forth. This arrangement was economical, since the better clocks were also the most expensive. The interfaces and connecting links between clocks in these hierarchies were also configured to maintain the accuracy and precision of updating clocks down in the hierarchy. With multiple systems operating interactively, a hierarchy is almost impossible to configure or maintain. A new approach to synchronization to a common global standard is required.

Absolute Common Time

Absolute common time for DoD systems is the time scale known as Coordinated Universal Time (UTC) as maintained by the U.S. Naval Observatory, designated UTC (USNO). Use of a UTC time scale presents some problems for the military user, in that it is not uniform. Leap seconds are introduced to keep UTC within 0.9 seconds of solar time corrected for nonuniform earth rotation, the UT1 time scale, which is needed for celestial navigation and inertial systems [8]. A problem has been the distribution of leap second information to the military user, so the time step may be introduced at the proper moment. GPS does provide leap second information within this navigation message, so that GPS receivers may compensate for this change automatically. This provides a means of distributing the occurrence and direction (+ or -) of the leap second. Another, more significant problem has been the ability of existing systems to accept or correct for leap seconds. Most of these legacy systems must be manually reset or corrected. This manual entry problem is still a significant issue on the use of UTC as a common time within the existing systems infrastructure.

For allied or coalition military operations, such as NATO, an absolute common time references designation has been partially addressed in that NATO common time is required to be UTC [9]. This designation usually indicates the final international resolved UTC time scale, which is a postprocessed scale after collecting considerable data internationally and computing an accurate, stable, long-term reference. However, for military purposes, real-time coordination and operations requires a real-time physical clock as a reference. UTC sources differ in accuracy and availability from nation to nation. Consequently, a common time reference for NATO and Allied operations will be resolved for those operations.

Multiple User Systems

As systems were required to be more interactive and operate as part of a larger system or group of systems, the implementation of clocks and required synchronization within these systems becomes more difficult to clearly define. A generic ship and aircraft system is shown in Figure 6. The clock symbols show some of the clocks contained in these systems, since virtually all electronic systems contain clocks and oscillators. The overall system time requirements depend not only on the clocks used, but also on how they are used. Clocks control the time of the system elements, but the manner in which they are applied controls the timing of the system.

Within the same platform, systems are still predominately organized as relative, self-contained systems. A radar system and weapons system employs its own internal time for operation. Moving data processed with one internal time to another determines the relations between the clocks and sets the timing paths. "Timing" is then more accurately defined as the ability of information to move through the systems. Limits on timing of the multiple systems to pass information are determined by instrument delays, uncalibrated transmission delays (latencies) between units, the interfaces between the systems, and information processing delays. The interaction of these elements, which would seem to play a minor role in system operation, has major effects in overall inter-operability.

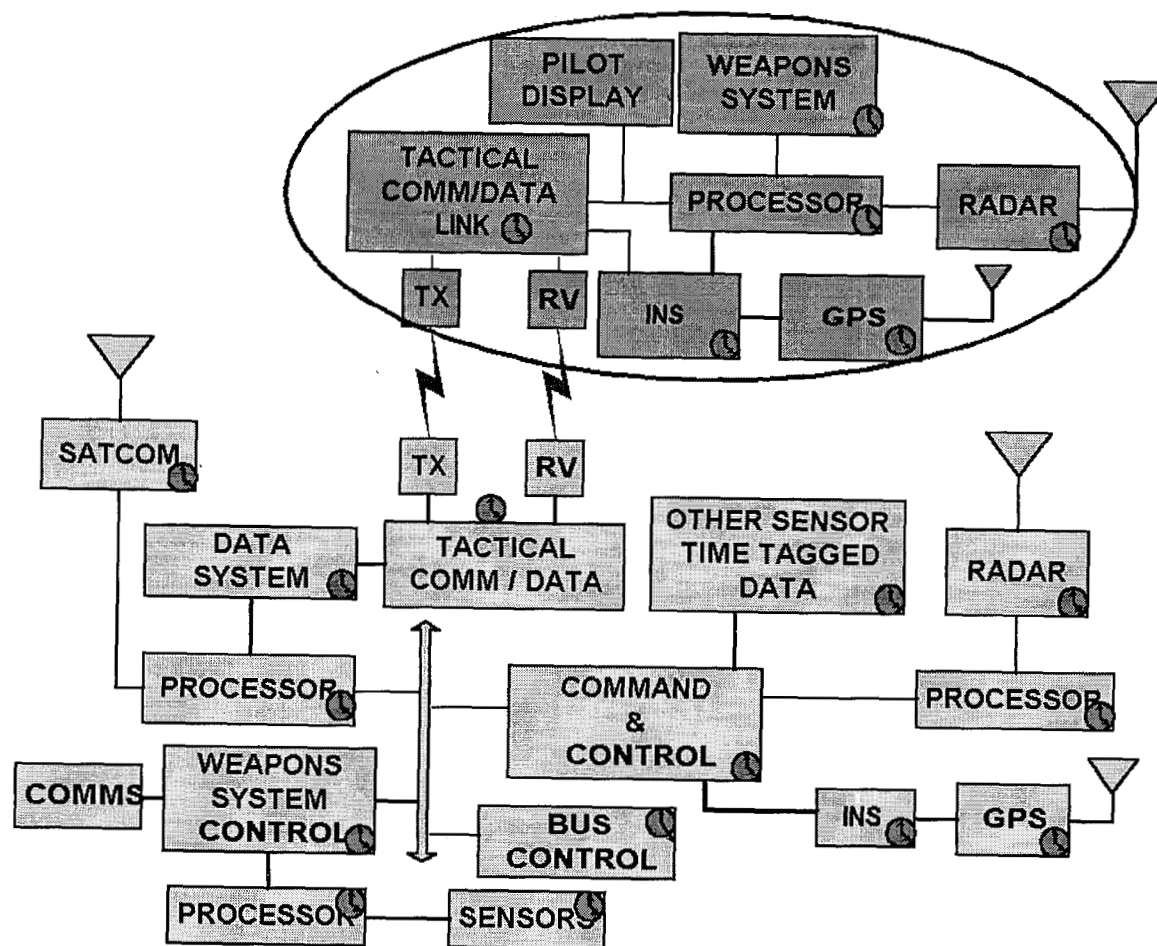


Figure 6. Generic Ship and Aircraft Systems

Given the profusion of the clock applications and time utilization within systems compounded by interaction with other systems, it is not surprising that timing requirements are difficult to define and specify. System level timing dependency and usage has been categorized to attempt to clarify the application within a specific system. These categories and limitations bearing on the time accuracy or precision needed in the category are as follows:

1. Positional Reference Time: Time tagging observations of platform positions or sensor measurements relating to positional information. The velocities and dynamics of the particular vehicle's motion determine the associated accuracies and precision limits and requirements.

2. Time Interval (Δt): Measurements of Δt for RF or optical measurements to determine range between objects or distance based on time of propagation of the signal at the speed of light. The associated accuracies and precision required are more stringent.
3. Communication Signal Synchronization: Data transfer links ranging from the local systems to synchronizing systems over global distances require both measurement of intervals and longer-term synchronization to maintain signal lock. Acquisition and demodulation of signal waveforms, bandwidths involved, modulation rates, and types determine time and timing requirements. The dynamics of these systems are limits relative to the speed of light.
4. Data Processing: Calculation of information and transmission through processing nodes and networks require timing and clocks. Processing delays for the calculations to take place dominate timing limits. Even asynchronous data transfer needs timing and set limits.

GPS TIME DISSEMINATION

GPS provides the primary worldwide, highly accurate capability for time dissemination to diverse remote units of the DoD. Different techniques for time dissemination are used within the scientific and timekeeping community, such as common-view time transfer that can intercompare clocks over intercontinental distances with nanosecond precision [10]. The DoD user relies primarily upon passive time dissemination as a product of positioning and navigation, as illustrated in Figure 7.

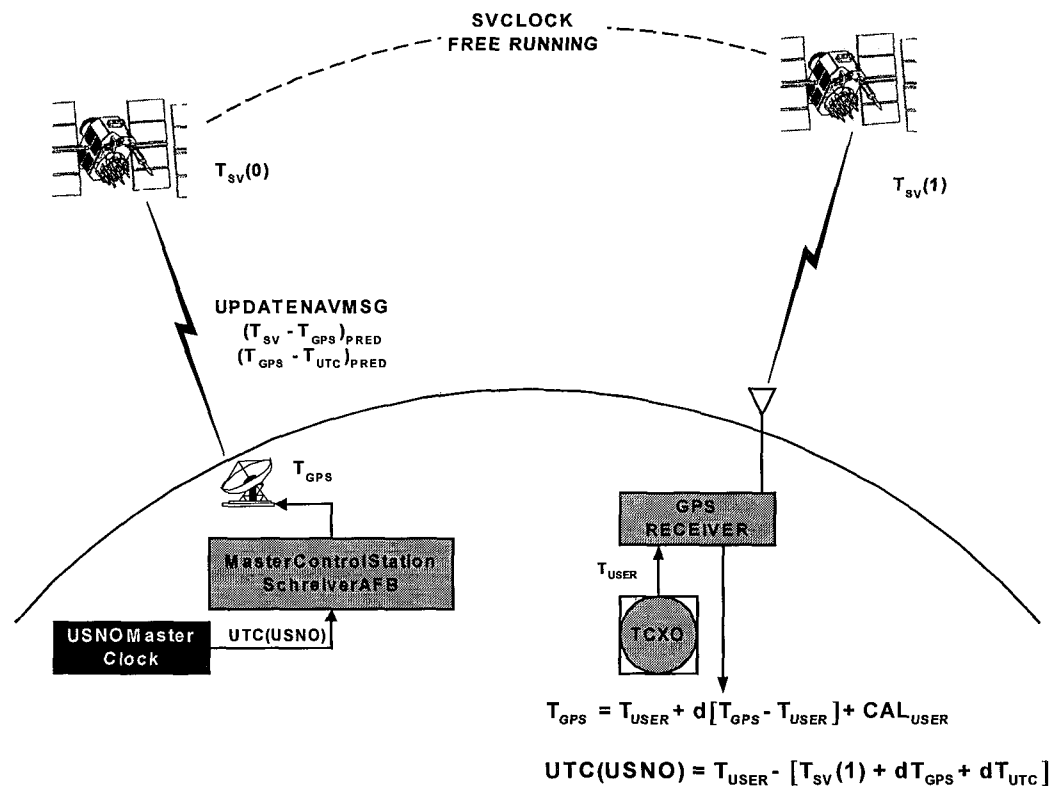


Figure 7. GPS Time Dissemination

This capability is made possible as a result of the highly synchronous nature of "GPS Time" [11]. GPS Time is the basis for accurate GPS measurements. It is continuously generated by the system Kalman filter at 15-min intervals from the constant monitoring of the atomic clocks in the satellites and monitor stations, as a composite, or weighted average of all these highly stable atomic clocks. The offset and rate of GPS Time from UTC (USNO) are determined from the constant monitored by USNO and correction terms included in the NAVSTAR satellite navigation message. The user can then correct GPS Time resulting from his navigation solution to an accurate time in UTC (USNO). To use this accurate time, the implementation of the receiver and instrumentation must be configured to output precise timing signals and data. The distribution system or circuitry being driven by these outputs must also be capable of maintaining the precision. GPS can then provide an accurate reference time to units across an operational theater and synchronize the variety of platforms and systems engaged.

With GPS capability and instrumentation for civilian time applications becoming so inexpensive, small civilian receivers have been integrated into a variety of timing equipment to discipline clocks primarily for telecommunications. These commercial integrated time subsystems can provide atomic clock level performance, so they are being used to replace more expensive clocks and are available off the shelf. Newer telecommunication and data processing equipment for military systems, that now emphasize commercial best practices and off-the-shelf acquisition, sometimes contain these embedded GPS receivers. These embedded civilian receivers then introduce hidden vulnerabilities into military systems. With accurate UTC (USNO) time now generally available to systems worldwide, legacy systems designed around relative time concepts may now utilize an accurate common absolute time and complement a systems-wide synchronized architecture.

CTR TECHNICAL ARCHITECTURE

The general view of the generation, dissemination, and utilization of time in military systems can be as shown in Figure 8. UTC (USNO) is the main element of Absolute CTR that was established as the reference time for use with all U.S. military systems.

The primary time dissemination system in the second element is GPS. By incorporating absolute time as the reference for local and tactical systems, they can then provide alternative time dissemination capability. A new implementation of Two-Way Satellite Time and Frequency Transfer (TWSTFT) has been developed for use with communications satellites [12]. TWSTFT can disseminate time with nanosecond accuracy globally; however, the technique is a point-to-point capability, vice the generally available broadcast capability of GPS. However, TWSTFT and the capability of tactical area relative systems, such as the Joint Tactical Information Distribution System (JTIDS), could be incorporated into an overall CTR architecture to develop an assured ability to synchronize systems to the CTR.

The final major block of the architecture contains the systems and their user infrastructure. The system-user infrastructure shown in Figure 6 can be represented as a distribution of clocks and oscillators.

This representative view, shown in Figure 9, illustrates the complete connection from the absolute reference, GPS, and the system clocks. The connecting links between the clock symbols represent their time comparison relationship, not necessarily data links or system operational data links. As discussed in an earlier section, relative system links may already provide the means to intercompare the clocks. GPS shown in the middle of the diagram represents dissemination of time by connecting directly to the systems. The other represents an embedded GPS receiver.

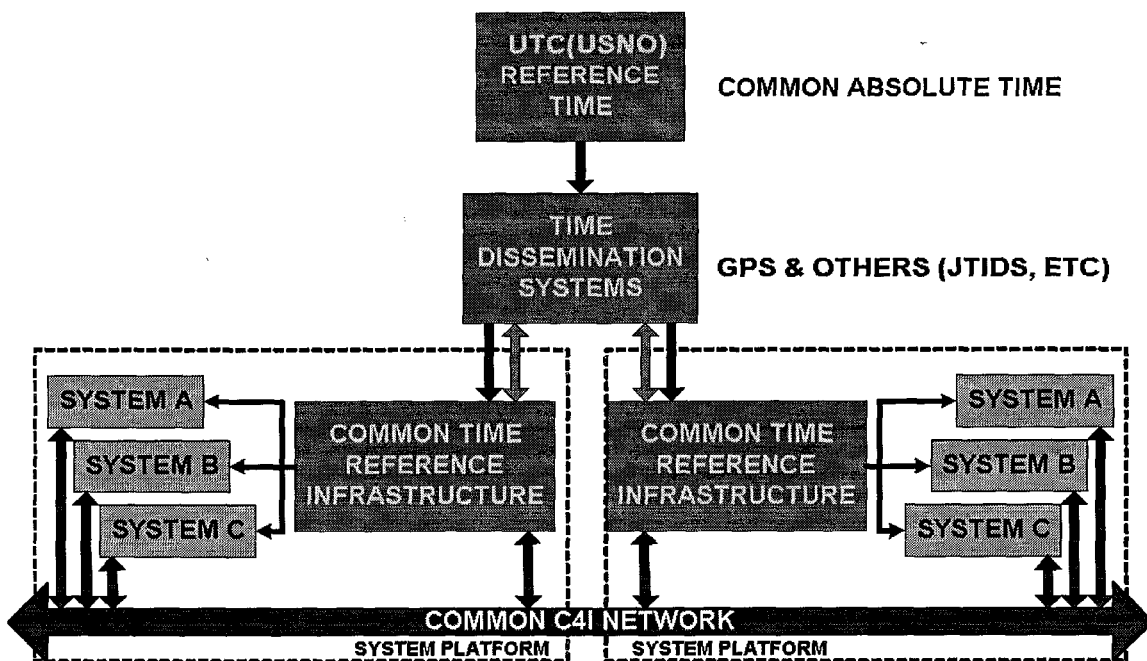


Figure 8. CTR Overall View

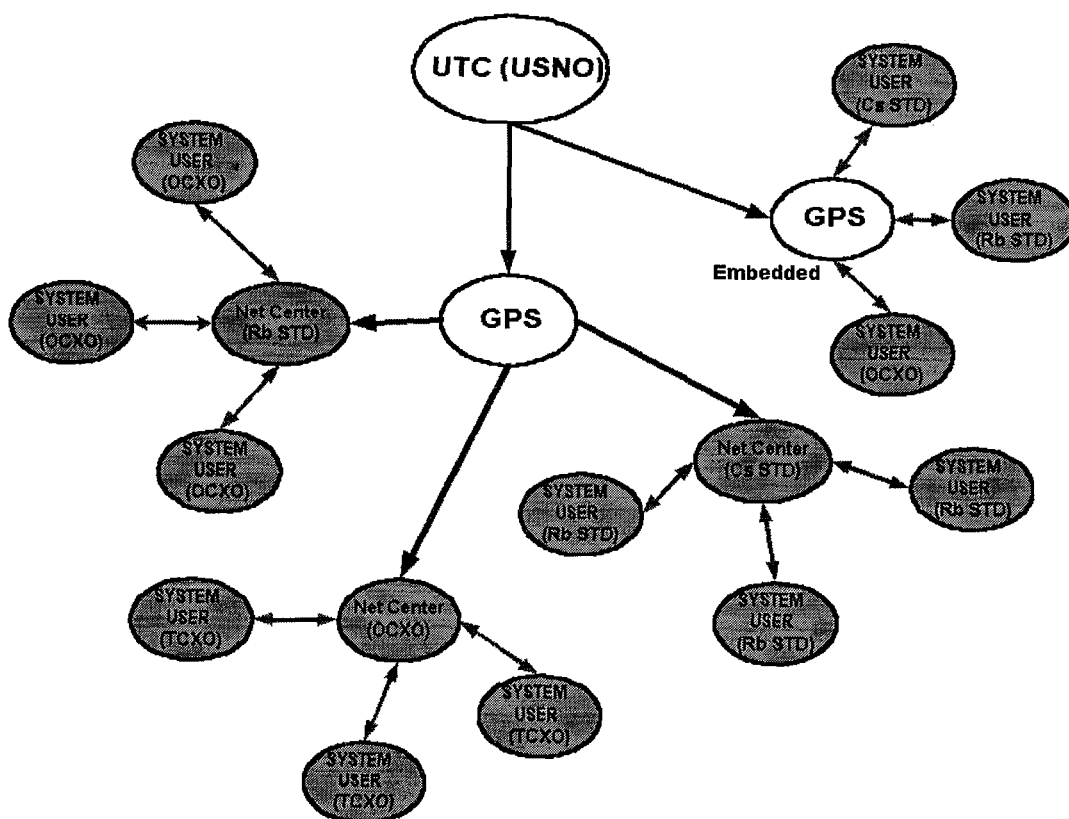


Figure 9. System-User Infrastructure of Clocks

group of clocks would then be combined with comparison, interfacing, and management equipment capable of maintaining an independent local CTR. This local CTR, shown by the markers, would then be maintained in synchronism with the absolute CTR via the time dissemination element. This element could consist of GPS receivers and other means, such as TWSTFT or through a local comparison through JTIDS to Task Group participants. The dissemination systems, including alternatives, would be active participants in the composite time group maintaining time throughout the systems infrastructure and other task group elements.

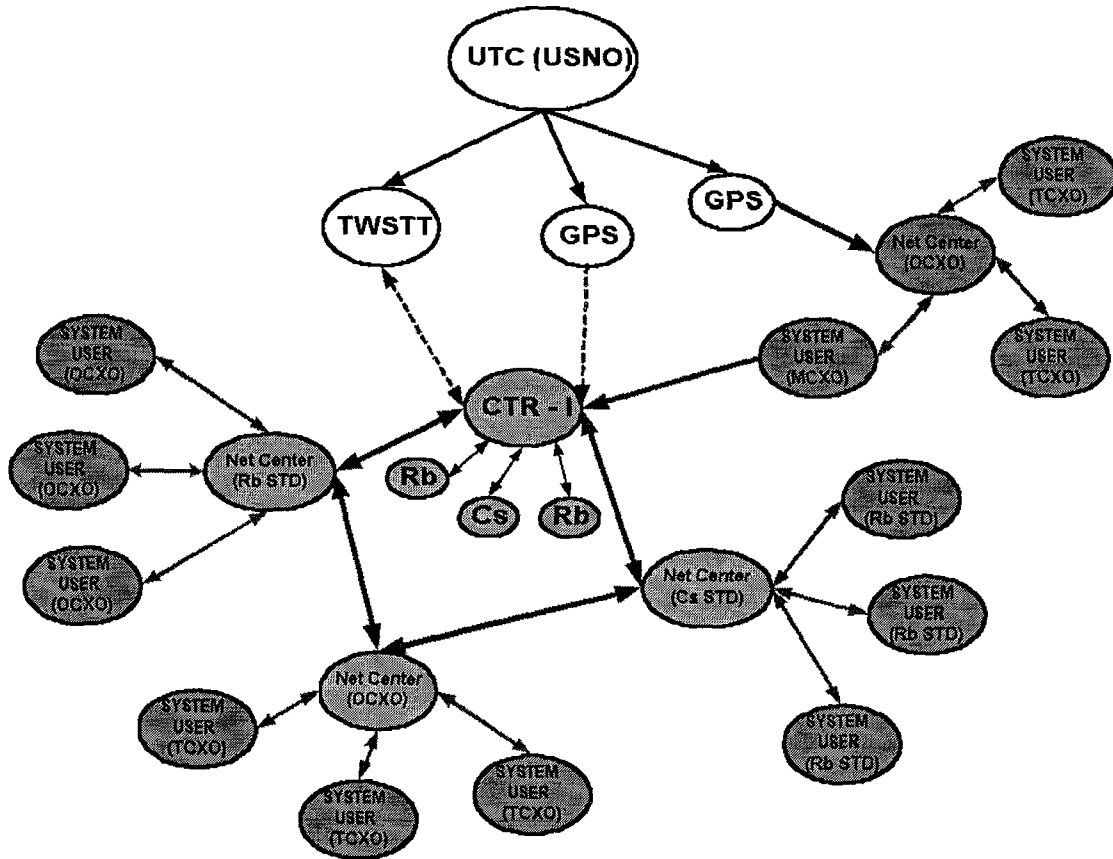


Figure 10. CTR Approach Combining Existing Clocks

CTR TECHNOLOGY ELEMENTS

The CTR functional infrastructure incorporating existing clock assets is shown in Figure 11. This functional diagram shows the elements of the architecture necessary for generation, comparison, maintenance, and distribution of the CTR within the platform and systems.

Central to the CTR infrastructure are the GPS receivers, which have been deployed on most Naval Ships and are being deployed on aircraft, ground forces, weapons, and fixed sites of all services. The preponderance of these receivers is intended for positioning and navigation purposes. Receivers for supporting time are in use, many of which, as discussed earlier, being embedded within system components. Submarines have a dedicated system to distribute time to clocks on board [13], and the Block 3 Upgrade to the Navigation Sensor System Interface onboard combatants includes a time distribution function [14].

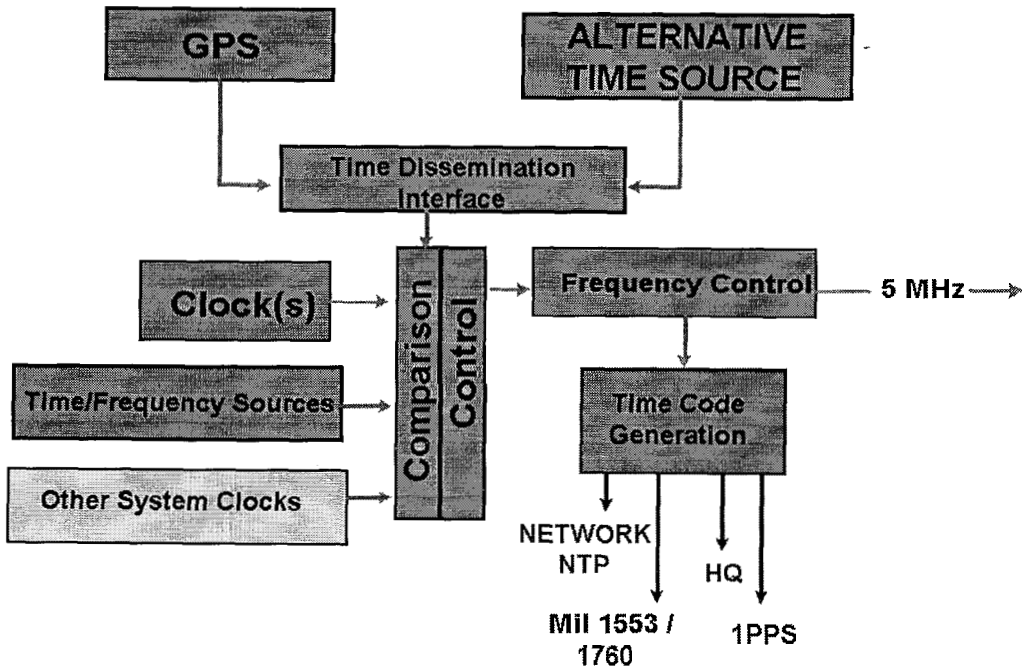


Figure 11. CTR Functional Infrastructure

Most GPS installations reflect time as a product of navigation and modifications currently being investigated are focusing on more deeply integrated navigation systems for increased positioning accuracy or resistance to electronic countermeasures. Time interfaces either rely on the GPS Precise Time and Time Interval Interface GPS-ICD-060 [15], which actually provides three different interfaces made up of older interface standards, or other instrumentation standards. Other GPS Interface Control Documents, such as GPS-ICD-153, address some time interfacing aspects as well, but not as a general capability. Time interfaces developed for instrumentation, such as the IRIG Time interfaces [16], the Mil Std-188-115 [17] and DOD-STD-1399 [18], are used. Most of the military interfaces have been derived from unique systems interfaces devised for relative system operations. These were subsequently adopted by developing systems or to instrument special capabilities that have spread to other applications. A good example is the Havequick interface. JTIDS is another with a unique interface. They are used for point-to-point distribution.

To effectively provide a robust time interface with sufficient performance for the primary dissemination system, GPS, and possible alternatives, consideration of an optimum interface or set of interfaces should be developed. Prior efforts to establish a single standardized interface, such as the STANAG 4430, Precise and Time and Frequency Interface for Military Electronics Systems [19], to replace the multiplicity of interfaces used has met with very limited success. How successful any new standard would be depends upon the extent the CTR infrastructure would be implemented. Nevertheless, a standardized interface would enable implementation of a synchronous infrastructure and reduce the multiplicity and maintenance of the many legacy interfaces.

Precise Clocks

Precise Clocks are typically the first subject raised in any discussion of PT&F and are a major consideration for military applications. However, the CTR approach is structured to take advantage of existing precise clocks already distributed throughout military systems. Supplemental clocks resulting from efforts into new technology clocks can play a role in

implementing the capability. The actual mix of clocks available on subject platforms may require supplement to form an accurate composite time group sufficient to meet the needs of the systems they serve. New technology efforts may supply this supplement, though they are mainly focused on increased capability for very difficult problem areas in maintaining time, such as small field radios, handheld units, and those for weapons [20].

A consideration in the use of new clock technology is the general decline in the availability of high performance or unique clocks and oscillators. The telecommunication market has created a large demand for low cost and, often, lower quality oscillators. Accuracy is provided by inexpensive GPS receivers in higher performance applications. Consequently, development of precise clocks both crystal-driven and atomic is being conducted by service R&D agencies. Small rubidium clocks, of lesser performance than previously generally available units, are also being utilized in the telecommunications market. For larger platforms, these small rubidium units may be a viable supplementary capability for some uses.

Intercomparison Subsystems

The key component technology that the CTR infrastructure requires is the ability to intercompare the clocks within and between the systems. Unless the actual clock performance can be measured *in situ*, the ability to maintain a synchronous infrastructure accurate to a CTR will be very difficult to achieve. Combining clocks to a common composite time maintained closely to the absolute CTR will require specific continuous knowledge of the participating clock performances.

Measuring actual clock performance in the environment it has to operate in, will determine the clock performance effects of clock sensitivities [21,22] and the subsequent effect on the system. From the clock equation introduced earlier, the environmental induced error,

$$\int_0^t E(t)dt + t\sigma(t)$$

integrates over the duration of the environmental changes and is a function of many different factors. The most significant environmental factors are temperature, vibration, and variable magnetic fields [23]. These factors can have significant effects on quartz crystal oscillators. Actual performance between similar clocks can also have variable values of frequency offset, R, and frequency aging, A, terms. These effects are within what would be considered normal operating limits and not abnormal. Complete clock failure resulting in loss of signal is not as common as abnormal jumps in frequency, phase, or aging terms, leading to anomalous performance. This anomalous behavior is difficult to identify without actual measurements and can have serious performance results. The more deterministic terms of clock performance having been established, the random noise component, characteristic of the clock establishes its basic behavior. This term is expressed in the time domain as the square root of the Allan variance, or Allan deviation, and is shown in Figure 12 for the major different clock types. This component determines the ultimate stability of the clock signal and the ability to determine and predict performance. This term may change over the life of the unit, reflects environmental effects, and varies between similar units, even the same type unit manufactured by the same manufacturer. Characterization of the clocks in under operating conditions is key to management of synchronization and is, in turn, highly dependent on the ability to compare clocks.

Whatever intercomparison technique is used [4,24,25], they can serve other possible uses. Automated precision comparison techniques can be used to monitor calibration of both clocks and distribution systems. They may also identify degrading performance and establish an accurate perturbation free means of switching clocks. The most significant use is to establish a basis for forming a composite time from the participating clocks.

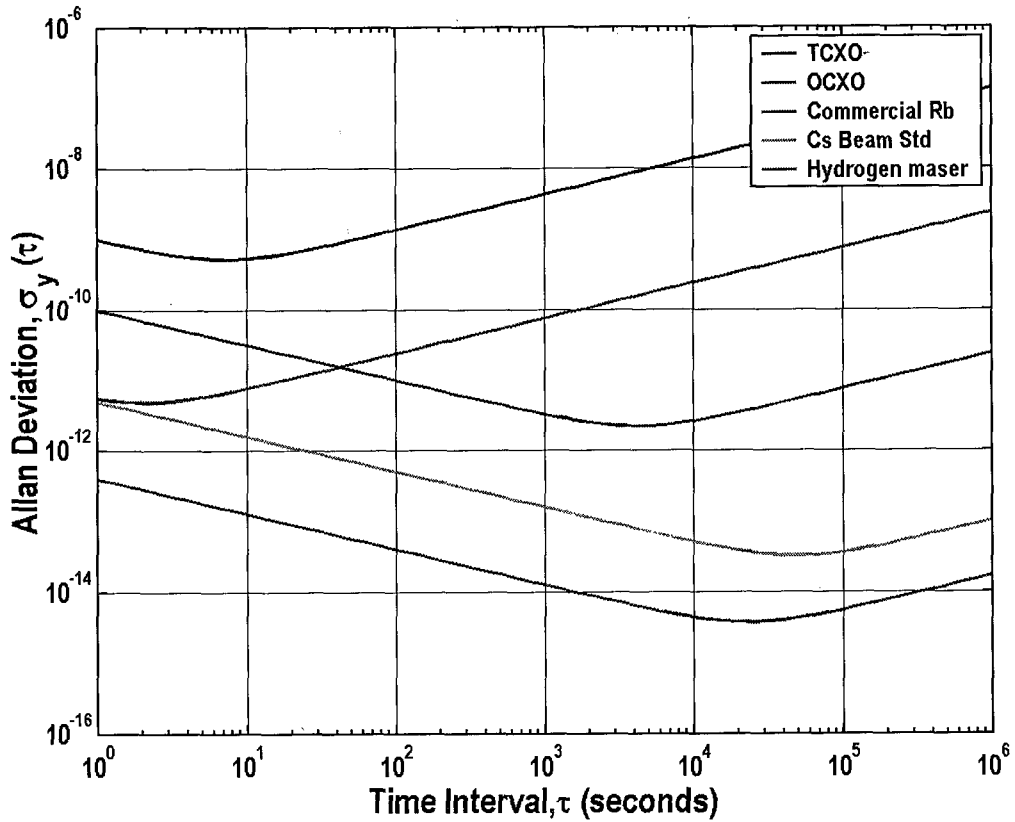


Figure 12. Allan Deviation of the Major Clock Types

Distribution Media

Connecting the CTR infrastructure within the systems will require distribution systems and different media. Implementation of signal distribution along with the need to provide clock signals for intercomparison could result in an overly complex and expensive distribution system for large platforms. Specific implementation of this architecture within the existing systems will need to be tailored to the specific unit.

The technique for distribution consists of various types of cabling and communications media [26]. Calibration of the media and interconnections will be a significant implementation issue. Calibration of fixed media, such as dedicated cabling, will not be as significant a problem as digital data and computer networks, which could be especially difficult. These networks are basically asynchronous, involving processing delays and network switching that can be unpredictable. Techniques for time comparison and synchronization with these networks have been developed, such as the Network Time Protocol (NTP), to provide a means of synchronizing computers through IP networks [27]. Within the limits of the network, NTP can maintain time within computer systems synchronized to millisecond levels. SONET systems offer the potential of providing a synchronous means of more accurate time distribution over digital networks [28].

Distribution media that present unique problems are Electronic Transfer Devices. These devices can be categorized with handheld radios and GPS receivers as far as the technical problems involved. Used for updating avionics prior to takeoff and physical transfer of data between equipment, the ability to maintain accurate time over the intervals necessary is highly dependent on the internal oscillators. Interfacing them into the CTR infrastructure is another consideration that must be addressed.

Composite Time Generation

The formation of a composite time from the existing system clocks will be possible with continuous precision comparisons. The resulting performance of the composite time would be dependent upon the actual clocks involved. Composite time is a form of a "Clock Ensemble" [4,29]. Clock Ensembles are used to generate time scales in major timing centers, such as USNO, to establish the most accurate time scale possible. This technique involves comparing the output of a large number of identical clocks of known characteristics and applying an ensembling algorithm to form a stable, predictable time more stable than the individual clocks. Similarities of the clocks are used to model and tune their operation, and the final determining factor is the number of clocks for stability improvement. For CTR composite time [30], the number and similarity of units to be used cannot be assured within the system clocks available. Consequently, ensembling for increased performance is not a specific objective, but would take advantage of the other major benefit of ensembling, which is to be insensitive to clock failure. This benefit will increase the overall reliability of the timing system. Forming a mean time that is necessary for synchronization could be adapted to a group composite.

The random noise characteristics of the major clock types that affect establishing a mean composite time are shown in Figure 12. Ensembling the specific clocks shown in Figure 12 would result in one or another clock dominating performance at different ranges of averaging times. The approach to forming a composite from a mixed clock group would be dependent upon specific algorithm to be applied, the physical interconnection and establishing local clocks for comparison reference, and maintenance of the resulting composite. An approach is diagrammed in Figure 13. This diagram shows a core group of clocks associated with CTR control and management. These core clocks would provide the reference for intercomparison, maintaining the mean time, and generating a physical signal representing the mean time, if necessary.

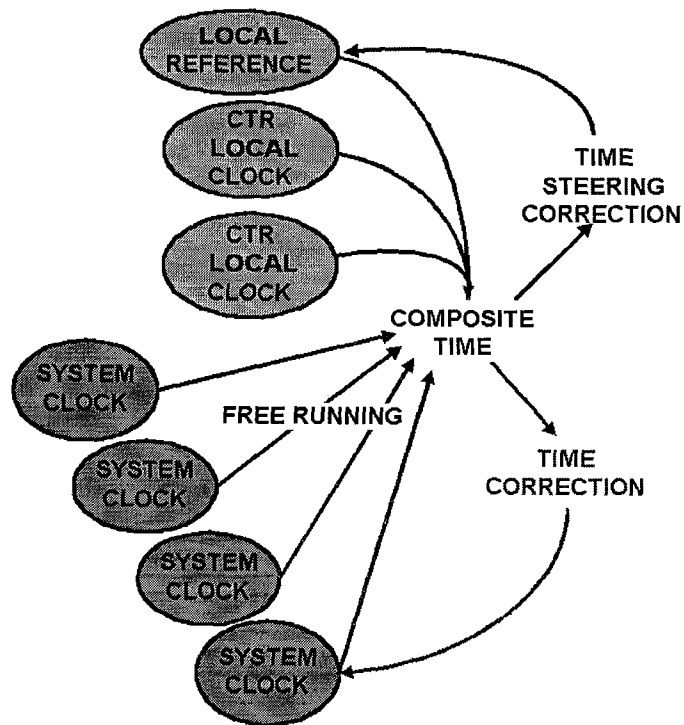


Figure 13. Composite Time Generation Approach

The actual composite time could be kept in the form of a "Paper Clock." In this case, there isn't an actual physical signal generated, but only correction terms to be applied to other clock signals to bring them onto a common time. Examples of this type of Paper Clock operation are the international UTC time scale and GPS Time. In both of these cases, a physical signal is not derived in the process of determining the time scale, as in the case of UTC, and for GPS the Master Control Station produces corrections that are applied with the free-running clocks in the system's satellites. However, these cases also result in large numbers of time users generating physical signals synchronized to the Paper Clock time. Generation of an actual physical signal, as is necessary for some communication systems, could then require a physical distribution system to provide this signal to the user systems.

TESTBED DEVELOPMENT

To investigate and determine the technologies necessary for CTR implementation, a Technology Demonstration Testbed (TDT) is being developed. This Testbed will be configured in the Laboratory to simulate with hardware and software the implementation necessary for the generic platform's infrastructure. The various technology areas discussed above will be analytically and experimentally investigated for demonstration with the TDT. The elements of this TDT will be used to design and develop a prototype installation for actual field-testing in follow-on efforts.

Requirements Definition

To determine the utility of this concept, the compilation and more detailed knowledge of the various systems timing needs and requirements are necessary. The systems needs and requirements must be better defined and clarified, since system's designers have built their systems on old basic assumptions about time and frequency availability and usage. These requirements are difficult to obtain and limited sets have been generated. A more comprehensive database is being collected throughout this effort. An approach to clarifying these requirements is to specifically test the existing systems capabilities in time generation and maintenance.

Legacy System Testing

A number of efforts are underway to develop inter-operable systems and alternatives to GPS, such as the JTIDS/GPS integration effort to ensure the compatibility of these two systems to support GPS acquisition. Coordination with these other efforts could take the form of participation in related testing. For example, the Ballistic Missile Defense Office is sponsoring calibrated testing of JTIDS implementation with the Aegis weapons system for missile detection and tracking. Part of that test could be used to determine time-transfer capability of the integrated system. If the test is configured for appropriate timing measurements, coordination and analysis of that test could provide data on time and its performance in these systems. Coordination of these testing efforts can provide extremely valuable data on system timing performance and common needs. Other specific tests are also being planned.

Laboratory Demonstration Testbed

From the concept of distributed time standards, and the results of identifying of timing requirements combined with data collected from system testing efforts, a Technology Demonstration Testbed (TDT) is being configured. This TDT will simulate, with hard-

ware and software in the Laboratory, the implementation of a common time reference infrastructure in generic platforms. The various technology areas discussed above will be analytically and experimentally investigated for demonstration with the TDT. The elements of this TDT will be validated to the point that the results could be used to design and develop a prototype installation for actual field-testing.

SUMMARY

GPS has had a major impact on the capability to determine position and navigate military platforms and systems. The impact of providing Time is just beginning to be recognized and may have an even more significant extension of military capability and operations. To take advantage of having precise time and synchronization of remote and dispersed forces with an absolute common reference, a systems infrastructure incorporating legacy systems is being developed. This infrastructure "System of Systems" approach can incorporate the old with the new. The resulting military capability will achieve inter-operability at the most basic level, Time.

The challenges to effecting a Systems approach to a CTR are more than just technical. Since they cross system and program boundaries, implementation will be programmatically difficult. To establish benefits and effectiveness, new methods for demonstration and test under operational conditions will be necessary.

REFERENCES

- [1] Cebrowski, and Garstka 1998, "*Network centric warfare: its origin and future,*" Proceedings of the U.S. Naval Institute, January 1998, pp. 28-35.
- [2] "*2000 CJCS Master Positioning, Navigation and Timing Plan,*" CJCSI 6130.01B of 15 June 2000.
- [3] J. R. Vig, "*Quartz crystal resonators and oscillators for frequency control and timing applications - a tutorial,*" CECOM Technical Report SLCET-TR-
- [4] "*Handbook selection and use of precise frequency and time systems,*" International Telecommunication Union, Radiocommunication Bureau, 1997.
- [5] W. R. Fried 1979, "*JTIDS relative navigation – architecture, error characteristics, and operational benefits,*" IEEE NAECON Proceedings, May 1979.
- [6] "*General specification for crystal oscillators,*" Military Standard MIL-O-55310, U.S. Department of Defense.
- [7] J. E. Abate, E. W. Butterline, R. A. Carley, P. Greendyke, A. M. Montenegro, C. Near, S. H. Richman, and G. P. Zampetti 1989, "*AT&T's new approach to the synchronization of telecommunication networks,*" IEEE Communications Magazine, April 1989.
- [8] "*Standard frequency and time-signal emission,*" ITU-R Recommendation TF. 460-5, 1997.
- [9] "*NATO military operational requirement for the provision of precise time,*" MMC-SFM-081-93, 28 July 1993.
- [10] W. Lewandowski, and C. Thomas 1991, "*GPS time transfer,*" Proceedings of the IEEE, 79, No. 7, July 1991.
- [11] K. R. Brown 1991 "*The theory of the GPS composite clock,*" Proceeding of the ION GPS-91, 11-13 September 1991, Albuquerque, New Mexico, USA, pp. 223-241.
- [12] G. P. Landis, J. D. White, A. Gifford, R. L. Beard, and J. A. Murray 1997, "*A new*

- two-way time transfer modem,"* Proceedings of the 21st Annual Precise Time and Time Interval (PTTI) Applications and Planning Meeting, 28-30 November 1996, Redondo Beach, California, USA, pp.131-136.
- [13] "Performance specification For time frequency distribution system," TFDS-PERFSPEC-01-U-R0C0, N66001-97-R-0004, 21 November 1996, NRaD, Code D831, San Diego, California, USA.
 - [14] P. T. Shaw, and W. Pettus, "An integrated approach to electronic navigation," Oceans 2000 MTS/IEEE Conference Proceedings, Marine Technology Society, 1828 L Street, N.W., Suite 906, Washington, D.C. 20036, USA.
 - [15] "Precise time and time interval interfaces," NAVSTAR Global Positioning System (GPS) Interface Control Document, GPS-ICD-060, Rev. B, 1986.
 - [16] "IRIG serial time code formats," Timing IRIG Standard 200-98, May 1998, Timing Committee, Telecommunications And Timing Group, Range Commanders Council, U.S. Army White Sands Missile Range, New Mexico, USA.
 - [17] "Interoperability and performance standards for communications timing and synchronization," Military Standard MIL-STD-188-115, U.S. Department of Defense.
 - [18] "Interface standard for shipboard systems, precise time and time interval (PTTI)," Military Standard DOD-STD-1399 (Navy), Section 441, U.S. Department of Defense, 1 June 1982.
 - [19] "Precise time and frequency interface for military electronic systems," STA-NAG 4430.
 - [20] "Special technology area review on frequency control devices," Acquisition DoD Advisory Group on Electron Devices, Office of the Undersecretary of Defense, Aquisition and Technology, Washington, D. C., 1 February 1996.
 - [21] "IEEE standard definitions of physical quantities for fundamental frequency and time metrology – random instabilities," IEEE Standard 1139-1999, 26 March 1999.
 - [22] H. Hellwig 1990, "Environmental sensitivities of precision frequency sources," IEEE Transactions on Instrumentation and Measurement, IM-39, No. 2, April 1990.
 - [23] "IEEE guide for measurement of environmental sensitivities of standard frequency generators," IEEE Standard 1193-1994, 27 February 1995.
 - [24] S. R. Stein, D. Glaze, J. Levine, J. Gray, D. Hilliard, D. Howe, and L. Erb 1982, "Performance of an automated high accuracy phase measurement system," Proceedings of the 36th Annual Symposium on Frequency Control, 2-4 June 1982, Philadelphia, Pennsylvania, USA, pp. 314-320.
 - [25] J. Levine 1999, "Introduction to time and frequency metrology," Review of Scientific Instruments, 70, No. 6, June 1999.
 - [26] U. D. Black 1983, Data Communications, Networks and Distributed Processing, Reston Publishing Co., Inc., A Prentice-Hall Company, Reston, Virginia, USA.
 - [27] D. L. Mills 1998, "Precise time synchronization, Network Time Protocol version 4," briefing 14 Sep 1998.
 - [28] U. Black, and S. Waters 1997, SONET and T1, Architectures for Digital Transport Networks, Prentice Hall PTR, Upper Saddle River, New Jersey, USA.
 - [29] D. Allan, J. E. Gray, and H. E. Machlan 1974, "The National Bureau of Standards atomic time scale: generation, stability, accuracy and accessibility," in Time and frequency: Theory and Fundamentals, NBS Monograph 140, pp. 205-231.
 - [30] S. R. Stein, G. A. Gifford, and L. A. Breakiron 1990, "Report on the timescale

algorithm test bed at USNO," Proceedings of the 21st Annual Precise Time and Time Interval (PTTI) Applications and Planning Meeting, 28-30 November 1989, Redondo Beach, California, USA, pp. 269-287.

Questions and Answers

THOMAS CLARK (NASA Goddard Space Flight Center): Both what you and Chris [Gregerson] have said has been very interesting. If we compare them with the material that was presented last night at our after-soup talk, I counted up the fact that the train systems, where the common time reference and time dissemination ended up evolving to the conductors on the trains, accounted for 45 losses of life in the 1800s. You cited the Scud missile accounting for 28, so these things are real problems and they are not new.

It strikes me that while the DoD may be taking the lead on this that the problem is not unique to the DoD. Those of you who fly out today, the time reference on the commercial airliner that you fly out on will be the dash clock that the pilot has, which he sets from his wristwatch. There is no time code written on to the flight data recorders, so the reconstruction of problems like Alaska 262 and the event chain to even do any diagnostic is rendered much more difficult by the lack of any precise time available on the aircraft. That need for precise time in the civilian airline community also extends to things like ground control. When your plane is taxiing today, since the time reference exists only in the pilot's mind for the aircraft, that is not in any way conveyed to the ground control system at the airport. It has very little correlation with the time system that used by the navigators back on the ground that are telling the airplane where to go.

That's just one example. I wonder, in all of your deliberations within DoD, if the need for the same type of study by the civilian community and, in reality, the need for some inter-operability between the military and the DoD is being considered. Because it is not just your problem, it's everyone in the audience's problem when you fly out of Dulles Airport this afternoon. This comment, followed by a question: are you talking to anyone outside of DoD? That's really my question, Ron.

RONALD BEARD: Actually, yes. I think that is a very large consideration in the WAAS system and inter-operability. The military aircraft have to fly to a civilian air station in order to get where they are going, so they need to be inter-operable with them, and the airlines are also very concerned about this inter-operability and that sort of thing. I defer a lot of that to Bill Klepczynski, who is involved in that sort of thing.

WILLIAM KLEPCZYNSKI (Innovative Solutions International): Thank you. There is within the satellite-based augmentation systems a working group called the Inter-operability Working Group. One of the issues that we work on is how do we synchronize the different augmentation systems like EGNOS, WAAS, and MSAS. That issue is being discussed now, and a working plan is being established now. I think on December 12th or so, the EGNOS people are going to be working on it.

DEVELOPMENT AND EVALUATION OF GPS SPACE CLOCKS FOR GPS III AND BEYOND

Andy Wu and Bill Feess

The Aerospace Corporation

2350 E. El Segundo Blvd., El Segundo - M5/688, CA 920245-4691

Tel: (310) 336-0437, Fax: (310) 336-5076

Andy.wu@aero.org

Abstract

The current GPS has exceeded its globally averaged position and timing accuracy of 16 m (50 % spherical error) and 100 ns (1 σ) as stated in the 1990 GPS System Operation Requirements Document (SORD). The 1999 GPS Operational Requirements Documents (ORD) set a new goal for the GPS III and beyond. The 1999 ORD specifies the ranging accuracy 1.5 m threshold and 0.5 m objective. The 95% time transfer accuracy threshold and objective are 20 ns and 10 ns, respectively. This paper will evaluate how the current clocks and the clocks being developed can support the ORD threshold and objective. The paper will include the following topics: (1) atomic clocks on the GPS Block II space vehicles, (2) estimated accuracy of the IIF Rb clock by Perkin Elmer and digital Cs clock by Datum-Beverly and assessment of their performance against the ORD threshold range requirements, (3) description of the new space clocks being developed jointly by the GPS JPO, Aerospace, and NRL, and evaluation of their predicted performance to see if they can support the ORD objective of 0.5 m (rms), and (4) Prediction of the GPS signal-in-space accuracy, including all the space and control segments errors, using IIF Rb and Cs clocks. The predictions are based on replacing the NIMA estimated GPS II/IIA/IIR clock data, contained in the actual tracking data of the GPS monitor stations and the NIMA tracking stations, by simulated IIF Rb and Cs clock data. A Kalman filter similar to that of the OCS then processes the resulting tracking data and the estimated results are compared with NIMA estimates treated as truth. Evaluations of the various options to see whether the ORD objective can be achieved based on the predicted signal-in-space accuracy are included.

1. ATOMIC CLOCKS ON THE GPS BLOCK II SPACE VEHICLES

Atomic Frequency Standards (AFSs) or clocks in the GPS satellites are essential in providing GPS users accurate position velocity and time determinations. Two rubidium (Rb) clocks and two cesium (Cs) clocks were used in the GPS Block II/IIA satellites. Rockwell produced the Rb clocks using Efratom physics packages, and the Cs clocks were provided by three different companies. Frequency and Time Systems (FTS) supplied the majority of the Cs clocks. Second source units were provided for flight validation by Kernco, which provided three units, and by FEI, which furnished two units. These clocks are the first ones produced in any quantity for space operation, and have experienced lower-than-expected life, even though no GPS II/IIA satellite has been lost due to clock failure. Designed in the late 70's and early 80's, these now out-of-date units are no longer produced by any of those companies [1].

Two Rb clocks and one Cs clock were originally planned for each satellite in the GPS Block IIR program. The selected Rb clocks resulted from second source development performed at EG&G during Block II/IIA procurement. However, after several years of unsuccessful attempts by the IIR Cs clock contractor to space-qualify a production unit, a three-Rb-clock-configuration was selected for the IIR program to maintain schedule. Testing of the first two GPS Block IIR satellites on-orbit and results from a dedicated Rb clock life-test ongoing at the Naval Research Laboratory (NRL) indicate that the Rb clock is performing nicely (much better than specification), and indications of mission success are excellent.

A clock configuration consisting of three Cs clocks and one Rb clock has been chosen for the GPS Block IIF spacecraft. The electronics packages of all spaceborne clocks so far have used analog technology, but Datum-Beverly (formerly FTS) will produce the IIF Cs clock using a digital electronics approach based on their commercial digital clock design. The development of the digital Cs clock was initiated by the GPS Joint Program Office and NRL to produce prototypes demonstrating the application of digital electronics technology to space-qualified atomic clocks. The GPS Block IIF contractor, Boeing North America (BNA), took over this project midway, including funding, after being convinced that the new digital Cs clock will meet their IIF requirements. This is a success story in the transfer of commercial technology to space applications being supported by continuing R&D for GPS. The history of atomic clock deployment on board GPS satellites is summarized in Table 1.

GPS Program	RAFS	CAFS
Block II/IIA	two (Rockwell)	two (FTS, Kernco, FEI)
Block IIR	three (EG&G)	none
Block IIF	one (Perkin Elmer)	three (Datum-Beverly)

Table 1. Clocks on GPS Satellites

2. GPS BLOCK IIF CLOCK ACCURACY ASSESSMENT

The IIF current baseline is to operate satellites in the cross-link navigation update mode such that with each upload to one satellite, corrections for the rest of constellation are also uploaded. These corrections are then relayed to the corresponding satellite through the cross-links. The Block IIF contractor, Boeing, offers a minimum update rate of once every 3 hours.

User Range Error (*URE*) is defined as the rms value of the total Space/Control segment or signal-in-space (SIS) range error components. User Equipment Error (*UEE*) is defined as the rms value of the total User segment range error components. User Equivalent Range Error (*UERE*) is the total statistical system ranging error (rms), defined as the root-sum-square (rss) of *URE* and *UEE*:

$$UERE = (\text{URE}^2 + \text{UEE}^2)^{1/2} \quad (1)$$

The 1990 GPS System Operation Requirements Document (SORD) specifies the position and timing accuracy requirements as:

Position: 16 m (50% spherical error), globally averaged.

Transfer of UTC: 100 ns (one standard deviation), globally averaged.

The derived UERE is 7 m, URE is 6 m, and UEE is 3.6 m.

The URE requirement for the IIF system operating in the cross-link navigation update mode as documented in the *GPS IIF System Specification, SS-YSY-600*, is:

URE <3 m (rms) at less than 3 hours Age of Data (AOD), with a goal of URE \leq 1 m (rms).

The 1999 GPS Operational Requirements Document (ORD) specifies the ranging and timing accuracy as:

UERE threshold (\leq 1.5 m (rms)) [URE threshold (\leq 1.25 m (rms)) and UEE threshold \leq 0.8 m (rms)]

UERE objective (\leq 0.5 m (rms))

Time transfer threshold (\leq 20 nsec (95%)) [Time transfer to a surveyed site]

Time transfer objective (\leq 10 nsec (95%))

In general the ranging accuracy requirement seems more stringent than the time transfer requirement; however, the timing accuracy included the UTC to GPS uncertainty.

The goal of the GPS JPO is to reduce ranging and timing errors as much as possible by exploring all possible means to do so.

SIS URE includes clock random errors, clock errors due to orbital temperature variations (about $\pm 3^{\circ}\text{C}$ with a period of 12 hours), and magnetic field effects due to three electro-magnets in the attitude determination and control system, L-band signals group delay differentials, ephemeris errors, and other small errors. It is assumed here that the URE budget is allocated equally to the above-mentioned four major independent error sources, so that the goal is to limit the GPS clock random error contribution to less than 1/2 of URE. The rms IIF range error contributions from random clock noise can be estimated using the clocks' measured Allan deviations from several engineering and production units , and are shown in Figure 1. The estimated range error contribution of the IIF Rb clock is about six times smaller than that of IIF Cs clock. Examination of the precision of the IIF clocks to verify whether they can support the various $1/2^*\text{URE}$ requirements mentioned above with 3-hour updates yields the results provided in Table 2. For the ORD objective, $1/2^*\text{UERE}$ instead of $1/2^*\text{URE}$ is used, since the current UEE of 0.8 m is larger than UERE of 0.5 m, and thus the URE cannot be computed.

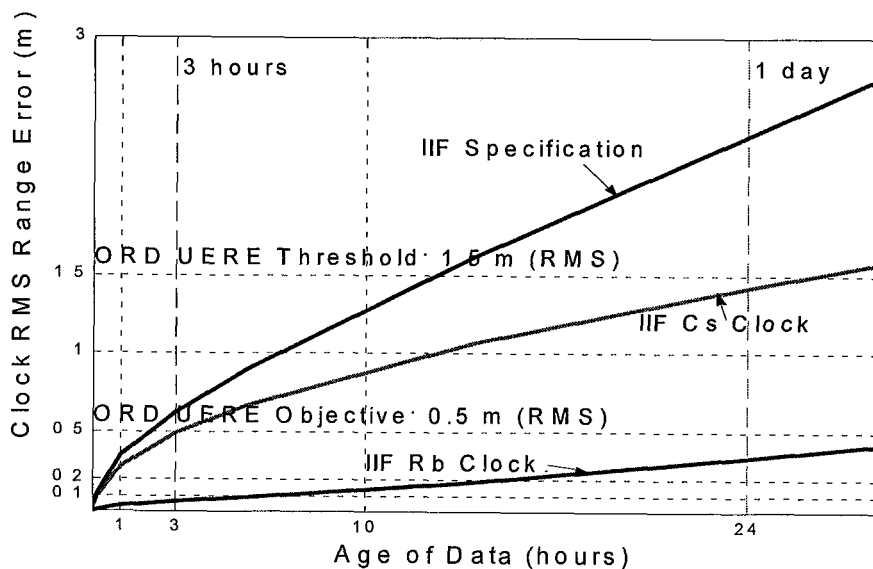


Figure 1. Estimated IIF Clocks Range Error

Clock Type	Estimated Clock Range Error	1990 SORD	GPS IIF AOD \leq 3hrs	1999 ORD Threshold	1999 ORD Objective
	m (rms) at AOD of 3 hours	$\frac{1}{2} \times \text{URE} \leq 3 \text{ m}$	$\frac{1}{2} \times \text{URE} \leq 1.5 \text{ m}$	$\frac{1}{2} \times \text{URE} \leq 0.75 \text{ m}$	$\frac{1}{2} \times \text{UERE} \leq 0.25 \text{ m}$
IIF Cs	0.49	yes	yes	yes	no
IIF Rb	0.06	yes	yes	yes	yes

Table 2. Support of IIF Clocks with 3-hour Updates to Meet URE/UERE Requirements

It can be observed from Table 2 that:

1. Both IIF Cs and Rb clocks can support IIF system requirements,
2. The IIF Cs clock with 3-hour updates can support the 1999 ORD Threshold requirement, but it will not support the 1999 ORD Objective, and
3. The IIF Rb clock with 3-hour updates can support both the 1999 ORD Threshold and Objective requirements.

Other characteristics of the IIF Cs and Rb clocks are provided in Table 3 for information.

	IIF Rb Clock	IIF Cs Clock
Weight	14 (lb)	27 (lb)
Envelope	7.5X6X12.1 (in ³)	7.5X6X16.5 (in ³)
Temperature controller	Built-in	None
Power	< 39 watts	< 25 watts
Temperature coefficient	5E-14 Δf/f/°C	1E-13 Δf/f/°C
Design Life	15 years	10 years

Table 3. GPS Block IIF Clock Comparison

The IIF Rb clock provides advantages over the IIF Cs clock except power. To preserve the legacy of better-performing Rb clocks from Block IIR, Boeing is being tasked under a special study to consider a minimum of two Rb clocks for each IIF space vehicle.

3. NEW CLOCK TECHNOLOGY ROADMAP PROGRAM

The GPS program has a dual clock technology requirement as documented in Section 3.2.7.2 of the System Requirements Document for GPS Block IIF system (SRD-GPS-IIF). This requirement was set to mitigate the risk that one of the clock types cannot be space-qualified. This requirement saved the GPS Block IIR program when the Cs clock, the preferred choice from the Block II/IIA experience, failed in multiple attempts to pass space qualification tests. Another advantage of this requirement is performance improvement through competing technologies.

Since the IIF Cs clock cannot support the 1999 ORD range error objective, a new clock technology program is needed to sustain the GPS system for future applications. The GPS JPO, Aerospace, and the Naval Research Laboratory (NRL) jointly developed the new clock technology roadmap program [1, 2] which was endorsed by atomic clock experts from a number of US Government organizations and FFRDCs in a GPS Spacecraft Clock Coordination Meeting held at NRL on 17 June 1999. The proposed effort includes:

1. Evolving the current design of the Block IIF Rb clock, which relies on an analog technology electronics package, to reduce clock variability and environmental sensitivity,
2. Developing space-qualifiable new technology clocks based on proven ground clock technologies,
3. Building flight demonstration models (FDMs) for qualification tests,
4. Conducting ground tests of the FDMs to monitor their characteristics and performance in a simulated space environment for space flight selection,
5. Developing and building an on-board clock comparison subsystem to evaluate the on-orbit performance of the FDM selected for space flight,
6. Providing funding to Boeing for integration of the on-board clock comparison subsystem with the SV and performance evaluation, and
7. Making available the spaceworthy new technology clocks for future GPS applications.

The new technology clocks being developed are [1-3]:

3.1 Advanced Digital Rb Clock, by Perkin Elmer (formerly EG&G) and NRL

This project will take space-qualified Rb clock technology, as implemented in the GPS Blocks IIR and IIF programs, to the limit of what present state of art allows. It will do so by: (a) modifying slightly the physics package to incorporate technical advances either already implemented in tactical Rb clock or suggested by the experience accumulated while manufacturing the Blocks IIR and IIF clocks, (b) modifying radically the clock electronics package to incorporate a state-of-art 6.8 GHz signal source, direct digital signal synthesis, digital servo loop, and microprocessor monitoring and control of all critical clock parameters.

The resulting clock is expected to have a stability performance about twice as good as that of the Block IIF clock. It will be more producible by incorporating automated setup, checkout, test, and calibration processes. It will have a smaller aging coefficient and lower environmental sensitivities (particularly thermal) than the current Rb clock. This project presents a low technical risk.

3.2 Optically Pumped Cs Beam Clock, by Datum-Beverly (formerly FTS) [4-6]

This task will introduce optical methods, instead of conventional magnetic methods, for state preparation and signal detection in the Cs clock. This concept has been demonstrated in the current US time and frequency standard, NIST-7, at the Time and Frequency Division of the National Institute of Standards and Technology (NIST), in Boulder, CO. It allows more efficient use of the Cs atoms emitted by the Cs oven, thereby potentially prolonging the useful life of the Cs beam tube, while at the same time increasing the flux of detected atoms, and thus improving the short-term stability of the clock. This clock is expected to have frequency stability comparable to that of the analog Block IIF Rb clock. The technical risk presented by this project is moderate, because of the challenge of identifying a source of laser diodes with appropriate stability, availability, and radiation hardness.

3.3 Space Linear Ion Trap System (LITS), by the Jet Propulsion Laboratory (JPL) [2, 3]

JPL will design and build a small, light, and space-qualifiable version of the linear mercury ion trap clocks developed for the NASA's Deep Space Network. JPL has built several operational ground units that display very good frequency stability. A significant difference between the way trapped mercury ion clocks and Cs or Rb clocks operate is that in the latter, microwave interrogate the Cs or Rb atoms continuously, while in the former, interrogation of the mercury atoms takes place in a low duty-cycle discontinuous fashion. Because of this a better quality local oscillator than that for Cs or Rb clocks has to be used. JPL plans to use the best available

BVA-cut quartz crystal oscillator, and interrogate the physics package approximately every 3 seconds. The expected stability of the LITS is about 10 times better than that of the advanced digital Rb clock. The technical risk involved with this redesign is moderate, with no evidence of fundamental problems.

The estimated new clock contributions to range error are provided in Figure 2. With 3-hour cross-link updates, all three new clocks can support the 1999 ORD range objective of 0.5 m (rms). With 24-hour updates, both the Advanced Digital Rb Clock and the Linear Ion Trap Clock can also support the 1999 ORD objective, while the Optically Pumped Cs Clock can support the 1999 ORD range objective only marginally.

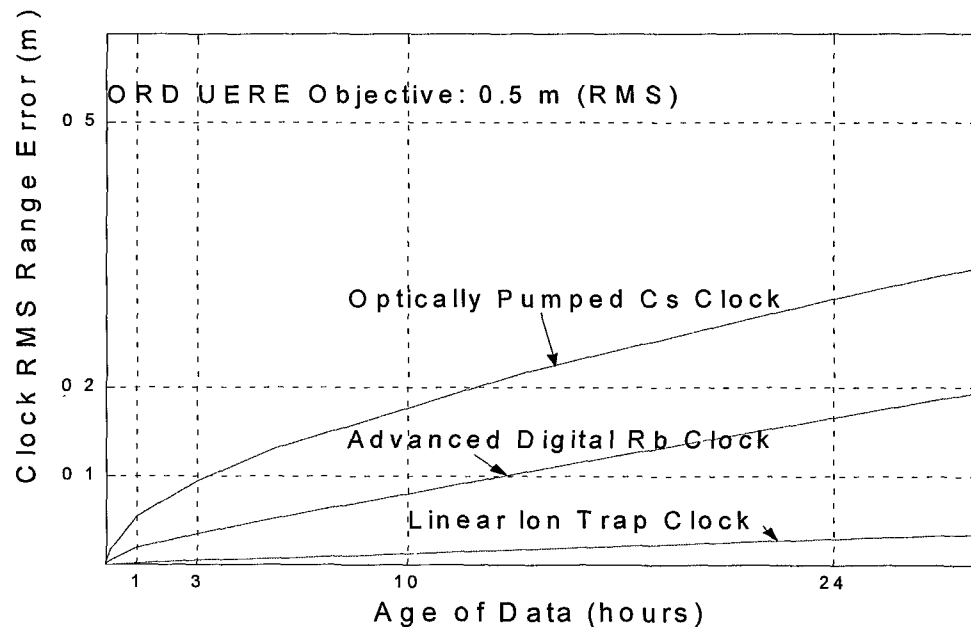


Figure 2. New Technology Clock Estimated Range Error Contributions

Educated guesses about the characteristics of the new clock technologies discussed above are provided in Table 4 below [3].

Clock Type	Technical risk	Estimated range error @ 3 hr (cm)	Estimated range error @ 24 hr (cm)	Weight (lb)	Dimensions (in)	Power (w)
Advanced Rb clock	Low	3.5	16	14	7.6x6x12	35
Optically Pumped Cs clock	Moderate	9.5	30	29	7.5x6x18	25
Linear Ion Trap clock	Moderate	0.5	2.9	25	16x10x8	25

Table 4. Expected Characteristics of New Technology Clocks

The current new clock technology roadmap schedule indicates that the flight demonstration

models (FDMs) of the Digital Rb Clock and the Optically Pumped Cs Clock will be ready for on-orbit test on a Block IIF space vehicle in late 2004, and, if successful, will be ready for future GPS application in 2007. The FDM of the JPL LITS will be ready for on-orbit test in 2006 and could be available for future GPS application in 2009.

Other clock technologies being monitored/considered for GPS applications are:

1. Small space hydrogen masers
2. Laser-cooled Cs clocks
3. Double-bulb Rb masers.

4. PROJECTED GPS SIGNAL-IN-SPACE (SIS) RANGE ACCURACY

NIMA routinely postprocesses GPS tracking data received from the GPS monitor stations and NIMA tracking stations to provide the best estimates of ephemeris, clock offset, and other states of every GPS satellites in the constellation. These NIMA estimates of satellite ephemeris and clock offset at 15-minute intervals have commonly been regarded as truth in the GPS community. Aerospace has developed a procedure to replace the NIMA estimated GPS II/IIA/IIR clock data, contained in the actual tracking data provided and used by NIMA, by simulated IIF Rb clock and Cs clock data. A Kalman filter similar to that of the GPS Operational Control Segment (OCS) then processes the resulting tracking data. The Aerospace filter estimates ephemeris and clock offset for each satellite and propagates these estimates forward in time. The propagated ephemeris and clock predictions for every satellite in the constellation are compared with the NIMA truth data to compute the globally average SIS URE for the near earth GPS user using the formula [8] as provided below:

$$SIS - URE = (Variance(R - C) + 0.0192 * [Variance(IT) + Variance(CT)])^{1/2} \quad (2)$$

where R, IT, CT, C = radial, in-track, and cross-track ephemeris errors and clock errors.

The projected GPS SIS URE accuracy data with IIF Rb and Cs clocks, II/IIA Cs clock, and a perfect clock, using 2-week GPS tracking data in October 98, as a function of age of data is shown in Figure 3. The projected SIS URE for the IIF constellation with mixed Cs and Rb clocks is expected to be somewhere between the IIF Cs and IIF Rb curves. These results were obtained without changing the filter or its tuning parameters.

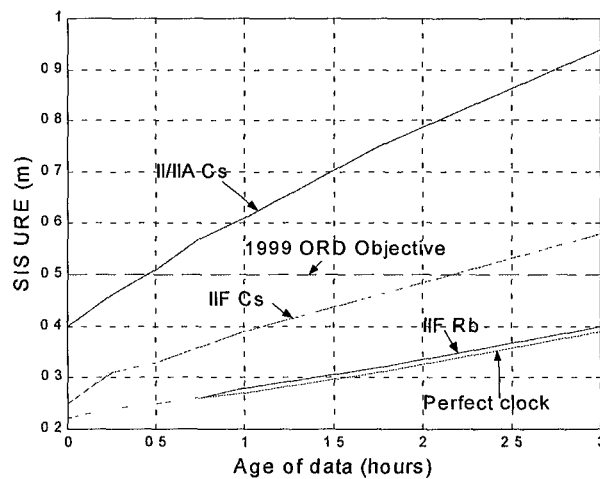


Figure 3. Projected GPS SIS URE

By comparing curves with IIR Rb and the perfect clock, it is evident that ephemeris and other errors dominate GPS SIS URE if the GPS Block IIF Rb or better clock is used. With IIF Rb or better clock, it offers an opportunity to reduce further the projected GPS SIS range accuracy by:

1. Retuning the Kalman filter
2. Improving multi-path mitigation and atmospheric modeling at the monitor stations
3. Identifying and estimating the errors not being modeled currently
4. Improving ephemeris estimation and prediction accuracy
5. Others.

Once the SIS URE range accuracy is improved by addressing the issues suggested above, it might become evident that the SIS URE can be further reduced with a much better clock. This shows that development of better clocks is a necessary first step to further improve the SIS URE.

5. COMMENTS ON THE PROJECTED GPS SIS URE

The IIF current baseline is to operate satellites in the cross-link navigation update mode with a minimum update rate of once every 3 hours. It is seen from Figure 3 that the SIS URE for the IIF with Cs and Rb clocks and with age of data of 3 hours are 0.58 m and 0.40 m respectively. To achieve the ORD range threshold of 1.5 m, the UEE allocation can be 1.38 m and 1.45 m for IIF with Cs and Rb clocks respectively. These UEE budgets can be met with today's user equipment technology, so the ORD range accuracy threshold can be achieved with today's technology.

In the 1999 ORD a benchmark user with user equipment error (UEE) of 0.8 m (rms) is assumed to specify the GPS range rms accuracy threshold of 1.5 m. Since UEE of 0.8 m is already greater than the ORD range accuracy objective of 0.5 m, it is obvious that further user equipment development and improvement are needed in order to meet the ORD range accuracy objective.

When the GPS Block IIF cross-link system works properly without interference and degradation, it is conceivable that the constellation can be refreshed every OCS Kalman cycle, i.e., every 15 minutes. Assuming that more advanced GPS receivers become available in the future, the projected signal-in-space accuracy as a function of age of broadcast data, as provided in Figure 3, can be used to see whether the ORD objective can be achieved. Based on the projected SIS URE as shown in Figure 3, the allocation of the UEE to achieve the ORD range accuracy objective of 0.5 m is plotted in Figure 4.

It is evident that from Figure 4 that:

1. GPS with IIF Rb clocks can support ORD range objective with 3-hour cross-link updates if UEE is 0.3 m or less,
2. GPS with IIF Rb clocks can support ORD range objective with 15-minute cross-link updates if UEE is 0.43 m or less,
3. GPS with IIF Cs clocks can support ORD range objective with 15-minute cross-link updates if UEE is 0.39 m or less,
4. GPS with IIF Cs clocks can support ORD range objective with 1.1-hour cross-link updates if UEE is 0.30 m or less, and
5. GPS with IIF Cs clocks cannot support ORD range objective if the cross-link update is 2.2-hour or longer.

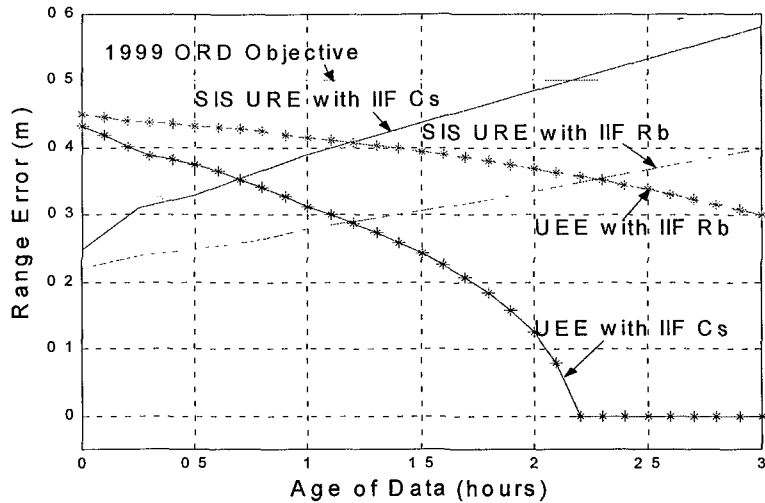


Figure 4. User Equipment Error (UEE) Allocation

6. CONCLUSIONS

1. Development of new space clocks is well underway. Digital Rb clock and Optically Pumped Cs clock could be ready for future GPS application in 2007, and JPL LITS could be ready in 2009.
2. The projected SIS URE based on the IIF Rb clock shows that development of advance clocks is the first step in improving GPS user range accuracy.
3. Improvement of current IIF cross-link system and development of more advanced GPS receivers are needed to meet the ORD range objective of 0.5 m and beyond.

REFERENCES

- [1] D. Martoccia, R. Beard, and A. Wu 1996, in "Atomic frequency standards Roadmap for the future GPS satellites," Proceedings of ION-GPS-96.
- [2] R. Beard 1998, *GPS Advanced Clock Roadmap Program, Preliminary Program Plan*, dated 7 July 1998.
- [3] W. Buell, Y. Chan, and B. Jaduszliwer 1999, "New clock technologies," an Aerospace interoffice correspondence to Andy Wu, dated 13 January 1999.
- [4] M. Garvey 1999, "Optically pumped cesium atomic clock for space applications," an unsolicited proposal to NRL from Datum-Beverly, dated 21 October 1999.
- [5] Y. Chan, and W. Buell 1999, "Comments on FTS optically pumped Cs beam clock proposal," an Aerospace interoffice correspondence to Andy Wu, dated 29 October 1999.

- [6] B. Jaduszliwer 1999, “*Datum/FTS optically pumped cesium atomic clock for space applications*,” an Aerospace interoffice correspondence to Andy Wu, dated 10 November 1999.
- [7] R. Beard 2000, “*Testing of the new technology clock*,” Powerpoint charts, dated 10 March 2000.
- [8] H. Bernstein 1983, “*Calculations of User Range Error (URE) variances from a Global Positioning Satellite (GPS)*,” The Aerospace Corporation TOR-0083 (3476-02)-1, 20 June 1983.

Questions and Answers

MICHAEL GARVEY (Datum): Andy, you had one of your slides which talked about contributors to URE that were not clock-related. I wondered if you had put them in order of priority, and maybe if you could go back to that slide and comment what the really big ones are.

ANDY WU: Oh, I see that. What we should do?

GARVEY: Yes, that is the one. Are those in order of priority and maybe could you put—?

WU: I think so, yes. We can do this, and this is not easy. We cannot do that, I guess, monitor cesiums, the receiver guy has to do that, and just send it down.

THOMAS CLARK (NASA Goddard Space Flight Center): I am surprised, and perhaps others are, that for the IIF satellites the rubidium is showing a factor of two to three or so better than the cesiums. I'm a little curious why. Is it that the performance has been tuned for short-versus-long term?

WU: That is just on the test results.

CLARK: Okay, so this is the actual implementation of the hardware?

WU: Yes, it is.

CLARK: I was wondering if there was some new breakthrough in rubidium physics that accounted for this rather than—

WU: I guess the rubidium for the 2-hour today was showing something like this. So it is no surprise to us that they did that. It is better than the cesium today. Most rubidiums are, surprisingly enough. Also, in the 2-hour rubidiums, there is a mechanism for them to get rid of the frequency drift and the frequency offset. So in 2 hours a rubidium looks just like a cesium. The drift is small; it has been removed now.

DENNIS McCARTHY (USNO): I am wondering, on some of these things that you showed us, the sources of error. Some of these issues have already been addressed to some extent by the International GPS Service in which they produced, characteristically, now operationally, orbits and even clocks that are much better than you typically see from anything available operationally from the operational GPS. Is there any effort at all in what you are describing here to make use of that capability that is provided by the IGS?

WU: Yes, we are aware of them. Most of that would be incorporated by the OCS, but slowly. It is not high priority right now; there is something else to worry about.

McCARTHY: When you say slowly, how slowly?

WU: Three or four years, unfortunately. It takes a long time. They have other problems to worry about.

GLOBAL POSITIONING SYSTEM (GPS) MODERNIZATION

**Lt. Col. C. McGinn, Capt. S. Rajotte
U.S. Air Force
GPS Joint Program Office
Los Angeles AFB, CA, USA**

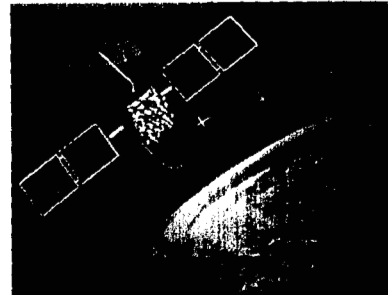
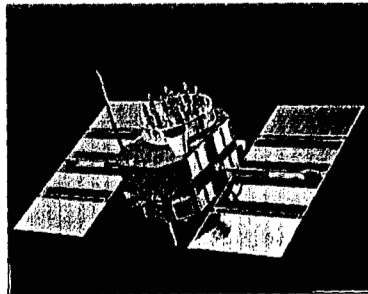
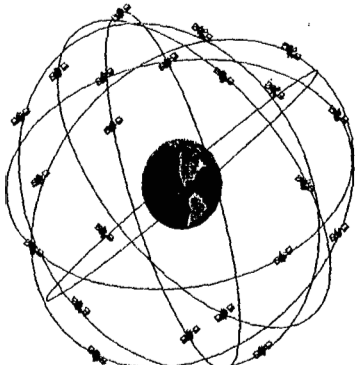
**D. Latterman
Science Applications International Corporation (SAIC)
Torrance, CA 90501, USA**

Abstract

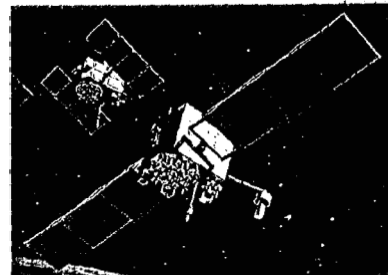
The Global Positioning System (GPS) signal is now the primary means of obtaining precise time to an internationally accepted standard. Precise timing applications have become dependent on this space-based source of precise time and, therefore, depend on the constellation of satellites that provide it worldwide, anytime. This paper describes the efforts by the GPS Joint Program Office within the U.S. Department of Defense to modernize the GPS signal services to meet future military and civil user requirements. GPS timing users and timing receiver developers and integrators need to be aware of these new capabilities and when they will be available. This paper starts with a brief review of the system design and an overview of the current constellation status. The GPS Modernization program to modify the current block of satellites being placed into service and the next generation currently in design to provide additional system capabilities will be described. Next, the paper discusses the GPS-III program to look at future user requirements beyond the next 20 years for precise positioning and timing services. The paper summarizes what these new capabilities will mean to the GPS timing users and provides some suggestions on what GPS timing users can do to make their future needs known. The paper concludes with some challenges to the user community to support the continued mission of GPS to provide precise positioning and time to all users free of direct charge.

GPS OVERVIEW

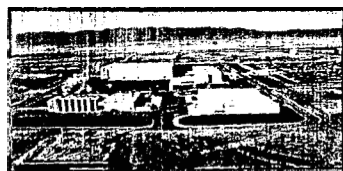
GPS Space Systems



- 24-satellite (nominal) constellation
- Six orbital planes, four satellites per plane
- Semi-synchronous, circular orbits (~11,000 mi)

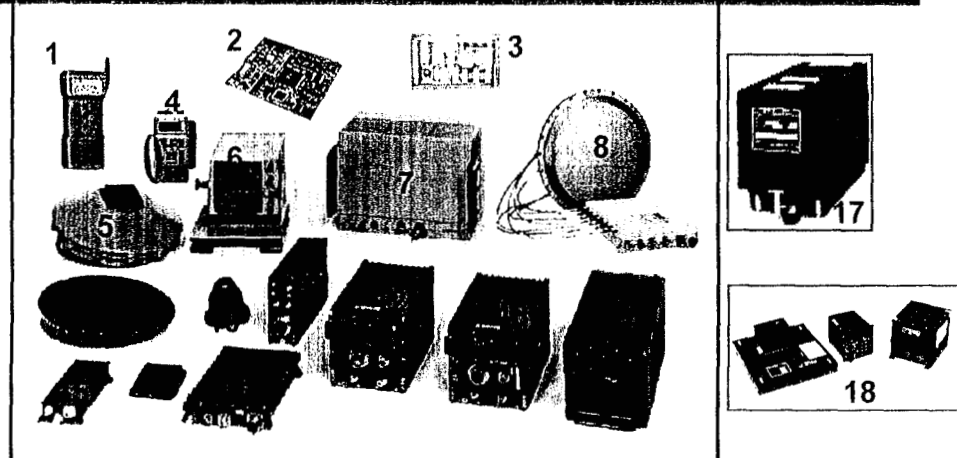


GPS Operational Control Segment



- Master Control Station (MCS): Satellite control; system operations
- Alternate Master Control Station (AMCS): Training; back-up (VAFB - FY04)
- Monitor Station (MS): Collect range data, monitor navigation signal
- ◆ NIMA Tracking Station (TS): Collect range data, monitor navigation signal
- Ground Antenna (GA): Transmit data/commands; collect telemetry

GPS User Equipment (UE)

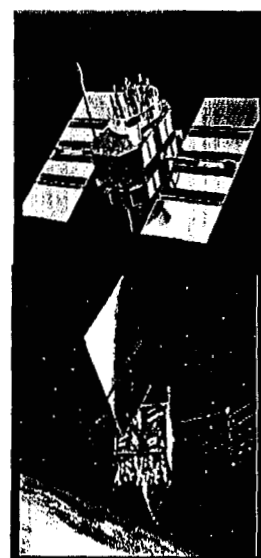


- | | |
|---|--|
| 1. Combat Survivor/Evader Locator (CSEL)
2. GPS Receiver Applications Module (GRAM) with SAASM
3. Selective Availability Anti-Spoofing Module (SAASM)
4. Precision Lightweight GPS Receiver (PLGR)
5. FRPA Ground Plane (FRPA-GP)
6. Standard Control Display Unit (CDU)
7. Receiver 3S
8. GPS Antenna System (GAS) -1 | 9. Controlled Radiation Pattern Antenna (CRPA)
10. Fixed Radiation Pattern Antenna (FRPA)
11. Miniature Airborne GPS Receiver (MAGR)
12. Receiver OH (MIL-STD-1553)
13. Receiver UH (ARINC 429)
14. Receiver 3A
15. Antenna Electronics AE-4
16. Antenna Electronics AE-1/AE-1A
17. Embedded GPS / INS (EGI)
18. Doppler-GPS Navigation System (DGNS) |
|---|--|

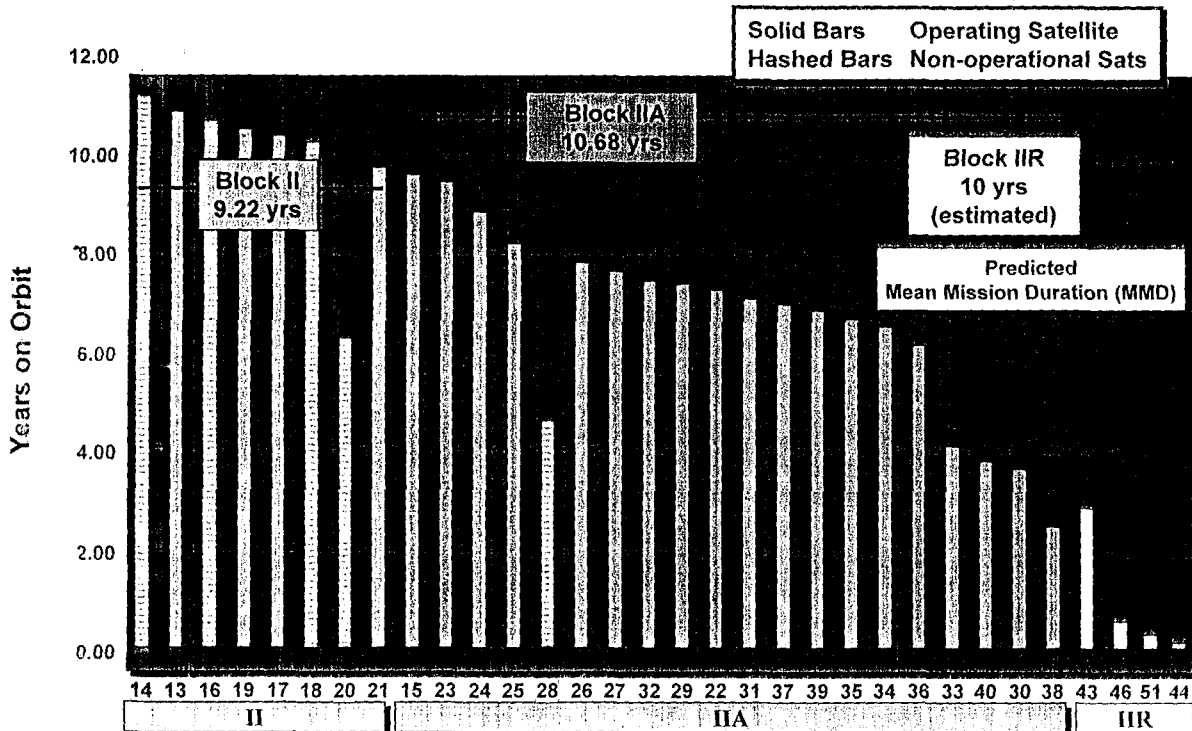
CONSTELLATION STATUS

28 Operating Satellites

- 23 Block II/IIA operational satellites
 - Block IIA life expectancy was extended two years (to 10.68 years)
- 5 Block IIR satellites on orbit
 - Last launch 10 Nov 00
 - 16 of 21 Block IIR satellites available
 - Modernizing up to 12 Block IIR satellites
- Next Launch: 30 Jan 01
- Tentative launch dates: Jun 01
- Continuously assessing constellation health to determine launch need



GPS Constellation Snapshot



RECENT PROGRAM CHANGES

Vice Presidential Announcements Second And Third Civil Frequencies

- "Enhancements to the Global Positioning System that will Benefit Civilian Users Worldwide" - 30 Mar 98
 - **Second civil signal** on L2 at 1227 MHz
 - Improve accuracy of the overall system
 - Redundant signal for safety critical users
 - **Third civil signal** for safety of life services by 2005 at frequency to be determined
 - New signals intended to be added to the Block IIF satellites
- "New GPS Modernization" Initiative - 25 Jan 99
 - Location of third civil frequency at 1176.45 MHz
 - Spectrum allocated for Aeronautical Radio Navigation Services (ARNS)
 - Beginning with a satellite scheduled for launch in 2005

Use Of Selective Availability (SA) Discontinued

Presidential Decision - 1 May 00

- US stopped the intentional degradation of the GPS signals available to the public (called Selective Availability or SA) on 1 May 00
- Decision based on a recommendation by the SecDef
 - In coordination with the Departments of Transportation, Commerce, the Director of Central Intelligence (DCI), and other Executive Branch Departments and Agencies
 - Worldwide transportation safety, scientific, and commercial interests could be best served by discontinuation of SA
 - Supported by threat assessments which conclude that setting SA to zero at this time would have minimal impact on national security
 - Demonstrated capability to selectively deny GPS signals on a regional basis when our national security is threatened
- Increase in accuracy will allow new GPS applications to emerge and continue to enhance the lives of people around the world

SA is off !!

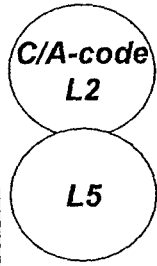
Why Modernize GPS?

- Better support the warfighter in the evolving threat environment
 - More signal power = more anti-jam
 - More secure new military code structure
 - More User Equipment anti-jam capability = more protection
 - Better able to deny an enemy use of GPS



**Joint Requirements Oversight Council (JROC)
validated requirements in Jun 99**

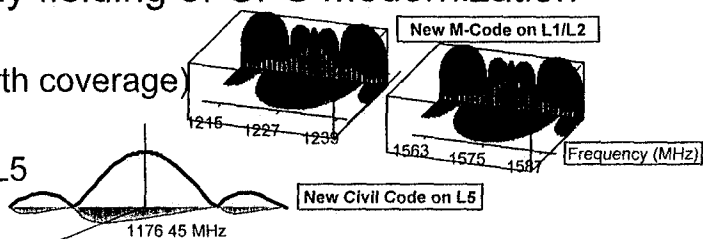
- Better support to civil GPS customers
 - New civil signals for improved accuracy, integrity and continuity of service = robustness
 - Global utility = economic enabler



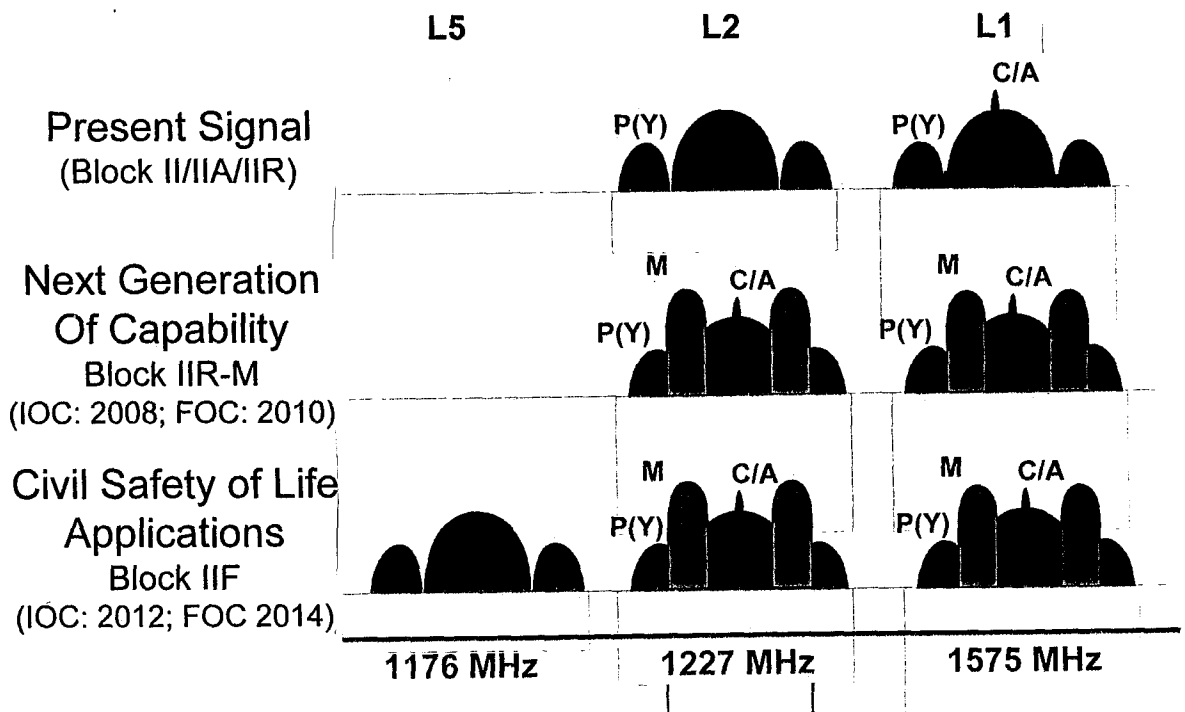
**Presidential Decision Directive - Mar 96
Vice Presidential Announcements - Mar 98 and Jan 99**

GPS Modernization Strategy Goals

- Commitment to early fielding of GPS Modernization capabilities
 - Military M-code (earth coverage)
 - C/A code on L2
 - New civil signal on L5
 - More signal power
- Keep the GPS constellation healthy
- Backward compatibility
- Ensure the right strategy to design and field the best GPS System for the user's needs in the long term
 - Better match to user requirements
 - Reduce total cost of ownership
 - Design-in flexibility for future changes
 - Provide multiple decision points for tailoring to meet evolving requirements

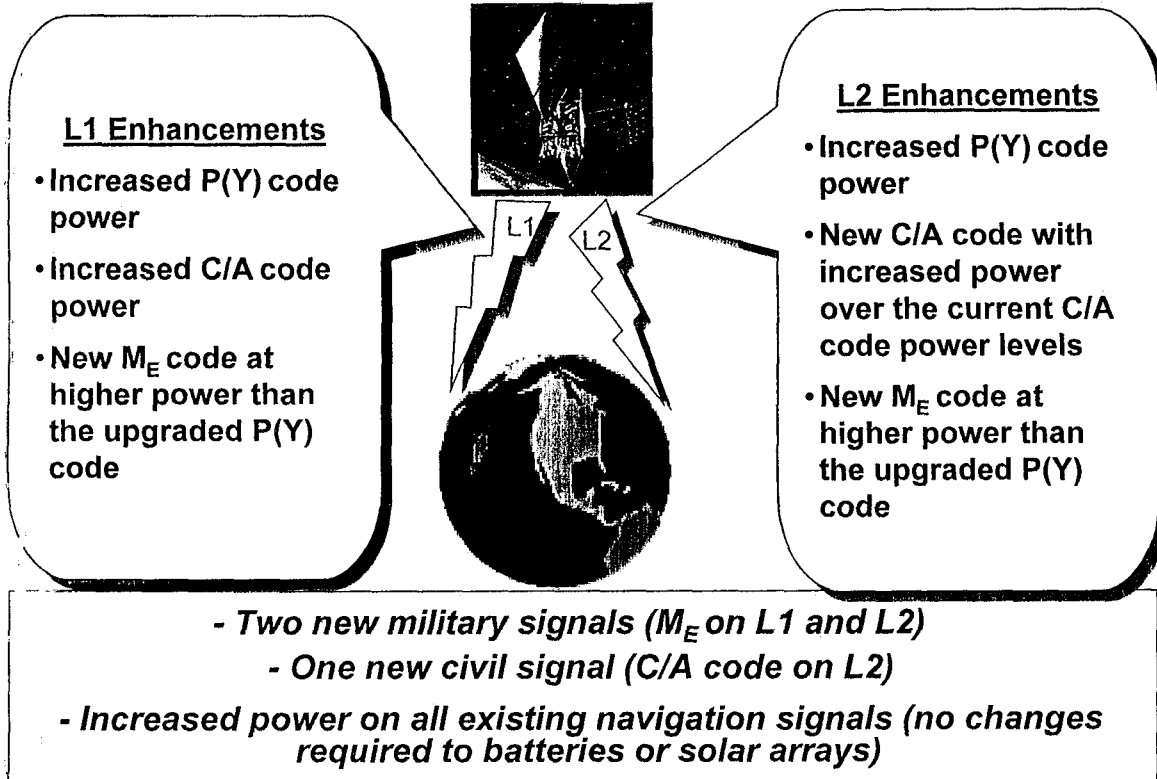


Modernized Signal Evolution

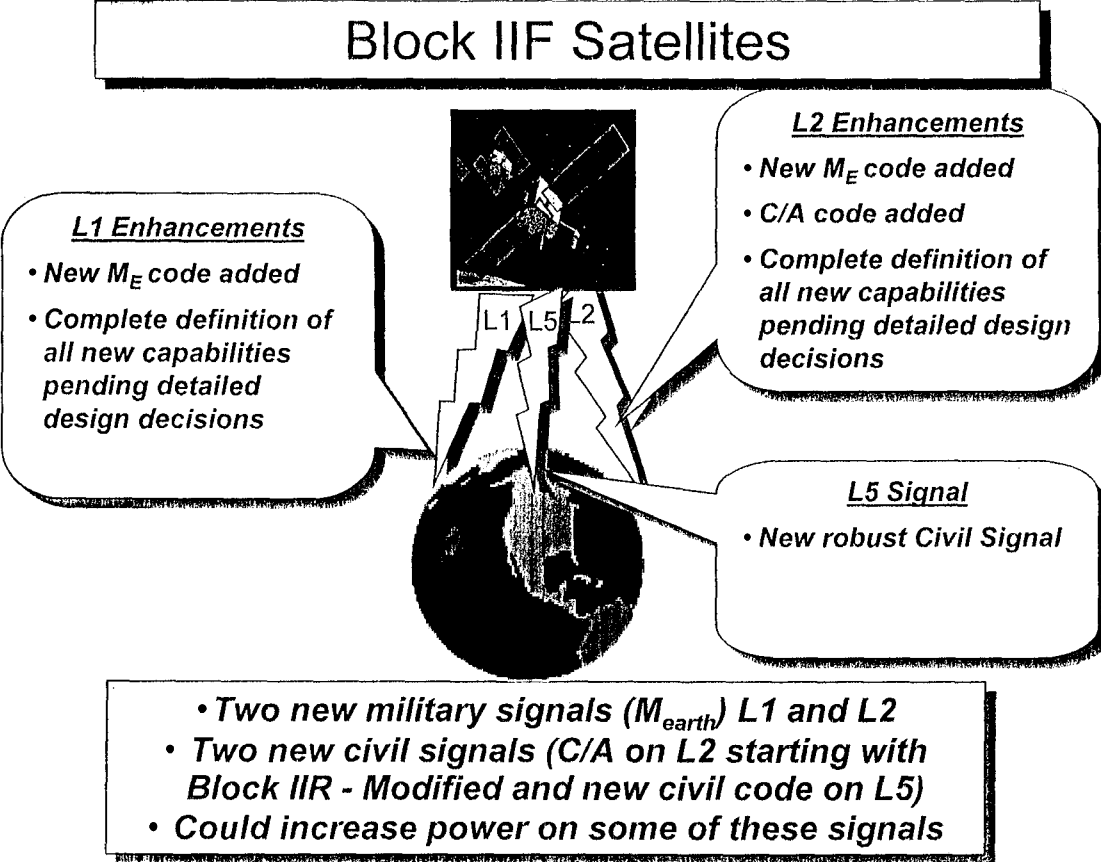


GPS MODERNIZATION PROGRAM

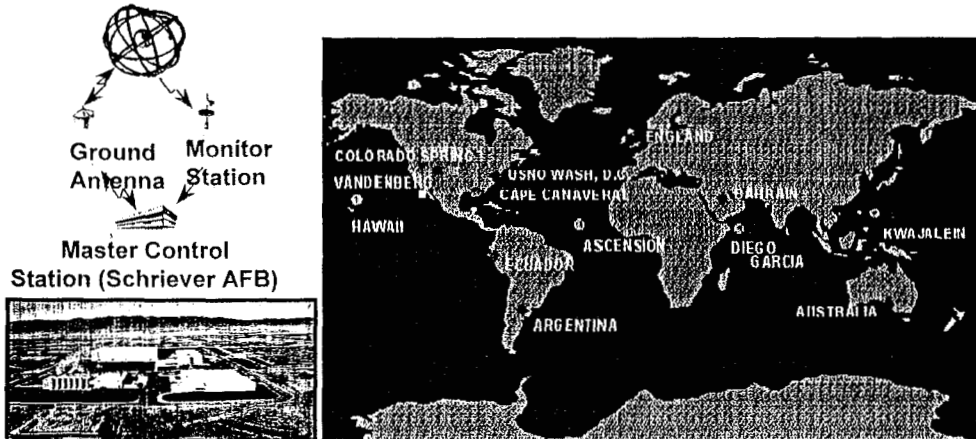
Block IIR- Modified Satellites



Block IIF Satellites



GPS Operational Control Segment

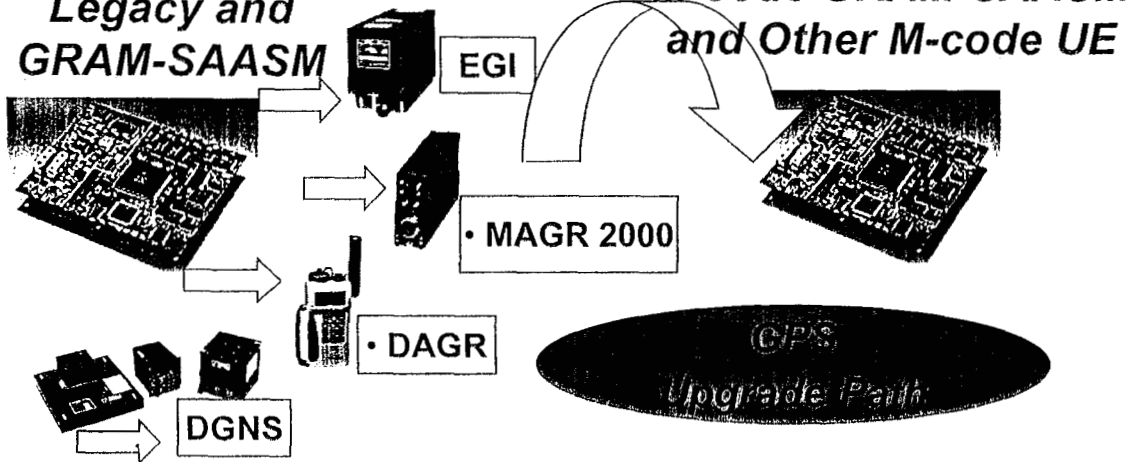


Incremental software versions and hardware upgrades to support modernization requirements

User Equipment Modernization Path

Near Term

Legacy and GRAM-SAASM



Open system architecture allows easier upgrades for future capability

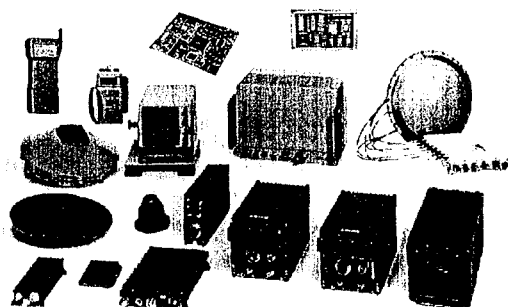
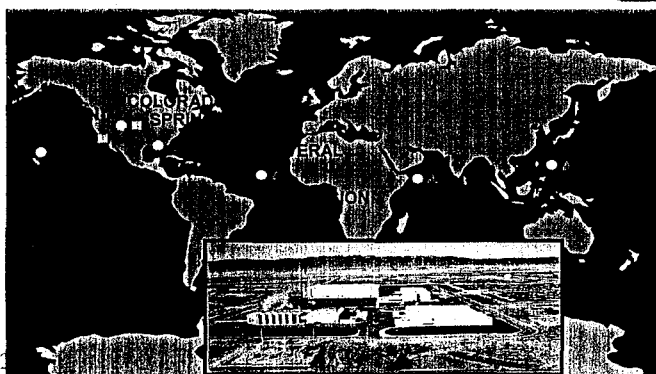
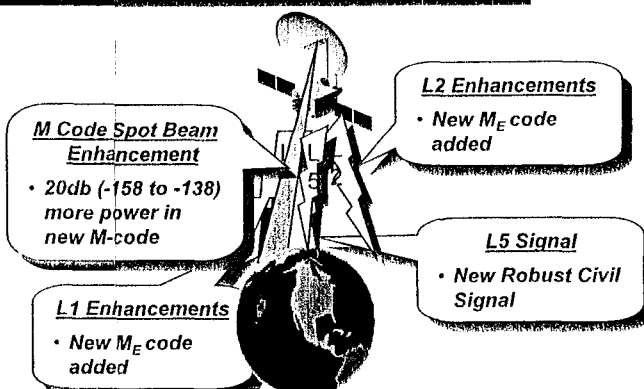
GPS Modernization and GPS-III Program Approval

- Operational Requirements Document (ORD) signed
- Amendment to President's Budget (PB) sent to Congress
- Congressional approval for GPS Modernization and GPS-III Program as "New Starts" received
 - Block IIR Modification letter contract awarded - Aug 00
 - Block IIF Undefinitized Contract Change for Modernization development issued on current contract - Aug 00
 - GPS-III Systems Architecture and Requirements Definition (SARD) Phase contracts for GPS-III competitively awarded to two contractors - Nov 00

GPS III Program

Involves looking at the whole system

- Space
- Control
- User Equipment



GPS III Program Objectives

Ensure best GPS system for the nation for the next 30 years

- Plan and grow system capabilities to meet future user needs for precise positioning and timing services
 - GPS ORD objective values as the target
- Procure most cost-effective system to meet future military and civilian requirements through 2030
 - Reduce Total Ownership Costs
 - Conscientious cost - benefit analyses for future requirements
- Make optimal use of system augmentations and complementary systems
- Re-look at entire GPS system architecture
 - Identify system-level trades for all system segments - space, control segment and user equipment

GPS III Program Approach

- System Architecture / Requirements Definition (SA/RD)
 - Space, UE and OCS system-level trades - open, iterative process
 - Define system architecture to lead into a System Requirements Review (SRR)
- Preliminary Design and Risk Reduction (PD/RR)
 - Competitive Source Selection after SA/RD phase
 - Two qualified sources compete for system design to reduce risk in Engineering, Manufacturing and Design (EMD) phase
- EMD / Production
 - Down-select to single contractor at Preliminary Design Review (PDR) - FY03
 - Conduct risk analysis for EMD
 - Solidify EMD Phase strategy

Three phase approach -
flexible, allows future changes, reduces risk

WHAT DOES THIS MEAN TO THE GPS TIMING USER?

System-Level Time Transfer Accuracy Requirements

System Operational Requirements Document (SORD) Jan 90

Time transfer data in the UTC coordinate system
for Precise Time and Time Interval (PTTI)
for Global Timing System users
with an error of less than **100 nsec** (1-sigma)
and availability of 0.98 (Para 4.1.1.1.c)

Operational Requirements Document (ORD) AFSPC/ACC 003-92-I/II/III - Global Positioning System - Feb 00

... the OCS shall maintain a steady state (sampled over 1 year)
time transfer accuracy of the GPS signal to
an error of less than or equal to
20 nsec (95 percent) relative to UTC(USNO) (**threshold**) and
10 nsec (95 percent) relative to UTC(USNO) (**objective**)
Key Performance Parameter (KPP) (Para 4.1.10.1)

GPS Modernization and GPS-III Implications for the Timing Users

Military User

- More anti-jam resistance – higher signal power
 - More secure access to the military code – m-code
 - Faster PPS signal acquisition – m-code
 - Separation from civil signal service – m-code
 - Backward compatibility with current signal architecture – m-code
-
- More anti-jam resistance – higher signal power
 - More accurate time transfer – GPS-III system architecture

Modernization

Civil User

- More interference resistance – higher signal power
-- spectrum protection for L5
 - More robust signal service – C/A code on L2; L5 signal
 - More accurate time transfer – SA off
-
- More accurate time transfer – GPS-III system architecture

Modernization

Modernization Impacts on the User

- Backward compatibility
 - New capabilities will not interfere with current capabilities
 - Current signal services will continue to be supported
 - Changes will be required to take advantage of new capabilities
- Equipment changes required to take advantage of capabilities offered by new signal architectures
 - M-code capable user equipment for the military user
 - Dual frequency C/A code and L5 capable civil receivers for civil applications requiring more robustness of service
- Start planning now for transition to future capabilities
 - M-code / C/A-code on L2 – IOC 2008; FOC 2010
 - L5 – IOC 2014; FOC 2016

User Involvement



- Participate through the formal DoD requirements process
 - Using Command – mission needs (MNS)
 - USNO -- DoD Precise Time/Time Interval (PTTI) manager
 - AFSPC – GPS operational requirements (ORD)
- Participate through the more informal civil requirements process
 - DoD / DoT Interagency GPS Executive Board (IGEB) – individual agency requirements processes
 - GPS Civil Signal Interface Committee (CGSIC)
 - Federal Radio Navigation Plan (FRNP) coordination process
- Take active role industry / professional associations
 - GPS Industry Council (GIC)
 - Radio Telecommunications Committee – Aeronautical / Maritime (RTCA/ RTCM)

CHALLENGES

GPS JPO Challenges

- Maintaining a healthy constellation while adding system capabilities
 - Constellation sustainment strategies
 - Operational Control Segment (OCS) upgrades
 - Testing / validating new signals - design and operations
- Adequate expression of future GPS user needs - military and civil
 - Best way to understand military operational needs and civil “value added” needs
- Flexibility in procurement strategies to allow for future growth
 - Ability to forecast GPS user requirements through 2030
- Reducing Total Ownership Costs
 - Weigh costs and benefits to make the right system trade-offs

GPS User Challenges

- Promote compatibility among precise positioning and timing services; protect critical frequency spectrum
- Use current system capabilities to the maximum extent – be innovative and creative!
- Advocate military and civil future requirements
 - Take an active role in the formal requirements processes
 - Leverage informal involvement and professional activities
- Plan to use future GPS capabilities to the fullest extent
- Build strong military and civil advocacy for precise positioning and timing services and applications

*Innovate!!
...use GPS to its fullest capability*

Questions and Answers

HUGO FRUEHAUF (Zyfer, Inc.): How much is JPO interfacing with the Galileo folks?

CAPT. STEVEN RAJOTTE: Actually, I refer that to Don Latterman, who works for SAIC. He's our lead technical for the GPS modernization program.

DONALD LATTERMANN: Actually, we are working a lot with the Galileo folks informally. The State Department right now is handling formal negotiations with the EU on Galileo, and we have been participating actively in that process. However, we have had some informal tactical discussions, one on one with the EU, trying to come to agreement on common standards and put some issues on the table in terms of inter-operability and common standards in architectures. The State Department is really taking the lead on that. We follow technically and programmatically; however, the political environment works the issues. Then we're following State's lead on that.

FRUEHAUF: How much complaining are you getting from Galileo concerning the increase to power on M-code since the original level of GPS was very carefully selected for tons of reasons as to its spectrum noise?

LATTERMAN: Well, obviously right now, we are looking at the influence of higher-power requirements across the board, not only as far as interfering with the Europeans, but also looking at how that is compatible with our current both military and civil architectures. The 20 additional dB spot beam is being deferred to GPS III, so we can really look at that whole architecture and all those issues that we would also look at in the consideration for Galileo. We kind of pushed that decision out as far as to whose systems' architecture is concerned so as to take a hard look at it.

FREQUENCY STABILITY REQUIREMENTS FOR NARROW BAND RECEIVERS

W. Klepczynski

Innovative Solutions International

1608 Spring Hill Road, Suite 200

Vienna, VA 22182, USA

Tel: 703-841-2669; 410-798-8457

Bill.CTR.Klepczynski@faa.gov; Wklepczy@aol.com

P. Ward

P.O. Box 38451

Dallas, TX 75238, USA

Tel: 214-348-9446

pward@flash.net

Abstract

Very-narrow-band Global Positioning System (GPS) receivers have recently been proposed in order to help mitigate the effects of scintillation. This paper will revisit the stability requirements placed on the local oscillator of such receivers.

INTRODUCTION

The need to have good local oscillator short- and medium-term stability for phase tracking receivers has been well documented, especially for space communications [1]. Recently there has been great interest in improving the tolerance of WAAS/GPS Reference Station receivers to the effects of ionospheric scintillation in order to improve their robustness. One means that has been suggested to accomplish this is to narrow the bandwidth of the receiver. Morrissey et al. [2] undertook a study to quantify scintillation effects, through simulation, on a WAAS reference receiver in order to determine optimum estimates for certain key parameters, such as loop bandwidth, discriminator type, and tracking loop order that would maximize performance of the receiver.

However, one parameter that was not varied or simulated in their study was local oscillator stability. Obviously, this was because an atomic frequency standard, similar to the one used at the WAAS Reference Stations, was used as the local oscillator for the receiver being tested. But it must be kept in mind that the short-term performance of a local oscillator plays a more significant role when estimating the performance of a narrow bandwidth receiver than long-term performance. It should also be kept in mind that the short-term performance of an atomic frequency standard depends solely on the performance of the crystal oscillator selected by the manufacturer of the atomic frequency standard. The short-term performance of an

atomic frequency standard will be dominated by the performance of the crystal for up to several seconds, depending on the attack time of the cesium standard in question.

Studies by Van Dierdonck and Hua [3] have shown that selection of a local oscillator for a Scintillation Monitor Receiver is very critical to its performance. Several types of ovenized crystal oscillators of different cuts (SC and AT) and different fundamental frequencies were evaluated before one was chosen for their purposes.

The use of receivers with narrower bandwidths seems to be on the increase for many applications. Therefore, it was thought that a short note showing the effects of oscillator stability, more properly instability, on receiver phase-lock loop (PLL) performance would be helpful. It is noted that PLL performance is linked directly to oscillator performance. Several types of input disturbances cause a certain jitter in the error detector of the tracking loops. It has been observed that PLL tend to loose lock when the phase jitter out of the error detector exceeds 1 radian [4].

MEASUREMENT ERRORS

The dominant sources of phase error in a GPS receiver PLL are phase jitter and dynamic stress error [5]. The 3σ values of this PLL error and its rule-of-thumb tracking threshold are computed by:

$$3\sigma_{PLL} = 3\sigma_j + \theta_e < 45^\circ \quad (1)$$

where:

σ_j = 1σ phase jitter from all sources except dynamic stress error, and
 θ_e = dynamic stress error in the PLL tracking loop.

Equation (1) shows that the dynamic stress error is a 3σ effect and is additive to the phase jitter. The phase jitter is the root-sum-square of every source of uncorrelated phase error, such as thermal noise and oscillator noise. Oscillator noise includes both jitter induced by vibration and jitter caused by oscillator instability. The 1-sigma (σ) rule of thumb for the PLL tracking error is given by:

$$\sigma_{PLL} = \sqrt{(\sigma_t^2 + \sigma_v^2 + \sigma_A^2)} + \theta_e/3 \leq 15^\circ \quad (2)$$

where:

σ_t = 1-sigma thermal noise in degrees,
 σ_v = 1-sigma vibration-induced oscillator jitter in degrees, and
 σ_A = Allan-variance-induced oscillator jitter in degrees.

Fuchser [4] has shown that the equation for the short-term Allan variance for a second-order PLL is

$$\sigma_A(\tau) = 2.5(\Delta\theta/\omega_L\tau) \quad (3)$$

where:

$\Delta\theta$ = root mean square jitter into phase discriminator due to oscillator (rad),
 ω_L = L-band input frequency = $2pf_L$ (rad/sec), and
 τ = short-term stability gate time for Allan variance measurement (sec).

The equation for a third-order PLL is similar:

$$\sigma_A(\tau) = 2.25(\Delta\theta/\omega_L\tau) \quad (4)$$

If the Allan variance has already been determined for an oscillator for the short-term gate time, t , then the Allan-deviation-induced jitter in degrees can be computed from the above equations. The short-term gate time used in the Allan variance measurement must be evaluated at the noise bandwidth of the carrier loop filter $\tau = 1/B_n$. Rearranging terms, we get for a second-order PLL:

$$\theta_{A2} = 144(\sigma_A(\tau)f_L/B_n) \text{ deg} \quad (5)$$

and for a third-order PLL, we get:

$$\theta_{A3} = 160(\sigma_A(\tau)f_L/B_n) \text{ deg.} \quad (6)$$

OSCILLATOR INSTABILITY

In order to evaluate Equations (5) and (6), data for a number of oscillators was obtained from [6] and manufacturer's specifications. Data obtained from [6] were for a poor quality crystal and a high quality crystal. The specifications for one manufacturer of a cesium frequency standard also contained the short-term performance of its crystals. Its performance fell in between that of the high and poor quality crystals, as indicated in Figure 1. The specifications of a second manufacturer did not contain the short-term performance of its crystals used in its standard, but it is assumed that it would be comparable in performance to that of the other manufacturer. The data used in this study are shown in Table I. Figure 1 is a plot of these values.

Tau	Log (tau)	Cesium A	Standard Cesium B	High Perf. Cesium B	Good XO	Poor XO
0.001	-3		1.0E-09	1.0E-09	5.0E-11	8.0E-08
0.01	-2		7.5E-11	7.5E-11	5.0E-12	9.0E-09
0.1	-1		1.2E-11	1.2E-11	5.0E-13	5.0E-10
1	0	2.0E-11	1.2E-11	5.0E-12	1.0E-13	5.0E-11
10	1	2.1E-11	8.5E-12	3.5E-12	1.0E-13	5.0E-11
100	2	5.0E-12	2.7E-12	8.5E-13	5.0E-13	5.0E-11
1000	3	1.6E-12	8.5E-13	2.7E-13	7.0E-13	1.0E-10
10000	4	5.0E-13	2.7E-13	8.5E-14	5.0E-12	3.0E-10

Table I - Sigma (Allan variance) for various values of tau (interval) for five different kinds of frequency standards. These include a high quality crystal oscillator, one of not so good a quality, a cesium frequency standard from one manufacturer, and two cesium frequency standards for a second manufacturer, one a high performance standard and one a normal standard.

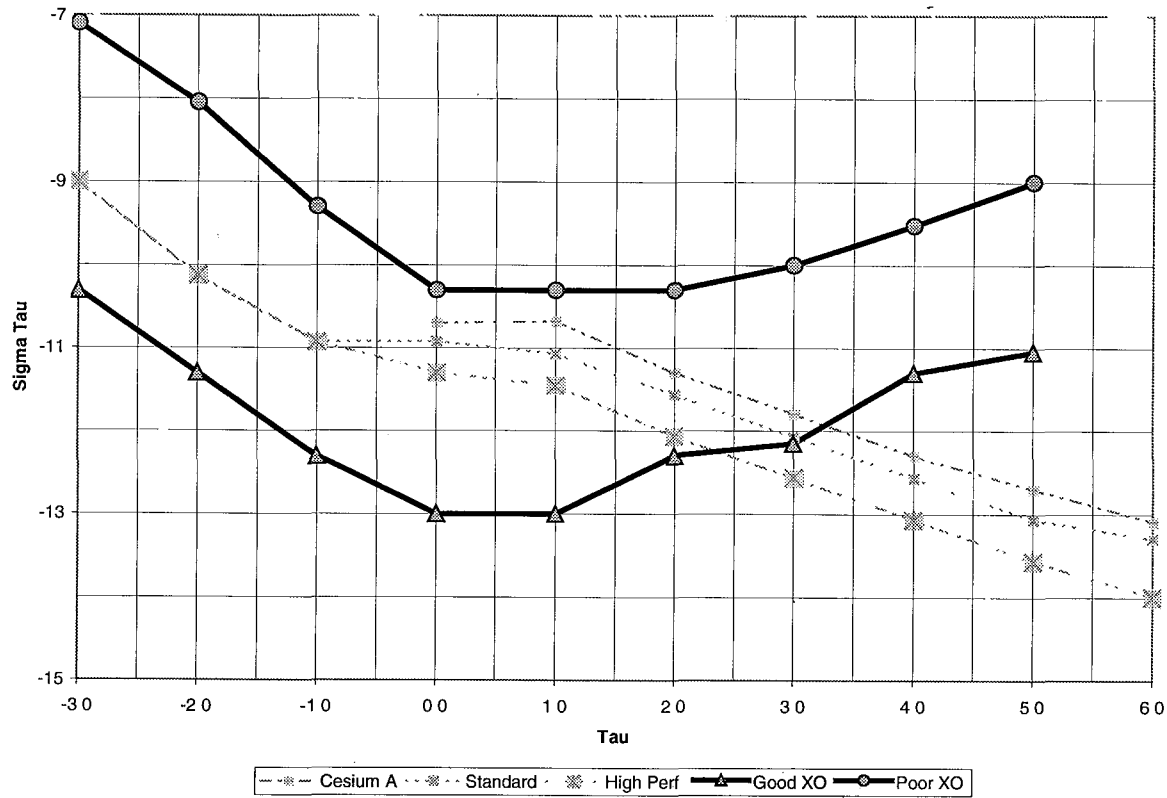


Figure 1 - Graph of the Allan variances for five different kinds of frequency standards. These include a high quality crystal oscillator, one of not so good a quality, a cesium frequency standard from one manufacturer, and two cesium frequency standards for a second manufacturer, one a high performance standard and one a normal standard.

DISCUSSION

Values of the Allan variance for a representative number of samples corresponding to various values of receiver bandwidth were derived from the tabular data contained in Table I. Tables II-V show the values of the Bandwidth for which the values of τ and the corresponding values

Bandwidth	Tau	L1 High	Theta A 2 Med	Poor
15	0.07	0.018	0.358	22.063
10	0.10	0.011	0.272	11.344
5	0.20	0.019	0.494	17.571
3	0.33	0.025	0.724	20.828
1	1.00	0.023	1.134	11.344
0.2	5.00	0.113	5.672	56.719
0.05	20.00	2.202	4.274	213.201

Table II - Values of the Allan-variance-induced oscillator jitter. Values were computed for a second-order PLL (θ_{A2}) and the GPS L1 frequency using Equation (5).

of the Allan-variance-*induced oscillator jitter* were computed using Equations (5) and (6). The computations were done for second- and third-order PLL and both GPS frequencies, L1 and L2.

Bandwidth	Tau	L1 High	Theta A 3 Med	Poor
15	0.07	0.020	0.398	24.515
10	0.10	0.013	0.302	12.604
5	0.20	0.021	0.549	19.523
3	0.33	0.028	0.804	23.142
1	1.00	0.025	1.260	12.604
0.2	5.00	0.126	6.302	63.021
0.05	20.00	2.447	4.748	236.890

Table III - Values of the Allan-variance-induced oscillator jitter. Values were computed for a third-order PLL (θ_{A3}) and the GPS L1 frequency using Equation (6).

Bandwidth	Tau	L2 High	Theta A 2 Med	Poor
15	0.07	0.014	0.279	17.192
10	0.10	0.009	0.212	8.839
5	0.20	0.015	0.385	13.691
3	0.33	0.019	0.564	16.229
1	1.00	0.018	0.884	8.839
0.2	5.00	0.088	4.420	44.197
0.05	20.00	1.716	3.330	166.130

Table IV - Values of the Allan-variance-induced oscillator jitter. Values were computed for a second-order PLL (θ_{A2}) and the GPS L2 frequency using Equation (5).

Bandwidth	Tau	L2 High	Theta A 3 Med	Poor
15	0.07	0.015	0.310	19.102
10	0.10	0.010	0.236	9.821
5	0.20	0.016	0.428	15.213
3	0.33	0.022	0.627	18.032
1	1.00	0.020	0.982	9.821
0.2	5.00	0.098	4.911	49.107
0.05	20.00	1.906	3.700	184.589

Table V - Values of the Allan-variance-induced oscillator jitter. Values were computed for a third-order PLL (θ_{A3}) and the GPS L2 frequency using Equation (6).

From Tables II-V it is obvious that the values of the oscillator-induced jitter arising from the poor crystal oscillators is greater than 15 degrees. This amount of jitter should be sufficient to cause the receiver carrier-tracking loop to lose phase lock. It should be pointed out that the oscillator-induced jitter is a very small order effect to the code tracking loop and that both the code and carrier tracking loops must be tracking in order for a GPS receiver to maintain lock.

However, it is not immediately obvious that the listed amount of oscillator-induced jitter for the crystal oscillators associated with a cesium-beam frequency standard would be large enough to induce a receiver to lose lock. Obviously, a reference oscillator with a short-term Allan deviation characteristic that is more than an order of magnitude worse than this example will cause PLL tracking problems, as the data in Tables II-V indicate. In this case, it would depend on the magnitude of other forms of contributing jitter, such as thermal noise and vibration-induced jitter. For the WAAS Reference Station receivers, vibration jitter should not be a large factor, since the receivers are located in a relatively benign environment. It should be kept in mind that some tracking loop disturbances could be tolerated if the tracking loop bandwidth is large enough to track these disturbances. For high quality crystals there should never be a problem of oscillator-induced jitter causing loss of lock in a GPS receiver.

It should also be pointed out that a frequency-locked loop (FLL) is very insensitive to oscillator-induced jitter. Some receivers derive delta range measurements from a receiver carrier-tracking loop operating in FLL. However, these measurements are about an order of magnitude (or more) less accurate than from a PLL. The best solution, as pointed out in [8], is an FLL-assisted PLL.

CONCLUSIONS

It is obvious that poor crystals should not be used with narrow bandwidth systems. However, the user must exercise caution in putting together a system that includes atomic frequency standards. The user must carefully investigate the performance of the crystal that is being used within the atomic standard. The user must learn its short-term characteristics. The user must also investigate the thermal noise characteristics of the receiver that is being used and also investigate the environmental conditions in which the receiver will be located. Otherwise, it is likely that the user's receiver will occasionally lose lock.

Other system characteristics must also be investigated that have not been considered here. It should be pointed out that problems might arise when the carrier-to-noise power ratios (C/N_0) decrease toward the thermal noise threshold.

In conclusion, the design of modern codeless receivers operate at a significantly reduced signal-to-noise ratio (SNR), which requires the tracking loop bandwidths to be extremely narrow [7]. Oscillator instability can be a significant factor and must be considered. The oscillator specification for Allan deviation is important for all receiver designs and must not be overlooked or assumed.

REFERENCES

- [1] R. Sydnor, J. J. Caldwell, and B. E. Rose 1966, "Frequency stability requirements for space communications and tracking systems," Proceedings of the IEEE, 54, 231-236.
- [2] T. N. Morrissey, K. W. Shallberg, A. J. Van Dierondonck, T. Kim, and M. J. Nicholson 1999, "GPS receiver performance characterization under simulated ionospheric scintillation environments," Proceedings of the National Technical Meeting, Institute of Navigation, January 1999.
- [3] A. J. Van Dierondonck, and Q. D. Hua 1998, "Crystal oscillator noise effects on the measurement of ionospheric phase scintillation using GPS," Proceedings of the 1998 International Frequency Control Symposium, 27-29 May 1998, Pasadena, California, USA, pp. 298-305.
- [4] T. Fuchser 1976, "Oscillator stability for carrier phase lock," Memorandum, Texas Instruments, Inc., February 1976.
- [5] P. Ward 1996, "Satellite signal acquisition and tracking," Understanding GPS Principles and Applications, pp. 119-1208, Artech House, 1996.
- [6] R. L. Sydnor 1997, "Characteristics of various frequency standards," Handbook on the Selection and Use of Precise Frequency and Time Systems, pp. 111-118, ITU RadioCommunication Bureau, 1997.
- [7] P. Ward 1996, "GPS satellite signal characteristics," Understanding GPS Principles and Applications, pp. 83-117, Artech House, 1996.
- [8] P. Ward, "Performance comparisons between FLL, PLL and a novel FLL-assisted-PLL carrier tracking loop under RF interference conditions," Proceedings of ION GPS-98 Meeting, Institute of Navigation, September 1998.

Additional Readings

- A. K. Tetewsky, J. B. Lozow, and K. W. Flueckiger 1999, "Determining specifications for an external GPS reference oscillator," Proceedings of ION GPS-99, pp. 339-352, September 1999.
- T. Fuchser 1978, "Short term stability measurements for tracking Loops (2nd and 3rd order)," GPS Trade Study Report, Texas Instruments, Inc., June 1978.
- J. Rutman 1977, "Oscillator specifications: a review of classical and new ideas," Proceedings of the 31st Annual Symposium on Frequency Control, 1-3 June 1977, Ft. Monmouth, New Jersey, USA, pp. 291-301.

Questions and Answers

HUGO FRUEHAUF (Zyfer, Inc.): You are speaking of the receivers at the WAAS stations, are you?

WILLIAM KLEPCZYNSKI: Yes.

FRUEHAUF: You're not speaking of general GPS receivers.

KLEPCZYNSKI: Well, I think in general, we couldn't do that.

FRUEHAUF: But your narrow bandwidth front end is the WAAS receiver?

KLEPCZYNSKI: Right. This is the one specifically for the WAAS receiver. But that is something I keep in mind because you go to the ION meetings, and they start talking about receivers, narrowing the bandwidth of the receivers, for all sorts of reasons, other reasons other than for simulations. But they should have to keep in mind the stability.

THE NANOKERNEL¹

David L. Mills²
University of Delaware

Poul-Henning Kamp²
FreeBSD Project

Abstract

Internet timekeeping has come a long way since first demonstrated almost two decades ago. In that era most computer clocks were driven by the power grid and wandered several seconds per day relative to UTC. As computers and the Internet became ever faster, hardware and software synchronization technology became much more sophisticated. The Network Time Protocol (NTP) evolved over four versions with ever better accuracy now limited only by the underlying computer hardware clock and adjustment mechanism.

The clock frequency in modern workstations is stabilized by an uncompensated quartz or surface acoustic wave (SAW) resonator, which are sensitive to temperature, power supply and component variations. Using NTP and traditional Unix kernels, incidental timing errors with an uncompensated clock oscillator is in the order of a few hundred microseconds relative to a precision source. Using new kernel software described in this paper, much better performance can be achieved. Experiments described in this paper demonstrate that errors with a modern workstation and uncompensated clock oscillator are in the order of a microsecond relative to a GPS receiver or other precision timing source.

1. INTRODUCTION

Several years ago the software algorithms to discipline the Unix system clock were overhauled to provide improved accuracy, stability, and resolution [5]. In addition, means were added to discipline the clock directly from a precision timing source, such as a GPS receiver or cesium oscillator. The software was integrated with several operating system kernels of the day and eventually adopted as standard in Digital Tru64 (Alpha), Sun Solaris, Linux, and FreeBSD. The best performance achieved with workstations of the day was a few hundred microseconds in time and a few parts-per-million (PPM) in frequency, so a clock resolution of one microsecond seemed completely adequate.

With workstations and networks of today reaching speeds in the gigahertz range, it is clear the solution of several years ago is rapidly becoming obsolete. Improved modelling techniques have resulted in better discipline algorithms which are more responsive to phase and frequency characteristics of computer clocks [3]. Faster processors and a standardized application program interface (API) allow more flexible and precise timing of external signals [7]. Faster network speeds and lower jitter provide more accurate timekeeping over the Internet [4].

-
1. Sponsored by: DARPA Information Technology Office Contract F30602-98-1-0225 and Digital Equipment Corporation Research Agreement 1417.
 2. David L. Mills is with the Electrical and Computer Engineering Department, University of Delaware, Newark, DE 19716, mills@udel.edu, <http://www.eecis.udel.edu/~mills>; Poul-Henning Kamp is with the FreeBSD Project, Valbygrdsvej 8, DK-4200 Slagelse, Denmark. phk@freebsd.org.

This paper describes new algorithms and kernel software providing much improved time and frequency resolution, together with a more agile and precise clock discipline mechanism. It discusses the analysis and design of the algorithms and the results of proof-of-performance experiments. The software has been implemented and tested in all the kernels mentioned above and is now standard in the Linux and FreeBSD public distributions.

The kernel software replaces the clock discipline algorithm in a synchronization daemon, such as the Network Time Protocol [6], with equivalent functionality in the kernel. It provides a resolution of 1 ns in time and .001 PPM in frequency. While clock corrections are recomputed about once per minute in the daemon, they are recomputed once per second and amortized at every tick interrupt in the kernel. This avoids errors that accumulate between updates due to the intrinsic hardware clock frequency error.

The new software can be compiled for 64-bit machines using native instructions or for 32-bit machines using a macro package for double precision arithmetic. The software can be compiled for kernels where the time variable is represented in seconds and nanoseconds and for kernels in which this variable is represented in seconds and microseconds. In either case the resolution of the clock is limited only by the resolution of the clock hardware. Even if the resolution is only to the microsecond, the software provides extensive signal grooming and averaging to minimize reading errors.

The remaining sections of this paper are organized as follows. Section 2 describes the characteristics of typical computer clock oscillators, which are based on the Allan deviation statistic used in the most recent NTP algorithms. Section 3 describes the software design, which is based on two interacting hybrid phase-lock/frequency-lock (PLL/FLL) feedback loops. Section 4 describes the software implementation, which is integrated in the kernels mentioned above. Section 5 summarizes the results of proof-of-performance experiments which validate the claims in this paper. Section 6 concludes with suggestions for further improvements.

2. COMPUTER CLOCK CHARACTERIZATION

In order to understand how the new kernel algorithms operate, it is necessary to understand the design of a typical computer clock and how the time and frequency is controlled. The accuracy attainable with NTP, or any other protocol that provides periodic offset measurements, depends strongly on the stability of the clock oscillator and the precision of its adjustment mechanism. The clock frequency in modern workstations is stabilized by an uncompensated quartz or surface acoustic wave (SAW) resonator, which is affected by temperature, power supply and component variations. The most significant affect is the temperature dependency, which is typically in the order of one PPM in frequency per degree Celsius.

In typical computer clock designs the clock oscillator drives a counter that produces processor interrupts at fixed tick intervals in the range 1-20 ms. At each tick interrupt a software clock variable is updated by the number of microseconds or nanoseconds in the tick interval. The means used by the traditional Unix kernel to adjust the clock time is the `adjtime()` kernel routine, which causes a fixed value, typically 5 μ s, to be added to or subtracted from the clock time at each tick interrupt. The `adjtime()` function computes how long these increments must be continued in order to amortize the adjustment specified. In order to provide a frequency offset, the NTP daemon calls the `adjtime()` routine at intervals of one second. Since the intrinsic clock oscillator frequency error can range to several hundred PPM, this can result in sawtooth-like time errors ranging to several hundred microseconds. This was the prime motivation to avoid the `adjtime()` routine and implement the clock discipline directly in the kernel.

Almost all modern processors provide means to measure intervals for benchmarking and profiling. These means typically take the form of a processor cycle counter (PCC), which can be read by a machine instruction. Upon receiving a request to read the clock, the kernel uses the PCC to compute the number of microseconds or nanoseconds since the last tick interrupt. Since the PCC and clock oscillator may not run at the

same frequency and, in the case of multiprocessor systems, there may be more than one PCC, the kernel must carefully mitigate the differences and develop a stable, monotonically increasing timescale.

It is well known that the behavior of an oscillator can be characterized in terms of its Allan deviation, which is a function of stability, interpreted as first-order frequency differences, and averaging interval [1]. In order to determine this statistic for a typical uncompensated computer oscillator, sample offsets relative to a cesium standard were measured with the computer oscillator allowed to free-run over periods ranging from 1.5 to 10 days. These data were saved in files and later used to construct plots in log-log coordinates showing stability versus averaging interval.

In [3] a simple model is developed which characterizes the performance of each individual time server. The model characterizes each combination of synchronization source and clock oscillator by two intersecting straight lines in log-log coordinates. In general, network and computer latency variations produce jitter, which is modelled as white phase noise and appears as a straight line with slope -1 on the plot. On the other hand, oscillator frequency variations produce wander, which is modelled as random-walk frequency noise and appears as a straight line with slope $+0.5$. The intersection of the two straight lines is called the Allan intercept, which serves to characterize the particular combination of source and oscillator. It represents the optimum averaging interval for the best oscillator stability. If the averaging interval is less than this, errors due to source jitter dominate, while if greater, errors due to oscillator wander dominate.

The averaging interval is roughly equal to the frequency time constant used in the clock discipline algorithm, and this is related to the interval between NTP poll messages sent across the network. With a minimum poll interval of 16 s in the current NTP design, the averaging interval is about 4,000 s, which is on the high side of the optimum range, and the match gets worse with larger poll intervals. Thus, the best accuracy is achieved at the minimum poll interval, but this may result in unacceptable network overhead. Therefore, when the NTP daemon is started, it uses a relatively small poll interval in order to respond quickly to the particular oscillator frequency offset, then gradually increases the interval to an upper limit. Depending on desired accuracy and allowable network overhead, the upper limit could be a small as a few seconds or as large as a day or more.

A phase-lock loop (PLL) functions best with poll intervals below the Allan intercept where jitter predominates, while a frequency-lock loop (FLL) functions best above the intercept where wander predominates. As the result of previous research [2][3], a hybrid PLL/FLL clock discipline algorithm has been designed, implemented, and tested in the NTP version 4 software for Unix, Windows, and VMS. A kernel implementation based on this design is described in the following section.

3. SOFTWARE DESIGN

The nanokernel software design is based on the NTP implementation, but includes two separate but interlocking feedback loops. The PLL/FLL discipline operates with periodic updates produced by a synchronization daemon such as NTP, while the PPS discipline operates with an external PPS signal and modified serial or parallel port driver. Both algorithms include grooming provisions that significantly reduce the impact of source selection jitter or *clockhopping* and network delay transients. In addition, the PPS algorithm can continue to discipline the clock frequency even if other synchronization sources or the daemon itself crash.

3.1 PLL/FLL Discipline

The PLL/FLL kernel discipline is specially tailored for typical Internet delay jitter and clock oscillator wander. However, the kernel embodiment provides better accuracy and stability than the NTP discipline, as well as a wider operating range. Both the kernel discipline and NTP discipline operate in the same manner except for one important detail. The NTP discipline uses the kernel `adjtime()` system call, which has an inherent resolution of 1 μ s in time and 5 PPM in frequency and amortizes adjustments once every

second. The kernel discipline has an inherent resolution of 1 ns in time and .001 PPM in frequency and amortizes adjustments at every tick interrupt.

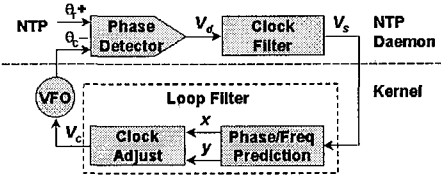


Figure 1. Clock Discipline Feedback Loop

groomed by the NTP clock filter and related algorithms to produce the phase update V_s used by the loop filter in the kernel to produce the phase prediction x and frequency prediction y . These predictions are used to produce clock adjustment updates at intervals of 1 s which result in the correction term V_c . This value represents the increment in time necessary to correct the clock at the end of the next second. The various performance data displayed later were derived from the phase update V_s , since this is a common measuring point for both the daemon and kernel.

The x and y predictions are developed from the phase update V_s as shown in Figure 2. As in the NTP algorithm, the phase and frequency are disciplined separately in both PLL and FLL modes. In both modes x is the value V_s , but the actual phase adjustment is calculated by the clock adjust process using an exponential average with an adjustable weight factor. The weight factor is calculated as the reciprocal of the time constant specified by the API. The value can range from 1 s to an upper limit determined by the Allan intercept. In PLL mode it is important for the best stability that the update interval does not significantly exceed the time constant for an extended period.

In PLL mode, y is computed using an integration process as required by PLL engineering principles; however, the integration gain is reduced by the square of the time constant, so adjustments become essentially ineffective with poll intervals above 1024 s. In FLL mode, y is computed directly using an exponential average with weight 0.25. This value, which was determined from simulation with real and synthetic data, is a compromise between rapid frequency adaptation and adequate glitch suppression. In operation, PLL mode is preferred at small update intervals and time constants, and FLL mode at large intervals and time constants. The optimum crossover point between the PLL and FLL modes, as determined by simulation and analysis, is the Allan intercept. As a compromise, the PLL/FLL algorithm operates in PLL mode for update intervals of 256 s and smaller and in FLL mode for intervals of 1024 s and larger. Between 256 s and 1024 s the mode is specified by the API.

3.2 PPS Discipline

In order to reduce incidental errors to the lowest practical value, it is necessary to use a precision source, such as a GPS receiver or precision oscillator. The kernels mentioned above have been modified for this purpose. For serial drivers the PPS signal is connected to the DCD pin via a level converter; for parallel drivers the signal is connected directly to the ACK pin. A comprehensive API has been designed and implemented for this function. It is currently the subject of a Internet Engineering Task Force proposed standard [7].

Both the kernel discipline and NTP discipline operate as a hybrid of phase-lock and frequency-lock feedback loops. Figure 1 shows the functional components of the kernel discipline. In the NTP discipline the components below the dotted line are implemented in the daemon. The phase difference V_d between the reference source θ_r and clock θ_c is determined by the NTP daemon. The value is then

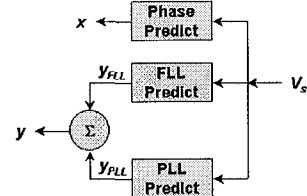


Figure 2. FLL/PLL Prediction Functions

The PPS algorithm shown in Figure 3 is functionally separate from the PLL/FLL discipline; however, the two disciplines have interlocking control functions designed to provide seamless switching between them as necessary. The PPS discipline is called at each PPS on-time signal transition with arguments including a clock timestamp and a virtual nanosecond counter sample. The virtual counter can be implemented using the PCC in modern computer architectures or a dedicated counter in older architectures. The intent of the design is to discipline the clock phase using the timestamp and the clock frequency using the virtual counter. This makes it possible, for example, to stabilize the clock frequency using a precision PPS source, while using an external time source, such as a radio or satellite clock or even another time server, to discipline the phase. With frequency reliably disciplined, the interval between updates from the external source can be greatly increased. Also, should the external source fail, the clock will continue to provide accurate time limited only by the accuracy of the precision source.

At each PPS on-time transitional the offset in the second is determined relative to the clock phase. A range gate rejects errors more than 500 μ s from the nominal interval of 1 s, while a frequency discriminator rejects errors more than 500 PPM from the nominal frequency of 1 Hz; however, the design tolerates occasional dropouts and rejects noise spikes. The virtual counter samples are processed by an ambiguity resolver that corrects for counter rollover and certain anomalies when a tick interrupt occurs in the vicinity of the second rollover or when the PPS interrupt occurs while processing a tick interrupt. The latter appears to be a feature of at least some Unix kernels which rank the serial port interrupt priority above the tick interrupt priority.

PPS samples are then processed by a 3-stage shift register. The median value of these samples is the raw phase signal and the maximum difference between them is the raw jitter signal. The PPS phase correction is computed as the exponential average of the raw phase with weight equal to the reciprocal of the calibration interval described below. In addition, a jitter statistic is computed as the exponential average of the raw jitter with weight 0.25 and reported as the jitter value in the API. Occasional electrical transients due to light switches, air conditioners, and water pumps are a principal hazard to PPS discipline performance. A spike (*popcorn*) suppressor rejects phase outliers with amplitude greater than 4 times the jitter statistic. This value, as well as the jitter averaging weight, was determined by simulation with real and synthetic PPS signals.

The PPS frequency is computed directly from the difference between the virtual counter values at the beginning and end of the calibration interval, which varies from 4 s to a maximum specified by the API. When the system is first started, the clock oscillator frequency error can be quite large, in some cases 200 PPM or more. In order to avoid ambiguities, the counter differences must not exceed the tick interval, which can be less than a millisecond in some kernels. The choice of minimum calibration interval of 4 s insures that the differences remain valid for frequency errors up to 250 PPM with a 1-ms tick interval.

The actual PPS frequency is calculated by dividing the virtual counter difference by the calibration interval in seconds. In order to avoid divide instructions and intricate residuals management, the calibration interval is always a power of 2, so division reduces to a shift. However, due to signal dropouts or noise spikes, either the length may not be a power of 2 or the signal may appear outside the valid frequency range, so the interval is ignored. The required frequency adjustment is computed and clamped not to exceed 100 PPM. This acts as a damper in case of abrupt changes that can occur at reboot, for example.

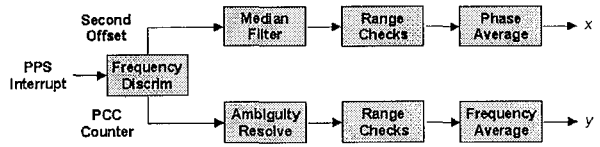


Figure 3. PPS Discipline

4. SOFTWARE IMPLEMENTATION AND OPERATION

Figure 4 shows the general organization of the kernel software. Updates produced by the NTP daemon are processed by the `hardupdate()` routine, while PPS signal interrupts are processed by the `hardpps()` routine. The values in both routines are calculated using extended precision arithmetic to preserve nanosecond resolution and avoid overflows over the range of clock oscillator frequencies from 50 Hz to above 1000 Hz. The actual corrections are redetermined once per second and linearly amortized over the second at each hardware tick interrupt. In contrast to the NTP daemon, where most computations use floating-double data types, the kernel is limited to integer data types.

Both the `hardupdate()` and `hardpps()` routines discipline the computer clock in nanoseconds in time and nanoseconds per second in frequency. There are two programs which implement the kernel algorithms, `ktime.c` and `micro.c`. The `ktime.c` program includes code fragments that implement the `hardupdate()` and `hardpps()` routines, as well as the `ntp_gettime()` and `ntp_adjtime()` system calls that implement the API. The `micro.c` program implements a nanosecond clock using the tick interrupt augmented by the virtual counter described above. In its present form, it can be compiled only for 64-bit architectures. In this program the `nano_time()` routine measures the intrinsic processor clock frequency, then interpolates the nanoseconds by scaling the PCC to one second in nanoseconds. The unavoidable divide instruction is the only one in the nanokernel software. The routine also supports a microsecond clock for legacy purposes.

Since the PPS signal is inherently ambiguous, the seconds numbering is established by another NTP server or a local radio clock using the PLL/FLL discipline. The PPS frequency determination is independent of any other means to discipline the clock frequency and operates continuously. When the NTP daemon recognizes from the API that the PPS frequency has settled down, it switches the clock frequency discipline to the PPS signal, but continues to discipline the clock phase using the PLL/FLL algorithm. The sometimes intricate mitigation rules that control the detailed sequencing are beyond the scope of this paper; they are given in the software documentation [8].

5. PERFORMANCE EVALUATION

Following previous practice [3], the `ktime.c` and `micro.c` routines have been embedded in a special purpose, discrete event simulator. In this context it is possible to verify correct operation over a wide range of operating conditions likely to be found in current and future computer systems and networks and which cannot be easily duplicated with in-situ implementations. It operates with internally synthesized data or raw data files produced by the NTP daemon during regular operation. For this purpose raw time offsets are recorded with NTP operating in an open-loop configuration and later played back to the simulator. Synthetic data having similar statistics are generated as described in [3]. The simulator can measure the response to time and frequency transients, monitor for unexpected interactions between the simulated clock oscillator, PCC and PPS signals, and verify correct monotonic behavior as the various counters interact due to small frequency variations.

In order to calibrate the performance of the routines in a functioning system, they were implemented in the kernels for several architectures, including Alpha, Intel, and SPARC. Detailed performance data have been collected for three systems: Rackety is a busy SPARC IPC time server running SunOS 4.1.3 and connected to four radio clocks - dual redundant GPS receivers and dual redundant WWVB receivers. The PPS signal is derived from one of the GPS receivers. Churhky is a Digital Alpha 433au personal workstation running

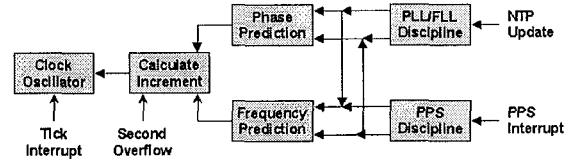


Figure 4. Kernel Clock Discipline

Tru64 4.0d and connected to a GPS receiver with PPS signal. Hepzibah is an Intel Pentium II 233 laboratory machine running FreeBSD 3.4 and connected to a GPS receiver with PPS signal.

Figure 5 shows the typical behavior of hepzibah. In this particular configuration the PPS signal was connected via a parallel port and a special kernel driver. The characteristic is decidedly spiky, in spite of the signal grooming algorithms used in the PPS discipline. The jitter budget includes contributions from the source (less than 100 ns), clock resolution (about 4 ns), and the hardware and software interrupt latencies. The interesting thing about this figure is that the jitter spikes are as often positive as negative. If due only to interrupt latencies, the spikes would be negative. There is no obvious explanation for this behavior other than to remark the standard (RMS) error is less than a microsecond.

While hepzibah has no applications or services other than NTP, rackety is a much slower machine dedicated to NTP service. It services an arrival stream of some 15 packets per second from an estimated client population well over 1000. The radio clocks are connected to a an 8-input multiplexor which services other ancillary devices as well. The hardware interrupt load produced by the multiplexor and network interface is severe, especially since the SPARC IPC is only a 25-MHz machine. The large negative time offset spikes shown in Figure 6 are clearly the result of interrupt latencies for the four radio clocks, the PPS signal, and the network interface.

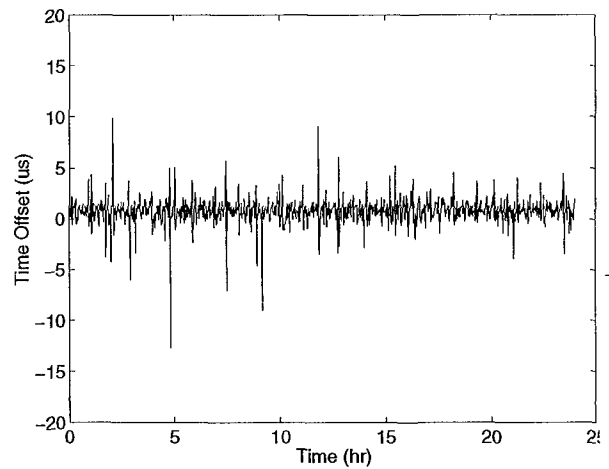


Figure 5. Time Offset for Hepzibah

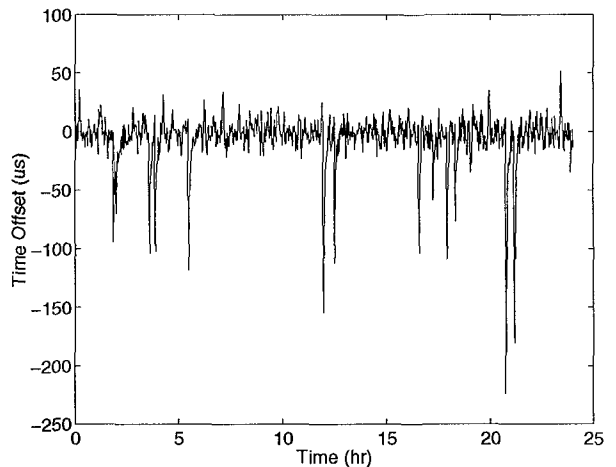


Figure 6. Time Offset for Rackety

Figure 7 shows the typical behavior for churchy, the fastest machine of the bunch. The PCC for this machine is derived from a SAW oscillator. Ordinarily, one would expect low phase noise from this type of oscillator, but the characteristics shown in the figure argue otherwise. To the trained eye, the characteristic is dominated by flicker noise. The source of this unexpected behavior is yet to be determined.

6. CONCLUSIONS

This paper demonstrates that modern computers can maintain nominal accuracy relative to precision time sources of a microsecond or two, assuming systematic latencies due to signal conditioning, interrupt processing, and timestamp capture can be calibrated out. In order to achieve this level of performance, a

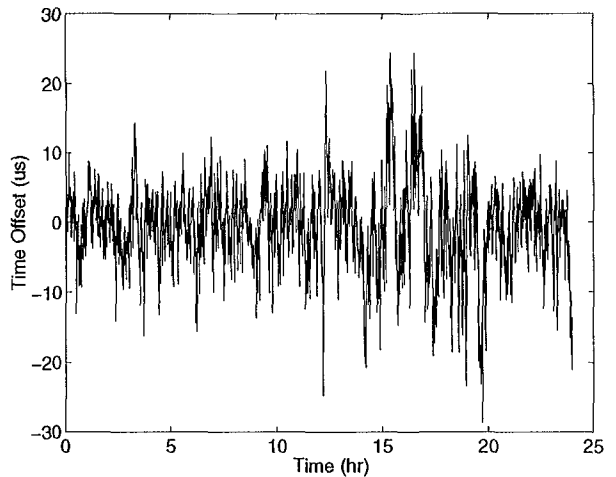


Figure 7. Time Offset for Churchy

hybrid PLL/FLL discipline loop is used for NTP control together with separate time and frequency loops for PPS discipline. The level of performance is probably near the best that can be achieved with an unstabilized clock oscillator. Where a fast computer with precision hardware clock is available, the performance can be improved to the order of a few tens of nanoseconds at the API. This was verified using a machine where the system clock was derived from a rubidium oscillator and FPGA counter; however, this setup would not ordinarily be considered practical. The practical accuracy expectations of individual applications will vary depending on the mix of applications and operating system scheduling latencies.

Observations of the kernel disciplines in actual operation suggest a few areas where further improvements may be possible. One of these is the grooming algorithm used in the PPS discipline. The complexity of the median calculation increases rapidly with the number of register stages, which is only three in the current design. However, the NTP discipline operates in user space, so its resource commitments are more flexible. The NTP daemon includes a PPS driver with a 60-stage register. The algorithm sorts the offsets, then iteratively trims off the sample furthest from the median until a prespecified fraction of the original samples are left. Finally, it presents the average of these samples to the kernel PLL/FLL discipline.

The PPS driver provides significantly less jitter than the kernel PPS discipline; however, the performance advantage due to the quick response of the kernel discipline is lost. While the current minimum daemon update interval is currently limited to 16 s in the interest of minimizing kernel overhead, it might be acceptable in fast machines to reduce that interval to 1 s. Should this be done, it would be practical to do almost all discipline loop processing in user space and move the per-second processing to the daemon, where more flexible processor and memory resource commitments are possible.

7. REFERENCES

Note: Papers and reports by D.L. Mills can be found in PostScript and PDF forma at www.eecis.udel.edu/~mills.

- [1] Allan, D.W. Time and frequency (time-domain) estimation and prediction of precision clocks and oscillators. *IEEE Trans. on Ultrasound, Ferroelectrics, and Frequency Control UFFC-34*, 6 (November 1987), 647-654. Also in: Sullivan, D.B., D.W. Allan, D.A. Howe and F.L. Walls (Eds.). *Characterization of Clocks and Oscillators. NIST Technical Note 1337*, U.S. Department of Commerce, 1990, 121-128.
- [2] Levine, J. An algorithm to synchronize the time of a computer to universal time. *IEEE Trans. Networking* 3, 1 (February 1995), 42-50.
- [3] Mills, D.L. Adaptive hybrid clock discipline algorithm for the Network Time Protocol. *IEEE/ACM Trans. Networking* 6, 5 (October 1998), 505-514.
- [4] Mills, D.L. The network computer as precision timekeeper. *Proc. Precision Time and Time Interval (PTTI) Applications and Planning Meeting* (Reston VA, December 1996), 96-108.
- [5] Mills, D.L. Unix kernel modifications for precision time synchronization. Electrical Engineering Report 94-10-1, University of Delaware, October 1994, 24 pp.
- [6] Mills, D.L. Network Time Protocol (Version 3) specification, implementation and analysis. Network Working Group Report RFC-1305, University of Delaware, March 1992, 113 pp.
- [7] Mogul, J., D. Mills, J. Brittenson, J. Stone and U. Windl. Pulse-per-second API for Unix-like operating systems, version 1. Request for Comments RFC-2783, Internet Engineering Task Force, March 2000, 31 pp.
- [8] Network Time Protocol Version 4 software distribution, including sources and documentation. Available via the web at www.ntp.org.

USING THE NETWORK TIME PROTOCOL (NTP) TO TRANSMIT INTERNATIONAL ATOMIC TIME (TAI)

Judah Levine

**Time and Frequency Division and JILA
National Institute of Standards and Technology
And University of Colorado
Boulder, CO 80305, USA**

David Mills

**Electrical Engineering Department
University of Delaware
Newark, DE 19716, USA**

Abstract

Although Coordinated Universal Time (UTC) is the time scale that is transmitted by almost all time services, this scale is awkward to use in the vicinity of a leap second. Many computer systems cannot represent the epoch corresponding to a positive leap second (23:59:60), and remain synchronized to UTC by stopping the clock at 23:59:59 for 1 extra second whenever a leap second is to be added. This makes it impossible to assign unambiguous time tags to events that happen during this period. In addition, computing the length of a time interval that includes a leap second of either sign is difficult because simply subtracting the two UTC time stamps at the end-points of the interval does not account for the time interval occupied by the leap second itself. To address these issues, we have augmented the Network Time Protocol to allow a client system to reconstruct TAI from UTC and a table of leap seconds. This time scale has no discontinuity during the leap second. Intervals computed using TAI are unaffected by the additional time occupied by the UTC leap second, and the TAI time scale provides an unambiguous time tag to any event -- even one that happens during a UTC leap second. Although our solution is unique to servers that support the Network Time Protocol, it could be adapted to other time services and formats. Such systems could support time tags using either UTC or TAI, and would significantly reduce the problems that result from using UTC alone.

INTRODUCTION

The time services operated by National Metrology Institutes and timing laboratories generally transmit time

signals based on a local realization of Coordinated Universal Time (UTC). These local time scales, which are identified as UTC(*lab*), are based on the UTC time scale computed by the International Bureau of Weights and Measures (BIPM). Since 1972, the rate of the UTC time scale has been equal to the rate of International Atomic Time (TAI), a time scale that is computed by the BIPM using a worldwide ensemble of cesium clocks and hydrogen masers. The rate of TAI, in turn, is determined by the length of the second, which is defined based on the frequency of a hyperfine transition in the ground state of the cesium atom. In addition to serving as the basis for the definition of time, this transition frequency plays a central role in setting the values for other fundamental constants of physics.

The length of the day computed using the current value for the cesium second is somewhat shorter than the length of a day based on astronomical observations (specifically, the UT1 time scale). The difference is currently about 260 ms (a fractional difference of about 3×10^{-8}); if this difference were left uncorrected, UTC would gain somewhat less than 1 s per year relative to UT1. The rate of this divergence is increasing slowly.

This time divergence is bounded by introducing “leap seconds” into UTC so as to keep the absolute magnitude of the difference between UTC and UT1 less than 0.9 s. (The leap second is not added to TAI, so that the difference between UTC and TAI is exactly an integral number of seconds.) Since the length of a UTC day is significantly less than the UT1 value, small variations in the length of the UT1 day do not affect the sign of the difference. Therefore, leap seconds have always been inserted into UTC, and this is likely to continue for the foreseeable future. However, the definition of the process also supports deleting seconds from UTC, should that ever be necessary.

These leap seconds are usually added at the end of June or December; the most recent one was added to UTC at the end of 1998, and the difference TAI-UTC became 32 s at that time. No additional leap seconds are currently scheduled, although there will almost certainly be one announced during 2001.

THE PROBLEM

The last second of a normal UTC day is 23:59:59, and the first second of the next day is 00:00:00. When a leap second is to be added to UTC, an additional second, whose name is 23:59:60, is inserted between these two seconds. This procedure introduces two difficulties into timekeeping in general and computer-based timekeeping in particular.

The first problem is that most computers keep time internally in units of seconds since some epoch (such as 00:00:00 1 January 1970 UTC). (The conversion to and from other representations of the epoch is handled by the routines that display the internal value.) There is no way of representing 23:59:60 in this system, and most computer systems repeat the time value corresponding to 23:59:59 instead. Although the internal clock remains synchronized to UTC once the leap second is over, this solution effectively stops the clock during the leap second and results in two distinct seconds having the same time stamp.

The second problem is that an interval that includes a leap second is physically longer than a normal equivalent interval, but that difference is not reflected in a computation that simply subtracts the UTC time stamps at the end points of the interval. Measuring the rate of some physical process using the difference in UTC timestamps will therefore show a strange value whenever the interval includes a leap second. (This problem is not unique to leap seconds – leap years introduce the same problem in people’s ages.)

THE SOLUTION

Since TAI has the same rate as UTC but has no leap seconds, applications that are affected by the two problems mentioned above can address both of them using timestamps derived from TAI instead of from UTC. Since these two scales always differ by an exactly integral number of seconds, it is a relatively simple matter to compute one from the other once the value of the difference is known.

Although it would be possible to address these problems by switching digital time services to pure TAI, this is not desirable for several reasons. In the first place, the resulting change would disrupt the thousands of systems that are based on the existing UTC-based definition. In the second place, such a change would result in a significant (and ever-increasing) difference between timestamps transmitted by the digital time services and normal civilian time, which will continue to be based on UTC to maintain its coordination with UT1. Therefore, we have implemented a solution which continues to be based on UTC timestamps, but which also contains the integer offset value between UTC and TAI to allow any client process to compute TAI as needed. Our solution is based on the Network Time Protocol (NTP), but the principles could be adapted to other protocols without great difficulty.

The solution we have implemented contains three independent components: (1) publishing the epochs of past and future leap seconds, (2) transmitting this information from servers to their clients, and (3) supporting combined UTC and TAI time stamps within the client itself. We discuss the details of each component in the following sections.

PUBLIC LEAP-SECOND TABLES

All of the public stratum-1 Internet time servers operated by NIST have a publicly-readable file that contains information regarding all known leap seconds since the current system was defined in 1972. The name of the file is leap-seconds.list, and it is in directory “pub”. (This filename is a link to a second file, located in the same directory, which contains the leap second data. The name of this other file is leap-seconds.<timeval>, where <timeval> is the time at which the file was last modified in units of seconds since 1900.0. This is done so that users can detect when the file has been modified without actually having to read the file itself or even retrieve it from the NIST server.) You can get the current version of this file using anonymous ftp to any of our time servers. If you use a web browser, the URL would be: *ftp://<timeserver>/pub/leap-seconds.list*. The parameter <timeserver> is the name of any NIST-operated time server. (See our Web page *www.boulder.nist.gov/timefreq/service/time-servers.html* for a complete list.) For example, you could use the URL:

ftp://time-b.nist.gov/pub/leap-seconds.list

to get the current copy of the table of leap seconds.

The format of the table is described in the file itself. It is a simple text file. The symbol “#” introduces a comment, which continues from that point to the end of the current line. A line starting with #\\$ is a special

comment line. The parameter on this line gives the last modification date of the file in NTP format (i.e., as a number of seconds since 1900.0). There will always be only one such ## comment lines. The remainder of the file contains leap second data, one value per line. Two consecutive data lines in the current file are:

3076704000	31	# 1 Jul 1997
3124137600	32	# 1 Jan 1999

The first value on each line is the epoch at which a new leap second was (or will be) introduced into UTC. This parameter is expressed in seconds since 1900 – the timestamp format used by NTP. The second value gives the difference between TAI and UTC starting at that epoch. The difference specified on each line is in effect until the epoch given on a following line, or into the indefinite future if there is no subsequent entry. (The remaining characters are a comment that gives the civil date corresponding to the epoch specified by the first value.) In each case, the second parameter is to be added to a UTC time stamp to produce the equivalent TAI value. The correction affects only the integer-seconds portion of the NTP time stamp; the value of the seconds fraction is always unchanged.

It is straightforward to compute the Modified Julian Day (MJD) number from an NTP time stamp. To convert, divide the NTP timestamp by the number of seconds in 1 day, and add 15020, the MJD corresponding to 1900.0. Thus $3124137600/86400 + 15020 = 51179$, the MJD corresponding to 1 January 1999. All of these computations can be done using integer arithmetic, so that there are no issues of round-off or truncation.

The International Earth Rotation Service (IERS) in Paris is responsible for announcing leap seconds, and NIST will modify the files on the servers as soon as we receive this notice from the IERS. Leap seconds are normally announced several months in advance, and all of the NIST servers would normally be updated to include the new leap second within one week of our receiving the announcement. It is extremely unlikely that users would have less than one month of advance notice for an upcoming leap second.

TRANSMISSION FORMAT

Version 3 of the NTP time format (see RFC 1305) does not support any additional time parameters beyond the UTC timestamps that are part of the basic protocol. However, the additional space needed to transmit the difference between UTC and TAI is supported by the general format “extension fields” specified for NTP version 4. These extension fields are in addition to (and are added at the end of) an unmodified unauthenticated old-style timestamp packet, so that using them does not break previous versions of the client software that does not expect them or know what to do with them. (However, an association that used the version 3 authentication mechanism will not be compatible with a server that uses the new format to transmit the UTC – TAI offset, since this offset value will be mistaken for part of the old-format authenticator. This shouldn’t happen in principle, since a version-3 client does not know how to ask the server for these data, and they are transmitted only if the client asks for them.)

The extension fields defined in NTP version 4 are placed between a version 3 timestamp packet and a terminating authenticator. Each extension field is a multiple of 4 octets (32 bits), and the total length of all extension fields is rounded up to the next multiple of 8 octets (64 bits). Many different types of extension field are defined. The most significant bit of the first octet always specifies whether the packet is a request

(0) or a response (1). The next bit is set in the response to indicate an error condition and is clear otherwise. The remaining bits of this octet specify the version number of the protocol; the format described here has been assigned a version number of 1. The second octet specifies the type of the request and the next 2 specify the length of any associated data. The type that is relevant to this discussion is “TAI leap second table.” The details of the format are in [1].

To request the leap second table, a client sends a “TAI leap second table” packet (currently this is type 8) to the server with the response bit cleared (thereby indicating a request for data). The server responds with a table of 32-bit time stamps giving the times in NTP format when a leap second was (or will be) inserted. The table is in reverse chronological order – the time of the most recent leap second is transmitted first. The TAI – UTC difference associated with each of these time stamps is inferred from the transmitted length of the table, using the fact that the offset was 10 seconds when the current leap second system was instituted in 1972 and must be increased by 1 s at the time specified by each subsequent entry. In addition, the response contains a timestamp showing when the table was generated. If the first entry in the response is less than this value then this entry specifies the current TAI – UTC difference. If the first entry is greater than the file timestamp, then the first entry represents a future leap second that has been announced, but whose effective date has not yet arrived. Normally, the current offset is one less than the value inferred from the table length, and the next entry will give the effective date of the current TAI-UTC time difference. If the server is not synchronized to an authenticated source then the timestamp field is 0.

The extension field is terminated with a message authenticator code (MAC), which is designed to guarantee the provenance of the data. The authenticator is a message digest of the entire packet, and is computed using a 32-bit key value. Both symmetric-key and public-key methods can be used to authenticate the messages. The details are in [2]. While the authenticator is optional for a simple NTP time packet, it is required when an extension field is present.

This implementation depends on two assumptions: (1) that leap seconds are always integral values and (2) that all leap seconds will be positive. Both of these are basic to the current definition of UTC, but neither is a fundamental unchanging truth. The first assumption was not true before 1972, for example, and this method cannot be used to represent dates before 1972 for that reason. The second assumption might change if the current definition of the second changed, or if the way that definition is used to construct TAI and UTC were altered. This is not very likely in the short term, but neither the cesium definition nor the current method of calculating UTC will live forever.

CLIENT IMPLEMENTATION

The leap second table changes very slowly, and a client only needs to query a server infrequently – during a cold start and once a month or even less often during steady-state operation. Furthermore, a client could update its internal notion of the current offset value by incrementing it (or, in some future implementation, conceivably decrementing it) each time it executed its special internal leap second code. There are two different implementations, depending on how the client realizes the leap second.

If the client implements the leap second by stopping its clock for one extra second at a time that is equivalent

to 23:59:59, then it must increment the TAI – UTC difference at the start of the second copy of this second. Thus, the internal state of the system would be:

UTC Time	System Time	TAI-UTC value
23:59:58	23:59:58	N
23:59:59	23:59:59	N
23:59:60	23:59:59	N+1 (the leap second)
00:00:00	00:00:00	N+1
00:00:01	00:00:01	N+1

This is the more common case. On the other hand, if the client implements the leap second by stopping its clock for one extra second at a time that is equivalent to 00:00:00, then it must increment the TAI – UTC difference at the start of the second copy of this duplicated second. The internal state of the system in this case would be:

UTC Time	System Time	TAI-UTC value
23:59:58	23:59:58	N
23:59:59	23:59:59	N
23:59:60	00:00:00	N (the leap second)
00:00:00	00:00:00	N+1
00:00:01	00:00:01	N+1

The timestamp in the leap second file that is associated with this event is the value corresponding to the UTC time of 00:00:00 – that is, the first second after the leap second has been inserted. Based on the previous tables, a client process that uses the first method must increment its internal value of TAI-UTC when its internal clock reads one second before the time in the table (for the second time), while a client that uses the second method must increment its internal counter one second after the value of its internal clock reads the time in the table (for the first time). If the internal implementation includes a special flag which is set to indicate that a leap second is currently in progress, then the TAI – UTC difference can be incremented when that flag is set. In each case, the goal is to realize a time scale that does not show any discontinuity (either in time or time interval) across the leap second.

Since maintaining the system clock is a kernel function in all operating systems, the easiest way to implement these strategies is to modify the kernel clock software and to add the additional location that holds the TAI – UTC time difference in the kernel address space. This is usually straightforward in principle, although it requires the source code of the kernel to realize it.

It is also possible to realize this system without modifying the kernel by defining a system-wide overlay to the kernel clock. This is obviously less desirable in principle and has not been done to our knowledge. Another solution (which was used in many older systems) is to implement the time adjustment associated with a leap second by adjusting the effective frequency of the system clock, thereby slewing the system time over some interval in the vicinity of the actual leap second. Since the maximum slew rate supported by most kernels is of order 0.1% or less, a system that implements this method will require several minutes to accommodate the leap second, and its clock will be wrong by a varying fraction of a second during this interval. The only advantage of this implementation is that it produces a system clock that never goes backwards, so that there is no problem with timestamps that violate causality. Since the system clock moves

backwards for only 1 second in the other implementations, this is not a strong enough advantage to outweigh the problem that the clock is wrong for several minutes following the leap second.

The final aspect of the client implementation is the method that is used to provide the TAI – UTC time difference to a user process. In order to maintain backward compatibility with applications that do not use this parameter, most implementations provide a separate system call which provides both the UTC timestamp and the TAI-UTC offset as part of a single structure. It is then a simple matter for any client process to compute the TAI timestamp. A client process that uses UTC timestamps simply ignores the TAI – UTC offset parameter.

SUMMARY AND CONCLUSIONS

We have designed a system that can support simultaneously transmitting both UTC and TAI. A client process can use either or both of these time scales as appropriate – UTC where compatibility with other services or legal traceability is required and TAI where smoothness of time intervals and monotonic time stamps are more important. This dual system is fully compatible with the previous implementation of the Network Time Protocol, and servers that support these new capabilities can simultaneously provide timestamps in the old formats. Although our system is designed around the Network Time Protocol, it can be readily adapted to other formats. In particular, the list of leap seconds is publicly available from all of the NIST time servers, and access to this list does not depend on the Network Time Protocol or on the details of the system used by the client to realize its internal time scale.

Even when the system fully supports the additional machinery for the TAI – UTC time difference, applications that reference the system clock directly without using the TAI correction will continue to operate in UTC as before. While these applications will use timestamps that are fully compatible with other civilian time services, they will have to cope with the discontinuity in time and in time interval in the immediate vicinity of each leap second. In particular, timestamps that are internal to the operating system (the modification time of a file, for example) will continue to be expressed in a time scale derived from UTC.

Finally, we note that the user interface to the clock on most systems is designed so that consecutive requests for the system time will produce responses that are monotonically increasing – even if the increase is only 1 in the least significant bit of the response. This design goal cannot be completely consistent with the methods described above that are used to realize a leap second, although the resulting time offset is almost always too small to be significant.

REFERENCES

- [1] David Mills, “Public Key Cryptography for the Network Time Protocol,” Internet Draft, Draft-ietf-stime-NTPauth-00.txt, June 2000. Available on the Web at www.eecis.udel.edu/~mills/memos.htm.
- [2] David Mills, “Public Key Cryptography for the Network Time Protocol,” Electrical Engineering Report 00-5-1, May, 2000, University of Delaware Electrical Engineering Department. Available on the Web at www.eecis.udel.edu/~mills/reports.htm.

Questions and Answers

RICHARD SCHMIDT (USNO): Is it possible that your table could be limited to just two lines? Is it possible that your cache table of leap seconds could be limited to just two lines rather than the full historical table to limit the amount of data that you transfer?

JUDAH LEVINE: There are only 20-odd leap seconds, so the table is going 20 inches long. Generally speaking, you are almost never going to be interested in historical value. You are going to want the current value, and maybe the next value. So, I would guess the table entry is maximum 20-something inches long and, more likely, 2 inches long. And that's it. I think in our lifetime, there's going to be 100 leap seconds, at most. After that, it is going to be somebody else's problem.

ROBERT LUTWAK (Datum): I have a question from the perspective of other manufacturers who are building NTP servers who need to receive advance notice of the leap seconds. It is not unlikely that they may start to rely on this table as a way of getting advance notice of the leap seconds. In which case, maybe instead of just having it be a NIST incorporation in some extension fields, it really needs to be built into the standard of NTP. So when the manufacturers build it into hardware, they can rely on it for the future.

LEVINE: I agree with you at the 100% level. That is somewhat beyond my power to do. All I can say is that the extension field concept is built into the standard for NTP. The idea of using the TAI leap second offset is built into Mills's documentation of the standard. The tables are there, and obviously, we encourage other people to do it as well. We're not an enforcement agency.

But yes, it would be nice if this became an official standard, and we can only propose it in order for it to become an official standard. But we are committed to maintaining the system as prescribed. If you look at Mills's documentation, you can see the details of how these are defined. They are fundamental to NTP Version 4 because they are used for other purposes. That is, they are part of the authentication and the digital signature system. So there are many types of extension fields besides this issue of leap seconds. There is a lot of other stuff, there are a lot of other capabilities that you might need an extension field for.

DENNIS McCARTHY (USNO): Two things. One, I would just like to say that I agree that this would go a long way towards helping some problems. But it still doesn't alleviate the basic fundamental issues. So I didn't want people to have a feeling that this solves all the problems and now we can go on.

LEVINE: No, I didn't mean that at all.

McCARTHY: Yes, but I think it does help some of our software users that complain about UTC.

The other thing I was wondering is what about the possibility of having this table actually be maintained by something like IERS or BIPM or something like that where this would be an international conventional table of some sort. You know, you wouldn't have to worry about somebody updating it; it would just be there at the IERS or BIPM.

LEVINE: I think that is a fine idea. I would do everything I could to encourage whoever wanted the table to take the table. It's there, it's available by public ftp from our servers. If anybody thinks it is useful, go for it.

McCARTHY: Yes, we will have an IERS directing board meeting in 2 weeks or something. I was thinking that maybe we could even bring that up for discussion.

LEVINE: That's fine. Now, the only thing that is somewhat special about this table is that its time stamps are in NTP format. And so, if you want to convert them to Julian day numbers, you divide by 86,400 and add 15020, and we all know how to do that. And that's all it would take.

WLODZIMIERZ LEWANDOWSKI (BIPM, France): I would like to add that the BIPM could come to such a table. That could be discussed during the next CCTF meeting, and the dates are now official. It will be held on June 20 and 21, 2001. So I believe that the leap second will again be a subject of CCTF, and such issues that you have raised here could also be discussed.

NEW ISSUES IN TELECOMMUNICATIONS

**Ed Butterline
Symmetricom
San Jose, CA, USA**

Abstract

There are two new issues that are currently causing concern in telecommunications. These issues are the introduction of pure optic systems for transmission and switching and the Federal Communications Commission (FCC) edict that wireless network operators must provide a precise location of wireless emergency E-911 callers.

OPTICAL NETWORKS

Optical transmission equipment has been deployed in telecommunications for well over 15 years. This equipment has been used primarily to interconnect telephone central offices. Fiber-optic cables are currently the technology of choice when inter-office capacity is increased. At the fiber-optic cable terminal, signals on these cables are converted from optical to electrical for processing by switching equipment. The signals are then converted back to optical for transmission to the next central office.

The current network issue is that optical switching equipment has reached the point where it is considered practical for central office deployment. This means that networks between central offices may be operated on a pure optical basis. The network between the central office and the user or customer is expected to remain electrical for the near future.

Standards for the new optical switching equipment are being actively worked upon in ANSI committee T1X1.5. The accuracy of the clocks that will control the new optical equipment has yet to be determined. The concern of network operators is that new, higher performing, clocks may be required.

WIRELESS E-911 SERVICE

E-911 is a standard feature of the wireline telecommunications network. Network operators provide the Public Safety Answering Point (PSAP) the location of E-911 callers from a database showing where the callers line was installed. The timing provided at PSAPs is not very precise. In most cases, timing it is obtained from a WWVB signal. This is sufficient to meet the legal timing stamping of received calls.

Currently when an E-911 call is received from a wireless caller, the caller must verbally tell the PSAP where they are. In many cases they simply do not know where they are or are unable to coherently give the information. To overcome this scenario, the FCC has

prescribed that the wireless network operator must locate the caller and pass that information to the PSAP. There are several, highly contentious, proposals to provide the location information. One solution is to place a GPS receiver in the handset. Another is to use equipment in the base stations of the wireless network itself to locate the caller. There are two variations of the GPS in the handset solution. One uses GPS autonomously. The other uses GPS in conjunction with network-based equipment.

The time frame for initial implementation of a wireless solution is October 1, 2001 or an interval after the PSAP request for implementation. The two solutions have different time deadlines. The time schedule for the GPS in the handset solution is by October 1, 2001 all new service activations must have the feature. By December 1, 2005 the network operator must have made a good faith effort to have all handsets equipped with the feature.

The time schedule for the network based solution is six months after the PSAP has requested it, the network operator must provide Automatic Location Identification (ALI) for 50% of the calls. Eighteen months after the request, ALI must be provided for all calls.

The mandated ALI accuracy is different for the two solutions. The GPS in the handset solution must be accurate to 50m for 67% of the calls and to 150m for 95% of the calls. The network-based solution must be accurate to 100m for 67% of the calls and to 300m for 95% of the calls.

Most areas are served by more than one wireless network. There will probably be price differences between the solutions offered. The customer will decide if economics or being found quickly in an emergency is more important.

Questions and Answers

HUGO FRUEHAUF (Zyfer, Inc.): Realizing that the network solution is going to be more difficult to get accuracy, why aren't the specs the same for everybody? Why is it that the GPS guys just have the same specs?

ED BUTTERLINE (Symmetricom): One can only ask the FCC that question. I can give my personal thoughts on it, but they would be strictly my personal thoughts. The FCC has edicted thus and so, thou shalt be twice as accurate if you have decided as a carrier to go to the GPS in the handset. Then if you have decided I'm going to put some software, maybe even some locator boxes at every bay station to locate you, I don't know. It is a very contentious issue, and I can't comment on that.

MICHAEL GARVEY (Datum): Maybe these are obvious questions. GPS is not very reliable indoors, number one. And number two, suppose you have a receiver, a cell phone that is used to working in a network that does location within the network? Then you roam to a different situation where there is the expectation that it gets a GPS-derived position. Has the FCC addressed that?

BUTTERLINE: I'm not sure what they've done in that regard. I will comment just a little bit on GPS not working inside. I know one of the suppliers of a proprietary GPS in a handset solution and realize that the solutions are proprietary that are being proposed. They would say, gee whiz, if I had to make a E911 call standing here in this room, inside, my system would locate me to better than 50 meters. And you say, how can that be? You know if you had a handheld GPS system and you said "Tell me where I am?" you are not going to get a fix here in this room. But there are GPS signals that can make it into this room—certainly not four at a time to give you a precision fix. But the proprietary solution of one of the suppliers that has been demonstrated says I can do it indoors, and do it to a high degree of accuracy; and I will probably exceed the FCC's requirements. Proprietary solution; I can't go any more than that.

MATTHEW LONG (NRL): For the network solution, I was wondering if you could add a little more information about the direction-finding process that is used to locate the software user, and what kind of equipment would added to the typical cell site? I understand cell sites are a bit larger than the area that we are talking about.

BUTTERLINE: I can't give you a lot of information. I am sort of acting as a reporter on this. It is mainly because I want to keep a certain amount of distance. These are all proprietary solutions that are being proposed by various suppliers and equipment to the wireless telephone industry. They are very contentious, as my system is better than your system is better than his system. I understand that there would be certain equipment added to space stations that would allow them to get a fix to the FCC-required degree of location accuracy. Beyond that, I don't know. Realizing that CDMA systems have a GPS in every site, so how much more do they need? I don't know.

JEREMY ELSON (UCLA): So an interesting difference between these two systems, I think, is that if there is GPS in the handset, it is the user that knows where it is, whereas the network-made solutions know where you are. So there are some obvious privacy implications to anything that always knows where the user is. I am wondering if that came up at all in the GPS solution. The user theoretically has some control over when it sends location information back. Whereas in the network-made solution, the network knows where you are, whether you like it or not.

BUTTERLINE: That is a very good question. I think initially when this was proposed, when

the FCC came out with their requirements, it was strictly intended that to be a safety-of-life kind of thing. Manufacturers of wireless telephony equipment come up with a solution to do it; we are not going to tell you how to do it. Lately, one hears stories that people have gotten quite creative with this approach and will be keeping track of where you are. To the point of being able to send you a little message that says "We're having a big special over at Joe's Market today; you're only a quarter mile away, why don't you stop by and mention Code 10, and you'll get an extra discount?" That's a very contentious issue. It may very well be a way of the wireless network operator recapturing the cost of implementing this location service. I don't know, but it's a very interesting thing and the privacy issue is real.

PRIMARY REFERENCE CLOCKS USING INDOOR ANTENNAS

Don Mitchell
Truetime, Inc.
3750 Westwind Blvd., Santa Rosa, CA 95403, USA

Abstract

This paper discusses a new technology of synchronizing clocks and disciplining oscillators using CDMA cellular transmissions. Like cellular telephones, these receivers will operate in most buildings without rooftop antennas. They are reported accurate to within microseconds of UTC with stable frequencies available.

INTRODUCTION

UTC Time and Frequency Dissemination via the IS-95 CDMA Mobile Telecommunications Infrastructure

Base Station Transmissions in IS-95 CDMA Systems

- All use the same pilot pseudonoise (PN) spreading code
- All use the same carrier frequency (within an individual provider's system)

Base Station Transmissions in IS-95 CDMA Systems Must be Synchronized

- To control interface between cells:
 - ⇒ Cell-to-cell interference is controlled by having each base station transmit the pilot PN code with its own unique time offset relative to GPS time
 - ⇒ The pilot PN offsets must be maintained accurately or adjacent cells would interfere with each other

Base Station Transmissions in IS-95 CDMA Systems Must be Synchronized

- To allow a “soft hand-off” as the mobile user travels between cells.
 - ⇒ The mobile unit must be able to calculate the approximate time offset of the new base station’s pilot PN code in order to rapidly acquire and lock to it before losing the current base station
 - ⇒ If the base stations are synchronized, and the mobile user decodes the neighboring cell PN offset data that it receives from the currently tracked base station, this can be achieved

The IS-95 CDMA System Time Base is the GPS Time Scale Because...

- GPS is globally available
- GPS can maintain the required level of synchronization between base stations
 - ⇒ Less than 1 us while tracking a satellite
 - ⇒ Less than 10 us for up to 24 hours while in holdover (IS-95 spec) using either
 - A rubidium vapor local oscillator
 - An ultra-stable, ovenized quartz local oscillator with software temperature compensation

The IS-95 CDMA Signal Structure Supports Precision Recovery of GPS Time & Frequency

- Spread spectrum modulation at GPS-like chipping rate of 1.2288 Megachips/second
- Pilot PN code can be acquired using long integration time—no data modulation
 - ⇒ 32768 chip code repeats every 26.666...ms
 - ⇒ Base station pilot PN codes are offset from each other in 64 chip increments (52.08333....us)

The IS-95 CDMA Signal Structure Supports Precision Recovery of GPS Time & Frequency

- Cellular (881 MHz)/PCS (1960 MHz) carriers support GPS-like low-noise frequency recovery and aiding/smoothing of the code tracking loop
- Sync channel message: base station PN offset, UTC leap seconds and local time offset
 - ⇒ 1200 bits/second data is convolutionally encoded ($k=2$, $m=9$) to 2400 symbols/second
 - ⇒ Block interleaved with 2:1 redundancy to 4800 symbols/second
 - ⇒ CRC-30 performed on complete message
 - ⇒ Message repeated every 240 milliseconds

Received IS-95 Signal Level is Much Higher than GPS

- IS-95 coverage spec minimum is -100 dbm – at least 30 dB greater than GPS
- Cellular band carrier penetrates buildings to much greater degree than GPS
- Provides an excellent alternative in situations that are difficult for “direct” GPS

SUMMARY

CDMA “Indirect” GPS Performance Relative to “Direct” GPS

- Uncertainty in the propagation delay from base station to user limits absolute accuracy of the recovered UTC time to tens of microseconds.
- With stationary users, the time offset due to propagation delay is fixed and the repeatability and stability of the recovered UTC time is at the 100 ns level.
- With stationary users, the quality of the base station GPS receiver/oscillator system provides excellent transmitted frequency accuracy and stability which is virtually reproduced with a well-designed receiver.

Questions and Answers

JEREMY ELSON (UCLA): I am wondering if anybody has talked about trying to recover position by locking to, let's say, four CMA space stations the same as you would lock on to four GPS satellites.

DONALD MITCHELL: That's a good thought. You could certainly do that. Because if you're looking at the offsets that are received, then most certainly you could be able to determine your location by looking at the offsets that you receive from three carriers. You have four carriers, and it makes it even better. So yes, that's a possibility. Although, like I say, I am not aware of anybody doing that. That could be something that is going on.

I really wasn't aware of this until I heard about it, but I think the first real notice I had that somebody was actually doing something in this area was Ed Butterline at the ION in '99 bringing the subject up.

THE TIME LINK BETWEEN CSAO AND CRL

Li Huanxin and Wang Zhengming

Shaanxi Astronomical Observatory, the Chinese Academy of Sciences (CSAO)

P.O. Box 18, Lintong, Xi'an, Shaanxi, China

Tel: +86-29-3890435; Fax: +86-29-3890196

E-mail: lhx@ms.sxso.ac.cn

Abstract

There are and will be a few techniques for time link between CSAO and CRL. The TWSTFT was set up in October 1998 via a Japanese communication satellite. The CSAO-CRL TWSTFT data have been accumulated for more than 1 year since the date when the link was established. The regular operations for the time comparison are well done in 30 minutes twice a week. The GPS Common View has been a regular time link between CRL and CSAO for TAI computation since June 1996. It is expected that there will be a third technique for the time link with GPS/GLONASS multichannel receivers in the near future.

INTRODUCTION

It was in June 1996 when Shaanxi Astronomical Observatory (CSAO) imported a GPS receiver, TTR-6, with which the modernized time link with GPS common view (CV) has been carried on between CSAO and the Communication Research Laboratory (CRL), the Ministry of Post and Telecommunications for the computation of TAI on a routine basis. The data exchange between the two time labs and the data reduction for the time comparison at CSAO have been continued for 2 years.

Two-Way Satellite Time and Frequency Transfer (TWSTFT) is one of the most advanced techniques for time and frequency comparison. By use of synchronous satellites, TWSTFT can optimally offset the errors caused by the path effects and the time labs are able to acquire the real-time results of the comparison. In order to improve the international time synchronization, the Bureau International des Poids et Mesures (BIPM) is carrying out a project for establishing the International TWSTFT Network.

The cooperation on TWSTFT between the National Time Service Center of China at Shaanxi Astronomical Observatory, of the Chinese Academy of Sciences (CSAO), and the Communication Research Laboratory, of the Japanese Ministry of Post and Telecommunications (CRL) will play a very important rule in the International TWSTFT Network. Dr. Imae from CRL and Dr. Li Zhigang from CSAO started to discuss the possibility on the TWSTFT cooperation in March 1997 and the TWSTFT time link between CSAO and CRL via Japanese communication satellite was established in October 1998, when a set of Ku band ground station equipment, as well as related measurement devices, supplied by CRL were installed at CSAO. The TWSTFT laboratory at CSAO, which was established at the same time with the fund supplied by the Chinese National Science and Technology Department and the Chinese Academy of Sciences,

has made the time comparisons with CRL through the Japanese communication satellite JSAT1 since 25 October 1998. The CSAO-CRL TWSTFT data have been accumulated for more than 1 year since the link was established. The routine operations are undertaken every Tuesday and Friday with 30 minutes each time.

The period of validity for the CSAO - CRL TWSTFT cooperation project now being carried out, the agreement of which was signed three years ago, is five years and it is still in the early part of the period. Since the project started two years ago, the cooperation has greatly prompted the research work and improved the precision of the time comparison for both the two time labs.

Because of some trouble with RF Transceiver and Low Noise Converter (LNC), the TWSTFT had to be temporarily interrupted for the period September 1999-June 2000. A new step of the project has begun with a new satellite, changing Satellite from JSAT3 to JSAT1. The Satellite Company in Japan set the antenna for JSAT1 at CSAO on 18 July 2000. The TWSTFT between CSAO and CRL works again after 10 months' absence.

THE DATA ANALYSIS

The results of data reduction for GPS CV before the end of May 2000 show that the position error of the antenna at CSAO was large and should be redetermined. The standard variations (RMS) for the data points [UTC(CRL)-GPS]-[UTC(CSAO)-GPS] to their smoothing curves are about 15.1 ns on average for the period from January to April 2000 and 12.1 ns for May 2000 (after Selective Availability was removed). The accurate coordinates for the TTR-6 antenna at CSAO were introduced at the end of May 2000, which improves the precision of the time comparison. The rms's are about 6.84 ns in average for the period from June to August 2000. When the IGS TEC maps are used for calculating the time delay caused by the ionospheric refraction instead of the model, the rms's are reduced to 6.60 ns for the same period. However, it is still larger than it should be. The antenna of TTR-6 at CSAO has been tested and was verified to have some troubles, which causes fewer tracks, large noises, and jumps in the data of UTC(CSAO)-GPS.

To compare the TWSTT result UTC(CRL)-UTC(CSAO) [by Dr. Hirotaka Yukawa, CRL] with the GPS result UTC(CRL)-UTC(CSAO) [by CSAO], we use 55 groups of effective data for the period from January 1999 to August 1999. The profiles of TWSTFT results and GPS results coincide well. However, the larger fluctuations can be seen in the GPS time link, which is surely caused by the big noise in TTR-6 at CSAO (see Figure 1A).

On 18 July 2000 the TWSTFT between CRL and CSAO restarted. We have gotten better results for the last 5 months. The TWSTT results [by Dr. Hirotaka Yukawa, CRL] and GPS results for the period from 18 July to 24 October 2000 are shown in Figure 1B, from which the obvious improvement can be seen for the TWSTT results in the recent few months.

SOME EXPERIENCES AND SUGGESTIONS

Because the RF transceiver (RFU) and the Low Noise Converter (LNC) are on the roof of the building in the open air, they would be easily damaged by environmental conditions. This situation did make trouble for RF Transceiver and Low Noise Converter (LNC) at CSAO, so that the TWSTFT had to be interrupted for 10 months. Some Asian labs have met the same problem. There could be nothing to do but send the RFU away for repair. It is necessary to

hood the antenna and cover the RF Transceiver, as CRL and CSAO do. They can preserve the instruments from water.

To seal all the connectors with mastic tape is a good way to keeping water from leaking in. Applying UPS to the whole system, either outdoors or indoors, can ensure that the instruments are well protected in order to avoid unforeseen power supply breakdowns.

THE POSSIBILITY OF ESTABLISHING THE TWSTFT LINK BETWEEN ASIA AND EUROPE VIA CSAO

CSAO is among the first group of institutes that has been granted by the Chinese Academy of Sciences (CAS) to be one part of the CAS's Innovation Project. CSAO will become the national center for research and service in the field of time and frequency and is going to be renamed as the National Time Service Center (NTSC). Therefore, CSAO will get more support from the Chinese Government. At CSAO a team of scientists and technicians working on the subject of time transfer, including TWSTFT, have made much progress in their research work.

Because of CSAO's geographic position, it should be a nice "bridge" of TWSTFT links between Asia and Europe. Figure 2 shows that the satellites located at the longitude zone from 50°E to 60°E can be used and their elevations would be higher than 20° for CSAO and some European time labs.

We are looking forward to establishing a new TWSTFT time link between CSAO and one of the European time labs, such as TUG and CAO, in the near future.

ALL-IN-VIEW TIME LINK WITH GPS/GLONASS MULTI-CHANNEL RECEIVERS

Both CRL and CSAO have been equipped with GPS/GLONASS multichannel receivers, R100, the products of 3S Navigation. The receivers are under testing. According to the primary results at CRL, the precision for the GLONASS P-code is much higher than the GPS and GLONASS C/A-code. Moreover, the stability with GPS C/A-code is about 3 times better than that with GPS single channel receivers [1]. Better time comparison results are expected when R100 receivers are used on a routine basis, which can also be used as a primary calibration for the TWSTFT link.

REFERENCE

- [1] W. Lewandowski, and J. Azoubib 2000, "*Time transfer and TAI*," 2000 IEEE/EIA International Frequency Control Symposium and Eexhibition, 7-9 June 2000, Kansas City, Missouri, USA, pp. 586-597.

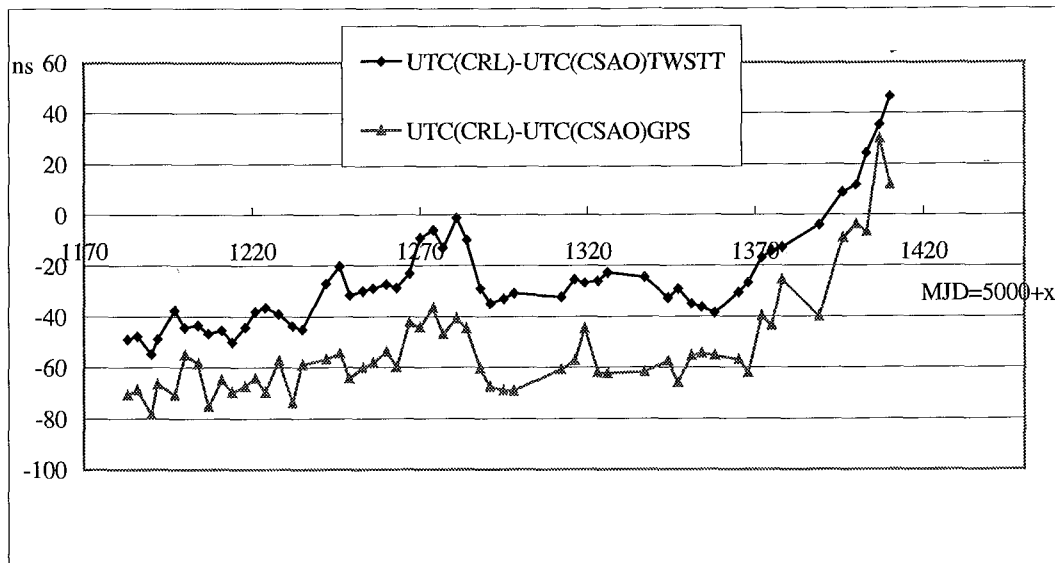


Figure 1A The comparison between TWSTT and GPS Common View (Jan.-Aug., 1999)

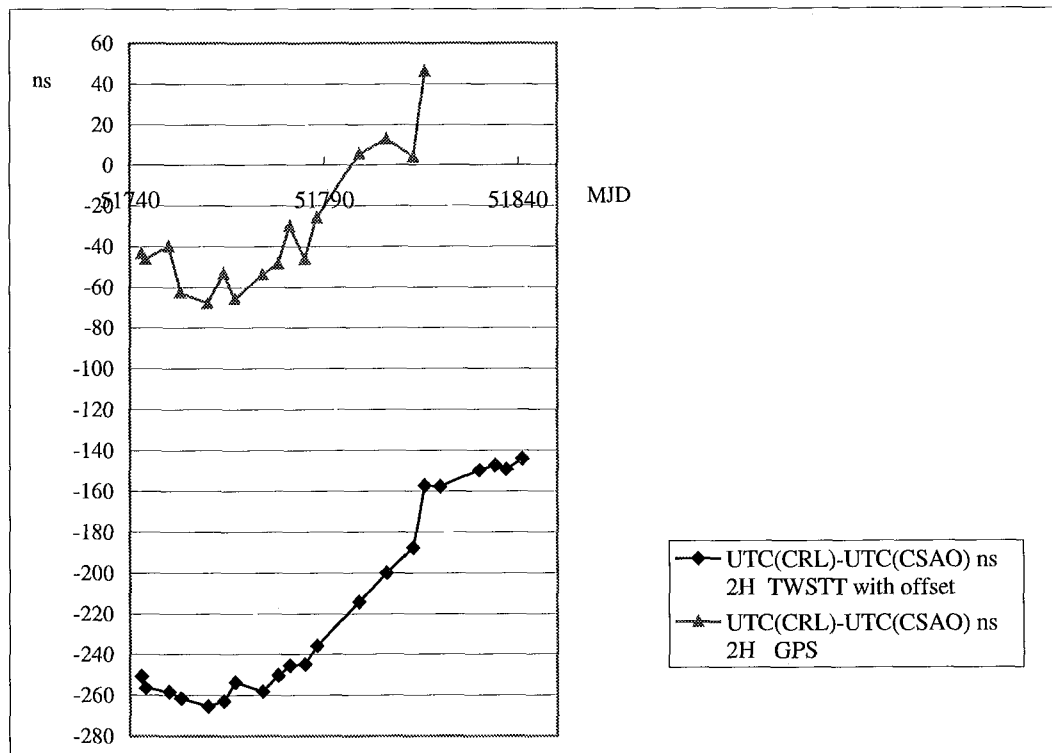


Figure 1B The comparison between TWSTT and GPS Common View (July 18-Oct.24,2000)

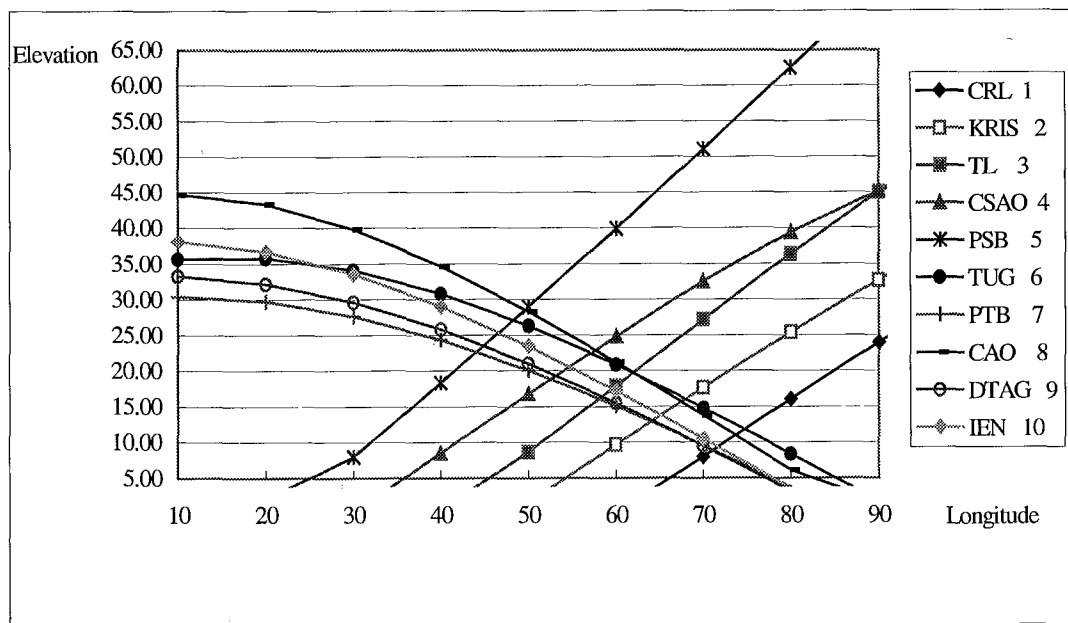


Figure 2 The elevation of satellite for some stations

TIME AND FREQUENCY ACTIVITIES AT THE CSIR — NATIONAL METROLOGY LABORATORY

**E. L. Marais
CSIR-NML**

P.O. Box 395, Pretoria, 0001, South Africa
Tel: +27 12 841 3013; Fax: +27 12 841 2131
E-mail: elmarais@csir.co.za

Abstract

The Time and Frequency Laboratory of the CSIR-National Metrology Laboratory (CSIR-NML) is responsible for the maintenance and development of the national standards in time and frequency. Specific responsibilities include time and frequency, phase angle, fast electrical-pulse characterization, and time-interval measurements. The fiber-optics laboratory also resides within the Time and Frequency Laboratory. This paper will discuss the various activities within the Laboratory.

INTRODUCTION

The CSIR is empowered by the Measuring Units and National Measuring Standards Act, 1973 (Act 76 of 1973), as amended, to keep and maintain all national measuring standards for South Africa. It performs this duty through the CSIR – National Metrology Laboratory (CSIR-NML).

The Time and Frequency Laboratory of the CSIR-NML is responsible for the maintenance and development of the standards in time and frequency. Specifically, the laboratory is responsible for the following standards: time, frequency, phase angle, pulse rise-time and pulse characterization, and time interval. Fiber-optic measurements also reside under the laboratory.

The national measuring standard for time in South Africa consists of two commercial cesium beam atomic clocks. Time transfer is performed using single and multi-channel Global Positioning System (GPS) and Global Navigation Satellite System (GLONASS) receivers. The CSIR-NML is the only contributor in Africa of time transfer data to the Bureau International des Poids et Mesures (BIPM).

In addition to its standards activities the Time and Frequency Laboratory also offers time services in the form of a dial-in Telephone Time Service (TTS), as well as an Internet time service. These services are provided free to any user in Southern Africa.

Recent developments at the CSIR-NML include the development and deployment of multi-channel GPS receivers, the deployment of a multi-channel dual frequency GPS / GLONASS receiver and the re-development of the TTS.

LABORATORY LAYOUT

The Time and Frequency Laboratory consists of four rooms on the top floor of one of the buildings of the Pretoria campus of the CSIR. These four rooms house the clock room, a calibration room, a computer room and a fiber-optics laboratory respectively. The rooms are all air-conditioned. The temperature in all rooms are kept at $(23 \pm 2)^\circ\text{C}$ and the humidity at $(50 \pm 15)\%\text{RH}$.

The calibration room houses the measurement standard for phase angle, a high bandwidth oscilloscope, a fast electrical pulse generator, and several general-purpose instruments. The clock room houses the clocks, the satellite receivers, a TV receiver, and monitoring equipment. The control room houses the time services, monitoring equipment, and a Web server. The fiber optic room houses the fiber optic measurement standards and related equipment. A small section of this room is designated as a development laboratory.

The satellite and television antennas are housed on the roof of the building. The lift tower provides excellent visibility with a mask of less than 5° in all directions. Several steel towers are situated elsewhere on the roof to give visibility to a number of other antennas. Access to the antennas is gained by access holes through the roof of the clock room and control room respectively.

The main satellite receivers reside in the clock room. Several experiments with GPS receivers are ongoing at present and most of these are performed in the control room.

TIME STANDARDS

The National Measurement Standard for Time in South Africa is a commercial cesium-beam atomic clock. This clock is maintained in continuous operation in the clock room of the Time and Frequency Laboratory.

CLOCKS

At present the clock room contains two commercial cesium clocks. One is designated as the master clock, and it is used as the primary reference clock for South Africa. The time and frequency accuracy of the master clock is disseminated to industry through time services and the issue of a monthly Time and Frequency Bulletin [1]. The status of the clocks is monitored on an ongoing basis, and the time transfer values logged to computer. Performance graphs of the clocks are drawn on a weekly and monthly basis, and paper copies of these graphs are archived.

SATELLITE RECEIVERS

The clock room also contains the satellite receivers used for international traceability. At present each clock is monitored by two GPS receivers, an Allan Osborne & Associates (AOA) receiver (either TTR5 or TTR5A) and a locally developed Motorola UT+ based receiver. In addition to these receivers, a dual system GPS (single frequency C/A code) / GLONASS (dual frequency C/A and P code) receiver (3S Navigation R100/30T) is used to monitor the master clock.

DISTRIBUTION EQUIPMENT

Distribution amplifiers are used to distribute the standard frequencies through the Time and Frequency rooms, and to other laboratories in the building requiring traceable signals. The satellite receivers all receive either 5 or 10 MHz signals, and a one pulse per second (1PPS) from the relevant clock in the clock room.

The calibration room, control room, and fiber-optic room receive 10 MHz signals, mainly for use as the external frequency reference for counters and signal generators. A 1 MHz signal is distributed to the control room, where it is used in the generation of lower frequency signals for the Telephone Time Service. 1 MHz and 5 MHz signals are distributed to the calibration laboratory where they are used as required.

A pulse distribution system for the 1PPS signal from the master clock distributes pulses to the calibration and the control room.

The Radio Frequency laboratory and the DC / Low frequency laboratory situated in the same building, each receives a 10 MHz feed, for use as an external clock reference.

OTHER EQUIPMENT

In addition to monitoring the transmissions from GPS and GLONASS, the vertical synchronization pulse from local television broadcasts is monitored. These values are measured every hour, at designated times, and then published (for office hours) in the monthly Time and Frequency bulletin. A project for making these values available in real time on the Internet is currently underway. Local accredited laboratories make use of these values to perform time transfer measurements; using CSIR-NML developed Auto Television Time Transfer Control Units (Auto-TTCUs).

TIME SERVICES

At present the Time and Frequency laboratory has two time services available to users in Southern Africa. These are the Telephone Time Service (TTS), a telephone-based service that can synchronize a wide range of instruments via a modem and computer, and the Internet time service, which provides synchronization via the Internet.

TELEPHONE TIME SERVICE

The TTS has been available to users in Southern Africa since the early 1990's. The service was started mainly as a replacement for the ZUO transmitter that was decommissioned in the late 1980's. At the time the laboratory was faced with financial pressures, and the service was offered on a pay-per-use basis. The structure of payment for this service was revised numerous times to attract new users, but the user basis dwindled nonetheless.

The service was upgraded in 1998 to be fully Y2K-compliant. At the time it was also decided to make the service available free of charge, and to comply fully with the specifications of the International Telecommunication Union (ITU) [2], which states that any time service should transmit Coordinated Universal Time (UTC). Up to that time the service was transmitting South African Standard Time. The

protocol adopted is a variation of the National Institute of Standards and Technology (NIST) Automated Computer Time Service (ACTS) protocol, and is used with permission. The number of users for this service is increasing rapidly. Major users are accredited laboratories, radio stations, the telecommunication authority, sporting clubs, and users that do not want to connect to the Internet due to security concerns.

INTERNET TIME SERVICE

In 1996 it was decided to offer an Internet-based time service. At present the laboratory provides two Internet Time servers, serving the Network Time Protocol (NTP) and the Time protocol. The number of users for this service is expanding on a daily basis, with most of the local Internet Service Providers (ISPs) making use of the servers.

The main server (tick.nml.csir.co.za) is running at Stratum 1, connected to the 1PPS output of the master clock. The other server (tock.nml.csir.co.za) is running at Stratum 2, using the Stratum 1 server as its primary synchronization source.

TIME AND FREQUENCY BULLETIN

The monthly Time and Frequency bulletin has been available since December 1994. The bulletin contains information on the measurements performed in the laboratory, notes on GPS performance and other information. It is available free of charge to anyone that wishes to receive a copy. All copies from January 1996 are also available on the Internet [3].

The measured values of CSIR - GPS as the time interval difference between the 1PPS of the master clock and the 1PPS of GPS as tracked by the 3S Navigation R100/30T receiver is reported. An All-in-View Common-View methodology is followed. All measurements above a mask angle of 15° are used. The daily value is the result of a linear fit to approximately 500 data points, reported to 0 h UTC each day.

CSIR - GLONASS measurements are reported as the least-squares linear interpolation of all measured values in a month, reported to 0 h UTC each day. The number of GLONASS observations is far less than those for GPS, and the calculated random uncertainty of the measured values is larger.

The computed values of UTC – UTC (CSIR) are reported for the previous month. The corrections for UTC (CSIR) are obtained from the BIPM Bulletin “T” [4]. The results are reported to 0 h UTC each day.

The bulletin also contains notes on GPS performance extracted from the United States Naval Observatory (USNO) series 4 bulletins [5]. A number of users in South Africa make use of stand-alone GPS equipment, and this information is used to ensure that no unusable satellites were used for measurements.

Television synchronization pulse measurements are reported for three local transmissions. The offset between the vertical synchronization pulse and the master clock 1PPS is measured and reported on the hour, every hour during the day.

In addition to these measurements, the calculated drift rate of the master clock is reported, as well as information on the TTS, the GPS common-view tracking schedule, leap second announcements, and the

relation between the International Atomic Time (TAI), UTC, and GPS time scales.

OTHER RESPONSIBILITIES

In addition to the responsibilities in time and frequency, the laboratory is also responsible for the national measurement standards for phase angle and for fast electrical pulse characterization, time interval, and fiber-optic measurements.

PHASE ANGLE

The national measurement standard for phase angle is a Clarke-Hess model 5500 phase standard, with a set of model 5002 phase bridges. The phase bridges are calibrated periodically and used to verify the phase standard annually. The laboratory also has a capability for phase measurement, utilizing commercial phase angle meters.

FAST ELECTRICAL PULSE CHARACTERIZATION

Fast electrical pulses are characterized using a high bandwidth oscilloscope, verified using a fast electrical pulse generator. As with phase angle, commercial equipment is being used.

TIME INTERVAL MEASUREMENT

The time-interval measurement and generation capability is based on commercially available equipment. For measurement of single shot events the laboratory can generate and measure signals of down to some tens of ps.

FIBER OPTICS

The fiber-optics laboratory was integrated with the Time and Frequency Laboratory in 1999, due to the similarity between measurements performed in the two laboratories. The services offered by the fiber-optics laboratory include calibration of fiber optic power meters, fiber-optic attenuators, Optical Time Domain Reflectometers (OTDR), wavelength meters, and optical delay lines.

FUTURE WORK

At present the focus in the Time and Frequency Laboratory is the reduction of time transfer uncertainties. To further reduce these uncertainties a geodetic quality GPS receiver will be acquired, and a project started to perform carrier-phase measurements using this receiver.

Further development of the Motorola-based GPS receivers are underway. The new M12 Oncore receiver from Motorola is being evaluated as a replacement for the current UT+ Oncore receivers. There are some drawbacks in using the UT+, which can possibly be overcome using the M12.

DISCLAIMER

Certain trade names and company products are mentioned in text of this paper. In no case does such mention imply recommendation or endorsement by the CSIR - National Metrology Laboratory, or the

CSIR, nor does it imply that the products are necessarily the best available for the purpose.

REFERENCES

- [1] Standard Time and Frequency Bulletin, CSIR - National Metrology Laboratory, Pretoria, South Africa, ISSN 1024-1612.
- [2] "Use of Time Scales in the Field of Standard-Frequency and Time Services," ITU-R Recommendation 485-2, 1990.
- [3] "Standard Time and Frequency Service Bulletin,"
<http://www.nml.csir.co.za/services/timepub/tfpubl.html>
- [4] BIPM Bulletin "T," <ftp://62.161.69.5/pub/tai/publication/cirt.xxx>
- [5] USNO Series 4 bulletins, <ftp://tycho.usno.navy.mil//pub/series/series4.xxxx>

Questions and Answers

FRANCOIS MEYER (Observatoire de Besançon, France): My question is about your NTP instrument called tick. What kind of hardware is used?

LOUIS MARAIS: We are running a Pentium 133 using a PDS 2.16 with general modifications by John Hay.

MEYER: Okay. And the 1PPS of an atomic clock is used to give the synchronization?

MARAIS: That's right.

MEYER: And what about possible 1-second or multiple of 1-second jumps in the — ?

MARAIS: We use GPS-based time to determine the time to ... (?) of the masers.

MEYER: And this is integrated in the NTP software?

MARAIS: No, it's not. We use an off-laboratory source for that. So we use a server on the CSIR campus that's not in our laboratory.

WLODZIMIERZ LEWANDOWSKI (BIPM, France): Do you have the TSA antenna temperature-stabilized?

MARAIS: Yes, we do.

LEWANDOWSKI: And this is connected on your 3S Navigation receiver right now?

MARAIS: Yes.

JACQUES AZOUBIB (BIPM, France): I am wondering why you aren't sending the BIPM your clock data? You have two clocks—

MARAIS: Yes, the other clock is three times worse than the HP. So I don't think it will add any value.

DETECTION OF THE GRAVITATIONAL REDSHIFT OF THE CESIUM FREQUENCY STANDARD AT CRL

Mizuhiko Hosokawa, Noboru Kotake,
and Kuniyasu Imamura, and Noriyuki Kurihara
Communications Research Laboratory
Nukui-kita 4-2-1, Koganei, Tokyo 184-8795, Japan
Tel: +81-42-327-7557; Fax: +81-42-327-6694
E-mail: hosokawa@crl.go.jp

Abstract

We have detected the gravitational redshift of a Cs frequency standard that has been transported from CRL Tokyo headquarters, at an altitude of 80 m, to Mt. Ohtakadoya LF standard frequency station, located at an altitude of 794 m, about 250 km far from the CRL Tokyo headquarters. In the Mt. Ohtakadoya LF station, three Cs clocks are equipped to be the references of standard frequency radio signal emission, and they are linked with UTC(CRL) by the GPS common-view time transfer. By using this link, we can compare the frequency of any standards in CRL Tokyo and the Mt. Ohtakadoya LF station with UTC(CRL). An HP5071A Cs frequency standard with a normal tube has been transported by car from the CRL Tokyo headquarters to the LF station on 27 April 2000. After the transport, we observed that the frequency of the Cs standard became higher by about 4.6×10^{-14} . According to General Theory of Relativity, a 700-m altitude difference will cause a 7.8×10^{-14} frequency difference. Considering the stability of the Cs standard and the accuracy of time transfer, the observed frequency shift shows an agreement with the theoretically predicted gravitational redshift.

INTRODUCTION

Detection of the relativistic effects by using portable atomic clocks has been conducted by many groups [1,2]. Today, there is little few significance in such measurements for the test of relativity. The theory of General Relativity has been tested in many cases and it is recognized as the reliable fundamental theory of precise space-time measurements within today's measurement accuracy [3]. Still, the detection of such effects would be important to prove the accuracy and stability of a system.

Recently, CRL has constructed a new LF frequency standard station at the top of Mt. Ohtakadoya, 250 km far from the CRL Tokyo headquarters and the altitude of that is 794 m. The LF station is equipped with three normal-tube HP5071A clocks, and a TTR-6 GPS receiver. In December 1999, one of the Cs standards went wrong and we fixed it. After that, we had watched the performance of this Cs standard for more than 1 month and then we transported the clock from the CRL Tokyo headquarters to the Mt. Ohtakadoya LF station. We call this clock Cs#28.

The altitude difference between these stations is about 700 m. These conditions seemed enough to detect the gravitational redshift. Following the precedents, we tried to detect the gravitational redshift of the frequency of Cs#28 from our regular time comparison data. In this paper, we will show the result of the frequency shift measurement.

GRAVITATIONAL REDSHIFT

The proper time of the atomic clock changes according to the gravitational potential where it placed. As the result, in the case of the transported clock near the earth's surface, the gravitational redshift is

$$\Delta f/f = 1.1 \times 10^{-16} \Delta h \quad (1)$$

where $\Delta f/f$ is the fractional shift of the frequency in Hz and Δh is the altitude difference between before and after the transport [3].

The clock room in CRL Tokyo is at an altitude of 80 m. That in the LF station is at an altitude of 790 m. The difference between them is about 710 m. Therefore, the expected gravitational redshift of the frequency is 7.8×10^{-14} .

EQUIPMENT AND ENVIRONMENT OF EACH STATION

CRL Tokyo Headquarters

At CRL Tokyo, we have nine HP5071A commercial cesium clocks with high-performance tubes. Using these clocks, we generate the synthesized atomic time scale UTC(CRL) that is used as the reference of the TTR-6 at CRL. The time difference between UTC(CRL) and every clock is measured every 4 hours. These measurement data are taken in a workstation and used as the basis of the calculation of the synthesized atomic time. In the clock room, the temperature and the humidity are kept to be 26 degrees and the 50 %, respectively. The room is equipped with an electromagnetic wave shield to shut down the intrusion of unfavorable perturbation.

Mt. Ohtakadoya LF Station

At the LF station, we usually have three HP5071A cesium standards with normal tubes. One of them is selected as the master clock in the station, while others are used as backup clocks. Here we denote the master clock as MC(LF). As at the Tokyo headquarters, the time difference between MC(LF) and other cesium clocks are measured every 4 hours. MC(LF) is also used as the reference of the TTR-6 GPS receiver in the LF station. The receiver is set to measure the GPS time according to the same BIPM schedule as at CRL. In the clock room of the LF station, the humidity is kept to be 50%, the same as that at the Tokyo headquarters. On the other hand, the temperature of that is 26 degrees, 3 degrees higher than that at the Tokyo headquarters. The station is equipped not only with an electromagnetic wave shield, but also a static magnetic shield.

Transport

On 27 April of this year, we transported the clock Cs#28 from the CRL headquarters to the Mt. Ohtakadoya LF station. The distance between them is about 250 km. The clock was transported by car. It took 6 hours from Tokyo headquarters to the LF station. During

that transport, a battery was provided so that the clock could be kept working without any discontinuity.

ESTIMATION OF FREQUENCY SHIFT

Using these data of the measurement and time transfer link, the frequency deviation of Cs#28 at each period and, thus, the frequency shift were obtained. Figure 3 shows the fractional frequency deviation of CS#28 from UTC(CRL), measured at CRL Tokyo in April before the transport. On 17 and 18 April, we put Cs#28 to the frequency tuning test. The effect of that test was apparent after a period. It is also shown that after the test, the frequency recovered to be the same as that before the test. Eliminating this period, the average deviation between CS#28 and UTC(CRL) is -14.3×10^{-14} .

In this period, GPS common-view link data show that the fractional frequency deviation of UTC(CRL) from MC(LF) is -5.0×10^{-14} (Figure 4). Hence, the deviation of Cs#28 from MC(LF) before the transport is -19.3×10^{-14} . Figure 5 shows the GPS common-view link between UTC(CRL) and MC(LF). On 3 May, we steered the frequency of UTC(CRL) by 2×10^{-14} . In the GPS common-view link, this steering is appeared as a frequency change of 1.8×10^{-14} . So it seems that the accuracy of the link would be a few parts in 10^{15} .

The fractional frequency deviation of Cs#28 from MC(LF) after the transport is shown in Figure 6. It seems that it took about 2 weeks until the frequency of Cs#28 settled. The average deviation after the period is -15.7×10^{-14} .

In addition to these frequency deviation measurements, we measured the frequency shift of a normal-tube HP5071A due to temperature variation. So far, we have obtained the typical temperature coefficient for a normal-tube HP5071A of -3×10^{-14} per 10 degrees (Figure 7). This result is obtained by a few days' measurements at each temperature. So it seems we have to confirm the measurement of the coefficient in the longer period. As far as we adopt this result, we can expect that the frequency shift due to the temperature variation of 3 degrees is expected to be about -1×10^{-14} .

For the evaluation of the uncertainty of the measurement, we use the Allan variance of the Cs standards. In the case of the frequency stability between UTC(CRL) and normal-tube HP5071A, the Allan variance in a 5-day average period is observed to be about 2×10^{-14} . That between two normal-tube HP5071As would be a bit worse, about 2.5×10^{-14} . The uncertainty of the GPS common-view link is much less than that, so that we can neglect it here. Using these values, we estimate that the total uncertainty in the frequency measurement would be 3.2×10^{-14} .

CONCLUSIONS AND DISCUSSION

Using the frequency deviations shown in the previous section, the result of the frequency shift of Cs#28 after the transport to the LF station is

$$-15.7 \times 10^{-14} - (-19.3 \times 10^{-14}) - (-1 \times 10^{-14}) = +4.6 \times 10^{-14}. \quad (2)$$

Considering the total uncertainty of 3.2×10^{-14} , this result of the frequency shift seems to be consistent with the theoretical value of 7.8×10^{-14} , though it is not such good agreement. Some factors are considered as problems of this trial. Just about 10 days before the transport, the frequency tuning test was conducted. Also, frequency steering of UTC(CRL) was conducted a

few days after the transport. These were mainly due to the fact that the detection of gravitational redshift was not originally planned when the clock was transported. Thus, we should plan the experiment more carefully next time. Also, we should examine the temperature effect more definitively. Furthermore, we should better check the frequency shift due to the difference of the static magnetic fields between Tokyo headquarters and the LF station. However, this shift would be small in so far as the C field servo motor of the clock works well and there is no interruption of the clock operation during transport. Therefore, in many aspects, further investigation will be needed.

However, we conclude that the link, equipment, and the environment in CRL Tokyo and the Mt. Ohtakadoya LF station are good enough for the detection of the gravitational redshift. In the future, we will have occasion to maintain or replace the clocks in the LF station. In that time we would like to continue the trial to detect the shift and to confirm the accuracy and the stability of the frequency standards system at CRL.

ACKNOWLEDGMENTS

The authors thank Ms. Y. Hanado and Ms. H. Usui at CRL for useful help in data analysis.

REFERENCES

- [1] J. C. Hafele, and R. E. Keating 1972, in "Around-the-world atomic clocks," *Science*, **177**, 166.
- [2] S. Iijima, and K. Fujiwara 1978, "*An experiment for the potential blue shift at the Norikura corona station,*" *Annals of the Tokyo Astronomical Observatory Second Series*, **XVII**, 1, 68.
- [3] B. Guinot 1997, "*International report: Application of general relativity to metrology,*" *Metrologia*, **34**, 261-290.

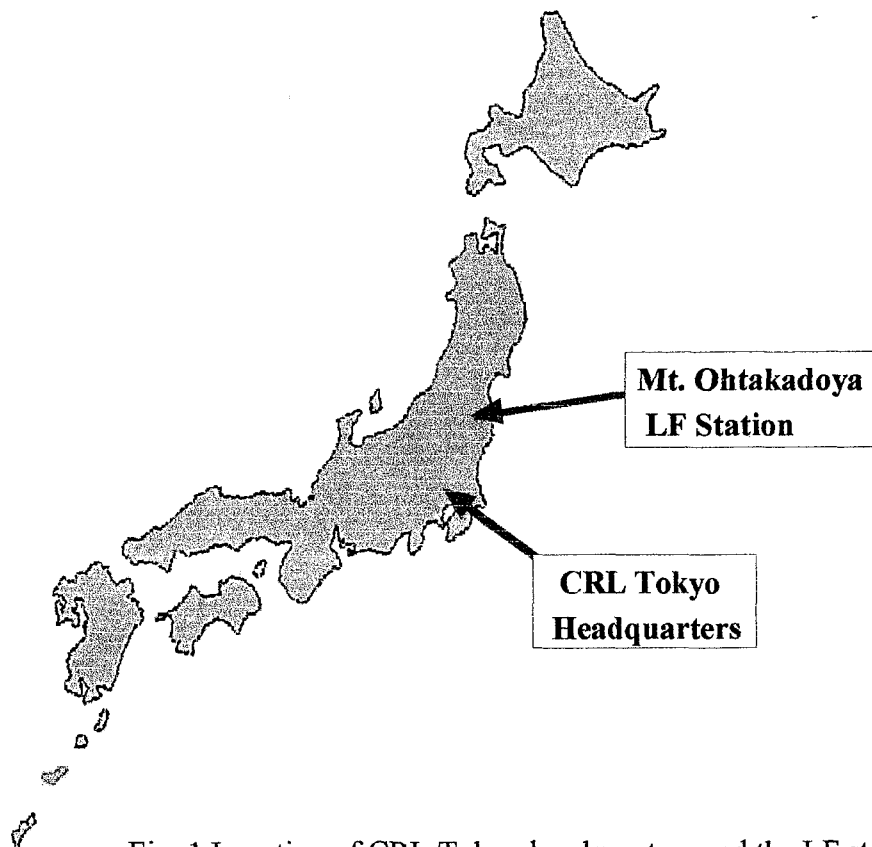


Fig. 1 Location of CRL Tokyo headquarters and the LF station

	CRL Headquarter	LF station
Altitude	80m	790m
Temperature	23°C	26°C
humidity	50%	50%
Shield	Electromagnetic wave	Electromagnetic wave and static magnetic field
Reference of TTR6	UTC(CRL)	MC(LF)

Table 1 Specifications of both stations

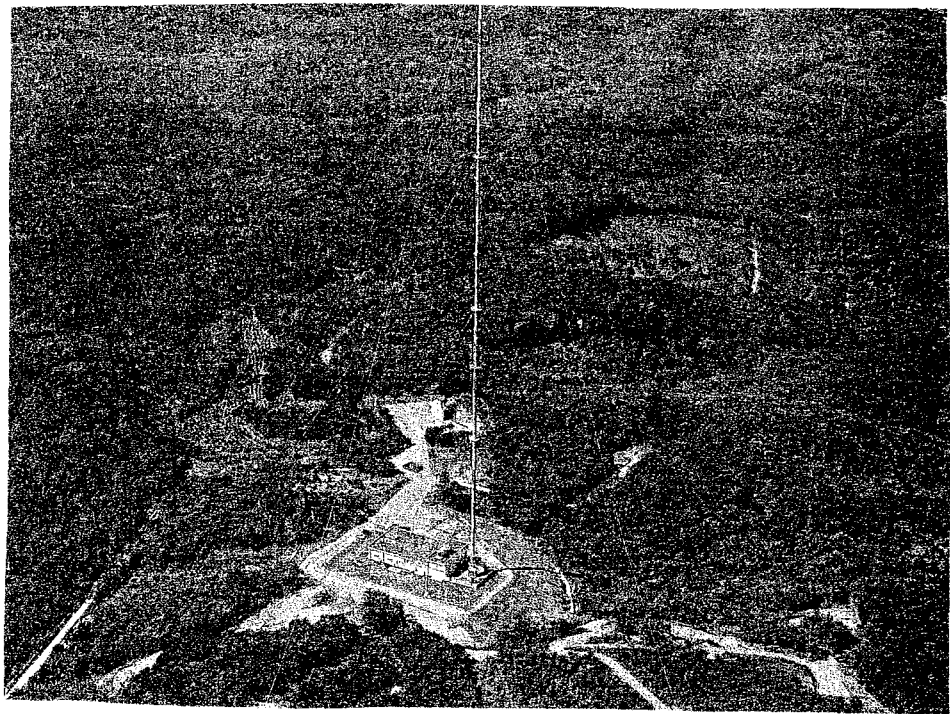


Fig. 2 LF station in Mt. Ohtakadoya

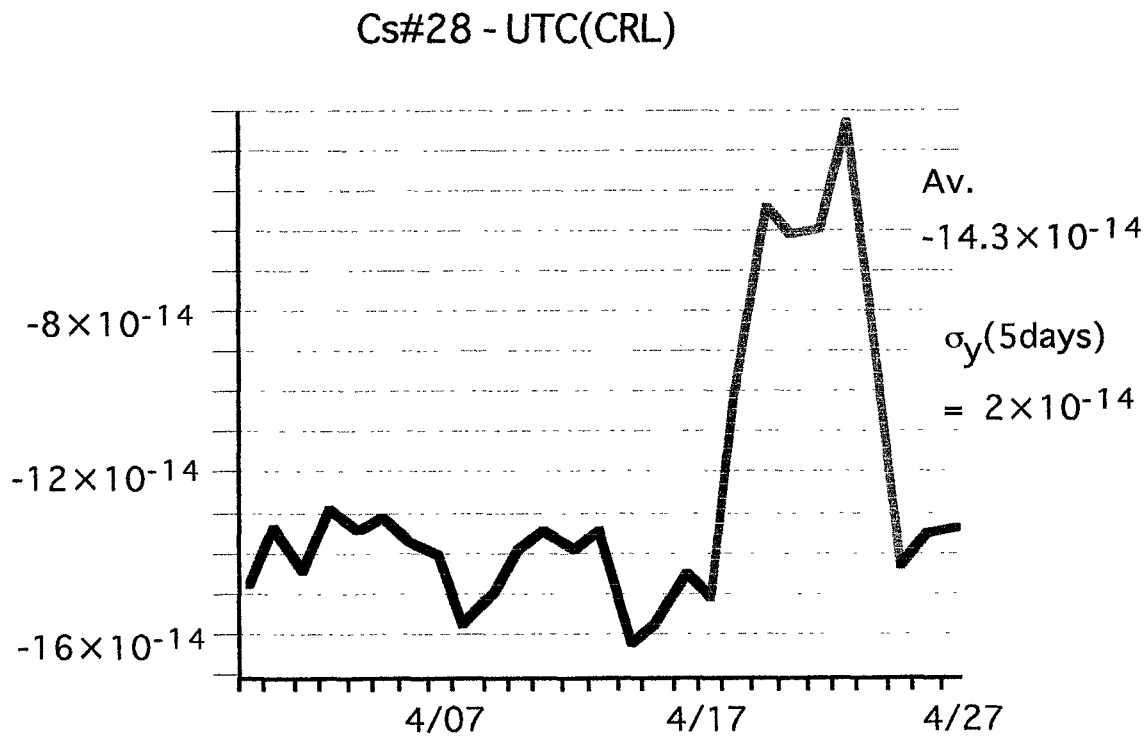


Fig. 3 Frequency deviation of Cs#28 from UTC(CRL) before transportation

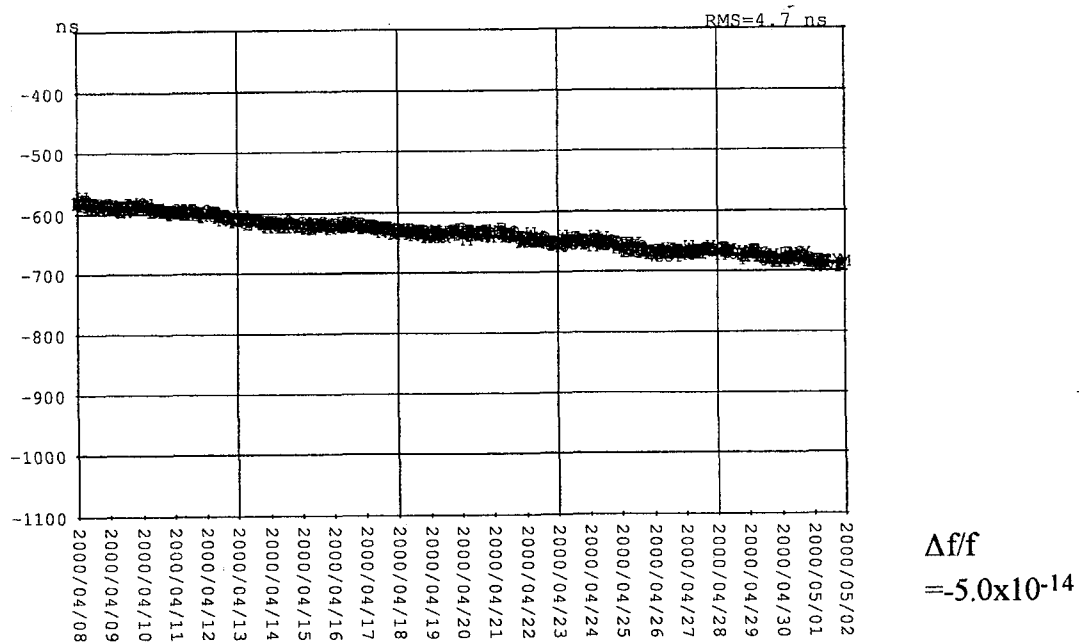


Fig. 4 GPS common-view link between UTC(CRL) and MC(LF Stat.) in April

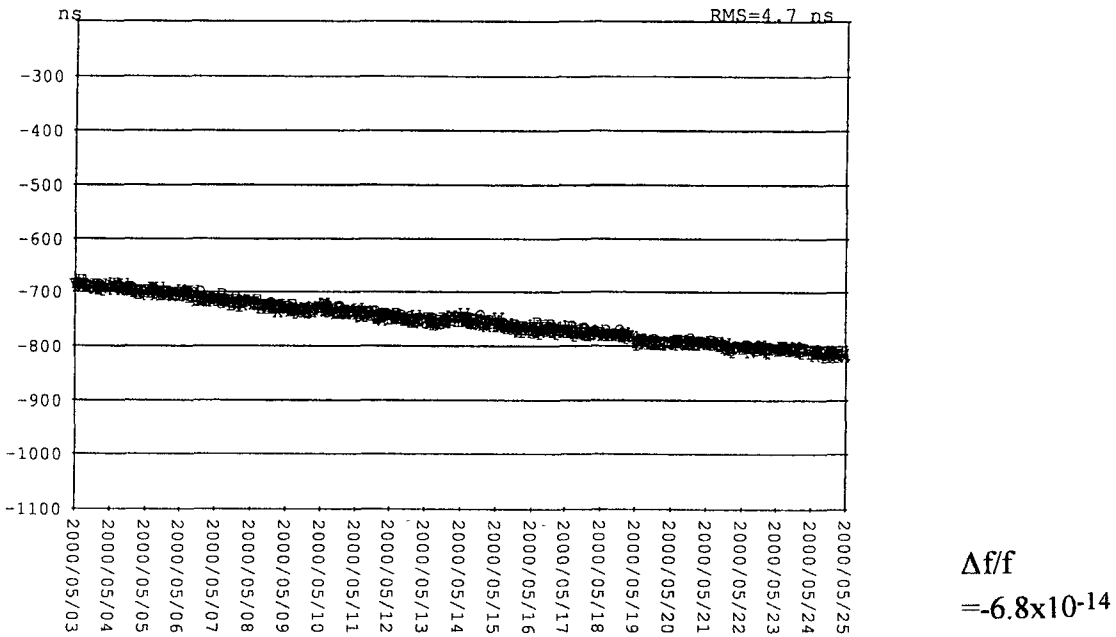


Fig. 5 GPS common-view link between UTC(CRL) and MC(LF Stat.) in May

Cs#28 - MC(LF St.)

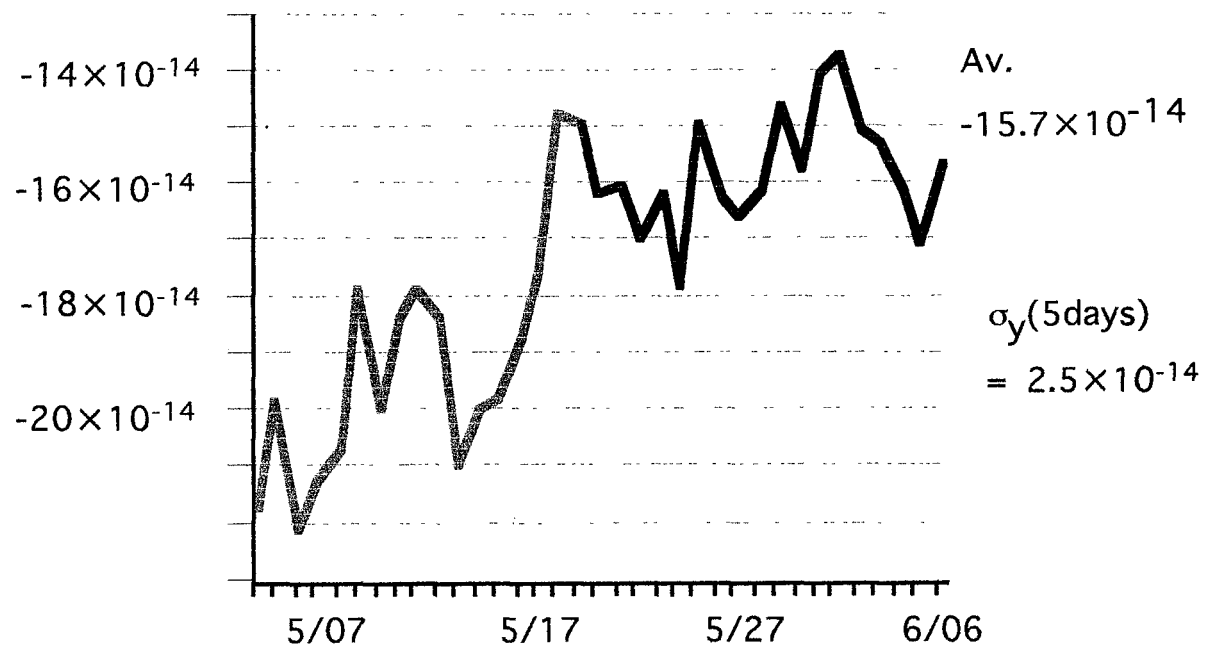


Fig. 6 Frequency deviation of Cs#28 from MC(LF) after the transportation

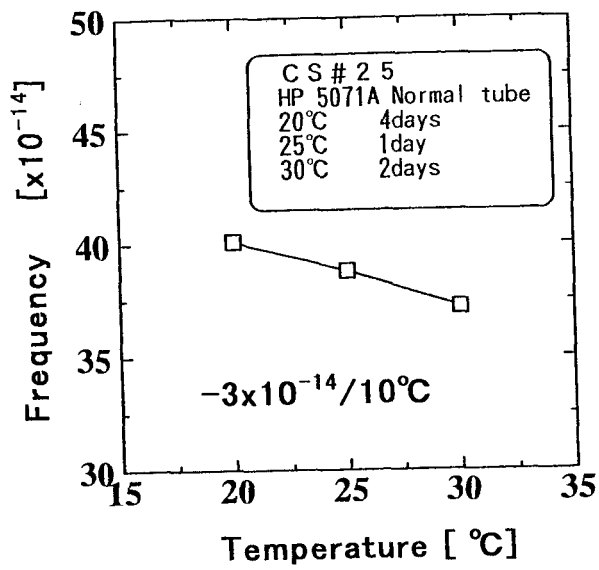


Fig. 7 Frequency shift of the same type Cs standard due to the temperature variation

MILLISECOND PULSAR OBSERVATION AT CRL

Y. Hanado, Y. Shibuya, M. Hosokawa, M. Sekido, and M. Imae
Communications Research Laboratory
4-2-1, Nukui-kitamachi, Koganei, Tokyo 184-8795, Japan

Abstract

We will report the current status of millisecond pulsar timing observation at CRL. Weekly observation of PSR1937+21 using the 34-m antenna at Kashima Space Research Center has been on going since November 1997. Recently we eliminated systematic trends that were apparent in the data, and estimated the pulsar parameters of PSR1937+21. Standard deviation of timing residuals is 2.4 μ s for about 3 hours' pulse-integration. The frequency stability of PSR1937+21 is 10^{-13} for an averaging time of one year, which demonstrates the possibility of constructing a pulsar time scale with a system using a small antenna.

INTRODUCTION

Pulsars are thought to be rotating neutron stars radiating radio beams from their oblique magnetic poles. Some pulsars have short pulse periods of millisecond order. These millisecond pulsars are known to keep the extremely stable pulse timings over long periods. The millisecond pulsar PSR1855+09 has a pulse period of 5.4 ms pulse rates, and its fractional frequency stability is about the order of 10^{-15} over 8 years, which is comparable to a cesium atomic clock [1; here after paper I].

From such rotational stability, millisecond pulsars are expected as reference time standards. The tie of pulsar time and atomic time are studied to construct a new stable time scale [2][3][4]. In addition, pulsar timing contributes to the various researches. Pulsar timing depends on the time scale and ephemeris used for the analysis, shown in paper (I), so it is useful for the comparison of some time scales and ephemerides. It also contributes to the reference frame tie. The pulsar's position determined by timing observation is based on the Earth orbit-oriented reference frame, and the position determined by VLBI observation is based on the extragalactic reference frame. By comparing both positions, the different reference frames are combined [5]. Pulsar timing is also expected as the probe for the interstellar medium and gravity in the propagation path.

Communications Research Laboratory (CRL) aims to apply millisecond pulsars to the construction of a new time scale; this entails theoretical research [6], VLBI observation [7], and timing observation. As for the timing observation, we developed an observation system that uses the 34-m antenna at Kashima. Signals from millisecond pulsars are quite weak and the 34-m antenna is not large enough to detect them, so we improved the system's sensitivity by using wide-band observation and longtime integration. The observation system has been completed, and observation of the millisecond pulsar PSR1937+21 has been on going since November of 1997.

However, we encountered some troubles in that the observed pulse phases showed systematic trends during a day and longer periods, which was reported in PTTI'98 [8]. We have checked our observation system and analysis program carefully, and recently found that these trends are caused by some reasons. The daily trend was caused by insufficient calibration of the Earth rotation, and long-term trend was caused by insufficient correction of observation time and frequency. We solved these problems, and by re-processing the data, obtained a frequency stability of 10^{-13} over 1 year and an estimate of the pulsar's parameters. In this paper, we report an recent progress in millisecond pulsar observation and observation results of PSR1937+21 at the 34-m antenna.

OBSERVATION SYSTEM

Figure 1 shows a block diagram of the observation system. We use the right-handed-circularly-polarized signal in S-band frequency. As for the antenna parameters in S-band, the system noise temperature is 71K, and the efficiency is 65%. An IF signal with 200MHz bandwidth was divided into four bands by the video converter, and each 50MHz bandwidth was divided into 256 channels by the acousto-optic spectrometer (AOS). The frequency resolution is about 200kHz. The 256 channels of each AOS unit were serially transported to the video averaging processor. The transportation trigger clock was synchronized to 1/100 of the pulsar period, giving a time resolution of 16 μ s for PSR1937+21. The video averaging processor works as an 8-bit A/D converter and an averaging processor. It can average a maximum of about 17 million pulses for each channel. The averaged signals were recorded at host computer #1. After the observation, dispersion delay corresponding to the observation frequency was calibrated in each channel; then the signals of all channels were combined.

The averaging trigger clock must be synchronized to the observed pulse period. The observed pulse period is not constant because of the Doppler effect, so host computer #2 calculated the predicted period and controlled the synthesizer in real time. The predicted value was calculated by the program TEMPO. TEMPO is the pulsar timing analysis package developed by the Princeton pulsar group [9], which can calculate the predicted period and pulse phase at any observatory. The observation time was obtained from the laboratory clock, which is phase-locked to a hydrogen maser. The averaging start time was measured by the time-interval counter. The time offset of the laboratory clock from UTC was monitored using a GPS receiver. All the oscillators were phase-locked to the hydrogen maser.

OBSERVATION OF PSR1937+21

TIMING RESIDUALS

Regular observation of the millisecond pulsar PSR1937+21 has been on going since November 1997. This pulsar is useful as a system performance check, because it is the brightest millisecond pulsar in the northern sky and has been observed at other stations for a long period of time. The observations are carried out once a week, and 8 hours per day. Figure 2 shows the pulse profile obtained from 50MHz bandwidth signals and 27 minutes of integration.

From such profiles, we determined the peak phases of the pulses, transformed them to the arrival time, compared them with the predicted time of arrivals (TOA), and obtained the residuals. The predicted TOAs were calculated by TEMPO. We adopted DE200 as the ephemeris and UTC as the reference

time scale. We used only the data of AOS #1 for the analysis, because other three units experienced hardware problems during the measurement period. Figure 3 shows the residuals, which is the same as results reported in PTTI'98. Figure 3(b) shows an example in 1 day picked up from Fig. 3(a). Some systematic trends are apparent. There is a drift on most observation days. We determined that the daily drift was caused by insufficient calibration of Earth rotation. The long-term trend was caused by a variety of reasons. Some were due to miscalibration of the observation frequency at the AOS. Others were due to insufficient calibration of the laboratory time offset. We fixed these problems and finally obtained a smooth line, which is shown in Fig. 4.

PARAMETER FITTING

The residuals in Fig. 4 still show a drift, so we carried out a parameter fitting for seven parameters: frequency f , frequency deviation df/dt , Right Ascension RA, Declination Dec, proper motion PRA, Pdec, and parallax p_x . We used the initial parameters derived from paper I. After the first fitting, the drift in Fig. 4 disappeared and the residuals were distributed without biases (Fig. 5). The standard deviation of the residuals is $6.4 \mu\text{s}$ for the 27-minute pulse-integration. We changed the initial parameters and did the fitting again; the parameters converged to the same values. Table 1 compares the parameters after fitting with those of paper I. Except for the frequency and its derivative, all values agree with Paper I within each error range. The frequency that is the reciprocal of the period agrees with paper I's value to 11 digits. The frequency derivative agrees to the order of 10^{-17} . A more reliable parallax will be obtained from the long years' observation.

FREQUENCY STABILITY

We estimated the frequency stability by the Allan variance of the residuals after fitting. At first we calculated the representative TOA for each observation day by averaging all TOAs in one day (Fig. 6). They corresponded to the TOAs obtained from the pulses after about 3 hours' integration. The standard deviation was $2.4 \mu\text{s}$ for the residuals of each day. From these residuals, we calculated the Allan variance for the time intervals of 7, 14, 21, ..., 364 day. Figure 7 shows the frequency stability. It seems to be proportional to $1/\tau$, which suggests the white PM system noise is dominant in this region. The stability at one year is about 1×10^{-13} , which is the expected order from our system's performance.

CONCLUSIONS

Continuous observation of PSR1937+21 at Kashima 34-m antenna has been on going since 1997. Timing residuals showed an unusual behavior at first, but the reasons have become clear recently. We solved them and then calculated the pulsar parameters from our data. The fitted parameters are about the same as those of paper I, which means the calculation was carried out properly. After parameter fitting, the residuals are distributed without bias. The standard deviation is $6.4 \mu\text{s}$ for the residuals obtained from the pulses after 27 minutes' integration, and $2.4 \mu\text{s}$ for the residuals obtained after about 3 hours' pulse-integration. They are the results obtained from the observation with 50MHz bandwidth, and if 200MHz bandwidth is available, the standard deviation will be about $1 \mu\text{s}$. The frequency stability is about 10^{-13} at 1 year. These results demonstrate the possibility of using our system for millisecond pulsar timing observation. We plan to improve the precision of our system

and use it to observe other millisecond pulsars for contributing to the construction of pulsar time scale.

ACKNOWLEDGMENTS

The authors thank Dr. Demetrios N. Matsakis of U. S. Naval observatory, and Dr. Matthew Bailes of Swinburne University of Technology for their kind advice.

REFERENCES

- [1] V. H. Kaspi, J. H. Taylor and M. F. Ryba, "High-precision timing of millisecond pulsars. III. Long-term monitoring of PSRs B1855+09 and B1937+21," *Astrophys. J.*, 428, pp.713-728, 1994.
- [2] B. Guinot and G. Petit, "Atomic time and the Rotation of Pulsars," *Astron. Astrophys.*, 248, pp. 292-296, 1991.
- [3] R. S. Foster and D. N. Matsakis, "Application of Millisecond Pulsar Timing to the Long-Term Stability of Clock Ensembles," Proceedings of the 27th Annual Precise Time and Time Interval (PTTI) Applications and Planning, 29 November-1 December 1995, San Diego, California, USA, pp. 447-455.
- [4] G. Petit and P. Tavella, "Pulsars and Time Scales," *Astron. Astrophys.*, 308, pp.290-298, 1996.
- [5] N. Bartel, J. F. Chandler, M. I. Ratner, I. I. Shapiro, R. Pan, and R. J. Cappalo, "Toward a frame Tie Via Millisecond Pulsar VLBI," *Astron. J.*, 112, No.4, pp. 1690-1696, 1996
- [6] M. Hosokawa, K. Ohnishi, and T. Fukushima, "Uncertainty of pulsar time scale due to the gravitational time delay of intervening stars and MACHOs," *Astron. Astrophys.*, 351, pp. 393-397, 1999.
- [7] M. Sekido, M. Imae, Y. Hanado, Y. P. Ilyasov, V. Oreshiko, A. E. Rodin, S. Hama, J. Nakajima, E. Kawai, Y. Koyama, T. kondo, N. Kurihara, and M. Hosokawa, "Astrometric VLBI observations of PSR0329+54," *Publ. Astron. Soc. Japan*, 51, pp. 595-601, 1999.
- [8] Y. Hanado, M. Imae, M. Hosokawa, M. Sekido, A. Kaneko, and Y. SHibuya, "Millisecond pulsar observation at CRL," Proceedings of the 30th Annual Precise Time and Time Interval (PTTI) Applications and Planning, 1-3 December 1998, Reston, Virginia, USA, pp. 89-97.
- [9] J. H. Taylor and J. M. Weisberg, "Further experimental tests of relativistic gravity using the binary pulsar 1913+16," *Astrophys. J.*, 345, pp.434-450, 1989.

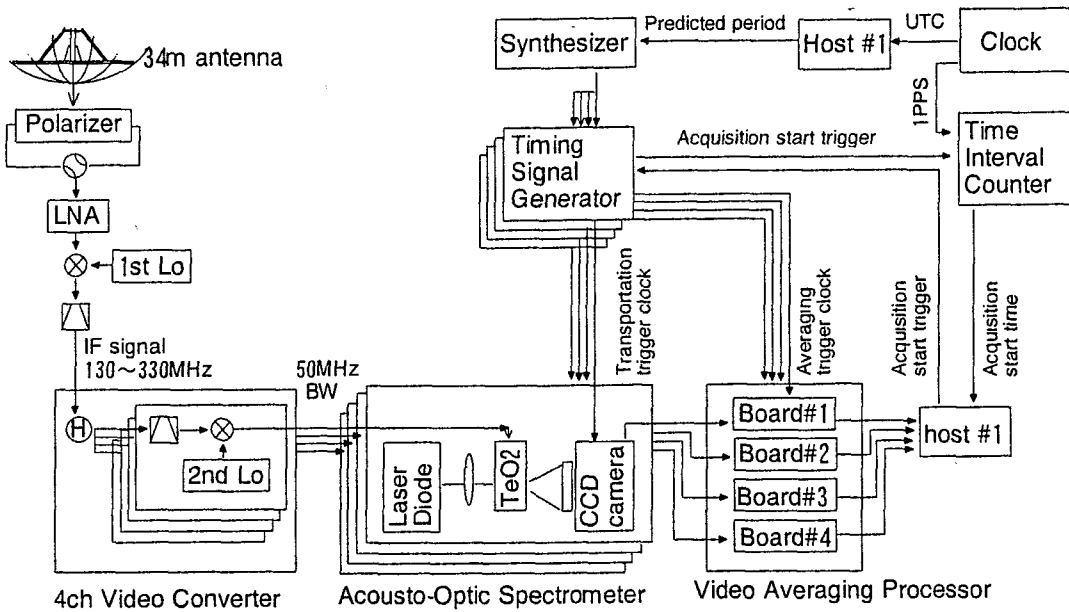


Figure 1: Millisecond pulsar observation system at CRL.

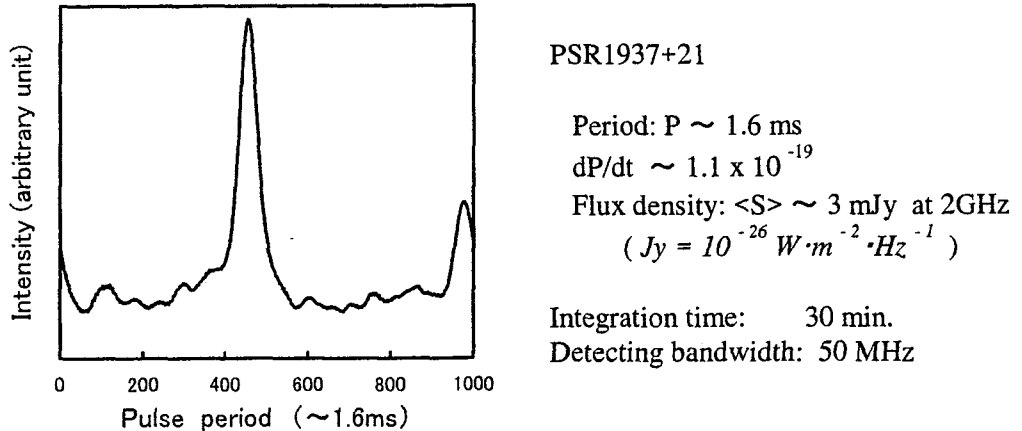


Figure 2: Pulse profile of MSP1937+21. Integration time is 27 minutes and observation bandwidth is 50MHz

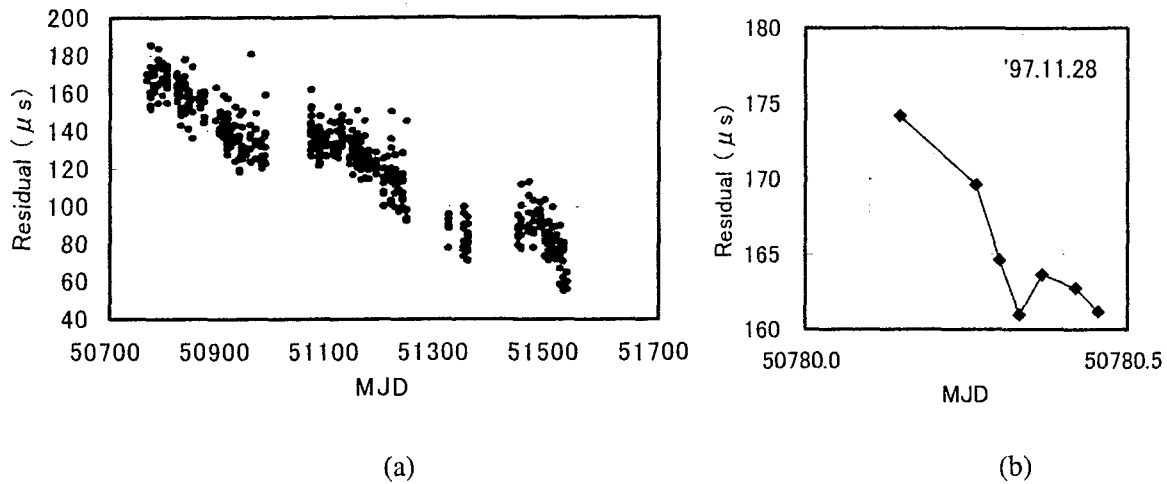


Figure 3: Timing residuals after the first analysis. Each residual is obtained from the peak phase of the pulse after the 27-minute integration. (a) Full data from Nov. '97 to Mar. '00. The windings are due to the insufficient calibration of observation time and frequency. (b) One day's example. The drift is due to the insufficient calibration of earth rotation parameter.

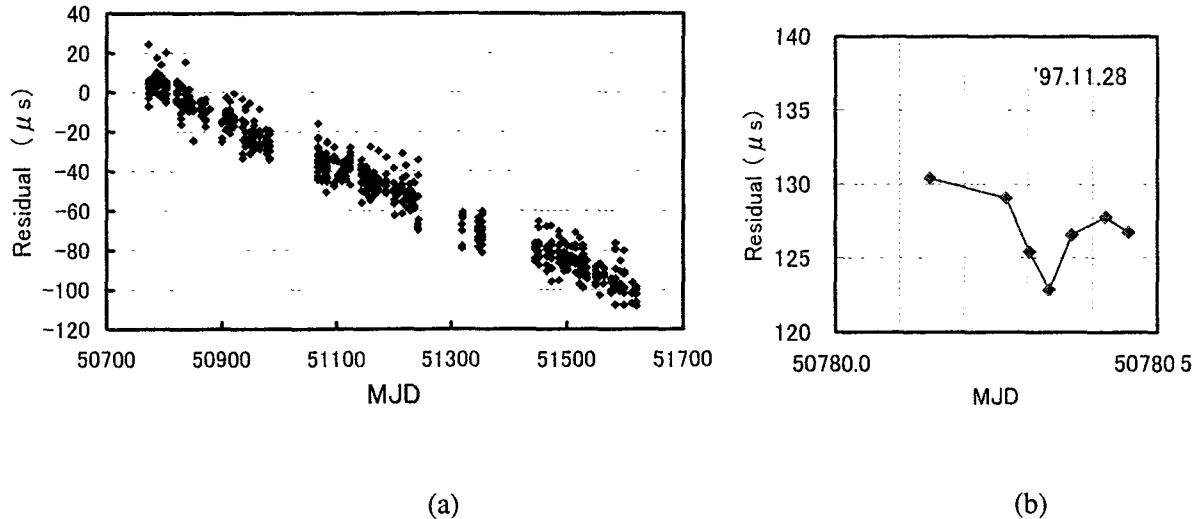


Figure 4: Timing residuals after fixing the problems. (a) Full data. (b) One day's example.

Table 1: Comparison of parameters obtained for PSR1937+21

	Kaspi, APJ,428,'94 Arecibo 305m antenna	CRL ('97nov.-'00Mar.) Kashima 34m antenna
RA	19h 39m 38s.560210	19h 39m38s.560300 (± 0.0002)
Dec	21°34'59".14166	21°34' 59".14042 (± 0.005)
Parallax (mas)	0.12	1.32 (± 1.8)
Pmotion(RA)(mas/yr)	-0.130	-0.284 (± 0.3)
Pmotion(Dec) (mas/yr)	-0.464	-0.378 (± 0.5)
Frequency (Hz)	641.9282626022265	641.9282626019291 ($\pm 3e^{-10}$)
dF/dt (s ⁻²)	$-4.331671 \times 10^{-14}$	$-4.331327 \times 10^{-14}$ ($\pm 9e^{-19}$)

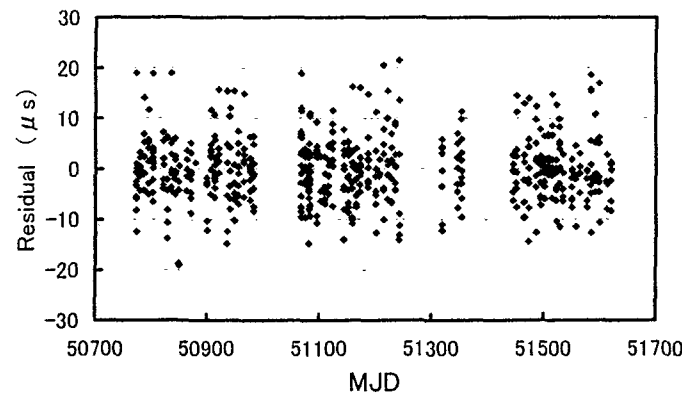


Figure 5: Timing residuals after the parameter fitting. Standard deviation is 6.4 μ s.

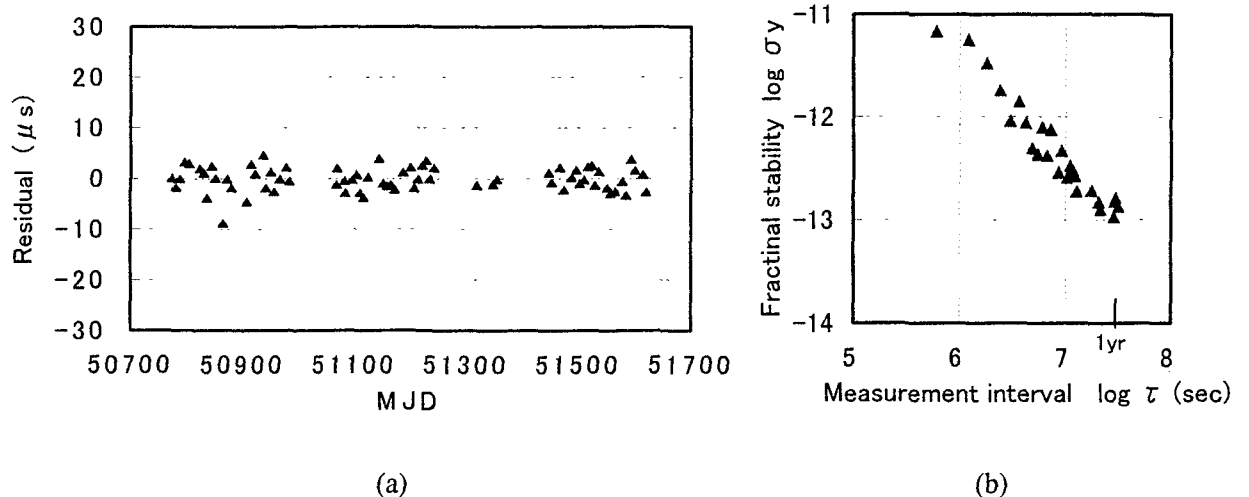


Figure 6. (a) Timing residuals for one day's averaging. Standard deviation is 2.4 μ s
(b) Allan variance.

PTTI 2000

ATTENDEES LIST

Franklin G. Ascarrunz
SpectraDynamics
1212 Main St.
Louisville, CO 80027
Tel: 303-665-1852
Fax: 303-604-6088
franklin@spectradynamics.com

Glenn J. Atkinson
Honeywell
4060 E. Bijou Street
Colorado Springs CO 80909
Tel: 719-637-6182
Fax: 719-380-7144
glenn.atkinson@atsc-dsc.com

Jean-Pierre Aubry
Oscilloquartz - SA
Br,vards 16
CH-2000 Neuchatel
Switzerland
Tel: 41-332-722-5555
Fax: 41-337-722-5556

Jacques Azoubib
BIPM
Pavillon de Breteuil
F-92312 Sevres Cedex
France
Tel: 33-1-45-077-062
Fax: 33-1-45-077-062
jazoubib@bipm.org

Françoise S. Baumont
Observatoire de la Côte d'Azur
Avenue N. Copernic
Grasse
France
Tel: 33-493-40-5338
Fax: 33-493-40-5332
baumont@obs-azur.fr

Ronald L. Beard
Naval Research Laboratory
4555 Overlook Avenue SW
Washington, DC
Tel: 202-404-7054
Fax: 202-767-2845
beard@juno.nrl.navy.mil

John E. Berberian
Agilent Technologies
5301 Stevens Creek Boulevard
Santa Clara, CA 95051
Tel: 408-553-2026
Fax: 408-553-6591
john_berberian@agilent.com

Bill Bollwerk
U.S. Naval Observatory
Alternate Master Clock
400 O'Malley Avenue
Ste 44
Schriever AFB, CO 80912-4044
Tel: 719-567-6740
Fax: 719-567-6763
bill.bollwerk@schriever.af.mil

Martin B. Bloch
FEIC
55 Charles Lindburg Blvd.
Uniondale, NY
Tel: 516-784-4500
Fax: 516-784-4340

Vincent Boyer
NIST
100 Bureau Drive, MS 8424
Gaithersburg, MD 20878-8424
Tel: 301-975-6583
Fax: 301-975-8272
Vincent.Boyer@nist.gov

Lee A. Breakiron
U.S. Naval Observatory
3450 Massachusetts Ave., NW
Washington, DC 20392-5420
Tel: 202-762-1092
Fax: 202-762-1511
lab@kepler.usno.navy.mil

James Buisson
AEI
3500 Lake Winds Lane
Bumpass, VA 23024
Tel: 202-404-7062
Fax: 202-767-2845
buisson@juno.nrl.navy.mil

Eric A. Burt
U.S. Naval Observatory
3450 Massachusetts Ave., NW
Washington, DC 20392-5420
Tel: 202-762-0308
Fax: 202-762-1421
burt@atom.usno.navy.mil

Ed Butterline
Symmetricom
1461 Carlisle Road
North Brunswick, NJ 08902
Tel: 732-246-7891
Fax: 732-246-7277
ebutterline@symmetricom.com

Malcolm D. Calhoun
Jet Propulsion Laboratory
4800 Oak Grove Drive
MS 298-100
Pasadena, CA 91109
Tel: 818-354-9763
Fax: 818-393-6773
malcolm.d.calhoun@jpl.nasa.gov

Glen E. Cameron
Syntomics LLC
9250 Bendix Road, North
Columbia, MD 21045-1800
Tel: 410-480-7205
Fax: 410-480-7202
glen.cameron@syntonicsscorp.com

Arnold Castro
Honeywell
4060 East Bijou Street
Colorado Springs, CO 80909
Tel: 719-637-6527
Fax: 719-380-7144
Arnold.Castro@atsc-dsc.com

Tom Celano
Timing Solutions Corporation
5335 Sterling Drive, Suite B
Boulder, CO 80301
Tel: 303-939-8481
Fax: 303-443-5152
tpcelano@timing.com

Harold Chadsey
U.S. Naval Observatory
3450 Massachusetts Ave., NW
Washington, DC 20392
Tel: 202-762-1092
Fax: 202-762-1511
hc@planck.usno.navy.mil

Gary Dieter
Boeing
440 Discoverer Ave.
Suite 38
Schriever AFB, CO 80912
Tel: 719-567-3176
Fax: 719-567-2664
Gary.L.Dieter@Boeing.com

David W. Fowler
USCG Navigation Center
7323 Telegraph Rd.
Alexandria, VA 22315-3940
Tel: 703-313-5872
Fax: 703-313-5805
dfowler@navcen.uscg.mil

Thomas A. Clark
NASA Goddard Space
Flight Center
Code 920.3
Greenbelt, MD 20771
Tel: 301-614-5866
clark@tomcat.gsfc.nasa.gov

Dennis J. Duven
JHU/APL
11100 Johns Hopkins Road
Laurel, MD 20723-6099
Tel: 240-228-6148
Fax: 240-228-6635
dennis_duven@jhuapl.edu

Nancy L. Franklin
DoD
17003 Longleaf Dr.
Bowie, MD 20716
Tel: 301-688-7390
nfrankli@csc.com

Leonard S. Cutler
Agilent Technologies
3500 Deer Creek
MS 26M-9
Palo Alto, CA 94304
Tel: 650-857-5259
Fax: 650-813-3384
len_cutler@agilent.com

James M. Early
Trimble
610 Herndon Pkwy.
Herndon, VA 20170
Tel: 703-464-1105
Fax: 703-904-1040
jim.early@trimble.com

David J. Fredlake
Timing Solutions Corporation
5335 Sterling Drive, Suite B
Boulder, CO 80301
Tel: 303-939-8481
Fax: 303-443-5152
djfredlake@timing.com

Rolf Dach
University Bern
Sidlerstrasse 5
CH-3012 Bern
Switzerland
Tel: 41-31-631-3802
Fax: 41-31-631-3869
dach@aiub.unibe.ch

Roger L. Easton
ROBARCO
Rt 2, Box 920
Canach, NH
Tel: 603-523-7532
Fax: 603-523-7532
easton@ncst.nrl.navy.mil

Gerald L. Freed
ITT Industries
100 Kingsland Rd
Clifton, NJ 07014-1993
Tel: 973-284-2104
Fax: 973-284-3394
gerald.freed@itt.com

Gerrit de Jong
NMI Van Swinden Laboratorium
97 Schoemakerstraat
2628 VK Delft
The Netherlands
Tel: 31-15-269-1623
Fax: 31-15-261-2971
gdejong@nmi.nl

Chris Ekstrom
U.S. Naval Observatory
3450 Massachusetts Ave., NW
Washington, DC 20392
Tel: 202-762-0066
Fax: 202-762-1421
ekstrom@atom.usno.navy.mil

Timothy J. Frei
TRW
One Space Park 01/1260
Redondo Beach, CA 90278
Tel: 310-813-3372
tim.frei@trw.com

Edoardo Detoma
Honeywell TSI
Corso Montecucco 95
10141 Torino
Italy
detomae@tin.it

Jeremy E. Elson
UCLA
923 2nd Street #G
Santa Monica, CA 90403
Tel: 310-395-6895
jelson@cs.ucla.edu

Hugo Fruehauf
Zyfer, Inc.
1585 S. Manchester Avenue
Anaheim, CA 92802-2907
Tel: 714-780-7960
Fax: 714-780-7760
hx@zyfer.com

William A. Diener
Jet Propulsion Laboratory
4800 Oak Grove Drive
MS 298-100
Pasadena, CA 91109
Tel: 818-354-6770
Fax: 818-393-6773
william.a.diener@jpl.nasa.gov

Sheila Faulkner
SFA, Inc.
3159 Patrick Henry Drive
Falls Church, VA 22044
Tel: 703-532-6411
Fax: 703-532-6338
bopenyan@aol.com

Ivan Galysh
Naval Research Laboratory
4555 Overlook Ave
Washington, DC 20375
Tel: 202-404-7060
Fax: 202-767-2845
galysh@juno.nrl.navy.mil

R. Michael Garvey
Datum
34 Tozer Road
Beverly, MA 01915
Tel: 978-927-8220
Fax: 978-927-4099
rmgarvey@datum.com

Robin P. Giffard
Agilent Technologies
3500 Deer Creek Road
MS 26-M3
Palo Alto, CA 96304
Tel: 650-485-5372
Fax: 650-485-3380
robin_giffard@agilent.com

Al Gifford
NIST
1101 Maryland Ave NE
Washington, DC 20002
Tel: 202-547-1816
algifford@aol.com

Jorge Gonzalez, Jr.
Jet Propulsion Laboratory
4800 Oak Grove Drive
MS 298-100
Pasadena, CA 91109
Tel: 818-354-6875
Fax: 818-393-6773
jorge.gonzalez-jr@jpl.nasa.gov

Clive Green
Quartzlock
Gothic, Plymouth Road
Totnes, Devon, TQ9 5LH
England
Tel: 44-1-803-862-062
Fax: 44-1-803-867-962
clivegreen@quartzlock.com

Charles A. Greenhall
Jet Propulsion Laboratory
4800 Oak Grove Drive
MS 298-100
Pasadena, CA 91109
Tel: 818-354-6944
Fax: 818-393-6773
charles.greenhall@jpl.nasa.gov

Christopher T. Gregerson
U.S. Naval Observatory
3450 Massachusetts Avenue, NW
Washington, DC 20392-5420
Tel: 202-762-1506
Fax: 202-762-1461
gregerson.chris@usno.navy.mil

Richard M. Hambly
CNS Systems, Inc.
363 Hawick Court
Severna Park, MD 21146-1409
Tel: 410-987-7835
Fax: 410-987-7836
rick@cnssys.com

Yuko Hanado
Communications Research Laboratory
4-2-1, Nukui-Kitamachi
184-8795 Koganei Tokyo
Japan
Tel: 81-42-327-7624
Fax: 81-42-327-6664
yuko@crl.go.jp

Wayne Hanson
NIST
325 Broadway
Boulder, CO
Tel: 303-497-5233
Fax: 303-497-3228
hanson@boulder.nist.gov

Guy Harles
SES/ASTRA
Chateau de Bergdorf
L-6815 Bergdorf
Luxembourg
Tel: 352-710-725-259
Fax: 352-710-725-416
guy_harles@ses-astra.com

David J. Harrington
TRW, Inc.
1 Space Park R5/2260
Redondo Beach, CA 90278
Tel: 310-814-7325
david.harrington@trw.com

Gregory E. Hatten
The Boeing Company
440 Discoverer Ave Ste 38
Schriever AFB, CO 80904
Tel: 719-567-2943
Fax: 719-567-2664
gregory.hatten@schriever.af.mil

Linda M. Herrell
Jet Propulsion Laboratory
4800 Oak Grove Drive
Pasadena, CA 91109
Tel: 818-354-0328
Fax: 818-393-6871
Linda.Herrell@jpl.nasa.gov

Eric S. Hodson
TASC
4801 Stonecraft Blvd.
Chantilly, VA 20151
Tel: 703-633-8300, x4408
Fax: 703-449-3400
eshodson@tasc.com

Safet Hodzic
Honeywell Technical Services Inc.
4060 E. Bijou St.
Colorado Springs, CO 80909
Tel: 719-637-6106
Fax: 719-380-7144
safet.hodzic@atsc-dsc.com

Douglas W. Hogarth
20241 194th PL NE
Woodinville, WA 98072-8889
Tel: 425-788-1507
doug@niceties.com

Mizuhiko Hosokawa
Communications Research Laboratory
4-2-1, Nukui-Kitamachi
184-8795 Koganei Tokyo
Japan
Tel: 81-42-327-7557
Fax: 81-42-327-6694
hosokawa@crl.go.jp

David A. Howe
NIST
325 Broadway
Boulder, CO 80305
Tel: 303-497-3277
Fax: 303-497-5996
dhowe@nist.gov

Steven T. Hutsell
U.S. Naval Observatory
Alternate Master Clock
400 O'Malley Avenue
Ste 44
Schriever AFB, CO 80912-4044
Tel: 719-567-6740
Fax: 719-567-6763
steven.hutsell@schriever.af.mil

Ben J. Jaramillo
U.S. Naval Observatory
3450 Massachusetts Avenue, NW
Washington, DC 20392-5420
Tel: 202-762-1538
Fax: 202-762-1461
jaramillo.ben@usno.navy.mil

Nicolette M. Jardine
U.S. Naval Observatory
Time Service Department
3450 Mass Ave. NW
Washington, DC 20392
Tel: 202-762-1414
Fax: 202-762-1511
jardine.nicolette@usno.navy.mil

Kenneth J. Johnston
U.S. Naval Observatory
3450 Massachusetts Avenue, NW
Washington, DC 20392-5420
Tel: 202-762-1513
Fax: 202-762-1461
kjj@astro.usno.navy.mil

Man Jong Lee
Korea Telecom
17 Woomyeon-dong, Seocho-gu
Seoul 137-792
Republic of Korea
Tel: 82-2-526-6283
Fax: 82-2-526-5216
mjlee@kt.co.kr

Sarunaz K. Karuza
The Aerospace Corporation
PO Box 92957
Los Angeles, CA 90009
Tel: 310-336-6837
Fax: 310-336-6225

William J. Klepczynski
ISI
3520 South River Terrace
Edgewater, MD 21037
Tel: 410-798-8457
Fax: 410-798-8567
bill.ctr.klepczynski@faa.gov

Paul Koppang
Datum
34 Tozer Road
Beverly, MA 01915
Tel: 978-927-8220
Fax: 978-927-4099
pkoppang@datum.com

Nicholas Koshelyaevsky
IMVP GP "VNIIFTRI"
141570 Mendelev Moscow
Russia
Tel: 7-95-534-8222
Fax: 7-95-535-1359
nkoshelyaevsky@imvp.aspnet.ru

James D. Kronman
TRW
1800 S. Robertson Blvd.
PMB 2032
Los Angeles, CA 90035-4352
bacchus@compuserve.com

Paul F. and Aline Kuhnle
3218 Kirkham Drive
Glendale, CA 91206
Tel: 818-790-5641
Fax: 818-952-5124
paulkuhnle@earthlink.net

Hans J. Kunze
NavCom Technology, Inc.
123 W. Torrance Blvd
Suite 101
Redondo Beach, CA 90277
Tel: 310-937-7460 x245
Fax: 310-937-7464
hkunze@navcomtech.com

Jack Kusters
Agilent Technologies
5301 Stevens Creek Blvd
M/S 51U/23
Santa Clara, CA 95052
Tel: 408-553-2042
Fax: 408-553-2123
jack_kusters@agilent.com

Francois Lahaye
Natural Resources, Canada
615 Booth Str.
Ottawa K1A 0E9 Ontario
Canada
Tel: 613-995-4488
Fax: 613-995-3215
lahaye@geod.nrcan.gc.ca

Paul Landis
NRL/SFA
4555 Overlook Avenue, SW
Washington, DC 20375
Tel: 202-404-7061
Fax: 202-767-2845
landis@juno.nrl.navy.mil

Werner R. Lange
Lange-Electronic GmbH
Ganghoferstr. 29
D-82216 Gernlinden
Germany
Tel: 49-8142-1041
Fax: 49-8142-1065
WLange@lange-electronic.de

Marie M. Largay
Naval Research Laboratory
4555 Overlook Avenue, SW
Washington, DC 20375
Tel: 202-404-4009
Fax: 202-767-2845
largay@juno.nrl.navy.mil

Donald Latterman
SAIC
21151 Western Avenue
Torrance, CA 90501
Tel: 310-781-8697
Fax: 310-781-8742
donald.latterman@saic.com

Judah Levine
National Institute of
Standards and Technology
325 Broadway
Boulder, CO 80305
Tel: 303-492-7785
Fax: 303-497-6461
jlevine@boulder.nist.gov

Wlodzimierz Lewandowski
BIPM
Pavillon de Breteuil
92310 Sevres
France
Tel: 33-1-45-07-70-63
Fax: 33-1-45-34-20-21
wlewandowski@bipm.fr

Frank Lifsey
ITT Industries
2560 Huntington Ave.
Alexandria, VA 22303
Tel: 202-279-2193
Fax: 703-329-3941
Frank.Lifsey@itt.com

Michael A. Lombardi
NIST
325 Broadway
Boulder, CO 80305
Tel: 303-497-3212
Fax: 303-497-3228
lombardi@boulder.nist.gov

Matthew G. Long
Naval Research Laboratory
Code 8131
4555 Overlook Avenue, SW
Washington, DC 20375-5320
Tel: 202-767-3839
Fax: 202-767-1317
long@ssdd.nrl.navy.mil

Matteo Luccio
GPS World
Raritan Plaza III
101 Fieldcrest Avenue
Edison, NJ 08837
Tel: 732-225-9500
Fax: 732-225-0211
mluccio@advanstar.com

Jerome A. Luine
TRW, Inc.
M5/1075 One Space Park
Redondo Beach, CA 90278
Tel: 310-812-0256
Fax: 310-812-0542
jerome.luine@trw.com

Edward M. Lukacs
U.S. Naval Observatory
3450 Massachusetts Ave., NW
Washington, DC 20392
Tel: 202-762-1092
Fax: 202-762-1511
eml@fermi.usno.navy.mil

Robert Lutwak
Datum
34 Tozer Road
Beverly, MA 01915
Tel: 978-927-8220
Fax: 978-927-4099
rlutwak@datum.com

Kenneth D. Lyon
Datum
34 Tozer Road
Beverly, MA 01915
Tel: 978-927-8220
Fax: 978-927-4099
klyon@datum.com

Werner Mache
BEV
Arltgasse 35
A-1160 Vienna
Austria
Tel: 43-1-491-10302
Fax: 43-1-492-0875
w.mache@bev-eich.gv.at

Leo A. Mallette
Boeing
2309 S. Santa Anita
Arcadia, CA 91006
Tel: 310-364-9243

Stephen Malys
NIMA
3467 Emy's Place
Monrovia, MD 21770
Tel: 301-227-7588
Fax: 301-227-5016
malys@nima.mil

Louis Marais
CSIR
PO Box 395
0001 Pretoria
South Africa
Tel: 27-12-841-3013
Fax: 27-12-841-2131
elmarais@csir.co.za

Demetrios N. Matsakis
U.S. Naval Observatory
Time Service Department
3450 Mass Ave. NW
Washington, DC 20392
Tel: 202-762-1587
Fax: 202-762-1511
dnm@orion.usno.navy.mil

Dennis D. McCarthy
U.S. Naval Observatory
3450 Mass Ave. NW
Washington, DC 20392
Tel: 202-762-1837
Fax: 202-762-1563
dmc@maia.usno.navy.mil

Thomas B. McCaskill
Naval Research Laboratory
4555 Overlook Avenue, SW
Washington, DC 20375
Tel: 202-404-7068
Fax: 202-767-2845
mccaskill@juno.nrl.navy.mil

Tim McCauley
ITT Industries
2560 Huntington Ave.
Alexandria, VA 22303
Tel: 202-279-2630
Fax: 703-329-3941
tim.mccauley@itt.com

Angela D. McKinley
U.S. Naval Observatory
3450 Massachusetts Ave., NW
Washington, DC 22007
Tel: 202-762-1457
Fax: 202-762-1511
mckinley.angela@usno.navy.mil

Kevin P. McMenamin
Agilent Technologies
8825 Stanford Blvd.
Columbia, MD 21045
Tel: 443-285-7741
Fax: 443-285-7830
kevin_mcmenamin@agilent.com

Marvin P. Meirs
FEIC
55 Charles Lindburg Blvd.
Uniondale, NY
Tel: 516-784-4500
Fax: 516-784-4340

Daniel R. Melick
Stanford Research Systems, Inc.
1290 D Reamwood Avenue
Sunnyvale, CA 94089
Tel: 408-744-9040
Fax: 408-744-9049
dan@thinksrs.com

François F. Meyer
Observatoire de Besançon
41b av. de l'Observatoire BP1615
25010 Besançon Cedex
France
Tel: 33-3-8166-6927
Fax: 33-3-8166-6944
fmeyer@obs-besancon.fr

David L. Mills
University of Delaware
Electrical and Computer
Engineering Department
Newark, DE 19716
Tel: 302-831-8247
Fax: 302-831-4316
mills@udel.edu

Mihran Miranian
U.S. Naval Observatory
3450 Massachusetts Ave., NW
Washington, DC 20392
Tel: 202-762-1092
Fax: 202-762-1511
mm@aitken.usno.navy.mil

Donald H. Mitchell
TrueTime, Inc.
3750 Westwind Blvd.
Santa Rosa, CA 95403
Tel: 707-528-1230, ext. 118
Fax: 707-527-6640
dmitchell@truetime.com

Bruce G. Montgomery Syntomics LLC 9250 Bendix Road, North Columbia, MD 21045-1800 Tel: 410-480-7203 Fax: 410-480-7202 Bruce.Montgomery@SyntomicsCorp.com	Keith Payea TrueTime, Inc. 3750 Westwind Blvd. Santa Rosa, CA 95403 Tel: 707-528-1230, x113 Fax: 7073527-6640 kpaya@truetime.com	Tom Radey JPL 4800 Oak Grove Drive MS 168-222 Pasadena, CA 91109 Tel: 818-384-2010 tom.radey@jpl.nasa.gov
T. Boyd Moore ITT Industries 2560 Huntington Ave. Alexandria, VA 22303 Tel: 202-279-2158 Fax: 703-329-3941 boyd.moore@itt.com	Alexander H. N. Pawlitzki Timetech GmbH Cuiestrasse 2 D-70563 Stuttgart Germany Tel: 49-711-678-080 Fax: 49-711-678-0899 alexander.pawlitzki@timetech.dr	Steven J. Rajotte NAVSTAR GPS JPO 2435 Vela Way Suite 1613 El Segundo, CA 90245-5500 Tel: 310-363-2431 Fax: 310-363-3844 steven.rajotte@losangeles.af.mil
Lisa M. Nelson NIST 325 S. Broadway, MS 847 Boulder, CO 80305-3328 Tel: 303-497-3446 Fax: 303-497-6461 lnelson@boulder.nist.gov	Rolando Penabade TRAK Microwave 4726 Eisenhower Blvd. Tampa, FL 33634 Tel: 813-901-7365 Fax: 813-901-7493 rpenabade@trak.com	Victor S. Reinhardt Boeing Space Systems PO Box 92919 Los Angeles, CA 90009 Tel: 310-416-4980
Robert A. Nelson Satellite Engineering Research Corporation 7701 Woodmont Ave., Ste 208 Bethesda, MD 20814 Tel: 301-657-9641 Fax: 301-657-9642 robtnelson@aol.com	Hsin-Min Peng Chunghwa Telecommunication Laboratories 12, Lane 551, Min-Tsu Road Sec. 5, Yang-Mei, Taoyuan Taiwan 326, R.O.C. Tel: 886-3-424-5174 Fax: 886-3-424-5178 hmpeng@ms.chttl.com.tw	Randall H. Reith ITT Industries 440 Discoverer Street Ste. 79 Schriever AFB, CO 80912-4479 Tel: 719-567-3952 Fax: 719-567-3927 randall.reith@schriever.af.mil
Jay Oaks Naval Research Laboratory 4555 Overlook Avenue, SW Washington, DC Tel: 202-767-1434	Bruce Penrod EndRun Technologies 520 Mendocino Avenue, Ste 380 Santa Rosa, CA 95401 Tel: 707-573-8633 Fax: 707-573-8619	William J. Riley Datum 34 Tozer Road Beverly, MA 01915 Tel: 978-927-8220 Fax: 978-927-4099 wriley@datum.com
Allen W. Osborne, III Allen Osborne Associates, Inc. 756 Lakefield Road Westlake Village, CA 91361 Tel: 805-495-8420 Fax: 805-373-6067 s_osborne@aoa-gps.com	Thomas Petsopoulos Naval Research Laboratory 4555 Overlook Avenue, SW Washington, DC 20375-5320 Tel: 202-404-3531 tpetsopoulos@space.nrl.navy.mil	Pascal Rochat Temex Neuchatel Vauseyon 29 Neuchatel Switzerland Tel: 41-32-732-1666 Fax: 41-32-732-1667 rochat@temex.ch
Peter Z. Paulovich SPAWAR Charleston PO Box 1376 Norfolk, VA 23501-1376 Tel: 757-396-0287 Fax: 757-396-0518 paulovip@spawar.navy.mil	Edward D. Powers U.S. Naval Observatory 3450 Massachusetts Ave., NW Washington, DC 20392 Tel: 202-762-1092 Fax: 202-762-1511 powers.edward@usno.navy.mil	Tom Rodilosso Naval Research Laboratory 4555 Overlook Ave., SW Washington, DC 20375 Tel: 202-404-4106 rodilosso@juno.nrl.navy.mil

Ron Roloff
Advanced Technical Resources LLC
8005 McKenstry Drive
Laurel, MD 20723
Tel: 301-725-5363
Fax: 301-953-0246
rroloff@clark.net

Fabian Roosbeek
Royal Observatory of Belgium
Avenue Circulaire, 3
1180 Brussels
Belgium
Tel: 32-2-373-02-46
Fax: 32-2-374-98-22
fabian.roosbeek@oma.be

Bill Ryan
DISA
10701 Parkridge Blvd.
Reston, VA 22191
Tel: 703-735-3177
Fax: 703-735-3354
ryanw@ncr.disa.mil

Wolfgang Schafer
TimeTech GmbH
Curiestrasse 2
D-70563 Stuttgart
Germany
Tel: 49-711-678-080
Fax: 49-711-678-0899
wolfgang.schaefer@timetech.de

Lara S. Schmidt
U.S. Naval Observatory
Time Service Department
3450 Mass Ave. NW
Washington, DC 20392
Tel: 202-762-0289
Fax: 202-762-1511
lss@ramsey.usno.navy.mil

Richard E. Schmidt
U.S. Naval Observatory
3450 Massachusetts Ave., NW
Washington, DC 20392
Tel: 202-762-1578
Fax: 202-762-1511
res@simon.usno.navy.mil

Debbie Scott
Meetings Verbatim
PO Box 941221
Atlanta, GA 31141
Tel: 404-814-1222
spicy1@mindspring.com

Ken Senior
U.S. Naval Observatory
3450 Massachusetts Ave., NW
Washington, DC 20392
Tel: 202-762-1092
Fax: 202-762-1511
ksenior@usno.navy.mil

Art Sepin
Synergy Systems, LLC
PO Box 262250
San Diego, CA 92196
Tel: 858-556-0666
Fax: 858-556-0768

George A. Shaton
DoD
3808 Palmetto Ct.
Ellicott City, MD 21042-4922
Tel: 301-688-7322

Charles M. Shenitz
Litton-TASC
131 National Business Parkway
Ste. 110
Annapolis Junction, MD 20701
Tel: 301-483-6000 x2078
Fax: 301 604-0500
cmshenitz@tasc.com

Dieter Sibold
Physikalisch-Technische Bundesanstalt
Bundesallee 100
Braunschweig D-38116
Germany
Tel: 49-531-592-8410
Fax: 49-531-592-8406
Dieter.Sibold@ptb.de

Gary Smith
Brandywine Communications
2133 South Hathaway St.
Santa Ana, CA 92705
Tel: 714-755-1050
Fax: 714-755-1070

Stephanie Smith
Meetings Verbatim
PO Box 941221
Atlanta, GA 31141
Tel: 404-814-1222

Robert W. Snow
Magellan Corporation
471 El Camino Real
Santa Clara, CA 95050
Tel: 408-615-5246
Fax: 408-615-5200
rsnow@magellangps.com

Clifford Snowe
Computer Sciences Raytheon
PO Box 4127, CSR 2100
Patrick AFB, FL 32925
Tel: 321-494-2800
Fax: 321-494-3949
snowec@rc.pafb.af.mil

Armin Soering
Deutsche Telekom AG
Am Kavalleriesand 3
Darmstadt 64295
Germany
Tel: 49-6151-83-4549
Fax: 49-6151-83-3834
Armin.Soering@telekom.de

Samuel R. Stein
Timing Solutions Corporation
5335 Sterling Drive, Suite B
Boulder, CO 80301
Tel: 303-939-8481
Fax: 303-443-5152
srstein@timing.com

Loyal D. Stewart
Honeywell Technology Solutions, Inc.
7515 Mission Dr.,
B1CG7
Lanham, MD 20706
Tel: 301-805-3939
Fax: 301-805-3974
loyal.stewart@honeywell-tsi.com

Michail Stolhand
CSC
Utah Test & Training Range
PO Box 217
Clearfield, UT 84089-0217
Tel: 801-777-4746
Fax: 801-775-2664
michail.stolhand@hill.af.mil

Donald R. Stribling
Honeywell
4060 East Bijou Street
Colorado Springs, CO 80909
Tel: 719-637-6780
Fax: 719-380-7144
don.stribling@atsc-dsc.com

Thomas B. Swanson
U.S. Naval Observatory
3450 Massachusetts Ave, NW
Washington, DC 20392
Tel: 202-762-1458
Fax: 202-762-1511
swanson@atom.usno.navy.mil

Richard L. Sydnor
JPL
2985 Zane Grey Terrace
Altadena, CA
sydnor@pacbell.net

Philip E. Talley, Jr.
SFA, Inc.
311 Eagle Crest
Macon, GA 31211-6013
Tel: 478-745-3415
ptalley.me50@gtalumni.org

Jack Taylor
Boeing
440 Discoverer Ave., Ste 38
Schriever AFB, CO 80912
Tel: 719-567-5953
Fax: 719-567-2664
Jack.Taylor2@boeing.com

Massimo Tinto
Jet Propulsion Laboratory
4800 Oak Grove Drive
Pasadena, CA 91109
Tel: 818-354-0798
Fax: 818-393-4643
Massimo.Tinto@jpl.nasa.gov

Robert L. Tjoelker
Jet Propulsion Laboratory
4800 Oak Grove Drive
MS 298-100
Pasadena, CA 91109
Tel: 818-354-1873
Fax: 818-393-6773
robert.l.tjoelker@jpl.nasa.gov

Bryan W. Tolman
University of Texas
PO Box 8029
Austin, TX 78713-8029
Tel: 512-835-3412
Fax: 512-835-3808
btolman@arlut.utexas.edu

Minh Q. Tran
U.S. Naval Observatory
3450 Mass Ave. NW
Washington, DC 20392
Tel: 202-762-0913
Fax: 202-762-1511
tran.minh@usno.navy.mil

John Vaccaro
PerkinElmer Optoelectronics
35 Congress St.
Salem, MA 01970
Tel: 978-745-0200
Fax: 978-745-0894
john.vaccaro@perkinelmer.com

Tom Van Baak
5171 150th Place SE
Bellevue, WA 98006
Tel: 425-378-1231
tvb@LeapSecond.com

Francine Vannicola
U.S. Naval Observatory
3450 Massachusetts Ave., NW
Washington, DC 20392-5420
Tel: 202-762-1455
Fax: 202-762-1511
fmv@usno.navy.mil

Francois Vernotte
Observatoire de Besancon
41 bis ave. de l'observatoire - BP 1615
25010 Besancon
France
Tel: 33-3-81-66-69-22
Fax: 33-3-81-66-69-44
francois@obs-besancon.fr

John R. Vig
Army CECOM
AMSEL-RD-C2-PT
Ft. Monmouth, NJ 07703
Tel: 732-427-4275
Fax: 732-427-4805
j.vig@ieee.org

Warren F. Walls
Femtosecond Systems, Inc.
4894 Van Gordon St.
Ste 301-N
Wheat Ridge, CO 80033-2170
Tel: 303-403-1213
Fax: 303-403-4044
WarrenW@phasenoise.com

S. Clark Wardrip
SFA, Inc.
726 Foxenwood Dr.
Santa Maria, CA 93455-4221
Tel: 805-937-6448
Fax: 805-937-9601
skyclark@aol.com

June E. Watanabe
Litton PRC
222 Sepulveda Blvd.
El Segundo, CA
Tel: 310-252-8028
watanabe_june@prc.com

Richard A. Watkins
Computer Sciences Corporation
PO Box 217
Clearfield, UT 84089-0217
Tel: 801-777-4865
rick.watkins@hill.af.mil

Werner Weidemann
Zyfer, Inc.
1585 S. Manchester Ave.
Anaheim, CA 92802
Tel: 714-780-7640
Fax: 714-780-7696
waw@zyfer.com

Marc A. Weiss
NIST
325 Broadway
Boulder, CO 80305
Tel: 303-497-3261
Fax: 303-497-3884
mweiss@nist.gov

Paul J. Wheeler
U.S. Naval Observatory
3450 Massachusetts Ave., NW
Washington, DC 20392
Tel: 202-762-1581
Fax: 202-762-1511

Joe White
U.S. Naval Research Laboratory
Code 8150.1
4555 Overlook Avenue, SW
Washington, DC 20375
Tel: 202-767-5111
Fax: 202-767-4050
white@juno.nrl.navy.mil

Lisa Withers
TrueTime, Inc.
3750 Westwind Blvd.
Santa Rosa, CA 95403
Tel: 707-528-1230
Fax: 707-527-6640
lwithers@trueitime.com

James L. Wright
Computer Sciences Raytheon
PO Box 4127, CSR 2500
Patrick AFB, FL 32925
Tel: 321-494-6379
Fax: 321-494-3057
james.wright@rc.patrick.af.mil

Andy Wu
The Aerospace Corporation
2350 E. El Segundo Blvd.
El Segundo, CA 90245-4691
Tel: 310-336-0437
Fax: 310-336-5076
andy.wu@aero.org

Victor S. Zhang
NIST
325 Broadway
Boulder, CO 80303
Tel: 303-497-3977
Fax: 303-497-6461
vzhang@boulder.nist.gov

Miao Zhu
Agilent Technologies
3500 Deer Creek Road
Palo Alto, CA 94304
Tel: 650-485-4414
Fax: 650-485-6241
miao_zhu@agilent.com